DTU Mechanical Engineering
Department of Mechanical Engineering

Heat pumps supplying district heating and ancillary services for the power system

Wiebke Meesenburg

PhD Thesis

Heat pumps supplying district heating and ancillary services to the power system
PhD thesis
2020

By
Wiebke Meesenburg

Published by: DTU Mechanical Engineering, Nils Koppels Allé 403, 2800 Kgs. Lyngby, Denmark
www.dtu.dk
ISSN: [0903-1685] (electronic version)
ISBN: [000-00-0000-000-0] (electronic version)

ISSN: [0903-1685] (printed version)
ISBN: [000-00-0000-000-0] (printed version)

Preface

This thesis was submitted as partial fulfilment of the requirements for the Ph.D. degree at the Technical University of Denmark (DTU).The thesis was completed at the Section of Thermal Energy, Department of Mechanical Engineering, Technical University of Denmark. The work was carried out from 1st October, 2016 to 31th December, 2019. The work was conducted under the supervision of Professor Brian Elmegaard and the co-supervision of Associate Professor Wiebke Brix Markussen and Researcher Torben Ommen. An external research stay was undertaken in the period from March 2018 to April 2018 at AIT, Group for Integrate Energy Systems in Vienna, Austria. The PhD project was part of the EnergyLab Nordhavn research project, which was financially funded by EUDP (Energy Technology Development and Demonstration programm), under the project title: "EnergyLab Nordhavn - New Urban Energy Infrastructures" (project number: 64014-0555). The participation at conferences and the external stay were financially supported by Otto Mønsteds Fond. All financial support is gratefully acknowledged.

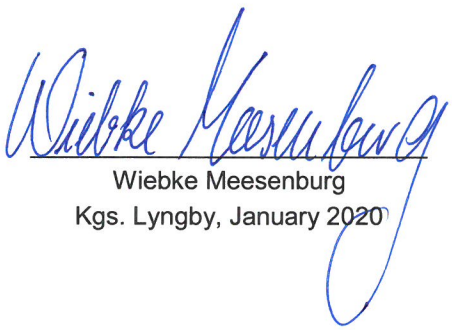

Wiebke Meesenburg
Kgs. Lyngby, January 2020

Acknowledgements

Undertaking this PhD has been an interesting and challenging experience that I am very grateful for. This work would not have been possible without the guidance and support of many people.

I want to thank my supervisor Brian Elmegaard for giving me the opportunity to work on this exiting project and his constant encouragement. I am especially thankful for his trust, which gave me the freedom to follow many of my own ideas, while always being available for discussions. I thank my co-supervisor Wiebke Brix Markussen for always being supportive, positive-minded and for understanding my language confusion better than anyone else. Thank you, Torben, for always having an open door, the patience to discuss any huge or tiny problem and for developing new ideas together.

This work has benefitted from proofreading, comments and abstract translation by my supervisors and Arne Jørgensen Egelund, Benjamin Zühlsdorf and Pernille Hartmund Jørgensen. Tusind tak.

I want to express my gratitude to Andreas Thingvad and Mattia Marinelli for the fruitful cooperation and for teaching me a lot about ancillary services and the electrotechnical view on things.

I was fortunate to be part of the EnergyLab Nordhavn project. I enjoyed the multiple interdisciplinary meetings and exchange with the other participants, as well as numerous tours through Nordhavn, which gave me the opportunity to show a little of what we did in the project to the real world out there. I am especially thankful for the well functioning cooperation with Hofor on the FlexHeat heat pump and on ultra-low temperature district heating. A special thank you goes to Tore Friis Gad Kjeld, for believing in flexible heat pumps just as much as I did and for a pleasant cooperation, even in stressful times. I also want to thank Jan Eric Thorsen from Danfoss for the cooperation on the booster heat pump substations and the ultra-low temperature district heating paper as well as for his enthusiasm and the nice e-mails, which always left me motivated. Further, I want to thank Matteo Caramaschi and Kasper Korsholm Østergaard from MetroTherm for the discussions on ultra-low temperature district heating and for challenging my ideas. I also want to acknowledge Christoffer Greisen, who did a great job in keeping this project together, and all of the participants of the PhD and PostDoc Forum for sharing ideas and thoughts.

I am grateful that I had the opportunity of collaborating with Johnson Controls. Especially, I want to thank Simon Stubkier, Per Skov and Dan Lyng for providing many useful insights and for fruitful discussions.

The external stay at the Austrian Institute of Technology in Vienna, was a valuable experience and I enjoyed the friendly atmosphere and the interesting discussions, which gave me another perspective on my work. I especially want to thank Ralf-Roman, Roman, and the female power office, Charlotte, Johanna and Olatz.

I want to acknowledge the participants of the coffee club for plenty of discussions and an insight into everybody's work. A big thank you goes to all my colleagues from the Section of Thermal Energy who contributed to an atmosphere that always made me want to go to work by sharing

enjoyable lunch times, having time for a chat, being patient with my Danish skills and by sharing many activities and experiences outside work together. A special thank you goes to my office mates: Pernille who went all the long PhD-way together with me, Benjamin for being the friend and expert I truly needed sometimes, Roberta for the ladies power and your cheerfulness, Valentin for never ever letting me forget to eat lunch and always reminding me of going home, Fabian for sharing chocolate with me (and sometimes even socks), Henrik for the collaboration in the EnergyLab Nordhavn project and great cakes and Brice for answering so many small questions.

It is good to be reminded once in a while that there is more to life than heat pumps. I want to thank the Exiles for this, for the ship that never sinks and for many memorable moments.

Ich möchte auch meinen Freunden in Deutschland (und im Rest der Welt) danken, die immer irgendwie da sind, auch wenn ich sie viel zu selten sehe.

Danke Mama, Papa und Maike dafür, dass ihr immer noch ein bisschen mehr an mich glaubt, als ich das selber kann. Für eure Liebe, Verständnis, das beste Home-office der Welt, mentale Unterstützung am Telefon und Geduld mit mir in allen stressigen Situationen. Und Danke Oma für das mathematische Talent.

René, die Stunden, die du mit mir diskutiert hast sind unzählbar, dein Feedback und Rat sind unersätzlich, und deine Ruhe und Gelassenheit haben mich manches Mal vor panischen Reaktionen bewahrt. Du passt auf mich auf, wenn ich es selbst nicht kann und bist mir dabei immer der beste Partner, Freund und Kollege, den ich mir wünschen kann. Danke.

Contents

Abstract

Transforming the energy system to a renewable energy system requires rethinking the structure of the system. One way to allocate large shares of renewable power production in the system is the coupling of different energy sectors in an integrated energy system. Large-scale heat pumps are expected to play a key role within these integrated energy systems, as they provide a link between the district heating sector and power sector. Thereby, they may unlock the thermal storage capacity of the district heating system to provide flexibility, while enabling the supply of heat from renewable heat sources. To analyse, whether and to what extend heat pumps may serve this purpose, the technical and economical feasibility of heat pumps supplying district heating and ancillary services for the power grid was assessed in this study, which was divided into three main parts.

The first part analysed, how the district heating system should be optimally designed to allow for the most feasible heat supply from heat pumps through a techno-economic approach. This allowed analysing the influence of the boundary conditions of the supplied area on the economic feasibility of the assessed heat pump based supply solutions. In the second part, the technical ability of large-scale ammonia heat pumps to supply frequency regulation was assessed. This was done using a dynamic model of a heat pump that was validated against measurements of an existing heat pump in Nordhavn, Copenhagen. It was assessed how the design of the heat pump system and the corresponding control structure influence the ability of the heat pump to operate flexibly to provide primary frequency regulation. Finally, the feasibility of providing frequency regulation from large-scale heat pumps was assessed and compared to a combined frequency regulation service delivered by the heat pump together with fast regulating electric vehicles. For this study, a simplified dynamic model of the overall heat pump and district heating system was used. This model further included the calculation of exergy and cost of all streams in the system. Based on these exergoeconomic data, a method to allocate cost to the two products of the heat pump, i.e. heat and ancillary services, was proposed. The following findings may be summarised based on the work presented in this thesis. Firstly, for future suburban and urban areas in Denmark supplied by heat pumps, the supply of low-temperature district heating from central large-scale heat pumps is most feasible. For areas with low linear heat demand densities, individual heat pumps become more feasible, while the feasibility of ultra-low temperature district heating suffers from the requirement of large space heating shares and additional cost for decentral heating units, despite the higher thermodynamic efficiency. Secondly, the dynamic behaviour of large-scale heat pumps and especially the ability to change load quickly is influenced strongly by the control structure of the system, controller parametrisation and the refrigerant mass in the system. A limiting factor of fast regulation of ammonia heat pumps is the risk of droplet formation in the suction line during fast ramp down. Within this work, it was shown that future fast regulating heat pumps should be designed, such that the refrigerant mass is minimised, especially in the vessels. Further, it is advantageous if the power uptake is controlled directly. Thirdly, it was shown that the assessed large-scale ammonia heat pump was able to follow a given frequency deviation and thereby may in principle provide frequency controlled reserve. If the allowed regulation time of the frequency regulation service is long enough, i.e. 150 s like FCR-N service in Eastern Denmark, the heat pump may provide frequency regulation on its own, which would maximise the obtainable income for the heat pump owner. If the heat pump is not fast enough to provide the service alone, e.g. for the required regulation times of 30 seconds in Western Denmark, it may be operated in combination with fast regulating bidirectional units, such as electric vehicles. This allows for a combined service provision and the exploitation of synergies between the different units, as the heat pump may generate an additional income from supplying ancillary services, while ensuring that the electric vehicles can bid a larger power capacity into the market. Finally, the proposed allocation method allows quantifying the influence of different operation strategies on the cost of the two different products of the system, i.e. heat and ancillary services. Overall, this work

showed that large-scale heat pumps may be equipped to be able to take over the intended role as flexible units between the heating and power system and that this operation mode can be economically feasible within the Danish market framework.

Resumé

Transformering af det nuværende energisystem til et bæredygtigt energisystem kræver en omstrukturering af systemet. En måde at allokere en stor andel af vedvarende strømproduktion i systemet, er gennem et integreret system med kobling af forskellige energisektorer. Det er forventet at storskala varmepumper spiller en afgørende rolle i et integreret energisystem, da de introducerer et link i mellem elsektoren og fjernevarmesektoren. Dermed kan de åbne for fleksibiliteten i fjernvarmenettets termiske lagerkapacitet, og samtidig sikre varmeforsyning fra vedvarende kilder. Dette studie er inddelt i tre dele, der alle har til formål at undersøge og vurdere, til hvilken grad varmepumper, i et teknisk og økonomisk perspektiv, kan levere både fjernvarme og systemydelser til elnettet.

I den første del er det, ud fra en teknoøkonomisk vinkel, undersøgt hvordan fjernevarmesystemet kan designes for at skabe optimal varmeforsyning med varmepumper. Dette inkluderede en økonomisk analyse af betydningen af forsyningsområdets randbetingelser for de mulige varmepumpeløsninger.

I den anden del blev den tekniske formåen af storskala ammoniak varmepumper undersøgt i forhold til frekvensregulering. Dette blev gjort med en dynamisk model, som forinden var valideret med data fra et eksisterende varmepumpeanlæg i Nordhavn. Undersøgelsen indebar hvordan designet af varmepumpen og den tilhørende styringsstrategi har indflydelse på mulighederne for at udnytte varmepumpen fleksibelt i forbindelse med primær frekvensregulering af elnettet.

I tredje del blev den økonomiske gevinst ved at udnytte storskala varmepumper til frekvensregulering holdt op i mod fordelen ved en kombinationen af storskala varmepumper og hurtig regulering ved hjælp af elbiler. Til dette studiet blev der benyttet en simpel, overordnet dynamisk model af en varmepumpe og fjernvarmenettet. Modellen inkluderede beregninger af exergi og omkostninger for alle dele af systemet. Baseret på disse exergoøkonimiske data, blev en metode til at allokere omkostningerne til hver af de to produkter, varme og reguleringsservices, forslået.

De følgende resultater er en opsummering baseret på ovenstående analyser. Først er det vist at den bedste varmepumpeløsning til varmeforsyning af fremtidige byområder, er et lavtemperatur fjernvarmenet forsynet med en storskala varmepumpe. For områder med lav varmebovstæthedsgrad, bliver individuelle varmepumper mere attraktive, mens den økonomiske gevinst bliver mindre fordelagtigt ved ultra-lavtemperaturfjernvarme på trods af deres højere effektivitet. Årsagen til det er en mindre andel af rumopvarmning og ekstra omkostninger for decentrale varmeforsynende enheder.

Dernæst er det også vist at de dynamiske effekter i en varmepumpe, og specielt muligheden for hurtig lastændring, er stærkt påvirket af systemets styringsstruktur, indstilling af styringsparametrene, og mængden af kølemiddel i systemet. Kondensering i sugegasledningen er en begrænsende faktor på hurtig nedregulering af ammoniak varmepumper. I studiet er det vist at fremtidige varmepumper til fleksibelt drift skal designes således at kølemiddelfyldningen minimeres, særligt i de indbyggede beholdere, samt at det er en fordel hvis effektoptaget er direkte styret. Endvidere blev det vist at en storskala ammoniak varmepumpe var i stand til at følge en given frekvensafvigelse, og at denne dermed i princippet kan levere frekvensstyret reserve. Hvis responstiden for frekvensregulering er lang nok, f.eks. 150 sekunder som ved FCN-R service i Østdanmark, kan varmepumpen alene levere frekvensregulering, hvilket vil maximere den mulige indkomst for ejeren af varmepumpen. Hvis varmepumpen ikke kan reguleres hurtigt nok til at levere den service selv, dvs. inden for en responstid på 30 sekunder for Vestdanmark, kan dette opnås i kombination med hurtigt regulerende enheder, såsom elbiler.

Dette kan medføre en kombineret levering a frekvens reguleringsydelser og udnyttelse af synergi mellem forskellige enheder, da varmepumpen kan genere ekstra indkomst fra systemydelser, samtidig med at elbilerne kan byde ind med en større kapacitet på elmarkedet. Endeligt, blev en exergoøkonomisk baseret metode til at allokere mulige ekstra omkostninger og indkomster for både varmeforsyning og systemydelser fra varmepumpen fremsat. Metoden gør det muligt at kvantificere

den økonomiske indflydelse fra forskellige styringsstrategier på de to forskellige leverancer fra systemet.
Overordnet set har dette arbejde vist at storskala varmepumper kan udstyres, så at det er muligt at opfylde den påtænkte rolle som fleksible enheder mellem varme- og elsektoren og at denne driftsform kan være økonomisk rentabel indenfor danske markedsvilkår.

Nomenclature

Abbreviations

aFRR	Automatic frequency restoration reserve
CHP	Combined heat and power
DEX	Direct expansion evaporator
DH	District heating
DHAT	District heating assessment tool
DHW	Domestic hot water
DK1	Regulation zone of Western Denmark
DK2	Regulation zone of Eastern Denmark
El. PH	Electric preheating
EU	European Union
EV	Electric vehicle
FCR	Frequency controlled reserve
FCR-D	Frequency controlled reserve, disturbance reserve
FCR-N	Frequency controlled reserve, normal operation reserve
FFR	Fast frequency regulation
GW	Groundwater
HP	Heat pump
HS	High-stage
LS	Low-stage
LTDH	Low-temperature district heating
mFRR	Manual frequency restoration reserve
MIMO	Multi-input-multi-output
NPV	Net present value
O&M	Operation and maintenance
PI	Proportional-Integral (controller)
PID	Proportional-Integral-Differential (controller)
PSO	Public Service obligation
RMS	Root mean square
SCOP	System coefficient of performance
SH	Space heating
SISO	Single-input-single-output
SOC	State-of-charge
TSO	Transmission service operator
ULTDH	Ultra-low temperature district heating
VLE	Vapour-liquid equilibrium

Latin symbols

A	Area, m²
$\boldsymbol{B}$	Vector of standardised regression coefficients, -
c	Specific cost, €/(kWh a)
$\bar{c}$	Weighted average price, €/(kWh a)
c_p	Specific heat capacity, kJ/(kg K)
C	Cost, €/a
$\dot{C}$	Cost stream associated with material stream, €/s
COP	Coefficient of performance, -
D	Diameter, m
e	Specific exergy of material stream, kJ/kg
e_{bias}	Normalised energy bias, -
E	Exergy content of control volume, J
$\dot{E}$	Exergy flow, kW
f	Frequency, Hz
h	Specific enthalpy, kJ/kg
k	Parameter, -
L	Length, m
m	Mass, kg
N	Number of layers, -
NRMSD	Normalised root-mean-square deviation, -
q_l	Linear heat demand density, MWh/(m a)
q_s	Specific annual heat demand, kWh/(m² a)
Q	Heat, J or MWh
$\dot{Q}$	Heat flow rate, W
R^2	Coefficient of determination, -
s	Share of total heat demand, -
t	Time, s or h
T	Temperature, °C or K
$\bar{T}$	Weighted average temperature, °C or K

V	Volume, m^3
$\dot{V}$	Volume flow rate, m^3/s
w	Characteristic width, m
W	Work, J or MWh

Greek symbols

β	Standardised regression coefficient, -
Δ	Difference in subsequent parameter, -
ϵ	Exergy efficiency, -
ϵ	Plot ratio, -
ϵ	Tolerance band, % or W/s
η	Efficiency, -
λ	Friction factor, -
ρ	Density, kg/m^3
σ	Standard deviation, -

Subscripts and superscripts

base	Scheduled power consumption or production
bat	Battery
booster	Booster heat pump
buildings	
cap	Capacity
cold	Cold control volume
con	Condensation
cs	Cross-sectional area
D	Destruction (Exergy analysis)
deg	Degradation
demand	Heat demand
der	Derivative
district	Related to the district
el	Electricity
eva	Evaporation
ex	Per unit of exergy
F	Fuel (Exergy analysis)
FCR-N,cap	Power capacity contracted for FCR-N
fixedOM	Fixed operation and maintenance costs
flex	Flexible operation
forw	Forward temperature
ground	Ground water temperature
HEX	Heat exchanger
hot	Hot control volume
in	Inlet of component
k	Index of component
L	Losses (Exergy analysis)
loss	Heat loss
min	Minimum
nom	Nominal
nonflex	Non-flexible operation
OFIC	Open flash intercooler
out	Outlet of component
P	Product (Exergy analysis)
Q	Related to heat flows (Exergy analysis)
r	Response
reg	Required regulation power
ret	Return temperature
sat	Saturation
seasonal	Seasonal average value
Sep	Separator
set	Set value
ss	Steady state
std	Standardised
tot	Total

$\dot{W}$	Power, W
x	Variable, -
$\boldsymbol{X}$	Standardised input parameter matrix, -
y	Normalised response, -
$\boldsymbol{Y}$	Standardised vector of the single valued output, -
$\dot{Z}$	Levelised cost stream of component, €/s

List of publications

Journal publications

[P1] Meesenburg, W., Ommen, T., Elmegaard, B., 2018. Dynamic exergoeconomic analysis of a heat pump system used for ancillary services in an integrated energy system. Energy 152, 154–165. https://doi.org/10.1016/j.energy.2018.03.093

[P2] Meesenburg, W., Ommen, T., Thorsen, J.E., Elmegaard, B., 2019. Economic feasibility of ultra-low temperature district heating systems in newly built areas supplied by renewable energy. Energy 116496. https://doi.org/10.1016/J.ENERGY.2019.116496

[P3] Meesenburg, W., Markussen, W.B., Ommen, T., Elmegaard, B., 2019. Optimizing control of two-stage ammonia heat pump for fast regulation. Submitted to Applied Energy

[P4] Meesenburg, W., Thingvad, A., Elmegaard, B., Marinelli, M., 2019 Combined provision of primary frequency regulation from Vehicle-to-Grid (V2G) capable electric vehicles and community-scale heat pump. Submitted to Sustainable Energy, Grids and Networks

Conference publications

[P5] Meesenburg, W., Kofler, R., Ommen, T., Markussen, W.B., Elmegaard, B., 2019. Design considerations for dynamically operated large-scale ammonia heat pumps, in: 25th IIR International Congress of Refrigeration. https://doi.org/10.18462/iir.icr.2019.1203

[P6] Meesenburg, W., Geyer, R., Terreros, O., Pieper, H., Ommen, T., Elmegaard, B., 2018. Feasibility of heat pumps supplying district heating systems: case study for Austria and Denmark, in: ISEC 2018, International Sustainable Energy Conference.

[P7] Meesenburg, W., Ommen, T., Markussen, W.B., Elmegaard, B., 2020. Influence of component sizing on the dynamic behaviour of fast-regulating two-stage ammonia heat pump. To be submitted to ECOS 2020, 33rd International Conference on Efficiency, Cost, Optimisation, Simulation and Environmental Impact of Energy Systems

Project deliverables

[P8] Meesenburg, W., Pieper, H., 2019. Delivery no.: D5.2a Criteria for selecting between large heat pumps for district and small heat pumps for individual buildings.

[P9] Kjeld, T.G., Meesenburg, W., 2019. Delivery no.: WP5.3 – Protocol for intelligent management of heat accumulators.

[P10] Kjeld, T.G., Meesenburg, W., 2019. EnergyLab Nordhavn - Deliverable no.: 5.5b Manual for optimised operation of an island district heating grid.

Other publications

[P11] Zühlsdorf, B., Meesenburg, W., Ommen, T.S., Thorsen, J.E., Markussen, W.B., Elmegaard, B., 2018. Improving the performance of booster heat pumps using zeotropic mixtures. Energy 154, 390–402. https://doi.org/10.1016/j.energy.2018.04.137

[P12] Zühlsdorf, B., Meesenburg, W., Jørgensen, P.H., Elmegaard, B., 2019. Industrial Heat Pumps in the Danish Energy System – Current Situation , Potentials and Outlook 37.

1 Introduction

This Chapter gives an overview of the background of the presented thesis, the EnergyLab Nordhavn project and the thesis statement, including research questions, objective and a short description of the chosen approach. Finally, a brief outline of the thesis is provided. Parts of the background chapter were adapted from previously published material, namely, chapter 1.1.1 was adapted from [P2] and [P6], and chapter 1.1.2 and 1.1.3 were extended based on [P3].

1.1 Background

The climate is under change due to greenhouse-gas emissions caused by human activity [1,2]. In order to keep the temperature increase caused by global warming well below 2 °C compared to pre-industrial levels, which has been defined as the aim by the United Nations in the Paris Agreement [3], greenhouse gas emissions need to be reduced. The European Union (EU) aims at reducing greenhouse gas emissions by 80 % by 2050 compared to 1990 levels [4]. All sectors are expected to contribute to this development and major reductions will be necessary in the power, domestic and industry sectors [5]. Denmark aims at reducing greenhouse gas emission by 70 % compared to 1990 by 2030 and at being climate neutral and fossil free in 2050 [6].

Heating and cooling in buildings, businesses and industry was responsible for 50 % of the final energy consumption, i.e. the total energy consumed by end users, in the EU in 2012 and it is projected to also be the largest energy sector within the EU in the future under different decarbonisation scenarios [7]. The largest share of the heating and cooling demand may be found in the residential area (45 %), followed by industry (37 %) and services (18 %). This underlines the importance of decarbonisation of the heating and cooling sector. Despite the importance of the heating and cooling sector, strategies for decarbonisation of this sector have only recently been addressed. While the scenarios proposed in the EU Energy Roadmap 2050 [5] focussed mainly on electrification and decentralised heat and cooling supply, the Heat Roadmap Europe study showed that by including district heating solutions the same emission reductions as in the EU Energy Roadmap 2050 may be obtained at around 15 % reduced cost [8]. In Denmark, district heating is acknowledged as a backbone of the energy system [9] and it is expected to play an important role in future integrated energy systems. This is because it may provide flexibility to the power sector and because it enables the use of large-scale heat sources that cannot be exploited by individual heating units [10].

These large-scale heat sources comprise ambient heat sources, such as geothermal heat, groundwater, sea water and air, and excess heat from industrial and commercial processes. The temperature level of these sources is often lower than the required temperatures for the end use, i.e. space heating and domestic hot water in the residential sector. Heat pumps enable using these low-temperature heat sources and increasing the temperature to the required level. Thereby, they help to supply heat from renewable sources. This is possible by using a reversed Rankine cycle. A simple one-stage vapour compression cycle is depicted in Figure 1-1. Within this cycle, a working fluid is circulated at two different pressure levels. The fluid takes up heat from the heat source in the evaporator and thereby evaporates at low pressure. The fluid is then compressed to a higher pressure in a mechanically driven compressor and rejects heat to the heat sink in the condenser at a higher temperature, while being desuperheated, condensed and subcooled. Finally, the fluid is expanded to the low stage pressure by passing the throttling valve. The heat sink is defined by the respective demand. For the case of a heat pump supplying district heating, the water flow in the district heating grid would be the heat sink.

The purpose of the heat pump cycle is to take up a certain heat flow rate at a low temperature, bring it to a higher temperature level using the electrically driven compressor, and rejecting the energy taken

up from the heat source and the compressor at a temperature level high enough to supply the desired service. The performance of this process is defined by how large the rejected heat flow rate is compared to the power used in the compressor for a given set of sink and source temperatures. The better the process, the more heat can be recovered from the low-temperature heat source, and thus less electric energy is needed to supply the same amount of heat at the same temperature on the sink side. This performance measure is called coefficient of performance (COP) and defined as:

$$\mathrm{COP} = \frac{\text{Heat output}}{\text{Power uptake}} = \frac{\dot{Q}_{\mathrm{out}}}{\dot{W}} \tag{1-1}$$

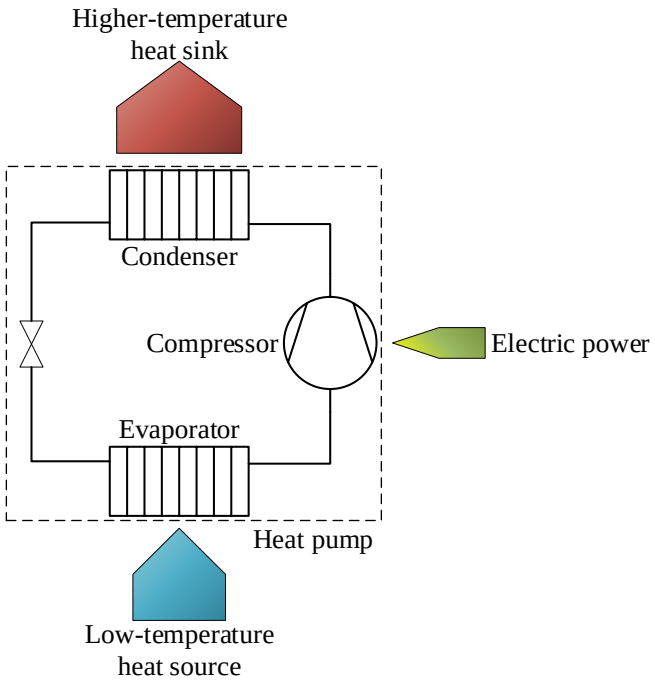

Figure 1-1 Basic one-stage heat pump cycle consisting of an evaporator, compressor, condenser and expansion valve

1.1.1 The role of district heating in integrated energy systems

In Denmark, most rural district heating networks were developed after the first oil crisis and were usually based on natural gas-fired units. District heating companies in Denmark are mostly cooperatives or municipality-owned and so directly or indirectly owned by the customers [11]. They are obliged to work on a non-profit basis and a national benchmark system is in place, ensuring that the most cost-effective and environmentally friendly solutions are promoted [12]. In combination with dedicated policy measures [12,13], this has led to a high penetration of district heating in Denmark (64 % in 2016 [9]). Today, many of the original natural gas units have been replaced by biomass-fired plants, and increasingly solar thermal plants and heat pumps. The main sources of biomass in Denmark are municipal waste, by-products from agricultural activities, like straw and manure, and wood-based biomass, of which approx. 50 % is imported [14]. An increase of biomass usage in Denmark would result in higher shares of imported biomass [15], which implies the risk of promoting non-sustainable land usage in other countries. As Denmark aims to achieve independency of fossil fuels, the available biomass resources might be needed in other sectors. Renewable electricity generation from non-biomass-based sources is thus expected to play a key role in the transition towards renewable supply of heat and electricity. To accommodate high shares of transient electricity generation in the energy system, the idea of an integrated energy system, utilizing synergies between different energy sectors is promoted in Denmark (e.g. [16]). This strategy has been widely acknowledged and current research

and demonstration projects, and recent policy changes [17] undergird the vision of an integrated energy system. Such systems are likely characterised by high shares of electricity generation from intermittent renewable energy sources and the need to exploit renewable heat sources. Lund et al. [18] define several criteria that a future district heating grid has to comply with, in order to play the expected central role: 1) The ability to supply low-temperature district heating for space heating and domestic hot water preparation, 2) reduction of grid losses, 3) exploitation of renewable and excess heat sources, 4) being an integrated part of the overall energy system and 5) suitable planning and policy instruments. The first three criteria are directly connected to lower district heating temperatures. To enable these, the supplied buildings need to be equipped with space heating and domestic hot water systems that can be supplied with low-temperatures, likely down to 45 °C to 55 °C. Reduction of system temperatures is expected to increase the distribution efficiency, due to reduced heat losses from the pipes [19,20]. The integration of renewable and excess heat sources is enhanced by low district heating temperatures too, as lower temperature sources can be used. These ambient and low-grade heat sources can be exploited by large-scale heat pumps, which benefit from lower district heating temperatures, as the coefficient of performance (COP) increases for lower temperature lifts. Heat pumps can also help to fulfil the fourth criterion, as they provide a link between the power and heating networks and might be able to balance the power grid by making use of the immanent thermal storage capacity of the district heating system. This may be found in thermal storages, the thermal mass of connected buildings [21] and the district heating pipelines [22]. Planning and policy instruments are needed in order to shape the system such that the first four criteria may be fulfilled.

As explained above the reduction in district heating supply and return temperatures is essential to increase the energy efficiency of central heat supply systems. Low-temperature district heating systems are systems with considerably reduced operation temperatures compared to conventional district heating systems. Design temperatures in these systems typically reach down to 50 °C to 55 °C, which still allows for direct supply of domestic hot water to the buildings by direct heat exchange [23]. In this case, the forward temperature is constrained by the minimum temperature required to avoid Legionella bacteria in the domestic hot water. If the district heating forward temperature is lowered further, the temperatures will not be high enough to supply domestic hot water directly. Instead, decentral heating units, e.g. heat pumps, are needed in the buildings to lift the temperature of the district heating forward flow. If the supply temperature is still high enough to provide space heating directly, these systems are typically referred to as ultra-low temperature district heating systems. Systems with even lower supply temperatures are referred to as cold district heating [24] or fifth generation district heating systems [25]. They require that both the heat for space heating and domestic hot water are lifted by a decentral heating unit. On the other hand, they allow the supply of cooling to customers as well and to make use of excess heat at temperatures too low to be used directly.

The type of district heating network needs to be considered, when looking at how heat pumps may be integrated with district heating networks in future systems. The feasibility of heat supply using heat pumps is expected to depend on the required supply temperatures, the system size, the available heat sources and location of implementation, i.e. central or decentral units.

1.1.2 Large-scale heat pumps in district heating

Large-scale heat pumps for district heating supply, using hydrofluorocarbons (HFC) or hydrochlorofluorocarbons (HCFC) as refrigerant, have been in operation in Sweden for several decades due to available excess electricity from nuclear power plants [26]. High global warming potential HFCs are being phased out for large-scale applications according to the Kigali amendment to the Montreal protocol [27]. Natural refrigerants are suggested as an alternative, where especially ammonia has been proven to be an efficient and safe refrigerant for large-scale applications and is widely used as refrigerant for heat pumps supplying district heating and large-scale refrigerant plants. This is e.g. the case in Denmark [28,29], where strict regulations have been in place with regard to refrigerants for

large-scale heat pumps and refrigeration installations. In Denmark, 47 large-scale heat pumps in district heating grids and 22 industrial applications for space or process heating, with a total installed capacity of approx. 120 MW, have been identified in 2018 [30]. The majority of these large-scale heat pumps, corresponding to approx. 111 MW installed capacity (93 %), use ammonia as refrigerant. The number of installed heat pumps in Danish district heating grids has been increasing in the last years and is expected to increase further [31]. This development is fostered by the Danish legislation in place, which requires district heating operators to choose the heat supply technology, which proves to be private- and socio-economically most beneficial [12]. Further, the boundary conditions for large-scale heat pumps have been improved lately through the phase-out of the public service obligation (PSO) tariff [32] and a reduction of the electricity tax [33], which reduces the electricity cost considerably. Further, heat pumps for district heating are eligible for energy efficiency promotion subsidies [34]. The increase in installed plants also benefits from research and demonstration projects and targeted collection and dissemination of knowledge, e.g. [35,36]. Hence today, large-scale heat pumps for district heating supply are known and acknowledged as feasible technology by all involved stakeholders. However, power-to-heat units, including heat pumps only contributed to 0.8 % of the total district heating production in Denmark in 2017 [37], corresponding to a heat production of 0.3 TWh in 2017. Lund & Persson [38] estimated the total available heat source potential for large-scale heat pumps as 18.3 TWh, excluding air as heat source, indicating a significant potential for further expansion of district heating supply from heat pumps. Bühler found that up to 1.36 TWh or 5.1 % percent of the overall Danish district heating demand could potentially be covered from industrial waste hea. Out of these 0.49 TWh would have to be recovered using heat pumps [39]

Several studies on the system perspective of integrating large-scale heat pumps into district heating systems have been conducted. Lund et al. [40] showed that there is a considerable socioeconomic potential of 100 M€/a towards the year 2025 of introducing large-scale heat pumps supplying district heating to the Danish energy system. They quantify the optimal capacity range between 2 GW to 4 GW thermal power, indicating a vast potential for large-scale heat pumps when compared to the capacity installed in district heating grids today, i.e. 100 MW. The potential for extending the installed heat pump capacity in district heating networks is supported by Kontu et al. [41] for Finland. They further point out that heat pumps are more feasible for heat supply in small-scale district heating networks, where they replace fossil fuel-based production. Bach et al. [42] analysed the potential for integration of heat pumps into the Greater Copenhagen district heating system, comparing the integration into transmission and distribution lines. Here, transmission lines refers to high-temperature (often >90 °C) long distance pipelines to transport heat to all subnetworks, while the distribution networks are operated at lower temperatures (60 °C to 90 °C) and distribute heat to the final customers. They outline that the integration into transmission lines may be advantageous, as this would allow overcoming the mismatch between heat source location and demand location. However, the heat pump performance and thus the economic feasibility are beneficial when integrated into the district heating distribution network, as the distribution system forward temperatures are considerably lower. The private economic feasibility of heat pumps is highly dependent on the regulatory and economic framework in place in the respective country, as e.g. shown by Popovski et al. [43] for a German case, where large-scale heat pumps cannot compete with coal-fired combined heat and power plants under the current boundary conditions. This is underlined by David et al. [44], who assessed the current state of large-scale heat pumps for district heating supply in Europe. They point out that while district heating systems are generally well promoted by policy makers, the economic feasibility of heat pumps, despite their socio-economic feasibility, is jeopardised by energy market policies without carbon penalty, and with subsidies for biomass and fossil fuels.

1.1.3 Flexible operation of heat pumps

Power-to-heat units take advantage of low electricity cost periods to supply heat at reduced cost. Thereby, they cost-effectively help the integration of renewable energies into the system [45]. Especially, large-scale heat pumps are expected to play a key role in future smart energy systems [10], as they provide the potential to combine intermittency-friendly operation with the efficient use of electricity for provision of heating and cooling [46]. In this way, large-scale heat pumps may help to accommodate larger shares of renewable power supply in the short and medium term and thereby support a flexible and cost effective operation of the energy system [47]. The Heat Roadmap Europe studies estimate that by 2050 up to 50 % of the European heat demand could be supplied by district heating, of which 20-35 % might be supplied by large-scale heat pumps [44]. This underlines the importance of understanding the challenges of highly intermittent operation of large-scale heat pumps as key units in future energy systems based on high shares of renewable power production.

While it is known that electric boilers can react very quickly to signals from the electricity grid [48], most large-scale heat pumps that have been installed to supply district heating, have been designed for base load or intermediate load operation and sudden load changes are typically avoided. According to experiences from Stockholm and Gothenburg in Sweden, it is technically feasible to use large-scale heat pumps for intra-day regulation [49][26], but the intermittent operation of heat-pumps can be constrained by mechanical wear of the components, as well as several minutes start-up time and low COP during start-up [50]. However, large-scale heat pumps have not been optimised to react quickly to signals from the electricity grid. Accordingly, there is a lack of knowledge about the flexible operation of heat pumps as pointed out by David et al. [44]. Also the effect on component wear and lifetime under flexible operation conditions needs further investigation [44]. It can however be expected that compressor parts, the electric motor and the gear box are influenced most by a more flexible operation [51].

While few experiences on flexible operation of large-scale heat pumps are available in literature, a multitude of publications about providing ancillary service using individual heat pumps is available. Fischer & Madani provided a comprehensive review on the possibility to supply ancillary services using individual heat pump pools [52]. They point out that the optimal design and the limitations of heat pumps for flexible operation need further investigation. In order to assess and understand these limitations, the dynamic behaviour of heat pumps needs to be taken into consideration.

1.1.4 Ancillary services in Denmark

The description of ancillary services to be supplied in Denmark is based on publicly available material from the Danish transmission system operator (TSO) Energinet [53,54]. Denmark is divided into two regulation zones. Western Denmark (DK1) is part of the continental European Power system (German load frequency control block) and Eastern Denmark (DK2) is part of the Nordic system. The TSO is responsible for operating the transmission system and for ensuring that the electricity generation and demand are in balance. The central elements for keeping the generation and demand in balance are the energy markets [55]. These markets include the day-ahead market, where electricity supplies and offers for the following day are settled. For Denmark, this is done via Nord Pool Elspot market or bilaterally between suppliers, producers or consumers. Further, they include the intra-day market – Nord Pool Elbas, which is a continuous trading platform that allows correcting the original schedules obtained from the day-ahead market. This is necessary if unforeseen changes on the production or demand side occur. And finally, the balancing power market is included, where a difference in consumption and production is bought by the TSO to balance the market. The TSO balances out imbalances in the grid by buying upward or down regulation power reserves on the regulation power market. Further, the TSO is responsible for trading of ancillary services.

Ancillary services are all services in the power system that help to keep the system robust and stable, when both, production and consumption, fluctuate and disturbances or faults occur. Stability in this

context refers to frequency stability, voltage stability and angular stability. Within this study, the focus was on frequency stability. Frequency stability indicates, whether the generation and demand are in balance, which is necessary on a second time scale. If a mismatch occurs, the frequency will deviate from its nominal value, i.e. it will increase in case that more power is fed into the grid than the current demand and it will decrease if the demand is larger than the current generation. The frequency deviates with the time it takes for the rotating mass in the system to accelerate or decelerate. Therefore, a large inertia in the power grid from synchronous generators and power demand helps to keep the frequency stable. It is however still necessary to establish a balance between production and consumption within a number of seconds. This is done by generation units that reserve capacity to increase or decrease production or by demand side units that adapt the electric power uptake to balance out frequency deviations and thereby restore frequency. The so provided regulation power is referred to as up-regulation, when the power generation is increased or the power uptake of the demand side unit is decreased. Hence, down-regulation refers to a decrease in generation or an increase of load on the demand side. These reserve capacities are categorised into the following services in Denmark, and are also summarised in Figure 1-2:

Fast frequency reserve (FFR) is a planned service in the Nordic synchronous grid. The definition of market terms and technical requirements is expected to be finalised in 2020. Here, the share of renewable low inertia power generation can be so high that the outage of the largest synchronous units constitutes a risk to the system. Instead of increasing the mechanical inertia in the grid, a fast frequency regulation market will be established to secure stability of the grid. The full activation time of these services is expected to be between 0.7 and 1.3 seconds and to support the grid during minimum 5 seconds (short service) or minimum 30 seconds (long service).

Frequency controlled reserve (FCR, FCR-D, FCR-N) or **primary reserve** services is delivered by units that automatically adapt their load according to frequency deviations in the grid. The primary reserve increases or decreases the production from the schedule proportional to the frequency deviation. When the power imbalance has been cancelled out, the frequency will stabilise at a new value. After the system has been stabilised, it is the role of the secondary reserve to bring the frequency back to 50 Hz. The immediate reaction to frequency deviations requires a frequency measurement at the respective unit. Different reserves are in place in Eastern and Western Denmark. **FCR** is the primary reserve in Western Denmark, which is defined according to the rules in the synchronous grid of Continental Europe, i.e. the regulation time needs to be between 15 to 30 seconds, and must be available for minimum 15 minutes after activation. **FCR-D** (disturbance reserve) is a primary frequency reserve in Eastern Denmark, which reacts when the frequency falls below 49.9 Hz. It is a fast reacting service, where half of the capacity response needs to be available after five seconds and the full response after 30 seconds. The service is a purely upwards regulation service. **FCR-N** (normal operation reserve) is a frequency regulation reserve in Eastern Denmark that is used to outbalance small mismatches in generation and demand during normal operation. It reacts to deviations from the nominal frequency within a frequency band of 49.9 to 50.1 Hz. The service is a symmetric service, and it is required that the response can be held during the complete contracted period. The full response must be available within 150 seconds. The minimum bid size of all primary regulation reserve services in Denmark is 0.3 MW.

Automatic frequency restoration reserve (aFRR – capacity), also referred to as **secondary reserve**, is an automatic power regulation, which is used to take over from the primary frequency reserve and thereby to free the respective capacity. It is the role of the secondary reserve to bring the system frequency back to its nominal value. This is done with an integral control that creates an opposite imbalance after the frequency has been stabilised, to drive the frequency back to 50 Hz. It also serves to balance out mismatches in the grid, which are too small to activate regulation power. aFFR is currently only in place in Western Denmark, a new aFRR market for Eastern Denmark is however planned for 2020. Service providing units get activated by a control signal, which is automatically sent

out by Energinet to the balance responsible party, who then calls the respective unit. aFRR is a symmetric service, i.e. the service provider needs to be able to regulate upwards and downwards. The minimum bid size is 1 MW and the full response must be available within 15 minutes in DK1 and within 5 minutes in DK2 (planned service).

Manual frequency restoration reserve (mFRR – capacity). Manual reserve refers to the capacity, which is reserved for manual balancing of the system in operation. These reserves are activated to keep the system in balance during longer periods of non-foreseen mismatch between generation and demand. Currently, Energinet purchases manual reserve for a five-year contract period and the service provider is compensated for being available. The market rules will however be redefined after 2020 and then be based on a combination of monthly contract and hour-based daily capacity procurement. The current minimum bid size is 5 MW, which may be either up- and/or down-regulation. The full capacity must be available 15 minutes after activation of the service.

Regulation power (mFRR - activation). Regulation power is an energy balance service and is called to keep the generation and demand in balance, if an unbalance is foreseen or if under operation unforeseen unbalances occur. It is further used for congestion management of the transmission grid in normal operation mode and when disturbances occur. Regulation power for both Danish regulation zones is traded on the Nordic regulation power market. In DK1, another regulation power service is in place, called special regulation, which aims at helping the Northern German TSO TenneT to avoid unbalances in the grid, which is typically a problem in case of high wind power generation, due to constraints in the German transmission system [56]. The regulation power reserve is only paid per amount of regulation energy that has been provided.

The voltage stability in the grid refers to keeping the voltage in the grid within certain boundaries to secure a high transmission efficiency, high robustness in operation and avoid damages on grid connected units that could ultimately lead to blackout. The voltage is controlled by a combination of passive and active compensation units connected to the transmission grid. The voltage can only be controlled locally, which requires that service providers are close to the constrained location. In future, all renewable energy generation units (production side) are required to deliver voltage regulation and to keep the delivered reactive power close to zero. A new concept for continuous voltage regulation is currently under development by Energinet. Both voltage and angular stability of the grid were beyond the scope of the current study, and were only mentioned here for completeness.

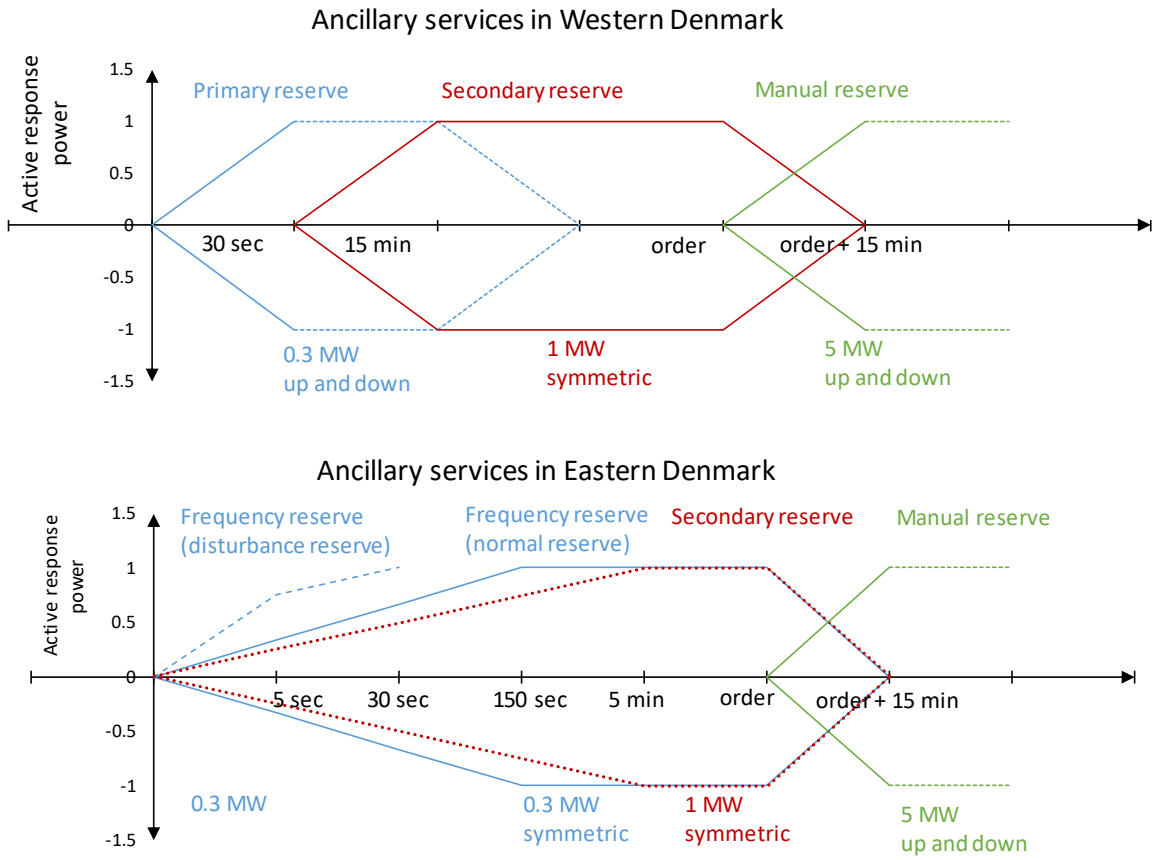

Figure 1-2 Summary of the regulation times (abscissa), minimum bid sizes, and service direction of ancillary services currently in place in Denmark and the planned secondary reserve in Eastern Denmark. The diagrams are based on data from [57]**.**

1.2 The EnergyLab Nordhavn project

The Nordhavn district [58] in Copenhagen is the largest metropolitan development project in Scandinavia. It's location within Copenhagen is depicted in Figure 1-3. It will be developed over the next 50 years and is expected to be home to 40,000 residents and 40,000 new jobs. The development plans to embrace sustainable city development, by aiming at green traffic, short distances, sustainable energy solutions and social diversity.

The EnergyLab Nordhavn [59] project is a large-scale research and demonstration project utilizing the urban development area of Nordhavn in Copenhagen as a living lab to develop and demonstrate future energy solutions. The project started in April 2015 and the first part finished in December 2019. The project aimed at providing a basis for design and dimensioning of energy infrastructure of future sustainable dense urban areas, by looking at smart energy technologies, business models and new operational solutions at scales from component level to energy system level.

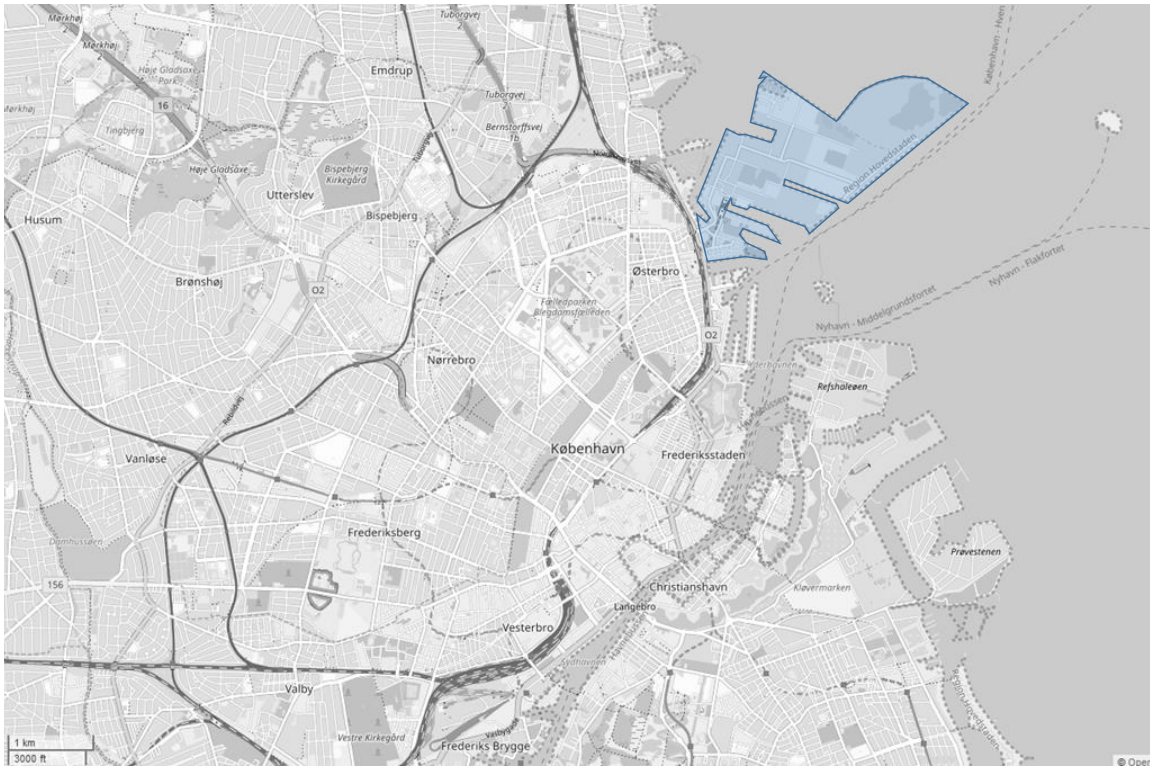

Figure 1-3 Location of Nordhavn area in Copenhagen, Denmark. Map taken from [60]

The project addressed the following main aspects:

- Data and measurements. A data collection and management system for EnergyLab Nordhavn integrated in PowerLabDK [61], named EnergyDataDK [62] was established to provide access to real-time and historic data from the demonstration facilities in Nordhavn.
- Smart energy buildings. The role of low-energy buildings as active energy-flexible elements in the energy systems was assessed and suitable control solutions for operation and monitoring of the building utilities were showcased, taking the behaviour of occupants into account.
- Smart network services. Various control-based solutions for smart networks and infrastructure were analysed.
- Smart thermal components. Components for energy efficient heat supply from various sources and for various applications were developed and analysed. These are characterised by the ability to be controlled according to external signals, allowing them to operate in a smart way.
- Thermal infrastructure. Various thermal infrastructure solutions were assessed, including the assessment of district heating design for highly energy efficient urban areas, smart management of renewable heat supply and heat storage, the interaction with energy flexible buildings, decentralised heat supply options and fuel-shift solutions.
- Electricity infrastructure. The aim was to develop robust and low maintenance electric infrastructure for low-energy districts, including a large-scale stationary battery used for ancillary services.
- Electric transportation infrastructure. Development and experimental validation of robust and smart infrastructure solutions for electric transportation in dense urban areas.
- Multi-carrier energy systems operation and markets. Multi-carrier energy markets and system operation were developed.
- Visibility and stakeholder engagement. A showroom was developed that was used to present the project outcome to guests from around the world. The showroom is integrated with EnergyHub and innovation hub.

The project included research training of nine PhD students and four postdocs. The findings of the EnergyLab Nordhavn projects are documented in various scientific publications [63–120], deliverables and a final report [121], which may also be accessed via the EnergyLab Nordhavn web page [59]. The work conducted for this PhD thesis was part of the "Thermal infrastructure" work package named above.

1.3 Thesis statement

As described above, the transformation of the energy system to a renewable energy system requires rethinking the structure of this system. In Denmark and other countries with a large share of heat supply from district heating, the district heating systems are expected to act as a backbone of the energy system. This has two major reasons. Firstly, district heating systems allow for exploitation of large-scale renewable and excess heat sources for space heating and domestic hot water preparation, which could not be exploited by individual heating units. Secondly, district heating systems may hold large amounts of flexibility in form of thermal storage capacity. This flexibility is needed to allow for integration of renewable generation units into the electricity system. In order to unlock the flexibility of thermal systems for the electricity sector, conversion units acting between the heating and electricity systems are needed.

This thesis is based on the expectation that the district heating grid and the electricity system may be coupled by heat pump systems such that synergies between the sectors may be obtained. In order to assess, whether and to what extent heat pumps may serve this purpose, it is important to assess how heat pumps should be implemented into the district heating system. Recently, there is a trend to lower system temperatures in district heating networks, which may lead to higher overall efficiencies. These lower district heating system temperatures may also benefit the supply of heat from heat pumps, as the needed temperature lift from the source temperature would be lower. The economic feasibility of the different district heating variants in combination with heat supply from heat pumps is unclear. In order to know, how newly developed city quarters should be supplied and thereby, which boundary conditions may be expected for future large-scale heat pumps in new areas, the feasibility of different district heating variants supplied by heat pumps needs to be assessed.

The main product of heat pumps is the heat supplied and possible incomes from delivering ancillary services are often seen as extra income. However, the ability of the system to react flexibly and thereby coupling the two sectors in a flexible way is defined by the thermal system. While the flexible operation of small-scale heat pumps has been demonstrated in many cases, there is a lack of knowledge about the flexible operation of large-scale heat pumps and how they should be designed to be able to react quickly. Further, a flexible operation may be suboptimal with regard to the overall energy efficiency of the heating system. The additional losses need to be quantified in order to be able to define a minimum price that needs to be obtained for the ancillary services to cover the additional cost associated with energy losses. Defining the cost of providing flexibility to the electric grid and heat to customers is not trivial due to the different nature of the two products. A suitable method that takes into account the thermodynamic losses of the system is missing, but could provide additional insight with regard to economic feasibility of flexible operation. Flexibility for the power grid through delivery of ancillary services may also be supplied by the heat pump in combination with other units. It is expected, that this allows making use of the strengths of the different technologies for a combined service.

From these underlying expectations, a thesis statement was formulated:

> *It is technically and economically feasible to supply low or ultra-low temperature district heating and ancillary services for the power grid using large-scale heat pumps. Depending on the specific services supplied, it may be required to combine the large-scale heat pump with other units to obtain the full provision of both services. Thereby, large-scale heat pumps are able to contribute to the sector coupling between the heating and power sector.*

1.3.1 Research questions and objectives

Based on the aforementioned aspects, this thesis aims at contributing to the development of integrating the heating and power sector and thereby supporting the vision and development of integrated energy systems based on 100 % renewable energy through addressing the following research questions:

- How should heat pumps be integrated with the district heating grid? And how does the optimal solution depend on the characteristics of the supplied area?
- How fast can conventionally designed large-scale heat pumps for district heating supply regulate their load and what are the limitations?
- How should future large-scale heat pump systems be designed in order to allow for flexible operation and the provision of ancillary services to the electricity system?
    - How does the control structure influence the dynamic behaviour?
    - How does the regulation time correlate with component sizing?
    - What is the influence of the cycle design on the regulation time?
- How should heat pumps be operated to allow for energy and cost-efficient sector coupling?
- How can the flexibility of a sector-coupling energy conversion unit be quantified and what is the associated cost of providing flexibility?
- Can synergies be found when combining flexibly operated heat pumps with faster regulating units for ancillary services?

The following objectives were derived from the research questions and were addressed within this thesis:

- Analysis of the influence of the characteristics of the supplied district heating area and type of heat source on the feasibility of low-temperature and ultra-low temperature district heating
- Development and validation of a model that allows predicting the dynamic behaviour and regulation time of large-scale ammonia heat pumps
- Analysis of the influence of component sizing, cycle design and control structure on the achievable regulation time
- Development of a method to assign cost to the two products of a flexibly operated power-to-heat unit, i.e. heat and frequency regulation
- Analysis of the economic feasibility of operating large-scale heat pumps flexibly as stand-alone units or in combination with fast-regulating units, such electric vehicles batteries

1.3.2 Approach

The work was divided into three main parts, corresponding to three different main methods applied, as depicted in Figure 1-4. The feasibility of different district heating variants and the influence of the characteristics of the supplied area on the feasibility were assessed using a techno-economic approach. The system was modelled based on generalised correlations that allowed varying the characteristics of the supplied area, without knowing the exact topology. The feasibility of the different district heating variants was assessed by calculating the levelised cost of heat for the customer and the socioeconomic net present value (NPV) of the system. This was done using an Excel/VBA based tool, which included calculation of the main thermodynamic performance parameters as well as calculation of the aforementioned economic measures.
The second part was the assessment of the dynamic behaviour of large-scale heat pumps for district heating supply. This analysis was limited to two-stage ammonia heat pumps, as these are most often used for district heating supply in Denmark. A dynamic model was developed in Modelica and implemented in Dymola using the TIL library. All component models were based on dynamic energy

and mass balances and steady-state momentum balances. Experiments were designed to assess the flexibility of a recently built heat pump in Copenhagen, Denmark. The experimental results were then used to validate the dynamic model. The model was used to assess how the ability of the heat pump to provide ancillary services could be enhanced by an improved control structure or different cycle design. In the third part, the feasibility of providing frequency regulation with large-scale heat pumps was assessed using a simplified dynamic model of a heat pump system in Nordhavn. Different possible operation strategies, including combined delivery of frequency regulation from different flexible units, were assessed. Further, a costing method for flexible operation of power-to-heat units was developed based on the exergoeconomic method, which was extended to be able to include the dynamic characteristics of the flexible operation of heat pumps. Here, it was accounted for the difference in direction of the service supplied and the exergy flow, which may be found when supplying ancillary services. This method was applied to the simplified dynamic model of the heat pump and the supplied district heating grid that was written in Modelica and implemented using Dymola.

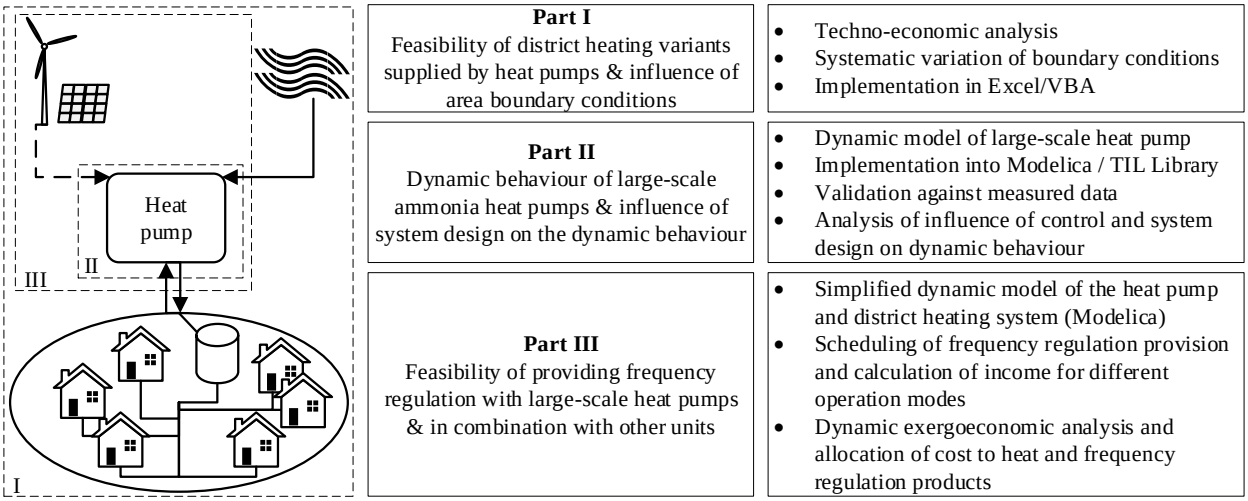

Figure 1-4 Overview of the different analyses conducted as part of this thesis and the applied methods

1.4 Thesis outline

The thesis is structured into five chapters, which are outlined in the following. Further, the underlying scientific publications are attached in the appendix.

Chapter 1 Gives an introduction to the background of this thesis and motivates the research questions and objectives answered by the thesis. Further, an overview of the applied methodological approach is given.

Chapter 2 The influence of the characteristics of the supplied district heating grid and heat supply unit on the feasibility of low-temperature and ultra-low temperature district heating is assessed. The state of the knowledge and the method used to assess the feasibility is described, before the method of the analysis are presented. Finally, an interpretation is given of the Levantkaj area case in the development area of Nordhavn, Copenhagen. At the end a discussion and summary of the chapter are given.

Chapter 3 The dynamic behaviour of a two-stage ammonia heat pump is assessed. The dynamic model is presented. The methods used for validation, analysis of the influence of the control structure and system design are given. The experimental measurements are described and the results are analysed. The dynamic model is validated against the experimental data. Model results for the validated case are analysed. The influence of control structure, cycle design and component sizing are assessed and recommendations for the design of flexibly operated large-scale ammonia heat pumps are derived. A discussion and summary of the chapter are given.

Chapter 4 The background of quantification of flexibility and the possibility of combining different flexible units for a combined regulation service is described and the technical and the economic feasibility is assessed. A simplified dynamic model was developed in Modelica. It was used to assess the feasibility of different operation strategies to supply FCR-N frequency regulation with large-scale heat pumps and combined frequency regulation provision from electric vehicles and a large-scale heat pump. An exergoeconomy-based method to assess the cost of flexible operation of sector-coupling units is proposed. The method is applied to a dynamic model of a district heating island system in Nordhavn. A discussion and summary of the chapter are given.

Chapter 5 The thesis is concluded by summarizing the main findings and recommendations for future work.

Appendix A Additional material related to Chapter 3

Appendix B Publications

2 Economic feasibility of heat pump integration into district heating systems

Newly developed areas are often characterised by buildings that need to comply with strict energy efficiency requirements, such as the urban development area in Nordhavn [58]. The area is being developed within several steps and is expected to be fully developed by 2060. For newly built areas, decisions on the kind of heat supply often need to be made very early in the planning phase. The heat supply of these new areas should be as energy and cost efficient as possible. Accordingly, it is expected that the space heating demand will be reduced to a minimum and domestic hot water will represent a larger share of the overall heat demand in these areas. Further, the building density is expected to be lower in the later development phases of the Nordhavn development. In the new areas, this will lead to relatively low linear heat demand densities, i.e. the total annual heat demand divided by the estimated trench length of the district heating grid. Therefore it should be assessed what the most feasible district heating design is, as this will define the boundary conditions for heat pumps in newly developed areas. Energy efficient district heating networks are characterised by lower system temperatures. The questions, how low these temperatures should be, which kind of central heat source should be chosen (if available), how decentral heat pumps should be implemented into ultra-low temperature district heating networks and how these results are influenced by the area characteristics, are answered in this chapter.

The work presented in this chapter was carried out in two parts.

- Comparison of the economic feasibility of low temperature district heating (LTDH) supplied from large-scale heat pumps using ambient heat sources, to LTDH supplied from wood-fired heat only boilers and to supply from different individual heating units. The feasibility was assessed for varying plot ratios, i.e. the ratio between the built space area and the land area supplied by DH, and thus linear heat demand densities (LHDD). Five central unit types were considered - air source heat pump, groundwater heat pump, seawater heat pump, wood pellet and wood chip boiler. Different district heating forward and return temperature cases (80 °C/50 °C, 70 °C/40 °C, 60 °C/30 °C) were analysed for two heat demand scenarios. The district heating solutions were compared to individual air-to-water heat pumps, brine-to-water (ground source) heat pumps and electric boilers. This work had the major aim to put the supply of district heating from central heat pumps into the perspective of another optional heat-only supply solution. The work presented in this part, has been published as a conference contribution [P6] and a project deliverable [P8].
- Assessment of the feasibility of ULTDH compared to LTDH and individual supply from air-source heat pumps. In this part both the plot ratio and the space heating share was varied. The nominal ULTDH temperatures were assumed to be 40 °C forward, 25 °C return, while the nominal LTDH was assumed to have 60 °C forward, 30 °C return. As central units, air-source heat pumps, groundwater heat pumps and industrial excess heat at different temperatures were considered. The following method description, and the results comparing LTDH, ULTDH and individual heat pumps, have been published as a journal publication [P2].

Both parts are based on the same method, which is described in section 2.2.

2.1 State-of-the-knowledge of feasibility of different types of district heating supplied by heat pumps

Several authors have studied the feasibility of low-temperature district heating (LTDH) or ultra-low temperature district heating (ULTDH). These studies have in common that they are conducted for a specific network, where the area characteristics are fixed and the system design is known.

Yang & Svendsen [19] found for a Danish case study that the lower temperatures of ULTDH allows further reduction of grid losses compared to LTDH. However, part of the heat used to provide domestic hot water (DHW) is replaced by electricity to run the decentral heat pumps, which results in a reduced exergy utilisation as the reduction of heat loss is outweighed by the additional electricity demand of the decentral heat pump, as shown by Elmegaard et al. [122]. Ommen et al. [77] investigated the influence of distribution temperatures on the performance of large-scale heat pumps and combined heat and power (CHP) plants as the central heat supply unit. The considered decentral heating unit is a heat pump using district heating water as heat source. The results showed that energy efficiency increases for ULTDH compared to LTDH, if supplied by a central heat pump, and decreases if supplied by a CHP plant.

The economic profitability of ULTDH and LTDH is challenged as the linear heat demand density (LHDD) is reduced, which generally decreases the profitability of district heating systems [123]. More detailed analyses of the economic performance of ULTDH have been conducted for specific district heating systems. Ommen et al. [20] examined the influence of district heating temperatures on the consumer cost in the Greater Copenhagen district heating network for supply from CHP only, and for integration of large-scale heat pumps into the supply portfolio. They show that reducing the district heating temperature to 60 °C leads to minimal consumer costs. Further reduction in district heating forward temperature results in increasing cost, as boosting of the temperature for DHW becomes necessary. Another Danish case study of a district heating network supplied by a ground-source heat pump supplemented with CHP and heat only boiler showed that the operational cost were lower for ULTDH than for LTDH [19]. A similar system was analysed for a German case [124], using air-source heat pumps as decentral heating units. The space heating share was 78 % of the overall heat demand. They found that the higher cost for decentral boosting for DHW preparation is offset by savings in heat distribution cost and central heat generation cost, due to a better COP of the central heat pump in the ULTDH case.

Vivian et al. [125] analysed the economic feasibility of ULTDH from a customer perspective for a network supplying mainly older buildings in Italy. As the existing buildings had higher temperature demands for space heating (SH) than the district heating forward temperature, the booster heat pumps had to provide SH in addition to DHW. They find that the levelised cost of heat in ULTDH systems decreases with increasing district heating supply temperatures, indicating that a LTDH solution might be beneficial. Köfinger et al. [126] studied different low- and ultra-low temperature district heating configurations for four cases in Austria. They recommend using booster units in combination with ULTDH when the heat source supply temperature is limited or when large amounts of DHW have to be stored in the buildings, e.g. in hotels. They emphasise that reduced heat losses and network investment cost prove to be especially beneficial in low heat demand density areas, this is however contradictory to the generally reduced feasibility of district heating solutions [123].

Lund et al. [127] compared the feasibility of ULTDH with LTDH on an energy system level from a societal point of view. They find that LTDH has the lowest socioeconomic cost but that ULTDH with booster heat pump substations may be feasible in specific cases under the right circumstances. Østergaard & Andersen [128] compare the operation cost of ULTDH and LTDH. They find that operation cost of ULTDH can be reduced compared to LTDH due to lower energy losses in the network. However, booster heat pump investment cost were not included in their analysis.

While most studies point towards LTDH as the more feasible system, some show economically feasible ULTDH systems. All of the above mentioned studies compared different ULTDH and LTDH solutions,

which were carried out for specific cases. Accordingly, a more systematic analysis of the influence of the different boundary conditions on the feasibility of ULTDH systems is needed to predict, which solutions should be evaluated for new development areas supplied by heat pumps. Therefore, this chapter aims at identifying how the characteristics of the supplied area and of the heat supply technologies influence the socioeconomic feasibility of the respective heat supply. This can be useful information in the early planning stages for new development areas. By identifying the feasibility of different district heating solutions in the nexus between the boundary conditions imposed by the supplied area and the available heat sources, the study addresses a techno-economic perspective, which is different to existing assessments based on energy system analysis as well as to studies of performance improvements of district heating cascade systems. The aim is to identify the most promising pathways of heat supply for future developments. The results of the studies mentioned above indicate that the feasibility of ULTDH is affected by many parameters, of which key items are listed in the following:

- SH- and DHW temperature requirements
- Heat demand density of the supplied area
- Share of SH demand of the overall heat demand
- Type of central district heating supply unit
- Price of heat supplied by district heating and price of electricity

In this chapter, the influence of these parameters on the economic feasibility of ULTDH compared to LTDH is assessed, in order to identify under which boundary conditions, one or another of these technologies should be applied. Further, the influence of the booster heat pump configuration and the corresponding operation and investment cost on the overall systems feasibility is analysed, to account for different possible ULTDH variants.

2.2 Method

To assess the economic feasibility of LTDH and ULTDH systems in Denmark under varying boundary conditions, an economic analysis was conducted using a Microsoft Excel/VBA based tool, based on the district heating assessment tool (DHAT), published by the Danish Energy Agency [129]. The DHAT is an MS Excel based tool that can be used to calculate the economic feasibility of establishing district heating in areas currently supplied by individual units. The tool includes technical data and price projections that are adjustable for different countries. It includes a cost-benefit analysis for the local society, customers, and the district heating company. It calculates the socioeconomic feasibility of the project according to Danish guidelines [130] and the levelised cost of energy (LCOE), including the total district heating network cost, and investment, fuel and operation and maintenance (O&M) cost for the supply units. The DHAT, as published by the Danish Energy Agency, was extended in this work to represent the variation of heat pump coefficient of performance (COP) for every hour of the year and investment and operation and maintenance cost in more detail to account for the characteristics of different heat sources. An estimation of the network cost and the heat losses were included to account for different district heating temperatures. Further, the calculation of the performance of ULTDH networks in combination with decentral heating units was added and the variation of boundary conditions was automated using VBA to allow calculating and analysing a large number of different scenarios. The following general assumptions were underlying the study: The analyses focused on newly developed areas supplied by a newly built central unit and the electricity used for driving the heat pumps stems from renewable sources. No detailed analysis of the actually expectable emissions from electricity generation has been included.

All changes made to the DHAT system are described in detail in section 2.2.2. The economic analysis conducted within the DHAT tool is further described in section 2.2.3.

A principle sketch of the assessed systems is given in Figure 2-1. All systems included energy supply in form of power supply, natural gas for the back-up unit and heat sources for the heat pump units.

Further, different central energy conversion units were considered, supplying the heat demand via the district heating network and transferring it in the customers substation. The system performance and economy were influenced by different physical- and policy boundary conditions, as indicated in Figure 2-1. The resulting levelised cost of heat obtained from the tool were compared to district heating prices published for Danish district heating networks [131] for verification.

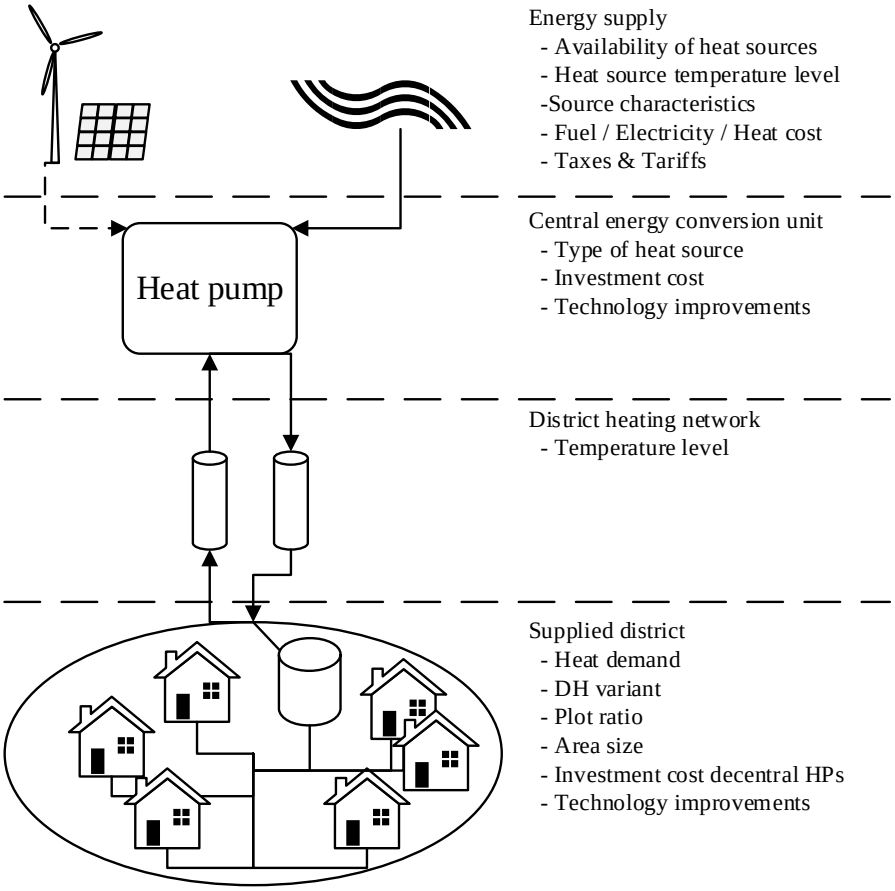

Figure 2-1 Overview of the system, including four main parts; energy supply, central energy conversion, district heating network and supplied district. Varied boundary conditions influencing the different parts of the system are given as bullet points.

2.2.1 Assessed system designs

In a first analysis the feasibility of the supply of LTDH from large-scale heat pumps was compared to three individual heat pump solutions and LTDH supplied by wood-chip and wood-pellet fired boilers. Different nominal district heating forward and return temperature cases (80 °C/50 °C, 70 °C/40 °C, 60 °C/30 °C) were analysed for two heat demand scenarios.

In the second analysis, three different ULTDH system designs were assessed, and compared to the performance of a LTDH system and to supply by individual air-to-water heat pumps. Figure 2-2 shows a sketch of the different system design cases.

Case 1) was LTDH with design system temperatures of 60 °C forward and 30 °C return. These temperatures specify the temperatures to be supplied to, and returned from, the last customer in the network. For all three ULTDH cases, temperatures of 40 °C forward and 25 °C return were assumed, using the above definition of forward and return temperature. They differed in the type and form of implementation of the decentral heat pumps. In case 2) “ULTDH-DH” the booster heat pump was using the district heating forward stream as sink and source. Substation and booster heat pump were implemented at building level. The advantages of this configuration were a high booster heat pump

COP of 5.23 and relatively high linear heat demand densities in the district heating network compared to case 3). Case 3) “ULTDH-air” used an air-source heat pump to supply DHW to the building. The COP was lower compared to case 2, with 2.9 to 3.3 (depending on the ambient temperature). In case 2) and 3) it was assumed that the DHW temperature supplied to the tanks in the building is 60 °C and the COPs were calculated as described in section 2.2.2.4. The last case, “ULTDH-DH-micro”, comprised micro-booster heat pumps at apartment level. In accordance with supplier data, the DHW temperatures were assumed to be as low as 53.5 °C and the micro-booster heat pump achieved an average COP of 6.7 for district heating supply temperatures of 40 °C [132]. In this case, anti-Legionella disinfection was carried out by shortly increasing DHW temperatures once or twice per week. The respective extra heat pump consumption was given by the manufacturer as 1 % of the calculated power consumption without disinfection [133] and was neglected.

For both analyses and all district heating temperature cases, weather compensation was applied for outdoor temperatures below 5 °C, increasing the district heating supply temperature by 1 K for a decrease of 1 K in outdoor temperature, up to a maximum compensation of 17 K [19], as depicted in Figure 2-3. The supply temperature of DHW from the individual DHW heat pumps was assumed to be unaffected by outdoor temperatures. It was assumed that the heat is transferred from the district heating grid to the building SH and DHW system via an indirect district heating substation. It was further assumed that the return temperature from the district heating substations could be kept constant throughout the year, which is a simplification, as the return temperature would usually vary as the forward temperatures vary. In all cases, the circulation losses within the buildings were assumed to be part of the specific heat demand of the buildings.

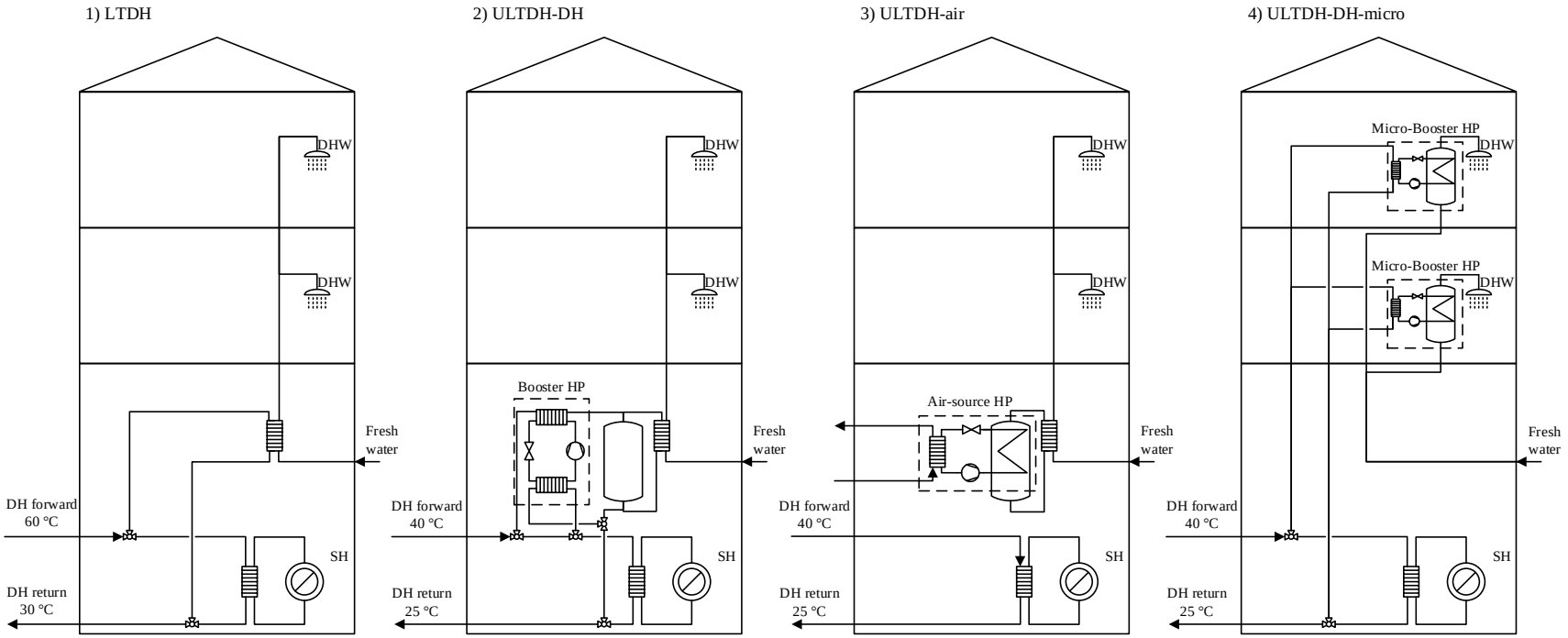

Figure 2-2 Four system design cases: 1) LTDH with indirect district heating substation at building level, 2) ULTDH with water-to-water booster heat pump at building level, 3) ULTDH with air-to-water heat pump at building level (the evaporator and compressor unit is usually placed outdoors, but was drawn inside for simplicity), 4) ULTDH with water-to-water booster heat pump at apartment level, including direct preheating of the fresh water.

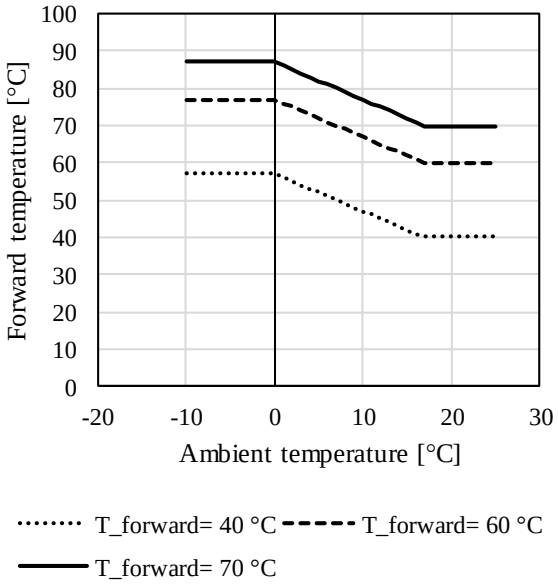

Figure 2-3 Weather compensation curves for three different nominal forward temperatures

2.2.1.1 Heat sources

Air-source evaporators and ground source systems were considered as central, natural heat sources. The cost of heat supplied to the evaporator, caused by pump or fan power consumption, was neglected. The sensitivity to this assumption was assessed (see section 3.5). Air-source heat pumps experience frosting at ambient temperatures of around 7 °C and lower, which leads to a reduction of COP due to defrosting and to a reduction of heating capacity, as frost formation on the evaporator reduces the heat transfer [134]. This effect was considered by reduction factors for COP and heating capacity for outdoor temperatures below 7 °C. The assumed reduction factor for the COP was 0.84 and for the heating capacity 0.85. These values are mean values of the data presented by Mader [134]. This simplified approach was chosen, as a more detailed modelling of the defrosting was beyond the scope of this study.

Further, excess heat at temperatures of 40 °C, 30 °C and 20 °C, was used as heat source for a central heat pump. It was assumed that all sources were cooled down to 10 °C by the heat pump. Lastly, a case of excess heat at temperatures high enough to supply ULTDH directly at all time was considered as an idealised situation. This was a theoretic case and the heat source was not further specified. In this case, the investment cost was reduced to that of a heat exchanger substation.

In principle, the excess heat cost is highly dependent on the type of process it originates from and the cost that occurs to make the excess heat available. The type of industrial process was beyond the chosen detail level for this study, and accordingly it was decided to vary the excess heat cost to be 0 €/MWh, 10 €/MWh and 20 €/MWh, and thereby assess how much the cost influences the overall feasibility, similar to the approach chosen by Bühler et al. [135].

2.2.2 Representation of district heating system

To assess under which circumstances ULTDH or LTDH is economically preferable, a generic representation of the district heating network and customer structure was developed. Accordingly, no detailed network analysis was conducted, but the calculation of heat demand, district heating grid investment, heat loss and pumping power were based on current regulations and estimations from existing district heating grids in Denmark and Sweden. The analysis was limited to newly developed, predominantly residential areas and the district area was fixed to 340 000 m^2, which is the area of the

Levantkaj city development area in Copenhagen [136]. To verify that a fixed district area is a feasible assumption, the influence of the district area on the result was tested.
The performance of the system was evaluated based on the seasonal system COP, which is defined in line with the definition of the seasonal COP for heat pumps [137]. It was calculated as the total annual heat supplied to the customers $Q_{tot,demand}$ divided by the total annual electricity input W_{tot}, which is the sum of the electricity input to the central heating units, decentral heating units and district heating pumping power.

$$\mathrm{COP}_{\mathrm{system,seasonal}} = \frac{Q_{\mathrm{tot,demand}}}{W_{\mathrm{tot}}} = \frac{\int_{\mathrm{year}} \dot{Q}_{\mathrm{tot,demand}}\, dt}{\int_{\mathrm{year}} \dot{W}_{\mathrm{tot}}\, dt} \tag{2-1}$$

2.2.2.1 Estimation of heat demand

The specific DHW demand q_{DHW} was assumed to be 20 kWh/m²/a [138]. The share of SH of the total heat demand s_{SH} was varied between 0.1 and 0.8 in steps of 0.1, representing different building energy efficiencies. The Danish 2020 building standard employs a SH share of 0 [139].

$$s_{\mathrm{SH}} = \frac{Q_{\mathrm{tot,SH}}}{Q_{\mathrm{tot,DHW}} + Q_{\mathrm{tot,SH}}} \tag{2-2}$$

The specific annual heat demand q_s was calculated from the specific DHW demand and the SH share.

$$q_s = q_{\mathrm{DHW}} + q_{\mathrm{SH}} = \frac{1}{1 - s_{\mathrm{SH}}} \cdot q_{\mathrm{DHW}} \tag{2-3}$$

The yearly SH demand profile was generated by weighting the heat demand according to the Danish Design Reference Year [140]. The DHW demand was determined by two components: The basic daily demand pattern, which was assumed to be the European standard tapping profile (XL load) [141] and a factor representing the seasonal variations of DHW demand. The seasonal correction factor was dependent on the outdoor temperature and was obtained by normalizing the measurements by Aronsson [142,143] with the corresponding mean temperatures of the same year.
The overall annual heat demand was calculated from the total heated building area. The heated building area $A_{\mathrm{buildings}}$ was calculated from the overall district area A_{district} and the plot ratio ϵ, which was considered an input for the analysis.

$$\epsilon = \frac{A_{\mathrm{buildings}}}{A_{\mathrm{district}}} \;\Leftrightarrow\; A_{\mathrm{buildings}} = \epsilon \cdot A_{\mathrm{district}} \tag{2-4}$$

The plot ratio was varied from 0.2 (rural) to 2 (urban) in steps of 0.2 to account for different building densities.

2.2.2.2 Estimation of network investment

The network investment cost was estimated from plot ratio, expected specific heat demand, effective width and estimated average pipe diameter, following the approach developed by Persson & Werner [144] and Frederiksen & Werner [143]. Piping cost were fitted to Danish empirical data [129].

2.2.2.3 Estimation of heat loss and pumping power

The heat loss is an important factor for the feasibility of DH, especially in heat sparse areas. The expectable heat loss from the network was estimated using an empirical approach. Figure 2-4 shows the heat loss of 187 district heating networks in Denmark as a function of their linear heat demand density q_l [131]. It is defined as the total annual heat demand divided by the estimated trench length *L* and it can be calculated from the annual specific heat demand, the plot ratio and the characteristic width, as described in [144].

$$q_l = \frac{Q_{tot}}{L} = q_s \cdot \epsilon \cdot w \tag{2-5}$$

Networks with linear heat demand densities above five were excluded. The heat loss was corrected according to forward and return temperatures. As can be seen in Figure 2-4 the data is spread out, which may be caused by different operation conditions and malfunctions in the systems. A power function was used to fit the data. To calculate the relative annual heat loss, the correction for the assumed network temperatures for LTDH and ULTDH was applied to the correlation found from this data. The full equation is:

$$\frac{Q_{loss}}{Q_{tot}} = 0.2748 \cdot q_l^{-0.653} \cdot \frac{T_{\mathrm{forw}} + T_{\mathrm{ret}} - 2 \cdot T_{\mathrm{ground}}}{\bar{T}_{\mathrm{forw}} + \bar{T}_{\mathrm{ret}} - 2 \cdot T_{\mathrm{ground}}} \tag{2-6}$$

$\bar{T}_{\mathrm{forw}} = 73.71$ °C and $\bar{T}_{\mathrm{ret}} = 40.52$ °C are the weighted average forward and return temperature (by heat load) of the Danish systems listed in the data base.

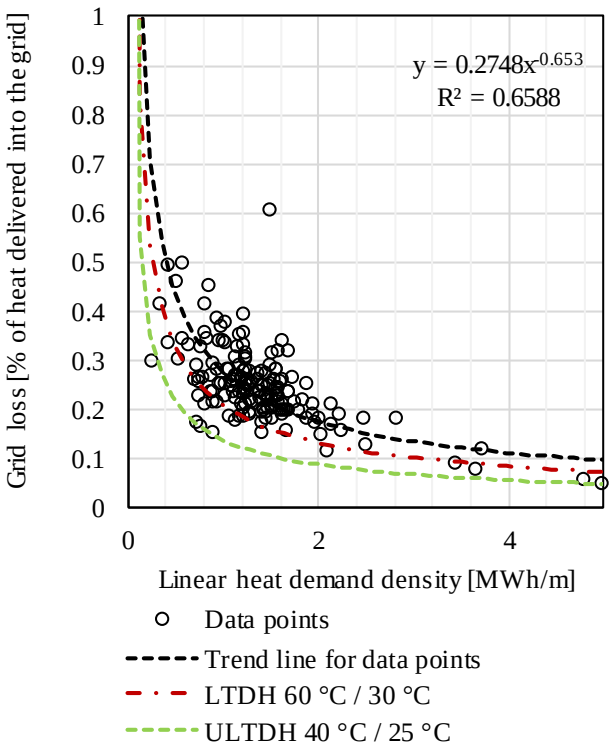

Figure 2-4 Heat loss data from existing district heating networks corrected to average forward and return temperatures in Denmark, 2017, and fitted power function based on data from [131]

The pumping power needed for a system depends on the system design. Any estimation made without knowing the detailed piping layout has large uncertainties. In general, the pumping power can be calculated as the product of the volume flow, the pressure drop and the pump's efficiency. The average volume flow through the primary pumps was estimated from the total heat delivered into the system and the forward and return temperatures at the central unit.

$$\dot{V} = \frac{\left(\frac{Q_{\mathrm{tot,delivered}}}{8760\ [h/a]}\right)}{c_{\mathrm{p,H_2O}} \cdot (T_{\mathrm{forw}} - T_{\mathrm{ret}}) \cdot \rho_{\mathrm{H_2O}}} \tag{2-7}$$

The pressure drop in the system was estimated assuming a constant pressure gradient in all the pipes of 100 Pa/m [143]. The corresponding pipe length was set to the estimated trench length L, which was calculated from equation (5), according to [144].

The pressure loss over the substations was assumed to be 1 bar [145]. The necessary energy for pumping per year was calculated as:

$$W_{\mathrm{pump}} = \Delta p_{\mathrm{DH}} \cdot \dot{V} \cdot \eta_{\mathrm{pump}} \cdot 8760 \left[\frac{\mathrm{h}}{\mathrm{a}}\right] \tag{2-8}$$

Here, Δp_{DH} denotes the overall pressure loss, $\dot{V}$ is the average volume flow and η_{pump} is the isentropic efficiency of the pump, which was assumed to be 0.8.

2.2.2.4 Representation of heat pump units

To calculate the seasonal COP of the heat pumps, the Danish Design Reference Year [140] temperature data was used as air-source temperature. The groundwater temperature was assumed to be 10 °C, the excess heat temperature was assumed to be 20 °C, 30 °C and 40 °C, and constant throughout the year. The source temperature for decentral heat pumps was given as the air temperature for the air-source heat pump and as the ULTDH forward temperature for the DH-source booster heat pump. The coefficient of performance (COP), defined as

$$\mathrm{COP} = \frac{\dot{\mathrm{Q}}_{\mathrm{HP}}}{\dot{W}_{\mathrm{HP}}} \tag{2-9}$$

was estimated from sink- and source temperatures, isentropic efficiency, compressor heat loss factor and the ratio of isentropic expansion- and -compression work, using the method described by Jensen et al. [146]. To determine these parameters, ammonia was assumed as refrigerant for large-scale heat pumps and isobutane for decentral units. The COP for all heat pumps was calculated for every hour of the year. Knowing the hourly COP and heat demand, the corresponding electric energy consumption was calculated. The seasonal COP of the heat pump units could then be calculated equivalent to the system's seasonal COP, (equation (1)).
The capacity of the central heat pump unit was set to be 80 % of the maximum hourly heating demand for LTDH. The backup electricity boiler capacity was 25 % of the maximum heat demand. For the ULTDH cases, the heat capacity of central heat pumps was set to the maximum district heating demand value.
For ULTDH-DH and ULTDH-DH-micro, the annual district heating demand was calculated as the difference of the total heat demand (including losses) minus the electric energy input to the booster heat pumps.

$$Q_{\mathrm{central}} = Q_{\mathrm{supply,tot}} - \frac{(1 - s_{\mathrm{SH}}) \cdot Q_{\mathrm{demand,tot}}}{\mathrm{COP}_{\mathrm{booster}}} \tag{2-10}$$

The heat capacity of the booster heat pump (ULTDH-DH) was constrained to be between 2 kW and 14 kW, which corresponded to previously demonstrated booster heat pump capacities (as of December 2018). The capacity of the micro-booster heat pump was fixed to 1.8 kW per installation.
In the ULTDH-air case, the district heating demand was the SH demand plus distribution losses. The heat supplied by the decentral heat pumps was the DHW heat demand. The capacity of the decentral units for ULTDH-DH and ULTDH-air was determined assuming a fixed number of full load hours of 2000 h/a, which is in line with [147] and was tested for sensitivity.

$$\dot{Q}_{\mathrm{booster,nom}} = \frac{\mathrm{Q_{DHW}}}{t_{\mathrm{fullload}}} \tag{2-11}$$

The air-source heat pump capacity did not have an upper boundary.

2.2.3 Economic evaluation

The economic feasibility of all assessed district heating configurations was compared based on the levelised cost of heat (LCOH) and socioeconomic net present value (NPV). Investment cost for central supply units, district heating grid incl. local substations, and decentral heat pumps were considered. Electricity price, and operation and maintenance (O&M) cost were included in the economic analysis. Taxes were based on Danish regulation as of September 2018.

2.2.3.1 Calculation of levelised cost of heat and socioeconomic net present value

The LCOH was calculated as the total cost over the project lifetime of 20 years divided by the total amount of heat delivered in the same period. The total cost was defined as all cost occurring during the project lifetime discounted to the first year of the project, i.e. 2023, including the residual values of components with a longer lifetime and investment into replacement of components with a shorter lifetime.
The socioeconomic NPV was calculated according to Danish guidelines [148] as the socioeconomic cost of the district heating project, i.e. all investment and operation costs plus emission cost, compared to individual heat supply with air-source heat pumps. Taxes and tariffs were not included in the socioeconomic cost.

2.2.3.2 Fuel cost and taxes

Electricity and emission price projections were based on projections from 2016 for the period 2012 – 2040 by Energinet.dk [149], where the emission prices were based on IEA projections [150]. Local conditions such as electricity tax, network- and system tariffs and distribution tariffs were considered.

2.2.3.3 Assumed cost data

The total investment cost of the system comprised the investment in central units, decentral heat pumps and the network itself. The functions for investment cost, and assumed lifetimes are listed in Table 2-1. Fixed- and variable O&M cost were taken from the Danish Technology Catalogue [151–153]. A linear cost function was used to describe the fixed O&M cost of booster heat pumps in €/unit/a, which was derived from [151], and uses $\dot{Q}_{\mathrm{booster,nom}}$ in MW.

$$C_{\mathrm{fixedOM,booster}} = 229.6 + 3852.6 \cdot \dot{Q}_{\mathrm{booster,nom}} \tag{2-12}$$

Table 2-1 Investment cost for energy conversion units. *Correlation fitted through cost data given in the stated sources

Technology	Investment cost function [M€/MW]	Lifetime [a]	Sources
Excess heat HEX installation	$0.260 \cdot \dot{Q}_{\mathrm{nom}}^{-0.1234}$	20	[154]
Central heat pump excess heat	$0.867 \cdot \dot{Q}_{\mathrm{nom}}^{-0.1234}$	25	[154][155]
Central heat pump groundwater	$1.112 \cdot \dot{Q}_{\mathrm{nom}}^{-0.23105}$	25	[154]
Central heat pump air	$0.937 \cdot \dot{Q}_{\mathrm{nom}}^{-0.1418}$	25	[154]
Central heat pump Sewage or sea water	$1.2166\ \dot{Q}_{nom}^{-0.33122}$	25	[156]
Wood chips boiler	0.9	20	[152]
Wood pellet boiler	0.48	20	[152]
Central Electric boiler	0.11	20	[152]
Central gas boiler	0.06	25	[152]
Indv. Air to water HP	0.95	15	[152]
Indv. Brine to water HP	1.52	20	[152]
Indv. Electric heater	0.86	30	[152]
Booster heat pump	$2.748 \cdot \dot{Q}_{\mathrm{nom}}^{-0.594}$	15	[89,125,157,158]*
District heating substation	$0.414 \cdot \dot{Q}_{\mathrm{nom}}^{-0.536}$	25	[151,157]*

2.3 Results for comparison of LTDH supplied by heat pumps and wood-fired boilers

The aim of the first part of the analysis was to compare the economic feasibility of LTDH supplied from large-scale heat pumps using ambient heat sources, to LTDH supplied from wood-fired heat only boilers and to supply from different individual heating units. Figure 2-5 shows the levelised cost of heat (LCOH) for four different central heat pump units, two central wood fired boilers and brine-to water heat pumps, air-to-water heat pumps and electric boilers as individual heating units. The results are plotted for different plot ratios and for district heating temperatures of 70 °C/ 40 °C. The cheapest individual heat supply unit with 56.2 €/MWh was air-to-water heat pumps and also brine-to-water heat pumps had only slightly higher levelised costs (56.8 €/MWh). The LCOH of individual electric boilers was significantly higher than for both individual heat pump solutions. All district heating options followed a similar trend, i.e. the cost were high for low plot ratios and decreased with increasing plot ratios. The central solutions supplying 70 °C forward, 40 °C return became feasible compared to individual heat pumps at plot ratios between 0.5 and 0.8. Further, it was observed that the feasibility of LTDH solutions benefitted from higher space heating shares, which is assessed in more detail in section 2.4.

The linear heat demand density (LHDD) at which the respective district heating solution becomes more feasible than the best individual supply solution is the minimum feasible LHDD. Figure 2-6 shows this minimum feasible LHDD for all district heating solutions that were assessed in this part of the study. The minimum feasible LHDD, and thereby the lowest plot ratios which may be supplied by district heating, decreased with decreasing supply temperatures for district heating networks supplied by central heat pumps. This is due to the higher COP that may be obtained in the central unit and due to reduced heat losses. Among the heat pumps, the sewage water heat pump had the lowest cost and accordingly could supply the lowest minimum LHDD. This is due to the comparably high heat source temperature, which were assumed to be constant throughout the year. Air-source heat pumps performed second best despite having the lowest COP (among the assessed sources) during the heating season. The reason for this was the lower investment cost compared to groundwater and seawater heat pumps. The trend for wood-fired boilers was in the opposite direction but less pronounced. Accordingly, district heating supplied from heat pumps could be feasible compared to wood-fired boilers and individual heat supply from heat pumps, especially for low density, low temperature networks.

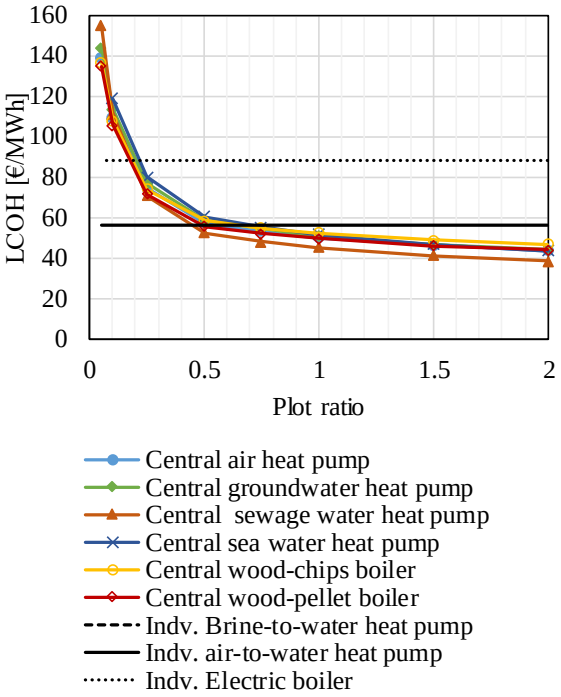

Figure 2-5 Levelised cost of energy over plot ratio for LTDH (70 C) with heat pumps and wood-fired boilers as central supply units and for supply from three different individual unit types, SH-share=0.13

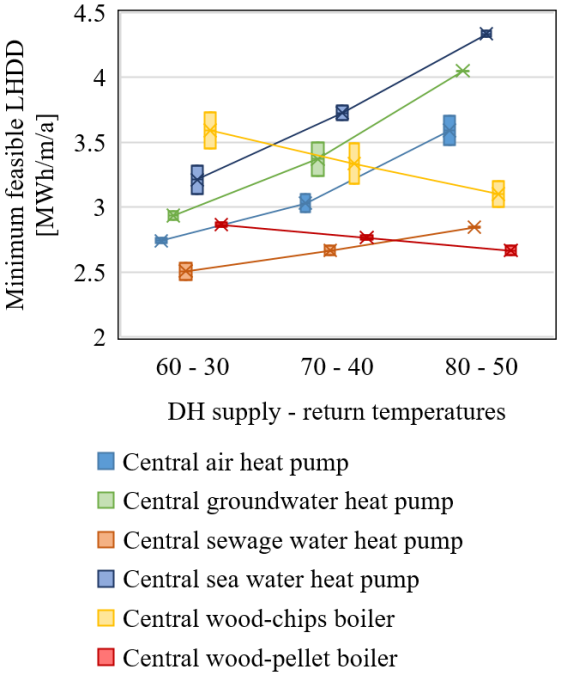

Figure 2-6 Minimum feasible linear heat demand density for LTDH supply compared to individual air-source heat pumps for three different temperature sets and different central supply units, the range of the results accounts of uncertainties with regard to the cost functions

2.4 Results for LTDH and ULTDH supplied by heat pumps

2.4.1 System performance

2.4.1.1 Duration load curves of heat production

Figure 2-7 shows the duration load curves of the heat production of four district heating cases. The heat demand was the same and thus the difference in heat supplied was small and only caused by differences in heat loss. For ULTDH-DH and ULTDH-DH-micro, district heating represented the heat source for the DHW heat pumps, depicted as the light grey area. Thus, the heat added to the system by the booster unit (black area) was equivalent to the power uptake of the units. In the ULTDH-air case, the decentral heat pump used air as heat source and thus the heat added to the system was all the heat supplied from the condenser.

The heat demand increased with increasing plot ratio, as more customers were supplied in the same area. An increase in the SH share led to a higher heat demand during the heating period, while the effect during summer was small as mainly DHW was needed. Accordingly, increasing SH shares led to more pronounced seasonal behaviour, i.e. a steeper load duration curve.

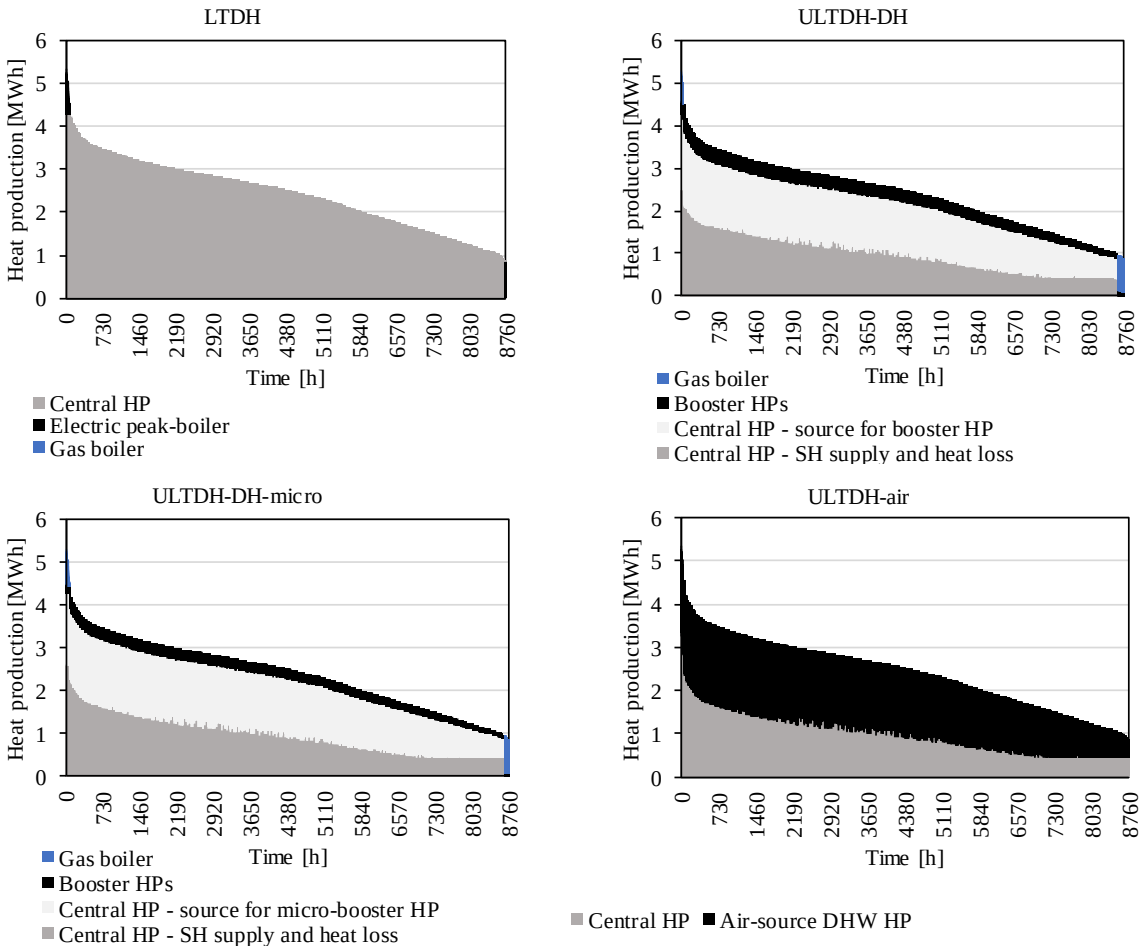

Figure 2-7 Duration curve for four district heating cases supplied by a central heat pump for plot ratio = 1.5, SH share = 0.5

2.4.1.2 Hourly variation of COP

The hourly values of COP of all heat pump units for ULTDH and LTDH are shown in Figure 2-8. The COP of the central units was higher for the ULTDH cases, as the supply temperature was lower compared to LTDH. A seasonal variation was observed for all units. It was most pronounced for air-

source heat pumps as the heat source (air) temperature varies strongly throughout the year. The variation of the other units was caused by increased forward temperatures during winter. This led to higher temperature lifts in the central units. The booster heat pump COP was affected, too, as sink and source inlet temperatures increased, while the supply temperature and the controlled return temperature stayed constant. In consequence, this led to an increased condensation pressure and thus reduced COP.

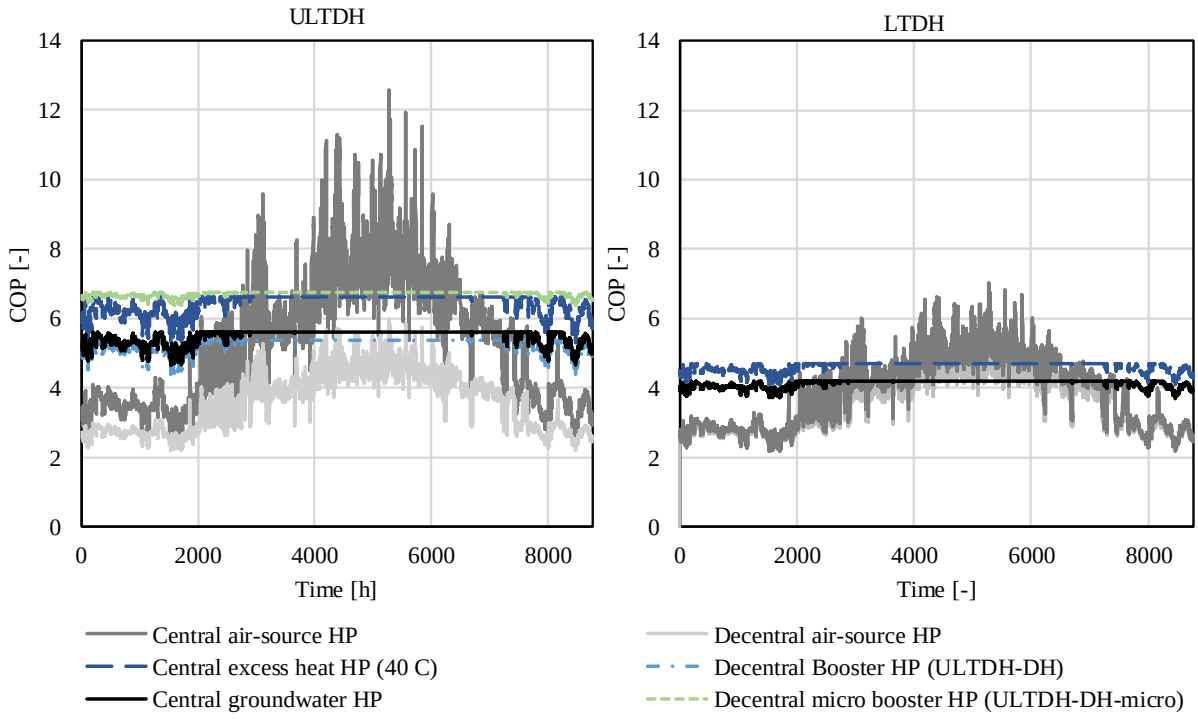

Figure 2-8 Hourly variation of COP for one year of all considered heat pump units for ULTDH and LTDH

2.4.1.3 Dependency of seasonal system COP on plot ratio and SH share

Figure 2-9 shows the seasonal system COP for excess heat of 40 °C and air-source heat pump as the central unit. The results for groundwater heat pump as central unit are not depicted, but show a similar trend to that of the air-source heat pump. For LTDH the seasonal system COP increased from 0.1 SH share and reached a maximum at a SH share of 0.6 and a plot ratio of 2 for heat pump using excess heat at 40 °C. For air-source heat pump and groundwater heat pump, the maximum was reached at a SH share of 0.3 and 0.6, respectively. For plot ratios larger than 0.7 the COP dropped again. Reductions in COP for low and high SH shares were connected to increased usage of the electric back-up boiler due to constraints of the heat pump capacity.

The maximum seasonal system COP for air-source heat pumps was shifted towards lower SH shares compared to the alternatives. For air-source heat pumps a reduction of seasonal heat demand peaks due to lower SH shares in winter was advantageous, because the amount of heat produced with a reduced COP due to low source temperatures and defrosting could be reduced.

The seasonal system COP increased with increasing SH share for all ULTDH solutions. For ULTDH-DH and ULTDH-DH-micro the DHW share of the heat supply had a lower COP than the heat supplied directly at 40 °C. This was due to the necessary additional electricity input to lift the temperatures to the desired level. Accordingly, larger shares of SH resulted in larger average COPs, as the share of directly supplied heat increased. However, increased SH shares meant less energy efficient buildings and a higher overall heat demand. The same trend was observed for ULTDH-air. Here, the system COP increased as the central heat pump had a better COP than the booster heat pump as shown in section 2.4.1.2.

For the excess heat case, the ULTDH solutions, which were supplied by excess heat directly, clearly outperformed LTDH, where a heat pump was needed to supply the necessary forward temperatures. ULTDH-DH-micro had the highest seasonal COPs, followed by ULTDH-DH and ULTDH air. This can be explained by the difference in COP between the micro-booster heat pump (6.7), the booster heat pump (5.2) and the decentral air-source heat pumps (2.9-3.3). For the booster heat pumps, a higher COP meant that more heat was supplied from the central source, and thus a higher share of heat was supplied directly from excess heat, which increased the overall seasonal COP.

For ULTDH supplied by a central air-source heat pump, the seasonal COP of the different district heating cases is much closer to each other and ULTDH-air performed best for most cases. For low SH shares, the COP of ULTDH-air was highly sensitive to the plot ratio, as can be seen from the larger spread of the data points in y-direction, indicated by the arrow in the diagram. This was caused by an increase in relative heat loss for very low heat demands. For SH shares of 0.4 and higher or plot ratios of 0.8 and higher ULTDH-air had the highest seasonal COP. This was because, in the ULTDH-DH and ULTDH-micro cases, DHW was produced by two heat pumps in a row, which led to a lower COP than the decentral air-source heat pump COP for the DHW demand share. The difference between ULTDH-DH-micro and ULTDH-DH is caused by the difference in booster heat pump COP.

For district heating supplied by a groundwater heat pump, the trends looked similar to those for the central air-source heat pump. LTDH yielded the highest seasonal COP up to SH shares of 0.4. For higher SH shares, ULTDH was more efficient. Among the three different ULTDH variants, ULTDH-air performed best followed by ULTDH-DH-micro and ULTDH-DH.

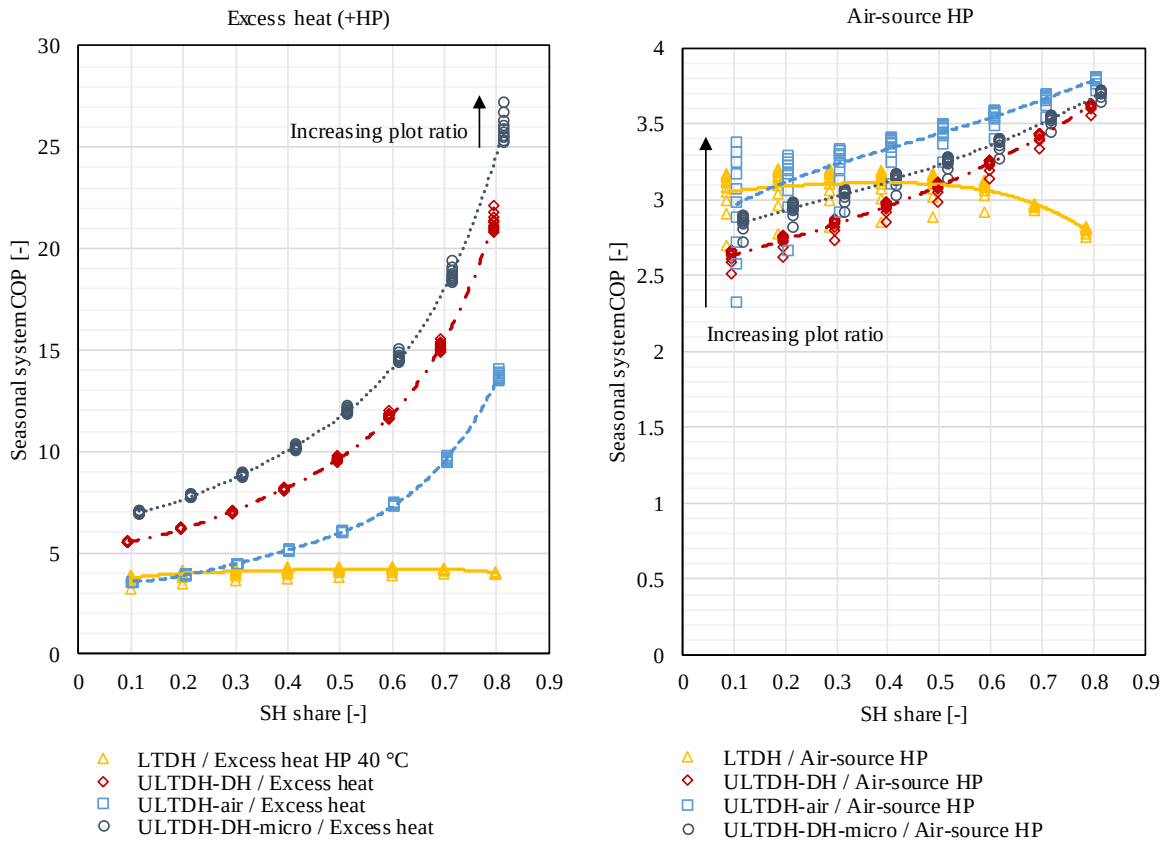

Figure 2-9 Seasonal system COP for four DH cases and two central heating units depending on the SH ratio. The data points presented are for plot ratios of 0.2, 0.4, ..., 2. Trend lines for the four different cases are shown.

2.4.2 Levelised cost of heat

The LCOH of 12 exemplary cases are depicted in Figure 2-10 a). The LCOH decreased with increasing plot ratio and with increasing SH share. The overall findings showed that LTDH was cheaper than the ULTDH systems in most calculated scenarios. The difference was largest for low SH demands, i.e. highly energy efficient buildings, and low plot ratios. Among the ULTDH solutions, ULTDH-DH-micro was only competitive for low plot ratios where the number of installed micro-booster units and alternative units was similar. For increasing plot ratios, multi-family buildings were considered and the booster heat pumps benefitted from economy of scale and thus ULTDH-DH got more beneficial. ULTDH-air could only be competitive for relatively high SH shares, as only the SH is distributed through DH, and thus all the cost of installing a network and a central unit was assigned to the SH cost only.

Figure 2-11 a) shows the most feasible supply options for varying SH share and plot ratio. Individual heat supply from air-source heat pumps was most feasible at low plot ratios and low SH shares. It was observed that the LHDD alone is not enough to describe the feasible area precisely, but instead both SH share and plot ratio should be considered. Figure 2-11 b) compares the most feasible district heating variants for direct excess heat supply to ULTDH, LTDH supplied by a heat pump using a 40 °C source and individual heat supply. In this case, ULTDH was beneficial compared to LTDH for buildings with a SH share of approximately 0.7 or more and for plot ratios above approximately 1.0 for ULTDH-DH and 1.8 for ULTDH-air.

Figure 2-12 compares the LCOH for different central heating units. The changes in LCOH between the different central units was small compared to the change due to different district heating system designs. The LCOH did not change significantly with decreasing excess heat temperatures for those cases, where a central heat pump was used, as it was assumed that all excess heat streams were cooled down to 10 °C. This heat source outlet temperature determined the evaporation pressure, and thus no COP improvement was obtained. For the ULTDH solutions, the investment cost for the central unit increased significantly, when the excess heat temperatures were too low to supply SH directly.

As the heat source was the main energy supply of the system, its cost could significantly influence the feasibility of the solution. For the case presented in Figure 2-12, heat pumps using excess heat at a cost of 10 €/MWh led to higher LCOH than both natural sources for all variants but ULTDH-air. Heat pumps using excess heat as source could lead to lower LCOH in case the cost of excess heat was reduced or the COP was increased, e.g. by allowing a higher source outlet temperature. The variation of excess heat cost did however not change the feasibility of the LTDH solutions compared to the ULTDH solutions.

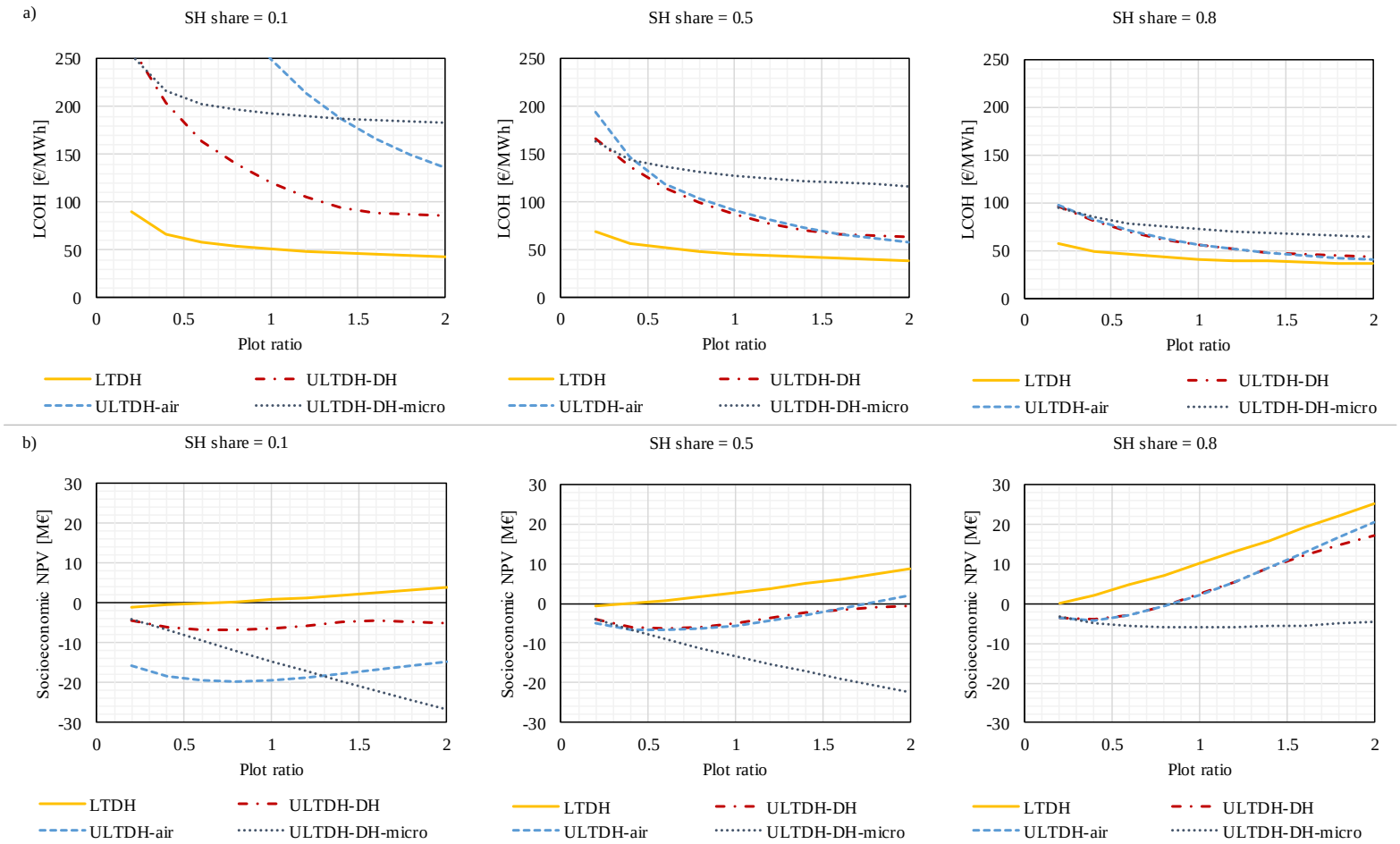

Figure 2-10 a) Levelised cost of heat depending on the plot ratio for three different SH shares, central heat source: Groundwater heat pump; b) Socioeconomic NPV depending on plot ratio for three different SH shares, central heat source: Groundwater heat pump

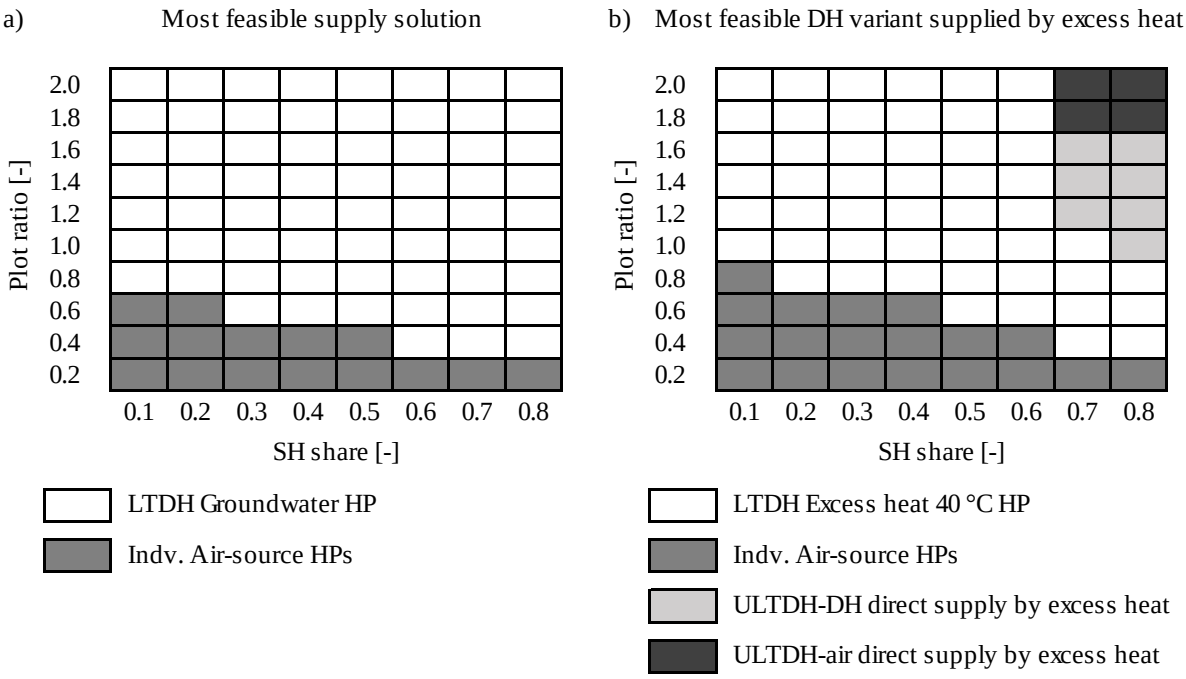

Figure 2-11 a) Most feasible supply solution comparing all technology combinations, b) most feasible district heating variant when the heat is supplied by excess heat directly for ULTDH and by a heat pump using 40 °C excess heat as heat source compared to supply from individual

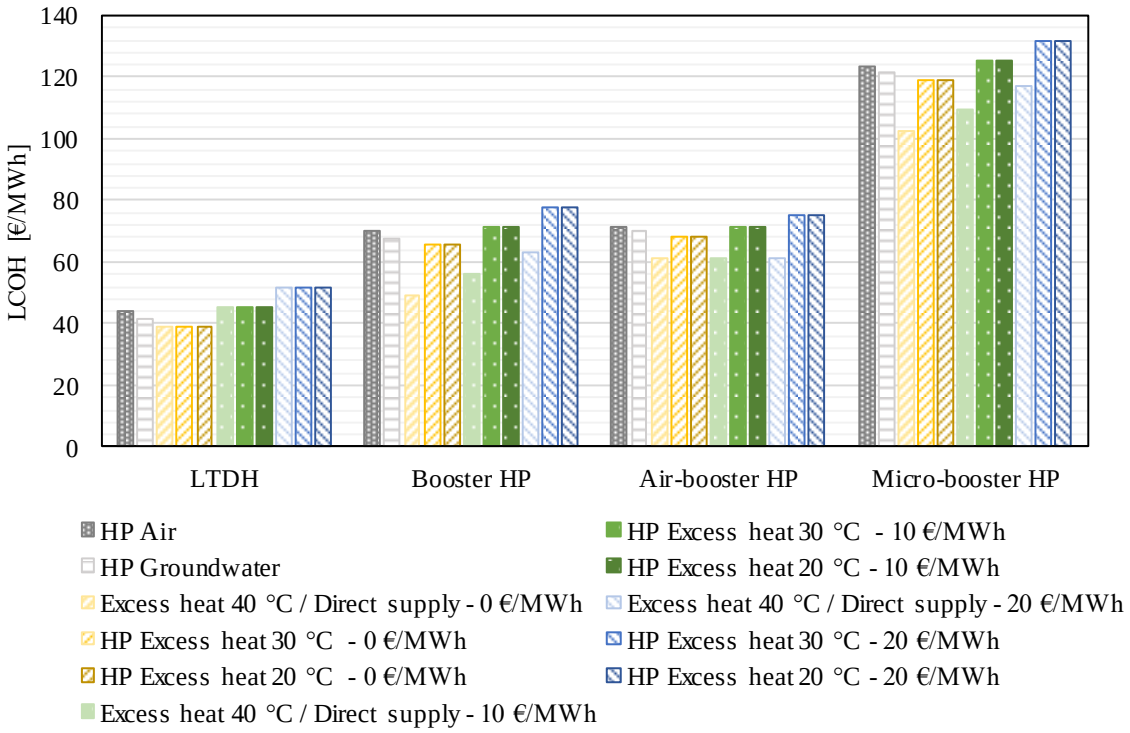

Figure 2-12 Levelised cost of heat for different central heat sources and excess heat cost for SH-share = 0.5 and plot ratio = 1.5

The influence of the supplied area size on the results was low compared to the other parameters presented. A reduction in area size resulted in higher specific costs for all solutions due to economy-of-scale effects. The increase in specific cost was largest for LTDH and lowest for ULTDH-DH-micro. This resulted in a slight shift, of where ULTDH solutions may be feasible towards lower heat demand densities.

2.4.3 Socioeconomic net present value

The socioeconomic NPV for the same cases shown in section 2.4.2 is depicted in Figure 2-10 b). The socioeconomic NPV is a relative value showing the difference between the district heating solution and heat supply based on individual air-source heat pumps. Accordingly, a positive value was equivalent to a socioeconomic PV larger than that of individual air-source heat pumps and a negative value meant that individual air-source heat pumps were most feasible. In the depicted cases, this was the case for a plot ratio below 0.63, 0.39 and 0.2 for SH shares of 0.1, 0.5 and 0.8, respectively.
Generally, the socioeconomic NPV increased with increasing plot ratio, if the LCOH of the district heating solution was below the LCOH of heat supply based on individual air-source heat pumps. This shows good agreement between the private consumer economy and the socioeconomic results. The gradient of the socioeconomic NPV curve depended on the gradient of the cost difference between the DH- and the individual solution, and the gradient of the overall heat supply with increasing plot ratio. This may result in a negative gradient, as in the case of ULTDH-DH-micro.

2.4.4 Cost composition

To understand what determines the economic feasibility of ULTDH and LTDH, the cost composition of the district heating solutions was analysed. Figure 2-13 shows the cost composition for the four district heating solutions, supplied by a groundwater heat pump, for SH shares of 0.5 and 0.8 and plot ratios of 0.6 and 2. The same trends were observed for all types of central heat pumps.
For all four cases depicted in Figure 2-13, LTDH was economically most feasible, despite the lower overall seasonal COP (see section 2.4.1). Among the ULTDH solutions, the total cost was lowest for ULTDH-air, followed by ULTDH-DH and ULTDH-DH-micro. The cost of the ULTDH-DH-micro was considerably higher compared to the alternatives, especially for the case with a plot ratio of 2. This had two major reasons. First, the investment cost of micro-booster units was 2.87 times the investment cost of the air-source heat pumps. This was due to the constant specific investment cost of the micro-booster heat pumps, which always came in the same size as they were installed in every apartment. The specific cost of the air source heat pump and the booster heat pump decreased due to economy-of-scale effects with increasing plot ratio, as the buildings got larger and thus the heat pump size increased. Second, the fixed O&M cost was 16.7 times higher than that for air-source heat pumps. This was due to the larger number of installed units that would have to be operated and maintained. The difference was less relevant for areas with lower plot ratio, where the number of apartments per building decreased. This is represented by the case of SH share of 0.8 and plot ratio of 0.6, where the total cost of the three ULTDH solutions were closer to each other.

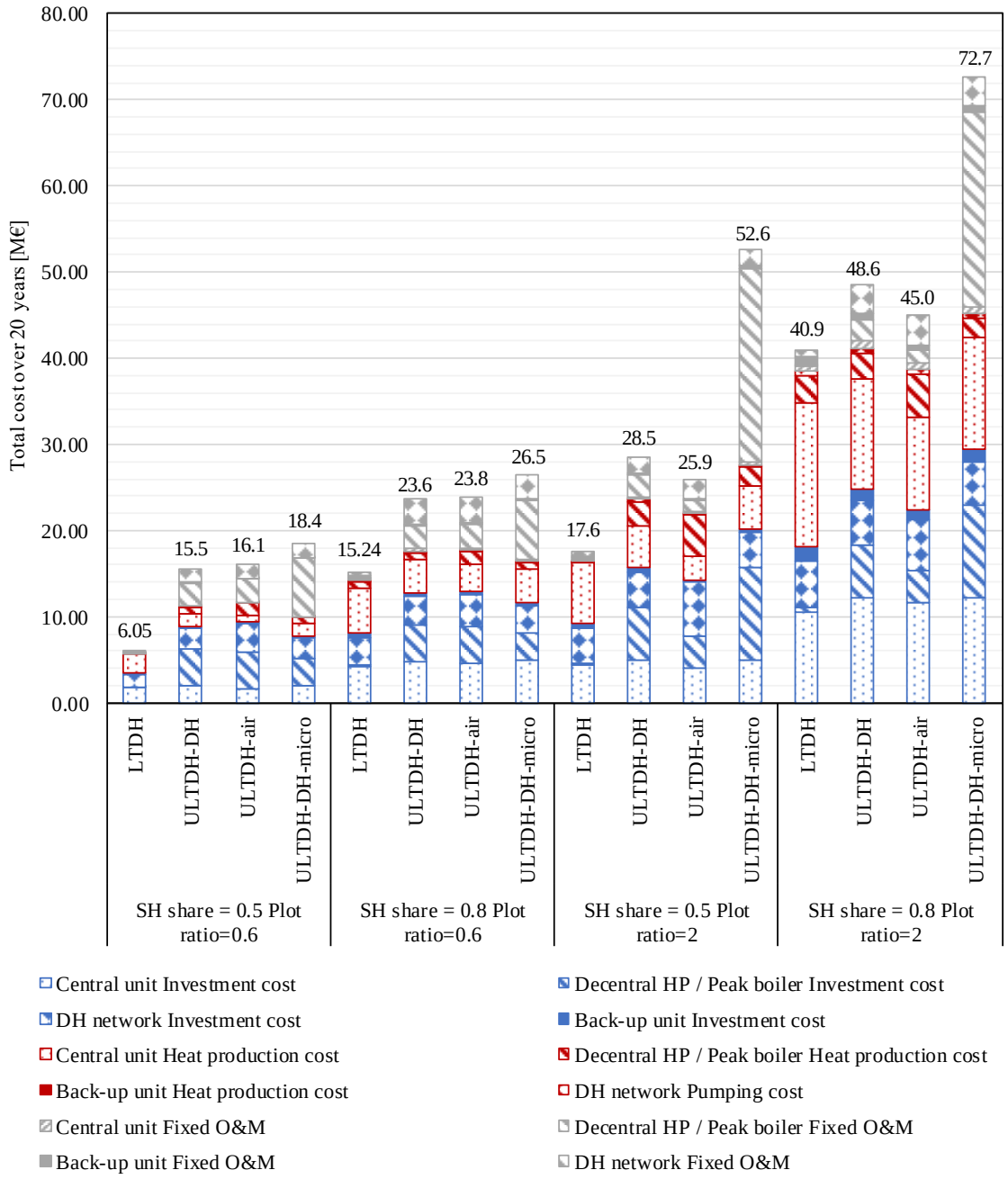

Figure 2-13 Cost composition for SH share= 0.5 and SH share= 0.8, plot ratio = 2 and plot ratio = 0.6, central heating source: Groundwater heat pump. Heat production cost includes variable O&M cost, fuel costs and taxes. Investment cost includes VAT, reinvestments and the residual value has been subtracted. district heating substation cost is included in fixed O&M cost of the district heating network.

The investment and O&M costs of the decentral heat pump units solely depended on the plot ratio, i.e. the total number of buildings and the number of apartments per building. Accordingly, the differences between the district heating variants were more pronounced for lower SH shares. With an increasing SH share the capacity of the central heat pump unit increased and accordingly, the investment cost of the central heating unit and the total heat production cost from the central heating unit increased. The heat production cost of the central unit included electricity cost,

variable O&M cost and taxes. The investment cost of the central unit supplying ULTDH at high plot ratios was slightly higher than for LTDH. This was caused by the assumption that the capacity of the central units for ULTDH should have capacity to cover the maximum district heating demand, while the capacity of the LTDH central unit was assumed to be only 80 % and instead an additional peak boiler was included. Accordingly, the lower investment cost in the central unit for LTDH led to relatively high heat production cost of the peak load boiler, indicating that the capacity of the central unit should be optimised.

2.4.5 Sensitivity analysis

2.4.5.1 Variation of investment cost

The heat pump investment cost were based on currently available technology and recent projects, but they might decrease due to higher production volumes in the future. The investment cost was varied for the central heat pumps, decentral heat pumps and the network. The results are presented in Figure 2-14 for a SH share of 0.8 and a plot ratio of 2, as this was the case, where the LCOH of ULTDH was closest to LTDH. The results are presented as the difference between the LCOH of the ULTDH solution and the LTDH solution, i.e. a negative value meant that ULTDH was more feasible than LTDH in terms of LCOH

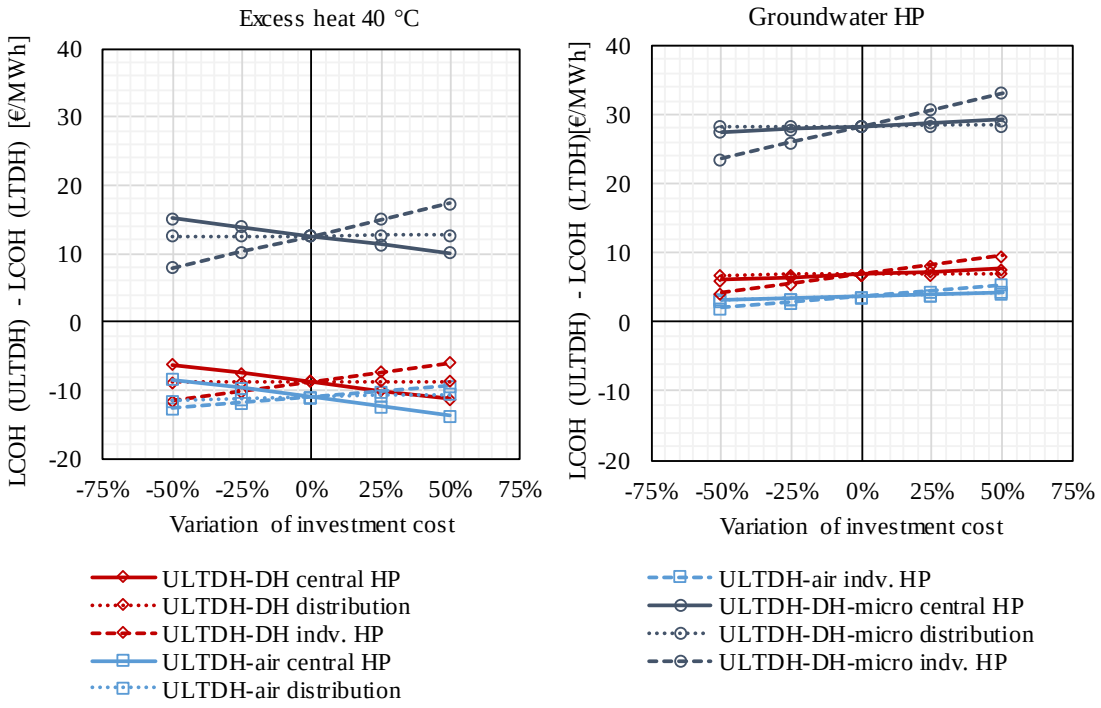

Figure 2-14 Variation of investment cost of central heating unit (central), decentral booster heat pumps (individual) and district heating network (distribution) for excess heat 40 °C (10 €/MWh) source heat pump / direct excess heat supply and groundwater heat pump as central heating units, plot ratio = 2 and SH share = 0.8

All investment cost changes resulted in a linear change in LCOH difference. The change in network investment was similar for all district heating variants and did not result in a significant change in the difference of LCOH. A lower investment in decentral heat pumps resulted in a decrease in LCOH difference. The effect was most significant for ULTDH-DH-micro, which had the highest decentral heat pump investment cost. An increase of the investment in the central unit

resulted in a decrease of the LCOH difference in the case of excess heat. This was because, the investment cost in the heat pump needed for LTDH supply were significantly higher than the cost of the central heat exchangers for direct use of excess heat in ULTDH. For groundwater heat pump as a central unit, both district heating solutions required the investment in a central heat pump and LTDH benefitted from economy of scale due to the larger necessary capacities. Accordingly, the LCOH difference increased with increasing central unit investment cost. The feasibility of LTDH or ULTDH did not change for the depicted cases.

2.4.5.2 Variation of COP

The COP of the central and decentral heat pumps were varied between -25 % and +50% [159] to account for possible innovations in heat pump technology. Such an increase might e.g. be obtained through the use of zeotropic mixtures as working fluids as proposed by Zühlsdorf et al. [89]. The results are presented in Figure 2-15 for the same cases shown in Figure 2-14. A reduction in COP of the central and decentral heat pumps had a larger influence on the LCOH difference than an increase. An increase in the decentral heat pump COP benefitted the ULTDH solutions. An increase in central heat pump COP benefitted the LTDH solution. ULTDH-air benefitted most from an increase in decentral heat pump COP, i.e. a higher share of heat that could be recovered from the outside air. Testing the influence of a decrease in decentral heat pump COP for ULTDH-air also gives an indication of how large the influence of neglecting the fan power consumption on the result may be. ULTDH-DH and ULTDH-DH-micro benefitted less from an increase in booster heat pump COP, which led to an increased heat production from the central heat pump and a larger capacity of the central heat pump.

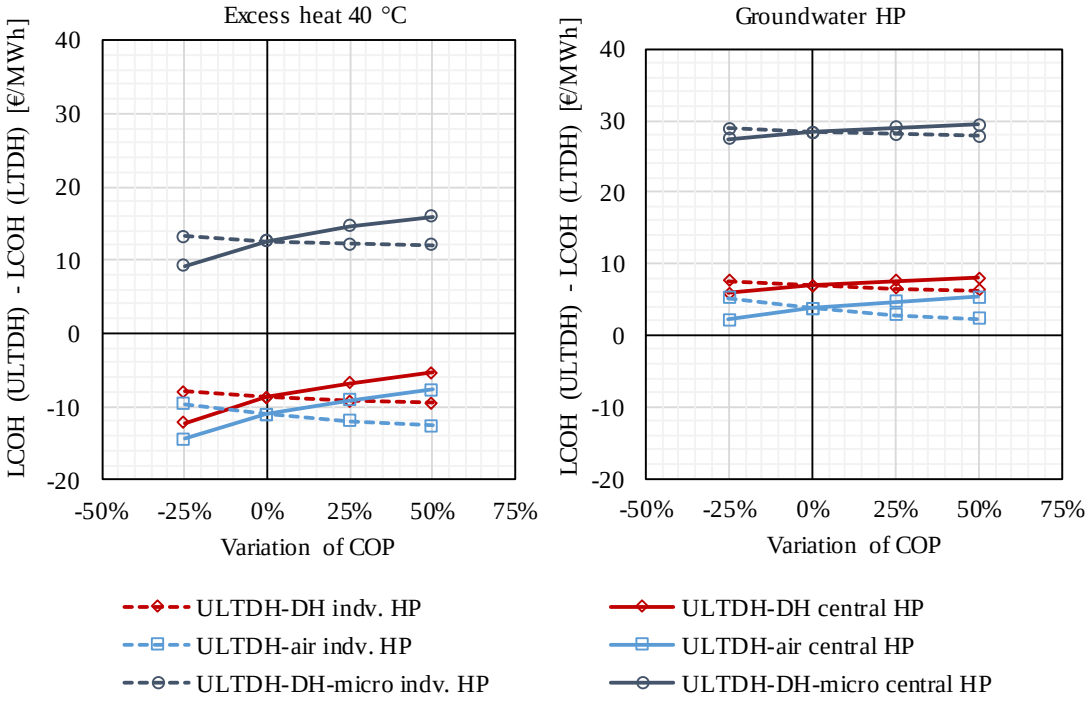

Figure 2-15 Variation of COP of central heat pump and booster units for excess heat 40 °C source heat pump / direct excess heat supply and groundwater heat pump as central heating units, plot ratio = 2 and SH share = 0.8

The influence of neglecting the fan power consumption of the air-source heat pumps on the overall feasibility of LTDH and ULTDH compared to heat supply by individual air-source heat pumps was

tested. Figure 2-16 shows the variation of the minimum plot ratio, for which LTDH is still feasible with increasing fan power consumption. The fan power was varied between 0 % and 11 % of the heat pump compressor power consumption. The minimum feasible plot ratio for LTDH decreased with increasing fan power ratio, as the operation cost of individual heat pumps increased and thus LTDH was competitive for less densely built areas. The effect is strongest for low SH shares, as the LCOH of LTDH and the LCOH of individual heat pumps cross each other at larger plot ratios, where the LCOH curve of LTDH is flatter than at lower plot ratios (compare Figure 2-10).

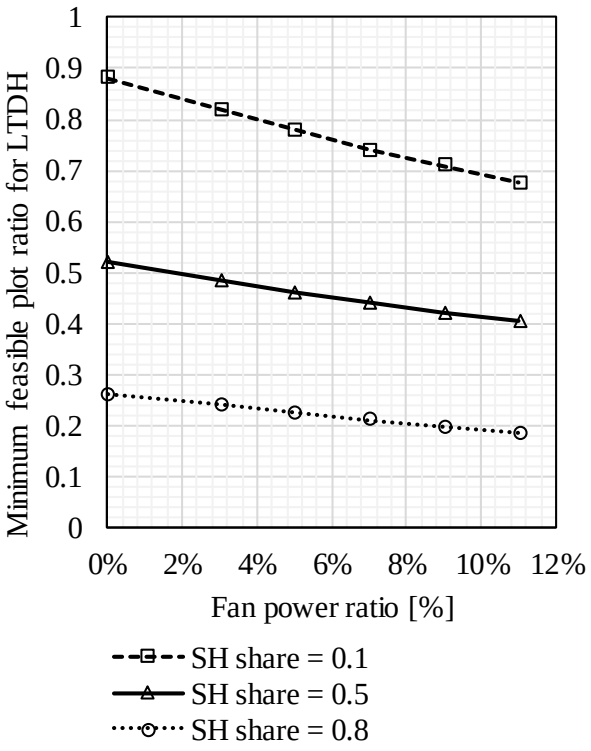

Figure 2-16 Variation of minimum feasible plot ratio for LTDH with fan power ratio for SH shares of 0.1, 0.5 and 0.8. Fan power ratio was defined as the total annual fan power consumption over the total annual compressor power.

2.4.5.3 Variation of electricity cost

The electricity cost was varied, as the future electricity price development is uncertain. A decrease in electricity price increased the LCOH difference slightly and thus benefitted the LTDH solution. ULTDH solutions benefitted from increased electricity prices, as the seasonal system COP is highest for the ULTDH options, i.e. less power is consumed per unit heat delivered. The effect was largest for ULTDH-DH-micro and least for ULTDH-air. The feasibility of the solution for the case of a SH share of 0.8 and a plot ratio of 2.0 did not change with a decrease or increase of the electricity price of 50 %.

2.4.5.4 Variation of full load hours of decentral heat pumps

The design full load hours per year for the decentral heat pump units of ULTDH-DH and ULTDH-air were varied from 1000 h to 4000 h. The results are presented in Figure 2-17. The LCOH difference decreased with increasing number of design full load hours, as the installed capacity and thereby the investment cost decreased. The trend was more pronounced for ULTDH-DH, than for ULTDH-air. Further, the decrease was lowest for the case with the highest SH share and

plot ratio. Accordingly, lower decentral heat pump capacities would benefit the ULTDH solutions compared to the LTDH, but in the assessed range, LTDH was still economically more feasible.

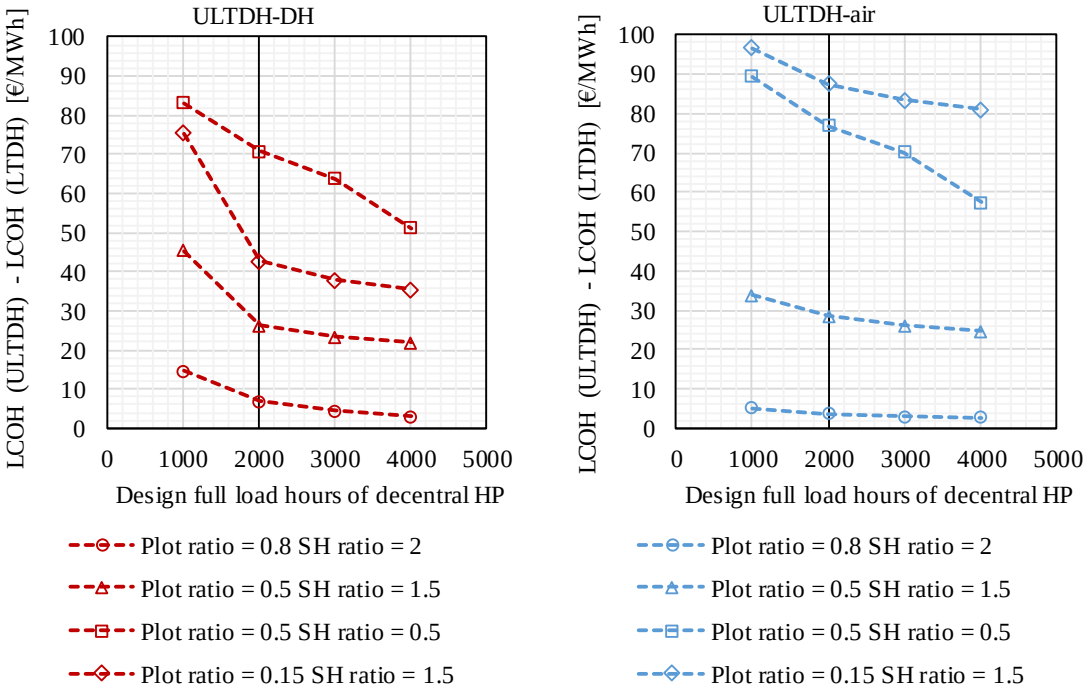

Figure 2-17 Variation of design full load hours of decentral heat pumps for groundwater heat pump as central heating unit for four cases

2.5 Case study Levantkaj

In the analysis that was described above, it was assessed whether a new development area like Nordhavn could beneficially be supplied by district heating. The later development steps of Nordhavn have not been planned in detail, thus plot ratios and building types are not yet known for all future development phases. It is however known for the next phase, the Levantkaj area in Nordhavn, Copenhagen that is expected to have a plot ratio 1.5. The Nordhavn area with the next development step is depicted in Figure 2-18. The results for economic feasibility of LTDH and ULTDH in terms of levelised cost of heat and socioeconomic NPV compared to supply from individual air-source heat pumps and a space heating share of 0.15 and 0.5, are presented in Figure 2-19 and Figure 2-20. For this case, LTDH supplied at 60 °C is the most feasible solution in terms of LCOH and socioeconomic NPV. The new buildings in Nordhavn, have to comply with the Danish building standard 2020 [139], however it is likely that the space heating demand will not be reduced to zero. The results for a space heating share of 0.15, which would correspond to a yearly space heating demand of only 3 kWh/m^2/a, indicate that LTDH would still be a feasible option. Among the calculated scenarios, the central groundwater heat pump had the highest socioeconomic NPV. ULTDH only reached a positive socioeconomic NPV for the case of direct excess heat supply and ULTDH-DH, assuming heat cost of 10 €/MWh for the excess heat. The availability of such a suitable excess heat source, that allows supplying excess heat directly to ULTDH is an unlikely scenario for the Levantkaj area. However, it may be possible to connect the area in cascade to the existing DH grid in the most southern area of Nordhavn.

Further, the results show that the supply of ULTDH benefits significantly from larger space heating demands. It is therefore important to precisely estimate the actual space heating demand of new buildings.

Figure 2-18 Nordhavn in Copenhagen, the next development step Levantkaj is marked in blue. Map taken from [60].

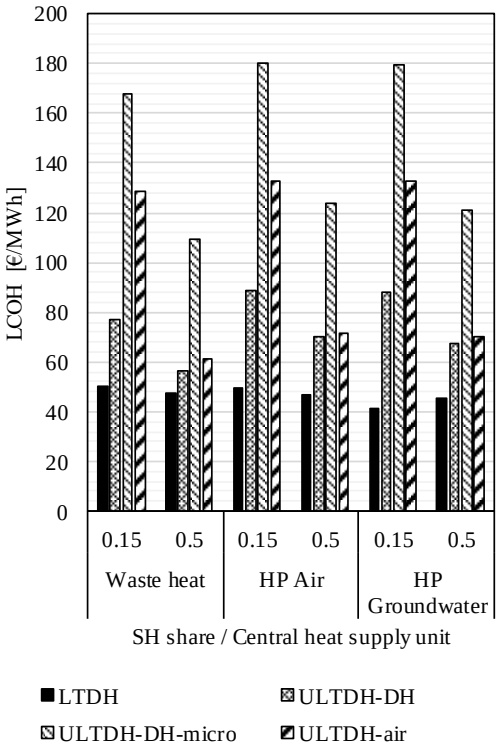

Figure 2-19 Levelised cost of heat for Levantkaj area for SH shares of 0.15 and 0.5, and excess heat 40°C, air and groundwater as central heat source

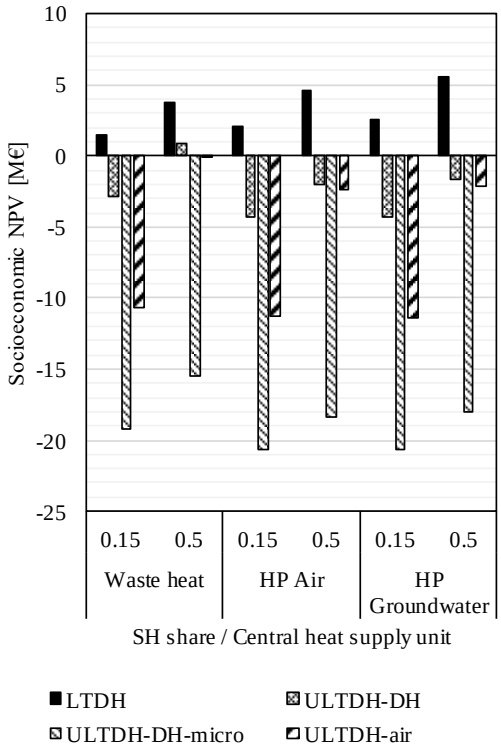

Figure 2-20 Socioeconomic net present value for Levantkaj area for SH shares of 0.15 and 0.5, and excess heat 40°C, air and groundwater as central heat source

2.6 Discussion

The aim of the current study was to deduce under which boundary conditions LTDH and ULTDH supplied by heat pumps could be feasible in Denmark. To answer this question, general correlations were used, which means that the results showed a general trend. Specific local conditions might change the results and a more thorough analysis would be needed for evaluating the feasibility of all heat supply solutions for a specific case. This would also allow for optimal sizing of the central unit with regard to the expected heat demand profile, which was not in the focus of the current study.

The first part of the study compared LTDH supply from central heat pumps, to supply from wood-fired boilers and different individual heating units. Comparing the results to current values from Denmark, it was found that distribution cost, LCOH and LHDD showed to be in good agreement with the values from realised projects [131]. Lower district heating temperatures and reductions in distribution costs were beneficial for LTDH supply compared to individual solutions. These may be obtained by new piping types, and cost efficient digging [160]. The economic feasibility of large-scale heat pumps benefitted from reduced supply temperatures. Further, heat pumps as central heat supply units currently benefit from the Danish owner structure and regulations, as these provide stable conditions for long-term investment into district heating systems and incentivises large-scale heat pumps.

The case of heat sparse areas is more common in suburban and rural networks, but a special case in an urban environment, where it mostly applies to newly developed areas with high building energy efficiency. These high building standards are expected to allow for lower heat supply temperatures and thereby reduced district heating temperatures. As shown, this benefits the economic feasibility of heat supply from large-scale heat units. Thus, low-temperature systems are a natural starting points for the employment of large-scale heat pumps. In order to change the heat supply to renewable, it is however of uttermost importance to change the supply of the existing district heating grids. This challenge has been addressed in recent projects, e.g. [29,161].

The second part of the study focused on large-scale heat pumps and excess heat as central heat sources. The excess heat source has not been specified further and might as well represent other natural heating sources. In this case, temperature variations of the excess heat source might occur, which should be considered, as they may influence the heat pump performance and necessary capacity. The case of 40 °C excess heat as heat source for a heat pump might also give an indication of the feasibility of new areas connected in cascade to the return line of existing networks.

The case of direct excess heat supply of ULTDH is a theoretical scenario, which was included as an extreme scenario that could maximise the benefit of ULTDH solutions. It should be noted that the existence of such a source, which can deliver 40 °C and higher forward temperatures e.g. as excess heat from industrial processes is a special case and if available, could be expected to not be free of charge and without demand for power.

As the network design was unknown for the conducted study, the pumping power and heat loss values could only be estimated. As the pumping power made up a minor part of the overall energy use, the uncertainty was deemed acceptable. The heat loss was obtained from average values of existing Danish networks. Newly built networks might perform better due to modern piping technology, but representative data for ULTDH networks is missing. Another simplification made, was that the return temperature could be kept constant. This is generally not achieved as the cooling of the district heating stream varies with the supply temperatures and the overall heat demand [143]. It may be expected that the return cannot be cooled down to the assumed values

during summer. The uncertainty introduced by this was integrated in the heat loss estimation, as it was based on empirical data. It might however, result in a decreased COP of the central heat pump during summer This effect was not considered in this study.

The economic feasibility of the ULTDH-air and ULTDH-DH suffered from the extra investment and O&M cost for the decentral heat pump units, even though the overall seasonal COP was higher than for LTDH if the LHDD of the supplied area were high enough. Accordingly, these cost components should be reduced. This may e.g. be achieved by reducing the capacity and thereby increasing the full load hours of the decentral units.

As presented in section 2.4.4, the fixed O&M cost for the booster units led to comparably high total cost of ULTDH-DH-micro. The cost function for the fixed O&M cost was based on experiences with existing individual air source and ground source heat pumps [151]. As the heat source for the micro-booster and booster heat pump is the district heating system, the O&M cost related to the source might be less compared to ambient heat sources, as pollution and other risks connected to the ambient sources might be avoided. Further, these units are prefabricated, which might allow for reduced O&M cost. This would decrease the LCOH difference between LTDH and ULTDH and increase the competitiveness of micro-booster heat pumps. However, reliable fixed O&M cost data based on existing booster and micro-booster heat pumps is missing and should be addressed in future studies to reduce uncertainties for future projects.

ULTDH could only be feasible under specific boundary conditions, i.e. a cheap heat source, which is available at temperatures high enough to supply SH directly, but not high enough for LTDH. It was shown that the cost for ULTDH are closest to LTDH when the network utilisation is high, i.e. for high plot ratios, i.e. a densely populated area and high SH shares. This is an unlikely scenario for newly built quarters in Denmark, as the future building regulations do not allow for such high SH shares [139]. It has however been observed that buildings do not always behave accordingly [162], which justifies the assessment of SH shares of up to 0.8. Another option to implement energy efficient ULTDH systems, while keeping the utilisation of the district heating network high, may be the combination with district cooling, in so called cold district heating systems, e.g. [24]. This would require further research with regard to optimal system design and development of suitable heat pump substations.

The fan power of all air-source heat pumps was neglected. The sensitivity of this assumption was tested for ULTDH-air and for individual air-source heat pumps. It was not tested for central air-source heat pumps, as they were not among the best performing technologies and thus a change in COP of central air-source heat pumps would not change the results with regard to feasibility of ULTDH compared to LTDH and individual heat pumps. Miara [163] determined in field tests that the fan power consumption of small-scale air-source heat pumps is typically below 7 % of the total power demand. Neglecting the fan power for the individual heat pumps led to more conservative results with regard to the feasibility of LTDH for low linear heat demand densities. The feasibility of ULTDH-air compared to the other ULTDH solutions did not change when assuming a reduction in COP corresponding to 7 % of the total heat pump power uptake.

The results presented here are in good agreement with the results presented for specific cases in literature. It was confirmed that the operation cost is lower for ULTDH than for LTDH, as also found by Yang and Svendsen [19] and Elmegaard et al. [122]. However, the increased investment and O&M cost for the ULTDH cases led to higher overall cost for the ULTDH cases. The case described by Best et al. [124], where they found that ULTDH was slightly better than LTDH considered a SH share of 0.8 and air-source heat pumps in a German case. According to the results presented here, this configuration might also be viable in Denmark, if the plot ratio of the

supplied area and the difference in central unit investment cost is large enough to balance out the extra investment in decentral units.
In the majority of the examined cases, LTDH was found to be economically more feasible than ULTDH. This was the case in terms of both LCOH and socioeconomic NPV. Both of these indicators evaluated the economy of the project from a public perspective. As the aim was to assess, which common heating solutions could make sense in future applications, this approach seemed most appropriate. It should be noticed that while the socioeconomic feasibility of heat supply solutions needs to be proven in order to realise a project in Denmark, this is not the case in most other countries and there, the feasibility in terms of business and customer economy would probably be the decisive factor.
For the case study of the Levantkaj area in Nordhavn, it should be noted that as Nordhavn is located at the seaside, seawater comprises one of the accessible sources. This source was only considered in the first part of this study, as the cost data was deemed too insecure, due to the lack of cost data for this type of system. A more thorough assessment of the available heat sources in Nordhavn and their optimal use has been published by Pieper et al. [94].
The later development steps of Nordhavn have not been planned in detail, thus plot ratios and building types are not yet known for future development phases. It is however known for the next phase, which is Levantkaj (plot ratio = 1.48), which has therefore been addressed in this study.
There are further challenges with regard to possible district heating supply in outer Nordhavn, as there are some island areas, where new heat supply solutions are expected to become necessary already in the next years. It is thus important, to have an idea of how the future heat supply in outer Nordhavn could look like. If this could be DH, the different island networks would later have to be integrated in a larger grid and thus it might be beneficial to plan for future constraints when planning these island solutions. This issue was further assessed in [164].

2.7 Chapter summary

In this chapter, it was assessed how the economic feasibility of different district heating variants supplied by heat pumps is influenced by the boundary conditions of the supplied area and the available heat sources. This question was assessed using a techno-economic approach to evaluate the levelised cost of heat, the socioeconomic NPV and the systems efficiency in terms of system COP for all assessed cases. This was done using a generalised approach that allowed identifying overarching trends, without having to know the district heating system topology in detail. The results indicated that for future suburban and urban (plot ratio above 0.6), newly built areas in Denmark supplied by heat pumps, heating supply from LTDH is economically most feasible. For these low supply temperatures, supply from central heat pumps, especially exploiting water based heat sources, is recommendable. Generally, the LCOH for all considered alternatives decreased with increasing plot ratio and increasing SH share for the assessed range of these variables. Therefore, for especially low linear heat demand densities, individual heat supply is preferable. If a cheap supply of ULTDH is available, such as direct heat supply from excess heat, ULTDH could be feasible compared to LTDH for high plot ratios of one or higher, and SH shares of 0.7 and higher. The economic feasibility of ULTDH suffered from additional investment- and fixed O&M cost of the decentral units that were not outbalanced by the lower operation cost. Compared to LTDH, ULTDH benefits from reduced overall cost of decentral units, including, increase in COP, decrease in investment cost and optimisation of installed capacity. The competitiveness of ULTDH systems is higher if the share of directly supplied energy is high, as the seasonal system COP increased with increasing SH share and plot ratio, i.e. increasing heat

demand and less energy efficient buildings. This contradicts the development towards more energy efficient buildings with low space heating demand.

3 Flexible operation of heat pumps

Within this chapter, the ability of large-scale ammonia heat pumps to operate flexibly and thereby act as a sector-coupling unit between the power and heating systems is assessed. Information on how fast large-scale heat pumps can actually start-up and shut-down, how they perform during load changes and what the limiting factors are to be able to react faster, is needed. This may serve as a basis to analyse the business case of different operation strategies of heat pumps as sector coupling units that provide flexibility to the system. The analysis is based on a dynamic model which was implemented into Dymola using the TIL library. The model was then calibrated to and validated against experimental data from the FlexHeat heat pump, recently installed in Nordhavn, Copenhagen. The validated model was used to analyse the dynamic behaviour of the plant and especially the regulation time, which is an important factor to be able to supply ancillary services to the power grid. The model description and validation is taken from [P3]. The description of control principles for vapour compression heat pumps (section 3.1.3) was elaborated as part of a special course on control of heat pumps conducted as part of the PhD studies.

The following analyses were conducted using the model and the results are presented after the method description in this chapter.

- *Quantification of the dynamic behaviour of the base-case heat pump*. The performance of the base-case model was analysed in steady-state for various operation conditions. Further, the dynamic behaviour was analysed. A risk for droplet formation in the suction line was identified. This part was published in [P3].
- *Optimisation of the control structure of the existing plant*. Based on a preliminary relative gain analysis suitable control structures for two-stage ammonia heat pumps were assessed. The most promising control structures were assessed using the dynamic model and compared to the base case in terms of regulation time and ability to avoid droplet formation. The effectiveness of the control structure to react to changes in the boundary conditions were analysed. This part was partly published in [P3].
- *Constructive changes to avoid droplet formation in the suction line*. The previous analysis showed that the risk of droplet formation in the suction line cannot fully be avoided by changing the control structure alone. In this part, constructive measures to ensure superheating of the fluid in the suction line were analysed. This part was published in [P5]. The result were however recalculated using an updated model.
- *Influence of component sizing on the regulation time*. It was analysed how the sizing of the different components influence the regulation time and COP and what limitations occur. This was done using a Monte Carlo approach and conducting a sensitivity analysis on the results. Design recommendation for future fast-regulating heat pumps were derived. This part is taken from [P7].
- *Influence of cycle design on the regulation time*. Different cycle designs for large-scale ammonia heat pumps were compared in terms of regulation time and COP, and design recommendations were derived. Parts of this section were published in [P5].

At the end of this chapter the results are discussed and a chapter summary is given.

3.1 Background

3.1.1 Two-stage ammonia heat pump cycle with open-flash intercooler

Figure 3-1 shows the principle sketch of a two-stage ammonia heat pump cycle with open flash intercooler and the corresponding log(p)-h diagram. The saturated vapour entering the low-stage compressor (1) is compressed (1→2) to an intermediate pressure level. The superheated fluid (2) is mixed with the fluid from state (9) before entering the intercooler, resulting in a mixed state (9*). Note that the mixing was omitted in Figure 3-1 to keep the sketch clear. In the intercooler, the fluid is split up into the liquid phase (10) and the vapour phase (3), which exit the intercooler separately. The ammonia is then compressed a second time (3→4). The superheated ammonia is desuperheated (4→5), condensed (5→6), and subcooled (7→8), while rejecting heat to the heat sink, here the district heating (DH) stream, which is warmed up. The receiver between condenser and subcooler serves to ensure that only liquid enters the subcooler. The subcooled liquid is then throttled to the intermediate pressure (8→9), and enters the intercooler. The liquid stream exiting the intercooler is throttled a second time down to the low pressure level(10→11). The stream enters the separator, where it is split up into liquid (12) and vapour phase (1). Ammonia heat pump cycles typically comprise a flooded evaporator in which the liquid ammonia is partly evaporated (12→13) while absorbing heat from the heat source. The stream passes then through the separator again, such that only the vapour phase enters the suction line to the compressor (1). The mass flow through the evaporator is driven by gravity, i.e. the separator needs to be placed above the evaporator, or by an auxiliary pump. The advantage of flooded evaporators is that the evaporator may be smaller, compared to a direct expansion evaporator and it can be ensured that the fluid entering the compressor is close to the saturation line. This ensures minimum superheating, which allows for lower power demand for compression, as in the case of ammonia the slope of the isentropic lines decreases for higher specific enthalpies (green lines in the log(p)-h diagram, Figure 3-1 right). Further the superheating at the compressor outlet is typically very high for ammonia, and thus minimum superheating in the suction line may help to keep the discharge temperature below the maximum allowable temperature of the compressor.

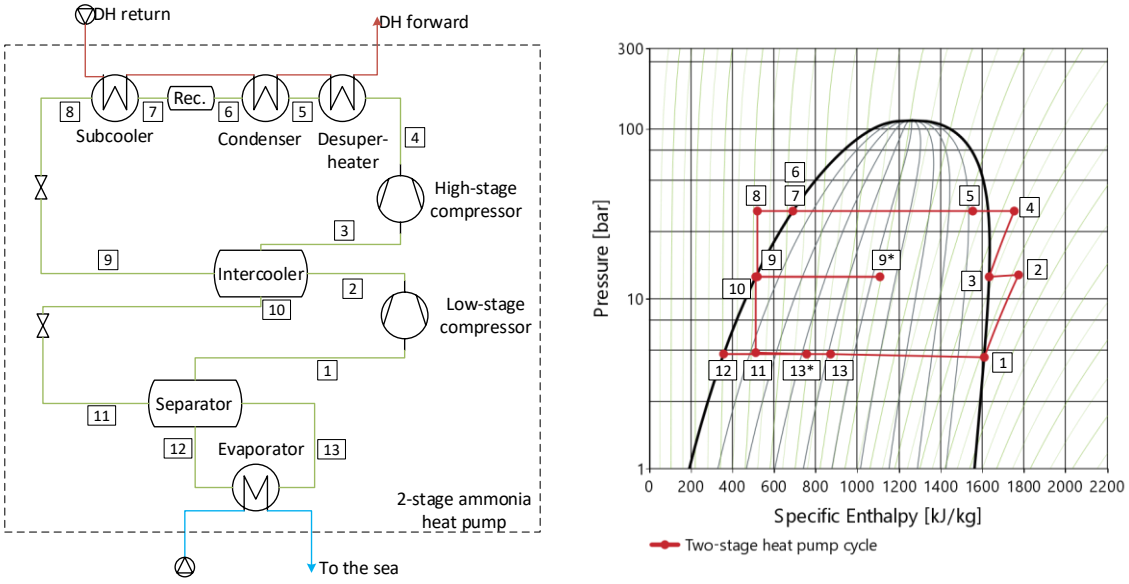

Figure 3-1 Principle structure of a two-stage ammonia heat pump with open-flash intercooler and the cycle representation in a (logarithmic) pressure - specific enthalpy diagram

3.1.2 Dynamic modelling of heat pumps

Steady-state model of heat pumps and refrigeration cycles are often used to design systems for a given case or to determine the seasonal behaviour of the heat pump. The aim of this study was to assess the dynamic behaviour of large-scale heat pumps and their ability to ramp quickly or follow a given frequency pattern for the provision of ancillary services. A steady-state simulation is not sufficient for this purpose, as the reaction time and the occurring phenomena during ramping are expected to be dominated by transient processes in the cycle. Hence, it is necessary to use a dynamic model to simulate the performance of the system, which per definition depicts the time dependent development of the modelled system. A dynamic model further allows to evaluate the influence of the system control on the system and may also be beneficially used for fault detection and diagnosis capability [165].

Dynamic models for refrigeration cycles have been a research topic approx. since the 1980's. Rasmussen et al. [166] described the dynamic behaviour of small-scale one-stage heat pumps (ca. 10.5 kW thermal) in detail. Apart from the cycling behaviour, they focused on the refrigerant migration in the heat pump during start-up and shut-down. Such a detailed analysis required the use of dynamic system models. Similar studies based on experimental and numerical assessment emphasised that component sizing and cycle design [167,168] as well as the operating conditions [169] influence the dynamic response time of heat pump systems. These statements generally hold true for larger heat pumps as well. Compared to small units, it is expected that larger heat pumps have larger inertia and therefore longer start-up and ramping times, and that the dynamics are influenced by a more complex cycle design and control system.

The prediction of this behaviour is possible using detailed dynamic models, which are based on fundamental physics and thereby are applicable to a large range of conditions and system configurations. The models may be applied to analyse system behaviour, design and optimise systems, model based control design, controller tuning by simulating the dynamic response, as well as for fault detection and diagnosis, as summarised by Rasmussen and Shenoy [170]. Li et al. [165] provide an extensive overview of research advances in the field of dynamic modelling of HVAC (heating, ventilation and air conditioning) equipment. They describe that dynamic models of refrigeration cycles are typically set up out of component models for the compressors, heat exchangers and the expansion valves. Typical modelling approaches include modelling the compressor using a steady-state mass balance and a dynamic energy balance to account for the heat stored in the component material. The underlying assumption behind the steady-state mass balance is that the time constant of the mass balance in the compressor is much shorter compared to other components and to the energy balance and may thus be neglected. The expansion valve is also commonly modelled as a quasi-steady-state component, i.e. the mass flow rate is updated instantaneously when the inlet or outlet state change. Two different modelling approaches are common for heat exchangers, finite volume models and moving boundary models. In the first case, the heat exchanger is divided into a certain number of constant volumes. The dynamic balance equations for mass and energy are solved for every volume, assuming an ideally mixed fluid in every volume. In the second case, the model is based on three variable control volumes, one for the superheated fluid, the two-phase fluid and the subcooled fluid, respectively. Moving boundary models are computationally more efficient than finite volume models because of the fewer control volumes. They do however tend to become instable for highly transient operation conditions, when a phase forms or disappears [165]. Another common simplification is to assume homogenous two-phase flow [171] and neglecting the refrigerants pressure drop [165].

Most of the models described in literature are based on component models that are dimensioned according to the plant that is modelled. This requires a lot of information about the size, volume, masses, refrigerant filling, etc. in order to be able to represent the systems dynamics correctly. There are however approaches to further generalise the description of the dynamic behaviour of heat pumps. Nunes et al. [172] proposed a dimensionless approach to describe vapour compression refrigeration systems and their steady-state and dynamic behaviour. They found that there is an optimal area factor, defined as the ratio of evaporator heat transfer area to the sum of evaporator heat transfer area and condenser heat transfer area (including desuperheating and subcooling), for a minimal pull-down time of the refrigeration system.
Different suitable numerical tools are available to efficiently simulate dynamic systems. Modelica [173] has been demonstrated to be a suitable platform for dynamic simulation of thermo-fluid problems, as pointed out by Li et al. [174]. Modelica is an open source object-oriented programming language and different open source and commercial libraries for thermodynamic modelling of refrigeration/heat pump cycles are available, e.g. TIL suite, ThermoCycle, Vapor Cycle Library.

3.1.3 Control principles for vapour compression heat pumps

The aim of controlling any system is to ensure high system performance and secure operation. In the case of heat pumps, system performance may be defined as accurately meeting the required heating (and possibly cooling) demand and the desired temperature. For flexibly operated heat pumps, the accurate regulation of the compressors' power uptake is of interest. The control system must further be able to react to disturbances of boundary conditions and keep the system in the desired operational state.
As described by Jensen & Skogestad [175], a simple refrigeration cycle has five degrees of freedom, namely the compressor power, the heat transfer in the condenser, the heat transfer in the evaporator, the valve opening and the active charge in the cycle. Ideally, the degree of freedom allows controlling five different variables. However, in practice mostly only the mass flow rate of the refrigerant, i.e. the compressor speed is controlled for load control and the superheating exiting the evaporator is controlled via the expansion valve. While the heat transfer in the heat exchangers and the refrigerant charge are set in the design phase, such that heat transfer, and thereby COP is maximised.
Goyal et al. [176] provide a comprehensive review of control methodologies for vapour compression and absorption heat pumps. They classify existing control approaches for vapour compression heat pumps into basic control, advanced control and intelligent control, as presented in Figure 3-2.
The conventional control methods are on/off control, which may be used to control an average heat flow over a longer period of time and to keep the temperature within a certain defined range. This control method relies on flexibility as to when the heat is supplied, that may be offered by thermal inertia of the supplied room or a storage tank, where the heat pump is started up, whenever the temperature falls under a given lower set value. This control cannot react to other changes in the boundary conditions than the controlled variable (here, the temperature).
The PID (Proportional-Integral-Differential) feedback control can accommodate external disturbances, as the system is constantly regulated during operation. Due to the integral element of the controller it may minimise the deviation between the set point value and the actual value of the control, which is not possible with a simple on/off control. This is enabled by variable speed drive for compressors and electric valves.

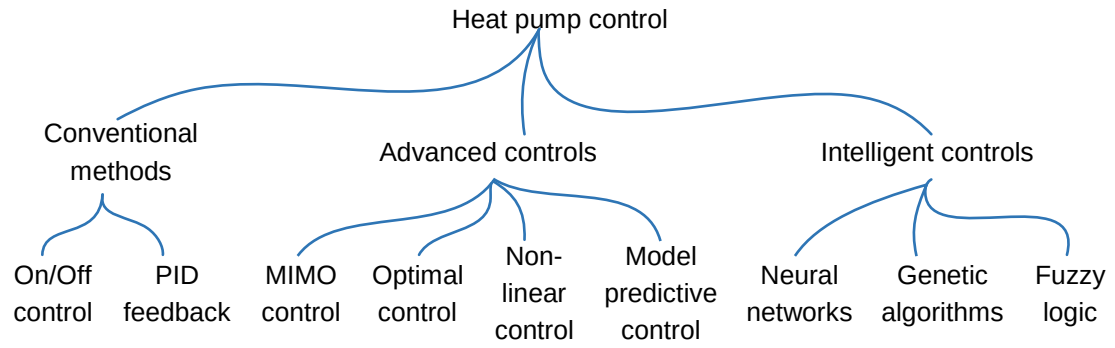

Figure 3-2 Classification of control methodologies for vapour compression heat pumps, adapted from [176]

If only one variable of a system is controlled via one manipulated variable, this is called a SISO (single-input-single-output) control structure. In usual technical systems, more than one variable needs to be controlled. If a system is controlled by several SISO loops, i.e. each control variable is controlled by one manipulated variable, this is called a multi-loop SISO control structure. In this case, every loop would include an individual controller. The underlying basics of designing a multi-loop SISO (single-input-single-output) control structure using PI(D) controllers will be described in the following sections.

The advanced control structures build upon the theory of multi-loop SISO control using PID controllers. When there is a strong coupling between the different SISO control loops in the system, the interactions between the different controllers decrease the performance of controllers. This is the case when the manipulated variables have a strong influence on more than one controlled variable. This can result in an increase of the time until steady-state is reached or in induction of oscillations in the system. To avoid this, multivariable control structures or MIMO (Multi-input-multi-output) can be used. Different variances of these exist, including decoupling control, optimal control and model predictive control. They have in common that the controller has several measurements of control variables and the corresponding set points as input and the values for several manipulated variables as output.

3.2 Method

3.2.1 Base case system layout

The heat pump assessed as base case in this study is a two-stage ammonia heat pump with a heating capacity of 800 kW, delivered by Johnson Controls and installed in the Nordhavn harbour area in Copenhagen, Denmark [177]. It uses brackish groundwater at 10.5 °C as heat source. The system rejects the cooled groundwater into the sea in accordance with the actual ground water flow. The heat pump is the main supply unit of a small-scale district heating grid supplying three cruise ship terminals and a high bay warehouse. It is able to deliver district heating forward temperatures of 60 °C to 82 °C. The heat supply unit is further equipped with a storage tank with an active volume of 100 m³ and two electric boilers with a capacity of 100 kW each. A sketch of the heat supply system can be seen in Figure 3-3.

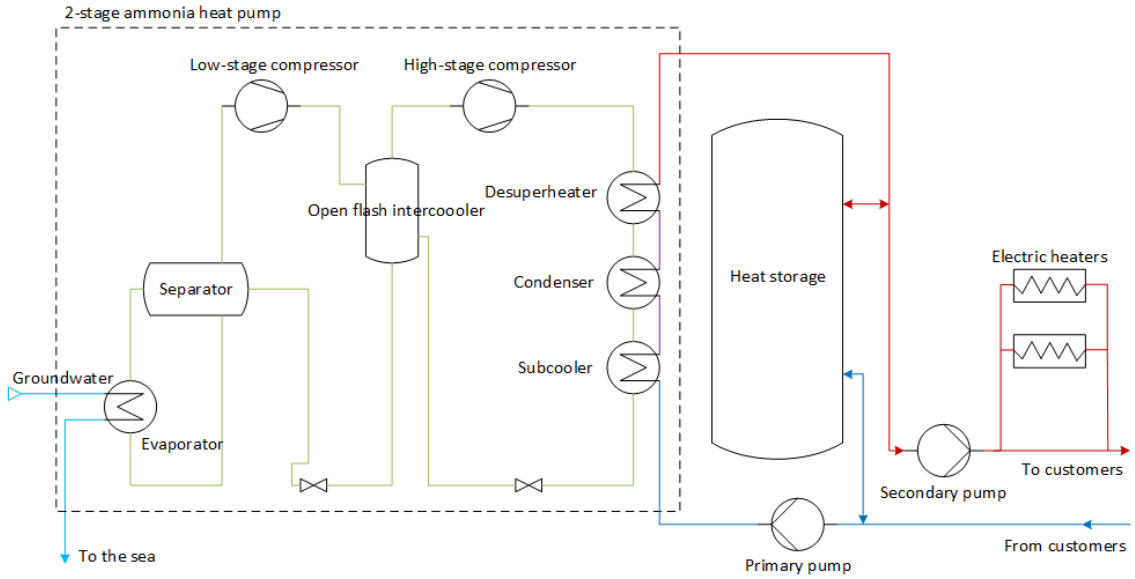

Figure 3-3 Diagram of the heat supply system comprising a 2-stage ammonia heat pump, a storage tank and two electric heaters

The heat pump unit is comprised of the following main components: flooded evaporator, separator, low- and high-stage piston compressor, open flash intercooler, desuperheater, condenser and subcooler and two throttling valves. The evaporator is a corrugated plate heat exchanger and the other three heat exchangers are shell-and-plate heat exchangers. Both compressors are equipped with variable speed drive, thus enabling part-load operation.
The heat pump heat output is controlled either directly or indirectly, by controlling the source outlet temperature from the evaporator to a set value, while keeping the source mass flow constant. In both cases the low-stage compressor speed is modified. The high-stage compressor speed is used to control the intermediate pressure to a fixed value. The district heating forward temperature from the heat pump is controlled indirectly, by controlling the condensation pressure using the sink mass flow as manipulated variable. The high-stage expansion valve controls the liquid level in a receiver between the condenser and the subcooler, thereby controlling the outlet quality from the condenser. The low-stage expansion valve controls the filling level of the open flash intercooler.

3.2.2 Experimental testing procedure

The first tests conducted were part-load tests of the heat pump for forward temperatures of 60 °C, 70 °C and 80 °C. Starting from full load the heating output was reduced to part-load and then ramped up to full load again, as schematically presented in Figure 3-4. This was done by changing the set value of the evaporator outlet temperature of the source flow. It was changed from 4.8 °C to 7.5 °C, 6.5 °C and 5.5 °C, which correspond to a load change from 100 % to 54 %, 65 % and 80 % at 70 °C DH forward temperature. The heat pump was operated in every condition until steady-state operation was reached. The values that were measured and logged during all tests are listed in Table 3-1.

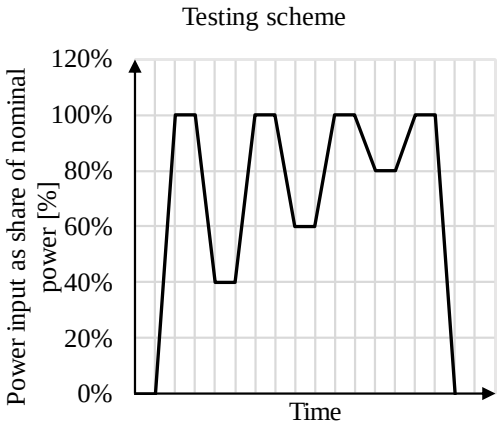

Figure 3-4 Idealised testing scheme for start-up, ramping and shut-down

Table 3-1 Logged data for experimental analysis, *derived from other measurements

Logged value		Unit
Operation mode		-
Heat output*		kW
Power uptake heat pump		kW
Power uptake system (incl. Pumps)		kW
COP (excl. Pumps)*		-
COP (incl. Pumps)*		-
Temperature (water)	Evaporator outlet	°C
	Evaporator inlet	°C
	Subcooler Inlet	°C
	Condenser Inlet	°C
	Desuperheater Inlet	°C
	Desuperheater outlet	°C
Gauge pressure (cycle)	Low-stage compressor inlet	bar
	Low-stage compressor outlet	bar
	High-stage compressor inlet	bar
	High-stage compressor outlet	bar
Temperature (cycle)	Low-stage compressor inlet	°C
	Low-stage compressor outlet	°C
	High-stage compressor inlet	°C
	Low-stage compressor outlet	°C

3.2.3 Model description

A dynamic model of the heat pump was implemented in the object-oriented modelling language Modelica [173]. It was implemented in the simulation software Dymola using the TIL library [178]. The model was set up based on component models of the two compressors, an evaporator, a desuperheater, a condenser and a subcooler, two expansion valves, an open-flash intercooler, a separator, an auxiliary pump and two suction pipes.

The components in the cycle are connected to each other via connectors. Via these connectors, the output mass flow from one component, together with the corresponding specific enthalpy and the pressure are given to the downstream component as input values. Further, the heat pump

control is included in the model. The fluid properties were calculated using the Refprop database [179]. In the following, the assumptions taken for the component models are presented.

3.2.3.1 Heat exchanger models

All four heat exchangers are modelled as corrugated plate heat exchangers. This simplification was made as no data or correlations were available for the three shell-and-plate heat exchangers on the high pressure side. For all heat exchangers a discretised model of parallel flow heat exchangers [178] was used. The model is a finite control volume model and uses the staggered grid approach, which allows the calculation of the interdependencies between mass, energy and impulse. The model is defined by *n* refrigerant control volumes, which are connected to *n* wall control volumes, which are connected to *n* liquid control volumes. The model includes dynamic energy, mass balances and a pressure drop correlation for the momentum balance for the water and refrigerant side. The energy balance in the wall between both fluids is dynamic, too. The flow direction was co-current in the evaporator and counter-current in all other heat exchangers. On the refrigerant side, the following correlations were applied: Ayub [180] was used for evaporation, Yan [181] for condensation and Martin [182] for single-phase flow. The pressure drop in the evaporator was assumed to be proportional to quadratic mass flow. The pressure drop in the heat exchangers on the high-pressure side was neglected. On the water side Martin's [182] correlations for heat transfer and pressure drop were used. The steady-state behaviour of the heat exchanger models was validated against performance data obtained from the Alfa Laval HEX software[183], as no measurements on the refrigerant side were available.

3.2.3.2 Compressor models

The high-stage compressor was based on the reciprocating compressor model included in the TIL library [178]. This model includes dynamic energy and mass balance equations for the suction and discharge chamber. Further, the re-expansion mass flow was calculated based on the cylinder dead space volume and the discharge valve delay, which were input parameters to the model.

The low-stage compressor model was based on polynomials for the isentropic efficiency, the volumetric efficiency and cooling of the compressor, including the effect of active cooling and heat loss to the environment. The volume of the component was disregarded and accordingly, the balance equations were steady-state, as no mass or energy can be stored inside the component. The polynomials were parametrised to fit Johnson Controls' SMC 112L (low-stage) and HPX (high-stage) compressors. The data was available from the Comp1 dimensioning software [184]. This model approach was based on the assumptions that the time constants of the compressors are low compared to the time constants of the overall cycle and that the stored mass and energy in the compressors may be disregarded.

A different approach was chosen for the low-stage compressor compared to the high-stage compressor as it was found unfeasible to adapt the dynamic model to the available compressor data for the low-pressure compressor, while the representation of the high-stage compressor was in good agreement with the available design data.

3.2.3.3 Other components

The separator and open flash intercooler were modelled as ideal separators.

In order to be able to solve the circular mass balance between the evaporator and separator, an additional pump component was used to fix the pressure increase between the separator and the evaporator. In the real system this increase in pressure is purely based on gravitational forces.

These were disregarded in the described model thus making the use of an additional pump component necessary.
The model versions were implemented. In the first one other pipe elements than the suction pipes were disregarded to reduce computational time. The pressure loss of all pipes (excl. suction lines) on the low pressure and intermediate pressure level were merged into a common pressure loss model to ensure the right inlet and outlet pressures for the compressors. The second version included all pipelines in the system to account for their influence on the systems dynamic behaviour and to test whether the simplification of neglecting the pipelines in the first model were justified.
The assumed geometries and input values of the model components are listed in Appendix A.1.

3.2.4 Model calibration and validation

Not all parameter values required by the component models in the TIL library could be determined by the given data for the real heat pump system, and thus some had to be estimated. Especially, the parameters of the low-stage compressor polynomial and the geometry parameters of the high-pressure side heat exchangers were uncertain. In order to calibrate and validate the model the following steps were performed:

1. Calibration of individual components against measured data using least-square method
2. Validation of the system against measured data during steady-state
3. Calibration of maximum ramping rate for low-stage compressor.
4. Validation of the dynamic behaviour of the heat pump

Here, calibration refers to tuning of the unknown parameters, such that the model represents the experimentally obtained measurement data. Validation refers to comparing the model results with corresponding experimental data. In order to obtain a valid result from the validation, a different data set than for the calibration was chosen. Both, calibration and validation were based on the same underlying procedure. The boundary conditions imposed to the system or component, such as the district heating return temperature and the heat source temperature for the overall system, were given to the model as a time dependent input. Further, inputs were necessary for the controller set values. These were unknown and thus estimated from the steady-state values of the measured data. Then the model was simulated and the obtained time dependent output was compared to the experimentally obtained output data. In the case of validation, the procedure finished at this stage. The calibration procedure continued by minimizing the error between the experimentally obtained result and the model result by varying the chosen tuning parameters and using a least-squares method.
The calibration procedure was divided into several steps for the individual components and the overall system. All unknown component parameters were calibrated using the component models instead of the overall system model. This enabled localising deviations in the model more easily and allows for numerically more efficient calibration of the overall model, as the number of calibration parameters that needed to be tuned using the complete system model was considerably reduced. A graphical representation of the validation and calibration procedure is given in the appendix A.1.
All steps were conducted using the Dymola calibration function [185]. The simulation results were compared to the results for dynamic behaviour of the real system. Further, a mean deviation over the whole validation simulation period was calculated as the normalised root-mean-square deviation (NRMSD), which was defined as:

$$NRMSD = \frac{\sqrt{\frac{\sum_t \left(y_{sim(t)} - y_{\exp(t)}\right)^2}{N_t}}}{\sqrt{\frac{\sum_t \left(y_{\exp(t)}\right)^2}{N_t}}} \quad (3\text{-}1)$$

3.2.5 Control structure design

The base case control structure is in line with the control structure of the experimental plant and is depicted in Figure 3-5. It is a multi-loop SISO control structure, where every control loop is controlled by a PI or PID controller. The groundwater flow was fixed to 24.1 kg/s. The low-stage compressor (LS comp.) controlled the evaporator outlet temperature on the source side and thereby indirectly the heat output and load of the heat pump. This set-up leads to higher evaporation outlet temperatures in part-load and thus a higher evaporation pressure, which is beneficial for the part-load COP (excl. pumps) of the system. The ramp rate of the low-stage compressor was limited to fit the experimentally found data by limiting the rate of change of the integral element to 0.05 s^{-2}. The high-stage compressor (HS comp.) was set to control the intermediate pressure to 13.6 bar (absolute).
The flow of the district heating water controlled the condensation pressure/temperature in the circuit and thereby indirectly the district heating forward temperature, as depicted in Figure 3-6. This meant it had to be known beforehand which condensation temperature should be chosen for a desired district heating forward temperature. This approach allows avoiding the delay of the forward temperature response to a change in mass flow. The temperature-offset values were determined experimentally for the real heat pump system and were used for validation. The high-stage valve (HS valve) in the model controlled the quality at the condenser outlet. This corresponds to a filling level control in the high-pressure receiver of a real system. The low-stage valve (LS valve) controlled the liquid level in the open intercooler.
This control structure was originally designed for high COP in both full load and part load, but is was not optimised for flexible operation of the heat pump. The changes listed in Table 3-2 were proposed and tested individually and combined for their impact on the dynamic behaviour of the system. Controlling the total power uptake directly was expected to enable the heat pump to respond more accurately to load change requirements and possibly supply frequency regulation services. The control of the evaporation pressure and the source outlet temperature are related to avoidance of droplet formation in the suction line during fast load changes or changes of the thermal boundary conditions. Other possible control structures were disregarded based on the results of a previously conducted relative gain analysis [186] and physical constraints, like e.g. the large time constant of controlling the supply temperature directly. All controllers were modelled as proportional-integral (PI) or proportional-integral-derivative (PID) controllers. The parameters as presented in Appendix A.1, were determined using the T-sum rule by Kuhn [187].

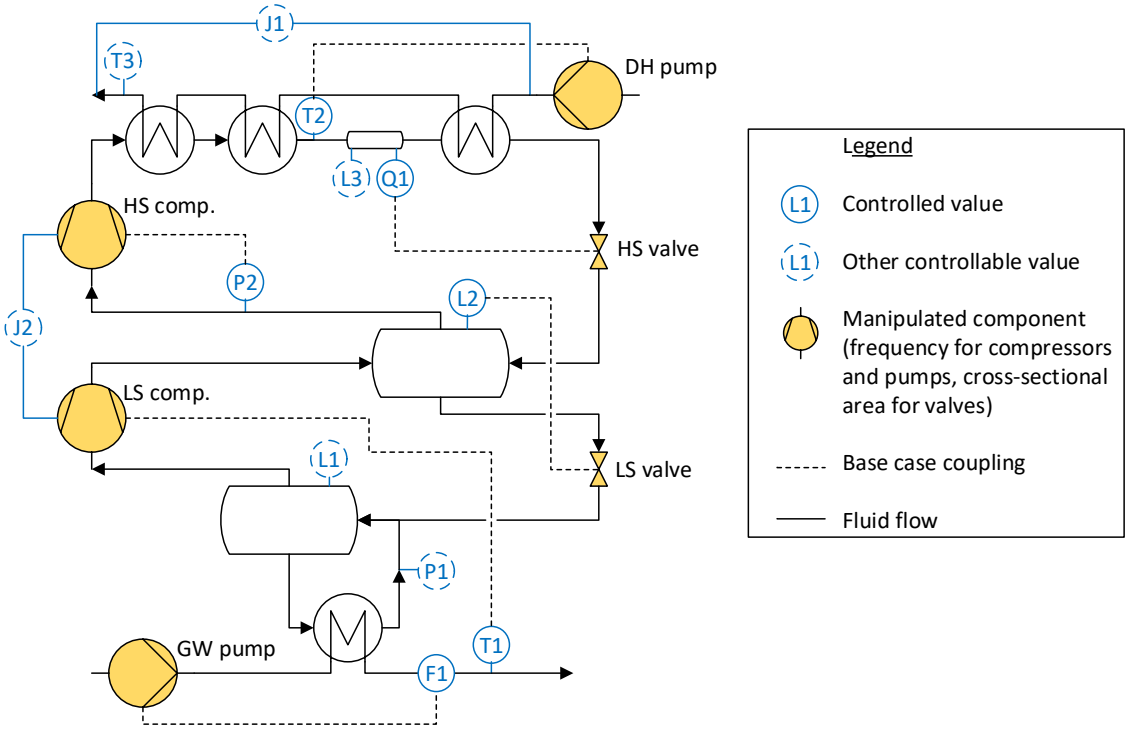

Figure 3-5 Sketch of the controlled variables in the base case and other controllable values mentioned in this thesis, the components that can be manipulated and the coupling of manipulated and controlled parameters for the base case scenario, with F - flow, P – pressure, T – temperature, L – liquid level, Q – vapour quality, J – Energy flow rate

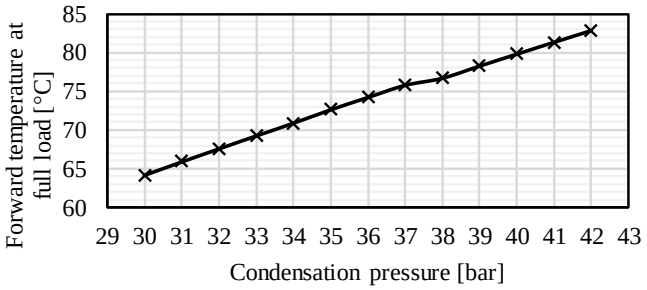

Figure 3-6 Forward temperature at full load over corresponding condensation pressure for base case control structure

Table 3-2 Variations in control structure that were tested

Manipulated variable	Controlled variable
LS compressor - *n*	$\dot{W}_{tot}$
LS valve – A_{cs}	p_{eva}, L_{Sep}
GW pump - *n*	p_{eva}, $T_{source,out}$

3.2.6 Constructive measures to ensure superheating in the suction line

The observed droplet formation in the suction line was a limiting factor to how fast the heat pump may be ramped down. There are a couple of possible constructive solutions that may enable controlling the superheating of the fluid in the suction line to values high enough to avoid the risk of sudden droplet formation during ramp-down. These constructive measures could help

to allow faster ramping of the heat pump and ensure robustness to sudden changes of the heat source temperature, which may be relevant for fluctuating heat sources, e.g. air. Here, three different constructive changes for the two-stage heat pump were assessed:

- Replacement of the flooded evaporator with a direct expansion evaporator (DEX) (Figure 3-7)
  In this case, the superheat after the evaporator could be controlled, to a value high enough to avoid liquid entering the compressor during ramp-down. The heat exchanger size of the evaporator was increased for this simulation by a factor 2, which was large enough to ensure superheating at the outlet, but it was not optimised. The superheat was controlled by the low-stage expansion valve.
- Implementation of an internal heat exchanger (IHX) to superheat the fluid in the suction line (Figure 3-8)
  This design would keep the flooded evaporator by installing an IHX to preheat the suction line using the liquid exiting the open-flash intercooler as heat source. The IHX was designed using manufacturer software to provide a superheating of 5 K. No further control was considered.
- Implementation of an electric preheating (el. PH) of the suction line (Figure 3-9)
  Ensuring superheated gas in the suction line by external electric heating is a flexible option, which may easily be added to existing systems and may allow adapting the superheating to the requirements of different operation modes. Due to simplicity for this study, a constant heating power of 2 kW throughout the simulation time was assumed.

Other options may also be relevant, but were not studied in detail. These include preheating the suction line using the heat source flow and the introduction of a controllable pressure loss in the suction line. The latter would however increase the pressure ratio of the compressor. The results of this analysis were recalculated for the thesis. Further, the calibrated lumped pressure drop on the low pressure stage from the validated model was disregarded, to make the different variants comparable. This resulted in slightly higher COP values.

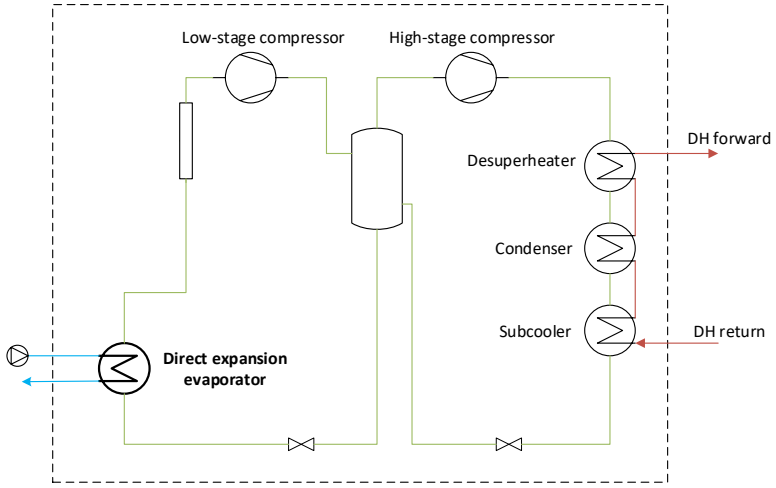

Figure 3-7 Two-stage ammonia heat pump cycle with direct expansion evaporator (DEX)

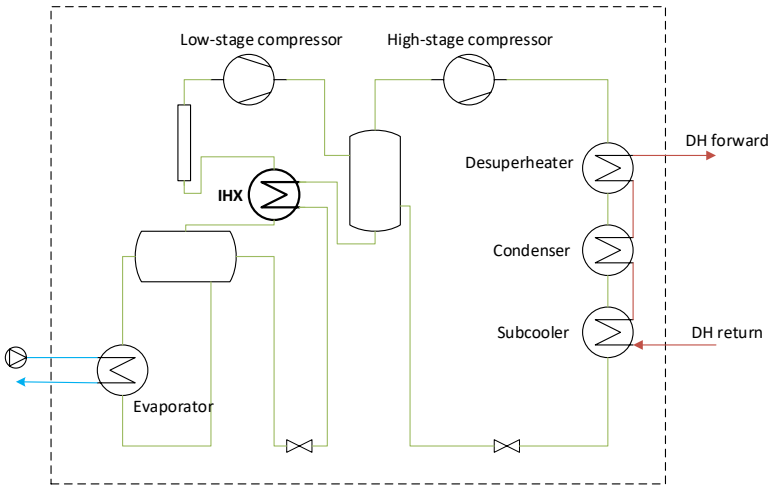

Figure 3-8 Two-stage ammonia heat pump cycle with flooded evaporator and internal heat exchanger between the liquid line exiting the intercooler and the low-stage suction line

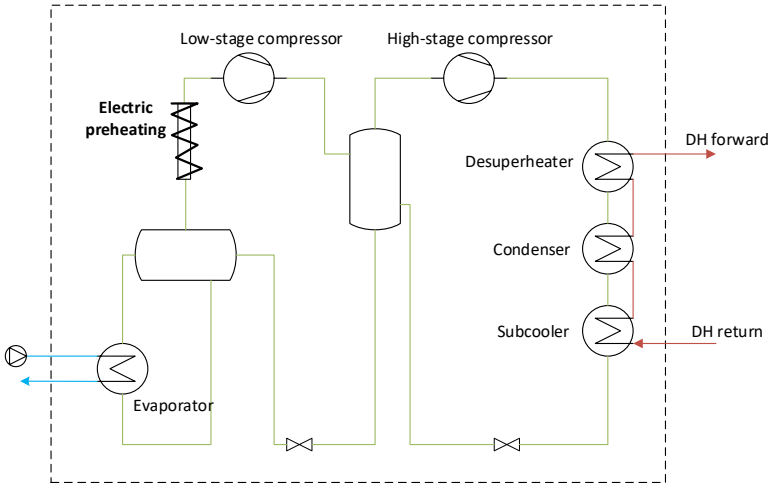

Figure 3-9 Two-stage ammonia heat pump cycle with electric preheating of the suction line

3.2.7 Monte Carlo approach and sensitivity analysis

In order to assess the influence of the component sizing on the regulation time a sensitivity analysis was conducted. It is expected that the heat exchanger areas, the ratio between heat exchanger area and the total refrigerant mass have the largest influence on the regulation time of the system [188]. Further, the type and size of compressor defines the dynamic behaviour of the system. This was however excluded, as other types than piston compressors were not part of the study and as the electric capacity of the heat pump was fixed here and thus the compressor size was given.

The analysis was conducted in two parts, corresponding to the two heat pump models, i.e. without pipes and including pipes (see section 3.2.3 for more details).

- In the first part the influence of the heats transfer and vessel sizes was analysed. To change the heat transfer area and the mass in the system, it was decided to vary the number of plates of all heat exchangers and the volume of the vessels, while the initial filling level of the vessels was kept constant to avoid too low liquid levels. The heat transfer area was varied by the number of plates, as this allowed changing the area without changing the aspect ratio and thereby the type of the plates.

- The second part focussed on analysing the influence of the length of all pipes in the system, including the receiver size.

The different geometry parameters were varied using MonteCarlo method [189], using the Modelica function “MonteCarloAnalysis” in the “Design” package. All values were varied by $\pm$ 30 %, assuming a random uniform distribution of all geometry input values. The number of random samples was set to 50. The model was simulated for 3000 s and a jump experiment was conducted at 2000 s, where the power set value was set from 250 kW (100 % load) to 175 kW (70 % load). The simulation time for the model with pipes was reduced to half and the jump was induced at 1000 s to save computational time.

A linear regression of the model outputs was conducted, assuming that the model can be described by the following structure:

$$\boldsymbol{Y} = \boldsymbol{X} \cdot \boldsymbol{B} \tag{3-2}$$

Where $\boldsymbol{Y}$ denotes the standardised vector of the single valued outputs, $\boldsymbol{X}$ is the standardised input parameter matrix and $\boldsymbol{B}$ is the vector of the standardised regression coefficients β_i. The input and output were standardised, according to the following formula [190]:

$$x_{std} = \frac{x - \bar{x}}{\sigma(x)} \tag{3-3}$$

$$\sigma(x) = \sqrt{\frac{1}{N}\sum_{i}^{N}(x_i - \bar{x})^2} \tag{3-4}$$

The standardised regression coefficients β_i contain information about the influence of the corresponding input variable on the output. A positive value denotes a positive linear correlation between the respective input parameter and the output, while a negative value denotes a negative linear correlation. The standardised β_i values are between -1 and 1. The closer the absolute value is to unity the larger is the influence of the corresponding parameter on the output. Values close to zero mean a negligible influence [191]. The square of the regression coefficient β_i^2 gives information about whether an input parameter has a significant influence on the model output. Here, the threshold below which the influence of the respective input parameter was assumed negligible was set to 0.01.

3.2.8 Variation of cycle design

In order to assess the influence of the cycle design on the ability of fast-regulation the results from the two-stage ammonia heat pump were compared to a one-stage set-up (Figure 3-10). In this set-up, the heat exchanger sizes were kept the same. This was a simplification, as the optimal sizing is expected to change, as the cycle changes. For the compressor the high-stage compressor model from the two-stage heat pump described above was used. The displacement volume was changed to the displacement volume of the low-stage compressor of the two-stage heat pump. The following control structure was implemented: The compressor controlled the power uptake of the heat pump, the expansion valve controlled the quality out of the condenser, the district heating mass flow rate controlled the condensation pressure and the source mass flow rate controlled the evaporation pressure. The controllers were parametrised according to conducted step experiments.

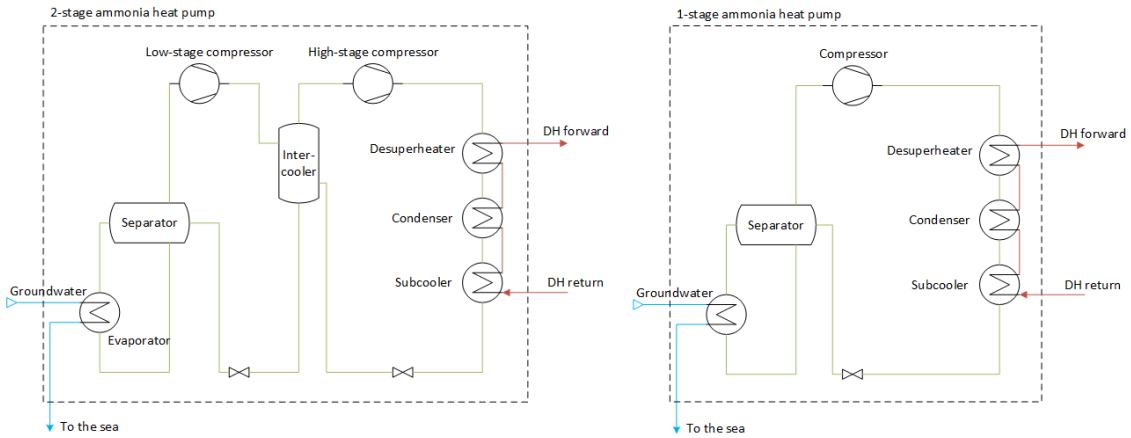

Figure 3-10 Two-stage ammonia heat pump cycle and one-stage ammonia heat pump cycle

3.2.9 Operation strategy

In order to deliver frequency regulation, the heat pumps need to adapt their electricity consumption quickly. Depending on the service provided, the heat pump will have to react constantly to frequency deviations during the regulation period or it will be asked to adapt the power uptake and keep this new power set value during a minimum regulation time. In order to assess whether the heat pump may possibly qualify to deliver ancillary services, both the ability to adapt the load quickly, according to the tests described below.

- Jump in the power uptake set value from full load to different part load levels and up again
- Regulation with the heat pump alone, i.e. the heat pump is operated at intermediate part-load and bids a capacity of half the difference between minimum and maximum load on the reserve market. This operation strategy is depicted in as case 1.
- Regulation with the heat pump and quick-starting unit. Here the heat pump is operated at full load and may provide a maximum regulation capacity of the difference between the minimum and maximum load. The heat pump would in this case only provide up-regulation to the grid. The down-regulation would be delivered by starting a quick starting unit, as e.g. an electric boiler. Note that up-and down regulation here are defined from an electricity generation perspective, i.e. taking up less power with the heat pump on the demand side corresponds to generating more power in a power plant. This operation strategy is depicted in as case 2.

The possibility to provide ancillary services by shutting the heat pump off and starting-it up again was disregarded here. The reasons for this were: Firstly, certain settling times need to be respected before the heat pump is allowed starting-up again, during these waiting times the heat pump is not able to react to new regulation signals and would therefore not qualify for services without a minimum regulation time larger than the required settling time. Secondly, symmetric services cannot be delivered from one heat pump alone when bidding the full electric capacity of the heat pump, but it would require two heat pumps with the same capacity. Thirdly, frequent start-up and shut-downs are expected to increase the wear of the system components and there is a risk of overheating the electric motors, when starting-up too frequently. Fourthly, continuous adaption of the load from 0% to 100% is not possible with the heat pump, but is required for continuous service supply.

Further, the ability follow the frequency deviations in the grid need to be tested, this was assessed in 4.3.1.

Tests with the existing two-stage heat pump have shown that the heat pump can operate at part loads of down to 40 % of full load. It was thus assumed that the heat pump capacity could be reduced by 60 % during regulation periods. These loads corresponded to nominal power uptakes of 100 kW to 250 kW. The frequency (normal) reserve market is the economically most attractive option and thus the aim of this study was to find out whether it could be possible to deliver the regulation power within 150 s. The electric capacity of the assessed heat pump is too low to bid into the markets. That means an exceptional allowance would be needed or the heat pump could be clustered with other flexible assets.

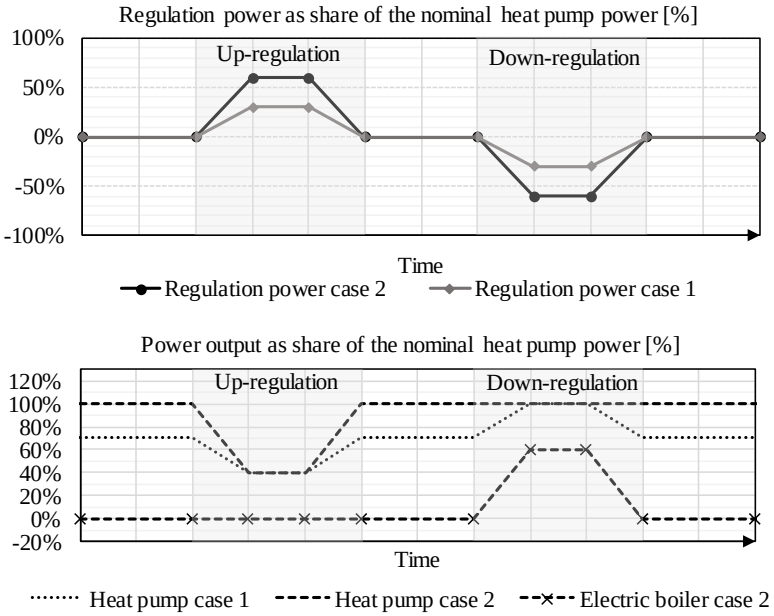

Figure 3-11 Schematic representation of the operation principles of the heat pump and electric boiler

3.2.10 Evaluation criteria

The time between the induced jump in load set value and reaching steady state (ss) was defined as the response time Δt_r.

$$\Delta t_r = t_{start} - t_{ss} \tag{3-5}$$

The steady-state COP was defined as the ratio of the steady state heat output $\dot{Q}_{ss}$ and power consumption $\dot{W}_{ss}$.

$$COP_{ss} = \frac{\dot{Q}_{ss}}{\dot{W}_{ss}} \tag{3-6}$$

The regulation time used as a measure to compare how fast the heat pump was able to regulate considering different control structures, was defined as the time after a step in set point value, until the power uptake remained within a tolerance band of $\pm\,\epsilon = 0.1$ % of full load and the power gradient was below $\epsilon_{\mathrm{der}} = 100\ W/s$.

$$\frac{\left|\dot{W}_{\mathrm{tot}} - \dot{W}_{\mathrm{set}}\right|}{\dot{W}_{\mathrm{fullload}}} < \epsilon \tag{3-7}$$

$$\frac{d\dot{W}_{\mathrm{tot}}}{dt} < \epsilon_{\mathrm{der}} \tag{3-8}$$

These tolerances were assumed, as the transmission system operator (TSO) does not make actual allowed tolerances for participation in the frequency regulation market available. The defined criterion, is a simple steady-state condition, it may however happen that the condition is true and then becomes false again before finally reaching steady-state. If this was the case, the latest time, when the condition became true was logged as regulation time.

3.3 Results

3.3.1 Behaviour of the test plant with base case control

Figure 3-12 shows the heat output flow rate and power uptake of the test plant during a load change experiment. A peak of the heat flow rate during start-up of the heat pump may be observed. This is caused by heat that is still stored in the heat exchangers on the high-temperature side. This exits the heat exchangers as soon as the district heating mass flow through the heat exchangers increases above zero. The heat flow rate and the power peak after ramping up, before the power uptake settles. During ramp down a large undershoot maybe observed, indicating that the control has not been optimised for fast ramping. The control of the heat pump has in fact been optimised to maximise COP also in part-load (steady-state). Further, below 45 % load the power uptake is unstable as part of the pistons of the compressors are decoupled. The shut-down of the heat pump is very fast. However, before starting up again, it is necessary for the refrigerant in the heat pump to settle, such that refrigerant that possibly accumulated in the suction line during shut-down falls back into the vessels. Further, the pressure equalises and refrigerant moves from the high pressure to the intermediate and low pressure side. Accordingly, a waiting time is introduced. This further serves to prevent undesired cycling operation of the heat pump.
The results of the load changing tests conducted with the test plant in terms of regulation time are presented in Figure 3-13. The load change is depicted on the abscissa, where positive values refer to a decrease in load and negative numbers refer to an increase in load. As shown in Figure 3-12, the load was always changed from full load down into part-load and up to full load again. A step from 100 % load to 60 % load would thus correspond to a load change of 40 % and a step from 70 % load to 100 % load corresponds to a load change of -30 %. Two different times are presented for every load change, the longer time refers to the actual measured values, while the shorter regulation times were calculated assuming that the undershoot of the power uptake may be balanced out by the electric boiler. This idealised case has not been validated experimentally. It may be observed that the heat pump alone is too slow to supply ancillary services. However, the behaviour of the heat pump indicates that the regulation is not optimised for fast ramping. An optimisation of the control is expected to result in less undershoot and faster regulation times.
The times for start-up and shut-down are not affected by the overshooting of the control. They are compared to the required ramping times in Eastern Denmark in Figure 3-14, where positive regulation power values refer to an up-regulation from the grid perspective, i.e. a load reduction of the demand side unit, and negative numbers refer to a down-regulation, i.e. heat pump load increase. The ramping times are depicted on the abscissa. It should however be considered, that due to the necessary waiting times, a start-stop operation of the heat pump for frequency regulation services is not viable.
Finally, the development of heat flow rate, power and COP during start-up was analysed. After the heat stored in the heat exchangers was ejected, the COP increased nearly linearly with

increasing heat flow rate during start-up, as shown in Figure 3-15 a). Figure 3-15 b) shows how the heat flow rate, power uptake and COP was reduced during start up. These values may be relevant when modelling the heat pump from an energy system perspective, where some cost or efficiency penalty is typically assigned to the start-up of a heat pump unit.

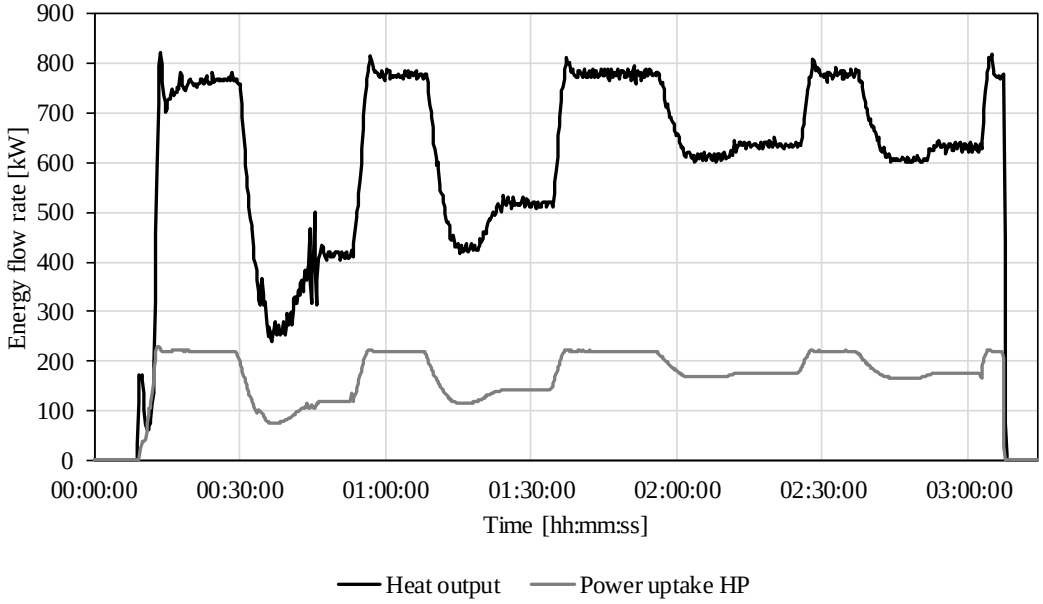

Figure 3-12 Heat output flow rate and power uptake of test plant for load changing test for 70 °C forward temperature

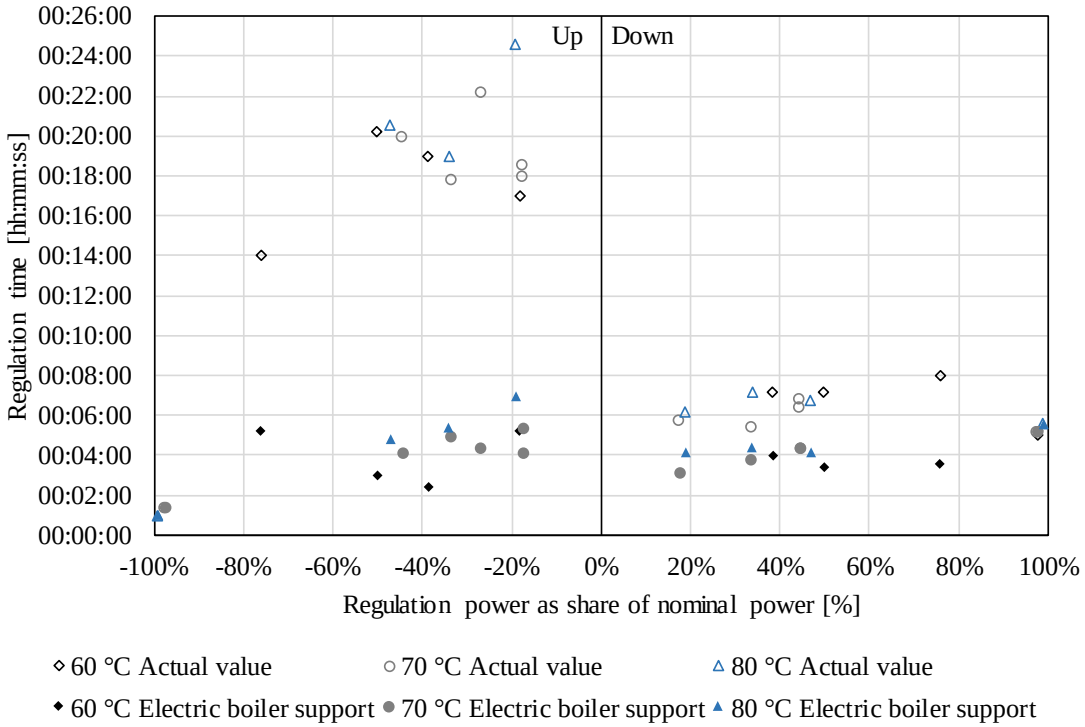

Figure 3-13 Regulation time and load for different forward temperatures, actual values measured with the heat pump, and idealised regulation times in case the undershoot could be balanced out by the electric boiler

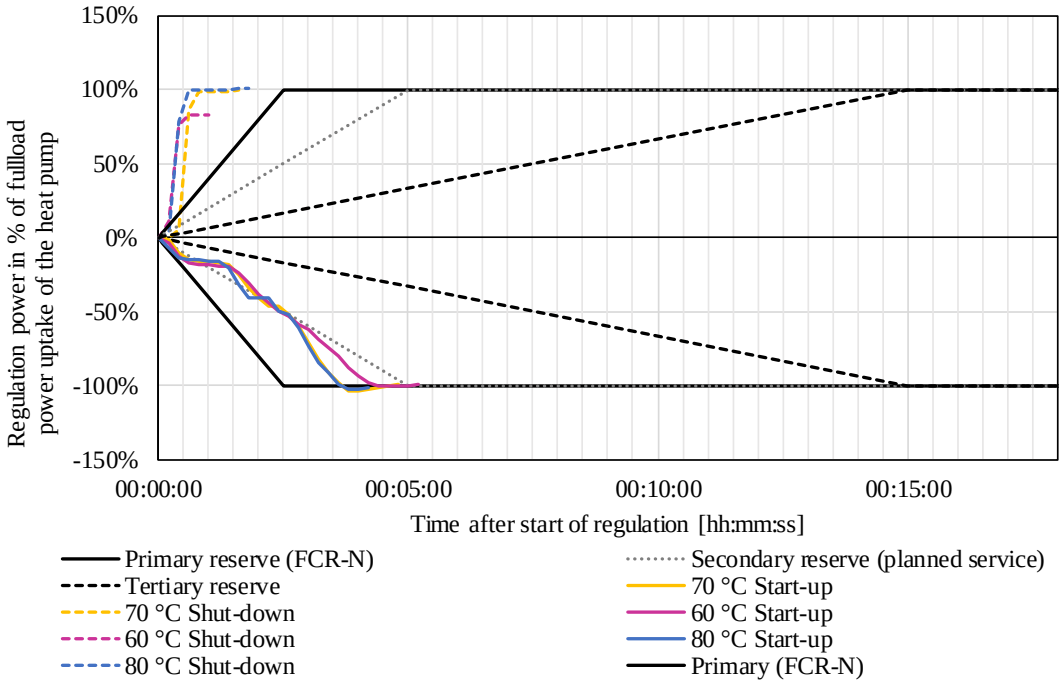

Figure 3-14 Start-up and shut-down times of FlexHeat heat pump compared to required regulation times in Eastern Denmark

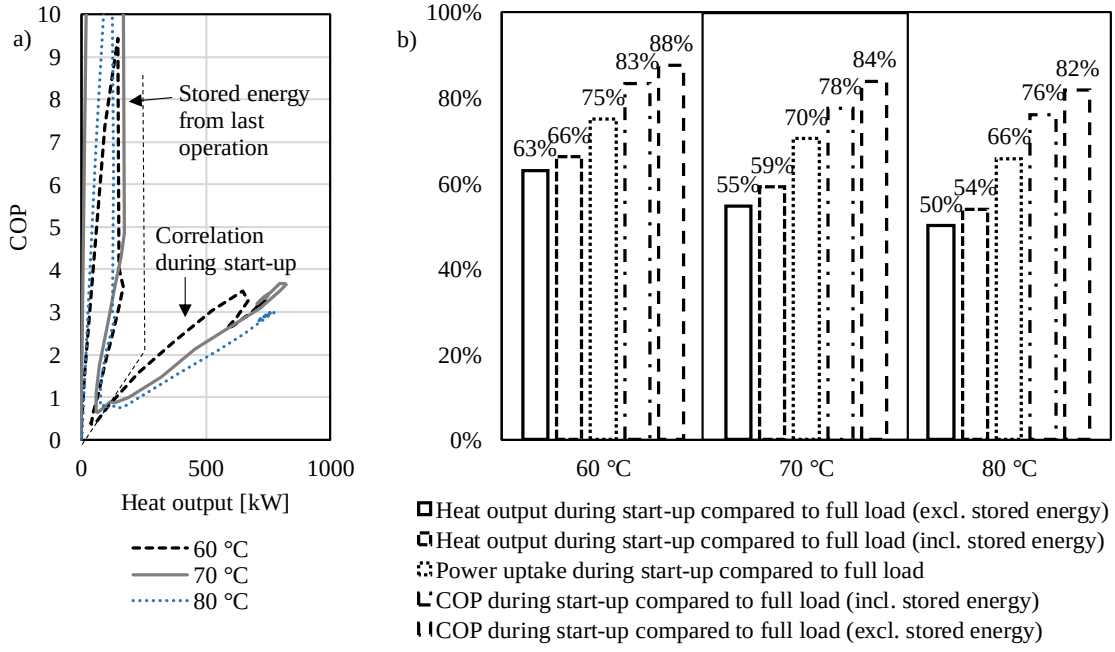

Figure 3-15 a) COP during start-up as a function of the heat output for three different forward temperatures, b) performance during start-up compared to full load

3.3.2 Validation against experimental data

Figure 3-16 shows the comparison of the simulated results and the experimentally obtained measurements from the real heat pump. The dynamic behaviour of the results is compared by showing the development over time (left graphs) and the overall correspondence between the values is compared using diagonal plots, showing the simulated results over the measured results for the same time step (right graphs). The results are presented for a forward temperature of 70 °C.

For the intermediate pressure at the low-stage compressor outlet and high-stage compressor inlet (Figure 3-16 c)) and the condensation pressure (Figure 3-16 d)), it may be observed that the time constant of the simulated response is smaller than for the measured response. This was due to neglecting the pipelines in the simulation. It was verified that including all pipelines in the simulation leads to slightly larger time constants, and gave an overshoot in intermediate and high-stage pressure, which is similar to the measured data. The inclusion of all pipelines resulted however in a numerically stiff model and computation time was accordingly high.

The characteristic overshoot of the evaporation pressure (Figure 3-16 e)) and the corresponding undershoot of the power uptake (Figure 3-16 b)) and heat flow rate (Figure 3-16 a)) is related to waiting times programmed in the real heat pump controller. For the model, the source outlet temperature obtained from the measured data was an input to the model. Thereby the waiting times were represented in the simulated results. The response of the evaporation pressure to load changes fits quite well to the modelled data. It can be seen that only discrete values for the measured pressure were available. A slight deviation between the steady state values may be observed. This is most likely due to uncertainties with regard to the actual pressure drop in the different components on the low-pressure side. All pressure drops were lumped into a pressure drop component, which does not account for the possibly different part load behaviour of individual pressure loss contributions. The reaction of the source outlet temperature (Figure 3-16 g)) fits less well. The time constant of the simulated response is smaller than the measured one. Since the evaporation pressure fits well, this difference may be accounted for delays and larger storage capacities on the water side.

The supply temperature (Figure 3-16 f)) fits well, considering the uncertainty induced by modelling plate heat exchangers instead of shell-and-plate heat exchangers. However, the dynamic behaviour is more similar to the measured dynamic behaviour after 3000 seconds, while the model seems to react faster than the measured data between 1000 and 3000 seconds.

The model was found to represent the general trends of the heat pump behaviour during load change well. However, some deviations were observed. The measured heat load dropped right before ramping up to full load (Figure 3-16 a)). This development was not identified in the simulated results. This may be explained by a slight difference in the control structure between the model and the real plant. During the measurements at the real plant the set value for the condensation pressure was changed according to the load. When ramping up, this was done before changing the set value for the source outlet temperature. The result was a decrease in mass flow and with it the heat flow rate prior to the event. The sink mass flow rate in the model was only changed as a reaction to the load changes, via the PI control for the condensation pressure, i.e. it changed after the heat pump started to ramp up. Therefore, no drop in heat flow rate before ramp up was observed.

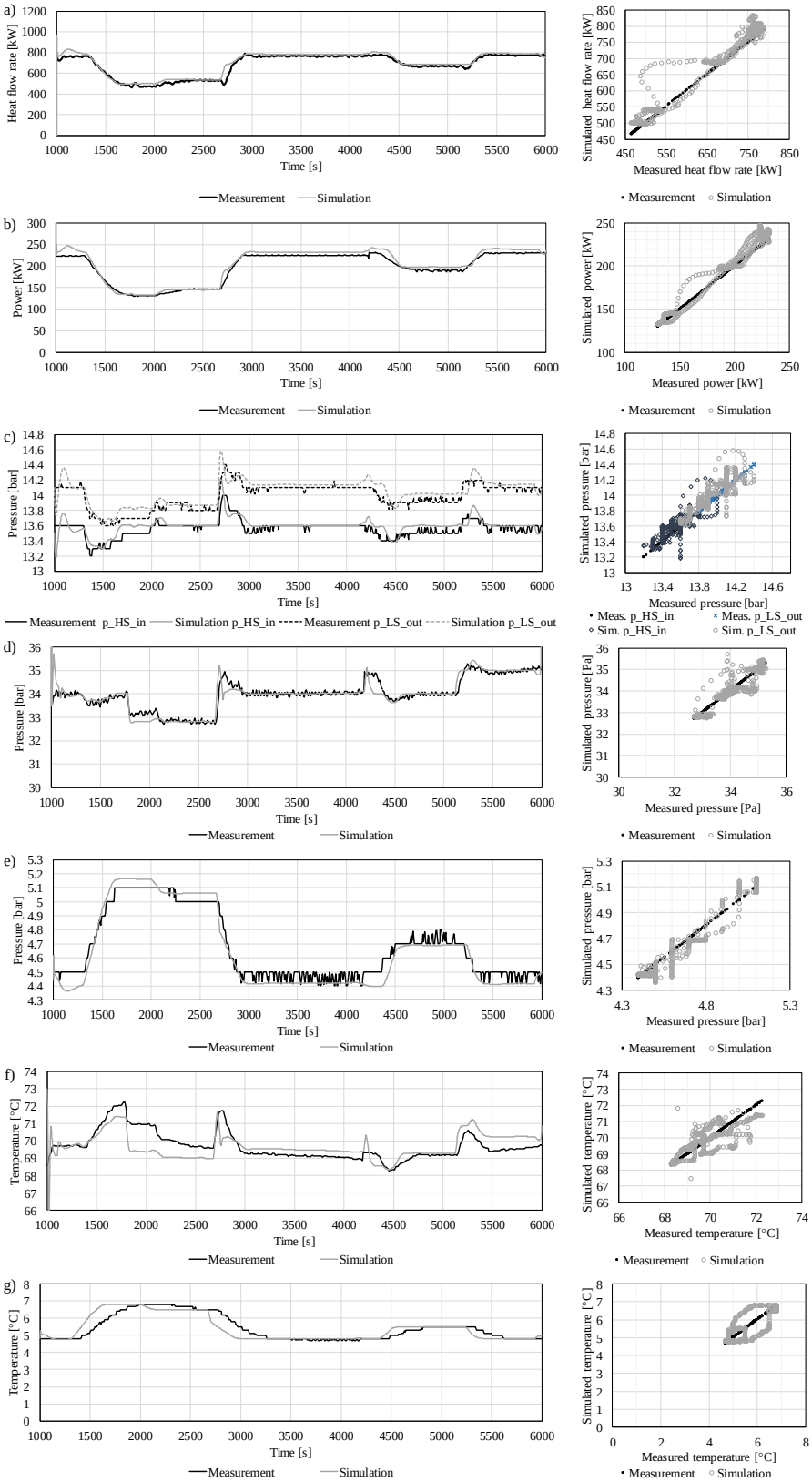

Figure 3-16 Comparison of simulation and measurement results over time (left) and as diagonal plot (right). From top to bottom: a) Heat flow rate, b) Power uptake, c) Intermediate pressure at low-stage compressor outlet and high-stage compressor inlet, d) Condensation pressure, e) Evaporator pressure, f) Forward temperature and g) Source outlet temperature.

Table 3-3 Root mean square of the measured data over the validated period (RMS measurement), root mean square of the difference (RMS difference) between measured data and simulated results and the mean deviation calculated as the ratio of RMS difference over RMS measurement.

	60 °C			70°C			80°C		
	RMS measurement	RMS difference	Mean deviation [%]	RMS measurement	RMS difference	Mean deviation [%]	RMS measurement	RMS difference	Mean deviation [%]
Qdot_tot [W]	529000	39100	**7.4%**	690000	41800	**6.1%**	639000	35400	**5.5%**
Wdot_tot [W]	137000	12900	**9.4%**	201000	12800	**6.4%**	192000	15900	**8.3%**
COP	3.93	0.38	**9.6%**	3.47	0.09	**2.5%**	3.35	0.18	**5.4%**
p_LS_in [Pa]	499000	15000	**3.0%**	468000	9340	**2.0%**	485000	15400	**3.2%**
p_LS_out [Pa]	1380000	19700	**1.4%**	1400000	12300	**0.9%**	1390000	16500	**1.2%**
p_HS_in [Pa]	1360000	18800	**1.4%**	1360000	10500	**0.8%**	1360000	15800	**1.2%**
p_HS_out [Pa]	2680000	116000	**4.3%**	3400000	34500	**1.0%**	388000	4800	**1.2%**
T_supply [K]	333	1.7	**0.5%**	343	0.8	**0.2%**	353	1.8	**0.5%**
T_eva_out [K]	280	0.5	**0.2%**	279	0.5	**0.2%**	279	0.4	**0.1%**

Table 3-3 summarises the deviations for all validated parameters for three different forward temperatures. The largest mean deviations were found for the power uptake $\dot{W}_{\mathrm{tot}}$ and the source outlet temperature $T_{\mathrm{eva,out}}$. The two are directly related through the control structure. The source outlet temperature reacted faster to a change of the low-stage compressor speed in the model compared to the measurements. This was fed back into the controller, the profile of the low-stage compressor speed followed and thereby the power uptake of the compressors.
The lowest mean deviations were calculated for the pressures in the system and the supply temperature. The low deviation of the pressures could be expected, since both condensation pressure and intermediate pressure are controlled and thus the deviations only come from differences in dynamic behaviour and uncertainties related to the exact timing of the condensation pressure set point change during measurements.

3.3.3 Performance of base case

The model was used to calculate the dynamic behaviour of the base-case system as response to load changes. Here, the source outlet temperature controller was optimised compared to the validation, by parametrizing the PI controller according to the T-sum rule [187]. Thereby, the overshoot and accordingly the regulation times could be reduced considerably.

3.3.3.1 Steady-state behaviour in part-load

Figure 3-17 shows the heat pump behaviour in part load in terms of COP, heat flow rate $\dot{Q}_{tot}$ and power uptake $\dot{W}_{\mathrm{tot}}$ for three different condensation pressure set points, corresponding to three different full load supply temperatures. As expected, the COP increased accordingly with decreasing supply temperature. It reached a maximum at 40 %, 38 % and 36 % load for condensation pressures of 29.3 bar, 33.2 bar and 38.5 bar – corresponding to supply temperatures of 62 °C, 70 °C and 77 °C – respectively. The power uptake increased with the condensation pressure, as the pressure ratio for the high-stage compressor increases. The heat flow rate behaves almost the same for all three supply temperatures. The heat uptake in the evaporator was fixed via the fixed source mass flow and the controlled source outlet temperature. As the power input increases with increasing pressure ratio of the high-stage compressor, the superheat out of the compressor increases, however the influence of this increase on the overall heat flow rate is comparably small. This means, the currently implemented control structure is feasible for the precise delivery of a certain desired heat flow rate. However, if the aim is to operate the heat pump according to the requirements of the electricity grid, it should be possible to control the power uptake precisely instead.
The quality of the heat supply as the main product of the heat pump is mainly defined by the supply temperature. Therefore, it is desirable that the supply temperature can be controlled precisely. However, the supply temperature was not controlled directly, but instead the condensation pressure was controlled. This was done to avoid large dead times in the supply temperature response to changes in the sink mass flow rate. Figure 3-18 shows the resulting deviation of the supply temperature over power uptake for different condensation pressure set points. The resulting supply temperatures are 2 °C to 3 °C higher at the lowest reported part load compared to full load power uptake. To be able to set the supply temperature more precisely, while not losing the advantage of condensation pressure control over direct supply temperature control, an offset function for the condensation pressure could be implemented. It would be a function of the desired supply temperature and the current heat pump load as inputs. It could then be used to calculate the necessary condensation pressure set point, which would then be an input to the existing controller.

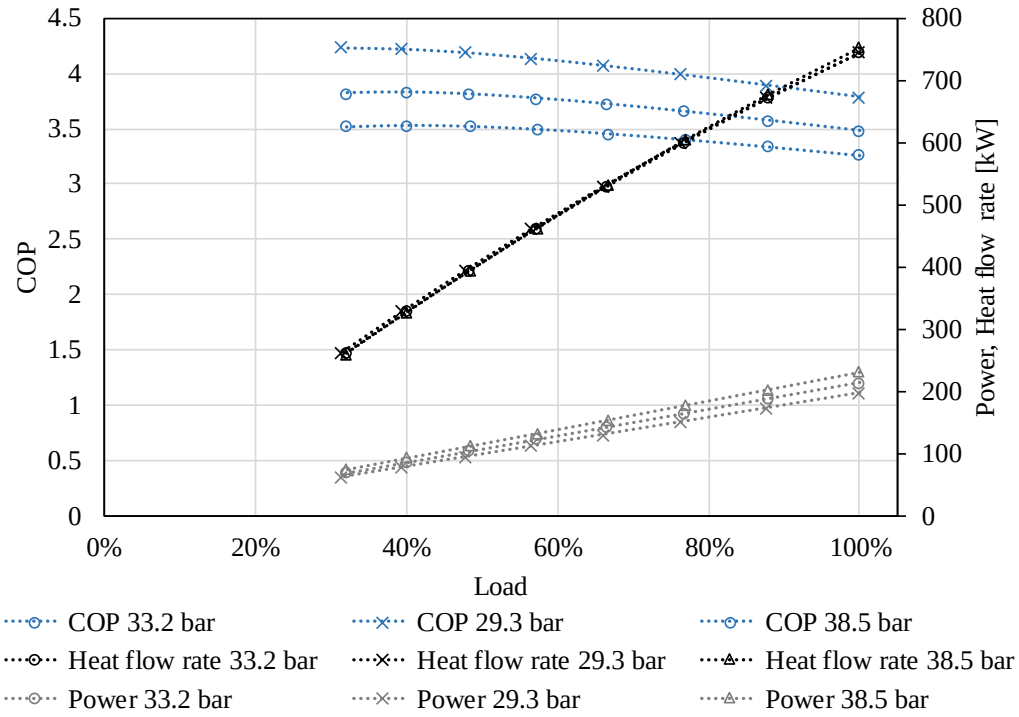

Figure 3-17 COP, heat flow rate and power uptake in steady-state for different part loads. The load was defined as the power uptake over the power uptake for a source outlet set temperature of 4.5 °C

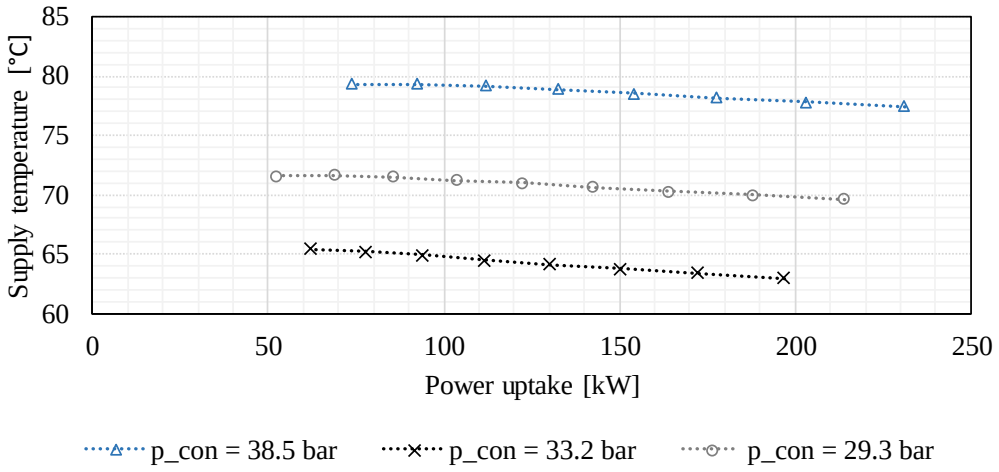

Figure 3-18 Supply temperature deviation in part load operation with base case control structure of condenser temperature for three different pressure set points

3.3.3.2 Regulation time of heat pump

An important measure with regard to heat pump flexibility is the regulation time that is needed until steady-state is reached after a load change. The regulation times were determined as described in section 3.2.10. They are presented for three supply temperatures, i.e. condensation pressure set points and different step sizes of the load change in Figure 3-19. A negative load change refers to ramping from full load into part load, e.g. a load change of -40 % corresponds to a change from 100 % load to 60 % load. A positive load change refers to ramping from part-load, up to full load again. Each point refers to an individual jump experiment. Figure 3-20 shows an example of a curve for the power uptake during a negative load change starting at 1300 seconds and a positive load change starting at 2700 seconds. The overshooting and following oscillations were more pronounced for larger load changes. This resulted in longer regulation times for larger load changes. All simulated regulation times were

above 400 seconds for a tolerance of 0.1 % of full load power and above 200 seconds for a tolerance of 1 %, and thus not feasible for FCR-N delivery. The regulation times were similar for up- and down-ramping. No clear dependency between the regulation time and the condensation pressure set point could be identified. For the smaller tolerance the regulation times were shortest for 33.2 bar condensation pressure set point, while the results for 29.3 bar and 38.5 bar condensation pressure were very similar. This was due to slightly larger oscillation for the 29.3 bar and 38.5 bar cases. The controller parametrisation is based on the assumption that the system has a similar response in all operation modes. For this study, it was based on the nominal operation conditions; accordingly, it may be better suited for 33.2 bar, as this is close to the nominal conditions.

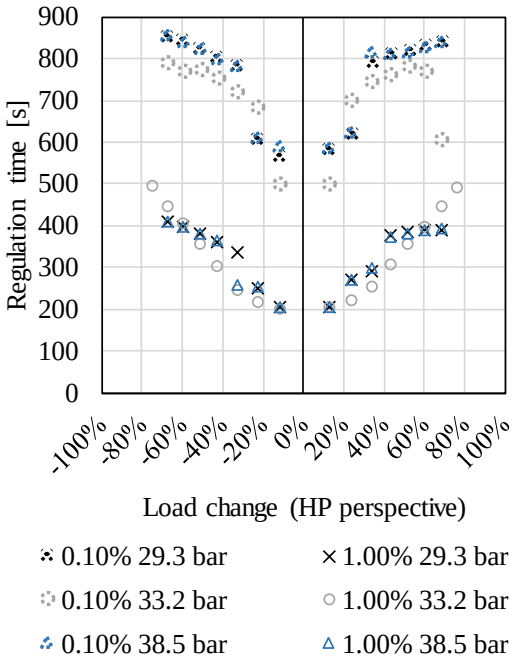

Figure 3-19 Regulation time for three different forward temperatures. A positive load change on the x-axis refers to increasing the power uptake of the heat pump, while a negative load change refers to decreasing the power uptake

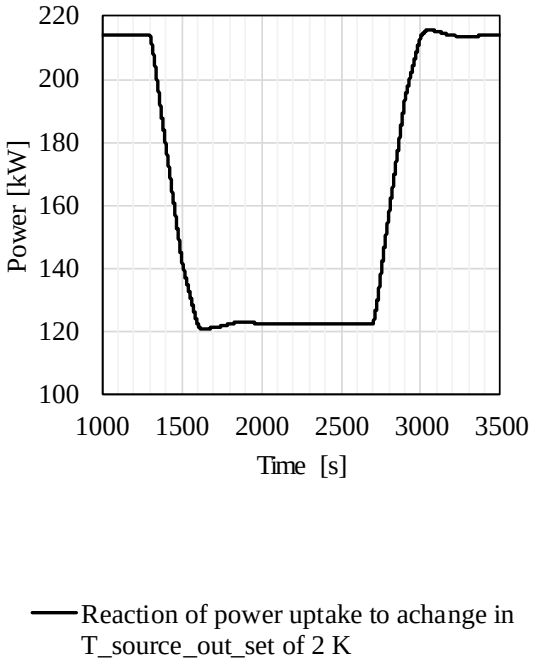

Figure 3-20 Response of the power uptake to a change in the set point of the source outlet temperature of 2 K, corresponding to 43 % points change, compared to full load

3.3.3.3 Risk of droplet formation in suction line

During ramp down and ramp up, the base case control structure of the heat pump load resulted in changed outlet temperature of the heat source stream. As can be seen in Figure 3-22, the saturation temperature in the low-stage compressor suction line rises above the suction line wall temperature during ramp-down of the heat pump. This is caused by the increase in evaporation pressure and thus saturation temperature, while the pipe walls are still cold from the operation before. This may result in sudden droplet formation in the suction line, due to condensation of the fluid at the cold surface. The droplets may harm the compressor and should therefore be avoided. A small increase in evaporation pressure, results in a relatively large increase in saturation temperature, as may be seen by the high gradient, $\frac{dT}{dp}$, at low ammonia pressures, as indicated by the tangents to the vapour pressure curve in the pressure-temperature diagram depicted in Figure 3-21.

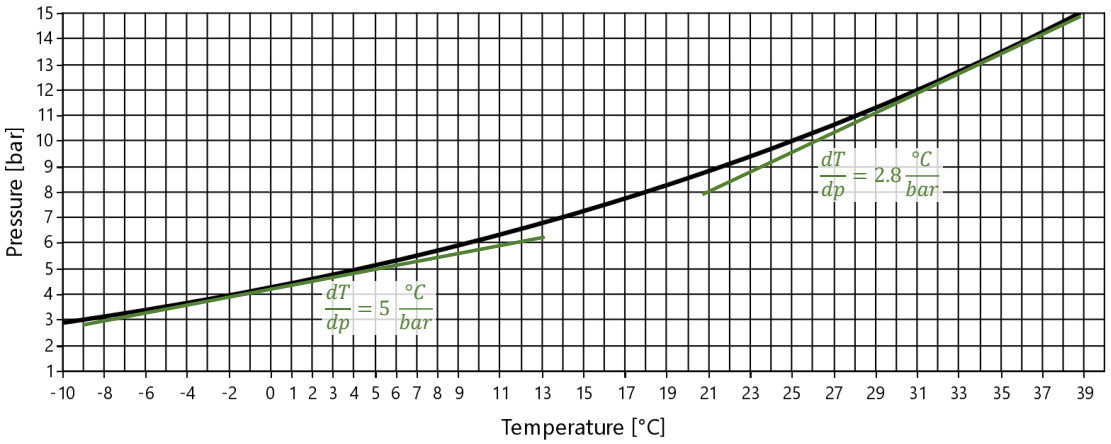

Figure 3-21 Vapour pressure curve of ammonia in a pressure- temperature diagram. The green tangents indicate how much the saturation temperature increases with pressure at different pressures.

A similar phenomenon may be observed in the high-stage suction line, even if the gradient of the saturation temperature is smaller compared to the low-stage suction line. The intermediate pressure dropped during ramp-down of the compressors. During the following increase in pressure back to the set value, the saturation temperature reacted faster to a change in pressure than the wall temperature and droplet formation in the suction line could occur. The saturation temperature was also calculated for the experimental pressure increase after the undershoot. The deviation in time constants between the simulated response and the measured response, as described in section 3.2.10, was enough to avoid droplet formation. Therefore, the high-pressure suction line was disregarded in the following. On the other hand, avoiding droplet formation in the low-pressure suction line is an important task to solve, in order to allow faster downward ramping of the heat pump without the risk of liquid entering the compressor.

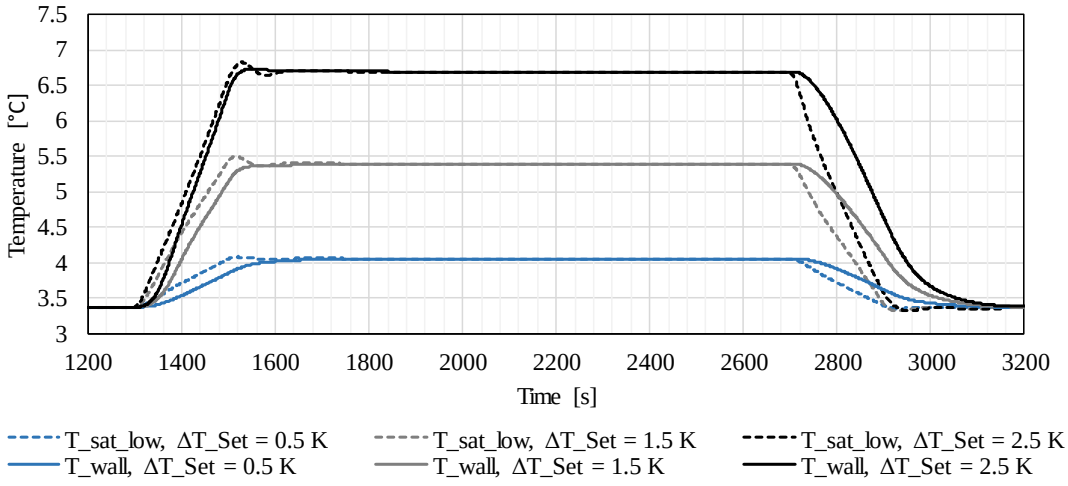

Figure 3-22 Saturation temperature of ammonia in the suction line (dashed) and suction line wall temperature (solid) (most downstream cell) during ramp-down (starting at 1300 s) and ramp-up (starting at 2700 s). If the wall temperature is below the saturation pressure, condensation may occur at the pipe surface, which may harm the compressor.

3.3.4 Optimisation of control structure

The control structure of the real system was designed to allow for maximum COP in part-load. It was however seen in the experimental data used for validation that the controllers were not optimally parametrised for fast regulation of the heat pump, which resulted in a prolonged undershoot of the power uptake and heat flow rate (compare Figure 3-16). The simulation with the base case control

structure, but with controller parametrisation according to simple tuning rules, already resulted in an improved dynamic behaviour. However, two limitations were identified that hinder the fast regulation of the heat pump. Firstly, the indirect control of the heat flow rate and thereby power uptake, makes it more difficult to control the power uptake precisely and induces a dead time into the load control. This was seen for both the control of the heat output and of the source outlet temperature. Secondly, droplet formation in the suction line during fast ramp down needs to be safely avoided in order to allow for fast ramping. Therefore, it was assessed whether a direct control of the power uptake instead of the implemented indirect load control could allow faster reaction of the system, and whether a low-pressure control could reduce the risk of condensation in the suction line.

3.3.4.1 Control of power uptake

In order to allow for faster regulation of the heat pump, within this work it was proposed to control the power uptake of the compressors directly via the low-stage compressors rotational speed, instead of indirectly via the source outlet temperature. By reducing the rotational speed of the low-stage compressor, the mass flow rate in the lower part of the two-stage cycle decreased and with it the pressure at the intermediate level. The high stage-compressor controller reacts to the decrease in intermediate pressure by decreasing the rotational speed. In this way, the high-stage compressor always follows the low-stage compressor. A reduction of mass flow rate through the heat exchangers on the low- and high-pressure side results in less heat uptake and heat output and thus a reduced heat load of the heat pump. This was expected to have two advantages. Firstly, the power uptake can be measured without the delay until a change in rotational speed can be measured as a change in temperature at the evaporator outlet. Secondly, when delivering regulation services, the power uptake could be controlled to follow the required ramping curve precisely.

The maximum change in power uptake of the heat pump depends on the operation strategy. As explained below the change could be either of the difference of the maximum and minimum load or 50 % of the difference. In the first case, all frequency up-regulation would be provided by the heat pump and the frequency down-regulation by turning on the electric boilers. In the second case, the heat pump would, as default, be operated at intermediate load and could then regulate up or down. The minimum load for the case study was fixed to 100 kW electric power. Accordingly, a maximum step change of -150 kW and -75 kW, respectively, would be obtained, as the full load of the compressors was considered to be 250 kW.

Figure 3-23 shows the power uptake for the base case control and the direct control of the power uptake with and without a constrained rate of change of the compressors rotational speed, as a reaction to a step in the load set value from 250 kW to 175 kW. The direct control of the power uptake in both cases was faster than the indirect control via the source outlet temperature (base case). The difference between the constrained power control and the base case control is the dead time induced by the temperature measurement, which leads to considerable oscillation before steady-state is reached, at 1385 seconds. For the direct control, the constrained ramping rate leads to minimal oscillations and thus the steady-state is reached at 1140 seconds. When the constraint on the ramping rate is removed, the power uptake overshoots slightly, but the regulation time can be reduced to 55 seconds.

For the larger step from 250 kW to 100 kW power uptake, the corresponding regulation times were longer. The base case regulation time was 475 seconds, the direct power control with ramping rate constraint was 320 seconds and without constraint, it was 115 seconds. All regulation times are summarised in Table 3-4. Accordingly, shifting from indirect to direct load control is not enough to be able to ramp fast enough for the supply of FCR-N frequency regulation, which requires a maximum regulation time of 150 s, if the ramping constraint was not reduced.

In all three cases, the risk of droplet formation during ramp down is apparent, as depicted in Figure 3-24. While the time during which droplet formation may occur is longer for the constrained controllers, the peak in the temperature difference between saturation temperature of the fluid and the wall

temperature is higher for the unconstrained controller. That means in none of the cases presented in Figure 3-24 the occurrence of sudden condensation could be excluded.

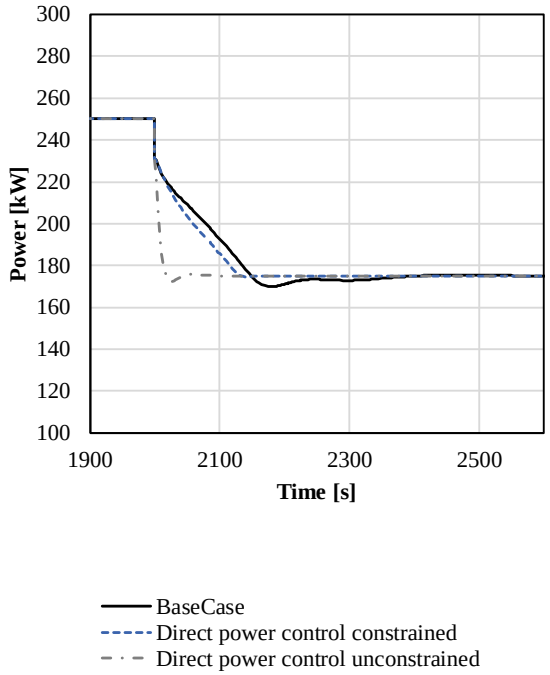

Figure 3-23 Response of power uptake of both compressors to a set value step of -75 kW for indirect load control (base case), direct load control with ramping rate constraint and direct load control without ramping rate constraint

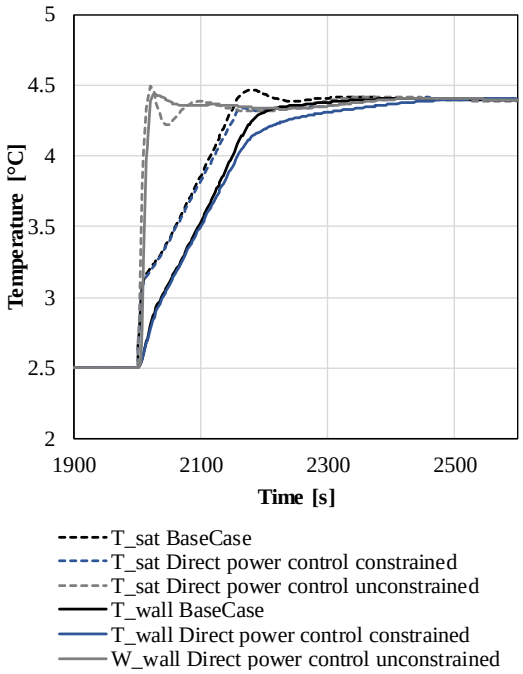

Figure 3-24 Response of saturation temperature and wall temperature of the low-pressure suction line to a set value step of -75 kW for indirect load control (base case), direct load control with ramping rate constraint and direct load control without ramping rate constraint

3.3.4.2 Low pressure control

To allow fast ramping, the risk of droplet formation in the suction line during ramp down needs to be avoided. The droplet formation occurs due to a sudden increase in pressure. Thus, one strategy may be to reduce the increase in pressure during ramp-down. This may be done by controlling the low-stage expansion valve, the source flow rate or both. Figure 3-24 compares the saturation and wall temperatures in the low-stage suction line for the following three cases and a step in the power set value of -75 kW:

- Direct control of power uptake
- Direct control of power uptake with evaporation pressure control via the low-stage expansion valve
- Direct control of power uptake with source outlet temperature control via the source mass flow rate

The steady-state increase in pressure is reduced by the source outlet temperature control and disappears for the low-pressure control. However, the pressure still peaks suddenly and then slowly approaches the new steady-state value. During this peak, the saturation temperature increases more rapidly than the wall temperature and therefore the risk of droplet formation could not be avoided. Another problem was observed when controlling the evaporation pressure with the low-stage expansion valve. In this case none of the vessels' liquid levels were controlled, which in most cases led to drainage of the separator. To avoid this, and thereby ensure stable conditions at the evaporator inlet, the level should be controlled. Figure 3-26 shows the results for a step in the power set value of -75 kW for direct control of the power uptake with:

- Liquid level control of the intercooler via the low-stage expansion valve and evaporation pressure control via the source mass flow rate
- Liquid level control of the separator via the low-stage expansion valve and evaporation pressure control via the source mass flow rate
- Liquid level control of the separator via the low-stage expansion valve and evaporation pressure control via the source mass flow rate with preheating of the suction line

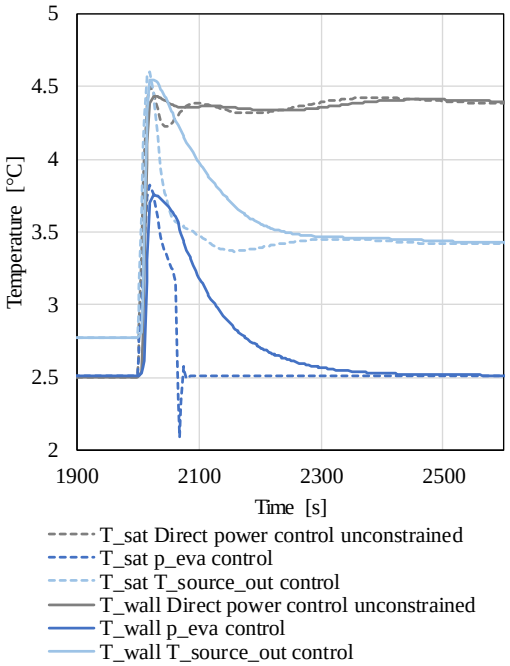

Figure 3-25 Response of saturation temperature and wall temperature of the low-pressure suction line to a set value step of -75 kW for direct load control, direct load control with evaporation pressure control (p_eva control), and direct load control with source outlet temperature control (T_Source_out control)

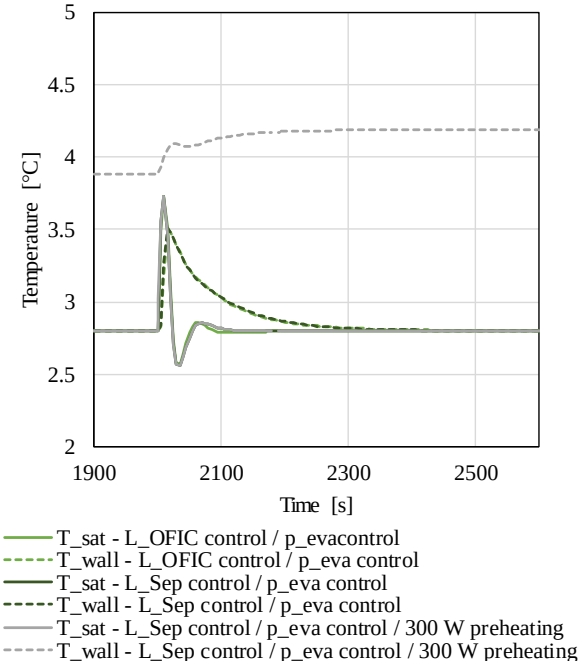

Figure 3-26 Response of saturation temperature and wall temperature of the low-pressure suction line to a set value step of -75 kW for direct load control with evaporation pressure control, with no, 100 W and 200 W preheating of the suction line

The peak in evaporation pressure was lower and shorter than for the control of the evaporation pressure via the expansion valve or source outlet temperature control. The saturation temperature increases shortly by 0.9 K, compared to 1.9 K for direct power control, 1.7 K for direct power control with source outlet temperature control and 1.2 K for direct power control with evaporation pressure control. Even though the peak in evaporation pressure was reduced, the saturation temperature still increased suddenly, while the suction line walls are colder and therefore the risk of droplet formation could not be excluded by a different control structure alone. It is not possible with a 1D discretised suction line model to predict precisely, whether this reduced increase would be enough to avoid condensation at the pipe surface.

To be sure that no droplet formation may occur, a preheating of the suction line is proposed. This may be electric or using another heat source. A preheating with 100 W to 500 W was simulated. The results for the minimum allowable preheating are also presented in Figure 3-26. 300 W preheating together with evaporation pressure control via the source mass flow rate is enough to avoid the risk of droplet formation for a load change of -75 kW. As presented in Table 3-4, this is not enough for a load change of 150 kW, where a preheating with 400 W is necessary to ensure that the suction line wall temperature is always higher than the saturation temperature. It was further found, that the peaks in saturation temperature are higher for the larger load change. It was 2.3 K for direct power control, 2.2 K for direct power control with evaporation pressure control, 1.8 K for direct power control with source outlet

temperature control, and 1.6 K for direct power control with evaporation pressure control via the source mass flow rate.

The regulation time, risk of droplet formation, full load COP and part load COP are summarised for all analysed control structures in Table 3-4. The control of evaporation pressure via the source mass flow rate together with a direct control of the power uptake allows for regulation times, which are in the same order of magnitude as the direct power uptake control alone. The only case where droplet formation in the suction line could be avoided was, when an additional preheating of the suction line was installed, as in all considered cases the evaporation pressure peaked. The regulation time for the direct power uptake control with evaporation pressure control and preheating of the suction line, resulted in regulation times of 54 seconds and 99 seconds for a step of – 30 % load and – 60 % load using the 1 % tolerance criterion, respectively. If this tolerance would be reduced to 0.1 %, the corresponding regulation times would be 97 seconds for -30 % load and 149 seconds for -60 % load.

Table 3-4 Summary of the regulation time, risk of droplet formation, full load and part load COP for a load reduction of 30 % and 60 % and different control structures

	Control structure	Reg. time 1 % tolerance [s]	Reg. time 0.1 % tolerance [s]	Risk of droplet formation	Full load COP	Part-load COP
250 kW to 175 kW, T_{supply} = 70 °C	BaseCase	385	570	yes	3.35	3.62
	Wdot constrained	140	140	yes	3.35	3.62
	Wdot unconstrained	55	90	yes	3.35	3.62
	p_eva control	85	110	yes	3.35	3.48
	T_source_out control	60	86	yes	3.37	3.55
	L_OFIC / p_eva control	45	86	yes	3.37	3.50
	L_Sep / p_eva control	54	97	yes	3.37	3.50
	L_Sep / p_eva control, 300 W preheating	54	97	no	3.37	3.49
250 kW to 100 kW, T_{supply} = 70 °C	BaseCase	475	670	yes	3.35	3.81
	Wdot constrained	320	320	yes	3.35	3.81
	Wdot unconstrained	115	115	yes	3.35	3.81
	p_eva control	145	145	yes	3.35	3.50
	T_source_out control	120	120	yes	3.37	3.61
	L_OFIC / p_eva control	84	103	yes	3.37	3.52
	L_Sep / p_eva control	87	156	yes	3.37	3.52
	L_Sep / p_eva control, 400 W preheating	99	149	no	3.37	3.50

3.3.4.3 Effectiveness of proposed control to changes in boundary conditions

The new control was designed to allow for rapid load change of the heat pump. However, the quality of service is defined by the deviation from the desired heat load and district heating supply temperature for the heat delivery. For the frequency regulation service the quality is defined by the accuracy by which the power uptake may be controlled. A well designed control should be able to control the control variables to the desired set values, also when the thermal boundary conditions change. Accordingly, the robustness of the control to changes in the boundary conditions of these variables was tested. For this purpose, steps of $\pm$ 0.5 K and $\pm$ 1 K were imposed to the heat source temperature and steps of $\pm$ 1 K and $\pm$ 3 K to the district heating return temperature. The results for the power load and the heat load are presented in Figure 3-27. The base case control results in deviations for both the power uptake and the heat flow rate for changes in the source temperature and the district heating temperature, as none of these are controlled explicitly. Further, also the steady-state supply temperature changes with changing source and DH return temperature for the base case control. The newly proposed control structure, achieves to control the power uptake to the desired values for changes in the source temperature and in the DH return temperature. The supplied heat flow rate is not affected by a change in the source inlet temperature. It does however change with the DH return temperature (Figure 3-27 c)). The supply temperature changes with the DH return temperature, but it is not influenced by the source temperature. The new control structure, which explicitly controls the power uptake, is more robust to changes in the thermal boundary conditions than the base case design. The precise control of the power uptake is important when delivering frequency regulation.

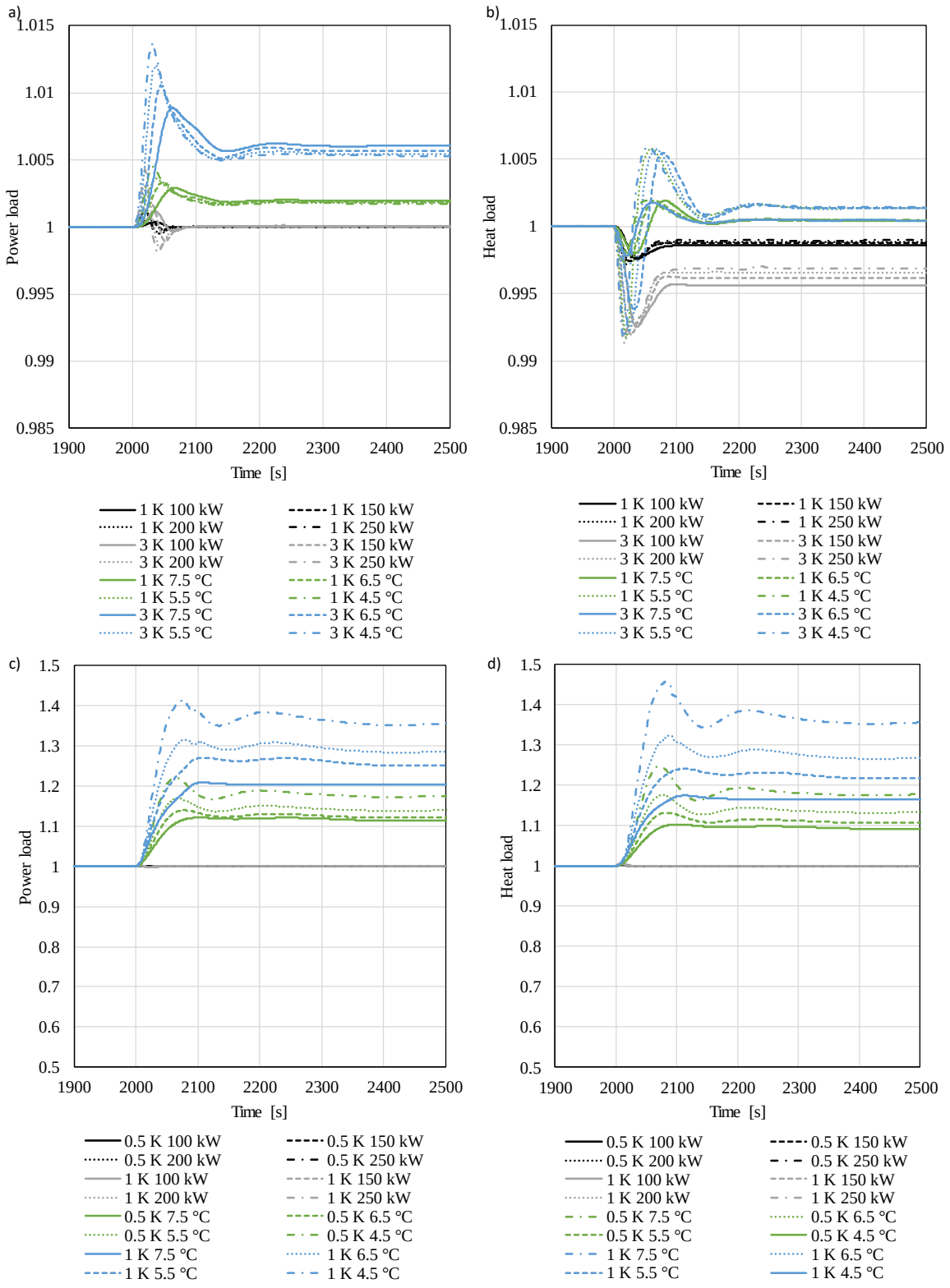

Figure 3-27 System reaction for base case control and newly proposed control to sudden changes in thermal boundary conditions and a condensation pressure set point of 33.2 bar. First number in legend refers to step height in return/source temperature, second number denotes set value for capacity control. a) Power load reaction to change in DH return temperature, b) heat load reaction to change in DH return temperature, c) power load reaction to change in source temperature, d) heat load reaction to change in source temperature.

3.3.5 Constructive changes to avoid droplet formation in the suction line

As seen in section 3.3.3.3, ramping quickly may result in sudden droplet formation in the suction line. The minimal preheating proposed in section 3.3.4, is likely to avoid droplet formation in the suction line at surfaces, which are preheated. However, not all surfaces may be preheated. This is e.g. the case for the suction chamber of the compressor. Here, the wall temperature is close to the fluid temperature. In order to be absolutely sure, that no sudden condensation may occur, the fluid entering the compressor needs to be superheated. Different constructive measures to secure superheated fluid in the suction line were tested with the model, namely, a direct expansion evaporator, an internal heat exchanger and electric preheating of the suction line. Figure 3-28 shows the results for the superheating of the fluid at the outlet of the suction line, i.e. the inlet of the low-stage compressor. All systems were designed for 5 K superheating. Further, a second case for electric preheating was considered with a constant heating of 2 kW, corresponding to 1.5 K superheating in full load, instead of 7.5 kW heating only during full load periods, corresponding to approx.. 5 K superheating. Note that the required electric preheating load is higher than in the case of suction line preheating (described in section 3.3.4), as the total refrigerant mass flow needs to be superheated. The effective superheating from the internal heat exchanger was slightly higher than the design value. With all shown design variants, it was possible to avoid the risk of droplet formation. The results from both electric preheating cases indicate that a lower set value for the superheating might be enough to avoid the risk of droplet formation. This is advantageous as the COP is considerably reduced by such a high amount of preheating and not in all cases it is possible to switch of the superheating control after ramp down. This is e.g. the case if continuous up- and down regulation of the heat pump is required, as e.g. for frequency controlled services.

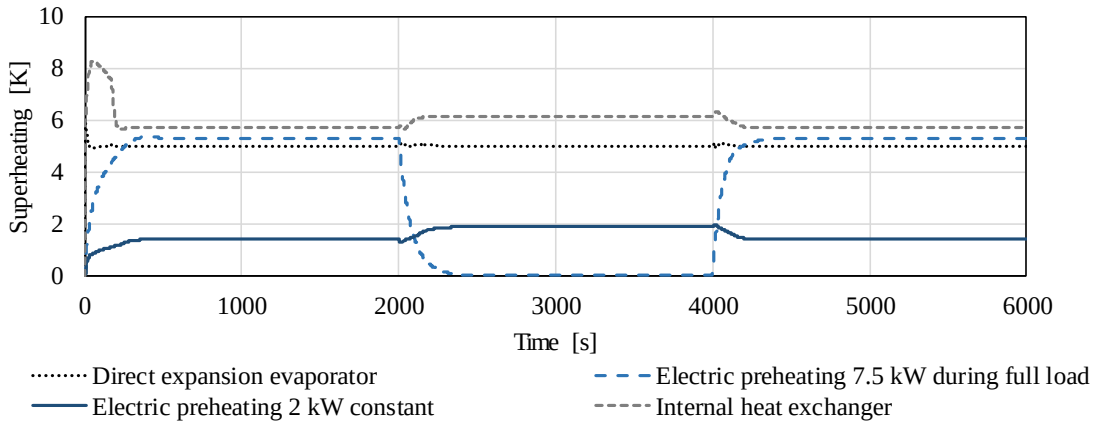

Figure 3-28 Superheating for three different strategies to avoid condensation in the suction line

A summary of the regulation times for up-and down regulation for a change in the source temperature value from 4.8 °C to 6.3 °C (down regulation), and from 6.3 °C to 4.8 °C(up regulation). Here, up- and down-regulation are defined from the heat pump perspective as an increase in power uptake and a decrease in power uptake, respectively. All design variants with a flooded evaporator and separator had similar regulation times, between 710 s and 720 s. The heat pump with direct expansion valve regulates considerably faster than the other variants and the refrigerant mass is lower compared to the cases with flooded evaporator and separator. It has however the drawback of a lower COP both in part load and full load. The highest COP is obtained using an internal heat exchanger, even though this resulted in the highest superheating in the suction line as well. The increase in performance is due to the increased cooling capacity in the evaporator obtained from the additional subcooling of the liquid exiting the intercooler.

Table 3-5 Regulation time, risk for droplet formation, COP and total refrigerant mass for up- and down regulation from full load (Source outlet temperature set value 4.8 °C) into part load (Source outlet temperature set value 6.3 °C)

Design	Regulation time down [s]	Regulation time up [s]	Risk of droplet formation [yes/no] [yes/no]	COP full load [-]	COP part load [-]	Total refrigerant mass [kg]
Direct expansion evaporator	287	296	no	3.35	3.46	86.4
Electric preheating 7.5 kW during full load	710	716	no	3.50	3.80	113.4
Electric preheating 2 kW constant	712	718	no	3.61	3.74	113.4
Internal heat exchanger	716	720	no	3.63	3.77	116.8

3.3.6 Influence of component sizing

The results of the Monte Carlo analysis to determine the influence of component sizing on the dynamic behaviour are presented in Figure 3-29 and Figure 3-30 in graphical form. The intercooler volume had a dominant influence on the regulation time compared to the other varied input parameters. No clear influence of the other parameters was identified from the plots. The results of the linear regression in form of the standardised regression coefficients β_i, β_i^2 and the coefficient of determination R^2 are given in Table 3-6. The dominant influence of the intercooler volume can be explained, by the large amount of refrigerants mass in the intercooler, which accounted for 63 % to 80 % of the total refrigerant mass for the different cases of the Monte Carlo analysis. This influence of the total refrigerant mass on the regulation time of the heat pump is represented in Figure 3-31. No clear dependency between the total heat exchanger area or the ratio of evaporator heat transfer area to total heat transfer area was observed.

The influence on the heat pump COP shows a different pattern, as depicted in Figure 3-30. A clear correlation between the number of plates, i.e. heat exchanger area, in the subcooler and the COP was identified. The overall change of COP was very little. This was surprising as the area of the heat exchangers in the system is expected to have an influence on the achievable COP. It may be explained, when looking at the control structure in place. Here, the optimised control structure presented in section 3.3.4 was considered. This was designed, such that both the evaporation pressure and condensation pressure were controlled, and accordingly the COP is affected little by the size variations. However, the heat exchangers still have to absorb or reject the same amount of heat. Accordingly, the decrease of evaporator size resulted in an increased source flow and source outlet temperature to compensate for the reduction in area. A decrease in the number of plates in the condenser resulted in an increase of the sink mass flow and the desired forward temperature was not reached anymore. Reducing the number of plates in the desuperheater and subcooler resulted in minor changes of the sink mass flow and the forward temperature. Changing the vessels sizes did not influence the heat pumps COP in steady-state. The limiting factors for changing the size of components using the given control structure were the maximum source mass flow and the allowable deviation from the set forward temperature. If the control structure was changed such that the supply temperature was kept constant, the variation of heat exchanger sizes on the high pressure side would result in a change of the condensation pressure.

Accordingly, it may be expected that the COP would also depend on the superheater and condenser area in this case.

Since the influence on the regulation time of the size of the intercooler was dominant over possible influences of other components, it was not possible to identify whether other factors than the total mass had an important influence on the regulation time. Therefore, the analysis was repeated with vessel sizes corresponding to 20 % of the original vessel sizes and an initial liquid level in the intercooler of 4 % instead of 8 %. Note that no detailed design study of such vessels with reduced volume and hold up was conducted. The results of the linear regression are presented in Table 3-7. It may be seen that the influence of the intercooler volume was less dominant than in the previous analysis and that the regulation time was positively correlated with the number of plates in the evaporator and subcooler, while it was negatively correlated with the number of plates in the condenser. The β_i^2-values of the separator volume and the number of plates in the desuperheater were below 0.01, i.e. the influence was negligible [191]. Figure 3-31 compares the regulation times obtained from the Monte Carlo analysis with the original and reduced vessel sizes. The reduction in the total mass of ammonia due to the reduction of vessel size and initial intercooler filling level resulted in considerably reduced regulation times. The reduction of refrigerant mass, especially in the intercooler, was therefore identified to have a significant potential to reduce regulation times.

The second Monte Carlo analysis conducted to assess the influence of the length of all pipes in the system revealed that the influence of the pipes on the system's dynamic behaviour was negligible compared to the influence of the mass stored in the vessels. This was true for the system with original vessel sizes and reduced vessel sizes. The only relevant influence found, was the size of the receiver. If this fell below 0.03 m^3 the damping factor induced by this volume element was so low, that the power uptake response undershot considerably. Such that it left the tolerance range again before converging to the steady-state value and the calculated regulation time increased, accordingly.

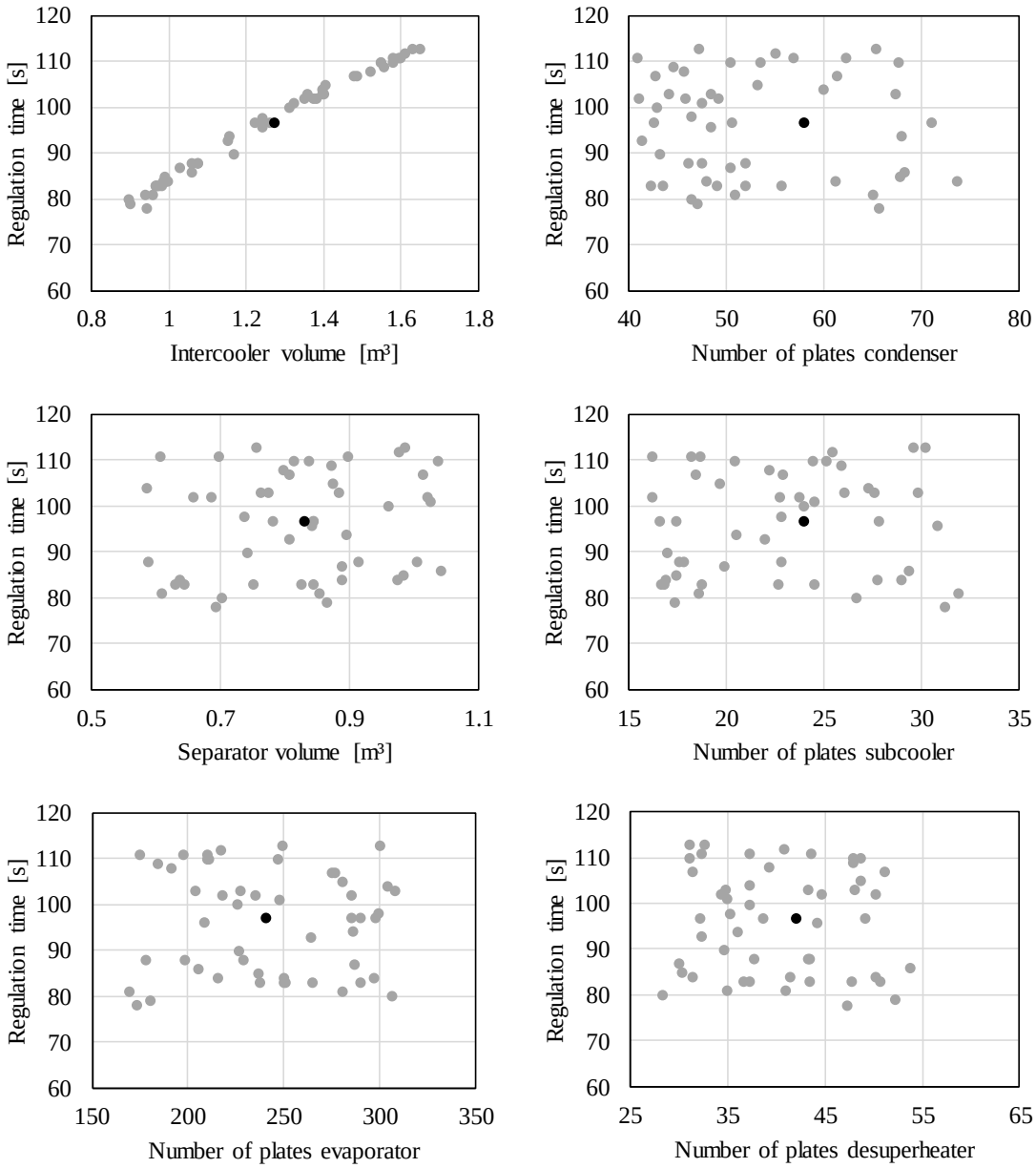

Figure 3-29 Influence of the varied input parameters on the regulation time of the system for all 50 draws of the Monte Carlo analysis (grey dots) and the original system design (black dot)

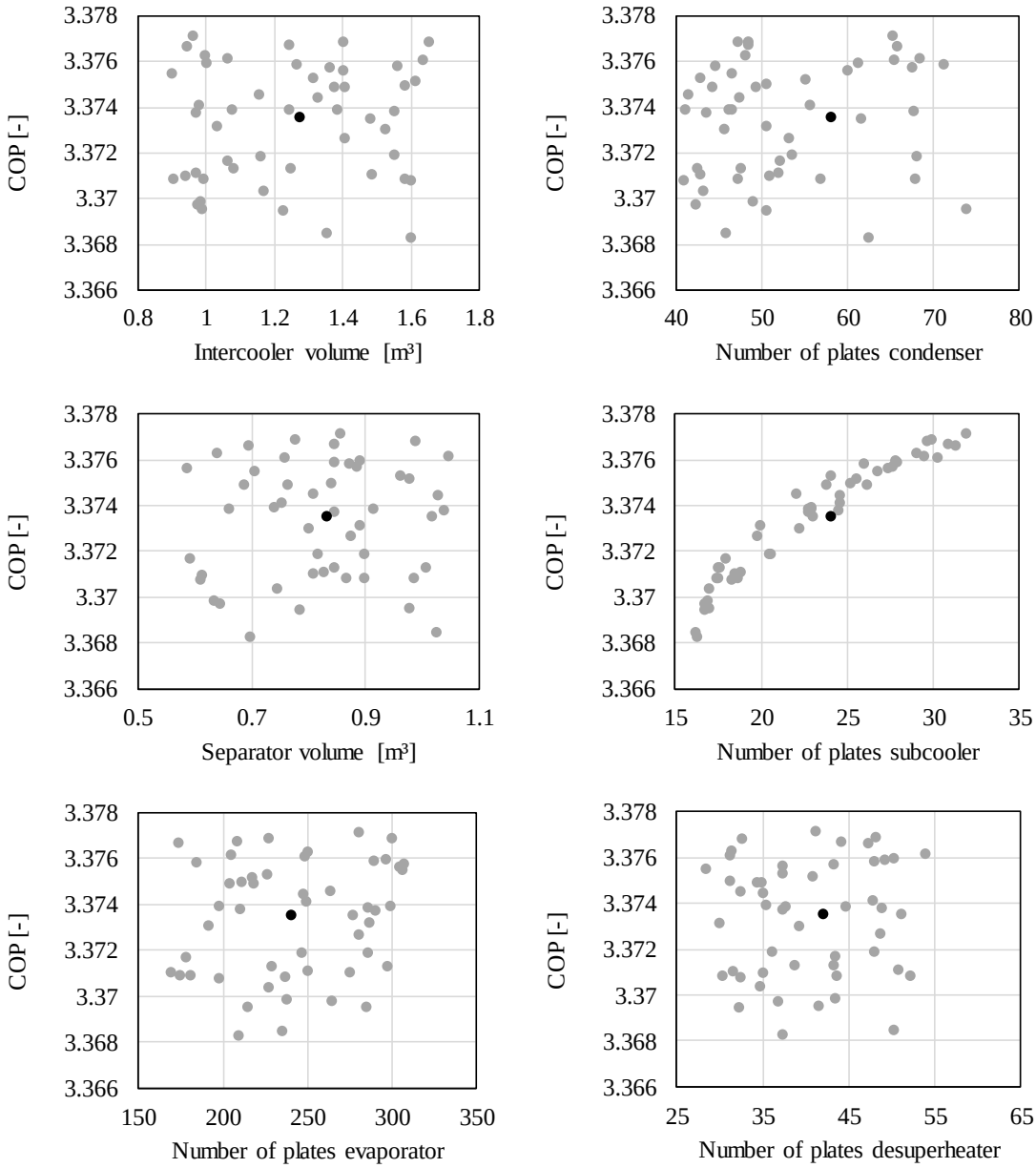

Figure 3-30 Influence of the varied input parameters on the heat pump COP for all 50 draws of the Monte Carlo analysis (grey dots) and the original system design (black dot)

Table 3-6 Regression parameters for sensitivity analysis on results from Monte Carlo analysis with the original size vessels

Varied input parameter	β_i	β_i^2	R^2
Intercooler volume	0.9993	0.9986	0.9929
Separator volume	0.0196	0.0004	
Number of plates evaporator	0.0551	0.0030	
Number of plates condenser	-0.0004	0.0000	
Number of plates subcooler	-0.0368	0.0014	
Number of plates desuperheater	-0.0076	0.0001	

Table 3-7 Regression parameters for sensitivity analysis on results from Monte Carlo analysis with the reduced size vessels

Varied input parameter	β_i	β_i^2	R^2
Intercooler volume	0.8512	0.7246	0.8966
Separator volume	0.0833	0.0069	
Number of plates evaporator	0.3255	0.1059	
Number of plates condenser	-0.2040	0.0416	
Number of plates subcooler	0.1603	0.0257	
Number of plates desuperheater	0.0814	0.0066	

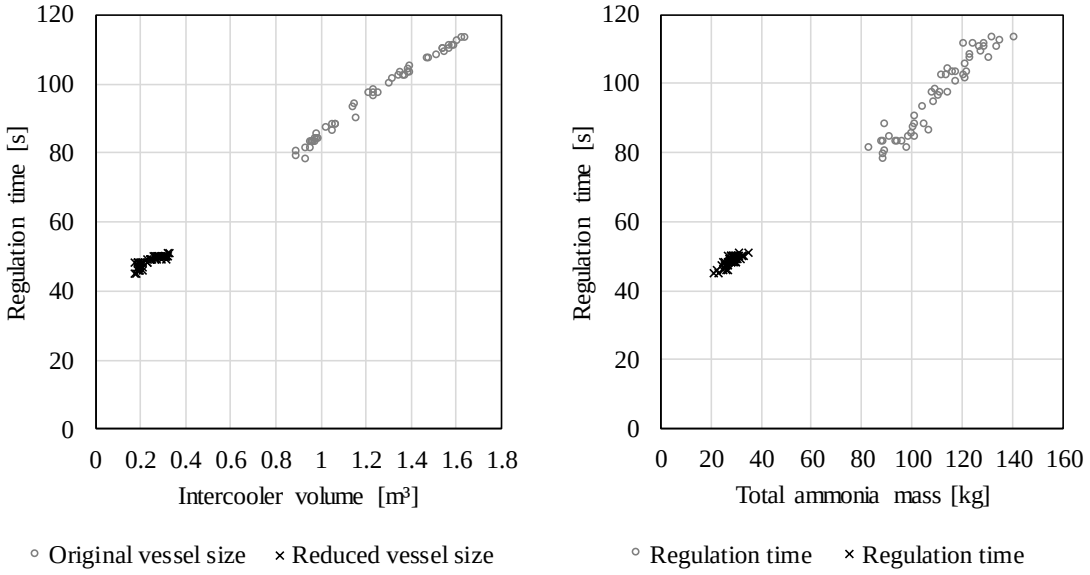

Figure 3-31 Comparison of the regulation times obtained in the Monte Carlo analysis for the original vessel size and the reduced vessels size, plotted as a function of the intercooler volume and the total ammonia mass in the system

3.3.7 Influence of cycle design

The response to a change in power uptake set value was compared for the one-stage heat pump and two-stage heat pump. The two-stage heat pump with original component sizing and the newly proposed control structure was considered. The responses of both systems to a set value change of -75 kW from full load and ramping up to full load again for 70 °C supply temperature were assessed. Table 3-8 summarises the regulation time, the full load and part load COP and the total refrigerants mass of both heat pumps. The one-stage heat pump has a higher regulation time, even though the overall refrigerant mass is considerably lower than for the two-stage heat pump. This is the case as the coupling between the different control loops for the one-stage heat pump are larger than for the two-stage heat pump. The two-stage heat pump benefits from the intermediate pressure level, which serves to decouple the control on the sink and the source side. This is not the case for the one-stage cycle, which results in larger regulation times. Figure 3-32 shows the response of the power uptake of both heat pumps to a reduction in the set value and an increase in set value. It should be noted that the integral time constants for both load controllers were set to the same value, 10 s, as the dynamic response varies considerably with this time constant. The time constant of the reaction of the two-stage heat pump was smaller than for the one-stage cycle. Further, a slight oscillation during ramping was observed. The development of the pressures at the compressor inlet and outlet for the same experiment is shown in Figure 3-33. The

intermediate and condensation pressure in the two-stage system overshoot during ramping of the system. Especially the intermediate pressure may be critical, as this might, in an extreme case, lead to sudden droplet formation in the high-stage suction line. The variations for the condensation pressure of the one-stage cycle are less, while the low stage pressure increases to a higher value in part-load than for the two-stage system. The response of the evaporation pressure in the one-stage cycle follows a first-order behaviour, while the evaporation pressure in the two stage cycle overshoots during ramp-down of the heat pump.

Table 3-8 Results for the response of the one-stage and two-stage heat pump to a step in power ste value of -75 kW.

	Unit	One-stage ammonia heat pump	Two-stage ammonia heat pump
Regulation time up	s	177	162
Regulation time down	s	176	163
COP at 250 kW power	-	3.18	3.41
COP at 175 kW power	-	3.21	3.54
Total refrigerant mass	kg	36	113

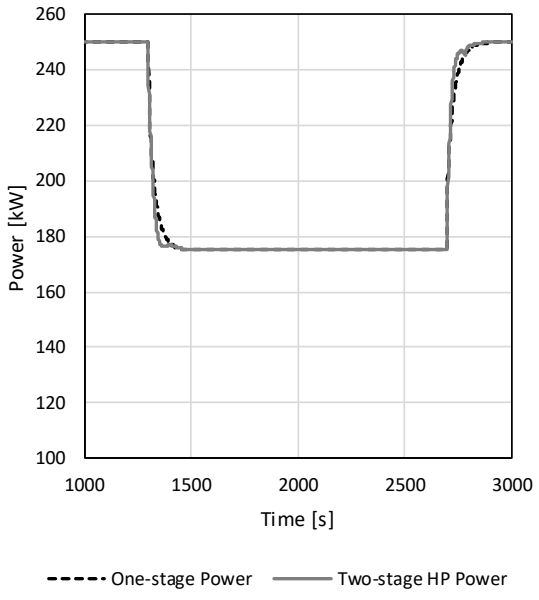

Figure 3-32 Response of power uptake for the one-stage and two-stage heat pump

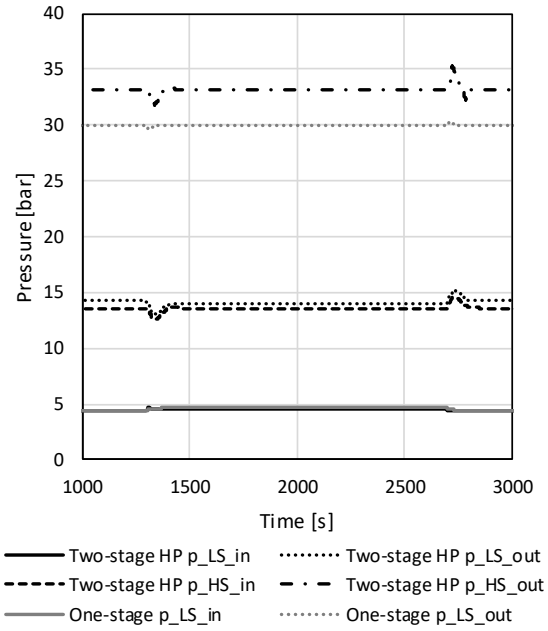

Figure 3-33 Response of inlet and outlet pressure of the compressors for the one-stage and two-stage heat pump.

3.4 Discussion

Future application of heat pumps and their expected role in integrated energy systems require that these systems are designed to be able to operate flexibly and according to variable boundary conditions. It may be expected that only a part of the heat pumps installed in future will be required to deliver ancillary services, i.e. the currently available best practice in design, which focusses on maximizing COP rather than optimizing regulation times, will still be the premise for many plants in the future. A dynamic model as the one presented in this study allows cost-efficient analysis of different control structures and system configurations, that would require major changes to the real system. Further, it allows testing the limitations of the system, such as the risk of droplet formation in the suction line without risking to damage the real system. Thereby validated dynamic models constitute an important tool in the development of high-performance heat pumps.
The present study focused on a two-stage ammonia heat pump operated with piston compressors. Even larger ammonia heat pumps often use screw compressors. The part-load regulation of these are different from piston compressors and future work should therefore include studies on the feasibility of different compressor types for fast regulation of heat pumps.
Within this work, the pumping power of the water source and the district heating water was neglected. Depending on the source, it may however be necessary to include the pumping power, to allow for the desired reduction or increase in power uptake.
Further, it has not been assessed how the component wear and the need for maintenance is influenced by flexible operation, as relevant data and experience from the test plant is missing.

3.4.1 Regulation time of the heat pump

A change in control structure was proposed. It would both minimise the risk for droplet formation in the suction line and allow for faster regulation of the heat pump. The latter is important, when heat pumps are supposed to react flexibly to changes in the electricity grid, e.g. by providing frequency regulation. The simulation results showed that the system response could be considerably improved by controlling the power uptake directly instead of indirectly via the source outlet control. By doing so, it would be possible to ramp down from 250 kW power to 175 kW power in 140 seconds, and from 250 kW to 100 kW in 320 seconds. If faster ramping rates for the compressor were implemented, the regulation time was reduced even further. If the proposed control strategy to avoid droplet formation in the suction line is taken into consideration, the heat pump could ramp from 250 kW to 175 kW within 97 seconds and from 250 kW to 100 kW in 149 seconds with the unconstrained direct power control. This means that the heat pump would regulate fast enough for manual reserves, which typically need to be delivered within 15 minutes, and for secondary reserves, which require ramping times of 5 minutes. Most primary frequency regulation services require ramping to the full activation power, i.e. the power bid into the market, in less than 30 seconds. Thus, the heat pump would not be able to react fast enough to supply these primary services. An exception is the Eastern Danish FCR-N frequency market, which demands ramping times below 150 seconds. Based on the presented results, it may be possible to supply this service with the heat pump alone, by bidding half of the capacity difference between minimum and maximum load on the market (here: 75 kW or 30 % load). The difference between the required regulation time and the calculated value for a jump of 150 kW (60 % load), was however so little, that further measures should be taken to ensure that the heat pump can operate safely and fast enough. Especially, since the calculated regulation time is highly dependent on the steady-state tolerance and the actually allowed tolerance is not known. Further, an additional unit, e.g. an electric boiler, would be required to deliver down-regulation.
As shown, one option to reduce the ramping time further, is to reduce the refrigerant mass in the system. This may be obtained by more careful design of the vessels in the system and reducing liquid hold-ups in the system. Another option would be to exchange the flooded evaporator with a direct expansion

evaporator. This would however result in a reduced COP, also when no frequency regulation is bid into the market. If the desired supply temperatures are low enough, a one-stage ammonia cycle may be used instead of a two-stage ammonia heat pump. This would result in a large reduction of the refrigeration charge, as the intercooler and additional pipelines are excluded. However, the single control loops in the one-stage cycle are coupled to a larger degree than in the two-stage cycle, i.e. more interaction between the control loops occur and thus the regulation time was not reduced compared to the two-stage cycle.
In reality, the specific heat pump would have to be combined with one or more other units to be able to bid on any of the Danish markets. If faster regulation is required, e.g. for different primary frequency reserves, the heat pump may be combined with faster regulating units, e.g. batteries, to provide a combined frequency regulation product. This will be further assessed in Chapter 4. Further, it should be noted that the flexible operation of heat pumps is enabled by the available heat storage capacity. This needs to be considered when evaluating, whether there is a business case in providing ancillary services from heat pumps. Additionally, the capacity of the heat pumps needs to be large enough in order to allow for reduction of power uptake and thereby heat production without supplying too little heat to the customers.

3.4.2 Droplet formation in the suction line

In order to avoid condensation in the suction lines during fast ramp down, the ramping rate may be restricted. If very fast regulation is required, restricting the ramping rate might not be an option. It was shown that by controlling the low pressure via the source mass flow rate, the peak in evaporation pressure may be considerably reduced, which helps reducing the risk of droplet formation in the suction line. Controlling the evaporation pressure via the expansion valve resulted in draining the separator in most cases, therefore it is advisable to stick to a classic liquid level control. In terms of regulation time, no significant difference in regulation time was seen between controlling the liquid level in the intercooler or in the separator. The separator liquid level control was chosen, to ensure stable conditions in the evaporator.
Fast ramping comes along with fast increases in the evaporation pressure, which increases the risk of condensation, even if the peak in evaporation pressure may be reduced. Preheating the suction line may help to avoid droplet formation in the suction line, as the wall is always kept at higher temperatures than the saturation temperature. In this case, the superheating of the ammonia is minimal and therefore attention needs to be paid to the compressor flange and suction chamber, which might be at fluid temperature, too, and thus condensation could occur here as well. These parts are more difficult to heat than the suction line. Alternatively, the fluid may be superheated before entering the compressor. Different constructive measures to do so were analysed. These are based on increasing the superheating before the compressor by heating the gas in the suction line or possibly by reducing the pressure. Superheating the fluid before compression will however result in increased compression work and thereby reduced COP. It was shown that the use of a direct expansion evaporator is beneficial in terms of regulation time, as the refrigerant mass is considerably reduced. In terms of COP, the implementation of an internal heat exchanger between the liquid line exiting the intercooler and the low-stage suction line yielded the best results. Implementing constructive changes in an existing plant to avoid droplet formation in the suction line may be economically and practically unfeasible. If these problems could be avoided by advanced control methods, a reduction of COP could possibly be avoided. It should further be mentioned that droplet formation in the low-stage suction line has been observed in real life operation of ammonia heat pumps, which occurs if the system is operated without superheating of the fluid in the suction line and the suction pressure increases rapidly [192]. However, no such observation is known to the author for the high-stage suction line. Accordingly, further studying of the effects in the intermediate stage is needed, including where pressure losses occur and any non-ideal behaviour of the intercooler. It should be noted that the problem of condensation in the suction

line is related to the negative influence of superheating on the COP of ammonia heat pumps. For other refrigerants the influence may be positive, and accordingly superheating the fluid in the evaporator and thus avoiding sudden condensation in the suction line would not be a problem, as also shown by Andersen [193].

3.5 Chapter summary

A dynamic model of a two-stage ammonia heat pump was implemented in Dymola. It was validated against experimental data from a recently built heat pump in Copenhagen. The control of the heat pump was not optimally parametrised, which required to calibrate the control parameters to the experimental case. The calculated mean error for all validated values was found to be between 0.1 % and 9.6 %. The parametrisation of the controllers was redone and the performance of the heat pump was calculated. A change in control structure was proposed to allow for faster ramping of the heat pump, while minimizing the risk of droplet formation in the suction line. By controlling the power uptake directly via the low-stage compressor and the evaporation pressure via the source flow rate, the regulation time of the heat pump could be considerably reduced. It was further showed, that the heat pump may follow a given frequency controlled operation pattern. In order to avoid droplet formation in the suction line during ramp-down, additional preheating of the suction line was necessary. The condensation at the pipe walls in the suction line may be avoided by electric preheating with 400 W. However, condensation might still occur at other cold surfaces, e.g. in the suction chamber. Therefore, different possible set ups to control superheating of the fluid in the suction line were analysed. All analysed cases could provide enough superheating to avoid condensation. A direct expansion evaporator set-up resulted in considerably reduced regulation times, but lower COP. The highest COP was obtained using an internal heat exchanger between the liquid line exiting the intercooler and the low-stage suction line. It was further assessed, how the component and pipe sizing influences the regulation time of the two-stage ammonia heat pump. It was found that there is considerable potential to reduce the regulation time by reducing the refrigerant mass in the system. Other influences were negligible compared to the refrigerant mass. Lastly, the influence of the cycle design was assessed by comparing a two-stage ammonia heat pump to a one-stage ammonia heat pump. It was found that no advantage in terms of regulation time is obtained by using a one-stage cycle instead of a two-stage cycle.

4 Feasibility of providing frequency regulation

Within this chapter, the economic feasibility of providing frequency regulation from large-scale heat pumps, alone and in combination with fast regulating bidirectional units, was assessed. As the delivery of ancillary services requires a modified operation of the heat pump system and creates losses in the system, a thermodynamic model of the heat pump system was used to analyse the performance under various operational schedules. This model has been developed for a dynamic exergoeconomic analysis, and the model description and explanation of the dynamic exergoeconomic method has been published prior in [P1]. The model was extended to simulate the combined delivery of frequency regulation from electric vehicles and the large-scale heat pump. The description of the model was adapted accordingly. The description of the requirements of FCR-N delivery and the combination of different flexibility assets, are part of [P4]. Here, the focus is on the heat pump operation. Nonetheless, a brief summary of the modelling approach of the electric vehicles (EVs) is given here (work on EVs conducted by Andreas Thingvad), to enhance the understanding of the combined system. A more detailed description of the modelling and results regarding electric vehicles may be found in [P4].
In order to ensure the comparability of the results of both studies for this chapter, the results of the two studies were updated for a common case. Five different operation modes, out of which three supplied FCR-N primary frequency regulation, were compared to each other.

4.1 Background

4.1.1 Related work

Within the EnergyLab Nordhavn project, the utility company HOFOR owning the FlexHeat heat pump, which was used for the case studies in this thesis, tested the components and the functionalities of the heat pump system in operation. Further, they developed an optimisation model, that allows to schedule the heat pump operation optimally, including the participation in different regulation markets. This model is described in [177]. It was used to compare the economic potential of manual reserve, secondary reserve (assuming similar prices as in Western Denmark, as the Eastern Denmark market is only planned for 2020), and primary reserve, i.e. FCR-N frequency regulation. The results showed that the expected income is highest for FCR-N delivery. This has two major reasons, firstly the service is regularly called and the capacity payments are high compared to the available payments for the other services. The delivery of secondary service yielded the second best result in terms of economy and would be interesting due to the longer ramping times allowed for service providers. The achievable prices are however uncertain for Eastern Denmark. Manual reserve resulted in the worst business case, as the hours, where this service was called throughout the year were few and the achievable payments were comparably low. A more detailed description of the conducted study may be found in [194][P10]. Based on these results, it was decided to focus on the provision of FCR-N frequency regulation for the analysis presented in this chapter.

4.1.2 Quantification of flexibility in the energy sector

Conventionally, frequency regulation services are provided by generation units. With increasing shares of distributed renewable energy resources and the replacement of conventional thermal power plants, new actors are required to deliver ancillary services. One option is to use demand side management to supply frequency regulation to the grid. Previous studies showed that the integration of the electricity and the heating sectors offers the possibility to decouple electricity supply and demand constraints and can provide balancing service to the power sector [195]. Stinner et al. [196] confirmed that balancing

services from lower voltage levels are necessary in energy systems with a high share of renewables to balance the distribution and transmission grids. Further, controlling the load of heat pumps flexibly can reduce CO_2 emissions and lower CO_2 abatement cost, while the overall electricity consumption may increase [197].
The considered conversion system provides two different products – the heat supplied to the district heating grid and ancillary services to the electricity grid. This may lead to additional income from providing a second product, but has several consequences for the operation of the heat pump. Firstly, the operation strategy has to take the demand of heat and power regulation into consideration. Secondly, the ability to provide flexibility comes at increased investment cost for a larger conversion system. Thirdly, the flexible operation leads to additional losses in the conversion system. The three consequences require investigations into the valuation of the different products and the additional cost of flexible operation.
Ulbig & Andersson define the operational flexibility of a power system as the technical ability of a power system to modulate the power feed-in or load over time [198]. Extending this definition to integrated energy systems, we propose to define flexibility as the technical ability of an energy conversion system to adapt the power feed-in, load or conversion into other forms of energy in order to optimise security of supply, cost and/or environmental impact of the overall energy system.
Different studies have been carried out to determine the value of flexibility provided by heat pumps and electric heaters. Three general approaches were identified: The first approach is to define an average flexibility value by considering the differences between supply and demand [195,199–201]. This approach is based on the idea that the unit adapts to the state of the system, and thus decreases the difference between supply and demand, providing a balancing service to the system.
The second approach takes the specifications regarding ramping rates and capacities of the different components into consideration. In this way, it evaluates the actual potential of a component to react to regulation needs of the system at a certain point in time with respect to the current state of component operation [198,200,202].
The third approach is to evaluate the flexibility of a unit by evaluating the cost effectiveness of an increase of flexibility. Blarke & Lund [203] define the cost effectiveness of the storage or relocation option as the shadow cost associated with increased flexibility of a certain unit. Meibom et al. [204] propose to evaluate the impact of heat pumps and electric boilers according to their influence on the price of regulating power.
All these approaches value flexibility according to the benefit of the power system or of the overall energy system. However, it is important to assess which cost is associated with providing ancillary services for the heat pump system operator, as this is valuable information when deciding on the operation strategy and the system design. The analysis of the actual changes induced to the conversion system and the associated costs requires a more detailed method than suggested by the above references.

4.1.3 Combination of flexibly operated units

The development towards an integrated energy system involves increasing interactions across energy infrastructures and optimising this integration to provide services at supply and demand level. One option is to use demand side management to supply frequency containment reserve to the grid. Demand side units often provide a link to a neighbouring energy sector with certain requirements and constraints. This requires a well-coordinated operation of these demand side units to be able to supply both the ancillary service and the primary service of the unit. In order to characterise the capability of different systems to provide operational flexibility, the following parameters can be used, as proposed by Makarov et al. [205] and modified by Ulbig & Andersson [198]:

- The power provision capacity, i.e. the load by which the current power uptake or supply of the unit may be decreased or increased

- The power ramp rate, which defines how fast a unit is able to change the power uptake or supply
- The energy provision capacity, which defines for how long the change in power uptake or supply can be maintained and thereby is a measure of the storage capacity of the system.

These measures may vary with the state of the system. As described by Ulbig & Andersson, combining different types of units results in combination of the strengths of the individual units. In other words, the aggregation of a fast ramping unit with small storage capacity and a slow ramping unit with large storage capacity will lead to a combined system that can react quickly and maintain the regulation for a longer period.
In this study, it is proposed to deliver primary frequency regulation from a combination of different demand side units. This approach is demonstrated for a combination of electric vehicles (EVs), which are able to regulate within seconds and in both directions, with large-scale heat pumps, which can access a large storage capacity. It is expected that in this way it may be possible to create a combined system, which can regulate fast and has a large storage capacity.

4.2 Methods to assess the feasibility of providing frequency regulation

Within this chapter, first, the analysed heat pump case is described. Second, an overview about the technical requirements to supply frequency regulation (FCR-N) is given and it is explained how the desired power response to frequency deviations was calculated. Third, a description of how the heat pump system and supplied district heating network were modelled for this study. Fourth, the implementation of combined delivery pf primary frequency regulation from the heat pump and fast regulating electric vehicles is described. Fifth, the economic evaluation of the different operation modes is explained and, sixth, a new allocation method for cost and income for power-to-heat units delivering ancillary services is proposed based on exergoeconomic principles. Finally, it is explained how the heat pump capacity and related cost were varied to test the influence on the economic feasibility.

4.2.1 Case description

The studied case was the FlexHeat heat pump system supplying a district heating island system at the Ocean Quay cruise ship terminal in Copenhagen [177]. The system was designed to supply three terminal buildings and a large warehouse with heat for space heating and domestic hot water. The heat pump replaced the formerly implemented oil burners and has a nominal capacity of 800 kW. Figure 4-1 shows a sketch of the described system and all water and electricity flows in the system. The heat source for the heat pump was groundwater delivered by the groundwater (GW) pump. Further, the system comprised a stratified storage tank with a volume of 120 m^3, a district heating (DH) pump and two electric boilers of 100 kW capacity each. The heat demand, including distribution losses, was considered as a lumped heat demand. Table 4-1 summarises the capacity of the components used in the assessed case.

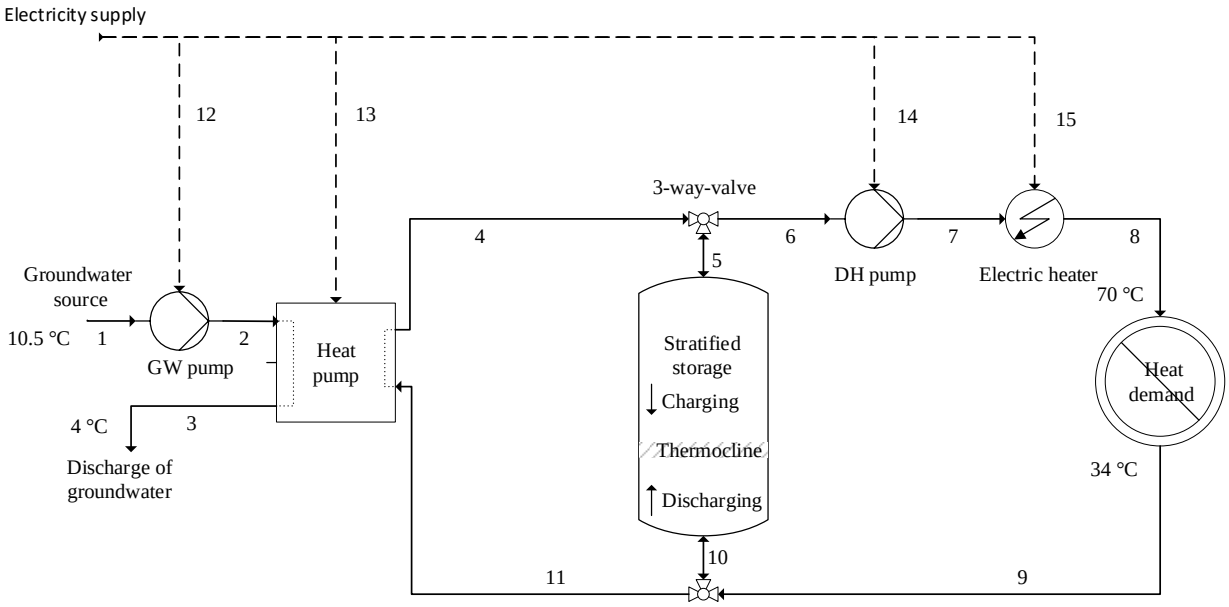

Figure 4-1 Sketch of the considered heat pump system located in Copenhagen, solid lines – water, dashed lines – electricity

Table 4-1 Specification of units in the considered system

Unit	Nominal capacity
Heat pump minimum heating capacity	350 kW
Heat pump nominal heating capacity	800 kW
Electric boiler capacity	2 · 100 W
District heating pump design flow	2 · 16.7 kg/s
Groundwater pump design flow	2 · 44.3 kg/s
Stratified Storage tank	120 m^3

The following operation modes of the heat pump system were compared:

- **Heat demand controlled:** Heat pump operation according to heat demand. The storage was only used when the heat demand was below the minimum heat pump load. The operation was not optimised with regard to fuel cost or energy efficiency and did not allow for frequency regulation.
- **Spot market optimised operation:** Heat pump operation optimised with regard to electricity spot market prices. This schedule was provided for 2018 by the utility company owning the heat pump [206].
- **Frequency regulation – HP max:** Heat pump providing frequency regulation as stand-alone unit, i.e. the heat pump was operated at intermediate load and was able to regulate up- and down according to the frequency of the grid. The hours of frequency regulation that may be provided were calculated from the expected heat demand.
- **Frequency regulation – HP 5 h:** Heat pump providing frequency regulation as stand-alone unit, i.e. the heat pump was operated at intermediate load and was able to regulate up- and down according to the frequency of the grid. The hours of frequency regulation were limited to maximum 5 hours, which were chosen to be between 00:00 and 05:00 am, as the expectable FCR-N capacity prices were highest for these hours in 2018, as depicted in Figure 4-2. The idea was to focus on the well-paid hours of the day and thereby increase the specific income per hour. This may be required in case the minimum required capacity payment from frequency regulation to cover the additional cost of the heat pump system were relatively high. It further

decreased the complexity of scheduling the service provision and helped to charge the storage tank to supply the heat demand of the expectable morning peak [143].

- **Frequency regulation – EV + HP:** Heat pump providing frequency regulation in combination with vehicle-to-grid capable electric vehicle batteries. The batteries were used to regulate within few seconds according to the frequency deviations, while the heat pump was operated at intermediate load and only adapted its load to offset the batteries power uptake when necessary, such that their state-of-charge remained within the allowable boundaries. The advantage of this approach is that the short regulation time of batteries may be combined with the storage capacity of the heat pump system. This may enable the supply of faster services than with the heat pump alone, while allowing the heat pump to regulate as slow as required for safe operation. This approach is further explained in 4.2.4.

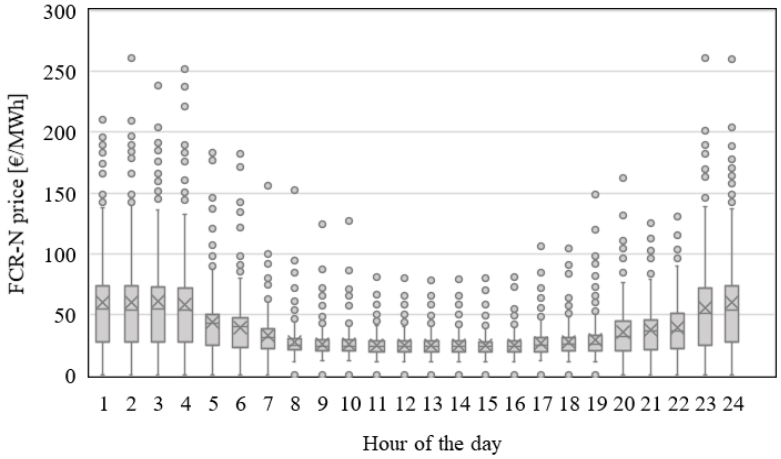

Figure 4-2 Distribution of average hourly FCR-N prices in 2018 for the hour of the day

To compare the results on an energy basis the seasonal heat pump COP and the seasonal system COP (SCOP) were defined as

$$\mathrm{COP}_{\mathrm{season}} = \frac{Q_{\mathrm{heat}}}{W_{\mathrm{HP}}} \tag{4-1}$$

$$\mathrm{SCOP}_{\mathrm{season}} = \frac{Q_{\mathrm{heat}}}{\sum_k W_{\mathrm{k}}} \tag{4-2}$$

where Q_{heat} denotes the annual amount of heat delivered into the DH network, W_{k} is the annual amount of electric energy supplied to component *k* and accordingly W_{HP} is the annual amount of electric energy supplied to the heat pump. In the sum all electrical components, i.e. the heat pump, the electric heater, the groundwater pump and the DH pump were considered.

4.2.2 Ability of different technologies to provide frequency regulation

4.2.2.1 Requirements for frequency regulation

One of the most critical ancillary services for the stability of the power system is the frequency containment reserve, which maintains the system frequency close to the nominal value by balancing the production with the consumption on the second time scale. Frequency Containment Reserve-Normal operation (FCR-N) is a primary frequency regulation reserve in Eastern Denmark. It has to be delivered within 150 s, and the minimum bid size is 0.3 MW, which can be delivered by both consumption and production units [54]. Because of the minimum bid size, the power of smaller units has to be pooled to a combined delivery, by an actor often referred to as the *aggregator*. FCR-N is a symmetrical service, which requires the provider to offer the same power capacity for upwards and downwards regulation. Frequency reserves must be provided linearly, with full activation for deviations

of ±100 mHz, without a deadband, as also presented in Figure 4-3. For a frequency value $f(t)$ in the range 49.9 Hz to 50.1 Hz at time *t*, the normalised response $y(t)$ is calculated as:

$$y(t) = (f(t) - 50\ \text{Hz}) / 0.1\ \text{Hz} \tag{4-3}$$

The power required by the service provider at time t is calculated as:

$$\dot{W}_{\text{reg}} = \dot{W}_{\text{base}}(t) + \dot{W}_{\text{FCR-N,cap}} \cdot y(t) \tag{4-4}$$

The value $\dot{W}_{\text{base}}(t)$ is the scheduled power consumption or production, based on the traded energy in MWh/h at the day ahead spot market or alternatively at the intra-day market. $\dot{W}_{FCR-N,cap}$ is the power capacity contracted for FCR-N, and is constant over the hour *h*. Despite FCR-N being a power service, it involves an electric energy uptake or delivery by the service providing unit, as the frequency can be too high or too low for continuous hours, representing a higher or lower electricity production compared to the consumption, respectively. This energy content or energy bias of the frequency is calculated by the TSO by integrating the frequency deviations for each hour. The normalised energy bias of hour *n*, $e_{\text{bias,n}}$ is calculated with a sample rate Δt of one second and the number of samples per hour is N = 3600 [207].

$$e_{\text{bias},n} = \frac{1}{N} \sum_{t=(n-1)\cdot N+1}^{n\cdot N} y(t) \cdot \Delta t \tag{4-5}$$

Considering demand side service providers, a negative energy content means that the service provider has been a net energy provider to the power system and is compensated with the price of the upwards regulation power price [54], which is equal or higher than the spot price. A positive energy content means that the service provider will have consumed more energy than scheduled, and has to pay the price for downwards regulation power for the imbalance to the transmission system operator (TSO). This is equal or lower than the spot market price. Since the frequency deviations in the long term should ideally be equal to zero, i.e. the energy bias equals out, the use of upwards and downwards regulation power prices reduces the cost of delivering the service, but the majority of revenues for service providers come from the capacity payment.

4.2.2.2 Quality of frequency regulation provision

As described in section 4.2.2.1, the required relation between the frequency deviation and the load adaption is linear. The ideal normalised response, calculated according to equation (4-4), is depicted in Figure 4-3.

This response may however only be reached if the service providing units are able to adapt the load according to the frequency deviation instantaneously without delay, i.e. if they reach steady-state instantaneously. This is not possible for real plants as measurements, communication, actuation and the reaction of the system will result in a slight delay. Accordingly, the power response will generally deviate from the ideal response.

The actually measured normalised power response curve can give information about how well the service-providing unit is able to adapt to the frequency. It was tested, how well the proposed unit combinations were able to meet the requirement of a linear response, by comparing the resulting normalised power response from frequency-controlled operation with the ideal normalised power response.

The normalised power response curve for the heat pump operation alone was calculated using the dynamic model of the heat pump, presented in section 3. This was done, by following the ideal power response to a given frequency deviation pattern with the dynamic heat pump model. The latter was done to observe the behaviour of the heat pump itself, while the behaviour of the electric motor and frequency converter were not modelled and studied. Based on a given frequency pattern for a two hours period [208], two different operation strategies were studied. For the first one, the power uptake

corresponding to the frequency pattern was given as input to the dynamic heat pump model and the reaction was simulated. For the second one, the slowest possible response was calculated and given as input for the power uptake set value to the heat pump. For both cases, it was assumed that the service was provided by the heat pump alone, i.e. the default power uptake was 175 kW (70 % load) and the heat pump could supply a maximum of 75 kW (30 % load) upwards and downwards regulation. The normalised power response curve for the electric vehicles was determined experimentally as described in detail in [P4]. To determine the response of the combined system of heat pump and electric vehicles, the required offset energy pattern was determined from the electric vehicle model for a given frequency pattern. The same frequency pattern was used to redo the experiment, while simulating that the required baseline power shift when the state-of-charge (SOC) runs out of the allowable range, could be provided by the heat pump.

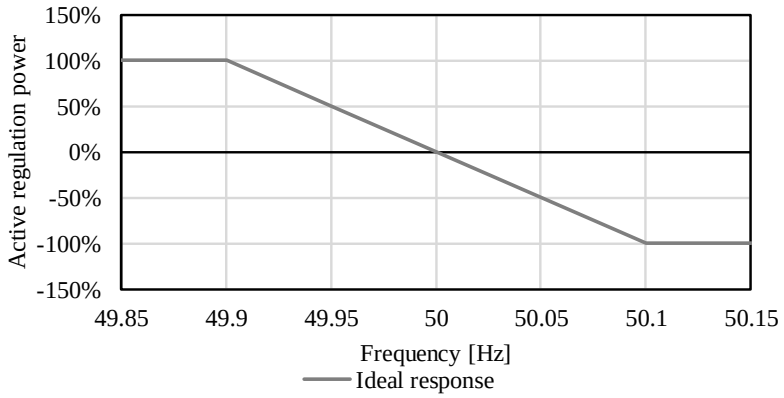

Figure 4-3 Ideal normalised response of the frequency regulation providing unit to frequency deviations. The active regulation power is defined positive for up-regulation, i.e. load reduction of demand side units.

4.2.3 Heat pump system model

The model of the system shown in Figure 4-1 was formulated in Modelica [173] and implemented in Dymola [209]. It contained seven main component models representing a heat pump, an electric boiler, a stratified storage tank, two pumps, a lumped heat demand model, two three-way-valves and a central control unit. The models for the heat demand, the heat pump, the control unit and stratified storage tank are further described below. All models were based on energy, mass and momentum balance equations. When not indicated differently, pressure losses were neglected. The pump model was adapted from an existing model from the TIL library [178]. The pump efficiency was implemented as a quadratic function and parametrised using manufacturer's data [210,211].

4.2.3.1 Heat demand model

The heat demand model was a simplified model of the demand side of the district heating system. It included the accumulated demand of all buildings supplied by the network and the heat losses in the distribution system. The demand was measured demand data of the system on hourly basis for the year 2018 [212]. Based on the demand data, the required mass flow for each time step was calculated and was used to control the district heating pump supplying the network. It was assumed that the building substations were able to cool the district heating water to a constant return temperature of 34 °C (Stream 9 Figure 4-1). The actually supplied heat was calculated from an energy balance in the model. The system pressure loss Δp was calculated for the longest pipeline from heat pump to substation from the known pipe geometries and the water mass flow, using equation (4-6).

$$\Delta p = \sum_i \lambda_i \cdot \frac{L_i}{D_i} \cdot \frac{\rho}{2} \cdot \left(\frac{\dot{m}_i}{\rho \cdot \pi \cdot \frac{D_i^2}{4}} \right)^2 \tag{4-6}$$

Here, i denotes the different pipe elements, λ_i is the friction factor, which was $\lambda_i = 64/Re$ for laminar flow and calculated according to *Colebrook*'s formula (e.g. [213]) for turbulent flow assuming hydraulically rough pipes. L_i is the length of the pipe element, D_i is the diameter, ρ is the water density, which was assumed to be the water density behind the electric heater, and $\dot{m}_i$ is the water mass flow. The pressure loss in the substation was neglected.

4.2.3.2 Heat pump model

The heat pump was a two-stage ammonia heat pump with open intercooler, as the one presented in Chapter 3. It was equipped with two variable speed drive piston compressors. Brackish groundwater at constantly 10.5 °C was the heat source. It was assumed that the groundwater could be cooled to 4 °C before being discharged into the sea. The heat pump was modelled as a black box. This was necessary, since the model was simulated for a whole year, i.e. 31,536,000 seconds, and a detailed dynamic model, as the one presented in chapter 3, would be too computationally demanding.
A dynamic energy balance for the heat pump was used to describe the model.

$$\frac{dQ_{HP}}{dt} = \dot{Q}_{eva} + \dot{W}_{HP} + \dot{Q}_{con} \tag{4-7}$$

The term $\frac{\mathrm{dQ_{HP}}}{\mathrm{dt}}$ represents the heat stored due to inertia in the heat pump. $\dot{Q}_{\mathrm{eva}}$ is the heat flow into the evaporator, $\dot{W}_{\mathrm{HP}}$ is the power uptake of both compressors and $\dot{Q}_{\mathrm{con}}$ represents the condenser heat load. In the black-box model the storage was determined as a function of the available heat output from the condenser to represent the dynamic start-up and load changing characteristics of the heat pump. Full heat production is not available during start-up compared to a theoretic instantaneous start-up, and heat will still be rejected after shut-off of the compressor (Figure 4-4). It was assumed that the dynamic heat load at the condenser follows a first order characteristic, which was included as function for the actual heat load $\dot{Q}_{\mathrm{con}}$ into the model. Other dynamic effects within the heat pump itself were neglected for the yearly calculation.

$$\frac{d\dot{Q}_{\mathrm{con}}}{dt} = \begin{cases} k_1 \cdot \left(\dot{Q}_{\mathrm{con,ss}} - \dot{Q}_{\mathrm{con}}\right) & \text{for } \left(\dot{Q}_{\mathrm{con,ss}} - \dot{Q}_{\mathrm{con}}\right) > 0 \ (\mathrm{ramp-up}) \\ k_2 \cdot \left(\dot{Q}_{\mathrm{con,ss}} - \dot{Q}_{\mathrm{con}}\right) & \text{for } \left(\dot{Q}_{\mathrm{con,ss}} - \dot{Q}_{\mathrm{con}}\right) \leq 0 \ (\mathrm{ramp-down}) \end{cases} \tag{4-8}$$

The parameters $k_1 = k_2 = 0.064$ were chosen to represent a start-up time (0 % to 100 % load) of five minutes, according to the times measured on the real plant, presented in section 3.3.1. The term $\dot{Q}_{\mathrm{con,ss}}$ represents the condenser heat load in steady state, which was calculated from the coefficient of performance (COP) in steady state. The COP was given as a function of the load and the sink and source temperatures. In this specific case, the source outlet temperature is directly correlated with the heat pump load, due to the control strategy in place and that the district heating return temperature and the source inlet temperature were assumed to be constant. Thus, the COP function could be simplified to only be dependent on the load and the district heating forward temperature. This function was obtained from the detailed dynamic model of the heat pump, described in section 3 and validated against measured COP data of the base-case, as presented in Figure 4-5.

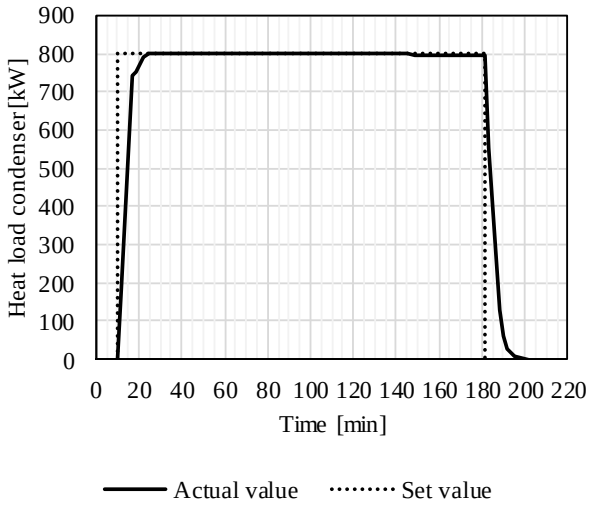

Figure 4-4 Steady state set value and actual value of condenser heat load for start-up and shut-down

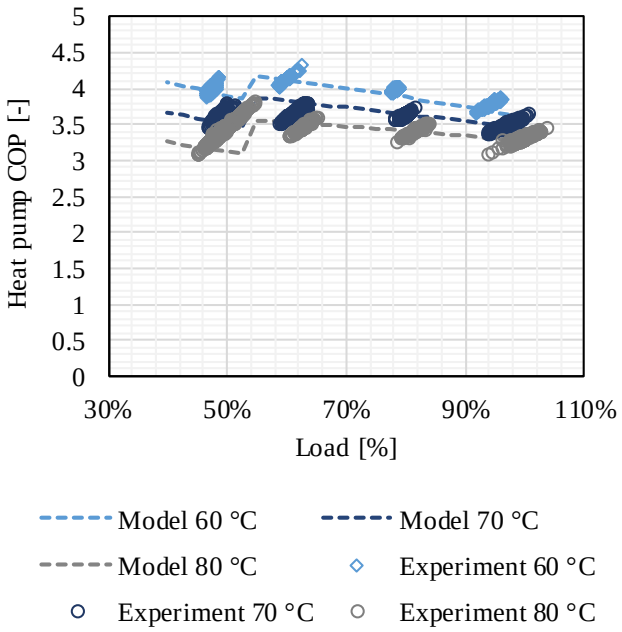

Figure 4-5 COP curves for 60 °C, 70 °C and 80 °C from the function used in the simplified model compared to experimental data, the step in the model function occurs assuming that half of the compressor cylinders are decoupled at 55 % load

The resulting actual COP was calculated from the condenser heat load and the power uptake of the heat pump compressor.

$$\mathrm{COP} = \frac{\dot{Q}_{\mathrm{con}}}{\dot{W}_{\mathrm{HP}}} \tag{4-9}$$

The model further included energy, mass and momentum balance (no pressure loss) equations for the evaporator and the condenser. The heat pump was controlled according to the desired power uptake for the different operation strategies.

4.2.3.3 Control unit

The described system was controlled using a central control unit, which contained the algorithm according to which the heat pump, the three-way-valve, the pumps and the electric heater were controlled. Via the three-way-valve at the top of the stratified storage tank, the charging and discharging

of the tank was controlled by setting a value for the ratio between the flow into the storage tank and the flow from the heat pump. The pumps were controlled to deliver the necessary mass flow to the heat demand model and the heat pump, respectively. The electric boiler heated the district heating supply flow to the required supply temperature if the temperature supplied by the storage or heat pump was too low. The required supply temperature was assumed to be 70 °C throughout the year. This was a simplification, as weather compensation would be required in the real system.
The model does not include the prices for regulating power, but aims at quantifying the true cost of providing this. The results may be compared to the actual prices in the regulating market.
The power uptake schedule for the spot market optimised operation, was given by the utility company. For all cases, where frequency regulation was delivered, the power uptake schedule for the different operation modes was calculated from historic frequency data in the DK2 grid for 2018 [208], as explained in section 4.2.2.1 and 4.2.2.2. For the yearly calculation, the power input values were given with a resolution of one hour. This was obtained from integrating the energy content of the frequency deviation during the respective hour, resulting in an average hourly load of the heat pump. For those hours, where no frequency regulation was provided, but heat demand needed to be covered, the heat pump operated at default load, i.e. 70 % or 175 kW power uptake.

4.2.3.4 Stratified storage tank

The stratified storage tank was modelled using a one dimensional discretisation [214] (Figure 4-8). The tank was divided into 100 layers from top to bottom. For each layer dynamic mass and energy balances were solved. It was assumed that the fluid inside each layer was ideally mixed and thus had constant properties. Heat losses to the environment and between layers were considered. Pressure differences across the tank were neglected as well as increased mixing between the layers during charging and discharging. The minimum and maximum amount of hot water was limited by the inlet design and was assumed to be 1/12 and 11/12 of the total stored mass, respectively.

4.2.4 Combined frequency regulation service by electric vehicles and heat pump system

4.2.4.1 Case description electric vehicles

The feasibility of combined frequency regulation delivery from a pool of fast regulating electric vehicles and the large-scale heat pump system described above was assessed for the delivery of FCR-N frequency containment reserve.
The idea is that the fast regulating vehicle-to-grid (V2G) ready batteries provide frequency regulation, by adapting the load quickly. The energy content of the frequency deviation is however covered by the heat pump, such that the batteries can be controlled to always be fully charged at the end of the grid connected period despite delivering the maximum capacity for frequency regulation. This combination allows exploiting the strength of both systems, i.e. the ability of V2G batteries to regulate quickly and the large energy storage capacity of the heat pump system. For this strategy, the heat pump is not required to be able to ramp quick enough for the supplied service. Thereby, it may be interesting for primary frequency regulation services with shorter regulation times as well. The aim of this analysis was to test, whether a combined service would result in synergy effects, i.e. reduced heat cost for the customers of the heat pump system and increased income from frequency regulation service provision from the electric vehicles.
In practice, the proposed combined operation would mean that the EVs regulated according to the grid frequency during the complete service provision period. The load of the heat pump was adapted once an hour according to the SOC of the EV batteries. If the SOC fell below the allowed minimum level, the heat pump was set to take up less power, such that the EVs could take up more power and thus charge. If the SOC increased above the maximum level, the heat pump load was increased, such that the batteries discharged. This internal redistribution of load does not affect the overall energy balance of

the combined system towards the electricity grid. Recently, a similar set-up has been proposed for the application of an integrated home energy system in [215].
It was assumed that the utility company owns the electric vehicles, and that these are available to deliver frequency regulation outside normal working hours, i.e. from 16.00 to 7.00. The electric vehicles where connected with a bidirectional V2G charger that can charge up to 10 kW from the grid or discharge up to 9 kW to the grid [216]. A similar case was demonstrated in the municipality of Bornholm [217] and by the utility company Frederiksberg Forsyning, Denmark [218].
The EVs were assumed to all have a battery capacity of 40 kWh. The daily electricity consumption for driving was assumed to be distributed according to a Gaussian distribution. The mean value was chosen equal to the average consumption of privately owned vehicles in Denmark, as corresponding data for the utility owned cars was missing, i.e. 9 kWh corresponding to 45 km per day [219] with a standard deviation of 1 kWh. Every EV should therefore have a high enough SOC at the end of the grid-connected period to ensure enough capacity for a higher driving consumption.

4.2.4.2 Modelling approach

Figure 4-6 gives an overview of the different models and calculation steps conducted to assess the feasibility of a combined frequency regulation service from EVs and the heat pump. To assess the performance of the system, the availability of the heat pump for the combined service was determined from the heat demand of the customers in the district heating grid. The availability of the heat pump was an input to the SOC model, which was used to calculate the required power response from the combined system and for electric vehicles delivering FCR-N alone, the corresponding SOC development and the actually required offset power from the heat pump for one year of operation. This model is further described below in section 4.2.4.4. The calculated operation schedule for the heat pump was given to the model described above in section 4.2.3. Finally, the economic performance of the combined system was evaluated in the same way as for the other operation modes, as described in section 4.2.5.

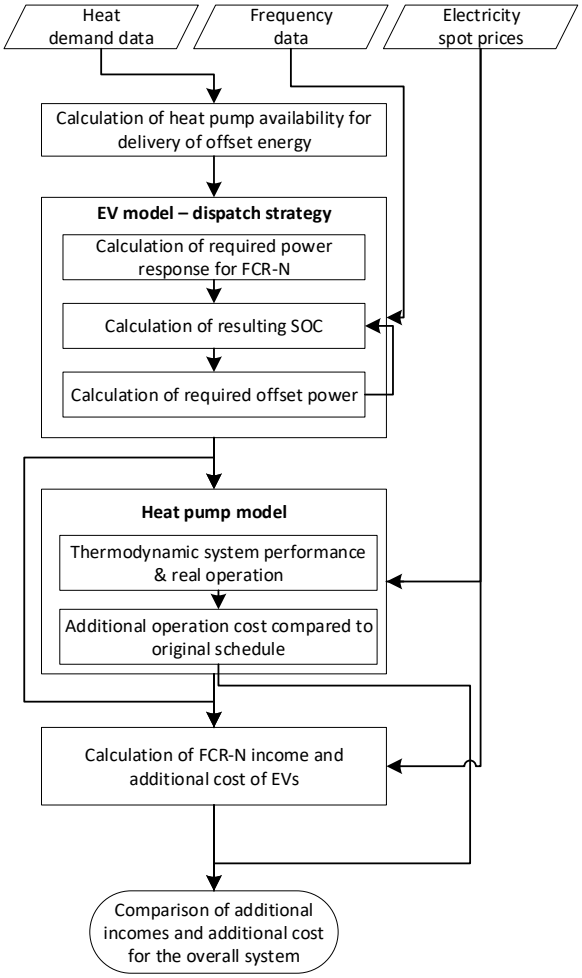

Figure 4-6 Overview of the workflow, including inputs, models and interaction between these

4.2.4.3 Determination of available heat pump offset operation

The available time per day t_{offset}, where the heat pump can be available to offset the EV electricity consumption is limited by the heat demand, the heat storage capacity and the minimum and maximum power uptake, which depend on the heat pump COP. The minimum and maximum power uptake was calculated from the given heat demand using equation (4-9), taking into account that the COP varies with the DH forward temperature. Considering that the frequency deviation and corresponding energy content cannot be known, when the heat pump has to bid the available capacity on the market, a conservative estimation is used. The minimum available hours can be calculated assuming that the heat pump is constantly required to regulate to full load, as in this case the heat storage would be filled most quickly. It was assumed that the minimum load is fixed to 40 % of full load for all forward temperatures and that the heat pump should be available for offsetting the EV operation every night. Accordingly, the maximum heat produced during offset operation needs to be less than or equal to the heat demand of the respective day, as a higher heat production would reduce the available offset operation time of the following day. Further, the heat produced during the offset operation cannot be higher than the sum of the demand during these hours and the available storage capacity. The corresponding minimum number of offset hours was rounded downwards to full hours.

$$t_{\text{offset}} \leq \min\left(\frac{Q_{\text{Demand,day}}}{\dot{Q}_{\text{fullload}}}, \frac{Q_{\text{cap,storage}} - \sum_{i=0}^{t} Q_{\text{demand,i}}}{\dot{Q}_{\text{fullload}}}\right) \quad (4\text{-}10)$$

Due to the limitations of the storage capacity within the district heating system and to avoid using the back-up electricity boiler for frequency regulation, which would results in a reduced system COP, the

heat pump was set to operate at the intermediate load between minimum part load and full load, that is:

$$\dot{W}_{\mathrm{set,nom}} = (\dot{W}_{\mathrm{min}} + \dot{W}_{\mathrm{fullload}})/2 = 175\ \mathrm{kW} \quad (4\text{-}11)$$

The load is changed upwards or downwards when a load shift is required by the SOC of the vehicle batteries. This results in a maximum absolute load shift of 75 kW, which is equivalent to a correction power of 3 kW up or down for 25 vehicles.

4.2.4.4 Electric vehicle model – Dispatch strategy

In the following a short overview of the electric vehicle and dispatch model is given. For a more detailed explanation, the reader is referred to [P4].

The electric vehicle model calculated the SOC of each EV battery during grid connected hours. The future frequency deviations cannot be predicted and thereby the future energy bias is not known. Therefore, the aggregator can only react to the current SOC. The proposed dispatching strategy was to change the baseline power uptake from zero to a negative or positive value when the SOC reaches an upper or lower threshold. Since the energy content per vehicle of the frequency deviation could be up to 6 kWh during one hour and the balancing power could only shift up to 3 kWh during one hour, it could take several hours before the SOC started moving in the wanted direction. It was therefore necessary to change the baseline before SOC reaches the actual physical limits of the battery.

The baseline power could be changed by the battery itself or by an additional unit, such as the heat pump. If the EV itself provided the baseline power shift, it meant that the EV was delivering or receiving energy to or from the grid over time and accordingly the SOC decreased or increased. The sum of the available offset capacity $\dot{W}_{\mathrm{EV,base}}$ and the bid power capacity $\dot{W}_{\mathrm{Cap}}$ could not be higher than the power capacity of the charger, i.e. $\dot{W}_{\mathrm{EV,base}} + \dot{W}_{\mathrm{Cap}} \leq 9\ \mathrm{kW}$. In a previous study it was shown, that reserving 3 kW to allow for offsetting the baseline power and bidding a 6 kW per EV for FCR-N, allows to maintain the SOC in the allowable range over the whole regulation period [220]. If the SOC increased above the upper limit, $\dot{W}_{\mathrm{EV,base}}$ was set to 3 kW of discharging, while if the SOC fell below the lower limit, $\dot{W}_{\mathrm{EV,base}}$ was set to 4 kW of charging. This was caused by the asymmetric characteristics of the tested charger that could charge with 10 kW and only discharge with 9 kW, so when 6 kW was contracted for FCR-N, there was 4 kW left for charging and 3 kW for discharging.

In case an external unit like the heat pump was used to shift the baseline power, the heat pump load was adapted, such that it took up the energy bias of the frequency deviation (equation 4-5), while the electric vehicles could still operate around a baseline power of zero. This allowed to bid the whole charger capacity, i.e. 9 kW, for FCR-N delivery. The operation principle of combined FCR-N delivery from the EVs and the heat pump is exemplified in Figure 4-7 for a period of 14 hours. When the required power response of the 25 electric vehicles resulted in surpassing of the SOC constraints, the base line power consumption of the electric vehicles was shifted. This shift was outbalanced by the heat pump that delivered offset energy by adapting its power uptake. Note that the SOC limits depicted here were arbitrarily chosen to exemplify the principle and do not represent the actually required levels. The number of hours that the heat pump could consume power during each night depended on the heat consumption of the area, i.e. it varied over the year. The FCR-N capacity was therefore $\dot{W}_{\mathrm{FCR-N,cap}} = 6\ \mathrm{kW} + \dot{W}_{\mathrm{HP,cap}}$, where $\dot{W}_{\mathrm{HP,cap}}$ was 0 kW when the heat pump was not available to shift the base line power and otherwise ±3 kW per vehicle.

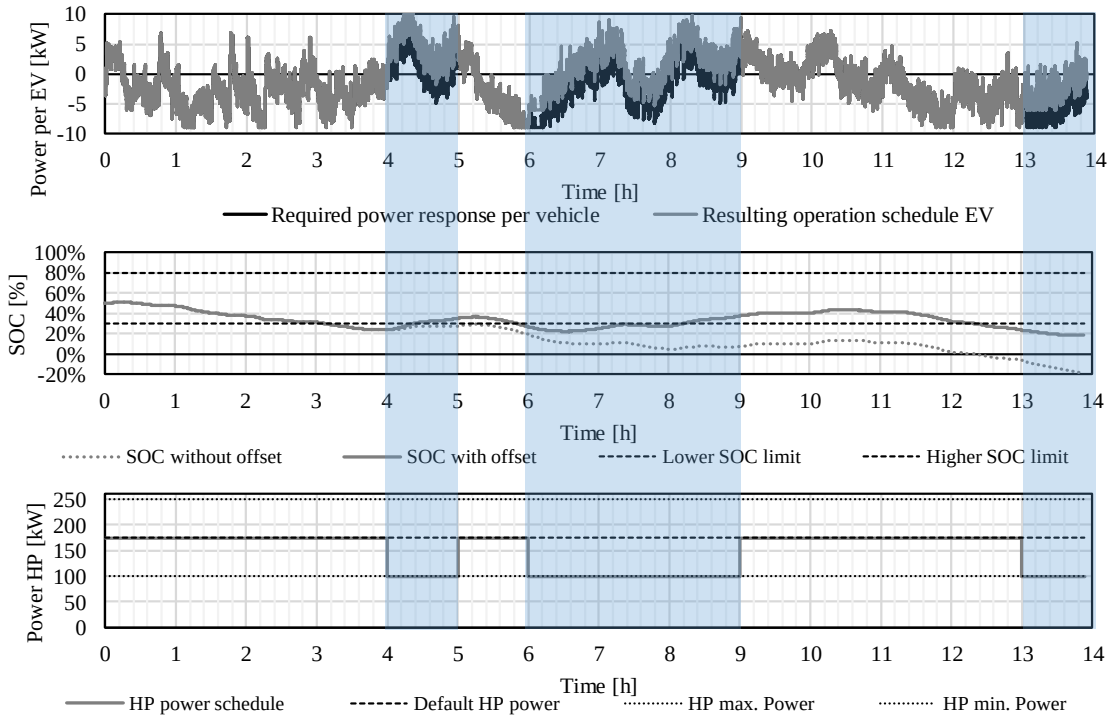

Figure 4-7 Principle of combined provision of FCR-N from EV and heat pump. Blue areas denote the time, where the power base line for the EV is shifted (upper diagram) as a reaction to the SOC surpassing the lower constraint (middle diagram) and the corresponding power uptake of the heat pump (lower diagram).

4.2.5 Economic evaluation of FCR-N provision

4.2.5.1 Calculation of heat production cost

The combined provision of frequency regulation can only be feasible if the additional cost of both the heat pump system and the electric vehicles can be covered. The additional income would reduce the heat generation cost. Therefore, the heat cost was chosen as decisive parameter. The economic performance of the heat pump was evaluated using three different measures. The first one was the fuel cost of the system, i.e. the weighted average electricity price over the simulated one-year period. It was calculated as the overall electricity cost divided by the overall electricity consumption in the same period.

$$\bar{c}_{\mathrm{el}} = \frac{C_{\mathrm{el,tot}}}{W_{\mathrm{tot}}} \tag{4-12}$$

The second one is the operational specific heat cost, which was calculated as the total electricity cost for one year divided by the total amount of heat delivered to the district heating customers.

$$\bar{c}_{\mathrm{heat,el}} = \frac{C_{\mathrm{el,tot}}}{Q_{\mathrm{tot}}} \tag{4-13}$$

The third measure is the total specific heat cost. To calculate the total specific heat cost, the obtained total yearly cost was divided by the overall amount of heat delivered per year to the customers. The total yearly heat generation cost included fuel cost, investment cost, capital cost and operation and maintenance cost of the components in the system. It was calculated using the model, as described in detail in section 4.2.6.2.

$$\bar{c}_{\mathrm{heat,tot}} = \frac{C_{\mathrm{heat,tot}}}{Q_{\mathrm{tot}}} \tag{4-14}$$

The electricity price used was the historic electricity spot market prices for Eastern Denmark for the year 2018 [221] including taxes and tariffs, as summarised in Table 4-2. The expected values for 2022

are given, too, as the public service obligation (PSO) fee is being phased out before 2022 and the energy tax on electricity is reduced, according to a political agreement.

Table 4-2 Taxes and tariffs for heat production from large-scale heat pumps in Denmark for 2018 and 2022

Type	Unit	2018	2022
PSO-tariff	€/MWh	13.58	0.00
TSO-tariff	€/MWh	5.11	5.11
System tariff	€/MWh	5.65	5.65
Reduced energy tax	€/MWh	34.54	20.83
Balance tariff	€/MWh	0.13	0.13
Distribution price (2018 average value)	€/MWh	15.73	15.73

4.2.5.2 Calculation of income from FCR-N provision

To calculate the income from capacity payments, historic FCR-N capacity payment prices for 2018 were used [221]. The yearly performance of the heat pump system for all five operation schedules was calculated using the heat pump system model. The difference in specific heat cost (including the additional cost of battery operation for the EV+HP case) was used to define the minimum capacity price that the system could bid into the FCR-N market. To calculate the income from capacity payments, a simple bidding strategy was applied. It was based on the assumption that the expected FCR-N capacity price in one specific hour was similar to the price in the same hour of the day before. It was assumed that in all hours, where the service could be provided the historic average value could be gained. This was a conservative assumption, as it might be possible to bid higher than average prices in the market. The same bidding strategy was assumed for all operation modes.

4.2.6 Dynamic exergoeconomic analysis

The provision of frequency regulation may result in a changed electricity use. At the same time, an additional income from frequency regulation services may be generated. In order to understand in detail, why the performance differs for the different operation modes, where losses occur and what these losses cost, the method of an exergoeconomic analysis was extended within this work to a dynamic exergoeconomic analysis of the system.

The method was further extended to assess the performance of a conversion unit in an integrated energy system, supplying a primary service (here: heat) and an ancillary service to a neighbouring energy sector. The method of exergoeconomic analysis is a combination of an exergy analysis and economic principles and is used to obtain information about how to design and operate energy conversion systems in a cost-effective way [222]. It enables the allocation of cost to multiple products of any energy conversion plant based on a framework that consistently connects economics and thermodynamics. Usually, an exergoeconomic analysis is conducted assuming steady state processes. A similar approach to the one chosen here, was described by Sayadi et al. [223], who conducted a dynamic exergy and exergoeconomic analysis for a building envelope. Sangi et al. [224] presented an approach to conduct a quasi-dynamic exergoeconomic analysis by analysing the result of each time step for a dynamic simulation of a building heating system.

In this study, both the time dependency of occurring losses was assessed and an approach based on integration over time was proposed to include the time dependent behaviour and non-concurrent loss effects in the yearly analysis. The results of the dynamic model, including the calculation of exergy and cost streams, allowed a detailed insight with regard to when losses occur and why. Further, the method was extended by the definition of exergy fuel and exergy product during dynamic operation for all components and a way to allocate cost to two services, heat and frequency regulation, based on the exergoeconomic method was proposed.

4.2.6.1 Exergy analysis

As reference state, the groundwater temperature (T_0 = 10.5 °C) at atmospheric pressure (p_0 = 1.013 bar) was chosen. The groundwater temperature was assumed to be constant throughout the year. All material streams were assumed to be water and no reactions occured at any place in the system. So, the chemical exergy would be equal for all streams and could be neglected [222].
To conduct the exergy analysis of the system, balance equations were formulated for all components. The balance equation for a general control volume can be formulated as

$$\frac{dE}{dt} = \sum_i \dot{m}_i \cdot e_i + \sum_j \dot{E}_{Q,j} + \sum_l \dot{W}_l - \dot{E}_L - \dot{E}_D \tag{4-15}$$

where *E* is the exergy content of the control volume. The first sum denotes the exergy content of the material streams entering and exiting the control volume which is calculated as the product of mass flow $\dot{m}$ and specific exergy e. The second sum is the sum of all exergy flows related to heat flows $\dot{E}_{Q,j}$ and the third sum considers power flows $\dot{W}_l$. $\dot{E}_L$ is the exergy loss to the environment and $\dot{E}_D$ denotes the exergy destruction within the control volume. All entering flows are accounted as positive by sign convention.
For the dynamic exergy analysis, exergy fuel and product were defined for all components (Table 4-3). The exergy efficiency of every component was calculated according to:

$$\epsilon_k = \frac{\dot{E}_{P,k}}{\dot{E}_{F,k}} \tag{4-16}$$

Heat pump
The exergy efficiency of the heat pump was defined as the increase of exergy of the district heating water in the condenser over the power input into the compressor. As the groundwater was cooled down from the reference state temperature in the evaporator, its exergy content increased. However, the cold stream was not a useful product in this case, as it was discharged into the environment and represented an exergy loss of the system. A cost can be assigned to the exergy loss by assuming that the exergy loss is covered through the supply of a corresponding amount of fuel (auxiliary equation) [225].

Three-way-valve
The three-way-valve controlled the mass flow to and from the stratified storage tank. The exergy fuel and product were different during charging or discharging of the tank. The purpose of mixing in the three-way-valve was to vary between two different heat sources (the heat pump and the storage) and not to heat up the stream from the storage using the stream from the heat pump. Thus the presented definition of exergy fuel and product is chosen [222].

Stratified storage tank
To define the exergy fuel and product of the stratified storage tank, the tank was divided into a hot and a cold control volume (Figure 4-8). It was assumed that the purpose of the tank is to store hot water, and that the cold water is only used to fill up the tank volume that is not occupied by the hot water. Both control volumes were variable in size and additional mass balances for the control volumes were needed.

$$m_{\mathrm{hot}} + m_{\mathrm{cold}} = \bar{\rho} \cdot V_{\mathrm{storage}} \tag{4-17}$$

$$m_{\mathrm{hot}} = \frac{N_{\mathrm{hot}}}{N} \cdot \bar{\rho} \cdot V_{\mathrm{storage}} \tag{4-18}$$

$m_{\mathrm{hot}}, m_{\mathrm{cold}}$ denote the mass of the hot and cold control volumes, respectively. N_{hot} is the number of layers with hot fluid which are defined as all layers with a temperature above 60 °C, $\bar{\rho}$ is the mean water density in the storage and V_{storage} is the overall volume of the storage tank. Calculating m_{hot} in the presented way, has the advantage that the mass flow from the hot to the cold volume due to decrease in temperature can be easily accounted for.

Table 4-3 Exergy fuel and -product and specific cost per unit of exergy fuel and product for the components used in the case study. Charging and discharging refer to charging/discharging of the storage tank. When there is no flow in or out of the tank, the equations for discharging are valid.

	Exergy fuel $\dot{E}_{F,i}$ Specific cost per unit of exergy fuel c_F		Exergy product $\dot{E}_{P,i}$ Specific cost per unit of exergy product c_P		Auxiliary equations
Heat pump	$\dot{E}_F = \begin{cases} \dot{W}_{13} + \frac{dE_{HP}}{dt} \\ \dot{W}_{13} \end{cases}$	: if $\frac{dE_{HP}}{dt} < 0$: else	$\dot{E}_P = \begin{cases} \dot{E}_4 - \dot{E}_{11} + \frac{dE_{HP}}{dt} \\ \dot{E}_4 - \dot{E}_{11} \end{cases}$	: if $\frac{dE_{HP}}{dt} > 0$: else	
	$c_F = c_{\mathrm{el}}$		$c_P = \frac{\dot{C}_4 - \dot{C}_{11}}{\dot{E}_4 - \dot{E}_{11}}$		$c_3 = c_F$
3-way-valve	$\dot{E}_F = \begin{cases} \dot{E}_4 \\ \dot{E}_4 + \dot{E}_5 \end{cases}$	: charging : discharging	$\dot{E}_P = \begin{cases} \dot{E}_5 + \dot{E}_6 \\ \dot{E}_6 \end{cases}$	: charging : discharging	
	$c_F = \begin{cases} \frac{\dot{C}_4}{\dot{E}_4} \\ \frac{\dot{C}_4 + \dot{C}_5}{\dot{E}_4 + \dot{E}_5} \end{cases}$	: charging : discharging	$c_P = \begin{cases} \frac{\dot{C}_5 + \dot{C}_6}{\dot{E}_5 + \dot{E}_6} \\ \frac{\dot{C}_6}{\dot{E}_6} \end{cases}$	: charging : discharging	$c_5 = c_6$ (for charging)
DH Pump	$\dot{E}_F = \dot{W}_{14}$		$\dot{E}_P = \dot{E}_7 - \dot{E}_6$		
	$c_F = c_{\mathrm{el}}$		$c_P = \frac{\dot{C}_7 - \dot{C}_6}{\dot{E}_7 - \dot{E}_6}$		
GW Pump	$\dot{E}_F = \dot{W}_{12}$		$\dot{E}_P = \dot{E}_2 - \dot{E}_1$		
	$c_F = c_{\mathrm{el}}$		$c_P = \frac{\dot{C}_2 - \dot{C}_1}{\dot{E}_2 - \dot{E}_1}$		
Electric heater	$\dot{E}_F = \dot{W}_{15}$		$\dot{E}_P = \dot{E}_8 - \dot{E}_7$		
	$c_F = c_{\mathrm{el}}$		$c_P = \frac{\dot{C}_8 - \dot{C}_7}{\dot{E}_8 - \dot{E}_7}$		
Stratified storage tank	$\dot{E}_F = \begin{cases} \dot{E}_5 \\ \frac{dE_{\mathrm{hot}}}{dt} \end{cases}$	: charging : discharging	$\dot{E}_P = \begin{cases} \frac{dE_{\mathrm{hot}}}{dt} \\ \dot{E}_5 \end{cases}$	: charging : discharging	
	$c_F = \begin{cases} \dot{C}_5 \\ \frac{dC_{\mathrm{hot}}}{dt} \end{cases}$	: charging : discharging	$c_P = \begin{cases} \frac{dC_{\mathrm{hot}}}{dt} \\ \dot{C}_5 \end{cases}$	: charging : discharging	$c_{10} = \frac{C_{\mathrm{cold}}}{E_{\mathrm{cold}}}$ (for charging)

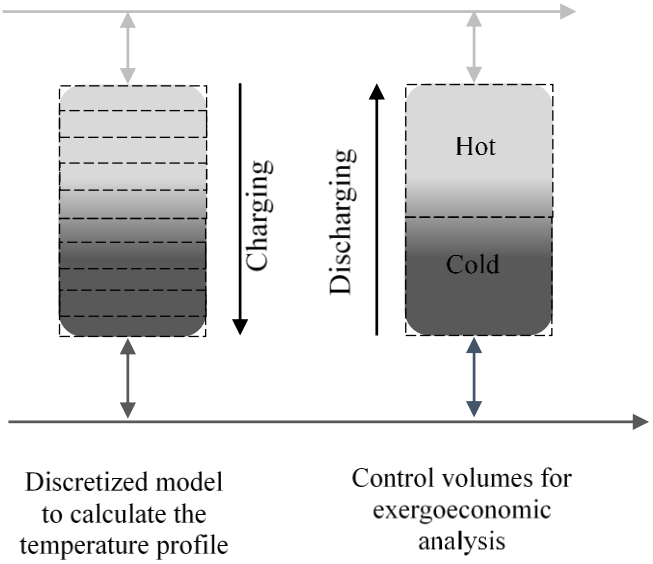

Figure 4-8 One-dimensional discretisation of storage tank and division into hot and cold control volume

The exergy fuel during charging was defined as the exergy of the hot water entering at the top of the tank and the product was the increase in stored exergy inside the hot control volume of the tank. The amount of stored exergy was calculated for both control volumes as

$$\frac{d(E_{hot} + E_{cold})}{dt} = \dot{m}_5 \cdot e_5 - \dot{m}_{10} \cdot e_{10} - \dot{E}_D \tag{4-19}$$

$$E_{\mathrm{hot}} = \sum_{n=1}^{N_{\mathrm{hot}}} (m_n \cdot e_n) \tag{4-20}$$

where E_{hot}, E_{cold} denote the exergy stored in the hot and cold volume respectively. m_n is the mass and e_n the specific exergy of layer n. The volume work due to variation of the control volume size was found to be small compared to the exergy of stored heat and was neglected. The heat loss from the storage is accounted for as exergy destruction $\dot{E}_D$. Assuming that the water in the tank behaves as an ideal liquid, the specific exergy e_n for every discretisation layer can be calculated from temperatures obtained from the energy balances for each control volume [226].

$$e_n = c_{p,\mathrm{H_2O}} \cdot (T_n - T_0) - T_0 \cdot c_{p,\mathrm{H_2O}} \cdot \ln\left(\frac{T_n}{T_0}\right) \tag{4-21}$$

An overall exergy efficiency for the storage was calculated as the ratio of the integrals of the output from - and the input into the hot control volume.

$$\epsilon_{storage,tot} = \frac{\int \dot{E}_{5,out}\, dt}{\int \dot{E}_{5,in}\, dt} \tag{4-22}$$

System exergy efficiency

The exergy efficiency of the overall system for every time step had to take the storage of exergy in the storage tank into consideration. During charging, the exergy stream into the storage represented a product of the system, whereas during discharging the exergy stream out of the tank was a fuel to the overall system:

$$\epsilon_{\text{system}} = \begin{cases} \dfrac{\dot{E}_{\text{heat}} + \dfrac{d(E_{\text{hot}} + dE_{cold})}{dt}}{\sum_k \dot{W}_k} & : \text{if charging} \\ \dfrac{\dot{E}_{\text{heat}}}{\sum_k \dot{W}_k + \left|\dfrac{dE_{\text{hot}} + dE_{cold}}{dt}\right|} & : \text{if discharging} \end{cases} \quad (4\text{-}23)$$

The annual mean exergy efficiency was calculated according to the following equation.

$$\epsilon_{\text{system,tot}} = \frac{E_{\text{heat}}}{\sum_k W_k} \quad (4\text{-}24)$$

E_{heat} denotes the overall amount of exergy of heat supplied per year and W_k is the overall amount of electric energy of component *k* per year.

4.2.6.2 Exergoeconomic analysis

Within an exergoeconomic analysis a cost is assigned to all exergy streams. This allows to determine the cost of exergy destruction in every component, which can give useful information about the sources of costs throughout the system and how they can be lowered [222].
In order to assign a cost to every exergy stream a dynamic cost balance for every component was set up.

$$\frac{dC}{dt} = \sum_i \dot{C}_i + \sum_k c_{\text{el}} \cdot \dot{W}_k + \dot{Z} \quad (4\text{-}25)$$

C denotes the cost that accumulates within the component, $\dot{C}_i$ is the cost streams associated with material streams, c_{el} is the electricity cost in the respective time step and $\dot{Z}$ denotes the levelised cost stream of the component. The cost stream of the component includes investment cost, capital cost, and operation and maintenance costs for the estimated lifetime of the respective component. It was calculated as described in [222]. However, the cost was not levelised to the full load hours per year but to the actual operation hours per year and $\dot{Z}$ was only considered when the respective component was in operation. The district heating network was existent and it was assumed that the operation and maintenance costs were the same for any kind of heat supplying system. Thus, the costs of the district heating network were neglected in the present work. The economic data used to calculate $\dot{Z}$ is summarised in Table 4-4 and Table 4-5. An average annual discount rate of 4 % and a nominal escalation rate of 2 % per year for operation and maintenance cost was assumed [227]. The assumed values for the first year of operation are given in Table 4-4.
The cost of electricity used in this study is historic spot market prices for Eastern Denmark 2018 from NordPool [221], including taxes and tariffs as presented in Table 4-2.

Table 4-4 Economic data case study

Unit	Capacity	Total capital investment [€]	Plant economic life[a]	Fixed O&M cost 1st year [€]	Source
Heat pump	800 kW	75,300	25	400	[152]
El. heater	200 kW	20,200	20	30	[152]
DH pump	2 · 16.7 kg/s	4,000	10	60	[210]
GW pump	2 · 44.3 kg/s	5,400	10	60	[210]
Storage tank	120 m³	4,200	40	90	[152]
Drilling		12,100	40	2,400	[153]

Table 4-5 Operation hours per year for all four tested operation modes

	Heat demand driven	Spot market optimised	FCR-N HP 5h/d	FCR-N HP max	FCR-N EV+ HP
Heat pump	4524	2787	3694	3072	3346
El. heater	3000	3000	3000	3000	3000
DH pump	8760	8760	8760	8760	8760
GW pump	4524	2787	3694	3072	3346
Storage tank	8760	8760	8760	8760	8760
Drilling	4524	2787	3694	3072	3346

4.2.6.3 Allocation of cost

The allocation of cost and additional income to both products of the heat pump system, i.e. heat supply and provision of demand flexibility, is a central question when operating energy conversion units in an integrated energy system. The characteristics of both products are different. Heat is an output from the system and so is the related heating service. Electricity is an input into the system, but the corresponding flexibility is a service provided by the system, see Figure 4-9. The cost of providing flexibility is not directly connected to the electricity stream and all extra cost will be reflected in the heat generation cost. However, as the source of cost difference was not the supply of heat but the additional exergy destruction due to the provision of flexibility, the cost should be allocated accordingly. The exergy destruction related to flexible operation does not only occur at the same time as the provision of regulation power. Thus, an integral approach to determine the cost related to flexible operation was required.

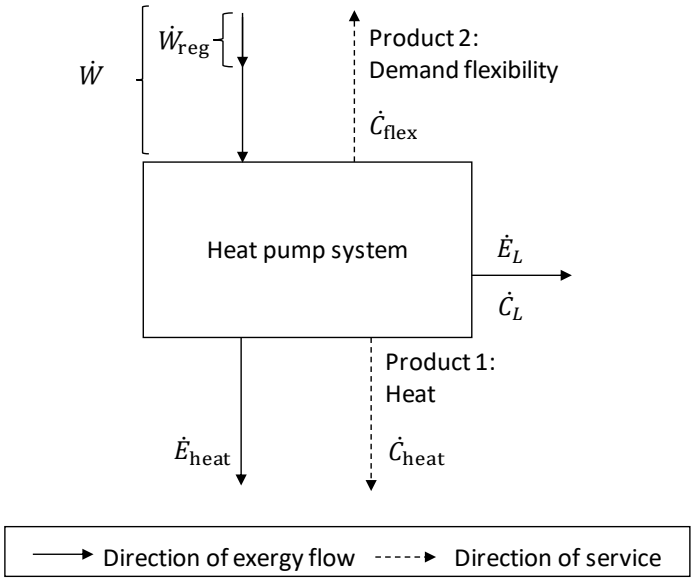

Figure 4-9 Direction of energy flow and product delivery for a conversion unit in an integrated energy system

As the flexibility provided to the electricity sector was not directly connected to an exergy product stream, the cost was allocated according to the increased exergy destruction due to flexible operation, which was given as the difference between the overall exergy destruction in the flexible

and the non-flexible case. Here, the non-flexible base case was chosen to be the spot market optimised operation. The specific cost per unit of exergy was calculated as:

$$c_{\mathrm{ex}} = \frac{(C_{\mathrm{heat}} + C_L)}{E_{\mathrm{heat}} + (E_{D,\mathrm{flex}} - E_{D,\mathrm{nonflex}})} \tag{4-26}$$

The overall cost exiting the system is the sum of the integrated cost of heat C_{heat} and of the exergy loss C_L. E_{heat} is the integrated amount of exergy supplied as heat to the DH grid and $E_{D,\mathrm{flex}}$, $E_{D,\mathrm{nonflex}}$ is the overall exergy destruction caused during flexible operation and non-flexible operation, respectively. All values were calculated by integrating the respective cost and exergy flow rates over one year.

Knowing the overall cost related to flexible operation per year, the specific cost per unit of regulating energy W_{reg} provided can be determined.

$$c_{\mathrm{flex}} = \frac{c_{\mathrm{ex}} \cdot (E_{D,\mathrm{flex}} - E_{D,\mathrm{nonflex}})}{W_{\mathrm{reg}}} \tag{4-27}$$

In order to be able to compare different units, the annual specific cost of flexible operation per kW available power capacity for frequency regulation $\dot{W}_{\mathrm{cap}}$ was calculated, too.

$$c_{\mathrm{flex,capacity}} = \frac{c_{\mathrm{ex}} \cdot (E_{D,\mathrm{flex}} - E_{D,\mathrm{nonflex}})}{\dot{W}_{\mathrm{cap}} \cdot 8760 \cdot 3600\ \mathrm{s/a}} \tag{4-28}$$

The heat generation cost is calculated from the overall cost delivered into the DH grid over the overall amount of heat.

$$c_{\mathrm{heat}} = \frac{c_{\mathrm{ex}} \cdot E_{\mathrm{heat}}}{Q_{\mathrm{heat}}} \tag{4-29}$$

4.2.7 Influence of heat pump capacity on result

It is expected that the design capacity of the heat pump has a large influence on the availability of the large-scale heat pump for supplying ancillary services. Therefore, the sensitivity of the economic feasibility on the design heat pump capacity was tested for the most feasible operation mode (FCR-N max HP) only. This was done by varying the design capacity from 600 kW to 900 kW in steps of 100 kW. The cost function of the heat pump and groundwater pumps were assumed to be a linear function of the capacity and the input cost were changed accordingly. The available hours for frequency regulation provision were calculated as described in section 4.2.4.3. The power uptake set values were calculated from historic grid frequency data for 2018, as described in section 4.2.2.

4.3 Results

4.3.1 Ability to follow a given frequency deviation pattern

The results presented in this section correspond to the method described in section 4.2.2. The results for the technical ability to provide frequency regulation with the heat pump alone are shown and compared to the results for frequency regulation from electric vehicles and the combined service from EVs and heat pump, taken from [P4].

4.3.1.1 Frequency regulation service provided by the heat pump alone

This applies to the cases FCR-N HP 5 h and FCR-N HP max. Depending on the operation strategy and the supplied reserve service to the power grid, the heat pump may be required to follow the

frequency deviations of the grid to supply the desired balancing service. This is typically the case for primary frequency reserve, which is a frequency-controlled service. From the results presented above, it was deemed that among the frequency-controlled services in Denmark, FCR-N is most likely to be supplied by large-scale heat pumps, as the allowed regulation times are relatively high with 150 s. Two cases were tested here, the slowest allowable response assuming FCR-N delivery and the response to an ideal active power response that was given as an input to the heat pump controller. The load over time for both cases is depicted in Figure 4-10.

Figure 4-11 shows the normalised power response of the heat pump response for both cases compared to the ideal response, where the active power of the heat pump is plotted against the grid frequency at the same point in time. It may be seen that the resulting deviation from the ideal response is slightly wider when the heat pump is allowed to ramp slowly than for the fast reacting heat pump. The normalised power response curve depicts data points for two hours of time. The upward deviations from the ideal response for the slow reacting heat pump and frequencies between 50.0 Hz and 50.1 Hz, occur, when the heat pump is suddenly required to ramp up, at 2770 s and 6360 s. In this case, the slow reacting heat pump (first case) does not follow the required load change as quickly as required, which results in deviations from the ideal response. The fast reacting heat pump (second case) operated safely without the risk of condensation in the suction line during load change. This was avoided due to the control structure proposed in section 3.2.5 and electric preheating of the suction line.

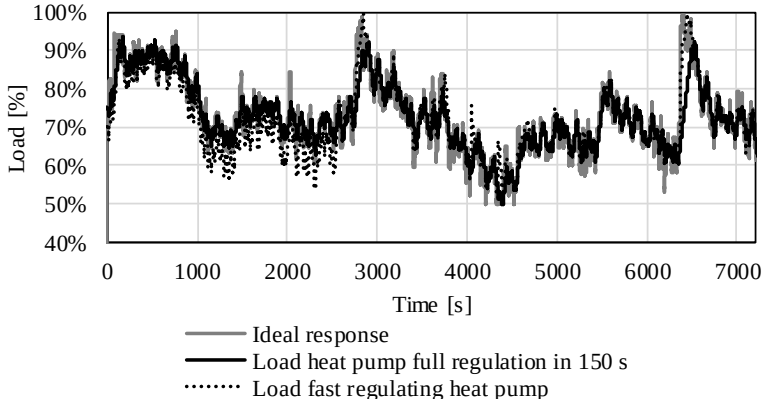

Figure 4-10 Ideal response and actual load of the heat pump for two regulation times as response to frequency deviations in the grid. Values were calculated for every 0.5 seconds.

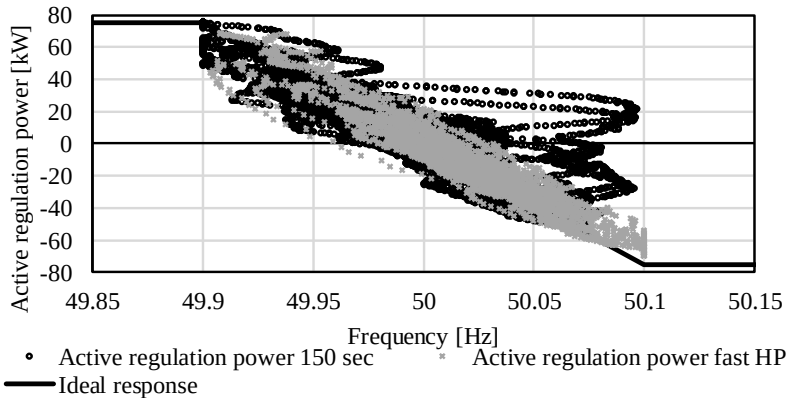

Figure 4-11 Normalised power response curve for heat pump with two regulation times and the ideal response. Values were calculated for every 0.5 seconds.

4.3.1.2 Frequency regulation service provided by electric vehicles and heat pump

The results for delivery of frequency regulation of the heat pump alone were compared to the experimental results[1] for electric vehicles and the heat pump delivering a combined service.
Figure 4-12 shows the ideal power uptake of the combined system, the actual response of the electric vehicles to the frequency as measured in the conducted experiment and the offset operation schedule of the large-scale heat pump, which was simulated. It may be seen that the electric vehicles are able to follow the ideal response precisely. There was only a two seconds delay between the frequency change and the power response on the grid side of the charger. The heat pump was only activated to deliver offset energy, when the SOC of the electric vehicle surpassed the upper or lower constraints.
The corresponding normalised power response are presented in Figure 4-13. Delivering FCR-N with the electric vehicles alone resulted in two additional lines of points, which occurred when the frequency power response was shifted up-or down by reserved power capacity of the electric vehicle itself. For FCR-N delivery from the combined service, the measured response followed the ideal response more closely. The two additional lines were avoided as the power base line shift of the electric vehicles was cancelled out by the offset energy delivered by the large-scale heat pump.

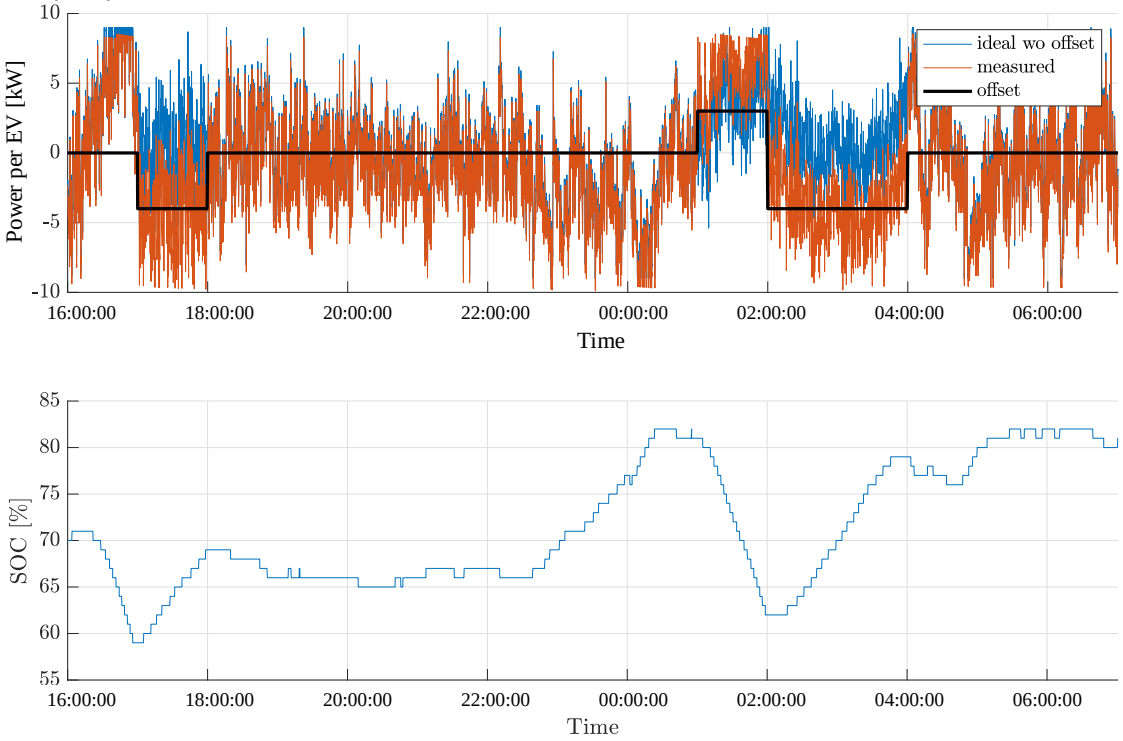

Figure 4-12 Experimental results for FCR-N delivery using electric vehicles and heat pump, upper: Response of electric vehicle and offset operation of heat pump, lower: corresponding state of charge of the electric vehicle battery [P4].

[1] The experiments were conducted by Andreas Thingvad and the results are presented in [P4].

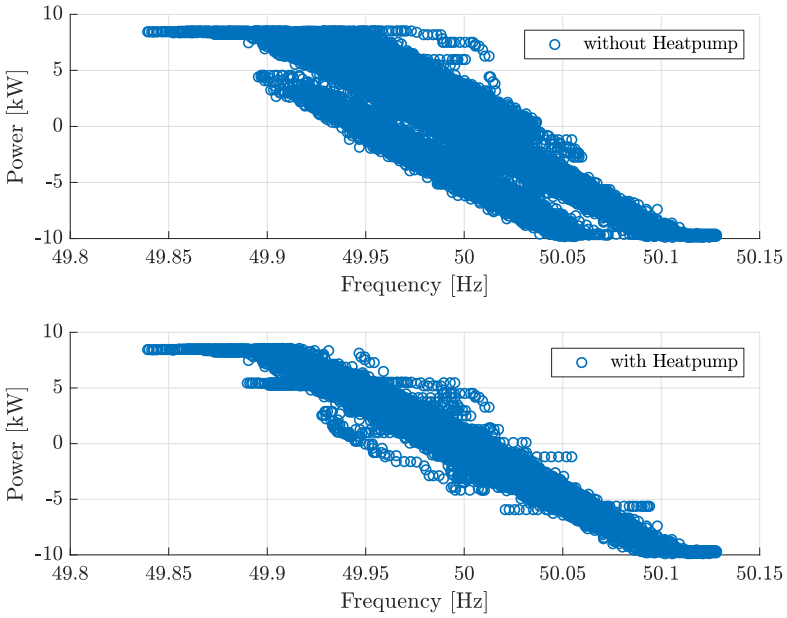

Figure 4-13 Active power uptake of one vehicle as a function of the grid frequency, upper: electric vehicle supplying regulation power alone, lower: heat pump offset the baseline power shift of the electric vehicle [P4].

4.3.2 Performance of different operation modes

Two different operation strategies were simulated for frequency delivery from the large-scale heat pump alone. Further, the combined delivery of FCR-N from electric vehicles and the large-scale heat pump was assessed. A spot market optimised operation schedule and the heat demand driven operation schedule were compared to the three cases with frequency regulation delivery. Figure 4-14 shows the heat demand and the heat pump heat output for all five operation schedules for January. The heat output in the heat demand driven operation followed the heat demand as long as the filling level of the storage was not out of range. When the storage level fell below the minimum level, the heat pump ramped up to full load and when it increased above the maximum level, the heat pump was switched off. In summer, the heat demand was lower than the minimum heat supply from the heat pump. Accordingly, the heat pump was operated at minimum load instead and the storage tank was charged, for the following days. In all other cases, the heat pump started up and shut down more often, as the operation was optimised according to spot market prices (Figure 4-14 b)), frequency regulation was delivered (Figure 4-14 c) and Figure 4-14 d)) or offset energy for electric vehicles supplying FCR-N was supplied (Figure 4-14 e)). For the spot market optimised operation mode, the heat pump was operated most often at 640 kW heat output, as the system COP (incl. pumps) was highest at this load.

Table 4-6 summarises the results of all analysed operation modes. The heat supplied to the customers was the same for all operation modes. The heat pump COP and the system COP differed however between the different operation modes. As shown above (Figure 4-5), the heat pump COP benefitted from part-load operation, such that the load of the heat pump influences the overall performance of the system.

The auxiliary heating from the electric boiler was highest for the heat demand driven operation, while the heat supplied by the heat pump was highest for the spot market optimised case. The seasonal system COP was however the same for both operation modes, as the losses from the storage were higher for the spot market case than for the heat demand driven case. Among the

cases with frequency regulation supply, the cases, where the heat pump delivered frequency regulation alone were beneficial in terms of system and heat pump COP compared to the EV+HP case. For the EV+HP case, the heat pump often delivered the full offset energy, i.e. operated at maximum or minimum load. Both have a relatively low COP compared to intermediate loads, see Figure 4-5.

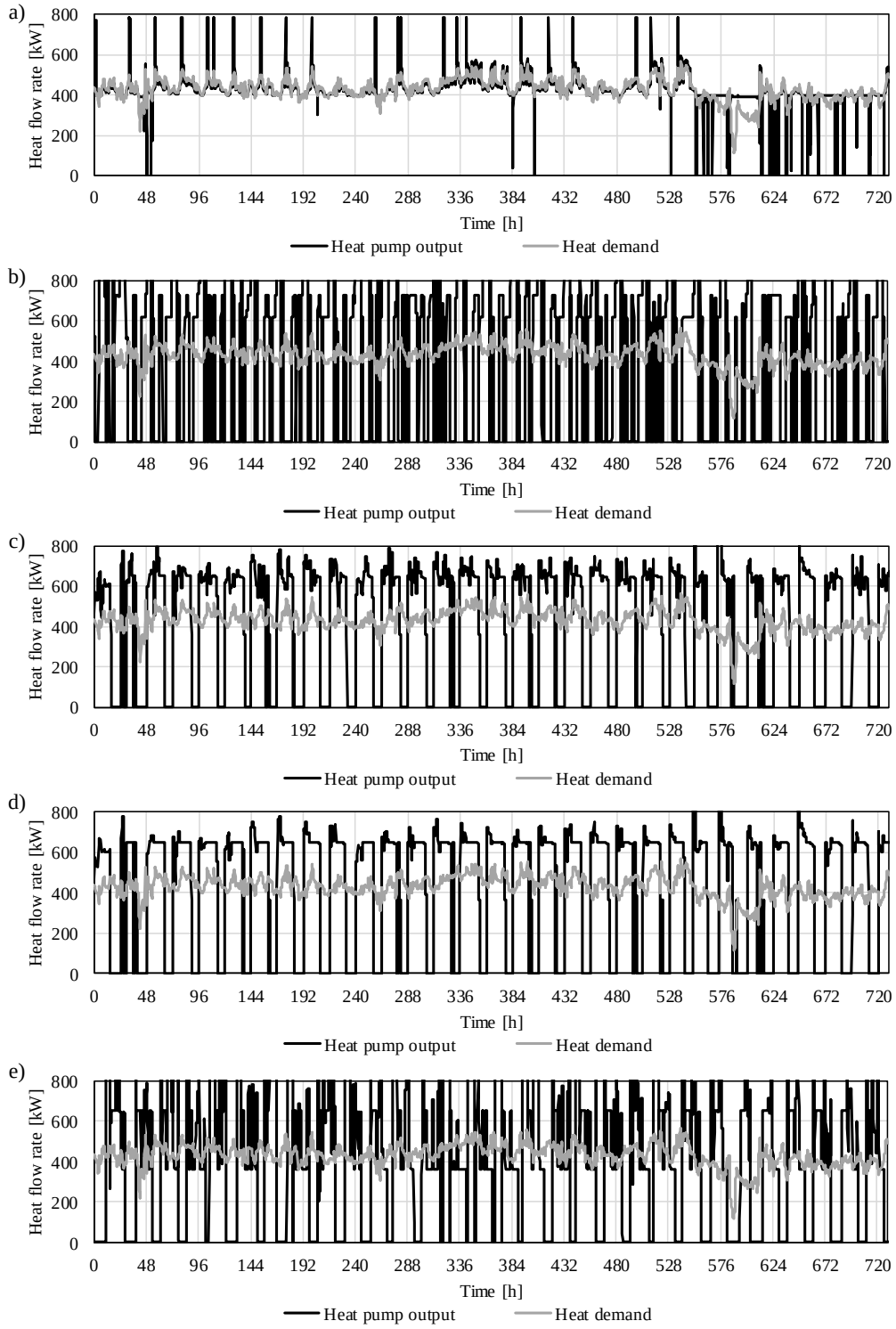

Figure 4-14 Heat pump heat output and heat demand for January 2018 a) Heat demand driven case, b) Spot market optimised operation schedule, c) FCR-N HP max, d) FCR-N HP 5 h, e) EV+HP

Table 4-6 Summary of thermodynamic and economic system performance for five different operation modes. El. – electric, EB – electric boiler, HP – heat pump

	Unit	Heat demand driven	Spot market optimal	FCR-N max	FCR-N 5 h	EV +HP
Total yearly el. energy	MWh	638	637	627	626	637
Total yearly heat supply	MWh	1,925	1,925	1,925	1,925	1,925
Yearly el. energy EB	MWh	19	10	15	15	12
Yearly el. energy HP	MWh	534	543	528	527	540
Yearly el. energy pumps	MWh	84	84	84	84	84
Yearly heat supply from HP	MWh	1,890	1,918	1,913	1,913	1,916
Regulation energy up	MWh	0	0	20	9	24
Regulation energy down	MWh	0	0	21	16	26
SCOP System	-	3.02	3.02	3.07	3.08	3.02
SCOP HP	-	3.60	3.55	3.65	3.65	3.56
Annual electricity cost	€	65,900	62,400	63,400	63,000	64,900
Overall annual cost (operation and investment)	€	84,800	81,300	82,200	81,900	83,700
Additional cost for 25 EVs	€	0	0	0	0	740
Income from FCR-N capacity payments (HP)	€	0	0	6200	5080	4440
Income from FCR-N regulation power price (HP)	€	0	0	200	80	310
Total cost incl. FCR-N payments and payment to EVs	€	84,800	81,300	75,800	76,700	79,700

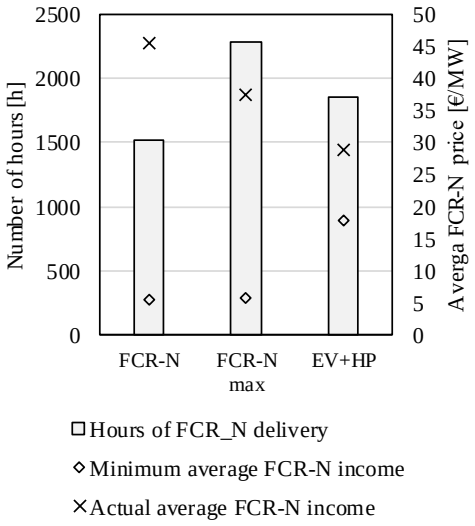

Figure 4-15 Number of hours were the system was available for FCR-N delivery, minimum required average income from FCR-N delivery and actually obtained average income from FCR-N delivery for three cases.

The largest amount of regulation energy was delivered by the heat pump in the EV+HP case, where 24 MWh of up regulation and 26 MWh of down regulation was provided. The amount of provided regulation energy for FCR-N delivery for maximum five hours a day compared to the maximum available number of hours per day, resulted in a reduction of 11 MWh in up-regulation, but only a reduction of 5 MWh of down regulation. The overall number of hours, where the heat pump was available for FCR-N delivery in the three cases is depicted in Figure 4-15. Further, the obtained average FCR-N payment per MW regulation power capacity and the minimum required average FCR-N payment for a positive business case are shown in Figure 4-15. The obtained average payment was highest for the heat pump alone when the frequency regulation period was limited to the five hours between 00:00 and 05:00 am, where the capacity payments were highest. The FCR-N HP max and the EV+HP case had the same number of hours, where the heat pump was theoretically available for FCR-N delivery. However, the amount of hours, when FCR-N was actually delivered from the heat pump alone was larger than for the combined service. This difference was mainly caused in the summer month, where the available offset time was very low. In this case, the few available operation hours were still bid into the market for the heat pump alone, which was not the case for the EV+HP case, where no power offset was required from the heat pump only for the last hour of service provision from the EVs. The reduced average payment for EV+HP wais caused by two effects. Firstly, the additional cost of conversion losses in the electric vehicles were subtracted from the income, as a minimum payment to the EV owner. Secondly, the operation period was shifted, such that the heat pump always started to operate at 00.00 in the morning for the FCR-N HP max case, while it always finished at 07:00 am for the EV+HP case. In the summer, where the heat pump often is only available for one hour of operation per day, considerably higher capacity prices may be obtained between 00:00 am and 01:00 am than between 06:00 am and 07:00 am. Seen over the whole year, FCR-N HP max was better to exploit those hours, where high capacity payments were available. The additional cost of conversion losses due to EV charging further resulted in a considerably increased minimum required average FCR-N price for the EV+HP case compared to FCR-N delivery from the HP alone. That means, the heat pump alone may bid smaller prices on the FCR-N market and thus might have a higher chance to get called.

For the combined delivery of FCR-N from electric vehicles and the large-scale heat pump, the difference between the obtained average FCR-N payments and the minimum required average FCR-N payments was 11 €/MW. This means, an average reduction of FCR-N payments of 38 % could be acceptable before the combined operation results in a negative business case, assuming the same number of service hours. For the delivery of FCR-N from the heat pump alone, the average prices could be reduced up to 88 % and 85 % of the calculated average payment for 2018, before the business case gets negative.

Figure 4-16 compares the specific electricity cost, the specific heat cost based only on the electricity purchase and based on both the operational and investment cost. Further, the specific heat cost, where the revenue from FCR-N provision was subtracted, is shown. The specific electricity cost, i.e. the average price at which one kWh of electricity was purchased, was lowest for the spot market optimised operation and highest for the operation according to the heat demand. Among the cases with FCR-N delivery, the service provided by the heat pump alone resulted in lower specific cost than the combined provision of FCR-N with electric vehicles. The same trend was seen for the specific heat cost exclusive FCR-N revenues. However, when the revenues from FCR-N payments were included, the operational and the total specific heat cost were lower for all cases of FCR-delivery than the spot market optimised operation and the heat demand driven operation. The lowest cost were obtained for FCR-N HP max.

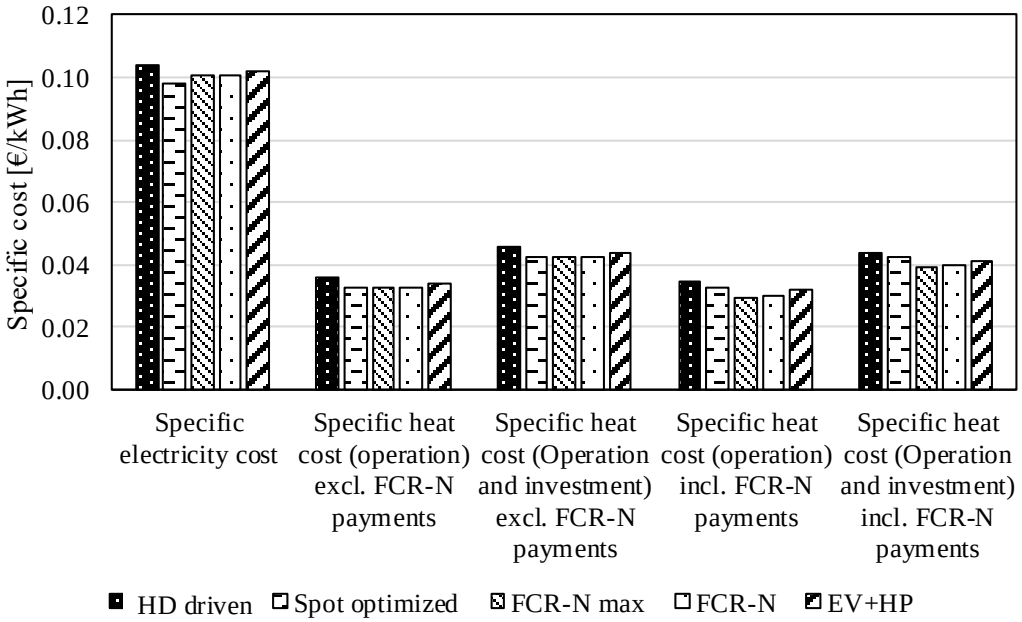

Figure 4-16 Comparison of specific energy cost for five different operation modes with and without income from FCR-N delivery. HD – Heat demand

4.3.3 Exergoeconomic analysis

The exergy efficiency of the heat pump for one case (FCR-N HP max) is depicted in Figure 4-17. The exergy efficiency peaked when the heat pump was shut down, as the power uptake decreased to zero, while heat was still ejected from the heat pump due to the thermal inertia of the components. During operation, the exergy efficiency varied with the load and due to dynamic behaviour. Figure 4-18 shows the steady-state exergy efficiency of the heat pump, which resembles the COP curves used as input to the model. The maximum exergy efficiency was reached at the minimum load, where all cylinders were still operating. The lowest efficiencies were obtained for maximum load and for 55 % load, when the cylinders were decoupled. Accordingly, the seasonal COP of those operation schedules, which resulted in operation at maximum or minimum load in many hours throughout the year, was lower than for operation scheduled that mainly resulted in part load operation at loads between 55 % and 100 %. This is the reason, why the EV+HP case performed worse compared to both FCR-N HP cases in terms of seasonal heat pump COP and seasonal system COP. The supply temperature was constant and thus, no variation in the exergy efficiency due to changes in supply temperature were observed.

The exergy analysis further allowed quantifying when and where losses occur in the system. To show the main loss mechanism, i.e. the exergy destruction, the first week of 2018 is depicted in Figure 4-19 and Figure 4-20 for the heat demand driven case and the FCR-N HP max case. In the heat demand driven case (Figure 4-19), the heat pump operated at minimum load or just above for most of the time, as the heat pump was oversized compared to the heat demand. The peaks in the power uptake occurred, when the charge of the storage fell below the allowed minimum value. The storage was constantly used to take up the additional heat production when the heat demand was below the minimum heat pump heat output.

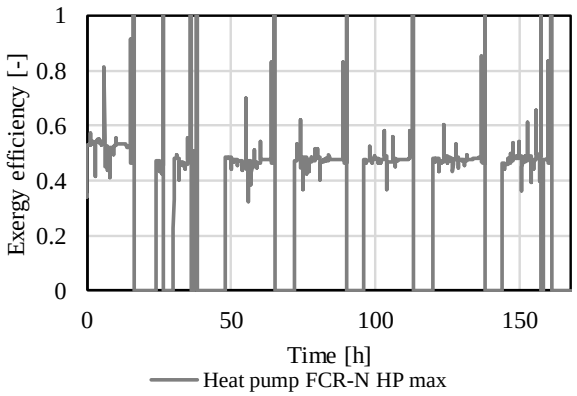

Figure 4-17 Exergy efficiency of heat pump for first week in 2018, case FCR-N HP max

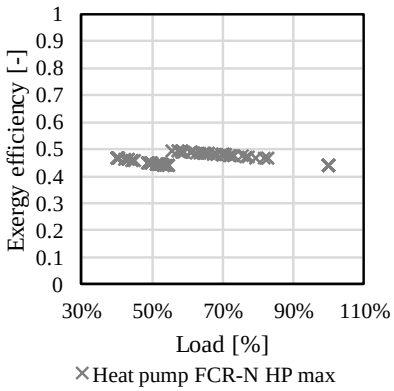

Figure 4-18 Exergy efficiency as a function of load in steady-state of heat pump for first week in 2018, case FCR-N HP max

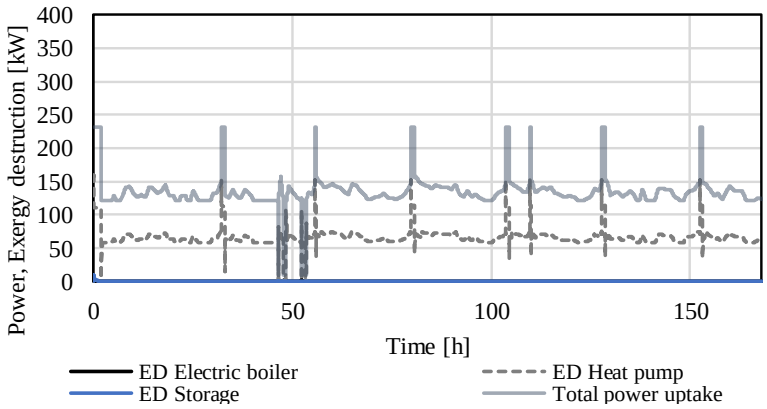

Figure 4-19 Total power uptake and exergy destruction in electric boiler, heat pump and storage during the first week of 2018 for heat demand driven operation schedule

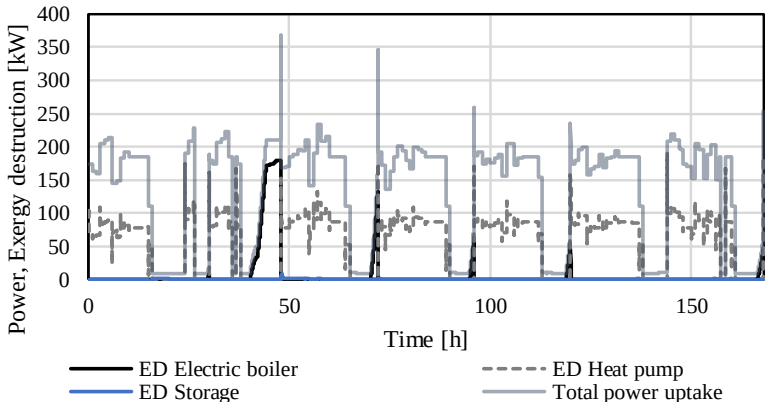

Figure 4-20 Total power uptake and exergy destruction in electric boiler, heat pump and storage during the first week of 2018 for FCR-N HP max operation schedule

The exergy destruction during operation according to heat demand was mainly caused by the heat pump In the graph for FCR-N HP max operation (Figure 4-20), the effect of shutting off the heat pump and supplying heat from the storage is depicted. Towards the end of the discharging period the temperature exiting the storage tank decreased and reheating of the supply flow with the electric heater became necessary. The remaining electricity during heat pump stand still was consumed by the pumps. The large electricity consumption in the electric boiler between 40 h and 50 h was caused by a mismatch of the operation profile, which was designed for FCR-N delivery during night hours. As the storage filling level was at minimum load as an initial condition, reheating with the electric boiler was necessary in the second night of the year. This was not necessary for the following nights, as the storage was charged a little more than the corresponding heat demand per day on most days of the year. This was due to the set point for charging the storage only changed once an hour and never before the full heat demand of the day was produced.

These exemplary operation patterns showed the main causes of exergy destruction in the system, which were the heat pump operation and reheating of the supply stream during heat supply from the storage, especially when the storage was discharged during longer periods, like for the heat demand driven case during summer. Further, losses occurred in the groundwater pumps and the district heating pumps, where the larger power uptake and thus absolute exergy destruction could be accounted to the groundwater pumps. The mixing in the three-way valve at the top of the storage tank and the T-piece at the bottom caused further exergy destruction. The absolute amount of these losses due to mixing was however three orders of magnitudes smaller than the overall exergy destruction in the system. The annual sum of exergy destruction in the different components for all five operation modes is compared in Figure 4-21. The lowest exergy destruction was caused by the FCR-N HP 5 h and FCR-N HP max operation modes with 309 MWh/a and 310 MWh/a, respectively. The exergy destruction for the other three cases was higher. For the EV+HP case and the spot market optimised operation, this was caused by more frequent operation of the heat pump at maximum and minimum load. In the heat demand driven case, heat was stored for longer periods in the storage tank, especially during summer, which resulted in increased electricity consumption in the electric boiler to reheat the supply stream, as also shown in Table 4-6. The corresponding cost of exergy destruction are depicted in Figure 4-22. The distribution was similar to the distribution of exergy destruction. Only the cost of exergy destruction in the network, which includes the three-way-valve and the T-piece, was considerably larger in the heat demand driven operation compared to the other cases. This was caused by the losses due to mixing in the three-way valve during discharging of the tank in summer. Here the cost were higher compared to winter operation, as the warm water was stored for a long period in the tank, meaning the constant cost stream $\dot{Z}$ of the storage tank accumulated at the exergy stored in the tank. Accordingly, losses during discharging caused larger cost compared to the other operation modes, where the heat was stored for maximum a day.

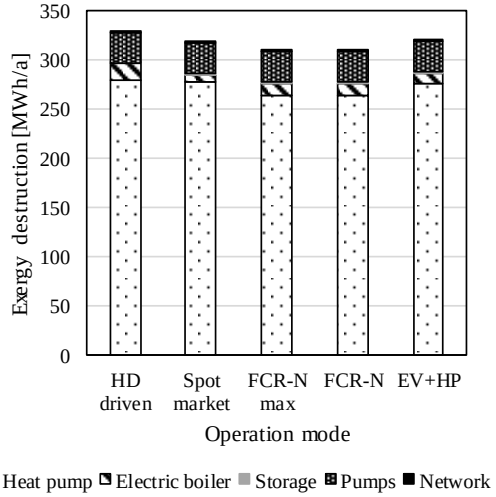

Figure 4-21 Annual exergy destruction in the heat pump system per component

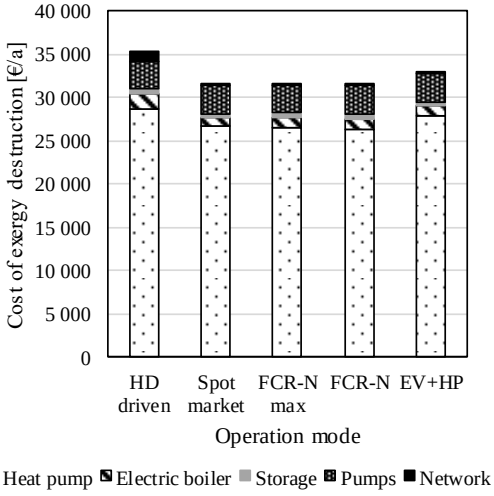

Figure 4-22 Annual cost of exergy destruction in the heat pump system per component

4.3.4 Allocation of cost and income

A method was proposed to allocate the cost of the system and the additional income to the two products of the system, heat and energy content of the frequency regulation. The underlying idea is to quantify the positive and negative effects of a newly proposed operation mode compared to a base case on the system performance and the associated cost. This allows locating where cost are caused in the system and which of the two products they should be allocated to. This can support the decision on how the heat pump should be operated, and which product needs to pay for additional cost or generates an income. This is useful information, especially if both services are marketed independently. Note, that in Denmark district heating companies are required to be non-profit, such that a possible income from frequency regulation would reduce the heat generation cost. This may however be different in other countries.

Table 4-7 summarises the results of the conducted analysis. The aim was to assess how the additional cost and income of frequency regulation should be divided between the different products. The spot market optimised operation was chosen as base case here, as this would be the economically most feasible option without the supply of frequency regulation. The base case was relevant, as the additional exergy destruction of the proposed operation was used as a factor to allocate the cost and income to the frequency regulation service.

The specific cost per unit exergy was largest for the HP FCR-N max case, followed by HP FCR-N 5h, EV+HP, and the heat demand driven case. The lowest specific exergy cost was obtained for the spot market optimised operation. The low value for the spot market optimised case compared to the other cases was caused by lower total annual cost, while the number of units of exergy ($\Delta E_D + E_{heat}$) lay between the other cases. This lower exergy destruction compared to the heat driven case was mainly due to shorter storage times for the spot market optimised operation, which resulted in less need for reheating of the supply stream and thus less exergy destruction in the electric boiler. The reduced exergy destruction that was seen for the FCR-N max and FCR-N 5 h cases was due to less exergy destruction in the heat pump, which also outbalanced a larger need for reheating of the supply stream compared to the spot market optimal case. The specific cost per unit exergy increased for all variants delivering frequency regulation compared to the base case as the exergy destruction decreased by a larger percentage than the overall annual

cost. Accordingly, the increased cost per unit exergy is mainly caused by a more efficient process, and thus less unit of exergy that the cost may be allocated to.

Looking at the resulting specific cost of heat and regulation energy, the specific cost of heat allocated according to the proposed method was lowest for the operation strategies without frequency regulation. The specific cost allocated to the regulation energy is positive for the FCR-N 5h and FCR-N max cases. That means, a cost reduction was generated just by changing the operation schedule, without considering the actual income from FCR-N payments. This does however result in an increase of the specific cost of heat based on the exergy-based allocation compared to the case without frequency regulation. In other words, if the overall exergy destruction is reduced by the flexible operation mode compared to the chosen base case, the ancillary service product will have a negative cost, which is covered by an increased cost of the heat product. This was not the case for the EV+HP case, where the exergy destruction is higher than for the spot market optimised operation and a cost was assigned to the regulation energy.

The income from FCR-N payments was allocated to the two products in the same way. The sign was chosen in agreement with the cost, such that positive values mean an income, while negative values denote a cost to the system. The specific income for heat reduced the overall specific cost of heat, while the income from changed operation allocated to the regulation energy was slightly reduced. Only for EV+HP an actual income was assigned to both products.

As a result, the overall heat prices are lower for the FCR-N max and FCR-N 5 h cases compared to the spot market optimised operation and an additional income is generated by supplying frequency regulation. According to the proposed allocation method, this could be used for other purposes than the reduction of heat cost, if the two products would be marketed independently.

The overall revenue for FCR-N max and FCR-N 5 h for the considered case was mainly caused by an increase in system efficiency. This result was however highly dependent on the chosen base case and would look different, if the base case was optimised with regard to system efficiency rather than electricity spot market cost. The largest specific revenue from regulation power was obtained for FCR-N HP operation with maximum five hours regulation period, followed by FCR-N HP max and the EV+HP operation.

Table 4-7 Overall results exergy analysis and allocation of cost and income according to exergy based allocation

	Unit	Heat demand driven	Spot market optimised	FCR-N max	FCR-N	EV+HP
Electric regulation energy up	MWh	0	0	20	9	24
Electric regulation energy down	MWh	0	0	21	16	26
Exergy of heat	MWh	245	249	249	250	249
Total power consumption	MWh	638	637	627	626	637
Total exergy destruction	MWh	330	318	310	309	320
Difference in exergy destruction compared to spot market optimised operation (ΔE_D)	MWh	12	0	-8	-9	2
Overall exergy efficiency	-	38%	39%	40%	40%	39%
Annual electricity cost	€	-65,900	-62,400	-63,400	-63,000	-64,900
Overall annual cost (operation and investment)	€	-84,800	-81,300	-82,200	-81,900	-83,700
Total cost incl. FCR-N payments and payment to EVs	€	-84,800	-81,300	-75,800	-76,700	-79,700
Cost per unit exergy (Allocation: $\Delta E_D + E_{heat}$)	€/MWh	-331	-327	-341	-340	-334
Specific cost of heat	€/MWh	-44	-42	-44	-44	-43
Specific cost of regulation power	€/MWh	-	-	68	125	-10
Income per unit exergy (Allocation: $\Delta E_D + E_{heat}$)	€/MWh	0	0	27	22	16
Specific income per unit heat	€/MWh	0	0	3	3	2
Specific income per unit regulation energy	€/MWh	-	-	-5	-8	0
Cost + income per unit exergy (Allocation: $\Delta E_D + E_{heat}$)	€/MWh	-331	-327	-315	-319	-318
Total specific cost of heat without FCR-N (no cost assigned to ancillary service product)	€/MWh	-44	-42	-43	-43	-43
Total specific cost of heat with FCR-N	€/MWh	-44	-42	-41	-41	-41
Total specific revenue of FCR-N per unit regulation energy	€/MWh	-	-	62	117	-10

4.3.5 Influence of heat pump capacity

The heat pump chosen as case study in this chapter may be considered over-dimensioned compared to the heat demand. Usually, heat pumps that are not intended to provide flexibility to the power system, are dimensioned to have a heat output capacity around 85 % of the peak heat demand [228]. In order to evaluate the importance of this assumption, the influence of the heat pump capacity on the feasibility to supply frequency regulation was assessed. The variation of COP with varying heat pump capacity is depicted in Figure 4-23 in relative terms compared to COP at nominal thermal capacity (800 kW). The COP fell with decreasing heat pump capacity. This was due to larger exergy destruction in the heat pump, as the average load was higher and thus the COP was lower.

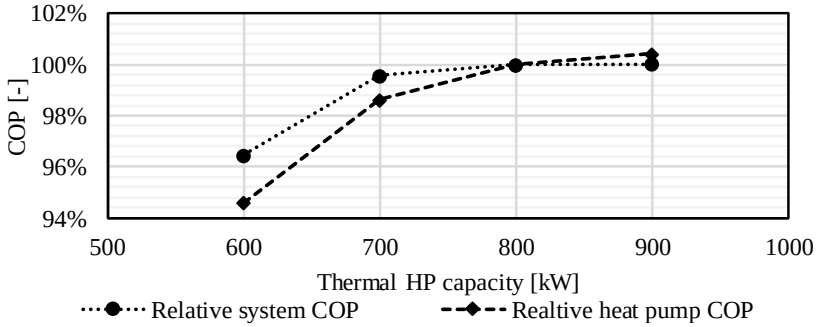

Figure 4-23 Relative COP compared to COP at nominal thermal capacity (800 kW) for varying heat pump capacity

The amount of scheduled hours of frequency regulation increased with decreasing heat pump capacity, before it reached a maximum and then decreased, as shown in Figure 4-24. As the capacity of the heat pump was reduced, while the heat demand of the system was kept constant, the required hours of heat production to fulfil the demand increased and thus the hours, when frequency regulation may be delivered, increased. The maximum was reached because the heat pump is required to run at full load more frequently for lower capacities to satisfy the heat demand. In these hours, the load may not be reduced and thus no flexibility may be delivered from the heat pump. The maximum amount of frequency regulation hours was found at 665 kW thermal capacity of the heat pump for the given heat demand of 1925 MWh/a, and a measured peak demand of 710 kWh/h.

The corresponding amount of energy provided during up- and down-regulation is depicted in Figure 4-24, too. The maximum was found at approx. 800 kW, i.e. the nominal capacity, as the number of service provision hours was smaller, but the energy content delivered during these hours was larger. Finally, the income from FCR-N capacity and regulation power payments is depicted. This increased slightly, when reducing the heat pump capacity to 700 kW thermal and then decreased for even lower capacities. For an increased capacity, the income fell rapidly as the amount of hours, where the heat pump was available for frequency regulation decreased.

Figure 4-25 shows the total yearly electricity consumption, total yearly electricity cost, total yearly levelised operation and investment cost and total yearly levelised operation and investment cost incl. income from frequency regulation. A minimum for the electricity consumption and the total annual electricity cost was found at 800 kW thermal capacity. Note that the location of all minima found here were approximate values and the actual minima may deviate from the rounded values considered within this study. The total annual cost (investment and operation) decreased with decreasing thermal capacity as the investment cost of the heat pump decreased. Accordingly, the

lowest total cost among the analysed cases without delivery of frequency regulation would be obtained for 600 kW thermal capacity. When taking the income from FCR-N payments into account, a minimum of the total annual cost including income was found at 700 kW thermal capacity. As shown in Figure 4-26, this was just below the maximum heat demand in the system. The corresponding total specific heat cost including all levelised cost and income from frequency regulation were 0.6 €/MWh lower for 700 kW thermal capacity compared to 800 kW thermal capacity. From the results, it may be concluded that considering the delivery of frequency regulation as an additional service from the heat pump shifts the optimal thermal capacity of the heat pump to larger values. For this case, the optimum capacity should be chosen close to the maximum expected heat demand per hour of the system. The optimum heat pump capacity of other, similar heat pump systems will depend on the shape of the sorted heat demand curve as well as the available storage capacity. This was not varied in the current study.

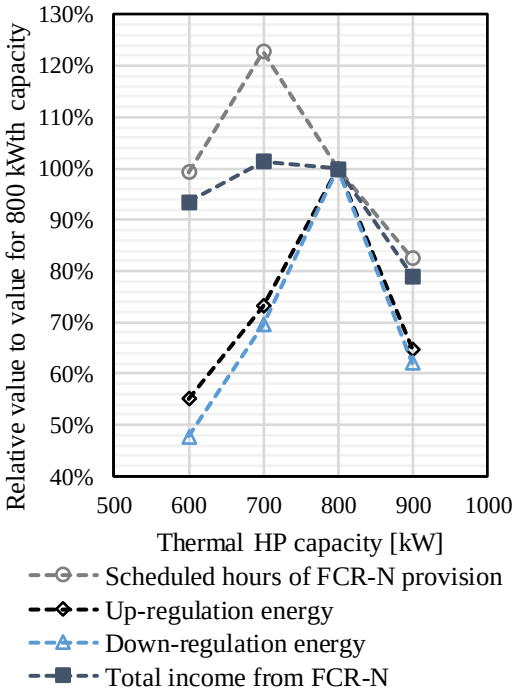

Figure 4-24 Yearly scheduled hours of FCR-N provision, total yearly regulation energy (up and down) for varying thermal heat pump capacity

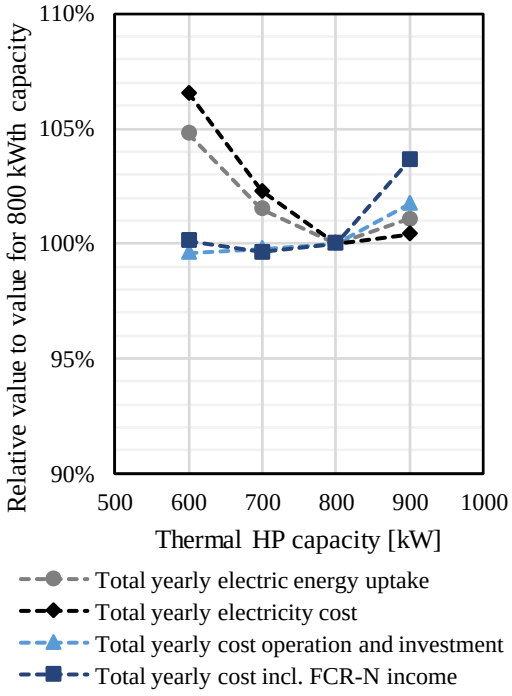

Figure 4-25 Total yearly electric energy uptake, electricity cost, total cost (operation and investment) and total cost incl. FCR-N income for varying thermal heat pump capacity

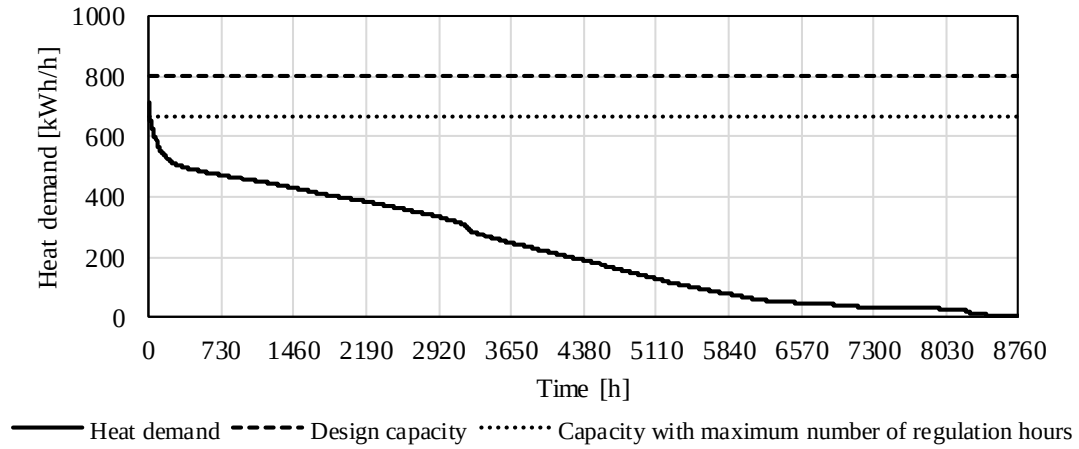

Figure 4-26 Sorted heat demand curve for FlexHeat network 2018 [212]**, design capacity of FlexHeat and capacity resulting in maximum of frequency regulation hours**

4.4 Discussion

4.4.1 Feasibility of different operation modes

4.4.1.1 Large-scale heat pump providing frequency regulation

The conducted analysis aimed at identifying the potential of primary frequency regulation supplied by large-scale heat pumps. Here, only the delivery of FCR-N in Eastern Denmark was analysed in detail, as the obtainable payments for this service are highest. FCR-N is a primary regulation service. It is however extraordinary as the required regulation time of maximum 150 seconds is high compared to other primary frequency regulation services. Accordingly, it may be possible to deliver this service from large-scale heat pumps. The simulation of the heat pump response showed that the heat pump was able to follow the frequency of the grid. Further, for the fast regulating heat pump, a clearly increased quality of frequency regulation was seen, defined by the smaller deviation of the response from the ideal response compared to the slowest allowed reaction of the heat pump. This result was however based on simulations of the system and still needs to be verified experimentally.

The analysis was conducted using historic data from 2018. It should be noted that 2018 was characterised by an extraordinarily hot and dry summer and by high FCR-N prices compared to the previous years. It may thus be expected that the heat pump would be available for frequency regulation for more hours in colder years, which may increase the obtainable capacity payments. Further, the available offset time was calculated from the maximum power uptake, i.e. full load conditions to avoid overcharging the heat storage tank. The resulting number of hours was a conservative estimate for winter days, where the heat pump is available many consecutive hours, as it is unlikely that the heat pump would be required to run at full load for the whole period. For future practical implementation, this scheduling approach may be improved using statistical methods or machine learning.

The techno-economic analysis showed that the delivery of FCR-N frequency regulation from the large-scale heat pump could generate an extra income for the heat pump operator and thereby reduce the heat cost for the customer. It should however be noted that the FlexHeat heat pump, used as a case in this study, is over-dimensioned compared to the heat demand, which results in

a low number of full load hours. Further, the flexible operation of the heat pump is enabled by the available extra capacity of the heat pump and storage. The variation of the heat pump capacity showed that a reduction of the heat pump capacity to values closer to the maximum expectable heat demand could improve the economic feasibility of the system. The sizing of storage compared to the heat demand and the influence on the feasibility of providing FCR-N frequency regulation was not assessed in detail within this study. It might however be worth to optimise both the heat pump and storage sizes for future systems already in the design phase, considering the planned flexible operation mode.

The heat generation cost could be reduced with all three strategies to deliver FCR-N even though all of these were based on rather simple schedules. An optimisation of the operation schedule including, when to bid on which market may further increase the income from ancillary services and decrease the electricity cost. It should be noted that the cost of increased wear due to frequency regulation was not assessed as part of this study. The information would however be relevant in order to evaluate the benefits and drawbacks of flexible operation on the heat pump system in more detail. Such an analysis is expected to require long time performance data of several heat pumps, which may be relevant for future performance studies.

4.4.1.2 Combination of fast regulating units and large-scale heat pump for combined frequency regulation services

The combination of electric vehicles, which are able to regulate quickly and a large-scale heat pump with a large energy storage capacity was found to be able to regulate quickly and precisely according to the grid frequency. The large-scale heat pump could balance out the deviations caused by the adaption of the EVs' baseline power uptake. Hence, the combination of these two types of units allowed an improved service delivery. It further allowed bidding on primary regulation markets with lower required regulation times, such as the primary reserve in DK 1, which requires full activation within 30 seconds. It is unlikely that large-scale ammonia heat pumps will be able to safely react within such a low regulation time, as shown in Chapter 3. Therefore, the combined operation mode may be of special interest, as it generally enables the heat pump in combination with fast regulating units to act on faster markets. In the assessed case of electric vehicles and heat pumps, a synergy effect was observed. The electric vehicles could bid a higher regulation power capacity on the market, i.e. receive more capacity payments, the quality of the response could be improved and the revenues from FCR-N for the heat pump were high enough to result in reduced heat supply cost for the customers. Here, it was assumed that the heat pump owner also owned the fleet of vehicles. In general, the units aggregated may not be owned by the same stakeholder and in this case, the question of how the revenues should be allocated to the different stakeholders is of interest.

The results showed that the average FCR-N price could be reduced by 38 % before the combined provision of frequency regulation from EVs and large-scale heat pump resulted in a negative business case. Considering that the average capacity prices in the three preceding years were 63 %, 32 % and 37 % lower than the average FCR-N payment obtained for 2018, respectively, this buffer cannot be considered sufficient. This means that future applications of the proposed operation strategy should be able to switch back to the normal spot market optimal operation strategy, when the FCR-N capacity payments are too low. It also means that this operation strategy is best suited for heat pumps that are already equipped with the necessary communication interface for frequency regulation services. This would help to minimise the additional investment cost. The offset operation of the heat pump resulted in additional cost due to higher average electricity prices and due to an increased electricity consumption. This

additional cost would however be reduced in future due to the expected decrease in PSO tariff and electricity tax, and thereby it would benefit the feasibility of combined FCR-N provision from EVs and large-scale heat pump.
The large-scale heat pump could also be combined with fast-regulating electric boilers for a combined service provision. One possible operation strategy would be to run the heat pump and offer up-regulation, i.e. load reduction down to minimum load. The down-regulation would then be delivered by the electric boiler. This set-up would allow bidding double the amount of power capacity into the frequency regulation market. However, the system COP is expected to be lower due to increased heat production using the electric boiler and the number of hours were the heat pump could be available for frequency regulation would be decreased. This is due to the larger default heat output from the system, which means that the daily heat demand is produced in less time and the heat storage is filled more quickly. This set-up would further require that the electric boiler could charge the storage, which was not possible in the presented case study. Therefore, this case was disregarded here. In future, it would however be interesting to look at the optimal combination of electric boilers and heat pumps in future systems supplying a combined frequency regulation service.

4.4.2 Allocation of cost and income

The allocation of cost to the provision of frequency regulation from a system on the demand side with a second product is not straightforward. This is due to the different directions of the flow of energy (from grid to the unit) and of the provided service (from unit to grid). Here, it was proposed to determine the cost and income due to frequency regulation according to the difference in exergy destruction in the system providing frequency regulation compared to a base case without provision of frequency regulation. This cost was then allocated to the delivered regulation energy, i.e. the energy content of the provided frequency regulation. This makes sense from a thermodynamic point of view, it is however contradictory to the principle of a capacity payment, where the payments is independent from the actually delivered energy. The proposed allocation was developed for power-to-heat units supplying both heat and frequency regulation and is based on a dynamic exergoeconomic analysis of the system. It provides insights into the cause of cost in the system, i.e. whether they occur due to heat production or due to the changed operation. Thereby, a thermodynamically based division of cost and income to the two products of the system is possible. This does however come at the cost of a more complex system analysis compared to a normal techno-economic analysis of the system. Note, that the allocation was done assuming that the system design is given. If the heat output capacity and storage size were optimised for the different cases, potential additional investment cost for a larger heat pump capacity to provide ancillary services should be taken into account. In this case, it could be argued that the additional investment cost should be fully allocated to the additional ancillary service product.
Despite the thermodynamic insights into cost generation of the system, some drawbacks were identified. First, the result is a comparative analysis and as such highly dependent on the chosen base case. This may be acceptable if a newly proposed operation schedule is compared to the operation schedule in place. However, the comparability of different plants is not straightforward, due to possibly different base cases. Here, a method that would not rely on a comparison to a base case could be beneficial.
Second, the allocation was only conducted for the heat pump system itself not for the units, that might be pooled together with the heat pump system, here the EV batteries. The case of combined

delivery of primary frequency regulation from different operating units would increase the complexity of such an analysis, but would not be able to capture the differences in terms of flexibility between the different units. Alternatively, a costing method based on the different flexibility measures, i.e. ramping time, energy storage capacity and power capacity, might result in an allocation of the revenues from combined service provision that would allow dividing the revenues to the different units. This is an important issue when the units delivering the combined service are not owned by the same company, as it was assumed for the present study.

4.5 Chapter summary

Within this chapter, the technical and economic feasibility of supplying ancillary services from large-scale heat pumps alone and in combination with fast regulating bidirectional units was assessed and compared to operation without FCR-N delivery. This was done using a simplified dynamic model of the heat pump system that was implemented in Modelica. The model also included the calculation of exergy and cost streams for all material streams, including investment cost of the components. This allowed assessing the losses and the corresponding cost in the heat pump system in detail. The different operation strategies were simulated for the whole year 2018 and the obtainable income from FCR-N delivery was calculated.

The results showed that all operation modes with delivery of frequency regulation, resulted in reduced heat cost, compared to the spot market optimised operation and the heat demand driven operation. The lowest specific heat cost were obtained for frequency regulation with the large-scale heat pump alone and in all hours, where the heat pump was available. If the maximum hours of service provision were limited to five hours during the night, the specific income per unit of regulation energy provided was highest, and the specific cost of heat was only slightly higher than for frequency regulation service from the heat pump alone in the maximum available number of hours. Limiting the hours of operation to those hours with high capacity payments might be a relevant strategy if the cost of flexible operation are high and the minimum required capacity payment that allowed an economic feasible delivery of frequency regulation was high, too.

The combined provision of frequency regulation from 25 electric vehicles and the large-scale heat pump did not require the heat pump to be able to regulate fast enough for the respective frequency regulation service. Thereby, the heat pump could act on fast regulation markets in combination with the electric vehicles, which would not be possible for the heat pump alone. The electric vehicles benefitted from the combined operation, as the energy content of the frequency deviation was delivered by the heat pump. The electric vehicles could bid a larger power capacity on the market and thereby generate a larger income. In this way, a synergy effect was generated. The income from a heat pump perspective was however less than for the delivery of the same service by the heat pump alone, if the required ramping times are longer than the ramping time of the heat pump.

The exergy analysis showed that the exergy destruction and the associated cost caused by the heat pump constituted the largest share among the different components. Further, the system efficiency suffered, when the heat pump was operated at minimum and maximum load as the exergy efficiency was lower than at intermediate loads. Storing heat for long periods caused additional losses and reheating of the supply temperature became necessary, which further reduced the overall exergy efficiency. The cost and income allocation according to the proposed exergoeconomy based method showed that the overall benefit of flexible operation compared to the heat driven operation for the assessed case could be accounted to the frequency regulation, while the effect on the specific cost of heat was minor. This would not be the case if the base case had a lower overall exergy destruction than the newly proposed operation.

5 Conclusion

The aim of this thesis was to contribute to the development of integrating the heating and power sector and thereby supporting the vision and development of integrated energy systems based on 100 % renewable energy. This was done through thermodynamic and economic analysis of, how the supplied district heating network should look like, how flexible heat pumps can operate and whether the provision of frequency regulation may be feasible. In order to assess these questions, first, the influence of the characteristics of the supplied district heating area on the feasibility of low-temperature and ultra-low temperature district heating with three different kinds of decentral heating units was assessed. This was done using a techno-economic approach to evaluate the levelised cost of heat, the socioeconomic NPV and the systems efficiency in terms of system COP for all assessed cases. A generalised modelling approach was chosen that allowed identifying overarching trends, without having to know the district heating system topology in detail. Second, a dynamic model of a two-stage ammonia heat pump was implemented in Dymola. It was validated against experimental data from a recently built heat pump in Copenhagen and used to assess the dynamic behaviour of a large-scale two-stage ammonia heat pump. Further, the influence of control structure, component sizing and cycle design on the achievable ramping times was assessed to derive recommendations for the design of fast-regulating large-scale ammonia heat pumps. Thirdly, the economic feasibility of providing frequency regulation with the heat pump alone or in combination with fast-regulating bidirectional EV batteries was assessed and compared to heat driven operation and electricity spot market optimised operation. Further, a method to allocate additional cost and income to the regulation energy provided and the heat supplied was proposed. This was based on an exergoeconomic approach.

These approaches allowed answering the research questions formulated in chapter 1:

- For future suburban and urban (plot ratio above 0.6), newly built areas in Denmark supplied by heat pumps, heating supply by low temperature district heating is economically most feasible. For these low supply temperatures, supply from central heat pumps, especially exploiting water based heat sources, is recommendable. Generally, the levelised cost of heat (LCOH) for all considered alternatives decreased with increasing plot ratio and increasing space heating share for the assessed range of these variables. Therefore, for especially low linear heat demand densities, individual heat supply is preferable.
- The feasibility of ultra-low temperature district heating (ULTDH) supplied by large-scale heat pumps suffered from additional investment- and fixed O&M cost of the decentral units that were not outbalanced by the lower operation cost. A sensitivity analysis showed that ULTDH would benefit from the availability of cheap direct heat supply, possibly from industrial excess heat, reduced overall cost of decentral units, high linear heat demand densities and especially high shares of space heating demand. The latter does however contradict the development towards highly energy efficient buildings.
- The achievable regulation times for large-scale ammonia heat pumps are highly dependent on the control structure, the controller design and the refrigerant mass in the system. By parametrizing the controllers in the system according to heuristic

parametrisation rules, it was possible to reduce the regulation time to 500 s to 900 s for load changes of ±12.5 % to ± 75 %, assuming a steady-state tolerance of 0.1 % of full load power. The regulation time could be further reduced by controlling the power uptake directly. The limiting factor for fast regulation was the risk of droplet formation in the suction line during ramp down as the evaporation pressure increases suddenly. This risk may be avoided by adaption of the control structure, such that the evaporation pressure is controlled to a constant value together with preheating of the suction line. With these measures, resulting regulation times of 97 s for ± 30 % load and 149 s for ± 60 % load were predicted.

- In order to reduce regulation time during load change of large-scale heat pumps and thereby enable supplying frequency regulation with these units, the following design changes should be considered:
    - An option to preheat the suction line or superheat the fluid in or prior to the suction line and in this way reduce the risk of droplet entering the compressor
    - Minimisation of refrigerant mass in the system, especially in the vessels (i.e. separator and intercooler), to reduce the time constant of the system
    - Design of the control explicitly for fast regulation.

  It may however be expected that only a part of the heat pumps installed in future will be required to deliver ancillary services, i.e. the currently available best practice in design, which focusses on maximizing COP rather than optimizing regulation times, will still be the premise for many plants in the future.
- The simulation of frequency regulation operation using the dynamic model of the heat pump predicted that the heat pump is able to follow the grid frequency with an acceptable deviation of the active response power from the required value for the delivery of FCR-N. For faster primary frequency regulations, the combination with fast-regulating bidirectional units, such as vehicle-to-grid ready batteries, could allow the heat pump to participate in the corresponding market, despite being too slow to act on these markets alone.
- The conducted analysis showed that the largest income from a heat pump owner perspective could be generated by supplying frequency regulation from the heat pump alone. A combined delivery of frequency regulation with EV batteries still resulted in reduced heat cost compared to the electricity spot market optimised operation and the heat demand driven operation. The availability of the heat pump system to supply frequency regulation depends on the sizing of the heat pump and storage system. For the analysed case study it was found that a thermal capacity of the heat pump of approx. the maximum expectable heat demand resulted in the lowest cost.
- The exergoeconomic approach chosen for allocating cost to the two products of the heat pump, allows quantifying additional losses and benefits and allocating the cost and income accordingly. The underlying exergoeconomic analysis gives an insight into where and when losses occur in the system, and what the associated cost are. For the analysed case, the cost and income allocation showed that the overall benefit of flexible operation compared to the heat driven operation may be accounted to the frequency regulation, while the effect on the specific cost of heat was minor.
- The combined provision of frequency regulation from electric vehicles and a large-scale heat pump does not require the heat pump to be able to regulate fast enough for the respective frequency regulation service. The electric vehicles benefit from the combined operation, as the energy content of the frequency deviation is delivered by the heat pump.

Hence, the electric vehicles can bid a larger power capacity on the market and thereby generate a larger income. In this way, a synergy effect is generated.

With regard to the thesis statement, it is concluded that large-scale heat pumps are able to contribute to the sector coupling between the heating and power service by providing frequency regulation to the power grid. The supply of heat from central heat pumps and district heating is socioeconomically beneficial compared to other implementation variants for suburban and urban areas. The provision of frequency regulation is technically feasible for tertiary, secondary and some kinds of primary reserve. Faster services may also be delivered by large-scale heat pumps in combination with fast-regulating units. Heat pump operators may generate an additional income from frequency regulation services, both from the heat pump alone and in combination with fast regulating units.

5.1 Recommendations for future work

Based on the presented work, a number of promising aspects for future research were identified, which are presented in the following:

- The higher seasonal system efficiency of ULTDH is not reflected in the economic feasibility of these systems. In order to become more competitive, future research should be directed towards reduction of cost of decentral units, including measures to improve the COP, reduction of investment cost and of O&M cost. For a more precise analysis of the O&M cost of booster heat pumps, representative data is missing. To be able to reduce these cost in future, a survey of currently expectable O&M cost could provide useful information. Further, research is needed to answer whether the combination of district heating and cooling could help to increase the utilisation of the central system structures and thereby decrease the specific cost. Further, the technical and economic potential to reduce the operational cost by flexible operation of the decentral units to allow for exploitation of low electricity spot market prices or of additional income from provision of ancillary services should be assessed in future studies.
- The optimisation of the dynamic behaviour of large-scale heat pumps is an important basis for the development of flexibly operating heat pumps. This is not only relevant for the provision of ancillary services, but the dynamic behaviour might also be of relevance when operating large-scale heat pumps with fluctuating heat source temperatures, as e.g. air-source heat pumps, or in combination with other heat pumps. Here, it is expected that further research on the optimal system design and control structure for dynamic operation of large-scale heat pump as part of complex systems may help to exploit the heat sources in a more optimal way.
- The proposed operation mode and changes to system design require validation. The system used for validation is currently being rebuilt and first tests look promising with regard to the achievable low ramping times. However, the ability of the system to follow a certain grid frequency still needs to be verified with the real plant.
- The results from the dynamic simulations of the heat pump showed a clear correlation between the refrigerant mass in the system and the regulation time of the heat pump. Accordingly, future fast regulating heat pumps should be designed for minimum refrigerant charge. This aim needs further research especially with regard to design of low-charge intercooler and separator, the dynamic behaviour of low-charge systems and suitable controller design.

- In this work, heat pumps with piston compressors were assessed. However, even larger ammonia heat pumps often operate with screw compressors. The part-load control is fundamentally different compared to piston compressors, such that the influence on the dynamic behaviour of the overall plant should be assessed in more detail in order to extend the results of the current analysis to further types of heat pumps.
- The presented work focussed on ammonia as refrigerant, as this is most common in large-scale heat pumps. The COP of ammonia heat pumps benefits from minimum superheating of the fluid after the evaporator, and this contradicts the requirement of superheating in the suction line in order to be able to ramp into part-load quickly. This problem might be avoided by the use of alternative refrigerants, which benefit from superheating after the evaporator, such a HFOs. A preliminary study has been conducted in [193], but further analysis of influence of the usually used turbo compressors, of the cycle design, which often included internal heat exchangers and of the economic feasibility of these systems in general and their flexible operation in particular is recommended.
- Data is missing on the long-term influence of flexible operation of large-scale heat pump on component wear and maintenance cost. This would most likely require long-term data from several large-scale heat pumps and should be addressed in future studies.
- The presented study of the economic feasibility of frequency regulation provision focussed on the provision of FCR-N frequency regulation, which is the technically and economically most promising service for large-scale heat pumps in Eastern Denmark. This service conditions are different from most other primary frequency regulation services, such that specific evaluations of the economic feasibility of other ancillary services should be considered.
- The combined deliver of frequency regulation from large-scale heat pump and electric vehicles showed that economic synergy effects can be obtained. The combination of heat pumps with other fast regulating units, e.g. electric boilers, for flexible operation needs further investigation.
- The proposed exergoeconomy-based allocation method for cost and income from heat and ancillary service supply was developed specifically for power-to-heat units. The analysis of the combined service provision from electric vehicles and large-scale heat pumps opened up for another allocation problem, i.e. the allocation of income between two different units, contributing with different flexibility measures to the service. In this case, assigning a certain price to the different flexibility measures may seem more feasible. Different allocation options should be compared in more detail, in order to allow for a suitable division of cost to the different aggregated units according to their contribution to the provided service and the cost of flexible operation.

References

[1] Cook J, Oreskes N, Doran PT, Anderegg WRL, Verheggen B, Maibach EW, et al. Consensus on consensus: a synthesis of consensus estimates on human-caused global warming. Environ Res Lett 2016;11:048002. doi:10.1088/1748-9326/11/4/048002.

[2] Governor's Office of Planning and Research - State of California. List of Worldwide Scientific Organizations 2019. http://www.opr.ca.gov/facts/list-of-scientific-organizations.html (accessed December 10, 2019).

[3] UNFCCC. Paris Agreement. Conf Parties Its Twenty-First Sess 2015:32. doi:FCCC/CP/2015/L.9/Rev.1.

[4] European Comission. A Roadmap for moving to a competitive low carbon economy in 2050 2011:1–14. https://eur-lex.europa.eu/LexUriServ/LexUriServ.do?uri=COM:2011:0112:FIN:EN:PDF.

[5] European Comission. Energy roadmap 2050 (COM(2011) 885 final 2012:1–9. doi:10.2833/10759.

[6] Mourier L. Aftale om klimalov 2019:14001.

[7] European Comission. Comission staff working document - Review of available information - Accompanying the document Communication from the Commission to the European Parliament, the Council, the European Economic and Social Committee and the Committee of the Regions on an EU 2016;COM(2016):1–99. doi:10.1017/CBO9781107415324.004.

[8] Connolly D, Lund H, Mathiesen BV, Werner S, Möller B, Persson U, et al. Heat Roadmap Europe: Combining district heating with heat savings to decarbonise the EU energy system. Energy Policy 2014;65:475–89. doi:10.1016/j.enpol.2013.10.035.

[9] Danish Energy Agency. Energy statistics 2016. Danish Energy Agency; 2018.

[10] Mathiesen BV, Lund H, Connolly D, Wenzel H, Østergaard PA, Möller B, et al. Smart Energy Systems for coherent 100% renewable energy and transport solutions. Appl Energy 2015;145:139–54. doi:10.1016/j.apenergy.2015.01.075.

[11] Dansk Fjernvarme. Heat generation in Denmark. vol. 16. 2013.

[12] Energi- Forsynings- og Klimaministeriet. Bekendtgørelse af lov om varmeforsyning 2014;2017:24.

[13] Danish Government. Reformopfølgning Regulering af fjernvarmesektoren 2016:4.

[14] Danish Energy Agency. Biomass | Energistyrelsen n.d. https://ens.dk/en/our-responsibilities/bioenergy/solid-biomass (accessed June 13, 2018).

[15] Danish Energy Agency. Analysis of Bioenergy in Denmark (Analyse af bioenergi i Danmark) 2014:160.

[16] Østergaard PA, Lund H, Mathiesen BV. Smart energy systems and 4th generation district heating. Int J Sustain Energy Plan Manag 2016;10:1–2. doi:10.5278/ijsepm.2016.10.1.

[17] Energi- Forsynings- og Klimaministeriet. Forslag til Lov om ændring af lov om fremme af vedvarende energi, lov om tilskud til fremme af vedvarende energi i virksomheders produktionsprocesser og lov om elforsyning 2016:11–3.

[18] Lund H, Werner S, Wiltshire R, Svendsen S, Thorsen JE, Hvelplund F, et al. 4th Generation District Heating (4GDH). Integrating smart thermal grids into future sustainable energy systems. Energy 2014;68:1–11. doi:10.1016/j.energy.2014.02.089.

[19] Yang X, Svendsen S. Ultra-low temperature district heating system with central heat pump and local boosters for low-heat-density area: Analyses on a real case in Denmark. Energy 2018;159:243–51. doi:10.1016/j.energy.2018.06.068.

[20] Ommen T, Markussen WB, Elmegaard B. Lowering district heating temperatures – Impact to system performance in current and future Danish energy scenarios. Energy 2016;94:273–91. doi:10.1016/j.energy.2015.10.063.

[21] Kyriaki Foteinaki. Models for flexible building operation in the Nordhavn district energy system. Technical University of Denmark, Department of Civil Engineering, 2019.

[22] Basciotti D, Judex F, Pol O, Schmidt R. Sensible heat storage in district heating networks: a novel control strategy using the network as storage. 6TH Int Renew Energy Storage Conf Exhib (IRES 2011) 2011.
[23] Brand M, Svendsen S, Thorsen JE, Christiansen CH. A direct Heat Exchanger Unit used for domestic hot water supply in a single-family house supplied by Low Energy District Heating. 12th Int. Symp. Dist. Heat. Cool., 2010, p. 60–8.
[24] Pellegrini M, Bianchini A. The innovative concept of cold district heating networks: A literature review. Energies 2018;11. doi:10.3390/en11010236.
[25] Buffa S, Cozzini M, D'Antoni M, Baratieri M, Fedrizzi R. 5th generation district heating and cooling systems: A review of existing cases in Europe. Renew Sustain Energy Rev 2019;104:504–22. doi:10.1016/j.rser.2018.12.059.
[26] Averfalk H, Ingvarsson P, Persson U, Gong M, Werner S. Large heat pumps in Swedish district heating systems. Renew Sustain Energy Rev 2017;79:1275–84. doi:10.1016/j.rser.2017.05.135.
[27] United Nations. Amendment to the Montreal Protocol on Substances that Deplete the Ozone Layer C.N.872.2016.TREATIES-XXVII.2.f 2016.
[28] Støchkel HK, Paaske BL, Clausen KS. Drejebog til store varmepumpeprojekter i fjernvarmesystemet 2017. https://ens.dk/sites/ens.dk/files/Varme/drejebog_for_store_varmepumper.pdf.
[29] Jørgensen PH, Ommen T, Markussen WB, Elmegaard B. Performance Optimization of a Large-Scale Ammonia Heat Pump in Off-Design Conditions. 8th IIR Conf. Ammon. CO2 Refrig. Technol. Ohrid, 2019, 2019. doi:10.18462/iir.
[30] Zühlsdorf B, Bühler F, Jørgensen PH, Brian Elmegaard. Industrial Heat Pumps, Second phase . IEA Heat pump Technology (HTP) Programme Annex 48, Task 1: Danish Report - Final Report. 2019.
[31] Paaske BL. Store varmepumper i fjernvarmen - Roadmap for electrificering i Danmark (Presentation at Dansk Energi) n.d.:1–23.
[32] Energiministeriet KB og. Aftale om afskaffelse af PSO-afgiften. 2016:9.
[33] Danish Government. Energiaftale af 29. juni 2018 2018:19.
[34] Klimaministeriet. Bekendtgørelse om tilskud til investeringer i eldrevne varmepumper til produktion af fjernvarme 2019;2018:1–7.
[35] Danish Energy Agency. Rejsehold for store varmepumper | Energistyrelsen n.d. https://ens.dk/ansvarsomraader/varme/rejsehold-store-varmepumper (accessed June 21, 2018).
[36] Støchkel HK, Paaske BL, Clausen KS. Drejebog til store varmepumpeprojekter i fjernvarmesystemet Udarbejdet for Energistyrelsen og Grøn Energi 2017. https://ens.dk/sites/ens.dk/files/Varme/drejebog_for_store_varmepumper.pdf (accessed March 19, 2018).
[37] Danish Energy Agency. Energistatistik 2017: Data, tabeller, statistikker og kort. 2018.
[38] Lund R, Persson U. Mapping of potential heat sources for heat pumps for district heating in Denmark. Energy 2015;46. doi:10.1016/j.energy.2015.12.127.
[39] Fabian Bühler. Energy efficiency in the industry: A study of the methods, potentials and interactions with the energy system (Doctoral Thesis). 2018.
[40] Lund R, Ilic DD, Trygg L. Socioeconomic potential for introducing large-scale heat pumps in district heating in Denmark. J Clean Prod 2016:1–20. doi:10.1016/j.jclepro.2016.07.135.
[41] Kontu K, Rinne S, Junnila S. Introducing modern heat pumps to existing district heating systems – Global lessons from viable decarbonizing of district heating in Finland. Energy 2019;166:862–70. doi:10.1016/j.energy.2018.10.077.
[42] Bach B, Werling J, Ommen T, Münster M, Morales JM, Elmegaard B. Integration of large-scale heat pumps in the district heating systems of Greater Copenhagen. Energy 2016;107:321–34. doi:10.1016/j.energy.2016.04.029.
[43] Popovski E, Aydemir A, Fleiter T, Bellstädt D, Büchele R, Steinbach J. The role and costs of large-scale heat pumps in decarbonising existing district heating networks – A case study for the city of Herten in Germany. Energy 2019;180:918–33. doi:10.1016/j.energy.2019.05.122.

[44] David A, Mathiesen BV, Averfalk H, Werner S, Lund H. Heat Roadmap Europe: Large-Scale Electric Heat Pumps in District Heating Systems. Energies 2017;10:578. doi:10.3390/en10040578.
[45] Bloess A, Schill WP, Zerrahn A. Power-to-heat for renewable energy integration: A review of technologies, modeling approaches, and flexibility potentials. Appl Energy 2018;212:1611–26. doi:10.1016/j.apenergy.2017.12.073.
[46] Blarke MB. Towards an intermittency-friendly energy system: Comparing electric boilers and heat pumps in distributed cogeneration. Appl Energy 2012;91:349–65. doi:10.1016/j.apenergy.2011.09.038.
[47] Blarke MB, Lund H. Large-scale heat pumps in sustainable energy systems: System and project perspectives. Therm Sci Eng Prog 2007;11:143–52. doi:10.2298/TSCI0703143B.
[48] Kuprat M, Bendig M, Pfeiffer K. Possible role of power-to-heat and power-to-gas as flexible loads in German medium voltage networks. Front Energy 2017;11:135–45. doi:10.1007/s11708-017-0472-8.
[49] Levihn F. CHP and heat pumps to balance renewable power production: Lessons from the district heating network in Stockholm. Energy 2017;137:670–8. doi:10.1016/j.energy.2017.01.118.
[50] Averfalk H, Ingvarsson P, Persson U, Werner S, Industry D. On the use of surplus electricity in district heating systems. Proc. from 14th Int. Symp. Dist. Heat. Cool. Sept. 6-10, 2014 Stock. Sweden, 2014, p. 7–12.
[51] Storesund J. Handbok för livslängdsarbete med energianläggningar - Utgåva 2 2004:2.5.5-1-2.5.5-11.
[52] Fischer D, Madani H. On heat pumps in smart grids: A review. REHVA J 2017;70:342–57. doi:http://dx.doi.org/10.1016/j.rser.2016.11.182.
[53] Energinet.dk. Rapport behovsvurdering for systemydelser 2020. 2019.
[54] Energinet.dk. Ancillary services to be delivered in Denmark 2017:1–49.
[55] Energinet.dk. Regulation A : Principles for the electricity market. Regulation 2007;1:1–13.
[56] BMWi. Bericht des Bundesministeriums für Wirtschaft und Energie nach § 63 Abs . 2a EnWG zur Wirksamkeit und Notwendigkeit der Maßnahmen 2014.
[57] Energinet.dk. Introduktion til systemydelser 2017:1–12.
[58] By&Havn. Forside - Nordhavn 2019. https://byoghavn.dk/nordhavn/ (accessed December 5, 2019).
[59] EnergyLab Nordhavn. EnergyLab Nordhavn fremtidens energi system 2018. http://energylabnordhavn.weebly.com/ (accessed July 18, 2018).
[60] OpenStreetMap.org. OpenStreetMap 2019. openstreetmap.org.
[61] PowerLabDK at Center for Electric Power and Energy (CEE) D. PowerLabDK 2019. http://www.powerlab.dk/ (accessed December 5, 2019).
[62] EnergyDataDK. energydata.dk 2019. https://energydata.dk/ (accessed December 5, 2019).
[63] Cai H, Hutter A, Olivero E, Roduit P, Ferrez P. Load shifting for tertiary control power provision. 2015 IEEE 5th Int. Conf. Power Eng. Energy Electr. Drives, IEEE; 2015, p. 469–75. doi:10.1109/PowerEng.2015.7266363.
[64] Le Ray G, Larsen EM, Pinson P. Evaluating price-based demand response in practice - with application to the EcoGrid EU Experiment. IEEE Trans Smart Grid 2016;9:1–1. doi:10.1109/TSG.2016.2610518.
[65] Zong Y, Böning GM, Santos RM, You S, Hu J, Han X. Challenges of implementing economic model predictive control strategy for buildings interacting with smart energy systems. Appl Therm Eng 2017;114:1476–86. doi:10.1016/J.APPLTHERMALENG .2016.11.141.
[66] Gianniou P, Foteinaki K, Heller A, Rode C. Intelligent Scheduling of a Grid-Connected Heat Pump in a Danish Detached House. Build. Simul. 2017, San Fr. United States, 2017.
[67] Klyapovskiy S, You S, Bindner HW, Cai H. Optimal Placement of a Heat Pump in an Integrated Power and Heat Energy System. 2017 Ninth Annu. IEEE Green Technol. Conf., IEEE; 2017, p. 246–53. doi:10.1109/GreenTech.2017.42.
[68] Cai H, You S, Bindner HW, Klyapovskiy S, Yang X, Li R. Optimal scheduling for electric

heat booster under day-ahead electricity and heat pricing. 2017 52nd Int. Univ. Power Eng. Conf., IEEE; 2017, p. 1–4. doi:10.1109/UPEC.2017.8232027.
[69] Gjelaj M, Traholt C, Hashemi S, Andersen PB. Cost-benefit analysis of a novel DC fast-charging station with a local battery storage for EVs. 2017 52nd Int. Univ. Power Eng. Conf., vol. 2017-, IEEE; 2017, p. 1–6. doi:10.1109/UPEC.2017.8231973.
[70] Zilio E, Foteinaki K, Gianniou P, Rode C. Impact of Weather and Occupancy on Energy Flexibility Potential of a Low-energyBuilding. Build. Simul. 2017, San Fr. United States, 2017.
[71] Awadelrahman MAA, Zong Y, Li H, Agert C, Awadelrahman MAA, Zong Y, et al. Economic Model Predictive Control for Hot Water Based Heating Systems in Smart Buildings. Energy Power Eng 2017;09:112–9. doi:10.4236/epe.2017.94B014.
[72] Gjelaj M, Traeholt C, Hashemi S, Andersen PB. Optimal design of DC fast-charging stations for EVs in low voltage grids. 2017 IEEE Transp. Electrif. Conf. Expo, IEEE; 2017, p. 684–9. doi:10.1109/ITEC.2017.7993352.
[73] Cai H, You S, Bindner HW, Klyapovskiy S. Load Situation Awareness Design for Integration in Multi-Energy System. 2017 IEEE Int. Conf. Energy Internet, IEEE; 2017, p. 42–7. doi:10.1109/ICEI.2017.15.
[74] Zong Y, Ahmed AMA, Wang J, You S, Træholt C, Xiao X, et al. Enhancing Wind Power Integration through Optimal Use of Flexibility in Multi-Carrier Energy Systems from the Danish Perspective. World J Eng Technol 2017;05:78–88. doi:10.4236/wjet.2017.54B009.
[75] Foteinaki K. Modeling energy flexibility of low energy buildings utilizing thermal mass. Proc 9th Int Conf Indoor Air Qual Vent & Energy Conserv Build 2016.
[76] Wang J, Zong Y, You S, Træholt C. A review of Danish integrated multi-energy system flexibility options for high wind power penetration. Clean Energy 2017;1:23–35. doi:10.1093/ce/zkx002.
[77] Ommen T, Thorsen JE, Markussen WB, Elmegaard B. Performance of ultra low temperature district heating systems with utility plant and booster heat pumps. Energy 2017;137:544–55. doi:10.1016/j.energy.2017.05.165.
[78] Klyapovskiy S, You S, Domens RC, Bindner HW, Cai H. Utilizing Flexibility Services from a Large Heat Pump to Postpone Grid Reinforcement. 2018 IEEE Student Conf. Electr. Mach. Syst., IEEE; 2018, p. 1–6. doi:10.1109/SCEMS.2018.8624702.
[79] Wang A, Li R, You S. Development of a data driven approach to explore the energy flexibility potential of building clusters. Appl Energy 2018;232:89–100. doi:10.1016/J.APENERGY.2018.09.187.
[80] Li R, You S. Exploring potential of energy flexibility in buildings for energy system services. CSEE J Power Energy Syst 2018;4:434–43. doi:10.17775/CSEEJPES.2018.00360.
[81] Foteinaki K, Li R, Heller A, Rode C. Heating system energy flexibility of low-energy residential buildings. Energy Build 2018;180:95–108. doi:10.1016/j.enbuild.2018.09.030.
[82] Pieper H, Ommen T, Buhler F, Paaske BL, Elmegaard B, Markussen WB. Allocation of investment costs for large-scale heat pumps supplying district heating. Energy Procedia 2018;147:358–67. doi:10.1016/j.egypro.2018.07.104.
[83] Mitridati L, Taylor JA. Power Systems Flexibility from District Heating Networks. 2018 Power Syst. Comput. Conf., IEEE; 2018, p. 1–7. doi:10.23919/PSCC.2018.8442617.
[84] Thorsen JE, Ommen T. Field experience with ULTDH substation for multifamily building. Energy Procedia 2018;149:197–205. doi:10.1016/j.egypro.2018.08.184.
[85] Mitridati L, Pinson P. A Bayesian Inference Approach to Unveil Supply Curves in Electricity Markets. IEEE Trans Power Syst 2018;33:2610–20. doi:10.1109/TPWRS.2017.2757980.
[86] Le Ray G. Data-driven Demand Response Characterization and Quantification. Proc 12th Ieee Power Energy Soc Powertech Conf 2017.
[87] Meesenburg W, Ommen T, Elmegaard B. Dynamic exergoeconomic analysis of a heat pump system used for ancillary services in an integrated energy system. Energy 2018;152:154–65. doi:10.1016/j.energy.2018.03.093.
[88] Gjelaj M, Hashemi S, Traeholt C, Andersen PB. Grid integration of DC fast-charging stations for EVs by using modular li-ion batteries. IET Gener Transm Distrib 2018;12:4368–76. doi:10.1049/iet-gtd.2017.1917.

[89] Zühlsdorf B, Meesenburg W, Ommen TS, Thorsen JE, Markussen WB, Elmegaard B. Improving the performance of booster heat pumps using zeotropic mixtures. Energy 2018;154:390–402. doi:10.1016/j.energy.2018.04.137.
[90] Cai H, Ziras C, You S, Li R, Honoré K, Bindner HW. Demand side management in urban district heating networks. Appl Energy 2018;230:506–18. doi:10.1016/j.apenergy.2018.08.105.
[91] Meesenburg W, Geyer R, Terreros O, Pieper H, Ommen T, Elmegaard B. Feasibility of heat pumps supplying district heating systems: case study for Austria and Denmark. ISEC 2018, Int. Sustain. Energy Converence, 2018.
[92] Cai H, You S, Wang J, Bindner HW, Klyapovskiy S. Technical assessment of electric heat boosters in low-temperature district heating based on combined heat and power analysis. Energy 2018;150:938–49. doi:10.1016/j.energy.2018.02.084.
[93] Finck C, Li R, Kramer R, Zeiler W. Quantifying demand flexibility of power-to-heat and thermal energy storage in the control of building heating systems. Appl Energy 2018;209:409–25. doi:10.1016/J.APENERGY.2017.11.036.
[94] Pieper H, Ommen T, Elmegaard B, Brix Markussen W. Assessment of a combination of three heat sources for heat pumps to supply district heating. Energy 2019;176:156–70. doi:10.1016/j.energy.2019.03.165.
[95] Gjelaj M, Toghroljerdi SH, Andersen PB, Træholt C. Grid Services Provision from Batteries within Charging Stations by using a StochasticPlanning Method of the EVs Demand. IET Smart Grid 2019;(Accepted/.
[96] Meesenburg W, Ommen T, Thorsen JE, Elmegaard B. Economic feasibility of ultra-low temperature district heating systems in newly built areas supplied by renewable energy. Submitt to Energy 2019.
[97] Gjelaj M, Traeholt C, Hashemi S, Andersen PB. DC Fast-charging stations for EVs controlled by a local battery storage in low voltage grids. 2017 IEEE Manchester PowerTech, IEEE; 2017, p. 1–6. doi:10.1109/PTC.2017.7980985.
[98] Guillaume Le Ray. On the Role of Smart Metering Data Analytics in the Energy Sector Digitization Process - DTU Findit. Technical University of Denmark, 2019.
[99] Wang J, You S, Zong Y, Cai H, Træholt C, Dong ZY. Investigation of real-time flexibility of combined heat and power plants in district heating applications. Appl Energy 2019;237:196–209. doi:10.1016/J.APENERGY.2019.01.017.
[100] Pieper H. Comparison of COP estimation methods for large-scale heat pumps in energy planning tools. Proc Ecos 2019 32nd Int Conf Effic Cost, Optim Simul Environ Impact Energy Syst 2019.
[101] Foteinaki K, Li R, Rode C, Andersen RK. Modelling household electricity load profiles based on Danish time-use survey data. Energy Build 2019;202:109355. doi:10.1016/j.enbuild.2019.109355.
[102] Sarran L, Christensen MH, Hviid CA, Radoszynski AM, Rode C, Pierre P. Data-driven study on individual occupant comfort using heating setpoints and windowopenings in new low-energy apartments – preliminary insights. E3S Web Conf 2019;111. doi:10.1051/e3sconf/201911104063.
[103] Gjelaj M. Planning Strategies for EV Fast-Charging Stations combined with Battery Storage Systems in Distribution Grids - DTU Findit. Technical University of Denmark , 2019.
[104] Pieper H. Modelling framework for integration of large-scale heat pumps in district heating using low-temperature heat sources: A case study of Tallinn, Estonia. Int J Sustain Energy Plan Manag 2019;20. doi:10.5278/ijsepm.2019.20.6.
[105] Mitridati L. A Bid-Validity Mechanism for Sequential Heat and Electricity Market Clearing 2019.
[106] Le Ray G, Pinson P. Online adaptive clustering algorithm for load profiling. Sustain Energy, Grids Networks 2019;17:100181. doi:10.1016/j.segan.2018.100181.
[107] Klyapovskiy S, You S, Cai H, Bindner HW. Integrated Planning of a Large-Scale Heat Pump in View of Heat and Power Networks. IEEE Trans Ind Appl 2019;55:5–15. doi:10.1109/TIA.2018.2864114.

[108] Wang J, Hashemi S, You S, Troholt C. Active and reactive power support of MV distribution systems using battery energy storage. 2017 IEEE Int. Conf. Ind. Technol., IEEE; 2017, p. 382–7. doi:10.1109/ICIT.2017.7913261.
[109] Mitridati LM-JM. Market-Based Coordination of Heat and Electricity Systems - DTU Findit. Technical University of Denmark, 2019.
[110] Klyapovskiy S, You S, Cai H, Bindner HW. Incorporate flexibility in distribution grid planning through a framework solution. Int J Electr Power Energy Syst 2019;111:66–78. doi:10.1016/j.ijepes.2019.03.069.
[111] Meesenburg W, Kofler R, Ommen T, Markussen WB, Elmegaard B. Design considerations for dynamically operated large-scale ammonia heat pumps. 25th IIR Int. Congr. Refrig., 2019. doi:10.18462/iir.icr.2019.1203.
[112] Foteinaki K, Li R, Heller A, Herget Christensen M, Rode C. Dynamic thermal response of low-energy residential buildings based on in-wall measurements. E3S Web Conf 2019;111:04002. doi:10.1051/e3sconf/201911104002.
[113] Ommen T. Generalized COP estimation of heat pump processes for operation off the design point of equipment. Proc 25th Iir Int Congr Refrig 2019. doi:10.18462/iir.icr.2019.0648.
[114] Ray G Le, Christensen MH, Pinson P. Detection and Characterization of Domestic Heat Pumps. 2019 IEEE Milan PowerTech, IEEE; 2019, p. 1–6. doi:10.1109/PTC.2019.8810930.
[115] Zong Y, Su W, Wang J, Rodek JK, Jiang C, Christensen M, et al. Model Predictive Control for Smart Buildings to Provide the Demand Side Flexibility inthe Multi-Carrier Energy Context: Current Status, Pros and Cons, Feasibility and Barriers. Energy Procedia 2019;158:3026–31. doi:https://doi.org/10.1016/j.egypro.2019.01.981.
[116] Gjelaj M, Arias NB, Traeholt C, Hashemi S. Multifunctional applications of batteries within fast-charging stations based on EV demand-prediction of the users' behaviour. J Eng 2019;2019:4869–73. doi:10.1049/joe.2018.9280.
[117] Sarran L. Impact of Building Design Parameters on Thermal Energy Flexibility in a Low-Energy Building. Build Simul 2017 2017.
[118] Li R. Enhancing demand side flexibility in Nordhavn buildings for integrated multi-energy systems. B Abstr Sustain 2017 2017.
[119] Yu X, You S, Jiang Y, Zong Y, Cai H. An evolving experience learned for modelling thermal dynamics of buildings from live experiments: the Flexhouse story. Energy Procedia 2017;141:233–9. doi:10.1016/J.EGYPRO.2017.11.098.
[120] Pinson P, Mitridati L, Ordoudis C, Ostergaard J. Towards fully renewable energy systems: Experience and trends in Denmark. CSEE J Power Energy Syst 2017;3:26–35. doi:10.17775/CSEEJPES.2017.0005.
[121] EnergyLab Nordhavn. Recommendations and main results 2019.
[122] Elmegaard B, Schmidt Ommen T, Markussen M, Iversen J. Integration of space heating and hot water supply in low temperature district heating. Energy Build 2016;124:255–64. doi:10.1016/j.enbuild.2015.09.003.
[123] Reidhav C, Werner S. Profitability of sparse district heating. Appl Energy 2008;85:867–77. doi:10.1016/j.apenergy.2008.01.006.
[124] Best I, Orozaliev J, Vajen K. Economic comparison of low-temperature and ultra-low-temperature district heating for new building developments with low heat demand densities in Germany. Int J Sustain Energy Plan Manag 2018;16:45–60. doi:10.5278/ijsepm.2018.16.4.
[125] Vivian J, Emmi G, Zarrella A, Jobard X, Pietruschka D, De Carli M. Evaluating the cost of heat for end users in ultra low temperature district heating networks with booster heat pumps. Energy 2018;153:788–800. doi:10.1016/j.energy.2018.04.081.
[126] Köfinger M, Basciotti D, Schmidt RR, Meissner E, Doczekal C, Giovannini A. Low temperature district heating in Austria: Energetic, ecologic and economic comparison of four case studies. Energy 2016;110:95–104. doi:10.1016/j.energy.2015.12.103.
[127] Lund R, Skaarup Østergaard D, Yang X, Vad Mathiesen B. Comparison of Low-temperature District Heating Concepts in a Long-Term Energy System Perspective. Int J

Sustain Energy Plan Manag 2017;12:5–18. doi:dx.doi.org/10.5278/ijsepm.2017.12.2.
[128] Østergaard PA, Andersen AN. Booster heat pumps and central heat pumps in district heating. Appl Energy 2016;184:1374–88. doi:10.1016/j.apenergy.2016.02.144.
[129] Rambøll. District Heating Assessment Tool 2017. https://ens.dk/sites/ens.dk/files/Globalcooperation/dhat_report-10-17.pdf (accessed November 21, 2017).
[130] Energistyrelsen. Vejledning i samfundsøkonomiske analyser på energiområdet 2005.
[131] Dansk Fjernvarme. Dansk Fjernvarmes statistik 2017 2018. http://www.danskfjernvarme.dk/viden-om/statistik-subsection/aarsstatistik/statistik-2017 (accessed June 20, 2018).
[132] Caramaschi M, Østergaard KK, Christiansen CH. Novel domestic hot water microbooster heat pump in ultra-low temperature district heating. 4th Int. Conf. Smart Energy Syst. 4th Gener. Dist. Heat., Aalborg, Denmark: 2018, p. 1–15.
[133] Caramaschi M, (MetroTherm). Personal communication 2019.
[134] Mader G. Economic analysis of air-water heat pump technologies with a screening method (Doctoral thesis). Stockholm, Sweden: KTH Royal Institute of Technology, School of Industrial Engineering and Management; 2015.
[135] Bühler F, Petrović S, Holm FM, Karlsson K, Elmegaard B. Spatiotemporal and economic analysis of industrial excess heat as a resource for district heating. Energy 2018;151:715–28. doi:10.1016/j.energy.2018.03.059.
[136] By & havn. Levantkaj 2018. http://www.nordhavnen.dk/kvarterer+i+nordhavnen/indre+nordhavn/levantkaj.aspx (accessed February 6, 2019).
[137] European Commission. EU Regulation No. 626/2011 - Energy labelling of air conditioners. Off J Eur Union 2011;L 178:1–72.
[138] HOFOR. Projektforslag til Københavns Kommune - Fjernvarmeforsyning af Nordhavn 2013.
[139] Hansen CF, Hansen ML. Executive Order on the Publication of the Danish Building Regulations 2015 (BR15) 2015;2015.
[140] Wang PG, Scharling M, Wittchen KB, Kern-Hansen C. Technical Report 13-19 2001 – 2010 Danish Design Reference Year - Reference Climate Dataset for Technical Dimensioning in Building , Construction and other Sectors 2013.
[141] Danish Standards Association, European committee for standardization. Heat pumps with electrically driven compressors - Testing, performance rating and requirements for marking of domestic hot water units. EN 16147:2017, 2017.
[142] Aronsson S. Fjärrvärmekunders värme- och effektbehov (Heat and heat power demands from district heating customers). Göteborg, Sweden: Department of Building Services Engineering, Chalmers University of Technology; 1996.
[143] Frederiksen S, Werner S. District heating and cooling. Studentlitteratur; 2013.
[144] Persson U, Werner S. Heat distribution and the future competitiveness of district heating. Appl Energy 2011;88:568–76. doi:10.1016/j.apenergy.2010.09.020.
[145] Euroheat & Power Board. Guidelines for District Heating Substations. Euroheat & Power 2008:68.
[146] Jensen JK, Ommen T, Markussen WB, Elmegaard B. Design of serially connected district heating heat pumps utilising a geothermal heat source. Energy 2017;137:865–77. doi:10.1016/j.energy.2017.03.164.
[147] Thorsen JE, Ommen T. Field experience with ULTDH substation for multifamily building. Energy Procedia 2018;149:197–205. doi:10.1016/j.egypro.2018.08.184.
[148] Energistyrelsen. Vejledning i samfundsøkonomiske analyser på energiområdet 2018. https://ens.dk/sites/ens.dk/files/Analyser/vejledning_i_samfundsoekonomiske_analyser_paa_energiomraadet_-_juni_2018_v1.1.pdf (accessed July 22, 2019).
[149] Danish Energy Agency. Finding your cheapest way to a low carbon future - The Danish Levelized Cost of Energy Calculator 2015. https://ens.dk/sites/ens.dk/files/Globalcooperation/vejledning_lcoe_calculator.pdf.
[150] International Energy Agency, Agency, Nuclear energy agency. Projected costs of generating electricity 2015 Edition 2015.
[151] Danish Energy Agency, Energinet. Technology Data for Individual Heating Installations

2016:166.
https://ens.dk/sites/ens.dk/files/Analyser/technology_data_catalogue_for_heating_installations_-_marts_2018.pdf.
[152] Energinet.dk. Technology Data for Energy Plants 2016. www.ens.dk (accessed October 12, 2017).
[153] Energinet.dk. Technology Data for Energy Plants 2012. https://ens.dk/sites/ens.dk/files/Analyser/technologydata_for_energy_plants_-_may_2012._updated_2015.pdf (accessed October 12, 2017).
[154] Pieper H, Ommen T, Bühler F, Paaske BL, Elmegaard B, Markussen WB. Allocation of investment costs for large-scale heat pumps supplying district heating. Energy Procedia 2017;147:358–67. doi:https://doi.org/10.1016/j.egypro.2018.07.104.
[155] Grosse R, Christopher B, Stefan W, Geyer R, Robbi S. Long term (2050) projections of techno-economic performance of large-scale heating and cooling in the EU. Publ Off Eur Union 2017;EUR28859 E:1–180. doi:10.2760/24422.
[156] Pieper H, Ommen T, Buhler F, Lava Paaske B, Elmegaard B, Brix Markussen W. Allocation of investment costs for large-scale heat pumps supplying district heating. Energy Procedia 2018;147:358–67. doi:10.1016/j.egypro.2018.07.104.
[157] Metrotherm. Installatørprisliste 2018. 2018.
[158] Wolf S, Fahl U, Blesl M, Voss A, Jakobs R. Analyse des Potenzials von Industrie-wärmepumpen in Deutschland - Endbericht. 2014.
[159] Danish Energy Agency, ENERGINET. Technology Data for Energy Plants Generation of Electricity and District Heating 2016:1–186. doi:ISBN: 978-87-7844-940-5.
[160] Zinko H, Bøhm B, Kristjansson H, Ottosson U, Rämä M, Sipilä K. District heating distribution in areas with low heat demand density. 2008.
[161] Ommen TS. Heat Pumps in CHP Systems High-efficiency Energy System Utilising Combined Heat and Power and Heat Pumps 2015.
[162] HOFOR. EnergyLab Nordhavn Deliverable no. T5.4a: Optimizing temperatures in low-temperature district heating networks. 2019.
[163] Miara M. Ergebnisse zu neuen Feldmessungen von elektrisch angetriebenen Kompressionswärmepumpen. Tagung des Dtsch. Klima- und Kältetechnischen Vereins, Aachen: 2012, p. AA VI.2.
[164] Grüner S, Sandersen CEP, Jørgensen PH. Deliverable: D5.6 - Scenarios and recommendations for heat supply to Nordhavn 2025 , 2035 and 2050. 2019.
[165] Li P, Qiao H, Li Y, Seem JE, Winkler J, Li X. Recent advances in dynamic modeling of HVAC equipment. Part 1: Equipment modeling. HVAC R Res 2014;20:136–49. doi:10.1080/10789669.2013.836877.
[166] R. W. Rasmussen, MacArthur JW, Grald EW, Nowakowski GA. Performance of Engine-Driven Heat Pumps under Cycling Conditions. Symp ASHRAE Trans 1987;93:1079–90.
[167] Murphy WE, Goldschmidt VW. Cyclic Characteristics of a Typical Residential Air Conditioner - Modeling of Start-Up Transients. ASHRAE Trans 1985;91.
[168] Goldschmidt VW, Hart GH. Heat pump System performance: Experimental and Theoretical Results. ASHRAE Trans 1982;88:479–89.
[169] MacArthur JW, Grald EW. Prediction of Cyclic Heat Pump Performance with a Fully Distributed Model and a Comparison with Experimental Data. Symp ASHRAE Trans 1987;93.
[170] Rasmussen BP, Shenoy B. Dynamic modeling for vapor compression systems-Part II: Simulation tutorial. HVAC R Res 2012;18:956–73. doi:10.1080/10789669.2011.582917.
[171] Qiao H, Aute V, Radermacher R. Transient modeling of a flash tank vapor injection heat pump system - Part I: Model development. Int J Refrig 2015;49:169–82. doi:10.1016/j.ijrefrig.2014.06.019.
[172] Nunes TK, Vargas JVC, Ordonez JC, Shah D, Martinho LCS. Modeling, simulation and optimization of a vapor compression refrigeration system dynamic and steady state response. Appl Energy 2015;158:540–55. doi:10.1016/j.apenergy.2015.08.098.
[173] Modelica Association. Modelica and the Modelica Standard Library 2017. http://www.modelica.org (accessed October 31, 2017).

[174] Li P, Li Y, Seem JE, Qiao H, Li X, Winkler J. Recent advances in dynamic modeling of HVAC equipment. Part 2: Modelica-based modeling. HVAC R Res 2014;20:150–61. doi:10.1080/10789669.2013.836876.
[175] Jensen JB, Skogestad S. Optimal operation of simple refrigeration cycles: Part I: Degrees of freedom and optimality of sub-cooling. Comput Chem Eng 2007;31:712–21. doi:10.1016/J.COMPCHEMENG.2006.12.003.
[176] Goyal A, Staedter MA, Garimella S. A review of control methodologies for vapor compression and absorption heat pumps. Int J Refrig 2019;97:1–20. doi:10.1016/J.IJREFRIG.2018.08.026.
[177] Kjeld TFG. EnergyLab Nordhavn Delivery no.: D5.5a - Optimum supply of an island district heating grid by a local heat plant. 2019.
[178] TLK Thermo GmbH & IfT. TIL 3.4 – Model library for thermal components and systems 2017.
[179] Lemmon EW, Huber ML, McLinden MO. REFPROP - Reference Fluid Thermodynamic and Transport Properties - NIST Standard reference Database 23, Version 9.1 2013.
[180] Ayub ZH, Khan TS, Salam S, Nawaz K, Ayub AH, Khan MS. Literature survey and a universal evaporation correlation for plate type heat exchangers. Int J Refrig 2018;99:408–18. doi:10.1016/j.ijrefrig.2018.09.008.
[181] Yan YY, Lio HC, Lin TF. Condensation heat transfer and pressure drop of refrigerant R-134a in a plate heat exchanger. Int J Heat Mass Transf 1999;42:993–1006. doi:10.1016/S0017-9310(98)00217-8.
[182] Martin H. A theoretical approach to predict the performance of chevron-type plate heat exchangers. Chem Eng Process Process Intensif 1996;35:301–10. doi:10.1016/0255-2701(95)04129-X.
[183] Alfa Laval AB. CAS 5 Version 5.62.0.01 2016.
[184] Johnson Controls - Sabroe. COMP1 - Heat pump quick selection tool n.d. https://www.sabroe.com/en/products/sales-tools/comp1/ (accessed November 18, 2019).
[185] Dassault Systèmes AB. Dymola User Manual Vol 2. vol. 2. n.d.
[186] Seborg DE, Edgar TF, Mellichamp DA, Doyle FJ. Process dynamics and control. Wiley; 2010.
[187] Kuhn U. Eine praxisnahe Einstellregel für PID-Regler: Die T-Summen-Regel (A practical parametrization rule for PID-conrollers: The T-sum-rule). Autom Prax 1995;37:10–6.
[188] Qiao H, Xu X, Aute V, Radermacher R. Transient modeling of a flash tank vapor injection heat pump system - Part II: Simulation results and experimental validation. Int J Refrig 2015;49:183–94. doi:10.1016/j.ijrefrig.2014.06.018.
[189] Metropolis N, Ulam S. The Monte Carlo Method. J Am Stat Assoc 1949;44:335–41. doi:10.1080/01621459.1949.10483310.
[190] Pawitan Y. In all likelihood : statistical modelling and inference using likelihood. Clarendon Press; 2001.
[191] Saltelli A, Ratto M, Andres T, Campolongo F, Cariboni J, Gatelli D, et al. Global Sensitivity Analysis. The Primer. John Wiley & Sons Ltd; 2008.
[192] Johnson Controls Denmark ApS. Personal communication with Simon Stubkier 2019.
[193] Martin Pihl Andersen. Dynamic modelling and control of a large-scale HFO heat pump. Master Thesis, Copenhagen: DTU Mechanichal Engineering; 2019.
[194] Kjeld TG, Meesenburg W. EnergyLab Nordhavn - Deliverable no.: 5.5b Manual for optimized operation of an island district heating grid. 2019.
[195] Carmo C, Detlefsen N, Nielsen M. Smart Grid enabled heat pumps: An empirical platform for investigating how residential heat pumps can support largescale integration of intermittent renewables. Energy Procedia 2014;61:1695–8. doi:10.1016/j.egypro.2014.12.194.
[196] Stinner S, Schlösser T, Huchtemann K, Müller D, Monti A. Primary energy evaluation of heat pumps considering dynamic boundary conditions in the energy system. Energy 2017;138:60–78. doi:10.1016/j.energy.2017.07.029.
[197] Patteeuw D, Reynders G, Bruninx K, Protopapadaki C, Delarue E, D'haeseleer W, et al. CO2-abatement cost of residential heat pumps with active demand response: Demand-

and supply-side effects. Appl Energy 2015;156:490–501. doi:10.1016/j.apenergy .2015.07.038.
[198] Ulbig A, Andersson G. Analyzing operational flexibility of electric power systems. Int J Electr Power Energy Syst 2015;72:155–64. doi:10.1016/j.ijepes.2015.02.028.
[199] Blarke MB. The missing link in sustainable energy - Techno-economic consequences of large-scale heat pumps in distributed generation infavor of a domestic integration strategy for sustainable enery n.d.
[200] Robbi S. LowEx-Fernwärme - Vergleichende Bewertung von Maßnahmen für eine effiziente, multifunktionale Fernwärmeversorgung (Doctoral thesis). Technische Universität Dresden, 2013.
[201] Schlachtberger DP, Becker S, Schramm S, Greiner M. Backup flexibility classes in emerging large-scale renewable electricity systems. Energy Convers Manag 2016;125:336–46. doi:10.1016/j.enconman.2016.04.020.
[202] Schlachtberger DP, Becker S, Schramm S, Greiner M. Backup flexibility classes in emerging large-scale renewable electricity systems. Energy Convers Manag 2016. doi:10.1016/j.enconman.2016.04.020.
[203] Blarke MB, Lund H. The effectiveness of storage and relocation options in renewable energy systems. Renew Energy 2008;33:1499–507. doi:10.1016/j.renene.2007.09.001.
[204] Meibom P, Kiviluoma J, Barth R, Brand H, Weber C, Larsen H V. Value of electric heat boilers and heat pumps for wind power integration. Wind Energy 2007;10:321–37. doi:10.1002/we.224.
[205] Makarov Y V., Loutan C, Ma J, Mello P de. Operational impacts of wind generation on California power systems. IEEE Trans POWER Syst 2009;24, No. 2:1039–50. doi:10.1109/NOMS.2002.1015622.
[206] Hofor A/S. Personal communication with Tore Friis Gad Kjeld 2019.
[207] Thingvad A, Ziras C, Hu J, Marinelli M. Assessing the energy content of system frequency and electric vehicle charging efficiency for ancillary service provision. 2017 52nd Int. Univ. Power Eng. Conf., vol. 2017-, IEEE; 2017, p. 1–6. doi:10.1109/UPEC.2017.8231947.
[208] PowerLabDK at Center for Electric Power and Energy (CEE) - Technical University of Denmark. Frequency data for DK 2 2018 2019.
[209] Dassault Systèmes. Dymola Systems Engineering 2017. https://www.3ds.com/products-services/catia/products/dymola/ (accessed October 31, 2017).
[210] Grundfos. Product data SP 46-4 2017. https://product-selection.grundfos.com/product-detail.catalogue.productfamilies.html?from_suid=151022228811006388052718785822&pumpsystemid=280760607&qcid=271031787 (accessed July 4, 2017).
[211] Grundfos. Product data NB 32 - 200/206 2017. https://product-selection.grundfos.com/product-detail.catalogue.productfamilies.html?from_suid=151022250390601434492979880763 7&pumpsystemid=290981485&qcid=293056119 (accessed October 30, 2017).
[212] HOFOR. Heat demand data for 3 cruise ship terminal buildings and a warehouse. Copenhagen: 2018.
[213] Spurk JH, Aksel N. Fluid Mechanics. Second Edi. 2008. doi:10.1007/978-3-540-73537-3.
[214] Rothuizen E, Markussen W, Elmegaard B, Madsen C, Olesen MF, Sølvsten M. High Efficient Heat Pump System Using Storage Tanks To Increase Cop By Means of the Isec Concept (Part I , Thermal Storage System). Proc 24th IIR Int Congr Refrig 2015:1–8.
[215] Angenendt G, Zurmühlen S, Figgener J, Kairies K, Uwe D. Providing frequency control reserve with photovoltaic battery energy storage systems and power-to-heat coupling. Energy 2020;194:116923. doi:10.1016/j.energy.2020.116923.
[216] Zecchino A, Thingvad A, Andersen PB, Marinelli M. Test and Modelling of Commercial V2G CHAdeMO Chargers to Assess the Suitability for Grid Services. World Electr Veh J 2019;10:21. doi:10.3390/wevj10020021.
[217] Trahand M. Nuvve V2G & deployments. 2nd Veh. Conf. - Electr. Veh. Renew. city, Amsterdam Univ. Appl. Sci., 2017.
[218] ACES. Project website 2016. www.aces-bornholm.eu,.
[219] Christiansen H. The Danish National Travel Survey 2017. https://www.cta.man.dtu.dk/

english/national-travel-survey.
[220] Thingvad A, Ziras C, Marinelli M. Economic value of electric vehicle reserve provision in the Nordic countries under driving requirements and charger losses. J Energy Storage 2019;21:826–34. doi:10.1016/j.est.2018.12.018.
[221] Energinet.dk. Energinet.dk - Markedsdata 2018. http://www.energinet.dk (accessed September 20, 2019).
[222] Bejan A, Tsatsaronis G, Moran M. Thermal design and optimization. John Wiley & Sons, Inc.; 1996.
[223] Sayadi S, Tsatsaronis G, Morosuk T. A New Approach for Applying Dynamic Exergy Analysis and Exergoeconomics to a Building Envelope 2016:1–17.
[224] Sangi R, Martín PM, Müller D. Thermoeconomic analysis of a building heating system. Energy 2016;111:351–63. doi:10.1016/j.energy.2016.05.112.
[225] Lazzaretto A, Tsatsaronis G. SPECO: A systematic and general methodology for calculating efficiencies and costs in thermal systems. Energy 2006;31:1257–89. doi:10.1016/j.energy.2005.03.011.
[226] Rosen MA, Dincer I. Thermal energy storage systems and applications. 2nd ed. Ontario, Canada: John Wiley & Sons, Inc.; 2011.
[227] Center for Klima og Energiøkonomi. Forudsætninger for samfundsøkonomiske analyser på energiområdet 2016;Version 3. https://ens.dk/sites/ens.dk/files/Analyser/samfundsoekonomiske_beregningsforudsaetninger_2016_v3.pdf.
[228] PlanEnergi. Personal Communication with Bjarke Lava Paaske 2018.

List of Figures

List of tables

Appendix A – Additional material

A.1. Graphical representation of the validation and calibration procedure applied to the dynamic model

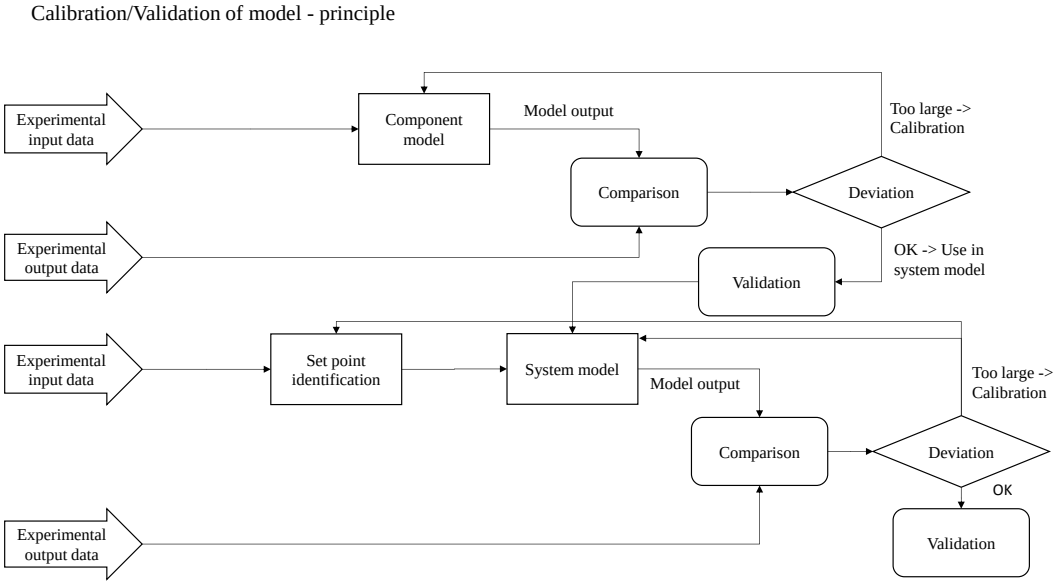

A.2. Component specifications for dynamic model of base-case heat pump

Table 0-1 Main component specifications. Calibrated parameters are marked with *.

Component	Parameter	Value	Reference
Low-stage compressor	Displacement	0.0094 m^3	[184]
High-stage-compressor	Displacement	0.0037 m^3	[184]
	Relative dead space	4 %	
	Charge valve delay	$0.4 \cdot 10^{-3}$ s	
	Total heat transfer coefficient*	250 W/K	
	Ambient temperature	20 °C	
Desuperheater	Heat transfer model VLE - Single-phase	Martin's correlation	[182]
	Heat transfer model VLE - Condensation	Yan's correlation	[181]
	Pressure drop model VLE	Assumption: $\Delta p = 0$	
	Heat transfer model water	Martin's correlation	[182]
	Pressure drop model water	Assumption: $\Delta p = 0$	
	Plate length	0.719 m	
	Plate width	0.326 m	
	Chevron-Angle*	30 °	
	Corrugation amplitude*	$1.33 \cdot 10^{-3}$ m	
	Corrugation wave length*	$15 \cdot 10^{-3}$ m	
	Plate thickness	$0.8 \cdot 10^{-3}$ m	
	Plate material	Stainless steel	

	Number of plates	42	
	Number of cells (discretisation	5	
Condenser	Heat transfer model VLE - Single-phase	Martin's correlation	[182]
	Heat transfer model VLE - Condensation	Yan's correlation	[181]
	Pressure drop model VLE	Assumption: $\Delta p = 0$	
	Heat transfer model water	Martin's correlation	[182]
	Pressure drop model water	Assumption: $\Delta p = 0$	
	Plate length	$0.719\ \mathrm{m}$	
	Plate width	0.326 m	
	Chevron-Angle*	30 °	
	Corrugation amplitude*	$0.83 \cdot 10^{-3}$ m	
	Corrugation wave length*	$13.9 \cdot 10^{-3}$ m	
	Plate thickness	$0.8 \cdot 10^{-3}$ m	
	Plate material	Stainless steel	
	Number of plates	58	
	Number of cells (discretisation	5	
Subcooler	Heat transfer model VLE - Single-phase	Martin's correlation	[182]
	Heat transfer model VLE - Condensation	Yan's correlation	[181]
	Pressure drop model VLE	Assumption: $\Delta p = 0$	
	Heat transfer model water	Martin's correlation	[182]
	Pressure drop model water	Assumption: $\Delta p = 0$	
	Plate length	$0.719\ \mathrm{m}$	
	Plate width	0.326 m	
	Chevron-Angle*	30 °	
	Corrugation amplitude*	$1.206 \cdot 10^{-3}$ m	
	Corrugation wave length*	$15 \cdot 10^{-3}$ m	
	Plate thickness	$0.8 \cdot 10^{-3}$ m	
	Plate material	Stainless steel	
	Number of plates	24	
	Number of cells (discretisation	5	
Evaporator	Heat transfer model VLE - Single-phase	Martin's correlation	[182]
	Heat transfer model VLE - Evaporation	Ayub's correlation	[180]
	Pressure drop model VLE	Quadratic mass flow dependent ($\dot{m}_{nom} = 0.69 \frac{kg}{s}$, $\Delta p_{nom} = 0.004\ \mathrm{bar}$)	
	Heat transfer model water	Martin's correlation	[182]
	Pressure drop model water	Assumption: $\Delta p = 0$	
	Plate length	$0.719\ \mathrm{m}$	
	Plate width	0.37 m	
	Chevron-Angle*	60 °	
	Corrugation amplitude*	$0.95 \cdot 10^{-3}$ m	
	Corrugation wave length*	$15 \cdot 10^{-3}$ m	

	Plate thickness	$0.6 \cdot 10^{-3}$ m
	Plate material	Titanium
	Number of plates	240
	Number of cells (discretisation	5
Open flash intercooler	Volume	1.27 m^3
	Initial fluid level	8 %
Separator	Volume	0.83 m^3
	Initial fluid level	4.3 %
Auxiliary pump	Efficiency	1
	Fixed pressure increase	0.004 bar
High-stage expansion valve	Effective flow area (full load)	$1.34 \cdot 10^{-5}$ m^2
Low-stage expansion valve	Effective flow area (full load)	$1.75 \cdot 10^{-5}$ m^2
PI-control source outlet temperature / low-stage compressor	Gain factor	-2.11
	Time constant	10 s
	Constrained ramp rate (integral part)*	0.05 $1/s^2$
PI-control intermediate pressure / high-stage compressor	Gain factor	$-1.04 \cdot 10^{-5}$
	Time constant	11.5 s
PI-control condensation pressure / sink mass flow	Gain factor	$0.16 \cdot 10^{-5}$
	Time constant	5 s
PI-control vapour quality at condenser outlet / high-stage expansion valve	Gain factor	$7.87 \cdot 10^{-5}$
	Time constant	20.75 s
PI-control fluid level in OFIC / low-stage expansion valve	Gain factor	$-2.56 \cdot 10^{-4}$
	Time constant	40 s
PI-control power / low-stage compressor	Gain factor	
	Time constant	
PID-control evaporation pressure / low-stage expansion valve	Gain factor	$1.30 \cdot 10^{-9}$
	Time constant (Integral)	2.65 s
	Time constant (Derivative)	0.67
PI-control source outlet temperature/ source mass flow rate	Gain factor	2.68
	Time constant	20 s

Appendix B – Publications

Dynamic exergoeconomic analysis of a heat pump system used for ancillary services in an integrated energy system

Energy 152 (2018) 154–165

Contents lists available at ScienceDirect

Energy

journal homepage: www.elsevier.com/locate/energy

Dynamic exergoeconomic analysis of a heat pump system used for ancillary services in an integrated energy system

Wiebke Meesenburg*, Torben Ommen, Brian Elmegaard

Department of Mechanical Engineering, Technical University of Denmark, Lyngby, Denmark

ARTICLE INFO

Article history:
Received 20 November 2017
Received in revised form
9 March 2018
Accepted 17 March 2018
Available online 20 March 2018

Keywords:
Dynamic exergoeconomic analysis
Integrated energy systems
Heat pump
Flexibility
Ancillary services

ABSTRACT

The integration of different energy sectors, such as the electricity and heating sector, is an effective way to integrate large shares of renewable energy into the energy system. Heat pumps allow efficient heat production based on electricity. As such, they may be used to provide two different services - the generation of heat and the provision of demand flexibility as ancillary services for the power system. The paper presents a method to assess the impact of providing demand flexibility on the performance of the conversion system based on a dynamic exergoeconomic analysis. A way to allocate the cost of heat and flexibility products based on the difference in exergy destruction was proposed. The method was applied to a case of a groundwater-source heat pump system supplying a district heating island system. It was found that providing demand flexibility causes higher exergy destruction, mainly due to heat losses during storage and the need to reheat the fluid using an electric heater. The major part of the additional exergy destruction was not related to heat pump regulation. When providing flexibility the overall cost of the system increased and according to the proposed allocation, demand flexibility accounted for 12% of the overall cost.

1. Introduction

The future Danish energy system will be characterized by high shares of transient renewable power production [1]. One of the main challenges imposed by this is to design future energy systems to be able to balance high shares of fluctuating power and to achieve an efficient use of the energy available. This challenge may be met by integrating the power, heating and mobility sectors. Synergies can be exploited, and it is expected that it will be possible to allocate higher shares of renewable energy, increase the overall energy efficiency of the system and help to ensure a reliable and resilient energy system [2].

The heating sector can absorb large amounts of electricity and additionally offers the possibility to store the energy as heat in heat storages, buildings and district heating systems [3]. Different technologies are available to couple the heating and electricity sector by converting one energy form into another, such as heat pumps and electric heaters. Mathiesen and Lund [4] found that large scale heat pumps are especially promising to efficiently integrate large amounts of renewable energy into the system. However, the ability and limitations of large heat pumps to provide demand flexibility need further investigation [5].

In this study, we focus on the integration between the heating and the power system by analyzing a heat pump system supplying a district heating island system. Further, the system acts as a controllable load in the power system, i.e. the heat pump electricity consumption changes according to signals from the power system operator [6]. Previous studies showed that the integration of the electricity and the heating sectors offers the possibility to decouple electricity supply and demand constraints and can provide balancing service to the power sector [7]. Stinner et al. [8] confirmed that balancing services from lower voltage levels are necessary in energy systems with a high share of renewables to balance the distribution and transmission grids. Further, controlling the load of heat pumps flexibly can reduce CO_2 emissions and lower CO_2 abatement cost, while the overall electricity consumption may increase [9].

The considered conversion system provides two different products – the heat supplied to the district heating grid and the ancillary service to the electricity grid. This has several consequences for the operation of the heat pump. Firstly, the operation strategy has to take the demand of heat and power regulation into consideration. Secondly, the ability to provide flexibility comes at

* Corresponding author.
E-mail address: wmeese@mek.dtu.dk (W. Meesenburg).

https://doi.org/10.1016/j.energy.2018.03.093
0360-5442/

the cost of increased investment cost for a larger conversion system. Thirdly, the flexible operation leads to additional losses in the conversion system. The three consequences open for investigations of the valuation of the different products and the additional cost of flexible operation.

Ulbig & Andersson define the operational flexibility of a power system as the technical ability of a power system to modulate the power feed-in or load over time [10]. Extending this definition to integrated energy systems, we propose to define flexibility as the technical ability of a energy conversion system to adapt the power feed-in, load or conversion into other forms of energy in order to optimize security of supply, cost and/or environmental impact of the overall energy system.

Different studies have been carried out in an effort to determine the value of flexibility provided by heat pumps and electric heaters. Three general approaches were identified.

The first approach is to define an average flexibility value by considering the differences between supply and demand [7], [11], [12]. This approach is based on the idea that the unit that adapts to the state of the system, and thus decreases the difference between supply and demand, provides a balancing service to the system.

The second approach takes the specifications regarding ramping rates and capacities of the different components into consideration. In this way it evaluates the actual potential of a component to react to regulation needs of the system at a certain point in time with respect to the current state of component operation [10–13].

The third approach is to evaluate the flexibility of a unit by evaluating the cost effectiveness of an increase of flexibility. Blarke & Lund [15] defined the cost effectiveness of the storage or relocation option as the shadow cost associated with increased flexibility of a certain unit. Meibom et al. [16] propose to evaluate the impact of heat pumps and electric boilers according to their influence on the price of regulating power.

All these approaches value flexibility according to the benefit of the power system or of the overall energy system. However, it is important to assess which cost is associated with providing ancillary services for the heat pump system operator, as this is valuable information when deciding on the operation strategy and the system design. The analysis of the actual changes induced to the conversion system and the associated costs requires a more detailed method than suggested by the above references.

In the present study, the performance of a conversion system was analyzed using an exergoeconomic approach. A dynamic model of the system was simulated and a dynamic exergoeconomic analysis was conducted in order to reveal the exergy destruction connected to the flexible operation of the system and where and when it occurs. The method of exergoeconomic analysis is a combination of an exergy analysis and economic principles and is used to obtain information about how to design and operate energy conversion systems in a cost-effective way [17]. It enables the allocation of cost to multiple products of any energy conversion plant based on a framework that consistently connects economics and thermodynamics. Usually, an exergoeconomic analysis is conducted assuming steady state processes. Sayadi et al. [18] conducted a dynamic exergy and exergoeconomic analysis for a building envelope. Sangi et al. [19] presented an approach, to conduct a quasi-dynamic exergoeconomic analysis by analyzing the result of each time step for a dynamic simulation of a building heating system.

In this paper, we used a dynamic exergoeconomic analysis to assess the system performance. The method is extended by the definition of exergy fuel and exergy product for the stratified storage tank and an approach to allocate the cost to both products of the system – heat and demand flexibility. In section 2 we describe the method, including a description of the case study, the mathematical model, exergy and exergoeconomic analysis. Section 3 presents the results found for the case study and section 4 discusses the results and the method that was used. Finally, in section 5 the conclusions are presented.

2. Method

The paper presents an approach to use dynamic exergoeconomic analysis to assess the performance of a conversion unit in an integrated energy system. Further, we propose a way to allocate the cost between heat and demand flexibility. The method is applied to a case presented in the following.

2.1. Case study

The case studied was a district heating island system that was designed for the Ocean Quay cruise ship terminal in Copenhagen. The system was designed to supply three terminal buildings and a large warehouse with heat for space heating and domestic hot water. The heat pump replaced the formerly implemented oil burners and has a nominal capacity of 800 kW. Fig. 1 shows a sketch of the described system and all water and electricity flows in the system. The heat source for the heat pump was groundwater delivered by the groundwater (GW) pump. Further, the system comprised a stratified storage tank of 120 m^3, a district heating (DH) pump and two electric boilers of 100 kW each. The heat demand, including distribution losses, was lumped into a heat demand model and it was assumed that the heat pump system should supply a constant temperature of 70 °C into the DH grid (Stream 8 in Fig. 1). Table 1 summarizes the capacity of the components used in the assessed case.

To compare the results on an energy basis we defined the seasonal heat pump COP and the seasonal system coefficient of performance (SCOP) as

$$\mathrm{COP}_{\mathrm{season}} = \frac{Q_{\mathrm{heat}}}{W_{\mathrm{HP}}} \tag{1}$$

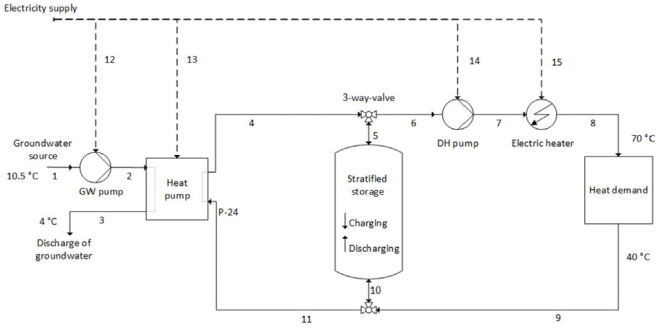

Fig. 1. Sketch of the considered heat pump system in, Copenhagen, solid lines – water, dashed lines – electricity.

Table 1
Specification of units in the considered system.

Unit	Capacity
Heat pump minimum heating capacity	150 kW
Heat pump nominal heating capacity	800 kW
Electric boiler capacity	2·100 kW
District heating pump design flow	2·16.7 $\frac{kg}{s}$
Groundwater pump design flow	2·44.3 $\frac{kg}{s}$
Stratified Storage tank	120 m^3

$$SCOP_{season} = \frac{Q_{heat}}{\sum_k W_k} \quad (2)$$

where Q_{heat} denotes the annual amount of heat delivered into the DH network, W_k is the annual amount of electric energy supplied to component *k and accordingly* W_{HP} *is the annual amount of electric energy supplied to the heat pump.* In the sum all electrical components, i.e. the heat pump, the electric heater, the groundwater pump and the DH pump were considered.

2.2. Model

The model was formulated in Modelica [20] and implemented in Dymola [21]. It contained seven main component models representing a heat pump, an electric boiler, a stratified storage tank, two pumps, a lumped heat demand model, two three-way-valves and a central control unit. Models for the heat demand, the heat pump, the control unit and stratified storage tank are further described below. All models were based on energy, mass and impulse balance equations. When not indicated differently, pressure losses were neglected. The pump model was adapted from an existing model from the TIL library [22]. The pump efficiency was implemented as a quadratic function, obtained from manufacturer's data [23,24].

2.2.1. Heat demand model

The heat demand model was a simplified model of the demand side of the system. It included the accumulated demand of all buildings and the heat losses in the distribution system. The demand was measured demand data of the system on hourly basis for the year 2012 [25]. In practice, the heat demand would be forecasted and the operation schedule of the day ahead would be optimized. However, for the current study a simplified approach was chosen. Based on the demand data, the required mass flow for each time step was calculated which was used to control the district heating pump supplying the network. It was assumed that the building substations are designed to cool the district heating water to a constant return temperature of 40 °C (Stream 9 Fig. 1). The actually supplied heat was calculated from an energy balance in the model. The system pressure loss was estimated to be at 3 bar, independently of the flow.

2.2.2. Heat pump model

The heat pump was a two stage ammonia heat pump with open intercooler. It was equipped with a piston compressor, which was controlled via a variable frequency drive. Brackish groundwater at 10.5 °C was the heat source. It was assumed that the groundwater can be cooled to 4 °C before being discharged into the sea.

A dynamic energy balance for the heat pump was used to describe the model.

$$\frac{dQ_{HP}}{dt} = \dot{Q}_{eva} + \dot{W}_{HP} + \dot{Q}_{con} \quad (3)$$

The term dQ_{HP}/dt represents the changed heat flow due to inertia in the heat pump. $\dot{Q}_{eva}$ is the heat flow in the evaporator, $\dot{W}_{HP}$ is the power uptake of the compressor and $\dot{Q}_{con}$ represent the condenser heat load.

The heat pump is implemented as a black box. Thus, a function for the actual heat output from the condenser during load changes was implemented to represent the dynamic start-up and load changing characteristics of the heat pump. Full heat production is not available during start-up compared to an theoretic instantaneous start-up, and heat will still be rejected after shut-off of the compressor (Fig. 2). It was assumed that the dynamic heat load at the condenser follows a first order characteristic, which was included as function for the actual heat load $\dot{Q}_{con}$ into the model.

$$\frac{d\dot{Q}_{con}}{dt} = \begin{cases} k_1 \cdot \left(\dot{Q}_{con,ss} - \dot{Q}_{con}\right) for \left(\dot{Q}_{con,ss} - \dot{Q}_{con}\right) > 0 (ramp-up) \\ k_2 \cdot \left(\dot{Q}_{con,ss} - \dot{Q}_{con}\right) for \left(\dot{Q}_{con,ss} - \dot{Q}_{con}\right) \leq 0 (ramp-down) \end{cases} \quad (4)$$

Table 2
Exergy fuel and -product and specific cost per unit of exergy fuel and product for the components used in the case study. Charging and discharging refer to charging/discharging of the storage tank. When there is no flow in or out of the tank, the equations for discharging are valid.

	Exergy fuel $\dot{E}_{F,i}$/Specific cost per unit of exergy fuel c_F	Exergy product $\dot{E}_{P,i}$/Specific cost per unit of exergy product c_P	Auxiliary equations
Heat pump	$\dot{E}_F = \begin{cases} \dot{W}_{13} + \frac{dE_{HP}}{dt} & : if \ \frac{dE_{HP}}{dt} < 0 \\ \dot{W}_{13} & : else \end{cases}$ $c_F = c_{el}$	$\dot{E}_P = \begin{cases} \dot{E}_4 - \dot{E}_{11} + \frac{dE_{HP}}{dt} & : if \ \frac{dE_{HP}}{dt} > 0 \\ \dot{E}_4 - \dot{E}_{11} & : else \end{cases}$ $c_P = \frac{\dot{C}_4 - \dot{C}_{11}}{\dot{E}_4 - \dot{E}_{11}}$	$c_3 = c_F$
3-way-valve	$\dot{E}_F = \begin{cases} \dot{E}_4 & : charging \\ \dot{E}_4 + \dot{E}_5 & : discharging \end{cases}$ $c_F = \begin{cases} \frac{\dot{C}_4}{\dot{E}_4} & : charging \\ \frac{\dot{C}_4 + \dot{C}_5}{\dot{E}_4 + \dot{E}_5} & : discharging \end{cases}$	$\dot{E}_P = \begin{cases} \dot{E}_5 + \dot{E}_6 & : charging \\ \dot{E}_6 & : discharging \end{cases}$ $c_P = \begin{cases} \frac{\dot{C}_5 + \dot{C}_6}{\dot{E}_5 + \dot{E}_6} & : charging \\ \frac{\dot{C}_6}{\dot{E}_6} & : discharging \end{cases}$	$c_5 = c_6$ (for charging)
DH Pump	$\dot{E}_F = \dot{W}_{14}$ $c_F = c_{el}$	$\dot{E}_P = \dot{E}_7 - \dot{E}_6$ $c_P = \frac{\dot{C}_7 - \dot{C}_6}{\dot{E}_7 - \dot{E}_6}$	
GW Pump	$\dot{E}_F = \dot{W}_{12}$ $c_F = c_{el}$	$\dot{E}_P = \dot{E}_2 - \dot{E}_1$ $c_P = \frac{\dot{C}_2 - \dot{C}_1}{\dot{E}_2 - \dot{E}_1}$	
Electric heater	$\dot{E}_F = \dot{W}_{15}$ $c_F = c_{el}$	$\dot{E}_P = \dot{E}_8 - \dot{E}_7$ $c_P = \frac{\dot{C}_8 - \dot{C}_7}{\dot{E}_8 - \dot{E}_7}$	
Stratified storage tank	$\dot{E}_F = \begin{cases} \dot{E}_5 & : charging \\ \frac{dE_{hot}}{dt} & : discharging \end{cases}$ $c_F = \begin{cases} \dot{C}_5 & : charging \\ \frac{dC_{hot}}{dt} & : discharging \end{cases}$	$\dot{E}_P = \begin{cases} \frac{dE_{hot}}{dt} & : charging \\ \dot{E}_5 & : discharging \end{cases}$ $c_P = \begin{cases} \frac{dC_{hot}}{dt} & : charging \\ \dot{C}_5 & : discharging \end{cases}$	$c_{10} = \frac{\dot{C}_{cold}}{\dot{E}_{cold}}$ (for charging)

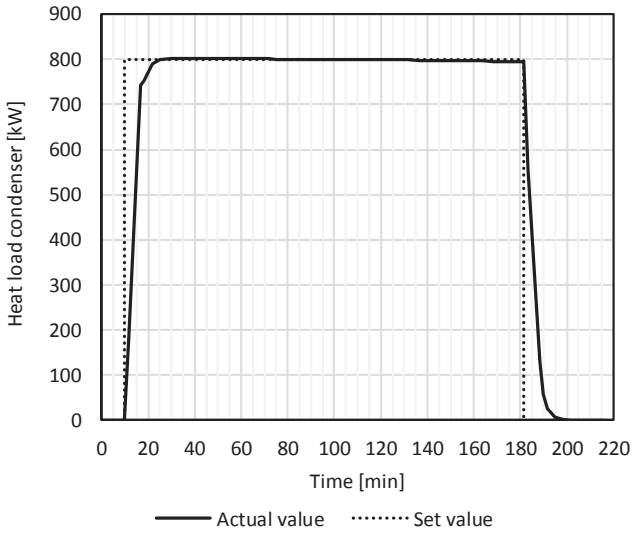

Fig. 2. Steady state set value and actual value of condenser heat load for start-up and shut-down.

The parameters $k_1 = 0.0016$ and $k_2 = 0.0018$ were chosen to represent a start-up time of 15 min and a shut-down time of 20 min. The term $\dot{Q}_{con,ss}$ represents the condenser heat load in steady state, which was calculated from the coefficient of performance (COP) in steady state. It was assumed that COP in steady-state depends solely on the sink and source temperatures and a given exergy efficiency ε_{ss} [26].

$$COP_{ss} = \left(1 - \frac{T_{m,source}}{T_0} * \left(\frac{1}{\varepsilon_{ss}} * \left(\frac{T_0}{T_{m,sink}} - 1\right) + 1\right)\right)^{-1} \quad (5)$$

$$T_{m,i} = \frac{T_{out,i} - T_{in,i}}{\ln\left(\frac{T_{out,i}}{T_{in,i}}\right)} \quad (6)$$

$$\dot{W}_{el,HP} = \frac{\dot{Q}_{con,ss}}{COP_{ss}} \quad (7)$$

$T_{m,i}$ is the logarithmic mean temperature and T_0 is the reference state temperature. ε_{ss} represents the steady-state exergy efficiency of the heat pump. It was assumed to have a constant value of 0.5. The part-load COP of a frequency controlled heat pump would typically increase for decreasing load, reaching a maximum at approx. 50% [27]. However, we assumed constant part load efficiency.

The resulting actual COP was calculated from the condenser heat load and the power uptake.

$$COP = \frac{\dot{Q}_{con}}{\dot{W}_{HP}} \quad (8)$$

The model further included energy, mass and impulse balance (no pressure loss) equations for the evaporator and the condenser. The heat pump was controlled according to the desired heat output at the condenser using an external control unit.

2.2.3. Control unit

The described system was controlled using a central control unit, which contained the algorithm according to which the heat pump, the three-way-valve, the pumps and the electric heater were controlled. Via the three-way-valve at the top of the stratified storage tank the charging and discharging of the tank was controlled, by setting a value for the ratio between the flow into the storage and the flow from the HP. The pumps were controlled to deliver the necessary mass flow to the heat demand model and the heat pump, respectively. The electric heater heated the DH supply flow to 70 °C if the temperature supplied was lower.

The operation of the heat pump was based on a simple, heuristic approach, which does not utilize variations in the electricity price, but is only based on the heat demand, the state of the storage and a regulation signal. This approach was chosen to focus on the effect of the provision of ancillary services for the electricity system. The algorithm changed the mode of operation of the system according to up- and down regulation signals, which were taken from data of hourly realized up- and down-regulation from the Transmission System Operator Energinet. dk's market data from 2012 [28]. The model does not include the prices for regulating power, but aims at quantifying the true cost of providing this. The results may be compared to the actual prices in the regulating market.

The up- and down regulation signals from Energinet are based on the generation side, i.e. an up-regulation signal means that the current demand is too high. The heat pump would react to this by reducing the power uptake. Accordingly, a down regulation signal would cause the heat pump to switch to full load. When the storage level and the current heat demand allowed for variation of the heat pump load, the heat pump was ramped up to full load in case of a down-regulation signal and shut-off for an up-regulation. This was done using a PI-controller ($k = 0.08$, $\tau = 50\,s$) where the desired heat output was the set value, the actual heat load was the input and the power uptake of the compressor was the output signal. In practice, the load of the heat pump could be increased or reduced to another value than full load or no production. However, the considered heat pump is small in terms of its electricity regulation ability and would have to be aggregated to actually act on the regulation market. Therefore, we chose to only consider the maximum provision of regulation power. Fig. 3 shows a flow diagram of the control algorithm for flexible operation. If no regulation signals were considered, the algorithm would follow only the left branch (regulating signal: none). The different paths of the algorithm ended up in 4 different operation modes for the heat pump:

2.2.4. Stratified storage tank

The stratified storage tank was modelled using a one dimensional discretization [29] (Fig. 4). The tank was divided into 100 layers from top to bottom. For each layer dynamic mass and energy balances were solved. It was assumed that the fluid inside each layer was ideally mixed and thus had constant properties. Heat losses to the environment and between layers were considered. Pressure differences across the tank were neglected as well as increased mixing between the layers during charging and discharging. The minimum and maximum amount of hot water is limited by the inlet design and was assumed to be 1/12 and 11/12 of the total stored mass, respectively.

2.3. Exergy analysis

As reference state the groundwater temperature ($T_0 = 10.5\,°C$) at atmospheric pressure ($p_0 = 1.013$ bar) was chosen. The groundwater temperature was assumed to be constant throughout the year. All material streams were assumed to be water and no reactions occur at any place in the system. So, the chemical exergy would be equal for all streams and can be neglected [17].

To conduct the exergy analysis of the system, balance equations were formulated for all components. The balance equation for a general control volume can be formulated as

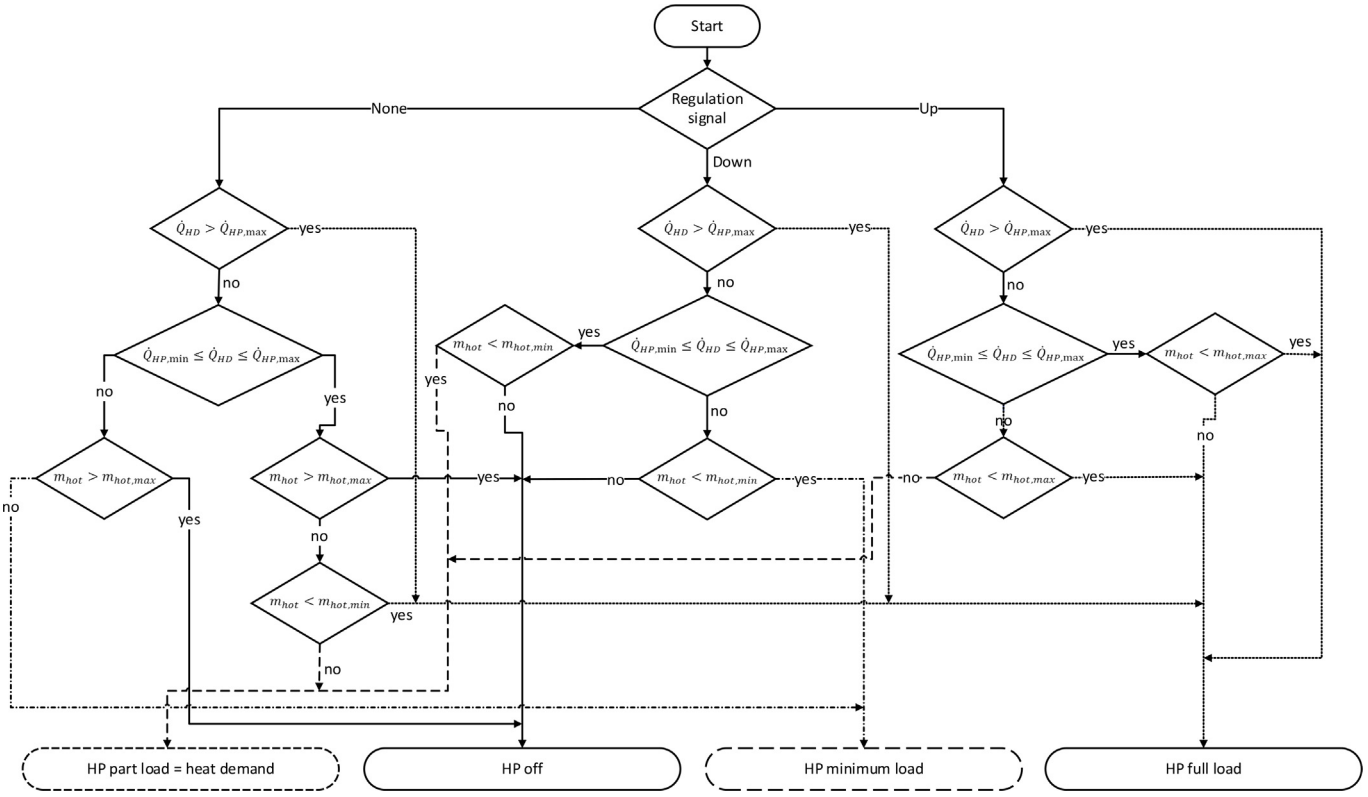

Fig. 3. Structure of control algorithm for flexible operation. HD- Heat demand, HP_min/max – Heat pump minimum load/full load, m_hot – mass of hot water in the storage, m_hot_min/max – minimum/maximum mass of hot water in the storage, HD – Heat demand.

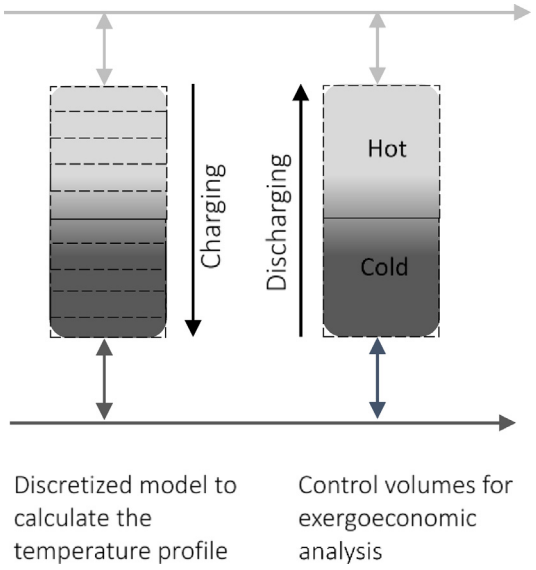

Fig. 4. One-dimensional discretization of storage tank and division into hot and cold control volume.

$$\frac{dE}{dt} = \sum_i \dot{m}_i \cdot e_i + \sum_j \dot{E}_{Q,j} + \sum_l \dot{W}_l - \dot{E}_L - \dot{E}_D \tag{9}$$

where E is the exergy content of the control volume, the first sum denotes the exergy content of the material streams entering and exiting the control volume which is calculated as the product of mass flow $\dot{m}$ and specific exergy e. The second sum is the sum of all exergy flows related to heat flows $\dot{E}_{Q,j}$ and the third sum considers power flows $\dot{W}_l$. $\dot{E}_L$ is the exergy loss to the environment and $\dot{E}_D$ denotes the exergy destruction within the control volume. All entering flows are accounted as positive by sign convention.

For the exergy analysis, exergy fuel and product were defined for all components (Table 2). The exergy efficiency of every component can be calculated according to:

$$\varepsilon_k = \frac{\dot{E}_{P,k}}{\dot{E}_{F,k}} \tag{10}$$

2.3.1. Heat pump

The exergy efficiency of the heat pump was defined as the increase of exergy of the DH water in the condenser over the power input into the compressor. As the groundwater was cooled down from the reference state temperature in the evaporator, it's exergy content increased. However, the cold stream was not a useful product in this case as it was discharged into the environment and represented an exergy loss of the system. A cost can be assigned to the exergy loss by assuming that the exergy loss is covered through the supply of a corresponding amount of fuel (auxiliary equation) [30].

2.3.2. Three-way-valve

The three-way-valve controlled the mass flow to and from the stratified storage tank. The exergy fuel and product were different during charging or discharging of the tank. The purpose of mixing in the three-way-valve was to vary between two different heat sources (the heat pump and the storage) and not to heat up the

stream from the storage using the stream from the heat pump. Thus the above definition of exergy fuel and product is chosen [17].

2.3.3. Stratified storage tank

To define the exergy fuel and product of the stratified storage tank, the tank was divided into a hot and a cold control volume (Fig. 4). We assumed that the purpose of the tank is to store hot water, and that the cold water is only used to fill up the tank volume that is not used by the hot water. Both control volumes were thus variable in size and additional mass balances for the control volumes are needed.

$$m_{hot} + m_{cold} = \overline{\rho} \cdot V_{storage} \tag{11}$$

$$m_{hot} = \frac{N_{hot}}{N} \cdot \overline{\rho} \cdot V_{storage} \tag{12}$$

m_{hot}, m_{cold} denote the mass of the hot and cold control volumes, respectively. N_{hot} is the number of layers with hot fluid which are defined as all layers with a temperature above 60 °C, $\overline{\rho}$ is the mean water density in the storage and $V_{storage}$ is the overall volume of the storage tank. Calculating m_{hot} in the presented way, has the advantage that the mass flow from the hot to the cold volume due to decrease in temperature can be easily accounted for.

The exergy fuel during charging was defined as the exergy of the hot water coming in at the top of the tank (stream 5) and the product was the increase in stored exergy inside the hot control volume of the tank. The amount of stored exergy was calculated for both control volumes as

$$\frac{d(E_{hot} + E_{cold})}{dt} = \dot{m}_5 \cdot e_5 - \dot{m}_{10} \cdot e_{10} - \dot{E}_D \tag{13}$$

$$E_{\mathrm{hot}} = \sum_{n=1}^{N_{\mathrm{hot}}} (m_n \cdot e_n) \tag{14}$$

where E_{hot}, E_{cold} denote the exergy stored in the hot and cold volume respectively. m_n is the mass and e_n the specific exergy of layer n. The volume work due to variation of the control volume size was found to be small compared to the exergy of stored heat and was neglected. The heat loss from the storage is accounted for as exergy destruction $\dot{E}_D$. Assuming that the water in the tank behaves as an ideal liquid, the specific exergy e_n for every discretization layer can be calculated from temperatures obtained from the energy balances for every control volume [31].

$$e_n = c_{p,\mathrm{H_2O}} \cdot (T_n - T_0) - T_0 \cdot c_{p,\mathrm{H_2O}} \cdot \ln\left(\frac{T_n}{T_0}\right) \tag{15}$$

An overall exergy efficiency for the storage was calculated as the ratio of the integrals of the output from - and the input into the hot control volume.

$$\varepsilon_{storage,tot} = \frac{\int \dot{E}_{5,out}\, dt}{\int \dot{E}_{5,in}\, dt} \tag{16}$$

2.3.4. System exergy efficiency

The exergy efficiency of the overall system for every time step had to take the storage of exergy in the storage tank into consideration. During charging the exergy stream into the storage represented a product of the system, whereas during discharging the exergy stream out of the tank was a fuel to the overall system:

$$\varepsilon_{\mathrm{system}} = \begin{cases} \dfrac{\dot{E}_{\mathrm{heat}} + \dfrac{d(E_{\mathrm{hot}} + dE_{cold})}{dt}}{\sum_k \dot{W}_k} & \text{if charging} \\ \dfrac{\dot{E}_{\mathrm{heat}}}{\sum_k \dot{W}_k + \left|\dfrac{dE_{\mathrm{hot}} + dE_{cold}}{dt}\right|} & \text{if discharging} \end{cases} \tag{17}$$

The annual mean exergy efficiency was calculated according to the following equation.

$$\varepsilon_{\mathrm{system,tot}} = \frac{E_{\mathrm{heat}}}{\sum_k W_k} \tag{18}$$

E_{heat} denotes the overall amount of exergy of heat supplied per year and W_k is the overall amount of electric energy of component k per year.

2.4. Exergoeconomic analysis

Within an exergoeconomic analysis a cost is assigned to all exergy streams. This allows to determine the cost of exergy destruction in every component, which can give useful information about the sources of costs throughout the system and how they can be lowered [17].

In order to assign a cost to every exergy stream a dynamic cost balance for every component was set up,

$$\frac{dC}{dt} = \sum_i \dot{C}_i + \sum_k c_{\mathrm{el}} \cdot \dot{W}_k + \dot{Z} \tag{19}$$

C denotes the cost that accumulates within the component, $\dot{C}_i$ is the cost streams associated with material streams, c_{el} is the electricity cost in the respective time step and $\dot{Z}$ denotes the levelized cost stream of the component. The cost stream of the component includes investment cost, capital cost, and operation and maintenance costs for the estimated lifetime of the respective component. It was calculated as described in Ref. [17]. However, the cost was not levelized to the full load hours per year but to the actual operation hours per year and $\dot{Z}$ was only considered when the respective component was in operation. The DH network was existent and we assumed that the operation and maintenance costs are the same for any kind of heat supplying system. Thus, the costs of the DH network were neglected in the present work.

The economic data used to calculate $\dot{Z}$ is summarized in Table 3. An average annual discount rate of 4% and a nominal escalation rate of 2% for operation and maintenance cost was assumed [32].

The cost of electricity used in this study is historic spot market prices for Eastern Denmark 2012 from NordPool [33]. 59 DKK/MWh transmission net tariff and 24 DKK/MWh system tariff were included [33]. Administration, and trading and unbalance cost were assumed to be 3 DKK/MWh and 2 DKK/MWh, respectively.

2.5. Allocation of cost

The allocation of cost to both products of the heat pump system, i.e. heat supply and provision of demand flexibility, is a central question when operating energy conversion units in an integrated energy system. The characteristics of both products are different. Heat is an output from the system and so is the related heating service. Electricity is an input into the system, but the corresponding flexibility is a service provided by the system, see Fig. 5. The cost of providing flexibility is not directly connected to the

Table 3
Economic data case study.

Unit	Capacity	Total capital investment [DKK]	Plant economic life [a]	Operation hours per year [h/a]		Fixed O&M cost 1st year [DKK]	Source
				Non-flex.	Flexible		
Heat pump	800 kW	560.000	25	7527	6917	3000	[34]
El. heater	200 kW	150.000	20	1233	3000	220	[34]
DH pump	2 × 16.7 kg/s	30.000	10	8760	8760	440	[23]
GW pump	2 × 44.3 kg/s	40.000	10	7527	6917	440	[23]
Storage tank	120 m^3	31.200	40	8760	8760	700	[34]
Drilling		900.000	40	7527	6917	18000	[35]

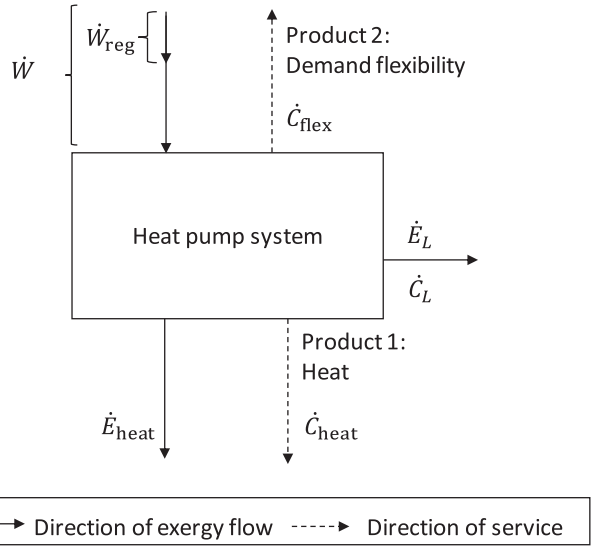

Fig. 5. Direction of energy flow and product delivery for a conversion unit in an integrated energy system.

electricity stream and all extra cost will be reflected in the heat generation cost. However, as the source of cost difference was not the supply of heat but the additional exergy destruction due to the provision of flexibility, the cost should be allocated accordingly. The exergy destruction related to flexible operation does not only occur at the same time as the provision of regulation power. Thus, we chose an integral approach to determine the cost related to flexible operation.

As the flexibility provided to the electricity sector was not directly connected to an exergy product stream, the cost was allocated according to the increased exergy destruction due to flexible operation, which was given as the difference between the overall exergy destruction in the flexible and the non-flexible case. The specific cost per unit of exergy was calculated as:

$$c_{ex} = \frac{(C_{heat} + C_L)}{E_{heat} + \left(E_{D,flex} - E_{D,nonflex}\right)} \tag{20}$$

The overall cost exiting the system is the sum of the integrated cost of heat C_{heat} and of the exergy loss C_L. E_{heat} is the integrated amount of exergy supplied as heat to the DH grid and $E_{D,flex}$, $E_{D,nonflex}$ is the overall exergy destruction caused during flexible operation and non-flexible operation, respectively. All values were calculated by integrating the respective cost and exergy flow rates over one year.

Knowing the overall cost related to flexible operation per year, the specific cost per unit of regulating energy W_{reg} provided can be determined.

$$c_{flex} = \frac{c_{ex} \cdot \left(E_{D,flex} - E_{D,nonflex}\right)}{W_{reg}} \tag{21}$$

In order to be able to compare different units, we also calculate the annual specific cost of flexible operation per kW installed electric capacity $\dot{W}_{installed}$.

$$c_{flex,\ capacity} = \frac{c_{ex} \cdot \left(E_{D,flex} - E_{D,nonflex}\right)}{\dot{W}_{installed} \cdot 8760 \cdot 3600\ s/a} \tag{22}$$

The heat generation cost is calculated from the overall cost delivered into the DH grid over the overall amount of heat.

$$c_{heat} = \frac{c_{ex} \cdot E_{heat}}{Q_{heat}} \tag{23}$$

3. Results

To calculate the performance of the system when operated flexibly the system was simulated and the exergoeconomic analysis was carried out for two different cases:

A. Non-flexible operation– the heat pump is not operated according to regulation requests from the grid, but only according to heat demand. This means the heat pump is mostly operating in part load.

B. Flexible operation according to regulatory signal – the heat pump is controlled according to the heat demand, the state of storage and a regulatory signal to provide flexibility. This control strategy was presented previously in chapter 2.2, Fig. 3.

Fig. 6 shows the heat load at the heat pump condenser for the non-flexible and flexible operation. The non-flexible operation followed the heat demand apart from the periods, where the heat demand was lower than the lowest allowable part load of the heat pump (150 kW). In that case, the heat pump was operated at minimum part-load until the storage was filled to the maximum, then the heat demand was supplied from the storage and the heat pump was switched off until the storage was emptied.

In the case of flexible operation the heat pump load changed frequently. When down- or up-regulation was requested, the system ramped up to full load or shut down, if possible. When there was no regulation signal, the heat load at the condenser followed the heat demand.

The overall power uptake was higher for flexible operation (Table 4). This was mainly due to reheating the water from the storage in the electric heater. The electric heater consumption increased from 37 MWh/year to 85 MWh/year. The power uptake of the heat pump was slightly lower during flexible operation. The seasonal heat pump COP was the same for both operation modes, whereas the seasonal SCOP was lower for the flexible case.

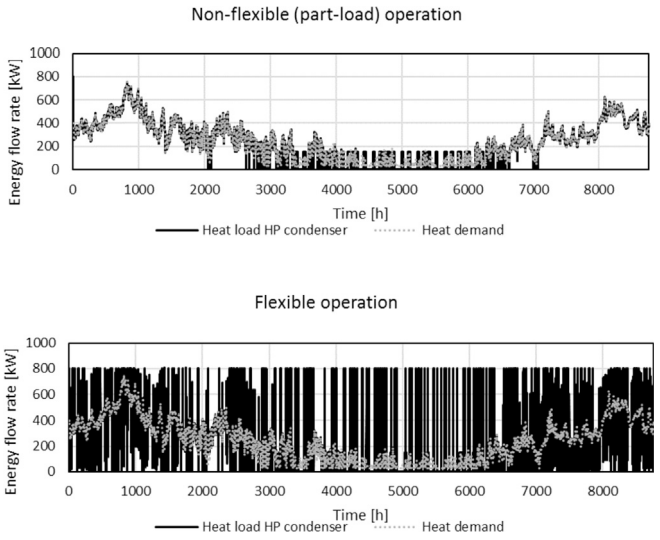

Fig. 6. Heat load at heat pump condenser and heat demand for non-flexible operation and flexible operation for one year (2012).

The overall exergy input into the system is given as the sum of all electric energy inputs into the system. The exergy provided to the heat pump accounts for 84.5% and 79.4% of the overall exergy input in the non-flexible and flexible case, respectively.

3.1. Exergy analysis

Fig. 7 shows the exergy destruction within the major components for a week in February. When the heat pump turned on, the exergy destruction in the heat pump increased rapidly and leveled out to a steady state value. The exergy destruction of the heat pump increased with the overall power input. When the heat pump turned off, the exergy destruction in the heat pump decreased to zero. The exergy efficiency peaked at these times because the heat supplied from the upper layers of the storage had a high enough temperature to supply the DH grid directly. When the temperature from the storage dropped, the electric heater was turned on to heat the supply flow to the desired temperature. The exergy efficiency decreased accordingly.

The component exergy efficiencies are presented in Fig. 8 for the same week. The heat pump exergy efficiency was constant during operation (Fig. 8 (a)). Peaks only occurred during ramping and shut-off. This is due to the heat stored in the heat pump components, which is still available during shut-down. The exergy efficiency of the electric heater is lower than the HP efficiency with approx. 17%.

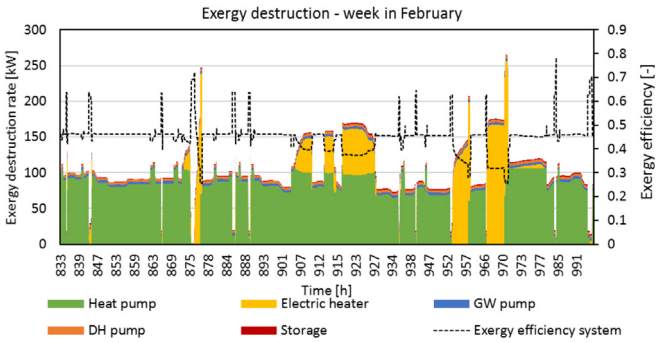

Fig. 7. Exergy destruction (ED) rates during flexible operation for major components.

The exergy efficiency of the groundwater pump was highest when the heat pump was operated at full load, i.e. at nominal conditions. Accordingly, the exergy efficiency decreased with decreasing mass flow.

The exergy efficiency of the storage was above 90% when the storage was charged or discharged (Fig. 8 (c)). Losses from the storage also occurred when the storage was not operated. Thus, the mean exergy efficiency of the storage was calculated as approx. 86.3%.

Fig. 9 shows the exergy content of the storage for the first thousand hours of the year for flexible operation. The amount of exergy stored as hot water increased during charging and the exergy content of the cold water decreased accordingly. When the storage was not charged or discharged over a longer period, the exergy content decreased slowly due to heat losses.

3.2. Exergoeconomic analysis

Fig. 10 shows the condenser load of the heat pump and the overall specific cost per unit of exergy that was delivered into the DH system. Further, the cost of electricity is shown. The yearly average for eastern Denmark for the year 2012 was 0.3757 DKK/kWh including the tariffs given in section 2.4.

The specific cost per unit exergy of the non-flexible operation followed the development of the electricity cost (Fig. 10). In the flexible operation case, the specific cost increased when the heat pump was turned off, as the heat had to be delivered from the storage tank and reheated in the electric boiler. The flow taken from the storage tank had a higher specific cost than that fed into it due to the cost of exergy destruction in the tank and the levelized cost of the tank. The cost was accounted to the exergy stored in the warm control volume of the tank. The exergy destruction and levelized cost of the electric boiler further increased the specific

Table 4
Energetic performance indicators.

		Non-flexible operation	Flexible operation
Heat pump electric energy consumption	[MWh/a]	582	577
Electric heater electric energy consumption	[MWh/a]	37	85
GW pump electric energy consumption	[MWh/a]	40	35
DH pump electric energy consumption	[MWh/a]	30	30
Total electric energy consumption	[MWh/a]	689	728
Heat supplied to DH system	[MWh/a]	2125	2125
Overall heat loss within the conversion system	[MWh/a]	5.9	41.2
Seasonal heat pump COP	[−]	3.60	3.60
Seasonal system COP (SCOP)	[−]	3.09	2.92
Exergy of heat	[MWh/a]	293	293
Total exergy destruction	[MWh/a]	360	399
Overall exergy loss	[MWh/a]	43.6	43.4
Overall exergy efficiency	[%]	42.6%	40.3%

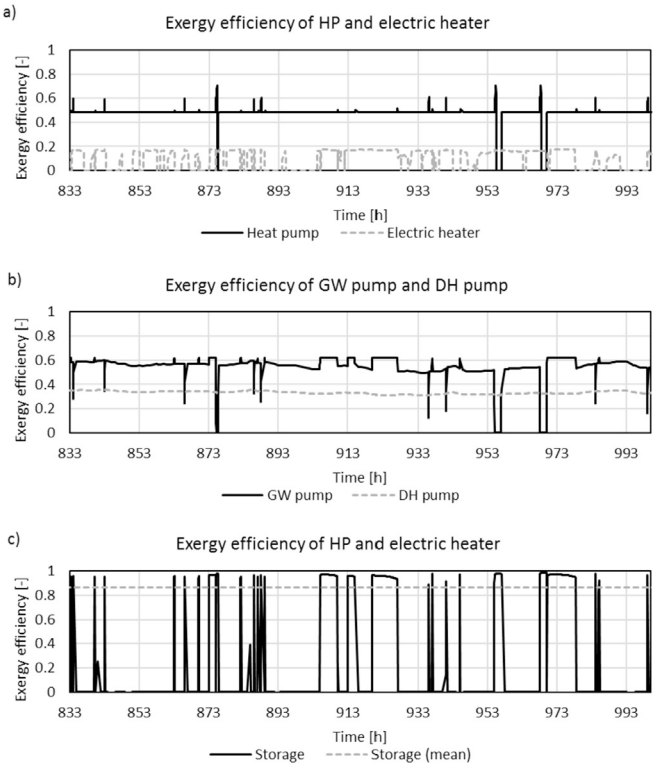

Fig. 8. Exergy efficiency of major components for flexible operation.

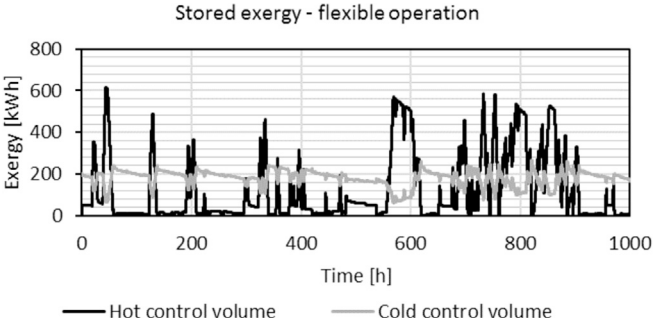

Fig. 9. Exergy content of hot and cold control volume of the stratified storage tank for the first 1000 h of the year 2012.

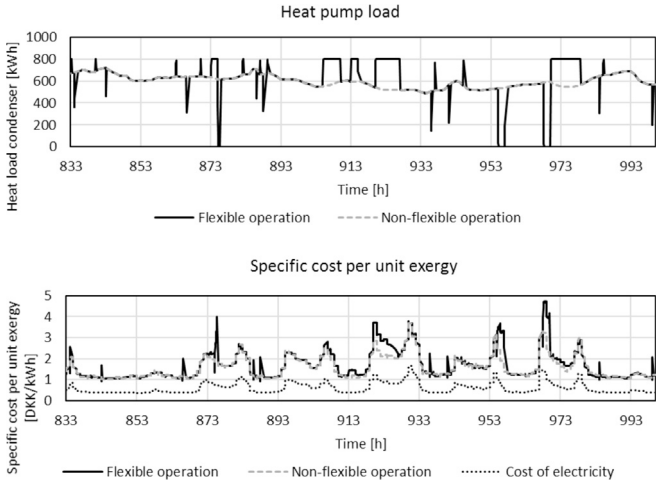

Fig. 10. Heat load condenser, overall product cost for non-flexible and flexible operation and cost of electricity for a week in February 2012.

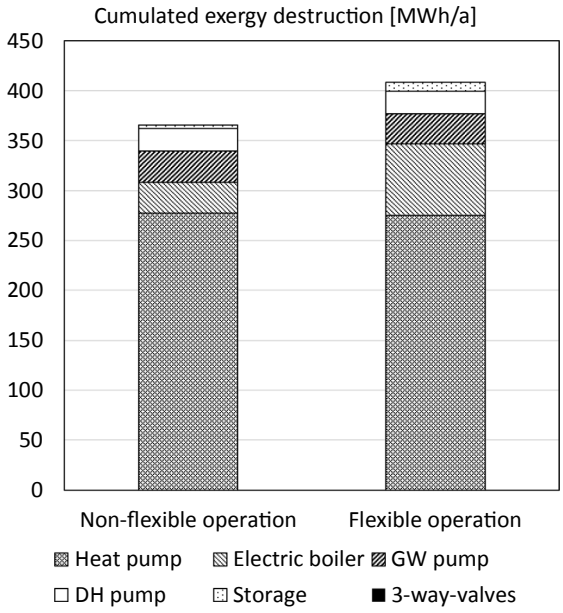

Fig. 11. Overall exergy destruction of all components per year for flexible and non-flexible operation.

cost. The specific cost did not differ significantly between the flexible and non-flexible operation while the heat pump is running. The mean specific fuel cost (spot market prices) during regulation was found to be slightly higher than the yearly average.

The regulation energy that was available from the heat pump system is shown in Table 5. The response rate given here is the ratio between the time where the system reacted to a regulation signal and the time where the system received a regulation signal. The response rate was lower for down-regulation, while the overall regulation energy was approx. six times larger than for up-regulation.

The specific cost of heat was lower for the flexible operation compared to the non-flexible operation, as 12% of the overall product cost were assigned to the provision of flexibility and the overall cost were reduced. The specific cost per kWh of regulation energy was 0.660 DKK/kWh. This corresponds to an annual cost of flexible operation per kW installed capacity (only heating units) of 65 DKK/kW/a. The average difference between the balancing price and the electricity spot price, i.e. the possible benefit by providing balancing services, was 0.133 DKK/kWh for down-regulation and 0.208 DKK/kWh for up-regulation for 2012 [28]. The corresponding values for 2017 were found to be even lower with 0.093 DKK/kWh for down-regulation and 0.153 for up-regulation. During individual hours the benefit of performing the service could be higher. For 2012 it was found that in 180 h out of 3101 h where balancing power was needed the benefit provided was larger than 0.660 DKK/kWh, this corresponds to 5.8% of the hours where balancing services where provided.

The overall cost input into the system is 443000 DKK/a for flexible operation and 464000 DKK/a for non-flexible operation. 37% and 43% of the overall cost of flexible and non-flexible operation, respectively, are the levelized cost of operation. The remaining part is the fuel cost of the system.

The exergy destruction and the related cost are presented in Figs. 11 and 12. The exergy destruction of the heat pump was very similar for both scenarios. This indicates that the increased exergy

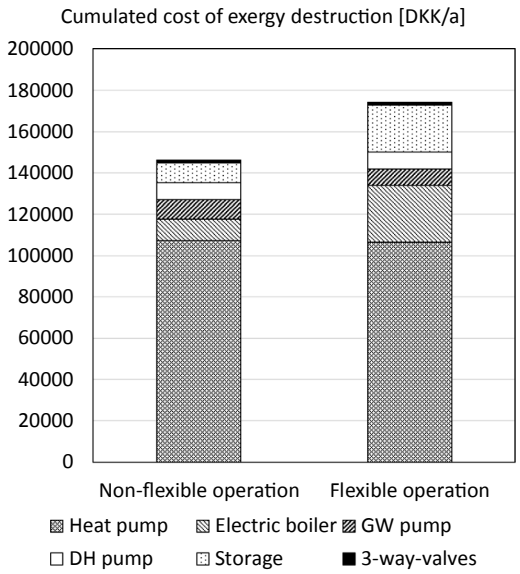

Fig. 12. Overall cost of exergy destruction of all components per year for flexible and non-flexible operation.

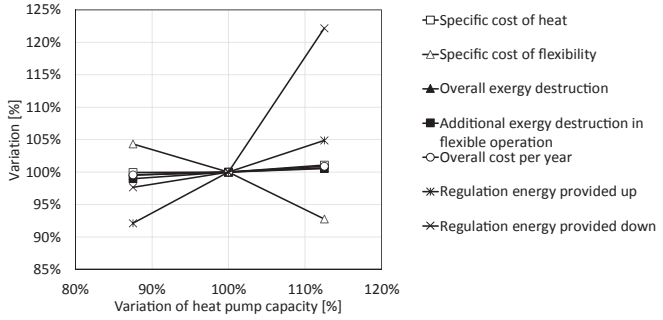

Fig. 13. Variation of specific product cost, response rate and exergy destruction in % over the heat pump capacity in %.

destruction during load changes did not have a significant influence on the overall exergy destruction of the heat pump. The exergy destruction in the groundwater pump was lower in the case of flexible operation, due to part-load operation.

The cumulated exergy destruction in the electric boiler was higher during flexible operation compared to non-flexible operation. This is due to an increased amount of heat, which was supplied from the storage and had to be heated up to fulfill the requirement of 70 °C supply temperature. The exergy destruction in the DH pump was similar for both cases, as the heat demand, and thus the mass flow rate were the same.

The exergy destruction in the storage occurs mainly due to heat losses and is low compared to the other components. The cost of exergy destruction in the storage was responsible for 16% and 7% of the overall cost of exergy destruction in flexible and non-flexible operation mode, respectively. The cost related to the exergy destruction in the storage was a larger share of the overall cost. This occurred as the fuel of the storage was the warm inlet, which had a high specific cost due to the cost of the upstream components assigned to it.

3.3. Influence of heat pump capacity

The system assessed here, was oversized for the given heat demand. This was done with the aim to be able to operate the system very flexibly. The simulation was repeated for an increase and decrease of the heat pump capacity of 100 kW each, keeping all other components and the heat demand the same. The results (Fig. 13) indicated that the specific cost of heat is almost constant for all three cases and the overall cost per year increases slightly with increasing HP capacity. Whereas, the specific cost of flexibility decreases considerably with increasing HP capacity. This is caused by two effects. Firstly, an increase in the additional exergy destruction due to flexible operation for larger heat pump capacities leads to a decrease in the specific cost per unit exergy. Secondly and more importantly, the amount of regulation energy provided increases with increased heat pump capacity.

The results for the overall exergy destruction and the additional exergy destruction due to flexible operation increased slightly for increased HP capacity. This is due to the lower minimum part-load capacity of the smaller heat pump and thus a higher share of heat that is directly supplied from the heat pump, avoiding exergy destruction in the storage and the electric boiler.

4. Discussion

A method was presented to value the two products of a heat pump system using a dynamic exergoeconomic analysis. The allocation of cost to the provision of ancillary services was based on the additional exergy destruction in the system. We found that this approach is well suited as it resembles the common exergy costing

Table 5
Amount of regulation energy and heat and specific cost of both products.

	Non-flexible operation	Flexible operation	Flexible operation - Winter	Flexible operation - Spring	Flexible operation - Summer	Flexible operation - Autumn
Heat [MWh/a]	2125	2125	965	540	155	464
Up-regulation [MWh/a]	0	67.8	18.5	14.2	15.6	19.5
Down-regulation [MWh/a]	0	11	0.99	0.72	5.49	4.02
Response rate Down-regulation [%]	0	37%	33%	48%	34%	39%
Response rate Up-regulation [%]	0	67%	27%	69%	100%	76%
Specific heat cost [DKK/kWh]	0.219	0.184	0.168	0.181	0.303	0.186
Cost of flexibility [DKK/kWh]	0	0.660	1.079	0.830	0.018	0.695
Overall cost [DKK]	465000	443000	183000	110000	47000	102000
Overall exergy of heat [MWh]	293	293	133	75	21	64
Overall exergy loss [MWh]	44	43	20	11	3	9
Overall exergy destruction [MWh]	360	399	160	103	44	93
Additional exergy destruction [MWh]		39	17	9	0	12

method closely, e.g. Ref. [30], and at the same time the problem of the different directions of exergy flow and service provision (Fig. 5) can be handled. Allocating the cost in the presented way, a cost could also be assigned to the flexibility when the overall fuel cost is be lower than in the reference case. The applied approach is based on exergoeconomic theory. Other approaches based on economics or more heuristic assumptions would also be possible and may reach other costs of the flexibility.

For the case study of a heat pump island system the flexible operation of the system caused higher exergy destruction and thus fuel consumption. The overall fuel cost and the specific fuel cost were found to be higher during regulation. This is due to the difference between the trends of the electricity spot market price and the regulation requests found in the data for Eastern Denmark in 2012. Also, the control algorithm did not consider any kind of optimization, but the system would react to a regulation request whenever possible. In this case the difference between the overall cost for flexible and non-flexible operation was approx. 21000 DKK/a.

Further, using the sport market price for the calculation implicates that a perfect prediction of the heat demand can be made. This is of course not possible in reality. The spot market price is also used to calculate the cost during regulation, thereby the cost difference between the flexible and non-flexible case is indeed an opportunity cost of providing flexibility. The comparison showed that the obtainable price at the balancing price was in most cases lower than the additional cost due to losses in the storage and the electric boiler.

The additional exergy destruction was mainly caused by heat losses in the storage, which led to reheating of the DH forward flow and thus exergy destruction in the electric boiler. This result reconfirms findings of previous studies on individual HP systems [36,37]. Reducing heat losses in the storage and the need for reheating, will improve the systems efficiency.

No significant difference in the exergy destruction of the heat pump was found. This is related to the assumption that part load characteristics of the heat pump are not considered. The part load performance depends on the capacity control type of the compressor [27], as well as the design of the heat exchangers.

The assumption that a largely overdimensioned system can provide more flexibility made when designing the system correlates with the results of the parameter variation that showed that the amount of regulation energy provided increased with increased HP capacity. On the contrary, both the overall cost per year and the exergy destruction in the system increase for larger HPs. Thus, the examination of the optimal component sizes for systems that are designed to provide flexibility may be a topic for further analysis.

The presented work gave an insight into the effect of providing ancillary services on the conversion unit, in this case a heat pump system. The advantage of this approach is that the actual thermodynamic and economic effect of providing flexibility to another sector can be assessed. In this way it is possible to assess the additional amount of electricity used and the part of the conversion units cost that is caused by providing another product. This is valuable information for the heat pump operator and it adds a different perspective to the discussion about how flexibility should be valued. So far the overall system benefit was mostly discussed (e.g. Refs. [4], [15], [38]) and the actual effect on the conversion unit was not considered.

5. Conclusion

Energy conversion units are an essential part of integrated energy systems. They are able to connect different sectors and provide services to both of them. In the case of electricity and heating sector, the conversion units provide heat to the heating system while acting as flexible demand for the electricity sector. A method to assess the impact of flexible operation of a heat pump system was presented, where allocation of the cost of both the heating and the flexibility products was based on a dynamic exergoeconomic analysis.

The method was applied to a heat pump island system located in Copenhagen. We found that operation according to regulation request resulted in higher exergy destruction and higher overall cost of the system. The additional exergy destruction was mainly caused by heat losses in the storage and reheating of the forward stream. The cost allocated to the flexible operation was 12% of the overall cost of the system.

Overall, the method gives important insights into the effect of integrating energy systems on the energy conversion units and can thus support the decision making process when considering how to design and operate a conversion unit.

Acknowledgements

This research project is financially funded by EUDP (Energy Technology Development and Demonstration) under the project "EnergyLab Nordhavn - New Urban Energy Infrastructures" (project number: 64014-0555).

Nomenclature

Abbreviations

COP	Coefficient of performance
DH	District heating
El	Electric
GW	Groundwater
SCOP	Seasonal system COP

Symbols

C	Cost [DKK]
c	Specific cost per unit exergy [DKK/J]
$\dot{C}$	Cost stream [DKK/s]
c_{p,H_2O}	Heat capacity water [J/(kg*K)]
E	Exergy [J]
e	Specific exergy per unit mass [J/kg]
$\dot{E}$	Exergy stream [W]
k_1, k_2	Parameters ramp-up function [−]
$\dot{m}$	Mass flow [kg/s]
m	Mass [kg]
N	Number of discretization layers [−]
p	Pressure [bar]
Q	Heat [J]
$\dot{Q}$	Heat flow rate [W]
T	Temperature [K]
t	Time [s]
$T_{m,i}$	Logarithmic mean temperature for stream i [K]
V	Volume [m^3]
$\dot{W}$	Electric power [W]
$\dot{Z}$	Levelized cost of capital investment, and operation and maintenance [DKK/s]

Greek symbols

ε	Exergy efficiency [−]
$\overline{\rho}$	Mean water density [kg/m^3]

Subscripts

0	Reference state

capacity	Per installed capacity
cold	Related to cold control volume of the tank
con	Condenser
D	Destruction
el	Electricity
eva	Evaporator
ex	Per unit of exergy
F	Fuel
flex	Flexible operation
heat	Heat supply into DH grid
hot	Related to hot control volume of the tank
HP	Heat pump
i	Material stream indicator
in	Inlet
installed	Installed capacity
j	Heat flow indicator
k	Component indicator
L	Loss
l	Electricity flow index
max	Maximum capacity
min	Minimum capacity
n	Discretization layer indicator
nonflex	Non-flexible operation
out	Outlet
P	Product
reg	Regulation energy
season	Seasonal
ss	Steady state
storage	Stratified storage tank
system	Conversion system
tot	Yearly mean value

References

[1] Lund H, Mathiesen BV. Energy system analysis of 100% renewable energy systems—The case of Denmark in years 2030 and 2050. Energy 2009;34:524–31. https://doi.org/10.1016/j.energy.2008.04.003.

[2] Mathiesen BV, Lund H, Connolly D, Wenzel H, Østergaard PA, Möller B, et al. Smart Energy Systems for coherent 100% renewable energy and transport solutions. Appl Energy 2015;145:139–54. https://doi.org/10.1016/j.apenergy.2015.01.075.

[3] Lund H, Werner S, Wiltshire R, Svendsen S, Thorsen JE, Hvelplund F, et al. 4th Generation District Heating (4GDH): integrating smart thermal grids into future sustainable energy systems. Energy 2014;68:1–11. https://doi.org/10.1016/j.energy.2014.02.089.

[4] Mathiesen BV, Lund H. Comparative analyses of seven technologies to facilitate the integration of fluctuating renewable energy sources. Renew Power Gener IET 2008;3:190–204. https://doi.org/10.1049/iet-rpg.

[5] David A, Mathiesen BV, Averfalk H, Werner S, Lund H. Heat roadmap Europe: large-scale electric heat pumps in district heating systems. Energies 2017;10:578. https://doi.org/10.3390/en10040578.

[6] Holttinen H, Cutululis NA, Gubina A, Keane A, Van Hulle F. Ancillary services: technical specifications, system needs and costs. 2012. Deliverable D 2.2.

[7] Carmo C, Detlefsen N, Nielsen M. Smart Grid enabled heat pumps: an empirical platform for investigating how residential heat pumps can support largescale integration of intermittent renewables. Energy Procedia 2014;61:1695–8. https://doi.org/10.1016/j.egypro.2014.12.194.

[8] Stinner S, Schlösser T, Huchtemann K, Müller D, Monti A. Primary energy evaluation of heat pumps considering dynamic boundary conditions in the energy system. Energy 2017;138:60–78. https://doi.org/10.1016/j.energy.2017.07.029.

[9] Patteeuw D, Reynders G, Bruninx K, Protopapadaki C, Delarue E, D'haeseleer W, et al. CO2-abatement cost of residential heat pumps with active demand response: demand- and supply-side effects. Appl Energy 2015;156:490–501. https://doi.org/10.1016/j.apenergy.2015.07.038.

[10] Ulbig A, Andersson G. Analyzing operational flexibility of electric power systems. Int J Electr Power Energy Syst 2015;72:155–64. https://doi.org/10.1016/j.ijepes.2015.02.028.

[11] Robbi S. LowEx-Fernwärme - Vergleichende Bewertung von Maßnahmen für eine effiziente, multifunktionale Fernwärmeversorgung (Doctoral thesis). Tech Universität Dresden; 2013.

[12] Schlachtberger DP, Becker S, Schramm S, Greiner M. Backup flexibility classes in emerging large-scale renewable electricity systems. Energy Convers Manag 2016;125:336–46. https://doi.org/10.1016/j.enconman.2016.04.020.

[13] Makarov YV, Loutan C, Ma J, Mello P de. Operational impacts of wind generation on California power systems. IEEE Trans POWER Syst 2009;24(2):1039–50. https://doi.org/10.1109/NOMS.2002.1015622.

[15] Blarke MB, Lund H. The effectiveness of storage and relocation options in renewable energy systems. Renew Energy 2008;33:1499–507. https://doi.org/10.1016/j.renene.2007.09.001.

[16] Meibom P, Kiviluoma J, Barth R, Brand H, Weber C, Larsen HV. Value of electric heat boilers and heat pumps for wind power integration. Wind Energy 2007;10:321–37. https://doi.org/10.1002/we.224.

[17] Bejan A, Tsatsaronis G, Moran M. Thermal design and optimization. John Wiley & Sons, Inc; 1996.

[18] Sayadi S, Tsatsaronis G, Morosuk T. A New Approach for applying dynamic exergy Analysis and exergoeconomics to a building envelope. 2016. p. 1–17.

[19] Sangi R, Martín PM, Müller D. Thermoeconomic analysis of a building heating system. Energy 2016;111:351–63. https://doi.org/10.1016/j.energy.2016.05.112.

[20] Modelica Association. Modelica and the Modelica standard library. 2017 (Accessed 31 October 2017), http://www.modelica.org.

[21] Dassault Systèmes. Dymola systems engineering. 2017 (Accessed 31 October 2017), https://www.3ds.com/products-services/catia/products/dymola/.

[22] TLK Thermo GmbH & IfT. TIL 3.4 – model library for thermal components and systems. 2017.

[23] Grundfos. Product data SP 46-4 2017. https://product-selection.grundfos.com/product-detail.catalogue.product families.html?from_suid=15102222881100638805271878582 2&pumpsystemid=280760607&qcid=271031787 (accessed July 4, 2017).

[24] Grundfos. Product data NB 32-200/206 2017. https://product-selection.grundfos.com/product-detail.catalogue.product families.html?from_suid=151022250390601434492979880763 7&pumpsystemid=290981485&qcid=293056119 (accessed October 30, 2017).

[25] HOFOR. Heat demand data for 3 cruise ship terminal buildings and a warehouse. Copenhagen. 2012.

[26] Jensen JK, Ommen T, Markussen WB, Elmegaard B. Design of serially connected district heating heat pumps utilising a geothermal heat source. Energy 2017. https://doi.org/10.1016/j.energy.2017.03.164.

[27] Pfeil HV. Intelligent capacity control potential for system efficiency improvements & energy savings. In: ICR 2015, Yokohama, Japan; 2015. https://doi.org/10.18462/iir.icr.2015.0016. p. ID:16.

[28] Energinet.dk. Energinet.dk - Markedsdata. 2012. http://www.energinet.dk. [Accessed 10 July 2017].

[29] Rothuizen E, Markussen W, Elmegaard B, Madsen C, Olesen MF, Sølvsten M. High efficient heat pump system using storage tanks to increase Cop by means of the Isec concept (Part I, Thermal storage system). Proc 24th IIR Int Congr Refrig. 2015. p. 1–8.

[30] Lazzaretto A, Tsatsaronis G. SPECO: a systematic and general methodology for calculating efficiencies and costs in thermal systems. Energy 2006;31:1257–89. https://doi.org/10.1016/j.energy.2005.03.011.

[31] Rosen MA, Dincer I. Thermal energy storage systems and applications. second ed. Ontario, Canada: John Wiley & Sons, Inc; 2011.

[32] Center for Klima og Energiøkonomi. Forudsætninger for samfundsøkonomiske analyser på energiområdet. 2016. Version 3, https://ens.dk/sites/ens.dk/files/Analyser/samfundsoekonomiske_beregningsforudsaetninger_2016_v3.pdf.

[33] Energinet.dk. Marketsdata. 2017 (Accessed 10 July 2017), www.energinet.dk.

[34] Energinet.dk. Technology data for energy plants. 2016. www.ens.dk. [Accessed 12 October 2017].

[35] Energinet.dk. Technology data for energy plants. 2012. https://ens.dk/sites/ens.dk/files/Analyser/technologydata_for_energy_plants_-_may_2012._updated_2015.pdf. [Accessed 12 October 2017].

[36] Baeten B, Rogiers F, Helsen L. Reduction of heat pump induced peak electricity use and required generation capacity through thermal energy storage and demand response. Appl Energy 2017:184–95. https://doi.org/10.1016/j.apenergy.2017.03.055.

[37] Arteconi A, Patteeuw D, Bruninx K, Delarue E, D 'haeseleer W, Helsen L. Active demand response with electric heating systems: impact of market penetration. Appl Energy 2016;177:636–48. https://doi.org/10.1016/j.apenergy.2016.05.146.

[38] Hedegaard K. Wind power integration with heat pumps, heat storages, and electric vehicles – energy systems analysis and modelling. 2013 (PhD thesis).

Economic feasibility of ultra-low temperature district heating systems in newly built areas supplied by renewable energy

Energy 191 (2020) 116496

Contents lists available at ScienceDirect

Energy

journal homepage: www.elsevier.com/locate/energy

Economic feasibility of ultra-low temperature district heating systems in newly built areas supplied by renewable energy

Wiebke Meesenburg [a, *], Torben Ommen [a], Jan Eric Thorsen [b], Brian Elmegaard [a]

[a] Technical University of Denmark, Department of Mechanical Engineering, Niels Koppels Allé 403, DK-2800, Kgs. Lyngby, Denmark
[b] Danfoss A/S, Nordborgvej 81, DK-6430 Nordborg, Denmark

ARTICLE INFO

Article history:
Received 29 April 2019
Received in revised form
27 October 2019
Accepted 5 November 2019
Available online 8 November 2019

ABSTRACT

Future district heating systems are expected to supply lower temperatures to increase system efficiency and enable exploitation of renewable heat sources. To answer whether it is beneficial to lower district heating temperatures below the level where it is still possible to supply domestic hot water directly, the economic feasibility of three ultra-low temperature district heating (ULTDH) concepts was compared to low temperature district heating (LTDH). The dependency of the economic feasibility on the boundary conditions of the supplied district heating area was assessed systematically and feasible boundary conditions were identified. For this purpose building plot ratio, specific heat demand and central heating unit were varied. The different solutions were compared based on levelised cost of heat, socioeconomic net present value and overall seasonal coefficient of performance. It was found that in most cases LTDH was economically preferred. ULTDH could be feasible if the linear heat demand density (LHDD) was high, if the cost of decentral units could be lowered or if the investment cost of the central heating unit was significantly lower compared to LTDH. Among the ULTDH solutions, apartment units were preferable for low LHDD, while units at building level performed better for larger LHDD.

1. Introduction

District heating (DH) is expected to play a key role in future renewable and energy efficient energy systems. Such systems are likely characterized by high shares of electricity generation from intermittent renewable energy sources and the need to exploit renewable heat sources. Lund et al. [1] define several criteria that a future DH grid has to comply with in order to play the expected central role: 1) The ability to supply low-temperature DH for space heating (SH) and domestic hot water (DHW) preparation, 2) reduction of grid losses, 3) exploitation of renewable and excess heat sources, 4) being an integrated part of the overall energy system and 5) suitable planning and policy instruments. The first three criteria are directly connected to lower DH temperatures. To enable these, the supplied buildings need to be equipped with SH and DHW systems that can be supplied with low-temperatures, likely down to 45 °C–55 °C. Reduction of system temperatures will increase the distribution efficiency, due to reduced heat losses from the pipes. The integration of renewable and excess heat sources is enhanced by low DH temperatures too, as lower temperature sources can be used. These ambient and low-grade heat sources can be exploited by large-scale heat pumps, which benefit from lower DH temperatures, as the coefficient of performance (COP) increases for lower temperature lifts. Heat pumps can also help to fulfil the fourth criterion, as they provide a link between the power and heating networks and might be able to balance the power grid by making use of the immanent thermal storage capacity of the DH-system. Planning and policy instruments are needed in order to shape the system such that the first four criteria may be fulfilled.

1.1. Low temperature- and ultra-low temperature district heating

Low temperature district heating denotes district heating with considerably lowered supply and return temperatures compared to conventional district heating. Design supply temperatures can reach down to 55 °C, which still allows direct supply of DHW to the buildings via direct heat exchange. In this case, the DH forward temperature is constrained by the minimum temperature required to avoid legionella in DHW. Ultra-low temperature district heating (ULTDH) systems are operated at even lower district heating

* Corresponding author.
E-mail address: wmeese@mek.dtu.dk (W. Meesenburg).

https://doi.org/10.1016/j.energy.2019.116496
0360-5442/

Nomenclature

Abbreviations

CHP	Combined heat and power
COP	Coefficient of performance
DH	District heating
DHW	Domestic hot water
HEX	Heat exchanger
HP	Heat pump
LCOH	Levelised cost of heat €/MWh
LTDH	Low temperature district heating
LHDD	Linear heat demand density above LTDH
NPV	Net present value €
O&M	Operation and maintenance
SH	Space heating
ULTDH	Ultra-low temperature district heating

Latin symbols

A	Area m^2
C	Cost €
c_p	Specific heat capacity $J/kg/K$
L	Pipe length m
p	Pressure Pa
Q	Heat Wh
$\dot{Q}$	Heat flow W
q	Specific heat demand $kWh/m^2/a$
q_l	Linear heat demand density $MWh/m/a$
s_{SH}	Space heating share –
T	Temperature $°C$
$\overline{T}$	Average temperature $°C$
t	Time h
$\dot{V}$	Volume flow m^3/h
W	Electric energy Wh
$\dot{W}$	Power W

Greek symbols

ε	Plot ratio –
ρ	Density kg/m^3

Subscripts

fixedOM	Fixed O&M cost
forw	DH forward
l	linear
nom	nominal
ret	DH return
s	Annual specific
tot	total

temperatures, that can reach down to around 40 °C forward temperature. These temperatures are high enough to supply SH directly, but decentral heating units are necessary to increase the DH temperature to supply DHW to the customers. This can be done using decentral heat pumps (HP). The lower DH temperature allows to further reduce grid losses compared to LTDH, as found for a Danish case study by Yang & Svendsen [2]. However, part of the heat used to provide DHW is replaced by electricity to run the decentral HPs, which results in a reduced exergy utilization as the reduction of heat loss is outweighed by the additional electricity demand of the decentral HP, as shown by Elmegaard et al. [3]. This result is in agreement with the results by Yang & Svendsen.

Ommen et al. [4] investigated the influence of distribution temperatures on the performance of large-scale heat pumps and combined heat and power (CHP) plants as the central heat supply unit. The considered decentral heating unit is a HP using DH water as heat source. The results showed that energy efficiency increases for ULTDH compared to LTDH, if supplied by a central HP, and decreases if supplied by a CHP plant.

1.2. Previous work on economic feasibility of ultra-low temperature district heating systems

The economic profitability of ULTDH and LTDH is challenged as the linear heat demand density (LHDD) is reduced, which generally decreases the profitability of DH systems [5]. More detailed analysis of the economic performance of ULTDH has been investigated for specific DH systems.

Ommen et al. [6] examin the influence of DH temperatures on the consumer cost in the Greater Copenhagen DH network for supply from CHP only, and for integration of large-scale HPs into the supply portfolio. They show that reducing the DH temperature to 60 °C leads to minimal consumer costs. Further reduction in DH forward temperature results in increasing cost, as boosting of the temperature for DHW becomes necessary.

Yang & Svendsen [2] conduct a Danish case study of a DH network supplied by a central ground-source heat pump supplemented with CHP and heat only boiler. They find that the operation cost of the system is lower for ULTDH than for LTDH. The heat losses in the LTDH case appear to be high with 25%–55%. Best et al. [7] compare the economic feasibility of ULTDH and LTDH for a similar network in Germany, which is supplied by a ground-source HP with a borehole thermal energy storage. The decentral units considered for ULTDH are air-source HPs. The share of SH was 78% of the overall heat demand, which is defined as SH- plus DHW demand. They find that the higher cost for decentral boosting for DHW preparation is offset by savings in heat distribution cost and central heat generation cost, due to a better COP of the central HP in the ULTDH case.

Vivian et al. [8] analyse the economic feasibility of ULTDH from a customer perspective for a network supplying mainly older buildings in Italy. As the existing buildings have higher temperature demands for SH than the DH forward temperature, the booster HPs have to provide SH in addition to DHW. They find that the levelised cost of heat in ULTDH systems decreases with increasing DH supply temperatures, indicating that a LTDH solution might be beneficial.

Köfinger et al. [9] study different low- and ultra-low temperature DH configurations for four cases in Austria. They recommend using booster units in combination with ULTDH when the heat source supply temperature has an upper constraint or when large amounts of DHW have to be stored in the buildings, e.g. in hotels. They emphasize that reduced heat losses and network investment cost prove to be especially beneficial in low heat density areas.

Lund et al. [10] compare the feasibility of ULTDH with LTDH on an energy system level from a societal point of view. They find that LTDH has the lowest socioeconomic cost but that ULTDH with booster heat pump substations may be feasible in specific cases under the right circumstances. Østergaard & Andersen [11] compare the operation cost of ULTDH and LTDH. They find that operation cost of ULTDH can be reduced compared to LTDH due to lower energy losses in the network. However, booster HP investment cost were not included in their analysis.

1.3. Scope of this study

While most studies point towards LTDH as the more feasible system, some show economically feasible ULTDH systems. All of the above mentioned studies compared different ULTDH and LTDH solutions which were carried out for specific cases. Accordingly, a more systematic analysis of the influence of the different boundary conditions on the feasibility of ULTDH systems is needed to predict which solutions should be evaluated for new development areas. Therefore, the present study aimed at identifying how the characteristics of the supplied area and of the heat supply technologies influence the socioeconomic feasibility of heat supply technologies. This can be useful information in the early planning stages for new development areas. By identifying the feasibility of different district heating solutions in the nexus between the boundary conditions imposed by the supplied area and the available heat sources, the study addresses a techno-economic perspective, which is different to existing assessments based on energy system analysis as well as to studies of performance improvements of district heating cascade systems. The aim is to identify the most promising pathways of heat supply to future developments. The results of the studies mentioned above indicate that the feasibility of ULTDH is affected by many parameters, of which key items are listed in the following:

- SH- and DHW temperature requirements
- Heat demand density of the supplied area
- Share of SH demand of the overall heat demand
- Type of central DH supply unit
- Price of heat supplied by DH and price of electricity

The current study assessed the influence of these parameters on the economic feasibility of ULTDH compared to LTDH, in order to identify under which boundary conditions, one or another of these technologies should be applied. Further, the influence of the booster HP configuration and the corresponding operation and investment cost on the overall systems feasibility was assessed, to account for different possible ULTDH variants. This was done by calculating the levelised cost of heat (LCOH) and the socioeconomic net present value (NPV), including all contributions from heat source to demand, assuming Danish prices and taxes. The analysis was based on a generalized modelling approach for the district heating network to be able to show trends of technology feasibility for networks under significantly different boundary conditions. The method is further described in section 2 as well as the different configurations that were assessed. The results are presented in section 3, before they are discussed in section 4. Final conclusions are presented in section 5.

2. Method

To assess the economic feasibility of ULTDH systems in Denmark under varying boundary conditions, an economic analysis was conducted using a Microsoft Excel/VBA based tool, based on the district heating assessment tool (DHAT), published by the Danish Energy Agency [12]. A principle sketch of the assessed systems is given in Fig. 1. All systems included energy supply in form of power supply, natural gas for the back-up unit and heat sources for the heat pump units. Further, different central energy conversion units were considered, supplying the heat demand via the DH network and transferring it in the customers substation. The whole system's performance and economy were influenced by different physical- and policy boundary conditions, as indicated in Fig. 1.

2.1. Assessed system designs

Three different ULTDH system designs were assessed, and compared to the performance of a LTDH system and to supply by individual air-to-water heat pumps. Fig. 2 shows a sketch of the different system design cases.

Case 1), was LTDH with design system temperatures of 60 °C forward and 30 °C return. These temperatures specify the temperatures to be supplied to, and returned from, the last customer in the network. For all three ULTDH cases temperatures of 40 °C forward and 25 °C return were assumed, using the above definition of forward and return. They differed in the type and form of implementation of the decentral HPs. In case 2) "ULTDH-DH" the booster HP was using the DH forward stream as sink and source. Substation and booster HP were implemented at building level. The advantages of this configuration were a high booster HP COP of 5.23 and relatively high LHDDs in the DH network compared to case 3). Case 3) "ULTDH-air" used an air-source HP to supply DHW to the building. The COP was lower compared to case 2, with 2.9–3.3. In case 2) and 3) it was assumed that the DHW temperature supplied to the tanks in the building is 60 °C and the COPs were calculated as described in section 2.2.4. The last case "ULTDH-DH-micro" comprised micro-booster HPs at apartment level. In accordance with supplier data, the DHW temperatures were assumed to be as low as 53.5 °C and the micro-booster HP achieved an average COP of 6.7 for DH supply temperatures of 40 °C [13]. In this case, anti-Legionella disinfection was carried out by shortly increasing DHW temperatures once or twice per week. The respective extra HP consumption was given by the manufacturer as 1% of the calculated power consumption without disinfection [14] and was neglected.

For all cases, weather compensation was applied for outdoor temperatures below 5 °C, increasing the DH supply temperature by 1 K for a decrease of 1 K in outdoor temperature, up to a maximum compensation of 17 K [2]. The supply temperatures of DHW from the individual DHW HPs was assumed to be unaffected by outdoor temperatures. It was assumed that the heat is transferred from the DH grid to the building SH and DHW system via an indirect DH substation. It was further assumed that the return temperature from the DH substations can be kept constant throughout the year, which is a simplification as the return temperature would usually vary as the forward temperatures vary. This is further discussed in chapter 4. In all cases, the circulation losses within the buildings were assumed to be part of the specific heat demand of the buildings.

2.1.1. Heat sources

Air-source evaporators and ground source systems were considered as natural heat sources. The cost of heat supplied to the evaporator, caused by pump or fan power consumption, was neglected. The sensitivity to this assumption was assessed (see section 3.5). Air-source heat pumps experience frosting at ambient temperatures of around 7 °C and lower, which leads to a reduction of COP due to defrosting and to a reduction of heating capacity, as frost formation on the evaporator reduces the heat transfer [15]. This effect was considered by reduction factors for COP and heating capacity for outdoor temperatures below 7 °C. The assumed reduction factor for the COP was 0.84 and for the heating capacity 0.85. These values are mean values of the data presented by Mader [15]. This simplified approach was chosen, as a more detailed modelling of the defrosting was beyond the scope of this study.

Further, excess heat at temperatures of 40 °C, 30 °C and 20 °C, was used as heat source for a central HP. It was assumed that all sources were cooled down to 10 °C by the HP. Lastly, a case of excess heat at temperatures high enough to supply ULTDH directly at all time was considered as an idealized situation. This was a theoretic

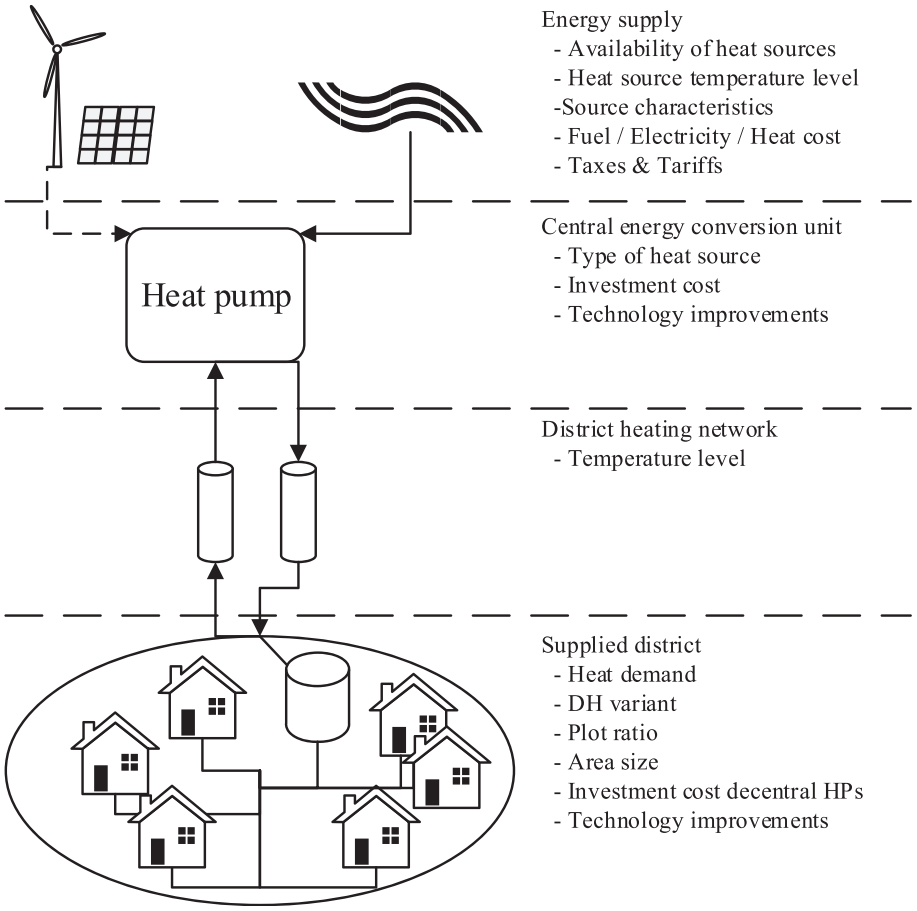

Fig. 1. Overview of the system, including four main parts; energy supply, central energy conversion, DH network and supplied district. Varied boundary conditions influencing the different parts of the system are given as bullet points.

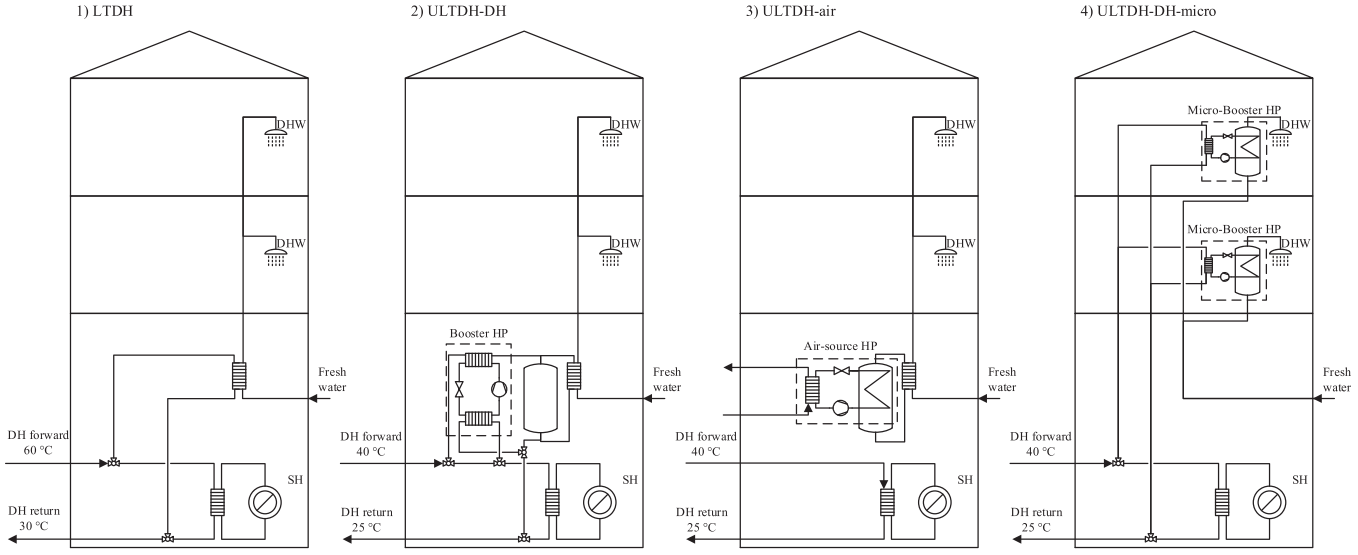

Fig. 2. Four system design cases: 1) LTDH with indirect DH substation at building level, 2) ULTDH with water-to-water booster HP at building level, 3) ULTDH with air-to-water HP at building level (the evaporator and compressor unit is usually placed outdoors, but was drawn inside for simplicity), 4) ULTDH with water-to-water booster HP at apartment level, including direct preheating of the fresh water.

case and the heat source was not further specified. In this case the investment cost was reduced to that of a heat exchanger substation.

In principle the excess heat cost is highly dependent on the type of process it originates from and the cost that occurs to make the excess heat available. The type of process was beyond the chosen detail level for this study, and accordingly it was decided to vary the

excess heat cost to be 0 €/MWh, 10 €/MWh and 20 €/MWh, and thereby assess how much the cost influences the overall feasibility, similar to the approach chosen by Bühler et al. [16].

2.2. Representation of DH system

To assess under which circumstance ULTDH or LTDH is economically preferable, a generic representation of the DH network and customer structure was developed. Accordingly, no detailed network analysis was conducted, but the calculation of heat demand, DH grid investment, heat loss and pumping power were based on current regulations and estimations from existing DH grids in Denmark and Sweden. The analysis was limited to newly developed, predominantly residential areas and the district area was fixed to 340 000 m^2, which is the area of the Levantkaj city development area in Copenhagen [17]. To verify that a fixed district area is a feasible assumption the influence of the district area on the result was tested.

The performance of the system was evaluated based on the seasonal system COP, which is defined in line with the definition of the seasonal COP for heat pumps [18]. It was calculated as the total annual heat supplied to the customers $Q_{tot,demand}$ divided by the total annual electricity input W_{tot}, which is the sum of the electricity input to the central heating units, decentral heating units and DH pumping power.

$$\mathrm{COP}_{\mathrm{system,\ seasonal}} = \frac{Q_{\mathrm{tot,demand}}}{W_{\mathrm{tot}}} = \frac{\int_{\mathrm{year}} \dot{Q}_{\mathrm{tot,demand}}\, dt}{\int_{\mathrm{year}} \dot{W}_{\mathrm{tot}}\, dt}$$

2.2.1. Estimation of heat demand

The specific DHW demand q_{DHW} was assumed to be 20 kWh/m^2/a [19]. The share of SH of the total heat demand s_{SH} was varied between 0.1 and 0.8 in steps of 0.1, representing different building energy efficiencies. The Danish 2020 building standard employs a SH share of 0 [20].

$$s_{\mathrm{SH}} = \frac{Q_{\mathrm{tot,SH}}}{Q_{\mathrm{tot,DHW}} + Q_{\mathrm{tot,SH}}}$$

The specific annual heat demand q_s was calculated from the specific DHW demand and the SH share.

$$q_s = q_{\mathrm{DHW}} + q_{\mathrm{SH}} = \frac{1}{1 - s_{\mathrm{SH}}} \cdot q_{\mathrm{DHW}}$$

The yearly SH demand profile was generated by weighting the heat demand according to the Danish Design Reference Year [21]. The DHW demand was determined by two components: The basic daily demand pattern, which was assumed to be the European standard tapping profile (XL load) [22] and a factor representing the seasonal variations of DHW demand. The seasonal correction factor was dependent on the outdoor temperature and was obtained by normalizing the measurements by Aronsson [23,24] with the corresponding mean temperatures of the same year.

The overall annual heat demand was calculated from the total heated building area. The heated building area $A_{\mathrm{buildings}}$ was calculated from the overall district area A_{district} and the plot ratio ε, which was considered an input for the analysis.

$$\varepsilon = \frac{A_{\mathrm{buildings}}}{A_{\mathrm{district}}} \quad \Leftrightarrow \quad A_{\mathrm{buildings}} = \varepsilon \cdot A_{\mathrm{district}}$$

The plot ratio was varied from 0.2 (rural) to 2 (urban) in steps of 0.2 to account for different building densities.

2.2.2. Estimation of network investment

The network investment cost was estimated from plot ratio, expected specific heat demand, effective width and estimated average pipe diameter, following the approach developed by Persson & Werner [25] and Frederiksen & Werner [24]. Piping cost were fitted to Danish empirical data [12].

2.2.3. Estimation of heat loss and pumping power

The heat loss is an important factor for the feasibility of DH, especially in heat sparse areas. The expectable heat loss from the network was estimated using an empirical approach. Fig. 3 shows the heat loss of 187 DH networks in Denmark as a function of their LHDD [26]. It is defined as the total annual heat demand divided by the estimated trench length L and it can be calculated from the annual specific heat demand, the plot ratio and the characteristic width, as described in Ref. [25].

$$q_l = \frac{Q_{tot}}{L} = q_s \cdot \varepsilon \cdot w$$

Networks with LHDD above five were excluded. The heat loss was corrected according to forward and return temperatures. As can be seen in Fig. 3 the data is spread out, which may be caused by different operation conditions and malfunctions in the systems. A power function was used to fit the data. To calculate the relative annual heat loss the correction for the assumed network

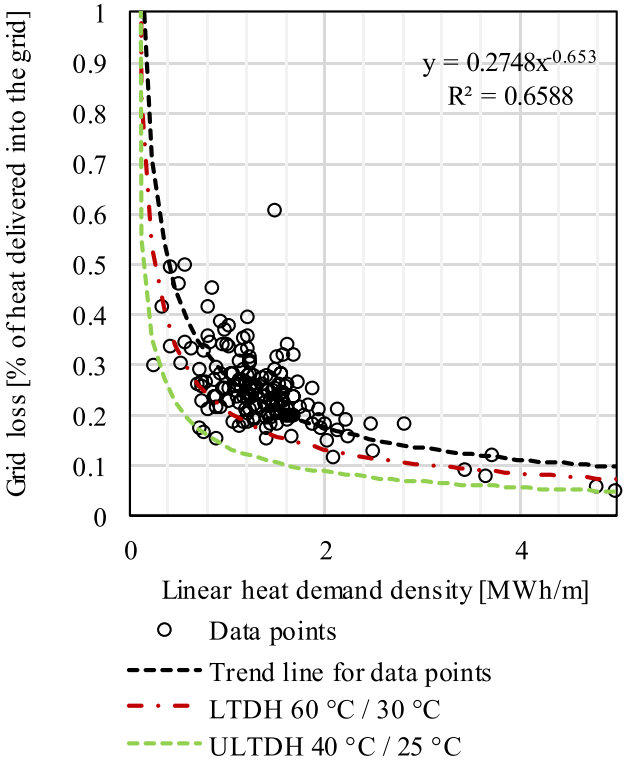

Fig. 3. Heat loss data from existing DH networks corrected to average forward and return temperatures in Denmark, 2017, and fitted power function based on data from Ref. [26].

temperatures for LTDH and ULTDH was applied to the correlation found from this data. The full equation is:

$$\frac{Q_{loss}}{Q_{tot}} = 0.2748 \cdot q_l^{-0.653} \cdot \frac{T_{forw} + T_{ret} - 2 \cdot T_{ground}}{\overline{T}_{forw} + \overline{T}_{ret}} - 2 \cdot T_{ground}$$

$\overline{T}_{forw} = 73.71\,^{\circ}C$ and $\overline{T}_{ret} = 40.52\,^{\circ}C$ are the weighted average forward and return temperature (by heat load) of the Danish systems listed in the data base.

The pumping power needed for a system depends on the system design. Any estimation made without knowing the detailed piping layout has large uncertainties. In general, the pumping power can be calculated as the product of the volume flow, the pressure drop and the pump's efficiency. The average volume flow through the primary pumps was estimated from the total heat delivered into the system and the forward and return temperatures at the central unit.

$$\dot{V} = \frac{\left(\frac{Q_{tot,delivered}}{8760\ [h/a]}\right)}{c_{p,H_2O} \cdot \left(T_{forw} - T_{ret}\right) \cdot \rho_{H_2O}}$$

The pressure drop in the system was estimated assuming a constant pressure gradient in all the pipes of 100 Pa/m [24]. The corresponding pipe length was set to the estimated trench length L, which was calculated from equation (5), according to Ref. [25].

The pressure loss over the substations was assumed to be 1 bar [27]. The necessary energy for pumping per year is calculated as:

$$W_{pump} = \Delta p_{DH} \cdot \dot{V} \cdot \eta_{pump} \cdot 8760 \left[\frac{h}{a}\right]$$

Here, Δp_{DH} denotes the overall pressure loss, $\dot{V}$ is the average volume flow and η_{pump} is the isentropic efficiency of the pump, which was assumed to be 0.8.

2.2.4. Representation of HP units

To calculate the seasonal COP of the HPs the Danish Design Reference Year [21] temperature data was used as air-source temperature. The groundwater temperature was assumed to be 10 °C, the excess heat temperature was assumed to be 20 °C, 30 °C and 40 °C, and constant throughout the year. The source temperature for decentral heat pumps was given as the air temperature for the air-source heat pump and as the ULTDH forward temperature for the DH-source booster HP. The coefficient of performance (COP), defined as

$$COP = \frac{\dot{Q}_{HP}}{\dot{W}_{HP}}$$

was estimated from sink- and source temperatures, isentropic efficiency, compressor heat loss factor and the ratio of isentropic expansion- and -compression work, using the method described by Jensen et al. [28]. To determine these parameters, ammonia was assumed as refrigerant for large-scale HPs and isobutane for decentral units. The COP for all HPs was calculated for every hour of the year. Knowing the hourly COP and heat demand, the corresponding electric energy consumption was calculated. The seasonal COP of the HP units could then be calculated equivalent to the system's seasonal COP, (equation (1)).

The capacity of the central heat pump unit was set to be 80% of the maximum hourly heating demand for LTDH. The backup electricity boiler capacity was 25% of the maximum heat demand. For the ULTDH cases, the heat capacity of central HPs was set to the maximum DH demand value. For ULTDH-DH and ULTDH-DH-micro, the annual DH demand was calculated as the difference of the total heat demand (including losses) minus the electric energy input to the booster HPs.

$$Q_{central} = Q_{supply,tot} - \frac{(1 - s_{SH}) \cdot Q_{demand,tot}}{COP_{booster}}$$

The heat capacity of the booster HP was constrained to be between 2 kW and 14 kW, which corresponded to previously demonstrated booster HP capacities (as of December 2018). The capacity of the micro-booster HP was fixed to 1.8 kW per installation. In the ULTDH-air case, the DH demand was the SH demand plus distribution losses. The heat supplied by the decentral HPs was the DHW heat demand. The capacity of the decentral units for ULTDH-DH and ULTDH-air was determined assuming a fixed number of full load hours of 2000 h/a, which is in line with [29] and was tested for sensitivity.

$$\dot{Q}_{booster,nom} = \frac{Q_{DHW}}{t_{fullload}}$$

The air-source HP capacity did not have an upper boundary.

2.3. Economic evaluation

The economic feasibility of all assessed DH configurations was compared based on LCOH and socioeconomic NPV. Investment cost for central supply units, DH grid incl. local substations, and decentral HPs were considered. Electricity price, and operation and maintenance (O&M) cost were included in the economic analysis. Taxes were based on Danish regulation as of September 2018.

2.3.1. Calculation of levelised cost of heat and socioeconomic net present value

The LCOH was calculated as the total cost over the project lifetime of 20 years divided by the total amount of heat delivered in the same period. The total cost was defined as all cost occurring during the project lifetime discounted to the first year of the project, i.e. 2023, including the residual values of components with a longer lifetime and investment into replacement of components with a shorter lifetime.

The socioeconomic NPV was calculated according to Danish guidelines [30] as the socioeconomic cost of the DH project, i.e. all investment and operation costs plus emission cost, compared to individual heat supply with air-source heat pumps. Taxes and tariffs were not included in the socioeconomic cost.

2.3.2. Fuel cost and taxes

Electricity and emission price projections were based on projections from 2016 for the period 2012–2040 by Energinet.dk [31], where the emission prices were based on IEA projections [32]. Local conditions such as electricity tax, network- and system tariffs and distribution tariffs were considered.

2.3.3. Assumed cost data

The total investment cost of the system comprised the investment in central units, decentral HPs and the network itself. The functions for investment cost, and assumed lifetimes are listed in Table 1. Fixed- and variable O&M cost were taken from the Danish Technology Catalogue [33–35]. A linear cost function was used to describe the fixed O&M cost of booster HPs in $€/unit/a$, which was derived from Ref. [33], and uses $\dot{Q}_{booster,nom}$ in MW.

$$C_{fixedOM,\ booster} = 229.6 + 3852.6 \cdot \dot{Q}_{booster,nom}$$

Table 1
Investment cost for energy conversion units. *Correlation fitted through cost data given in the stated sources.

Technology	Investment cost function [M€/MW]	Lifetime [a]	Sources
Excess heat HEX installation	$0.260 \cdot \dot{Q}_{nom}^{-0.1234}$	20	[36]
Central HP excess heat	$0.867 \cdot \dot{Q}_{nom}^{-0.1234}$	25	[36,37]
Central HP groundwater	$1.112 \cdot \dot{Q}_{nom}^{-0.23105}$	25	[36]
Central HP air	$0.937 \cdot \dot{Q}_{nom}^{-0.1418}$	25	[36]
Central electric boiler	0.11	20	[34]
Central gas boiler	0.06	25	[34]
Indv. Air to water HP	0.95	15	[34]
Booster HP	$2.748 \cdot \dot{Q}_{nom}^{-0.594}$	15	[8,38–40]*
DH substation	$0.414 \cdot \dot{Q}_{nom}^{-0.536}$	25	[33,39]*

3. Results

3.1. System performance

3.1.1. Duration load curves of heat production

Fig. 4 shows the duration load curves of the heat production of four DH cases. The heat demand was the same and thus the difference in heat supplied was small and only caused by differences in heat loss. For ULTDH-DH and ULTDH-DH-micro, DH represented the heat source for the DHW heat pumps, depicted as the light grey area. Thus, the heat added to the system by the booster unit (black area) was equivalent to the power uptake of the units. In the ULTDH-air case, the decentral heat pump used air as heat source and thus the heat added to the system was all the heat supplied from the condenser.

The heat demand increased with increasing plot ratio, as more customers were supplied in the same area. An increase in the SH share led to a higher heat demand during the heating period, while the effect during summer was small as mainly DHW was needed. Accordingly, increasing SH shares led to more pronounced seasonal behaviour, i.e. a steeper load duration curve.

3.1.2. Hourly variation of COP

The hourly values of COP of all HP units for ULTDH and LTDH are shown in Fig. 5. The COP of the central units was higher for the ULTDH cases, as the supply temperature was lower compared to LTDH. A seasonal variation was observed for all units. It was most pronounced for air-source heat pumps as the heat source (air)

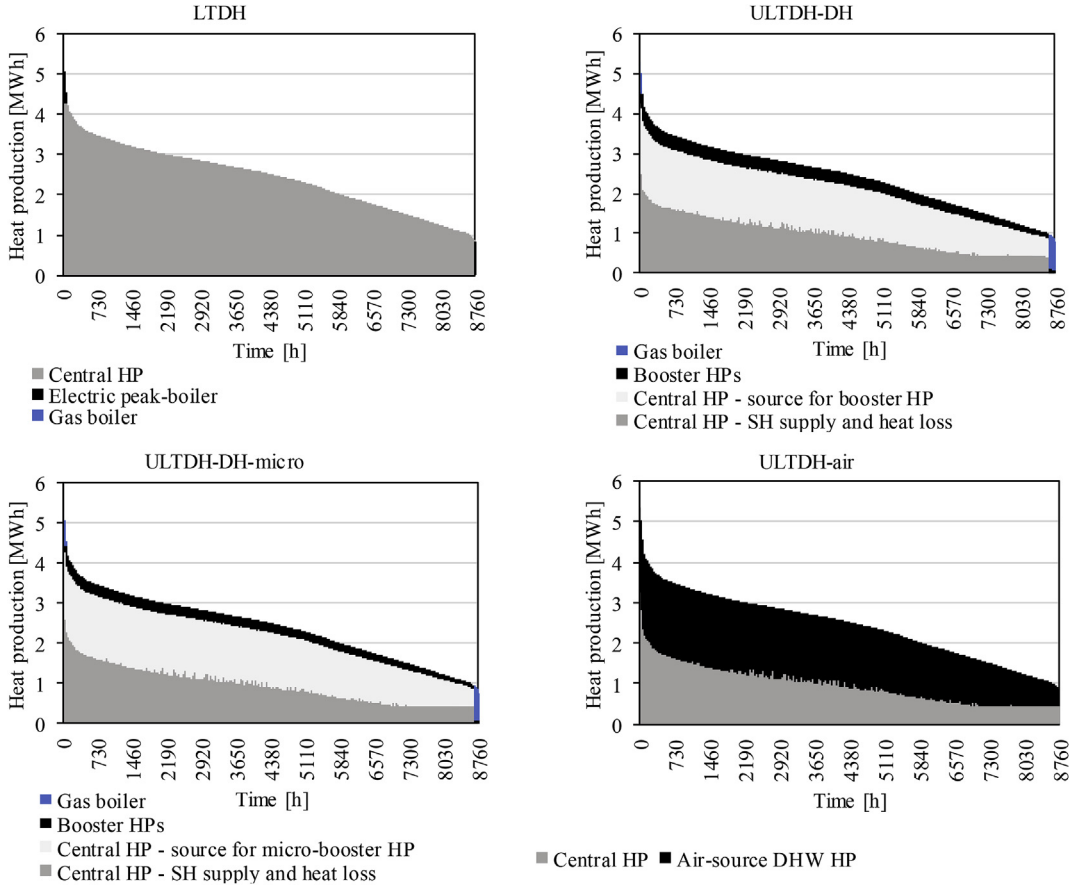

Fig. 4. Duration curve for four DH cases supplied by a central HP for plot ratio = 1.5, SH share = 0.5.

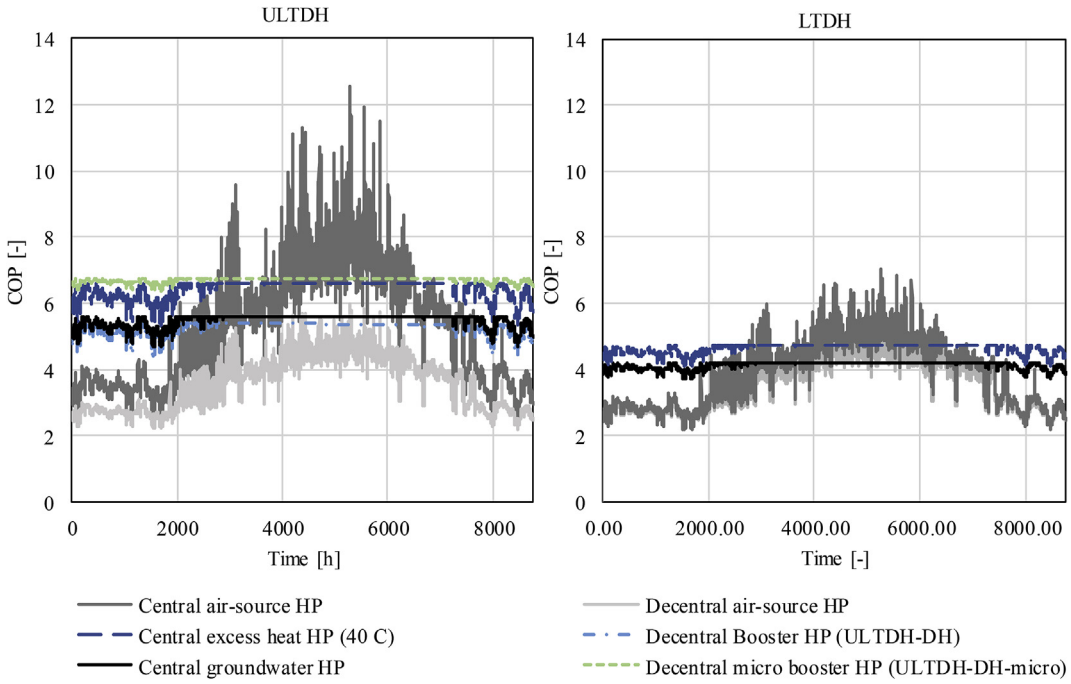

Fig. 5. Hourly variation of COP for one year of all considered heat pump units for ULTDH and LTDH.

temperature varied strongly throughout the year. The variation of the other units was caused by increased forward temperatures during winter. This led to higher temperature lifts in the central units. The booster HP COP was affected, too, as sink and source inlet temperatures increased, while the supply temperature and the controlled return temperature stayed constant. In consequence, this led to an increased condensation pressure and thus reduced COP.

3.1.3. Dependency of seasonal system COP on plot ratio and SH share

Fig. 6 shows the seasonal system COP for excess heat of 40 °C and air-source HP as the central unit. The results for groundwater HP as central unit are not depicted, but show a similar trend to that of the air-source HP. For LTDH the seasonal system COP increased from 0.1 SH share and reached a maximum at a SH share of 0.6 and a plot ratio of 2 for HP using excess heat at 40 °C. For air-source HP and groundwater HP, the maximum was reached at a SH share of 0.3 and 0.6, respectively. For plot ratios larger than 0.7 the COP dropped again. Reductions in COP for low and high SH shares were connected to increased usage of the electric back-up boiler due to constraints of the HP capacity.

The maximum seasonal system COP for air-source HPs was shifted towards lower SH shares compared to the alternatives. For air-source HPs a reduction of seasonal heat demand peaks due to lower SH shares in winter was advantageous, because the amount of heat produced with a reduced COP due to low source temperatures and defrosting could be reduced.

The seasonal system COP increased with increasing SH share for all ULTDH solutions. For ULTDH-DH and ULTDH-DH-micro the DHW share of the heat supply had a lower COP than the heat supplied directly at 40 °C. This was due to the necessary additional electricity input to lift the temperatures to the desired level. Accordingly, larger shares of SH resulted in larger average COPs, as the share of directly supplied heat increased. However, increased SH shares meant less energy efficient buildings and a higher overall heat demand. The same trend was observed for ULTDH-air. Here, the system COP increased as the central HP had a better COP than the booster HP as shown in section 3.1.2.

For the excess heat case, the ULTDH solutions, which were supplied by excess heat directly, clearly outperformed LTDH, where a HP was needed to supply the necessary forward temperatures. ULTDH-DH-micro had the highest seasonal COPs, followed by ULTDH-DH and ULTDH air. This can be explained by the difference in COP between the micro-booster HP (6.7), the booster HP (5.2) and the decentral air-source HPs (3.1–3.3). For the booster HPs, a higher COP meant that more heat was supplied from the central source, and thus a higher share of heat was supplied directly from excess heat, which increased the overall seasonal COP.

For ULTDH supplied by a central air-source HP, the seasonal COP of the different DH cases is much closer to each other and ULTDH-air performed best for most cases. For low SH shares the COP of ULTDH-air was highly sensitive to the plot ratio, indicated by the larger spread of the data points in y-direction indicated by the arrow in the diagram. This was caused by an increase in relative heat loss for very low heat demands. For SH shares of 0.4 and higher or plot ratios of 0.8 and higher ULTDH-air had the highest seasonal COP. This was because in the ULTDH-DH and ULTDH-micro cases, DHW was produced by two heat pumps in a row, which led to a lower COP than the decentral air-source HP COP for the DHW demand share. The difference between ULTDH-DH-micro and ULTDH-DH is caused by the difference in booster HP COP.

For DH supplied by a groundwater HP, the trends looked similar to those for the central air-source HP. LTDH yielded the highest seasonal COP up to SH shares of 0.4. For higher SH shares ULTDH was more efficient. Among the three different ULTDH variants, ULTDH-air performed best followed by ULTDH-DH-micro and ULTDH-DH.

3.2. Levelised cost of heat

The LCOH of 12 exemplary cases are depicted in Fig. 7 a). The LCOH decreased with increasing plot ratio and with increasing SH share. The overall findings showed that LTDH was cheaper than the

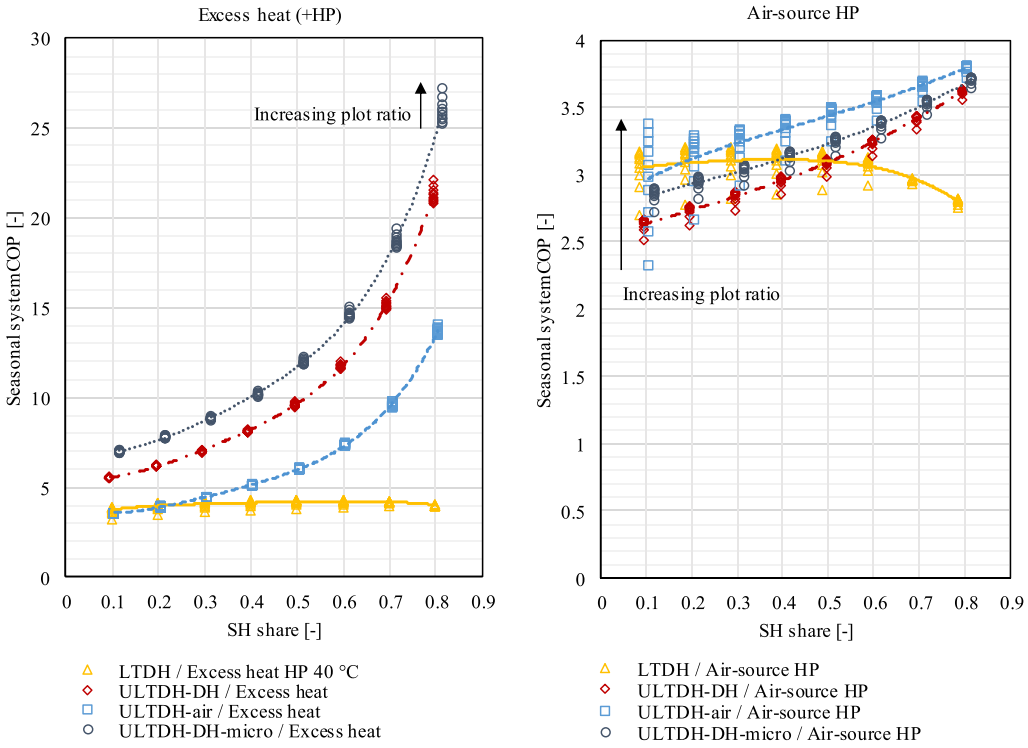

Fig. 6. Seasonal system COP for four DH cases and two central heating units depending on the SH ratio. The data points presented are for plot ratios of 0.2, 0.4, …, 2. Trend lines for the four different cases are shown.

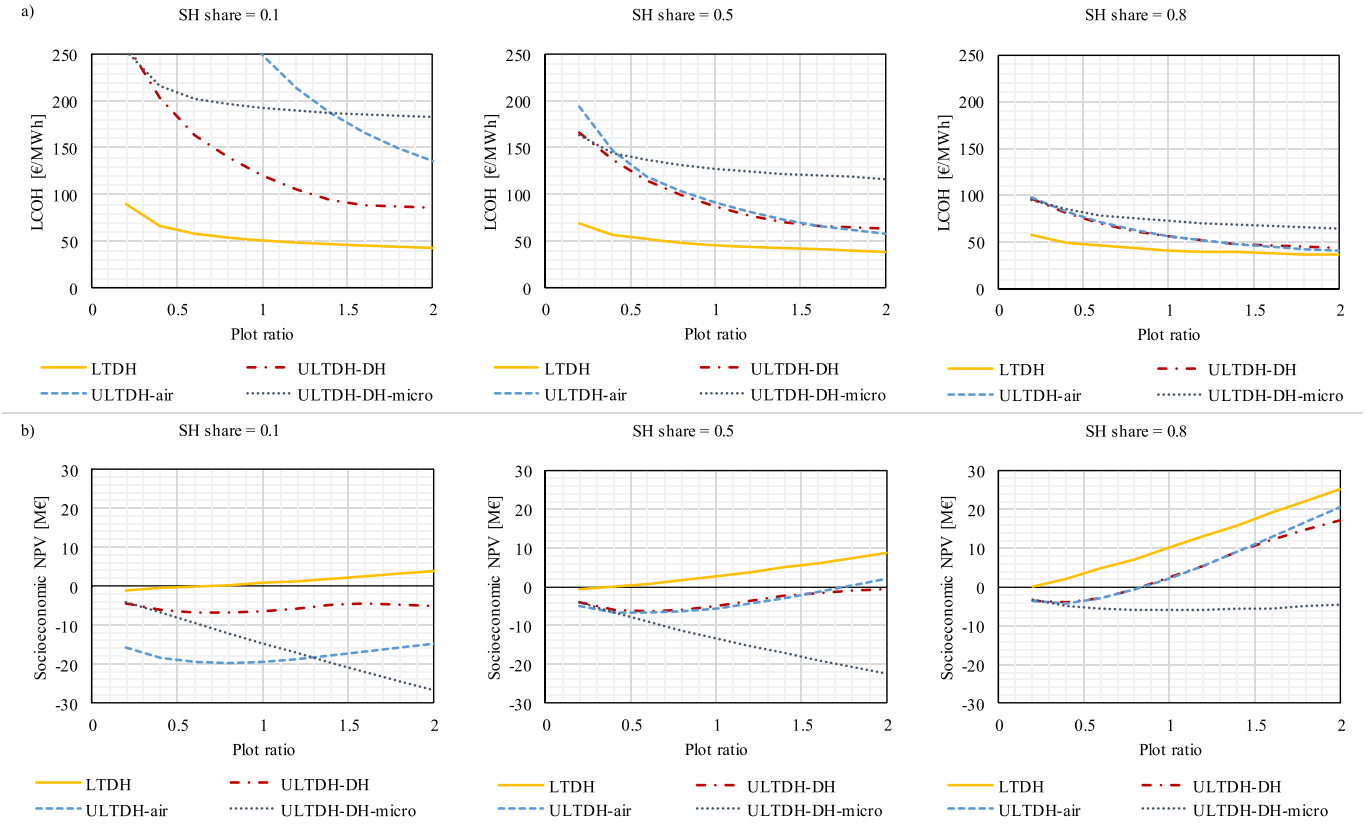

Fig. 7. a) Levelised cost of heat depending on the plot ratio for three different SH shares, central heat source: Groundwater HP; b) Socioeconomic NPV depending on plot ratio for three different SH shares, central heat source: Groundwater HP.

ULTDH systems in most calculated scenarios. The difference was largest for low SH demands, i.e. highly energy efficient buildings, and low plot ratios. Among the ULTDH solutions, ULTDH-DH-micro was only competitive for low plot ratios where the number of installed micro-booster units and alternative units was similar. For increasing plot ratios, multi-family buildings were considered and the booster HPs benefitted from economy of scale and thus ULTDH-DH got more beneficial. ULTDH-air could only be competitive for relatively high SH shares, as only the SH is distributed through DH, and thus all the cost of installing a network and a central unit was assigned to the SH cost only.

Fig. 8 a) shows the most feasible supply options for varying SH share and plot ratio. Individual heat supply from air-source heat pumps was most feasible at low plot ratios and low SH shares. It was observed that the LHDD alone is not enough to describe the feasible area precisely, but instead both SH share and plot ratio should be considered. Fig. 8 b) compares the most feasible DH variants for direct excess heat supply, LTDH supplied by a heat pump using a 40 °C source and individual heat supply. In this case, ULTDH was beneficial compared to LTDH for buildings with a SH share of approximately 0.7 or more and for plot ratios above approximately 1.0 for ULTDH-DH and 1.8 for ULTDH-air.

Fig. 9 compares the LCOH for different central heating units. The changes in LCOH between the different central units was small compared to the change due to different DH system designs. The LCOH did not change significantly with decreasing excess heat temperatures for those cases, where a central heat pump was used, as it was assumed that all excess heat streams were cooled down to 10 °C. This heat source outlet temperature determined the evaporation pressure, and thus no COP improvement was obtained. For the ULTDH solutions, the investment cost for the central unit increased significantly, when the excess heat temperatures were too low to supply SH directly.

As the heat source was the main energy supply of the system, its cost could significantly influence the feasibility of the solution. For the case presented in Fig. 9, HPs using excess heat at a cost of 10 €/MWh led to higher LCOH than both natural sources for all variants but ULTDH-air. HPs using excess heat as source could lead to lower LCOH in case the cost of excess heat was reduced or the COP was increased, e.g. by allowing a higher source outlet temperature. The variation of excess heat cost did however not change the feasibility of the LTDH solutions compared to the ULTDH solutions.

The influence of the supplied area size on the results was low compared to the other parameters presented. A reduction in area size resulted in higher specific costs for all solutions due to economy-of-scale effects. The increase in specific cost was largest for LTDH and lowest for ULTDH-DH-micro. This resulted in a slight shift of where ULTDH solutions may be feasible towards lower heat demand densities.

3.3. Socioeconomic net present value

The socioeconomic NPV for the same cases shown in section 3.2 is depicted in Fig. 7 b). The socioeconomic NPV is a relative value showing the difference between the DH solution and heat supply based on individual air-source heat pumps. Accordingly, a positive value was equivalent to a socioeconomic PV larger than that of individual air-source HPs and a negative value meant that individual air-source HPs were most feasible. In the depicted cases this was the case for a plot ratio below 0.63, 0.39 and 0.2 for SH shares of 0.1, 0.5 and 0.8, respectively.

Generally, the socioeconomic NPV increased with increasing plot ratio if the LCOH of the DH solution was below the LCOH of heat supply based on individual air-source HPs. This shows good agreement between the private consumer economy and the socioeconomic results. The gradient of the socioeconomic NPV curve depended on the gradient of the cost difference between the DH- and the individual solution, and the gradient of the overall heat supply with increasing plot ratio.

3.4. Cost composition

To understand what determines the economic feasibility of ULTDH and LTDH, the cost composition of the DH solutions was analysed. Fig. 10 shows the cost composition for the four DH solutions, supplied by a groundwater HP, for SH shares of 0.5 and 0.8

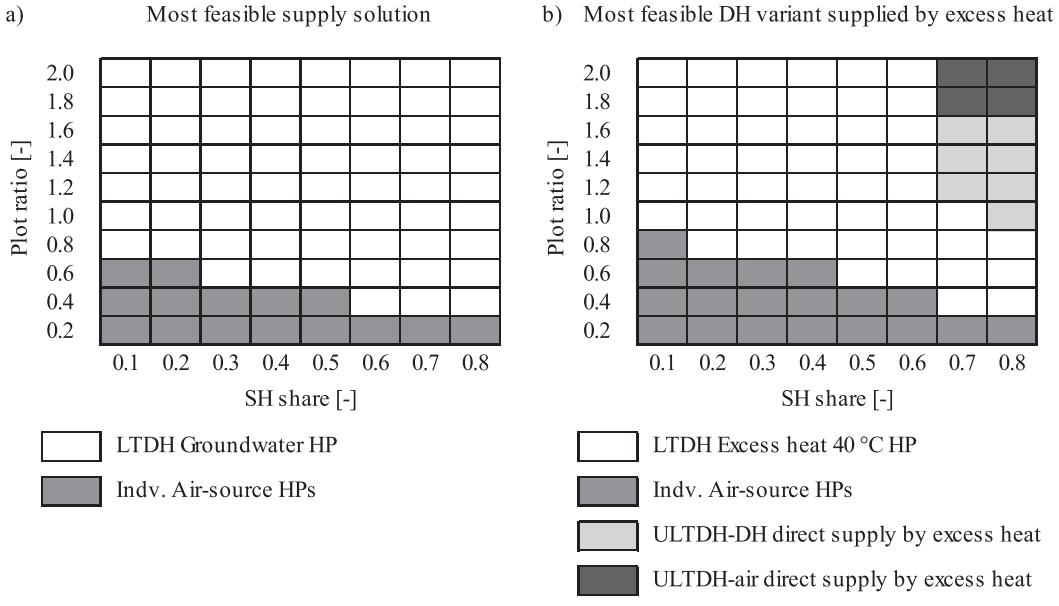

Fig. 8. a) Most feasible supply solution comparing all assessed technology combinations, b) most feasible DH variant when the heat is supplied by excess heat directly for ULTDH and by a heat pump using 40 °C excess heat as heat source compared to supply from individual.

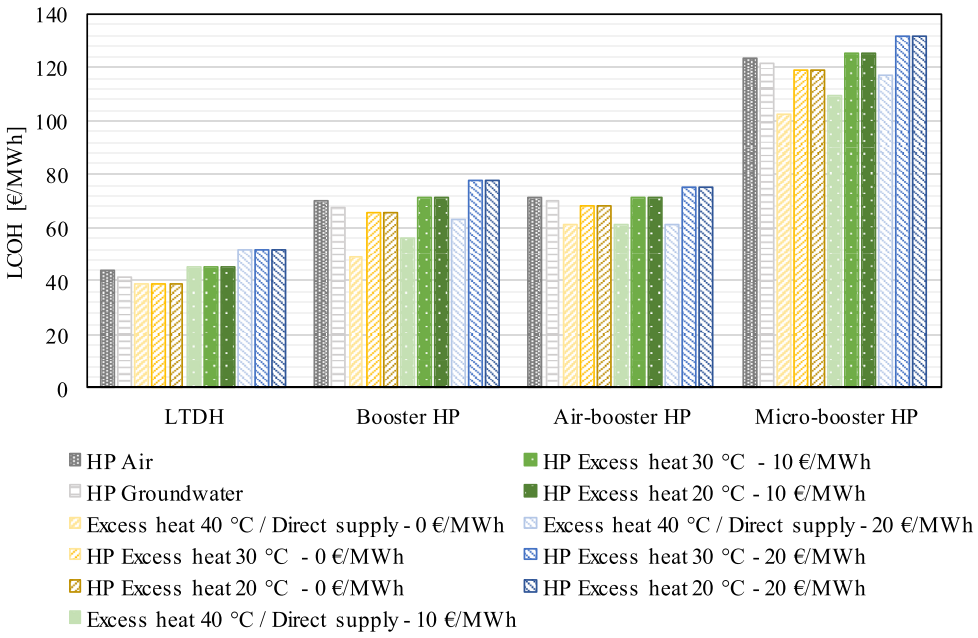

Fig. 9. Levelised cost of heat for different central heat sources and excess heat cost for SH-share = 0.5 and plot ratio = 1.5.

and plot ratios of 0.6 and 2. The same trends were observed for all central HPs.

For all four cases depicted in Fig. 10, LTDH was economically most feasible, despite the lower overall seasonal COP (see section 3.1). Among the ULTDH solutions, the total cost was lowest for ULTDH-air, followed by ULTDH-DH and ULTDH-DH-micro. The cost of the ULTDH-DH-micro was considerably higher compared to the alternatives, especially for the case with a plot ratio of 2. This had two major reasons. First, the investment cost of micro-booster units was 2.87 times the investment cost of the air-source HPs. This was due to the constant specific investment cost of the micro-booster HPs, which always came in the same size as they were installed in every apartment. The specific cost of the air source HP and the booster HP decreased due to economy-of-scale effects with increasing plot ratio, as the buildings got larger and thus the HP size increased. Second, the fixed O&M cost was 16.7 times higher than that for air-source HPs. This was due to the larger number of installed units that would have to be operated and maintained. The difference was less relevant for areas with lower plot ratio, where the number of apartments per building decreased. This is represented by the case of SH share of 0.8 and plot ratio of 0.6, where the total cost of the three ULTDH solutions were closer to each other.

The investment and O&M costs of the decentral HP units solely depended on the plot ratio, i.e. the total number of buildings and the number of apartments per building. Accordingly, the differences between the DH variants were more pronounced for lower SH shares. With an increasing SH share the capacity of the central heat pump unit increased and accordingly, the investment cost of the central heating unit and the total heat production cost from the central heating unit increased. The heat production cost of the central unit included electricity cost, variable O&M cost and taxes. The investment cost of the central unit supplying ULTDH at high plot ratios was slightly higher than for LTDH. This was caused by the assumption that the capacity of the central units for ULTDH should have capacity to cover the maximum DH demand, while the capacity of the LTDH central unit was assumed to be only 80% and instead an additional peak boiler was included. Accordingly, the lower investment cost in the central unit for LTDH led to relatively high heat production cost of the peak load boiler, indicating that the capacity of the central unit should be optimized.

3.5. Sensitivity analysis

3.5.1. Variation of investment cost

The HP investment cost were based on currently available technology and recent projects, but they might decrease due to higher production volumes in the future. The investment cost was varied for the central HPs, decentral HPs and the network. The results are presented in Fig. 11 for a SH share of 0.8 and a plot ratio of 2, as this was the cases were the LCOH of ULTDH was closest to LTDH. The results are presented as the difference between the LCOH of the ULTDH solution and the LTDH solution, i.e. a negative value meant that ULTDH is more feasible than LTDH in terms of LCOH.

All investment cost changes resulted in a linear change in LCOH difference. The change in network investment was similar for all DH variants and did not result in a significant change in the difference of LCOH. A lower investment in decentral HPs resulted in a decrease in LCOH difference. The effect was most significant for ULTDH-DH-micro, which had the highest decentral HP investment cost. An increase of the investment in the central unit resulted in a decrease of the LCOH difference in the case of excess heat, as the investment cost in the heat pump needed for LTDH supply were significantly higher than the cost of the central heat exchangers for direct use of excess heat in ULTDH. For groundwater HP as a central unit, both DH solutions required the investment in a central HP and LTDH benefitted from economy of scale due to the larger necessary capacities. Accordingly, the LCOH difference increased with increasing central unit investment cost. The feasibility of LTDH or ULTDH did not change for the depicted cases.

3.5.2. Variation of COP

The COP of the central and decentral HPs were varied between −25% and +50% [41] to account for possible innovations in heat pump technology. Such an increase might e.g. be obtained

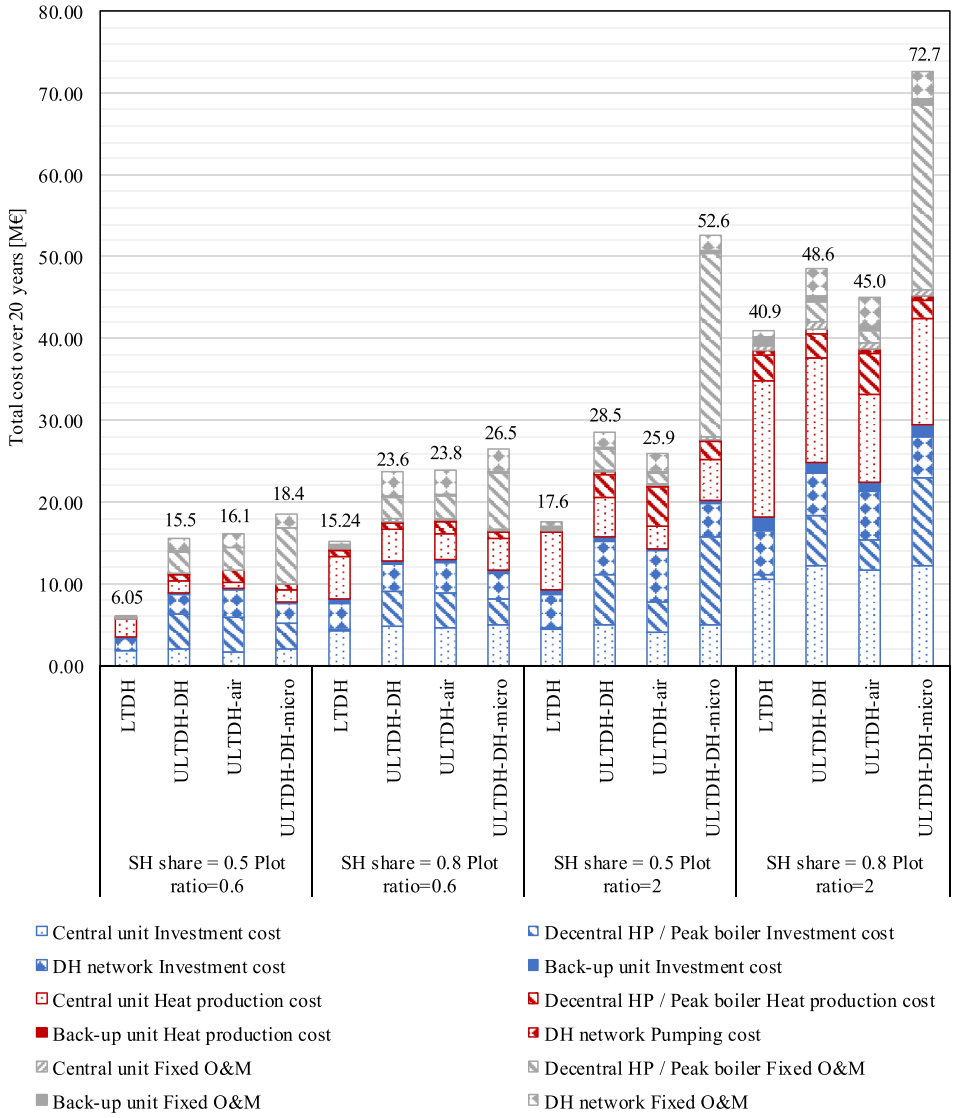

Fig. 10. Cost composition for SH share = 0.5 and SH share = 0.8, plot ratio = 2 and plot ratio = 0.6, central heating source: Groundwater HP. Heat production cost includes variable O&M cost, fuel costs and taxes. Investment cost includes VAT, reinvestments and the residual value has been subtracted. DH substation cost is included in fixed O&M cost of the DH network.

through the use of zeotropic mixtures as working fluids as proposed by Zühlsdorf et al. [38].The results are presented in Fig. 12 for the same cases shown in Fig. 11. A reduction in COP of the central and decentral HPs, had a larger influence on the LCOH difference than an increase. An increase in the decentral HP COP benefitted the ULTDH solutions. An increase in central HP COP benefitted the LTDH solution. ULTDH-air benefitted most from an increase in decentral HP COP, i.e. a higher share of heat that could be recovered from the outside air. Testing the influence of a decrease in decentral HP COP for ULTDH-air also gives an indication of how large the influence of neglecting the fan power consumption on the result may be. ULTDH-DH and ULTDH-DH-micro benefitted less from an increase in booster HP COP, which led to an increased heat production from the central HP and a larger capacity of the central HP.

The influence of neglecting the fan power consumption of the air-source HPs on the overall feasibility of LTDH and ULTDH compared to heat supply by individual air-source HPs was tested. Fig. 13 shows the variation of the minimum plot ratio for which LTDH is still feasible with increasing fan power consumption. The fan power was varied between 0% and 11% of the HP compressor power consumption. The minimum feasible plot ratio for LTDH was reduced with increasing fan power ratio, as the operation cost of individual HPs increased and thus LTDH was competitive for less densely built areas. The effect was strongest for low SH shares, as the LCOH of LTDH and the LCOH of individual HPs crossed each other at larger plot ratios, where the LCOH curve of LTDH was flatter than at lower plot ratios (compare Fig. 7).

3.5.3. *Variation of electricity cost*

The electricity cost was varied, as the future electricity price development is uncertain. A decrease in electricity price increased the LCOH difference slightly and thus benefitted the LTDH solution. ULTDH solutions benefitted from increased electricity prices, as the seasonal system COP was highest for the ULTDH options, i.e. less power is consumed per unit heat delivered. The effect was largest for ULTDH-DH-micro and least for ULTDH-air. The feasibility of the

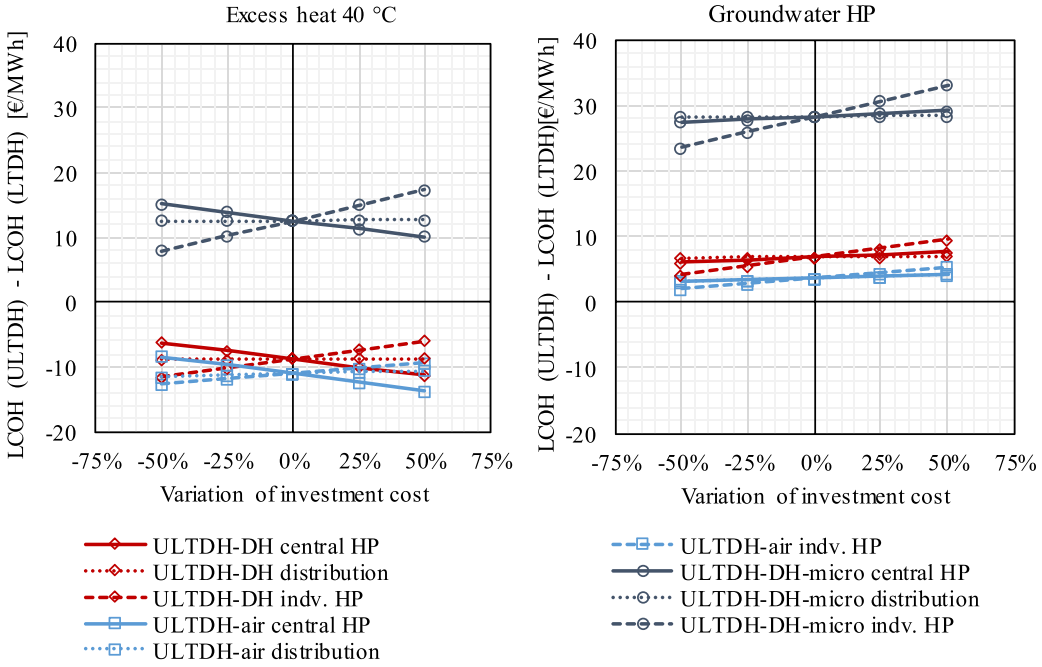

Fig. 11. Variation of investment cost of central heating unit (central), decentral booster HPs (individual) and DH network (distribution) for excess heat 40 °C source HP/direct excess heat supply and groundwater HP as central heating units, plot ratio = 2 and SH share = 0.8.

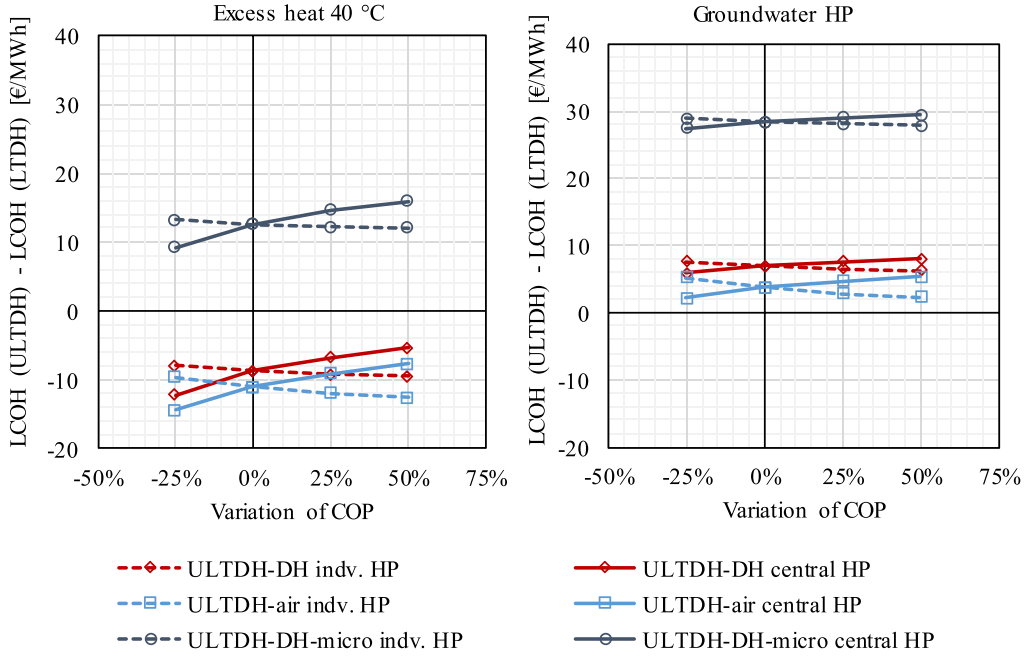

Fig. 12. Variation of COP of central HP and booster units for excess heat 40 °C source HP/direct excess heat supply and groundwater HP as central heating units, plot ratio = 2 and SH share = 0.8.

solution for the case of a SH share of 0.8 and a plot ratio of 2.0 did not change with a decrease or increase of the electricity price of 50%.

3.5.4. Variation of full load hours of decentral HPs

The design full load hours per year for the decentral HP units of ULTDH-DH and ULTDH-air were varied from 1000 h to 4000 h. The results are presented in Fig. 14. The LCOH difference decreased with increasing number of design full load hours, as the installed capacity and thereby the investment cost decreased. The trend was more pronounced for ULTDH-DH, than for ULTDH-air. Further, the decrease was lowest for the case with the highest SH share and plot ratio. Accordingly, lower decentral HP capacities would benefit the ULTDH solutions compared to the LTDH, but in the assessed range

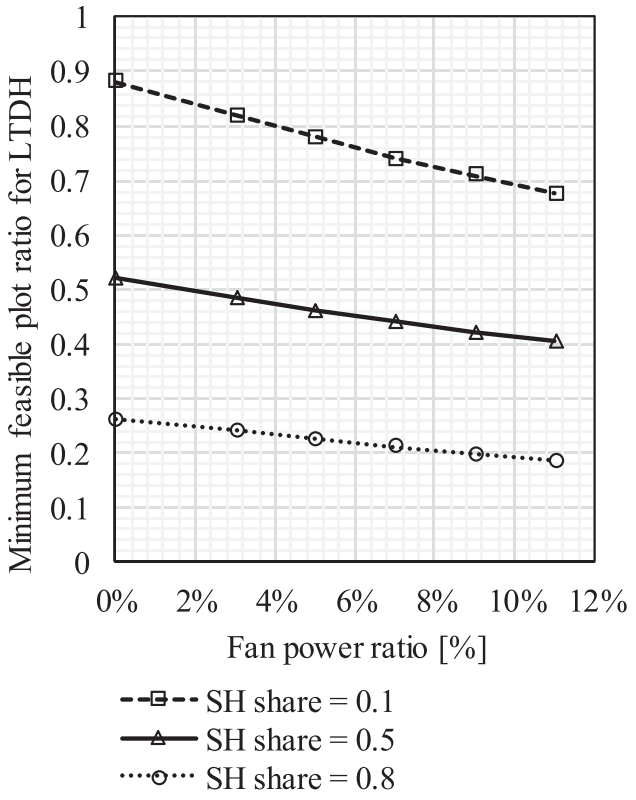

Fig. 13. Variation of minimum feasible plot ratio for LTDH with fan power ratio for SH shares of 0.1, 0.5 and 0.8. Fan power ratio was defined as the total annual fan power consumption over the total annual compressor power.

LTDH was still economically more feasible.

4. Discussion

The aim of the current study was to deduce under which boundary conditions ULTDH could be feasible compared to LTDH in Denmark. To answer this question, general correlations were used, which means that the results showed a general trend. Specific local conditions might change the results and a more thorough analysis would be needed for evaluating the feasibility of all heat supply solutions for a specific case. This would also allow for optimal sizing of the central unit with regard to the expected heat demand profile, which was not in the focus of the current study.

The current study focused on large-scale heat pumps and excess heat as central heat sources. The excess heat source has not been specified further and might as well represent other natural heating sources. In this case, seasonal temperature changes might occur, which should be considered, as they may influence the HP performance and necessary capacity. The case of 40 °C excess heat as heat source for a heat pump might also give an indication of the feasibility of new areas connected in cascade to the return line of existing networks.

The case of direct excess heat supply of ULTDH is a theoretical scenario, which was included as an extreme scenario that could maximise the benefit of ULTDH solutions. It should be noted that the existence of such a source, which can deliver 40 °C and higher forward temperatures e.g. as excess heat from industrial processes is a special case and if available, could be expected to not be free of charge and without demand for power.

As the network design was unknown for the conducted study, the pumping power and heat loss values could only be estimated. As the pumping power made up a minor part of the overall energy use, the uncertainty was deemed acceptable. The heat loss was obtained from average values of existing Danish networks. Newly built networks might perform better due to modern piping

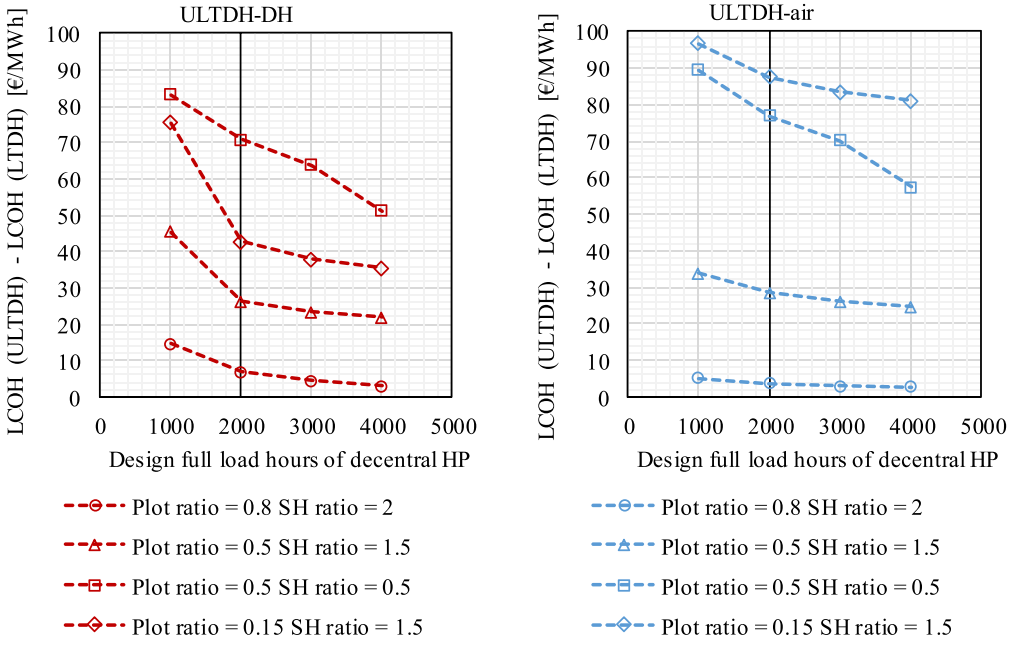

Fig. 14. Variation of design full load hours of decentral HPs for groundwater HP as central heating unit for four cases.

technology, but representative data for ULTDH networks is missing. Another simplification made is that the return temperature can be kept constant. This is generally not achieved as the cooling of the DH stream varies with the supply temperatures and the overall heat demand [24]. It may be expected that the return cannot be cooled down to the assumed values during summer. The uncertainty introduced by this was integrated in the heat loss estimation, as it was based on empirical data. It might however, result in a decreased COP of the central HP during summer, which was not considered in this study.

As presented in section 3.4 the fixed O&M cost for the booster units led to comparably high total cost of ULTDH-DH-micro. The cost function for the fixed O&M cost was based on experiences with existing individual air source and ground source HPs [33]. As the heat source for the micro-booster and booster HP is the DH system, the O&M cost related to the source might be less compared to ambient heat sources, as pollution and other risks connected to the ambient sources might be avoided. Further, these units are prefabricated, which might allow for reduced O&M cost. This would decrease the LCOH difference between LTDH and ULTDH and increase the competitiveness of micro-booster HPs. However, reliable fixed O&M cost data based on existing booster and micro-booster HPs is missing and should be addressed in future studies to reduce uncertainties for future projects.

The economic feasibility of the ULTDH-air and ULTDH-DH suffered from the extra investment and O&M cost for the decentral HP units, even though the overall seasonal COP was higher than for LTDH if the LHDD of the supplied area were high enough. Accordingly, these cost components should be reduced. This may e.g. be achieved by reducing the capacity and thereby increasing the full load hours of the decentral units.

ULTDH could only be feasible under specific boundary conditions, i.e. a cheap heat source, which is available at temperatures high enough to supply SH directly, but not high enough for LTDH. It was shown that the cost for ULTDH are closest to LTDH when the network utilization is high, i.e. for high plot ratios, i.e. a densely populated area and high SH shares. This is an unlikely scenario for newly built quarters in Denmark, as the future building regulations do not allow for such high SH shares [20]. It has however been observed that buildings do not always behave accordingly [43], which justifies the assessment of SH shares of up to 0.8. Another option to implement energy efficient ULTDH systems, while keeping the utilization of the DH network high may be the combination with district cooling, in so called cold district heating systems, e.g. Ref. [44]. This would require further research with regard to optimal system design and development of suitable heat pump substations.

The fan power of all air-source heat pumps was neglected. The sensitivity of this assumption was tested for ULTDH-air and for individual air-source heat pumps. It was not tested for central air-source HPs, as they were not among the best performing technologies and thus a change in COP of central air-source heat pumps would not change the results with regard to feasibility of ULTDH compared to LTDH and individual HPs. Miara [42] determined in field tests that the fan power consumption of small-scale air-source HPs is typically below 7% of the total power demand. Neglecting the fan power for the individual heat pumps led to more conservative results for the feasibility of LTDH for low linear heat demand densities. The feasibility of ULTDH-air compared to the other ULTDH solutions did not change when assuming a reduction in COP corresponding to 7% of the total HP power uptake.

The results presented here are in good agreement with the results presented for specific cases in literature. It was confirmed that the operation cost is lower for ULTDH than for LTDH, as also found by Yang and Svendsen [2] and Elmegaard et al. [3]. However, the increased investment and O&M cost for the ULTDH cases led to higher overall cost for the ULTDH cases. The case described by Best et al. [7] where they found that ULTDH was slightly better than LTDH considered a SH share of 0.8 and air-source HPs in a German case. According to the results presented here, this configuration might also be viable in Denmark if the plot ratio of the supplied area and the difference in central unit investment cost is large enough to balance out the extra investment in decentral units.

In the majority of the examined cases, LTDH was found to be economically more feasible than ULTDH. This was the case both in terms of LCOH and socioeconomic NPV. Both of these indicators evaluated the economy of the project from a public perspective. As the aim was to assess which common heating solutions could make sense in future applications, this approach seemed most feasible. It should be noticed that while the socioeconomic feasibility of heat supply solutions needs to be proven in order to realize a project in Denmark, this is not the case in most other countries and there the feasibility in terms of business and customer economy would probably be the decisive factor.

5. Conclusion

The aim of this study was to assess how the economic feasibility of LTDH and ULTDH systems is influenced by the boundary conditions of the supplied area and the available heat sources. For future suburban and urban (plot ratio above 0.6), newly built areas in Denmark supplied by heat pumps, heating supply from LTDH is economically most feasible. Generally, the LCOH for all considered alternatives decreased with increasing plot ratio and increasing SH share for the assessed range of these variables. Therefore, for especially low linear heat demand densities, individual heat supply is preferable. If a cheap supply of ULTDH is available, such as direct heat supply from excess heat, ULTDH could be feasible compared to LTDH for high plot ratios of 1 or higher and SH shares of 0.7 and higher. The economic feasibility of ULTDH suffered from additional investment- and fixed O&M cost of the decentral units that were not outbalanced by the lower operation cost. Compared to LTDH, ULTDH benefits from reduced overall cost of decentral units, including, increase in COP, decrease in investment cost and optimization of installed capacity. The competitiveness of ULTDH systems is higher if the share of directly supplied energy is high, as the seasonal system COP increased with increasing SH share and plot ratio, i.e. increasing heat demand and less energy efficient buildings. This does not correlate with the development towards more energy efficient buildings with low space heating demand.

The higher seasonal system efficiency of ULTDH are not reflected in the economic feasibility of these systems. In order to become more competitive, future research should be directed towards reduction of cost of decentral units, including measures to improve the COP, reduction of investment cost and of O&M cost. Further, research is needed to answer whether the combination of district heating and cooling could help to increase the utilization of the central system structures and thereby decrease the specific cost.

Acknowledgements

This research project is financially funded by EUDP (Energy Technology Development and Demonstration) under the project “EnergyLab Nordhavn - New Urban Energy Infrastructures” (project number: 64014-0555).

References

[1] Lund H, Werner S, Wiltshire R, Svendsen S, Thorsen JE, Hvelplund F, et al. 4th Generation District Heating (4GDH). Integrating smart thermal grids into

future sustainable energy systems. Energy 2014;68:1–11. https://doi.org/10.1016/j.energy.2014.02.089.
[2] Yang X, Svendsen S. Ultra-low temperature district heating system with central heat pump and local boosters for low-heat-density area: analyses on a real case in Denmark. Energy 2018;159:243–51. https://doi.org/10.1016/j.energy.2018.06.068.
[3] Elmegaard B, Schmidt Ommen T, Markussen M, Iversen J. Integration of space heating and hot water supply in low temperature district heating. Energy Build 2016;124:255–64. https://doi.org/10.1016/j.enbuild.2015.09.003.
[4] Ommen T, Thorsen JE, Markussen WB, Elmegaard B. Performance of ultra low temperature district heating systems with utility plant and booster heat pumps. Energy 2017;137:544–55. https://doi.org/10.1016/j.energy.2017.05.165.
[5] Reidhav C, Werner S. Profitability of sparse district heating. Appl Energy 2008;85:867–77. https://doi.org/10.1016/j.apenergy.2008.01.006.
[6] Ommen T, Markussen WB, Elmegaard B. Lowering district heating temperatures – impact to system performance in current and future Danish energy scenarios. Energy 2016;94:273–91. https://doi.org/10.1016/j.energy.2015.10.063.
[7] Best I, Orozaliev J, Vajen K. Economic comparison of low-temperature and ultra-low-temperature district heating for new building developments with low heat demand densities in Germany. Int J Sustain Energy Plan Manag 2018;16:45–60. https://doi.org/10.5278/ijsepm.2018.16.4.
[8] Vivian J, Emmi G, Zarrella A, Jobard X, Pietruschka D, De Carli M. Evaluating the cost of heat for end users in ultra low temperature district heating networks with booster heat pumps. Energy 2018;153:788–800. https://doi.org/10.1016/j.energy.2018.04.081.
[9] Köfinger M, Basciotti D, Schmidt RR, Meissner E, Doczekal C, Giovannini A. Low temperature district heating in Austria: energetic, ecologic and economic comparison of four case studies. Energy 2016;110:95–104. https://doi.org/10.1016/j.energy.2015.12.103.
[10] Lund R, Skaarup Østergaard D, Yang X, Vad Mathiesen B. Comparison of low-temperature district heating concepts in a long-term energy system perspective. Int J Sustain Energy Plan Manag 2017;12:5–18. dx.doi.org/10.5278/ijsepm.2017.12.2.
[11] Østergaard PA, Andersen AN. Booster heat pumps and central heat pumps in district heating. Appl Energy 2016;184:1374–88. https://doi.org/10.1016/j.apenergy.2016.02.144.
[12] Rambøll. District heating assessment tool. https://ens.dk/sites/ens.dk/files/Globalcooperation/dhat_report-10-17.pdf. [Accessed 21 November 2017].
[13] Caramaschi M, Østergaard KK, Christiansen CH. Novel domestic hot water microbooster heat pump in ultra-low temperature district heating. In: 4th int. Conf. Smart energy syst. 4th gener. Dist. Heat; 2018. p. 1–15. Aalborg, Denmark.
[14] Caramaschi M. (MetroTherm). Personal communication. 2019.
[15] Mader G. Economic analysis of air-water heat pump technologies with a screening method (Doctoral thesis). Stockholm, Sweden: KTH Royal Institute of Technology, School of Industrial Engineering and Management; 2015.
[16] Bühler F, Petrović S, Holm FM, Karlsson K, Elmegaard B. Spatiotemporal and economic analysis of industrial excess heat as a resource for district heating. Energy 2018;151:715–28. https://doi.org/10.1016/j.energy.2018.03.059.
[17] By & havn. Levantkaj. http://www.nordhavnen.dk/kvarterer+i+nordhavnen/indre+nordhavn/levantkaj.aspx. [Accessed 6 February 2019].
[18] European Commission. EU Regulation No. 626/2011 - energy labelling of air conditioners. Off J Eur Union 2011;L 178:1–72.
[19] HOFOR. Projektforslag til københavns kommune - fjernvarmeforsyning af Nordhavn 2013.
[20] Hansen CF, Hansen ML. Executive order on the publication of the Danish building regulations 2015 (BR15) 2015. 2015.
[21] Wang PG, Scharling M, Wittchen KB, Kern-Hansen C. reportTechnical report 13-19 2001 – 2010 Danish design reference year - reference climate dataset for technical dimensioning in building , construction and other sectors 2013.
[22] Danish Standards Association. European committee for standardization. Heat pumps with electrically driven compressors - Testing. performance rating and requirements for marking of domestic hot water units. EN 2017;16147. 2017.
[23] Aronsson S. Fjärrvärmekunders värme- och effektbehov (Heat and heat power demands from district heating customers). Sweden: Department of Building Services Engineering, Chalmers University of Technology; 1996. Göteborg.
[24] Frederiksen S, Werner S. District heating and cooling. Studentlitteratur; 2013.
[25] Persson U, Werner S. Heat distribution and the future competitiveness of district heating. Appl Energy 2011;88:568–76. https://doi.org/10.1016/j.apenergy.2010.09.020.
[26] Fjernvarme Dansk. Dansk fjernvarmes statistik 2017. http://www.danskfjernvarme.dk/viden-om/statistik-subsection/aarsstatistik/statistik-2017. [Accessed 20 June 2018].
[27] Euroheat, Power Board. Guidelines for district heating substationsvol. 68. Euroheat & Power; 2008.
[28] Jensen JK, Ommen T, Markussen WB, Elmegaard B. Design of serially connected district heating heat pumps utilising a geothermal heat source. Energy 2017;137:865–77. https://doi.org/10.1016/j.energy.2017.03.164.
[29] Thorsen JE, Ommen T. Field experience with ULTDH substation for multi-family building. Energy Procedia 2018;149:197–205. https://doi.org/10.1016/j.egypro.2018.08.184.
[30] Energistyrelsen. Vejledning i samfundsøkonomiske analyser på energiområdet. https://ens.dk/sites/ens.dk/files/Analyser/vejledning_i_samfundsoekonomiske_analyser_paa_energiomraadet_-_juni_2018_v1.1.pdf. [Accessed 22 July 2019].
[31] Danish Energy Agency. Finding your cheapest way to a low carbon future - the Danish Levelized Cost of Energy Calculator. https://ens.dk/sites/ens.dk/files/Globalcooperation/vejledning_lcoe_calculator.pdf; 2015.
[32] International Energy Agency, Agency. Nuclear energy agency. Projected costs of generating electricity. 2015. Edition 2015.
[33] Danish Energy Agency, Energinet. Technology data for individual heating installations 2016:166. https://ens.dk/sites/ens.dk/files/Analyser/technology_data_catalogue_for_heating_installations_-_marts_2018.pdf.
[34] Energinetdk. Technology data for energy plants. www.ens.dk. [Accessed 12 October 2017].
[35] Energinetdk. Technology data for energy plants. https://ens.dk/sites/ens.dk/files/Analyser/technologydata_for_energy_plants_-_may_2012._updated_2015.pdf. [Accessed 12 October 2017].
[36] Pieper H, Ommen T, Bühler F, Paaske BL, Elmegaard B, Markussen WB. Allocation of investment costs for large-scale heat pumps supplying district heating. Energy Procedia 2017;147:358–67. https://doi.org/10.1016/j.egypro.2018.07.104.
[37] Grosse R, Christopher B, Stefan W, Geyer R, Robbi S. Long term (2050) projections of techno-economic performance of large-scale heating and cooling in the EU. Publ Off Eur Union 2017:1–180. https://doi.org/10.2760/24422. EUR28859 E.
[38] Zühlsdorf B, Meesenburg W, Ommen TS, Thorsen JE, Markussen WB, Elmegaard B. Improving the performance of booster heat pumps using zeotropic mixtures. Energy 2018;154:390–402. https://doi.org/10.1016/j.energy.2018.04.137.
[39] Metrotherm. Installatørprisliste 2018 2018.
[40] Wolf S, Fahl U, Blesl M, Voss A, Jakobs R. Analyse des Potenzials von Industriewärmepumpen in Deutschland - Endbericht. 2014.
[41] Danish Energy Agency, ENERGINET. Technology Data for Energy Plants Generation of Electricity and District Heating 2016;1–186. 978-87-7844-940-5.
[42] Miara M. Ergebnisse zu neuen Feldmessungen von elektrisch angetriebenen Kompressionswärmepumpen. Tagung des Dtsch. Klima- und Kältetechnischen Vereins. 2012AA VI.2. Aachen.
[43] EnergyLab HOFOR. Nordhavn Deliverable no. T5.4a: optimizing temperatures in low-temperature district heating networks. 2019.
[44] Pellegrini M, Bianchini A. The innovative concept of cold district heating networks: a literature review. Energies 2018;11. https://doi.org/10.3390/en11010236.

Optimizing control of two-stage ammonia heat pump for fast regulation

Optimizing control of two-stage ammonia heat pump for fast regulation

Wiebke Meesenburg[1], Wiebke Brix Markussen[1], Torben Ommen[1], Brian Elmegaard[1]

[1] Technical University of Denmark, Departement of Mechanical Engineering, Section of Thermal Energy, Nils Koppels Allé 403, 2800 Kongens Lyngby, E-mail: wmeese@mek.dtu.dk, +45 45254118

Abstract

A significant share of heat pumps in integrated energy systems is expected to be able to operate flexibly and according to variable boundary conditions. The most common type of heat pumps supplying district heating in Denmark is the two-stage ammonia heat pump. The objective of this study was to assess, how the control strategy influences the dynamic behaviour of the heat pump and to investigate whether the heat pump could supply primary frequency regulation for the electricity grid. For this purpose, a dynamic model of this heat pump type with variable speed piston compressors was implemented in Modelica and validated against experimental data from a heat pump in Copenhagen, Denmark. The results showed that the best suited control structure for fast regulation included a direct control of the power uptake, evaporation pressure control, source outlet temperature control, and preheating of the suction line. It allowed regulation of the heat pump power input from 250 kW to 175 kW in 85 seconds and from 250 kW to 100 kW in 140 seconds without the risk of condensation in the low-stage suction line. This means primary frequency regulation, which requires ramping rates below 150 seconds, could be supplied with the assessed large-scale ammonia heat pump.

Keywords: Large-scale heat pump, frequency regulation, flexibility, dynamic model, control

Nomenclature

Abbreviations			y	Output value	
CHP	Combined heat and power (plant)		**Greek symbols**		
COP	Coefficient of performance		ϵ	Tolerance	[%]
DH	District heating		**Subscripts**		
GW	Ground water		con	Condensation	
GWP	Global warming potential		cs	Cross-section	
HFC	Hydrofluorocarbons		der	Derivative	
HS	High-stage		eva	Evaporation	
LS	Low-stage		exp	Experimentally obtained value	
NRMSD	Normalised root mean square deviation		fullload	Full load	
OFIC	Open flash intercooler		in	At inlet	
TSO	Transmission system operator		low	Low pressure	
Latin Symbols			out	At outlet	
A	Area	m^2	sat	Saturation	
L	Level	$[-]$	Sep	Separator	
N	Number of discretization steps	$[-]$	set	Set value	
n	Rotational speed	$[s^{-1}]$	sim	Simulated value	
p	Pressure	$[bar]$	source	Heat source	
$\dot{Q}$	Heat flow rate	$[kW]$	supply	Supply	
t	Time	$[s]$	tot	Total	
T	Temperature	$[°C]$	wall	Suction line wall	
$\dot{W}$	Power	$[kW]$			

1 Introduction

1.1 Large-scale heat pumps in district heating

Integrating the heating sector and the electricity sector has been identified as a promising approach to efficiently accommodate large shares of transient renewable energy like wind power [1-2]. It is especially promising as district heating grids and thermal storages in the grid provide a large amount of heat storage capacity and thus flexibility as to when the necessary heat is produced. The two systems are interlinked via combined heat and power (CHP) plants and via power-to-heat units, such as heat pumps and electric boilers.

Vapour compression heat pumps do not only provide a link between the heating sector and the power sector, but also enable the exploitation of natural heat sources and excess heat at temperatures below the supply temperature. Thereby, the use of renewable heat sources is enabled. Large-scale heat pumps for district heating supply, using chlorofluorocarbons and hydrofluorocarbons (HFC) refrigerants, have been in operation in Sweden for several decades [3].Because of their high global warming potential (GWP), HFCs are being phased out for large-scale applications according to the Kigali amendment to the Montreal protocol [4]. Natural refrigerants are suggested as alternative, and especially ammonia is widely used as refrigerant for heat pumps supplying district heating. This is e.g. the case in Denmark [5,6], where strict regulations with regard to the GWP of refrigerants are in place for large-scale heat pumps.

Several studies on the system perspective of integrating large-scale heat pumps into district heating systems have been conducted. Blarke et al. [7] found that heat pumps are more cost-competitive than electric boilers, and that they provide the potential to combine intermittency-friendly operation with the efficient use of electricity for provision of heating and cooling. In this way, large-scale heat pumps may help to accommodate larger shares of renewable power supply and reduce the need for central power plant and cross-national transmission capacities [8]. The Heat Roadmap Europe studies estimate that by 2050 up to 50 % of the European heat demand could be supplied by district heating, of which 20 % to 35 % might be supplied by large-scale heat pumps [9]. This underlines the importance of understanding the challenges of highly intermittent operation of large-scale heat pumps, as key unit in future energy systems based on high shares of renewable power production.

1.2 Flexibility of large-scale heat pumps

Power-to-heat units take advantage of low electricity cost periods to supply heat at reduced cost. Thereby, they cost-effectively assist the integration of renewable energy into the system [10]. Especially, large-scale heat pumps are expected to play a key role in future smart energy systems [11]. An even higher degree of integration and support for the power system may be obtained through provision of ancillary services, i.e. frequency regulation reserve. This would however require fast adaption of the heat pump power uptake. The required ramping times are different for different regulation zones. The frequency services in place in Eastern Denmark are summarised in Figure 1. The required regulation times until the full response power is reached is indicated on the x-axis for all services. The minimum bid size and required direction of services are given below the respective curve in the system. The frequency containment reserve –normal operation and the secondary reserve are symmetric services. That means the service providing unit on the demand side needs to be able to reduce and increase its power uptake by the power capacity bid into the market. For manual reserve the service provider may bid either up-regulation capacity or down-regulation capacity. Note that the up- and down-regulation for frequency regulation services are defined from a power generation perspective, i.e. consuming less electric power with a heat pump by operating in part-load denotes an up-regulation for the power grid.

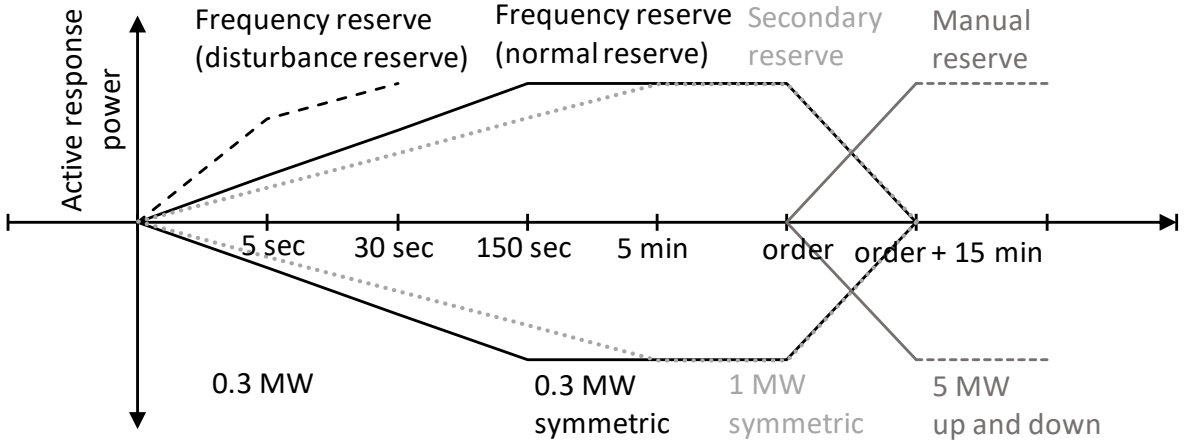

Figure 1 Requirements for frequency regulation reserves in DK-2 (Eastern Denmark): primary reserve (disturbance reserve (FCR-D) and normal reserve (FCR-N)), secondary reserve (aFRR), manual reserve (mFRR) [12]

While it is known that electric boilers can react very quickly to signals from the electricity grid [13], most large-scale heat pumps that have been installed to supply district heating, have been designed for base load operation. According to experiences from Stockholm and Gothenburg in Sweden, it is technically feasible to use large-scale heat pumps for intra-day regulation [3,14], but the intermittent operation of heat-pumps can be constrained by mechanical wear of the components, as well as several minutes start-up time and low COP during start-up [15]. However, large-scale heat pumps have not been optimised to react quickly to signals from the electricity grid. Accordingly, there is a lack of knowledge about the flexible operation of heat pumps as pointed out by David et al. [9]. Also the effect on component wear and lifetime under flexible operation conditions needs further investigation [9]. According to Storesund [16], it can be expected that compressor parts, the electric motor and the gear box are influenced most strongly by a more flexible operation.

While few experiences on flexible operation of large-scale heat pumps are available in literature, a number of publications focus on the provision of ancillary service using individual heat pumps. Fischer & Madani provided a comprehensive review on the possibility to supply ancillary services using pools of individual heat pump [17]. They point out that the optimal design and the limitations of heat pumps for flexible operation need further investigation. In order to assess and understand these limitations, the dynamic behaviour of heat pumps needs to be taken into consideration.

1.3 Dynamic modelling of heat pumps

Rasmussen et al. [18] described the dynamic behaviour of small-scale one-stage heat pumps (ca. 10.5 kW thermal) in detail. Apart from the cycling behaviour they focused on the refrigerant migration in the heat pump during start-up and shut-down. Such a detailed analysis requires the use of dynamic system models. Similar studies based on experimental and numerical assessment have emphasised that component sizing and cycle design [10-11] as well as the operating conditions [21] influence the dynamic response time of heat pump systems. These statements generally hold true for larger heat pumps as well. Compared to small units, it is expected that larger heat pumps have larger inertia and therefore longer start-up and ramping times, and that the dynamics are influenced by a more complex cycle design and control system.

The prediction of this behaviour is possible using detailed dynamic models, which are based on fundamental physics and thereby are applicable to a large range of conditions and system configurations. The models may be applied to analyse system behaviour, design and optimise systems, model based control design, controller tuning by simulating the dynamic response, as well as for fault detection and diagnosis, as summarised by Rasmussen and Shenoy [22]. Modelica [23] has been demonstrated to be a suitable platform for dynamic simulation of thermo-fluid problems, as pointed out by Li et al. [24].

1.4 Scope of this study

The aim of this study was to quantify the dynamic behaviour of a large-scale two-stage ammonia heat pump. Further, it was assessed whether it is possible to change the plant control such that existing heat pumps can ramp up and down fast enough to be eligible to supply frequency regulation services, without changing the components or cycle design of the system. Information on how fast large-scale heat pumps can actually start-up and shut-down, how they perform during regulation and what the limiting factors are to be able to react faster is needed. This may serve as a basis to analyse the business case of different operation strategies of heat pumps as sector coupling units that provide flexibility to the system.

The dynamic behaviour of the system and optimization of the control structure was done using a detailed dynamic model of an existing heat pump, which is located in Copenhagen, Denmark. The model was calibrated and validated against measured data from the physical system. It was then used to quantify the influence of the system's control structure and design on the dynamic behaviour and point to the limitations for fast regulation of the heat pump. The analysed control structures were selected from previously conducted relative gain analysis, where unfeasible structures were excluded. Further, the option of preheating the low-stage suction line was included, as it was shown that the risk of condensation in the suction line during fast ramp down is a problem that is difficult to solve solely based on controller design [25].

The system design, experimental test procedure, dynamic model, controller system design and assessed variations, the validation method, and the simulation approach are presented in chapter 2. The validation, results for the base case control and for alternative control structures focussing on the reduction of heat pump regulation time and on minimization of the risk of condensation in the suction line are presented in chapter 3 and discussed in chapter 4 before a conclusion is given in Chapter 5.

2 Method

2.1 System layout

The heat pump assessed in this study is a two-stage ammonia heat pump with a thermal capacity of 800 kW, delivered by Johnson Controls and installed in the Nordhavn harbour area in Copenhagen, Denmark [26]. It uses brackish groundwater at 10.5 °C as heat source. The system rejects the cooled groundwater into the sea. This is a special arrangement that is only possible, as there is a natural flow from the sea back into the aquifer. The heat pump is the main supply unit of a small-scale district heating grid supplying three cruise ship terminals and a high bay warehouse. The heat pump is able to deliver district heating forward temperatures of 60 °C to 82 °C. The heat supply unit is further equipped with a storage tank with a volume of 100 m³ and two electric boilers with a capacity of 100 kW each. A sketch of the heat supply system can be seen in Figure 2 and the corresponding pressure-enthalpy diagram of the cycle is presented in Figure 3.

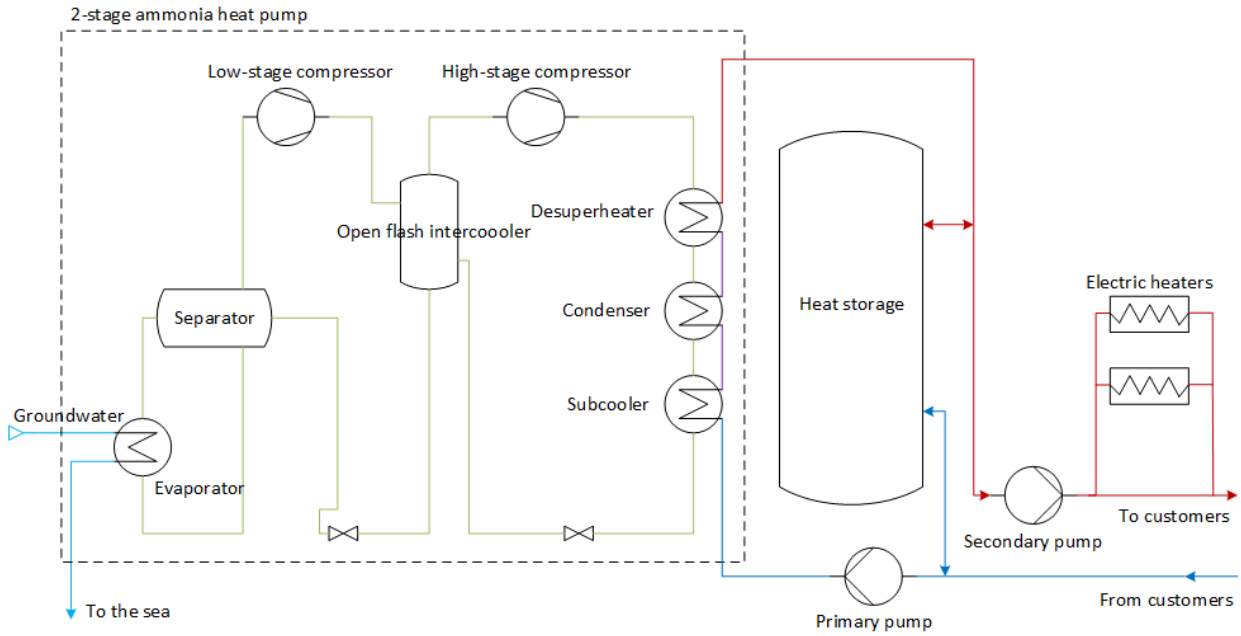

Figure 2 Diagram of the heat supply system comprising a 2-stage ammonia heat pump, a storage tank and two electric heaters

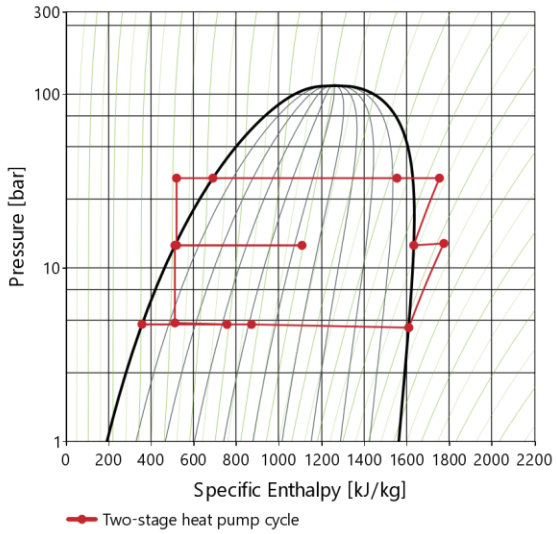

Figure 3 Pressure (logarithmic) - specific enthalpy diagram of the two-stage ammonia heat pump cycle in nominal conditions

The heat pump unit is comprised of the following main components: flooded evaporator, separator, low- and high-stage piston compressor, open flash intercooler, desuperheater, condenser and subcooler and two throttling valves. The evaporator is a corrugated plate heat exchanger and the other three heat exchangers are shell-and-plate heat exchangers. Both compressors are equipped with variable speed drive, thus enabling part-load operation.

The heat pump heat output is controlled indirectly, by controlling the source outlet temperature from the evaporator to a set value, while keeping the source mass flow constant. To control the source outlet temperature, the low-stage compressor speed is modified. The high-stage compressor speed is used to

control the intermediate pressure to a fixed value. The district heating forward temperature from the heat pump is controlled indirectly, by controlling the condensation pressure using the sink mass flow as manipulated variable. The high-stage expansion valve controls the liquid level in a receiver between the condenser and the subcooler, thereby controlling the outlet quality from the condenser. The low-stage expansion valve controls the filling level of the open flash intercooler. A PI-Diagram including the control structure may be found in section 2.3.4.

2.2 Test conditions

The first tests conducted were part-load tests of the heat pump for forward temperatures of 60 °C, 70 °C and 80 °C. Starting from full load the heating output was reduced to part-load and then ramped up to full load again, as schematically presented in Figure 4. This was done by changing the set value of the evaporator outlet temperature of the source flow. It was changed from 4.8 °C to 7.5 °C, 6.5 °C and 5.5 °C, which correspond to a load change from 100 % to 54 %, 65 % and 80 % at 70 °C DH forward temperature. The heat pump was operated in every condition until steady-state operation was reached. The values that were measured and logged during all tests are listed in Table 1.

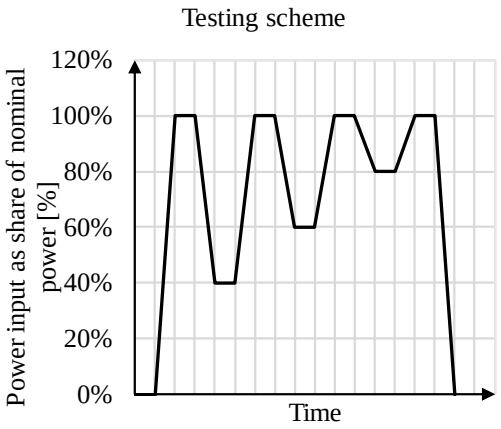

Figure 4 Idealised testing scheme for start-up, ramping and shut-down

*Table 1 Logged data for experimental analysis, *derived from other measurements*

Logged value		Unit
Operation mode		-
Heat output*		kW
Power uptake heat pump		kW
Power uptake system (incl. Pumps)		kW
COP (excl. Pumps)*		-
COP (incl. Pumps)*		-
Temperature (water)	Evaporator outlet	°C
	Evaporator inlet	°C
	Subcooler Inlet	°C
	Condenser Inlet	°C
	Desuperheater Inlet	°C
	Desuperheater outlet	°C
Gauge pressure (cycle)	Low-stage compressor inlet	bar
	Low-stage compressor outlet	bar
	High-stage compressor inlet	bar
	High-stage compressor outlet	bar
Temperature (cycle)	Low-stage compressor inlet	°C
	Low-stage compressor outlet	°C
	High-stage compressor inlet	°C
	Low-stage compressor outlet	°C

2.3 Dynamic model

A dynamic model of the heat pump was built in the object-oriented modelling language Modelica [23]. It was implemented in the simulation software Dymola using the TIL library [27]. The model was set up based on component models of the two compressors, an evaporator, a desuperheater, a condenser and a subcooler, two expansion valves, an open-flash intercooler, a separator, an auxiliary pump and two suction pipes. Other pipe elements were disregarded to reduce computational time. The pressure loss of all pipes (excl. suction lines) on the low pressure and intermediate pressure level were merged into a common pressure loss model to ensure the right inlet and outlet pressures for the compressors.

The components in the cycle were connected to each other via connectors. Via these connectors, the output mass flow from one component, together with the corresponding specific enthalpy and the pressure were given to the downstream component as input values. Further, the heat pump control was included in the model. The fluid properties were calculated using the *Refprop* database [28]. In the following, the assumptions taken for the component models are presented.

2.3.1 Heat exchanger models

All four heat exchangers were modelled as corrugated plate heat exchangers. This simplification was made as no data or correlations were available for the three shell-and-plate heat exchangers on the high pressure side. For all heat exchangers a discretised model of parallel flow heat exchangers [27] was used. The model was a finite control volume model and used the staggered grid approach, which allows the calculation of the interdependencies between mass, energy and momentum. The model was defined by *n* refrigerant control volumes, which were connected to *n* wall control volumes, which were connected

to *N* liquid control volumes. The model included dynamic energy, mass balances and a pressure drop correlation for the momentum balance for the water and refrigerant side. The energy balance in the wall between both fluids was dynamic, too. The flow direction was co-current in the evaporator and counter-current in all other heat exchangers. On the refrigerant side, the following correlations were applied: Ayub [29] was used for evaporation, Yan [30] for condensation and Martin [31] for single-phase flow. The pressure drop in the evaporator was assumed to be proportional to quadratic mass flow. The pressure drop in the heat exchangers on the high-pressure side was neglected. On the water side Martin's [31] correlations for heat transfer and pressure drop were used. The steady-state behaviour of the heat exchanger models was validated against performance data obtained from the Alfa Laval dimensioning tool [32], as no measurements on the refrigerant side were available.

2.3.2 Compressor models

The high-stage compressor was based on the *reciprocating compressor* model included in the TIL library [27]. This model includes dynamic energy and mass balance equations for the suction and discharge chamber. Further, the re-expansion mass flow was calculated based on the cylinder dead space volume and the discharge valve delay, which were input parameters to the model. The available model was adapted to Johnson Controls' *HPX* compressor by introducing a polynomial for the isentropic efficiency, calibrating the suction volume and the friction losses. The calibration procedure is further described in section 2.5.

The low-stage compressor model was based on polynomials for the isentropic efficiency, the volumetric efficiency and cooling of the compressor, including the effect of active cooling and heat loss to the environment. The volume of the component was disregarded and accordingly, the balance equations were steady-state, as no mass or energy can be stored inside the component. The polynomials were parametrised to fit Johnson Controls' *SMC 112L* (low-stage) compressor. The data for calibration and validation of both compressors was available from the Comp1 dimensioning software [33]. This model approach was based on the assumptions that the time constants of the compressors are low compared to the time constants of the overall cycle and that the stored mass and energy in the compressors may be disregarded.

A different approach was chosen for the low-stage compressor compared to the high-stage compressor as it was found unfeasible to adapt the dynamic model to the available compressor data for the low-pressure compressor, while the representation of the high-stage compressor was in good agreement with the available design data.

2.3.3 Other components

The separator and open flash intercooler were modelled as ideal separators.

In order to be able to solve the mass balances for the evaporator and the separator, an additional pump component was used to fix a pressure increase between the separator and the evaporator. In the real system this increase in pressure is purely based on gravitational forces. These were disregarded in the described model thus making the use of an additional pump component necessary.

The influence of not taking the pipes into account when modelling the heat pump system was tested by conducting a jump experiment for the model with and without pipe components and comparing the dynamic response.

The assumed geometries and input values of the model components are listed in **Error! Reference source not found.** in Appendix A.

2.3.4 Controller design

The base case control structure is depicted in Figure 5. The groundwater flow was fixed to 24.1 kg/s. The low-stage compressor (LS comp.) controlled the evaporator outlet temperature on the source side and thereby indirectly the heat output and load of the heat pump. This set-up leads to higher evaporation outlet temperatures in part-load and thus a higher evaporation pressure, which is beneficial for the part-load COP (excl. pumps) of the system. The ramp rate of the low-stage compressor was limited to fit the experimentally found data by limiting the rate of change of the integral element to 0.05 s^{-2}. The high-stage compressor (HS comp.) was set to control the intermediate pressure to 13.6 bar (absolute).

The flow of the district heating water controlled the condensation pressure/temperature in the cycle and thereby indirectly the district heating forward temperature. The relation between the condensation temperature and the desired district heating forward temperature thereby had to be known beforehand. This approach allows to avoid a delay in temperature control loop due to the system inherent delay of the forward temperature response to a change in mass flow. The temperature-offset values were determined experimentally for the real heat pump system and were used for validation. The high-stage valve (HS valve) controlled the quality at the condenser outlet. This corresponds to a filling level control in the high-pressure receiver of the real system. The low-stage valve (LS valve) controlled the liquid level in the open intercooler.

This control structure was originally designed for high COPs in both full load and part load, but it was not optimised for flexible operation of the heat pump. The changes listed in Table 2 were proposed and simulated individually and in combination for their impact on the dynamic behaviour of the system. Controlling the total power uptake directly was expected to enable the heat pump to respond more accurately to load change requirements and thereby increase the possibilities for supplying frequency regulation services. The control of the evaporation pressure and the source outlet temperature are related to avoid condensation in the suction line during fast load changes [25] or changes of the thermal boundary conditions. Other possible control structures were disregarded based on the results of a previously conducted relative gain analysis and physical constraints, like e.g. the large time constant of controlling the supply temperature directly.

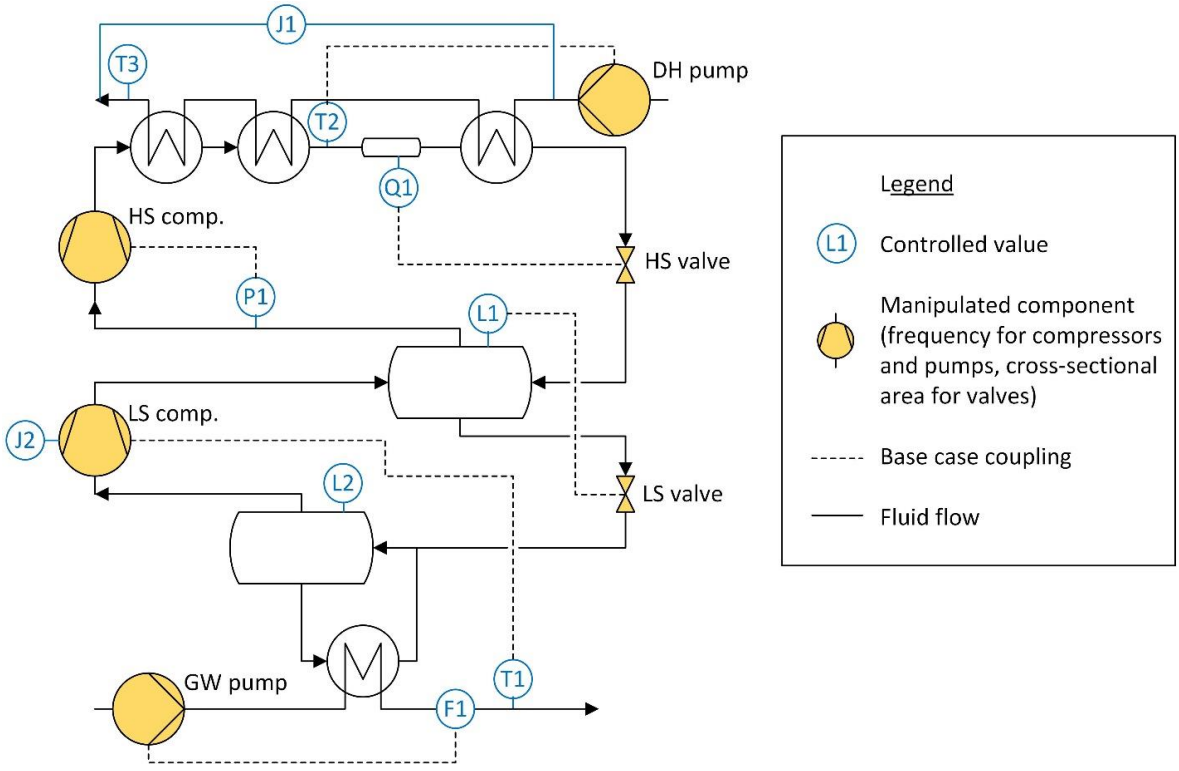

Figure 5 Sketch of the controllable values, the components that can be manipulated and the coupling of manipulated and controlled parameters for the base case scenario, with F - flow, P – pressure, T – temperature, L – liquid level, Q – vapour quality, J – Energy flow rate

Table 2 Variations in control structure that were tested

Manipulated variable	**Controlled variable**
LS compressor - n	$\dot{W}_{\mathrm{tot}}$
LS valve - A_{cs}	p_{eva} , L_{Sep}
GW pump - n	$T_{\mathrm{source,out}}$, p_{eva}

All controllers were modelled as proportional-integral (PI) or proportional-integral-derivative (PID) controllers. The applied parameters (presented in Appendix A) were determined using the T-sum rule by Kuhn [34].

2.4 Determination of regulation time

The regulation time used as a measure to compare how fast the heat pump was able to regulate considering different control structures, was defined as the time after a step in set point value, until the power uptake remained within a tolerance band of $\pm\,\epsilon = 1\,\%$ of full load and the power gradient was below $\epsilon_{\mathrm{der}} = 100\ W/s$.

$$\frac{\left|\dot{W}_{\mathrm{tot}} - \dot{W}_{\mathrm{set}}\right|}{\dot{W}_{\mathrm{fullload}}} < \epsilon \tag{1}$$

$$\frac{d\dot{W}_{\mathrm{tot}}}{dt} < \epsilon_{\mathrm{der}} \tag{2}$$

These tolerances were assumed as actual allowed tolerances for participation in the frequency regulation market are not made available by the transmission system operator (TSO). The defined criterion, is a simple steady-state condition, it may however happen that the condition is true and then becomes false again before finally reaching steady-state. If this was the case, the latest time, when the condition became true was logged as regulation time.

2.5 Model calibration and validation

Not all parameter values required by the component models in the TIL library could be determined by the given data for the real heat pump system, and thus some had to be estimated. Especially, the parameters of the low-stage compressor polynomial and the geometry parameters of the high-pressure side heat exchangers were uncertain. In order to calibrate and validate the model the following steps were performed:

1. Calibration of individual components against measured data using least-square method
2. Validation of the system against measured data during steady-state
3. Calibration of maximum ramping rate for low-stage compressor.
4. Validation of the dynamic behaviour of the heat pump

Here, calibration refers to tuning of the unknown parameters, such that the model represents the experimentally obtained measurement data. Validation refers to comparing the model results with corresponding experimental data. In order to obtain a valid result from the validation, a different data set than for the calibration was chosen. Both, calibration and validation were based on the same underlying procedure. The boundary conditions imposed to the system or component, such as the district heating return temperature and the heat source temperature for the overall system, were given to the model as a time dependent input. Further, inputs were necessary for the controller set values. These were unknown and thus estimated from the steady-state values of the measured data. Then the model was simulated and the obtained time dependent output was compared to the experimentally obtained output data. In the case of validation, the procedure finished at this stage. The calibration procedure continued by minimizing the error between the experimentally obtained result and the model result by varying the chosen tuning parameters and using a least-squares method.

The calibration procedure was divided into several steps for the individual components and the overall system. All unknown component parameters were calibrated using the component models instead of the overall system model. This enabled to localise deviations in the model more easily and allows for numerically more efficient calibration of the overall model, as the number of calibration parameters that needed to be tuned using the complete system model was considerably reduced.

All steps were conducted using the Dymola calibration function [35]. The simulation results were compared to the results for dynamic behaviour of the real system. Further, a mean deviation over the whole validation simulation period was calculated as the normalised root-mean-square deviation (NRMSD), defined as follows.

$$\mathrm{NRMSD} = \frac{\sqrt{\frac{\sum_t \left(y_{\mathrm{sim}}(t) - y_{\mathrm{exp}}(t)\right)^2}{N_t}}}{\sqrt{\frac{\sum_t \left(y_{\mathrm{exp}}(t)\right)^2}{N_t}}} \tag{3}$$

Here, $y_{\mathrm{sim}}(t)$ refers to the simulated value at time t, $y_{\mathrm{exp}}(t)$ is the measured value at time t, and N_t is the number of time steps.

2.6 Simulation approach

Before conducting the ramping experiments for calibration, validation and the proposed simulation experiments, the model was simulated for 1000 seconds before any changes were made to the model to ensure that the system was in steady–state.

Only ramping into part-load and up to full load again were studied within this study. This is in line with the proposed heat pump operation of providing frequency regulation by changing the load rather than shutting down completely and starting up again and thereby avoiding necessary settling and compressor waiting times.

After validation of the component and system models, the following experiments were conducted with the model.

- Reaction of the system to sudden load changes with improved controller parametrization compared to the validated control structure
- Reaction of the system to sudden changes in set value for DH forward temperature
- Assessment of the influence of control structures on the regulation time and risk of condensation in the suction line. The following controller changes were assessed:
    - Direct control of the heat pump power uptake
    - Control of the evaporation pressure
    - Control of the source outlet temperature
    - Control of the separator liquid level
    - Control of the evaporation pressure and the separator liquid level
    - Control of the evaporation pressure and the separator liquid level with preheating of the suction line

3 Results

This chapter presents the results of the model validation against experimental data, before more detailed results from the dynamic model are presented for the base case control structure. These include the part-load behaviour of the heat pump, the regulation time for different load changes and condensation pressures and the saturation temperature and wall temperature in the low-stage suction line as an indication of the risk of condensation. Finally, the control structure was varied, as describe above. The results for the regulation time and risk of condensation are presented in the last part of the result section.

3.1 Validation against experimental data

Figure 6 shows the comparison of the simulated results and the experimentally obtained measurements from the real heat pump. The dynamic behaviour of the results is compared by showing the development over time (left graphs) and the overall correspondence between the values is compared using diagonal plots, showing the simulated results over the measured results for the same time step (right graphs). The results are presented for a forward temperature of 70 °C.

For the intermediate pressure at the low-stage compressor outlet and high-stage compressor inlet (Figure 6 c)) and the condensation pressure(Figure 6 d)), it may be observed that the time constant of the simulated response is smaller than for the measured response. This was due to neglecting the pipelines in the simulation. It was verified that including all pipelines in the simulation leads to larger time constants, and showed an overshoot in the intermediate and high-stage pressure, which was similar to the measured data. The inclusion of all pipelines resulted tended however to be numerically stiff and computation time was accordingly high.

The characteristic overshoot of the evaporation pressure (Figure 6 e)) and the corresponding undershoot of the power uptake (Figure 6 b)) and heat flow rate (Figure 6 a)) is related to waiting times programmed in the real heat pump controller. For the model, the source outlet temperature obtained from the

measured data was an input to the model. Thereby the waiting times were represented in the simulated results. The response of the evaporation pressure to load changes fits quite well to the modelled data. It can be seen that only discrete values for the measured pressure were available. A slight deviation between the steady state values may be observed. This is most likely due to uncertainties with regard to the actual pressure drop in the different components on the low pressure side. All pressure drops were lumped into a pressure drop component, which does not account for the possibly different part load behaviour of individual pressure loss contributions. The reaction of the source outlet temperature (Figure 6 g)) fits less well. The time constant of the simulated response is smaller than the measured one. Since the evaporation pressure fits well, this difference may be accounted for delays and larger storage capacities on the water side.

The supply temperature (Figure 6 f)) fits well, considering the uncertainty induced by modelling plate heat exchangers instead of shell-and-plate heat exchangers. However, the dynamic behaviour is more similar to the measured dynamic behaviour after 3000 seconds, while the model seems to react faster than the measured data between 1000 and 3000 seconds.

The model was found to represent the general trends of the heat pump behaviour during load change well. However, some deviations were observed. The measured heat load dropped right before ramping up to full load (Figure 6 a)). This development was not identified in the simulated results. This may be explained by a slight difference in the control structure between the model and the real plant. During the measurements at the real plant the set value for the condensation pressure was changed according to the load. When ramping up, this was done before changing the set value for the source outlet temperature. The result was a decrease in mass flow and with it the heat flow rate prior to the event. The sink mass flow rate in the model was only changed as a reaction to the load changes, via the PI control for the condensation pressure, i.e. it changed after the heat pump started to ramp up. Therefore, no drop in heat flow rate before ramp up was observed.

Table 3 summarises the deviations for all validated parameters for three different forward temperatures. The largest mean deviations were found for the power uptake $\dot{W}_{\mathrm{tot}}$ and the source outlet temperature $T_{\mathrm{eva,out}}$. The two are directly related through the control structure. The source outlet temperature reacted faster to a change of the low-stage compressor speed in the model compared to the measurements. This was fed back into the controller, the profile of the low-stage compressor speed followed and thereby also the power uptake of the compressors. The lowest mean deviations were calculated for the pressures in the system and the supply temperature. The low deviation of the pressures could be expected, since both condensation pressure and intermediate pressure are controlled and thus the deviations only come from differences in dynamic behaviour and uncertainties related to the exact timing of the condensation pressure set point change during measurements.

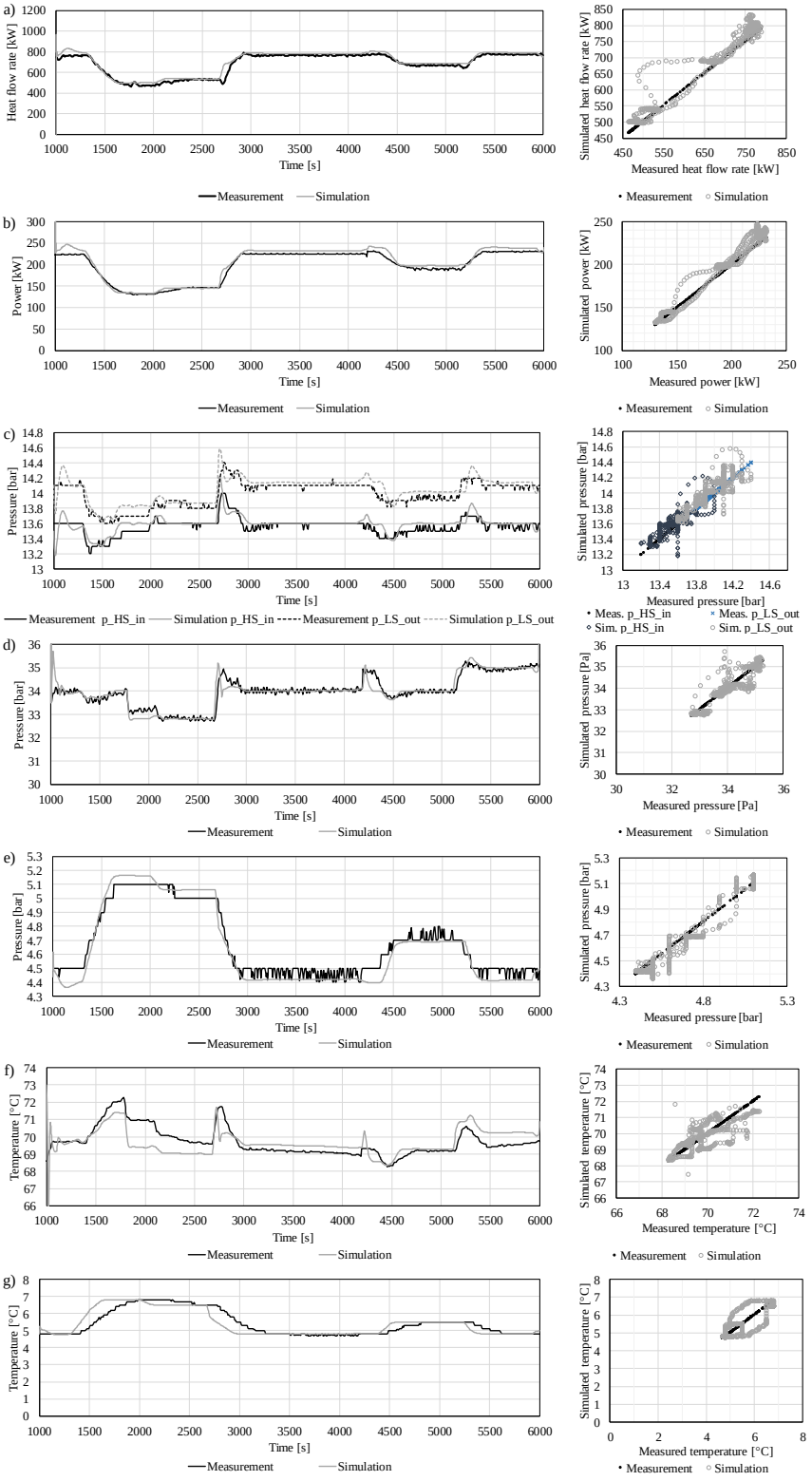

Figure 6 Comparison of simulation and measurement results over time (left) and as diagonal plot (right). From top to bottom the following is depicted: a) Heat flow rate, b) Power uptake, c) Intermediate pressure at low-stage compressor outlet and high-stage compressor inlet, d) Condensation pressure, e) Evaporator pressure, f) Forward temperature and g) Source outlet temperature.

Table 3 Root mean square of the measured data over the validated period (RMS measurement), root mean square of the difference (RMS difference) between measured data and simulated results and the mean deviation calculated as the ratio of RMS difference over RMS measurement.

	60			70			80		
	RMS measurement	RMS difference	Mean deviation [%]	RMS measurement	RMS difference	Mean deviation [%]	RMS measurement	RMS difference	Mean deviation [%]
$\dot{Q}_{\mathrm{tot}}$ [W]	529000	39100	**7.4%**	690000	41800	**6.1%**	639000	35400	**5.5%**
$\dot{W}_{\mathrm{tot}}$ [W]	137000	12900	**9.4%**	201000	12800	**6.4%**	192000	15900	**8.3%**
COP	3.93	0.38	**9.6%**	3.47	0.09	**2.5%**	3.35	0.18	**5.4%**
$p_{\mathrm{LS,in}}$ [Pa]	499000	15000	**3.0%**	468000	9340	**2.0%**	485000	15400	**3.2%**
$p_{\mathrm{LS,out}}$ [Pa]	1380000	19700	**1.4%**	1400000	12300	**0.9%**	1390000	16500	**1.2%**
$p_{\mathrm{HS,in}}$ [Pa]	1360000	18800	**1.4%**	1360000	10500	**0.8%**	1360000	15800	**1.2%**
$p_{\mathrm{HS,out}}$ [Pa]	2680000	116000	**4.3%**	3400000	34500	**1.0%**	388000	4800	**1.2%**
T_{supply} [K]	333	1.7	**0.5%**	343	0.8	**0.2%**	353	1.8	**0.5%**
$T_{\mathrm{eva,out}}$ [K]	280	0.5	**0.2%**	279	0.5	**0.2%**	279	0.4	**0.1%**

3.2 Base case scenario

The model was used to calculate the dynamic behaviour of the system as response to load changes. Here, the source outlet temperature controller was optimised compared to the validation, by parametrizing the PI controller according to the T-sum rule [34]. Thereby, the overshoot and accordingly the regulation times could be reduced considerably, an example is shown in Figure 10.

3.2.1 Steady-state behaviour in part-load

Figure 7 shows the heat pump behaviour in part load in terms of COP, heat flow rate $\dot{Q}_{tot}$ and power uptake $\dot{W}_{\mathrm{tot}}$ for three different condensation pressure set points, corresponding to three different full load supply temperatures. As expected, the COP increased with decreasing supply temperature. It reached a maximum at 40 %, 38 % and 36 % load for condensation pressures of 29.3 bar, 33.2 bar and 38.5 bar – corresponding to supply temperatures of 62 °C, 70 °C and 77 °C – respectively. The power uptake increased with the condensation pressure, as the pressure ratio for the high-stage compressor increases. The heat flow rate behaves almost the same for all three supply temperatures. The heat uptake in the evaporator was fixed via the fixed source mass flow and the controlled source outlet temperature. As the power input increases with increasing pressure ratio of the high-stage compressor, the superheat out of the compressor increases, however the influence of this increase on the overall heat flow rate is comparably small. This means, the currently implemented control structure is feasible for the precise delivery of a certain desired heat flow rate. However, if the aim is to operate the heat pump according to the requirements of the electricity grid, it should be possible to control the power uptake precisely instead.

The quality of the heat supply as the main product of the heat pump is mainly defined by the supply temperature. Therefore, it is desirable that the supply temperature can be controlled as precisely as possible. However, the supply temperature was not controlled directly, but instead the condensation pressure was controlled. This was done to avoid large dead times in the supply temperature response to changes in the sink mass flow rate. Figure 8 shows the resulting deviation of the supply temperature over power uptake for different condensation pressure set points. The resulting supply temperatures are 2 °C to 3 °C higher at the lowest reported part load compared to full load power uptake. To be able to set the supply temperature more precisely, while not losing the advantage of condensation pressure control over direct supply temperature control, an offset function for the condensation pressure could be implemented. It would be a function of the desired supply temperature and the current heat pump load as inputs. It could then be used to calculate the necessary condensation pressure set point, which could then be used as input to the existing controller.

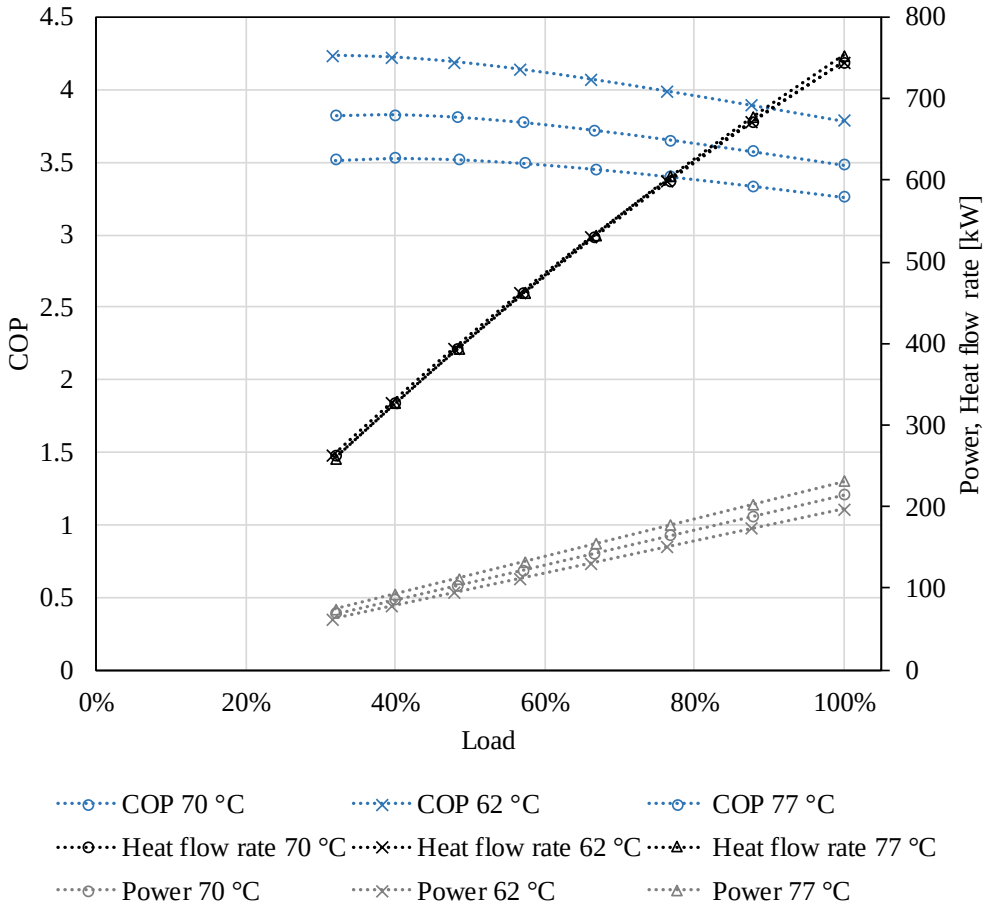

Figure 7 COP, heat flow rate and power uptake in steady-state for different part loads. The load was defined as the power uptake over the power uptake for a source outlet set temperature of 4.5 °C

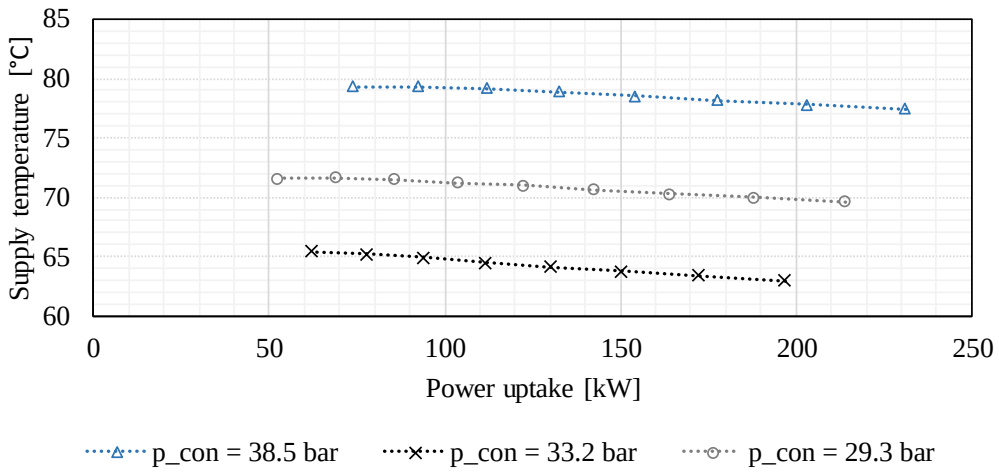

Figure 8 Supply temperature deviation in part load operation with base case control structure of condenser temperature for three different pressure set points

3.2.2 Regulation time of heat pump

An important measure with regard to heat pump flexibility is the regulation time that is needed until steady-state is reached after a load change. The regulation times were determined as described in section 2.4. They are presented for three supply temperatures, i.e. condensation pressure set points and different step sizes of the load change in Figure 9. A negative load change refers to ramping from full load into part load, e.g. a load change of -40 % corresponds to a change from 100 % load to 60 % load. A positive load change, refers to ramping from part-load, up to full load again. Figure 10 shows an example of a curve for the power uptake during a negative load change starting at 1300 seconds and a positive load change starting at 2700 seconds. The overshooting and following oscillations were more pronounced for larger load changes. This resulted in longer regulation times for larger load changes. All simulated regulation times were above 200 seconds, and thus not feasible for FCR-N delivery. The regulation times were similar for up and down ramping. No clear dependency between the regulation time and the condensation pressure set point could be identified.

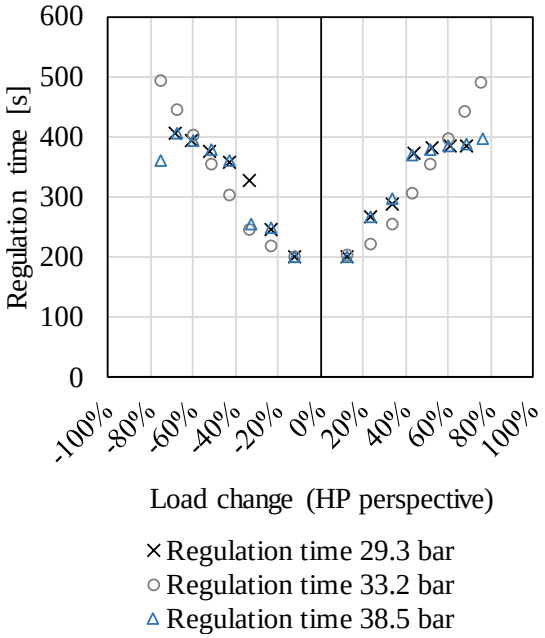

Figure 9 Regulation time for three different forward temperatures. A positive load change on the x-axis refers to increasing the power uptake of the heat pump, while a negative load change refers to decreasing the power uptake

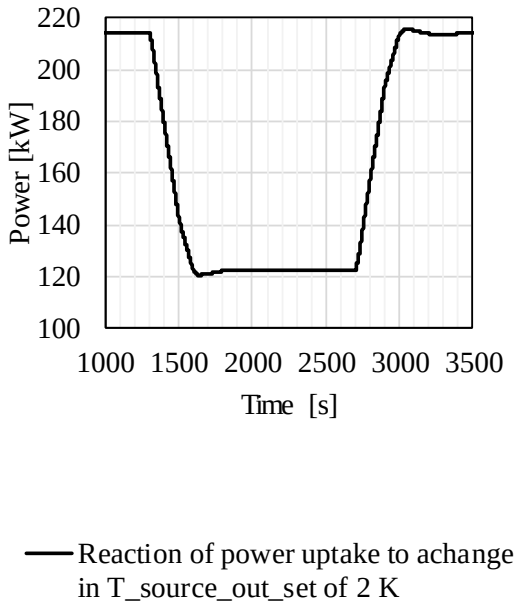

Figure 10 Response of the power uptake to a change in the set point of the source outlet temperature of 2 K, corresponding to 43 % points change, compared to full load

3.2.3 Risk of condensation in suction line

During ramp down and ramp up, the base case control structure of the heat pump load resulted in changed outlet temperature of the heat source stream. As can be seen in Figure 11 the saturation temperature in the low-stage compressor suction line rises above the suction line wall temperature during ramp down of the heat pump. This is caused by the increase in evaporation pressure and thus saturation temperature, while the pipe walls are still cold from the operation before. This may result in sudden condensation in the suction line, which may harm the compressor and should therefore be avoided. A similar phenomenon may be observed in the high-stage suction line. Here, the pressure dropped during ramp down of the compressors. During the following increase in pressure back to the set value, the saturation temperature reacted faster to a change in pressure than the wall temperature and condensation in the suction line could occur. The saturation temperature was also calculated for the experimental pressure increase after the undershoot. The slightly larger time constant of the measured response compared to the simulated response, as described in section 3.1, was slow enough, so that no condensation would occur. Therefore, the high-pressure suction line was disregarded in the following. On the other hand, avoiding condensation in the low-pressure suction line is an important task to solve, in order to allow faster downward ramping of the heat pump without the risk of liquid entering the compressor.

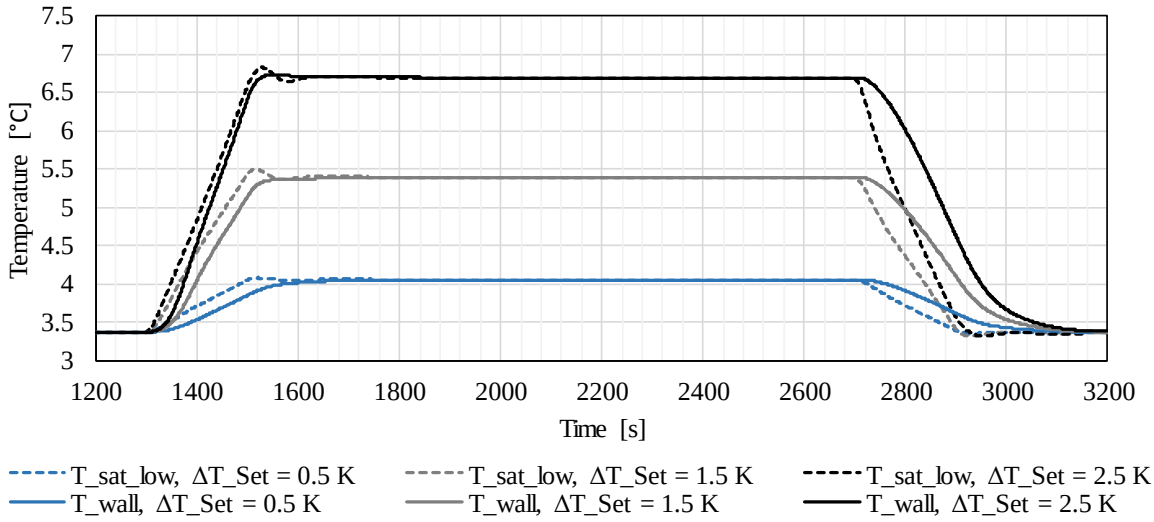

Figure 11 Saturation temperature of ammonia in the low-stage suction line (dashed) and suction line wall temperature (solid) (most downstream cell) during ramp-down (starting at 1300 s) and ramp-up (starting at 2700 s). If the wall temperature is below the saturation pressure, condensation may occur at the pipe surface, which may harm the compressor.

3.3 Influence of control strategy on dynamic behaviour

The control structure of the real system was designed to allow for maximum COP in part-load. It was however seen in the experimental data used for validation that the controllers were not optimally parametrised for fast regulation of the heat pump, which resulted in a prolonged underswing of the power uptake and heat flow rate (as shown in Figure 6). The simulation with the base case control structure, but with controller parametrization according to simple tuning rules (compare section 3.2), already resulted in an improved dynamic behaviour. However, two limitations were identified that hinder the fast regulation of the heat pump. Firstly, the indirect control of the heat flow rate and thereby power uptake, makes it more difficult to control the power uptake precisely and induces a dead time into the load control. This was seen for control of the heat output and of the source outlet temperature. Secondly, condensation in the suction line during fast ramp down needs to be safely avoided in order to allow for fast ramping. Therefore, it was assessed whether a direct control of the power uptake instead of the implemented indirect load control could allow faster reaction of the system, and whether a low-pressure control could reduce the risk of condensation in the suction line.

3.3.1 Control of power uptake

In order to allow for faster regulation of the heat pump, it was proposed to control the power uptake of the compressors directly via the low-stage compressors rotational speed, instead of indirectly via the source outlet temperature. By reducing the rotational speed of the low-stage compressor, the mass flow rate in the lower part of the two-stage cycle decreased and with it the pressure at the intermediate level. The high stage-compressor controller reacts to the decrease in intermediate pressure by decreasing the rotational speed. In this way the high-stage compressor always follows the low-stage compressor. A reduction of mass flow rate through the heat exchangers on the low- and high-pressure side results in less heat uptake and heat output and thus a reduced heat load of the heat pump. This was expected to have two advantages. Firstly, the power uptake can be measured more quickly compared to the evaporator outlet temperature, where a system immanent delay needs to be considered until a change in rotational speed can be measured as a change in temperature at the evaporator outlet. Secondly, when

delivering regulation services, the power uptake could be controlled to follow the required ramping curve precisely.

The maximum change in power uptake of the heat pump depends on the operation strategy. As explained below the change could be either of the difference of the maximum and minimum load or 50 % of the difference. In the first case, all frequency up-regulation would be provided by ramping-down the heat pump and the frequency down-regulation by turning on the electric boilers. In the second case, the heat pump would, as default, be operated at intermediate load and could then regulate up or down. The minimum load for the case study was fixed to 100 kW electric power. Accordingly, maximum a step changes of -150 kW and -75 kW respectively would be obtained, as the full load of the compressors was considered to be 250 kW. In principle, other operation strategies may be possible, but were not regarded in this study.

Figure 12 shows the power uptake for the base case control and the direct control of the power uptake with and without a constrained rate of change of the compressors rotational speed, as a reaction to a step in the load set value from 250 kW to 175 kW. The direct control of the power uptake in both cases was faster than the indirect control via the source outlet temperature (base case). The difference between the constrained power control and the base case control is the dead time induced by the temperature measurement, which leads to considerable oscillation before steady-state is reached, at 1385 seconds. For the direct control, the constrained ramping rate leads to minimal oscillations and thus the steady-state is reached at 1140 seconds. When the constraint on the ramping rate is removed, the power uptake overshoots slightly, but the regulation time can be reduced to 55 seconds.

For the larger step from 250 kW to 100 kW power uptake, the corresponding regulation times were longer. The base case regulation time was 475 seconds, the direct power control with ramping rate constraint was 320 seconds and without constraint it was 115 seconds. All regulation times are summarized in Table 4. Accordingly, shifting from indirect to direct load control is not enough to be able to ramp fast enough for the supply of FCR-N frequency regulation if the ramping constraint was not reduced.

In all three cases, the risk of condensation during ramp down is apparent, as depicted in Figure 13. While the time during which condensation may occur is longer for the constrained controllers, the peak in the temperature difference between saturation temperature of the fluid and the wall temperature is higher for the unconstrained controller. The occurrence of sudden condensation can be excluded in none of the cases.

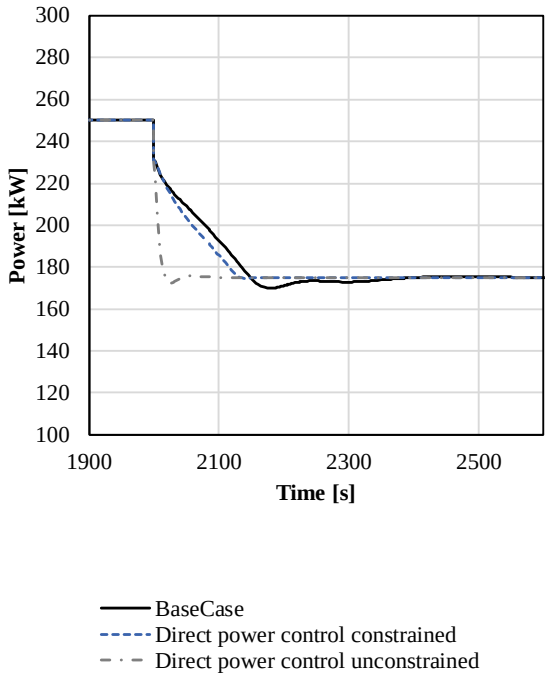

Figure 12 Response of power uptake of both compressors to a set value step of -75 kW for indirect load control (base case), direct load control with ramping rate constraint and direct load control without ramping rate constraint

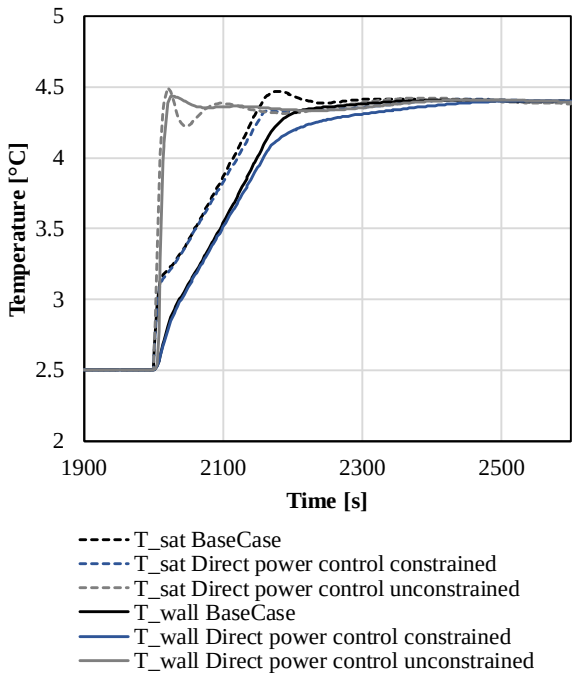

Figure 13 Response of saturation temperature and wall temperature of the low-pressure suction line to a set value step of -75 kW for indirect load control (base case), direct load control with and without ramping rate constraint

3.3.2 Low pressure control

To allow fast ramping, the risk of condensation in the suction line during ramp down needs to be avoided. The condensation occurs due to a sudden increase in pressure. Thus, one strategy may be to reduce the increase in pressure during ramp-down. This may be done by controlling the low-stage expansion valve, the source flow rate or both. Figure 14 compares the saturation and wall temperatures in the low-stage suction line for the following three cases, for a step in the power set value of -75 kW:

- Direct control of power uptake
- Direct control of power uptake with evaporation pressure control via the low-stage expansion valve
- Direct control of power uptake with source outlet temperature control via the source mass flow rate

The steady-state increase in pressure is reduced by the source outlet temperature control and disappears for the low-pressure control. However, the pressure still peaks suddenly and then slowly approaches the new steady-state value. During this peak, the saturation temperature increases more rapidly than the wall temperature and therefore the risk of condensation could not be avoided. Another problem was observed when controlling the evaporation pressure with the low-stage expansion valve. In this case none of the vessels' liquid levels were controlled, which in most cases led to drainage of the separator. To avoid this, and thereby ensure stable conditions at the evaporator inlet, the level should be controlled. Figure 14 shows the results for a step in the power set value of -75 kW for direct control of the power uptake with:

- Liquid level control of the separator via the low-stage expansion valve and source outlet temperature control via the source mass flow rate
- Liquid level control of the separator via the low-stage expansion valve and evaporation pressure control via the source mass flow rate
- Liquid level control of the separator via the low-stage expansion valve and evaporation pressure control via the source mass flow rate with preheating of the suction line

For all three cases, the peak in evaporation pressure was lower and shorter than for the control of the evaporation pressure via the expansion valve or for source outlet temperature control. The saturation temperature increases shortly by 0.9 K, compared to 1.9 K for direct power control, 1.7 K for direct power control with source outlet temperature control and 1.2 K for direct power control with evaporation pressure control. Even though the peak in evaporation pressure was reduced, the saturation temperature still increased suddenly, while the suction line walls are colder and therefore the risk of condensation could not be excluded by a different control structure alone. It wass not possible with a 1D discretised suction line model to predict precisely, whether this reduced increase would be enough to avoid condensation.

Table 4 Summary of the regulation time, risk for condensation, full load and part load COP for a load reduction of 30 % and 60 % and different control structures

	Control structure	Regulation time 1 % tolerance[s]	Risk of conden-sation	Full load COP	Part-load COP
250 kW to 175 kW, 70 °C supply temperature	BaseCase	385	yes	3.35	3.62
	Direct power - constrained	140	yes	3.35	3.62
	Direct power - unconstrained	55	yes	3.35	3.62
	p_{eva} control	85	yes	3.35	3.48
	$T_{\mathrm{source,out}}$ control	60	yes	3.37	3.55
	L_{OFIC} / p_{eva} control	45	yes	3.37	3.50
	L_{Sep} / p_{eva} control	54	yes	3.37	3.50
	L_{Sep} / p_{eva} control with preheating 300 W	54	no	3.37	3.49
250 kW to 100 kW, 70 °C supply temperature	BaseCase	475	yes	3.35	3.81
	Direct power - constrained	320	yes	3.35	3.81
	Direct power - unconstrained	115	yes	3.35	3.81
	p_{eva} control	145	yes	3.35	3.50
	$T_{\mathrm{source,out}}$ control	120	yes	3.37	3.61
	L_{OFIC} / p_{eva} control	84	yes	3.37	3.52
	L_{Sep} / p_{eva} control	87	yes	3.37	3.52
	L_{Sep} / p_{eva} control with preheating 400 W	99	no	3.37	3.50

To be sure that no condensation may occur, a preheating of the suction line is proposed. This may be electric or using another heat source. A preheating with 100 W to 500 W was simulated. The results for the minimum allowable preheating are also presented in Figure 15. 300 W preheating together with evaporation pressure control via the source mass flow rate was enough to avoid the risk of condensation for a load change of -75 kW. As presented in Table 4 this was not enough for a load change of 150 kW, where a preheating of 400 W was necessary to ensure that the suction line wall temperature was always higher than the saturation temperature. It was further found, that the peaks in saturation temperature were higher for the larger load change. It was 2.3 K for direct power control, 2.2 K for direct power control

with evaporation pressure control, 1.8 K for direct power control with source outlet temperature control, and 1.6 K for direct power control with evaporation pressure control via the source mass flow rate.

The regulation time, risk of condensation, full load COP and part load COP are summarised for all analysed control structures in Table 4. The control of evaporation pressure via the source mass flow rate together with a direct control of the power uptake allows for regulation times, which are in the same order of magnitude as the direct power uptake control alone. The only case where condensation in the suction line could be avoided was when an additional preheating of the suction line was installed, as in all considered cases the evaporation pressure peaked. The regulation time for the direct power uptake control with evaporation pressure control and preheating of the suction line, resulted in regulation times of 54 seconds and 99 seconds for a step of – 30 % load and – 60 % load using the 1 % tolerance criterion, respectively. If this tolerance would be reduced to 0.1 %, the corresponding regulation times would be 98 seconds for -30 % load and 145 seconds for -60 % load.

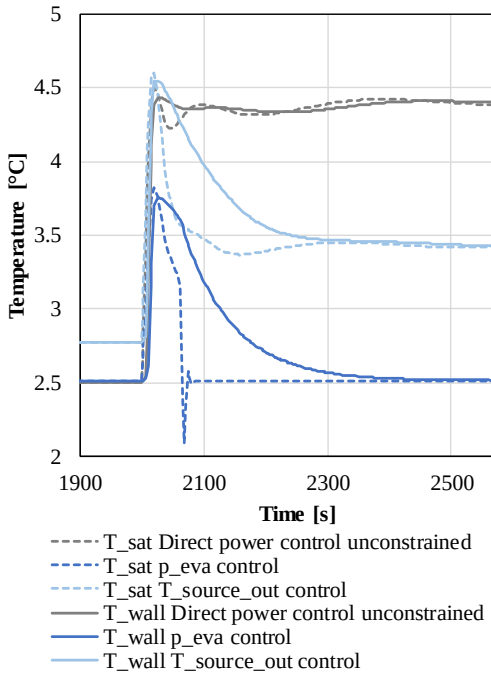

Figure 14 Response of saturation temperature and wall temperature of the low-pressure suction line to a set value step of -75 kW for direct load control, direct load control with evaporation pressure control (p_eva control), and direct load control with source outlet temperature control (T_Source_out control)

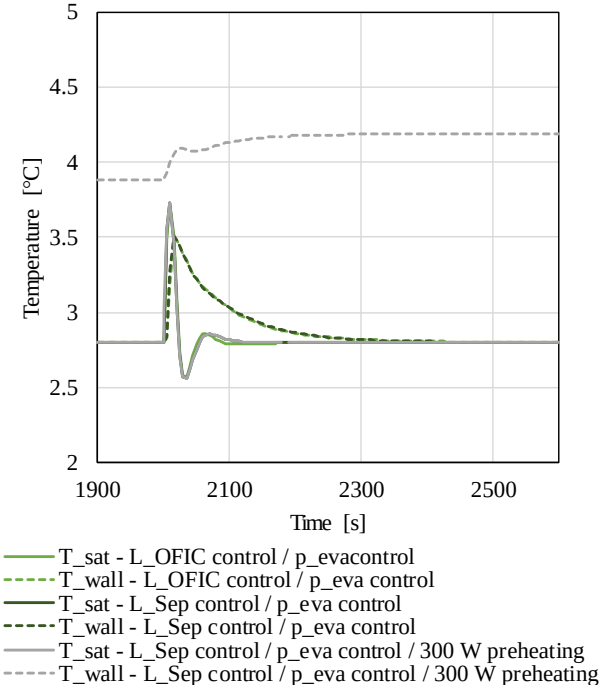

Figure 15 Response of saturation temperature and wall temperature of the low-pressure suction line to a set value step of -75 kW for direct load control with evaporation pressure control and source outlet temperature control, with no, 100 W and 200 W preheating of the suction line

4 Discussion

Future application of heat pumps and their expected role in integrated energy systems require that these systems are designed to be able to operate flexibly and according to variable boundary conditions. A dynamic model as the one presented in this study allows to cost-efficiently analyse different control structures and system configurations, that would require major changes to the real system. Further, it allows to test the limitations of the system, such as the risk of condensation in the suction line without

risking to damage the real system. Thereby validated dynamic models constitutes an important tool in the development of high-performance heat pumps.

The present study focused on a two-stage ammonia heat pump operated with piston compressors. Even larger ammonia heat pumps often use screw compressors. The regulation of these are different from piston compressors and future work should therefore include studies on the feasibility of different compressor types for fast regulation of heat pumps.

Within this work, the pumping power of the water source and the district heating water was neglected. Depending on the source, it may however be necessary to include the pumping power, to allow for the desired reduction or increase in power uptake.

4.1 Regulation time of the heat pump

A change in control structure was proposed. It would both minimise the risk for condensation in the suction line and allow for faster regulation of the heat pump. The latter is important when heat pumps are supposed to react flexibly to changes in the electricity grid, e.g. by providing frequency regulation. The simulation results showed that the system response could be considerably improved by controlling the power uptake directly instead of indirectly via the source outlet control. By doing so, it would be possible to ramp down from 250 kW power to 175 kW power in 140 seconds, and from 250 kW to 100 kW in 320 seconds. If faster ramping rates for the compressor were implemented, the regulation time was reduced even further. If the proposed control strategy to avoid condensation in the suction line is taken into consideration, the heat pump could ramp from 250 kW to 175 kW within 54 seconds and from 250 kW to 100 kW in 99 seconds with the unconstrained direct power control. This means that the heat pump would regulate fast enough to be able to act on the FCR-N frequency market, which demands ramping times below 150 seconds. If the tolerance for deviations this was decreased, the calculated regulation times would increase. The results showed that the proposed control structure with direct power uptake control, evaporation pressure control via the source mass flow rate and preheating of the suction line may still be fast enough to act on the FCR-N market, if the tolerance would be reduced to 0.1 % of full load power capacity.

In reality, the specific heat pump would have to be combined with one or more other units to be able to bid in the minimum required capacity of 300 kW. If faster regulation is required, e.g. for different primary frequency reserves, the heat pump may be combined with faster regulating units, e.g. batteries, to provide a combined frequency regulation product. Further, it should be noted that the flexible operation of heat pumps is enabled by the available heat storage capacity. This needs to be considered when evaluating whether there is a business case in providing ancillary services from heat pumps. Additionally, the capacity of the heat pumps needs to be large enough in order to allow for reduction of power uptake and thereby heat production without supplying too little heat to the customers.

4.2 Condensation in the suction line

In order to avoid condensation in the suction lines during fast ramp down, the ramping rate may be restricted. If very fast regulation is required, restricting the ramping rate might not be an option. It was shown that by controlling the low pressure via the source mass flow rate, the peak in evaporation pressure may be considerably reduced, which helps reducing the risk of condensation in the suction line. Controlling the evaporation pressure via the expansion valve resulted in draining the separator in most cases, therefore it is advisable to stick to a classic liquid level control. In terms of regulation time, no significant difference in regulation time was seen between controlling the liquid level in the intercooler or in the separator. The separator liquid level control was chosen, to ensure stable conditions in the evaporator.

Fast ramping comes along with fast increases in the evaporation pressure, which increases the risk of condensation, even if the peak in evaporation pressure may be reduced. Preheating the suction line may help to completely avoid condensation in the suction line, as the wall is always kept at higher temperatures than the saturation temperature. In this case, the superheating of the ammonia is minimal and therefore attention needs to be paid to the compressor flange and suction chamber, which might be at fluid temperature, too, and thus condensation could occur here as well. These parts are more difficult to heat than the suction line. Alternatively, the fluid may be superheated before entering the compressor. Different constructive measures to do so were analysed in [25]. These are based on increasing the superheating before the compressor by heating the gas in the suction line or possibly by reducing the pressure. Superheating the fluid before compression will however result in increased compression work and thereby reduced COP. Implementing constructive changes in an existing plant to avoid condensation in the suction line may be economically and practically unfeasible. If these problems could be avoided by advanced control methods, a reduction of COP could possibly be avoided. It should further be mentioned that condensation in the low-stage suction line has been observed in real life operation of ammonia heat pumps, which occurs if the system is operated without superheating of the fluid in the suction line and the suction pressure increases rapidly [178]. However, no such observation is known to the authors for the high-stage suction line. Accordingly, further studying of the effects in the intermediate stage is needed, including where pressure losses occur and the non-ideal behaviour of the intercooler. It should be noted that the problem of condensation in the suction line is related to the negative influence of superheating on the COP of ammonia heat pumps. For other refrigerants the influence may be positive, and accordingly superheating the fluid in the evaporator and thus avoiding sudden condensation in the suction line would not be a problem.

5 Conclusion

A dynamic model of a two-stage ammonia heat pump with piston compressors was implemented in Dymola. It was validated against experimental data from a recently installed heat pump in Copenhagen, Denmark. The validation showed a satisfying agreement between the experimental and simulated data. Uncertainties in the model were mainly related to unknown controller design of the real plant, uncertainties in high pressure heat exchanger modelling and lumped modelling of pressure loss on each pressure level. The model was then used to assess further control structures with the aim of finding a structure that would allow to regulate the heat pump fast enough to supply FCR-N primary frequency regulation, which requires regulation time of 150 seconds or less.

It was found that the most optimal control structure investigated allowed regulation of the heat pump power from 250 kW to 175 kW in 54 seconds and from 250 kW to 100 kW in 99 seconds without the risk of condensation in the low-stage suction line. To do so, the control structure was changed to a direct control of the power uptake plus controlling the evaporation pressure using the source mass flow rate, and preheating the suction line. The required preheating heat flow rate depended on the maximum expectable load reduction and was 300 W for -75 kW load change and 400 W for -150 kW load change. The maximum COP reduction through preheating was found to be less than 0.01 % at minimum load.

In conclusion, the results showed that it is possible to supply FCR-N primary frequency regulation with large-scale ammonia heat pumps with variable speed piston compressors.

Acknowledgements

We thank Tore Friis Gad Kjeld from the utility company HOFOR for conducting the measurements on the FlexHeat heat pump, and the heat pump manufacturer Johnson Controls for many fruitful discussions and insights. This research project is partially funded by EUDP (Energy Technology Development and

Demonstration) under the project ”EnergyLab Nordhavn - New Urban Energy Infrastructures” (project number: 64014-0555).

Bibliography

[1] Lund H. Large-scale integration of wind power into different energy systems. Energy 2005;30:2402–12. doi:10.1016/j.energy.2004.11.001.

[2] Lund H, Münster E. Integrated energy systems and local energy markets. Energy Policy 2006;34:1152–60. doi:10.1016/j.enpol.2004.10.004.

[3] Averfalk H, Ingvarsson P, Persson U, Gong M, Werner S. Large heat pumps in Swedish district heating systems. Renew Sustain Energy Rev 2017;79:1275–84. doi:10.1016/j.rser.2017.05.135.

[4] United Nations. Amendment to the Montreal Protocol on Substances that Deplete the Ozone Layer C.N.872.2016.TREATIES-XXVII.2.f 2016.

[5] Støchkel HK, Paaske BL, Clausen KS. Drejebog til store varmepumpeprojekter i fjernvarmesystemet. 2017.

[6] Jørgensen PH, Ommen T, Markussen WB, Elmegaard B. Performance Optimization of a Large-Scale Ammonia Heat Pump in Off-Design Conditions. 8th IIR Conf. Ammon. CO2 Refrig. Technol. Ohrid, 2019, 2019. doi:10.18462/iir.

[7] Blarke MB. Towards an intermittency-friendly energy system: Comparing electric boilers and heat pumps in distributed cogeneration. Appl Energy 2012;91:349–65. doi:10.1016/j.apenergy.2011.09.038.

[8] Blarke MB, Lund H. Large-scale heat pumps in sustainable energy systems: System and project perspectives. Therm Sci Eng Prog 2007;11:143–52. doi:10.2298/TSCI0703143B.

[9] David A, Mathiesen BV, Averfalk H, Werner S, Lund H. Heat Roadmap Europe: Large-Scale Electric Heat Pumps in District Heating Systems. Energies 2017;10:578. doi:10.3390/en10040578.

[10] Bloess A, Schill WP, Zerrahn A. Power-to-heat for renewable energy integration: A review of technologies, modeling approaches, and flexibility potentials. Appl Energy 2018;212:1611–26. doi:10.1016/j.apenergy.2017.12.073.

[11] Mathiesen BV, Lund H, Connolly D, Wenzel H, Østergaard PA, Möller B, et al. Smart Energy Systems for coherent 100% renewable energy and transport solutions. Appl Energy 2015;145:139–54. doi:10.1016/j.apenergy.2015.01.075.

[12] Energinet.dk. Introduktion til systemydelser 2017:1–12.

[13] Kuprat M, Bendig M, Pfeiffer K. Possible role of power-to-heat and power-to-gas as flexible loads in German medium voltage networks. Front Energy 2017;11:135–45. doi:10.1007/s11708-017-0472-8.

[14] Levihn F. CHP and heat pumps to balance renewable power production: Lessons from the district heating network in Stockholm. Energy 2017;137:670–8. doi:10.1016/j.energy.2017.01.118.

[15] Averfalk H, Ingvarsson P, Persson U, Werner S, Industry D. On the use of surplus electricity in district heating systems 2014:7–12.

[16] Storesund J. Handbok för livslängdsarbete med energianläggningar - Utgåva 2 2004:2.5.5-1-2.5.5-11.

[17] Fischer D, Madani H. On heat pumps in smart grids: A review. REHVA J 2017;70:342–57. doi:http://dx.doi.org/10.1016/j.rser.2016.11.182.

[18] R. W. Rasmussen, MacArthur JW, Grald EW, Nowakowski GA. Performance of Engine-Driven Heat Pumps under Cycling Conditions. Symp ASHRAE Trans 1987;93:1079–90.

[19] Murphy WE, Goldschmidt VW. Cyclic Characteristics of a Typical Residential Air Conditioner - Modeling of Start-Up Transients. ASHRAE Trans 1985;91.

[20] Goldschmidt VW, Hart GH. Heat pump System performance: Experimental and Theoretical Results. ASHRAE Trans 1982;88:479–89.

[21] MacArthur JW, Grald EW. Prediction of Cyclic Heat Pump Performance with a Fully Distributed Model and a Comparison with Experimental Data. Symp ASHRAE Trans 1987;93.

[22] Rasmussen BP, Shenoy B. Dynamic modeling for vapor compression systems-Part II: Simulation tutorial. HVAC R Res 2012;18:956–73. doi:10.1080/10789669.2011.582917.

[23] Modelica Association. Modelica and the Modelica Standard Library 2017. http://www.modelica.org (accessed October 31, 2017).

[24] Li P, Li Y, Seem JE, Qiao H, Li X, Winkler J. Recent advances in dynamic modeling of HVAC equipment. Part 2: Modelica-based modeling. HVAC R Res 2014;20:150–61. doi:10.1080/10789669.2013.836876.

[25] Meesenburg W, Kofler R, Ommen T, Markussen WB, Elmegaard B. Design considerations for dynamically operated large-scale ammonia heat pumps. 25th IIR Int. Congr. Refrig., 2019. doi:10.18462/iir.icr.2019.1203.

[26] Kjeld TFG. EnergyLab Nordhavn Delivery no.: D5.5a - Optimum supply of an island district heating grid by a local heat plant. 2019.

[27] TLK Thermo GmbH & IfT. TIL 3.4 – Model library for thermal components and systems 2017.

[28] Lemmon EW, Huber ML, McLinden MO. REFPROP - Reference Fluid Thermodynamic and Transport Properties - NIST Standard reference Database 23, Version 9.1 2013.

[29] Ayub ZH, Khan TS, Salam S, Nawaz K, Ayub AH, Khan MS. Literature survey and a universal evaporation correlation for plate type heat exchangers. Int J Refrig 2018;99:408–18. doi:10.1016/j.ijrefrig.2018.09.008.

[30] Yan YY, Lio HC, Lin TF. Condensation heat transfer and pressure drop of refrigerant R-134a in a plate heat exchanger. Int J Heat Mass Transf 1999;42:993–1006. doi:10.1016/S0017-9310(98)00217-8.

[31] Martin H. A theoretical approach to predict the performance of chevron-type plate heat exchangers. Chem Eng Process Process Intensif 1996;35:301–10. doi:10.1016/0255-2701(95)04129-X.

[32] Alfa Laval AB. CAS 5 Version 5.62.0.01 2016.

[33] Johnson Controls - Sabroe. COMP1 - Heat pump quick selection tool n.d. https://www.sabroe.com/en/products/sales-tools/comp1/ (accessed November 18, 2019).

[34] Kuhn U. Eine praxisnahe Einstellregel für PID-Regler: Die T-Summen-Regel (A practical parametrization rule for PID-conrollers: The T-sum-rule). Autom Prax 1995;37:10–6.

[35] Dassault Systèmes AB. Dymola User Manual Vol 2. vol. 2. n.d.

A Appendix

See Appendix A.2

Combined provision of primary frequency regulation from Vehicle-to-Grid (V2G) capable electric vehicles and community-scale heat pump

Combined provision of primary frequency regulation from Vehicle-to-Grid (V2G) capable electric vehicles and community-scale heat pump

Wiebke Meesenburg[1], Andreas Thingvad[2], Brian Elmegaard[1], and Mattia Marinelli[2]

[1]Department of Mechanical Engineering, Technical University of Denmark, Lyngby, Denmark
[2]Department of Electrical Engineering, Technical University of Denmark, 2800, Kgs. Lyngby, Denmark

***Abstract*—A combined delivery of frequency containment reserve (FCR) from a fleet of electric vehicles (EVs) and a large-scale heat pump is proposed to exploit synergies between the fast regulating batteries and the large heat storage capacity of the thermal system. The feasibility of the proposed strategy is assessed with a state of charge model for the EVs delivering FCR, based on one year of system frequency measurements including the conversion losses in the charger and a dynamic model of the heat pump system. Both models were previously validated against experimental data. The proposed operation of the EVs was experimentally validated as part of this study. The heat pump offsets the energy content of the frequency deviations for 25 electric vehicles and thereby enables the EVs to bid a larger power capacity on the primary frequency containment market without violating energy constraints of the battery capacity. The results for the case of 2018 shows that a synergy effect could be obtained, i.e. additional income of 4740 €/a from capacity and power price payments. This could not be generated by the EVs or the heat pump alone. This is enough to outweigh additional costs of 2960 €/a for heat pump operation and 750 €/a due to the increased conversion losses related to battery operation, and resulted in a total plus of 2130 €/a for the aggregation of the large scale heat pump and 25 EVs.**

***Index Terms*—Ancillary Services, large-scale heat pump, Electric Vehicles, Frequency Control, Vehicle-to-Grid**

I. Introduction

The future energy system will have to accommodate a higher share of distributed energy resources (DER) than today. At the same time, synergies can be found among the different sectors to secure the integration of DER and achieve a coordinated operation. An integrated energy system consisting of electricity, heat and transportation is increasingly recognised as the research paradigm to address these challenges [1][2]. It involves increasing interactions across energy infrastructures and optimising this integration to provide services at supply and demand level. Due to the increased share of transient DER that need to be accommodated in the energy system, and the replacement of conventional thermal power plants, ancillary services have to be delivered by new actors in the system. One option is to use demand side management to supply frequency containment reserve to the grid. Demand side units often provide a link to a neighbouring energy sector with certain requirements and constraints. This requires a well coordinated operation of these demand side units in order to be able to supply both the ancillary service and the primary service of the unit. In order to characterise the capability of different systems to provide operational flexibility, the following parameters can be used, as proposed by Makarov et al. [3] and modified by Ulbig & Andersson [4]:

- The power provision capacity, i.e. the load by which the current power uptake or supply of the unit may be decreased or increased
- The power ramp rate, which defines how fast a unit is able to change the power uptake or supply
- The energy provision capacity, which defines for how long the change in power uptake or supply can be maintained and thereby is a measure of the storage capacity of the system.

They show that combining different types of units results in combination of the strengths of the individual units. In the current study, it is proposed to deliver primary frequency regulation from a combination of different demand side units. This approach is demonstrated for a combination of electric vehicles (EVs), which are able to regulate within seconds and in both directions, with large-scale heat pumps, which can access a large storage capacity. It is expected that in this way it may be possible to create a combined system, which can regulate fast and has a large storage capacity.

The transportation sector accounts for 25 % of the global energy-related CO_2 emissions of which light-weight passenger vehicles account for over half [5]. Electrifying the private transportation sector allows to use renewable electricity as fuel and thereby it is expected to considerably reduce the transport related CO_2 emissions. Vehicle-to-Grid (V2G) research may serve to limit the self-induced adverse effects of EVs in terms of additional grid loading, but also to make the EV an active asset in supporting a stable, economic power system based on renewable energy. By controlling the charging power, it is possible to minimise the energy costs through adaptive or predictive charging [6]. The use of EVs for providing ancillary services to the power system can be an additional revenue for EV owners and can assist the integration of larger amounts of renewable sources [7, 8]. A high speed response of distributed battery-based energy resources can cover the regulation requirements of significantly larger thermal power plants with slower ramp rates, which are decreasing in numbers, as the generation is transitioning towards renewable

production [9]. EVs that charge using power electronics can regulate their power uptake quickly during the grid connected hours. However, an EV battery has a limited energy provision capacity and thus availability for frequency regulation delivery. Thingvad et al. [10] showed that it is necessary to reserve part of the maximum charging power capacity to be able to re-balance the state of charge (SOC) of the battery when delivering frequency regulation. This is necessary, as the grid frequency is often too high or too low during consecutive hours, leading to continuous charging or discharging of the battery as response to the frequency deviation. This may be avoided by bidding only a part of the capacity for frequency regulation and using the remainder for maintaining the SOC within a bounded range This would however result in a reduction of the possible revenues from capacity payments.

The heating and cooling sector is responsible for ca. 50 % of the final energy consumption in Europe, of which the largest share is still supplied by fossil fuels [11]. Different strategies have been proposed on how the European target of 80 % reduction in annual greenhouse gas emissions in 2050 compared to 1990 levels can be reached [12][13]. According to these, large-scale and domestic heat pumps are expected to play a key role in the future heat supply, as they enable the exploitation of low-temperature ambient or excess heat sources and provide a link to the electricity sector. Thereby, they unlock the thermal storage potential for providing flexibility, e.g. as ancillary services to the power sector. Large-scale heat pumps can access a large thermal storage potential that can be found in district heating networks [14], thermal storage and the buildings' thermal mass [15]. This may be used to provide flexibility to the electricity sector [16] by shifting the time of operation of the heat pump or by adapting the heat pump load. However, large-scale heat pumps are typically optimised to reach maximum energy efficiency and operate continuously in base-load, not to be able to change their load quickly. In order to secure safe operation, most large-scale heat pumps will take minutes to start up or change load. In Denmark, large-scale heat pumps typically use ammonia as refrigerant [17], as it provides a relatively high coefficient of performance (COP) while having no ozone depletion potential and no global warming potential [18]. In order to deliver district heating at forward temperatures of 60 °C to 90 °C, ammonia heat pumps are typically built as two-stage heat pumps with flooded evaporators. A previous study showed that the achievable ramping rates in this kind of system is limited by waiting times of the compressors which ensure a stable operation of the heat pump, and by the risk of condensation in the suction line during ramp-down [19]. Without further adaption of the system design and the control strategy, this kind of heat pump is expected to regulate too slowly to provide primary frequency regulation directly, i.e. the regulation time is larger than 150 seconds. However, as they are coupled to a large storage capacity on the thermal side they may still have a large potential to provide energy flexibility.

Scope of this study

The aim of this study was to assess the feasibility of combined supply of primary frequency regulation using two different technologies, each with their individual characteristics with respect to the system demand. This approach was applied to a specific case of a fast reacting pool of EVs with low energy capacity, and a slower large-scale heat pump integrated with the district heating network and a thermal storage tank, which provides a large storage capacity. The service supplied by the combined system was the Danish frequency containment reserve –normal operation (FCR-N), which is a frequency controlled service that requires ramping times below 150 seconds and is described in more detail in section II. The EV pool consist of 25 vehicles that are charged in an orchestrated way to allow for FCR-N delivery. The batteries of the V2G EVs should react quickly to changes in the grid frequency, while the heat pump should outbalance the energy bias of the frequency deviations, e_n^{bias}, to avoid that the EVs become fully charged or depleted. Thereby, the combination with the large-scale heat pump is expected to allow to bid the full EV power capacity for FCR-N, despite the heat pump not being fast enough to deliver FCR-N by itself. The aim was to identify whether a combined operation of these units may lead to increased provision of FCR-N, what constrains the combined operation, and whether a combined operation is economically feasible. In order to answer these questions, a model of the charging of 25 EVs and a model of a large-scale heat pump system were used to assess the feasibility of providing a combined service for one year of operation using 2018 data. The work was conducted in five steps:

- Analysis of the consumption of a district heating (DH) network in Copenhagen to calculate the number of hours that the heat pump is available to deliver offset electricity to the EV batteries, i.e. to balance out the energy bias of the frequency deviation .
- One year of grid frequency measurements and a stochastic driving consumption was used to calculate the SOC of 25 EVs. A SOC control strategy was implemented to change the base line power on an hourly basis according to SOC constraints. The control strategy was used to generate the offset schedule for the heat pump.
- The yearly heat pump operating cost was calculated using a thermodynamic system model and electricity spot market prices. It was compared to the cost of operating the heat pump according to the optimal schedule used by the operators.
- The income from supplying FCR-N service was calculated for delivering FCR-N from the EVs alone and combined with the heat pump. Additional operation cost and battery degradation were considered.
- The control method for maintaining the SOC was experimentally validated by delivering FCR-N with a single EV during 15 hours.

A description of the market framework for FCR-N, an overview of the different models used and the simulation approach is given in section II, together with a description of the assessed EV and heat pump system, model descriptions and experimental set-up. The results for the available offset power from the heat pump, the experimental test of following

a given frequency pattern with an EV, and the economic analysis for the combined delivery of FCR-N are presented in section III, the discussion may be found in section IV and the conclusion in section V.

II. Methods

A. Market framework for Frequency Containment Reserve Normal Operation

One of the most critical ancillary services for the stability of the power system is the frequency containment reserve, which maintains the system frequency close to the nominal value by balancing the production with the consumption on the second time scale. Frequency Containment Reserve-Normal operation (FCR-N) is a primary frequency regulation reserve in Eastern Denmark. It has to be delivered within 150 s, and the minimum bid size is 0.3 MW, which can be delivered by both consumption and production units [20]. Because of the minimum bid size, the power of each EV has to be pooled to a combined delivery, by an actor called the *aggregator*.

FCR-N is a symmetrical service, which requires the provider to offer the same power capacity for upwards and downwards regulation. Frequency reserves must be provided linearly, with full activation for deviations of $\pm$ 100 mHz, without a deadband. For a frequency value f_t in the range 49.9 Hz to 50.1 Hz at time t, the normalised response y_t is calculated as $y_t = (f_t - 50\text{ Hz})/0.1\text{ Hz}$.

The power required by the service provider at time t is calculated as $P_t = P_h^{\text{cap}} \cdot y_t + P_h^{\text{base}}$.

The value P_h^{base} is the scheduled power consumption or production, based on the traded energy in MWh/h at the day ahead spot market or alternatively at the intra-day market. P_h^{cap} is the power capacity contracted for FCR-N, and is constant over the hour, h.

Despite FCR-N being a power service, it involves an electric energy uptake or delivery by the service providing unit, as the frequency can be too high or too low for continuous hours, representing a higher or lower electricity production compared to the consumption, respectively. This energy content or energy bias of the frequency is calculated by the TSO by integrating the frequency deviations for each hour. The energy bias of hour n, e_n^{bias}, is calculated with Eq. 1, with a sample rate of $t_s = 1$ s and the number of samples per hour $N = 3600$ [21].

$$e_n^{\text{bias}} = \frac{1}{N} \sum_{t=N\cdot(n-1)+1}^{n\cdot N} y_t \cdot t_s \tag{1}$$

Considering demand side service providers, a negative energy content means that the service provider has been a net energy provider to the power system and is compensated with the price of the upwards regulation power price [€/MWh][20], which is equal or higher than the spot price. A positive energy content means that the service provider will have consumed more energy than scheduled, and has to pay the price for downwards regulation power [€/MWh] for the imbalance to the transmission system operator (TSO). This is equal or lower than the spot price. Since the frequency deviations in the long term should be equal to zero and the energy bias equals out, the use of upwards and downwards regulation power prices reduces the cost of delivering the service, but the actual revenue for service providers comes from the capacity payment.

B. Case description

1) EV case description: For the following analysis it was assumed that the local utility company, which owns and operates a large-scale heat pump for district heating supply, also owns a fleet of 25 EVs. It was assumed that the EVs are grid-connected between outside normal working hours (16:00-07:00) with a bidirectional V2G charger that can charge up to 10 kW from the grid or discharge up to 9 kW to the grid [22]. During this period they are available for delivering FCR-N. A similar case was demonstrated in the municipality of Bornholm [23] and by the utility company Frederiksberg Forsyning, Denmark [24].

The EVs were assumed to all have a battery capacity of 40 kWh. The daily electricity consumption for driving daily was assumed to be distributed according to a Gaussian distribution. The mean value was chosen equal to the average consumption of privately owned vehicles in Denmark, as corresponding data for the utility owned cars was missing, i.e. 9 kWh corresponding to 45 km per day [25] with a standard deviation of 1 kWh. Every EV should therefore have a high enough SOC at the end of the grid-connected period to ensure enough capacity for a higher driving consumption.

2) Heat pump system description: The heat pump system comprised the heat pump itself, a hot water storage tank with a storage volume of 100 m^3 and two electric boilers downstream of the storage with a capacity of 100 kW each. Figure 1 shows a sketch of the system. The system supplies heat to a small scale DH network with heat for space heating and domestic hot water. The heat pump assessed in the current study was a two-stage ammonia heat pump, with a heating capacity of 800 kW, corresponding to a rated power of 250 kW. The heat pump used groundwater at 10.5 °C as a heat source. The heat pump could supply forward temperatures of 60 °C to 84 °C. The load could be varied between 100 % and 40 % of full load, i.e. a power uptake of 250 kW down to 100 kW.

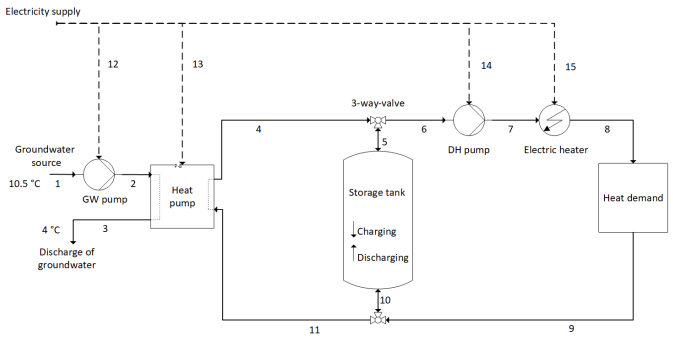

Fig. 1. Sketch of the heat pump system including heat pump, storage tank, electric boiler, groundwater pump, district heating pump and district heating network (heat demand)

C. Modelling of EVs and heat pump

Fig. 2 gives an overview of the different models and calculation steps conducted in this study and how information is interchanged between these.

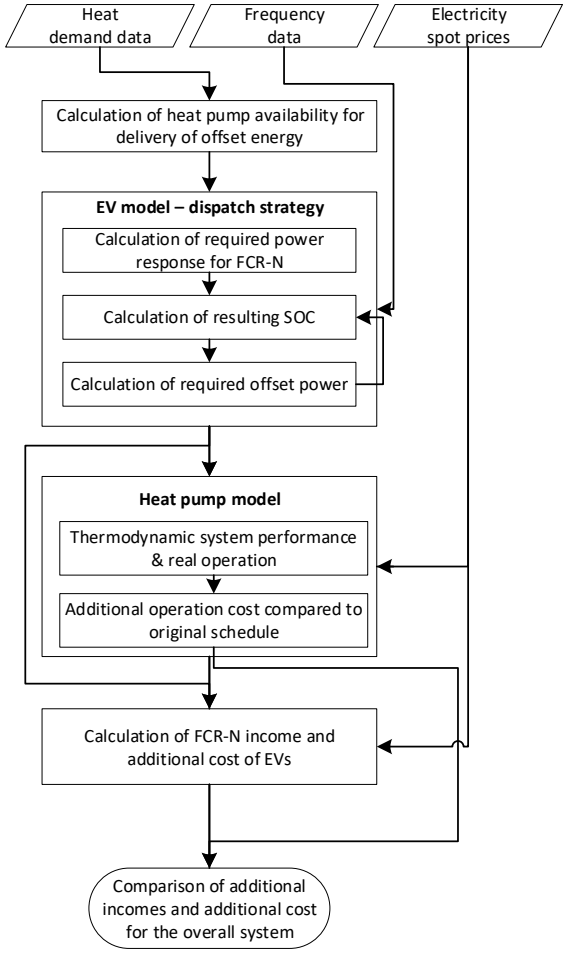

Fig. 2. Overview of the the workflow, including inputs, models and interaction between these

1) EV model: Dispatching Strategy: The following SOC-simulation is intended to calculate the SOC of each EV during the entire year of operation to verify that the bidding/dispatching strategy does not result in violation of the energy constraints. The future frequency deviations cannot be predicted and thereby the future energy bias is not known. Therefore, the aggregator can only react to the current SOC.

Initially the baseline power, P_{base}, is set equal to zero. The proposed dispatching strategy is to change P_{base} to a negative or positive value when the SOC reaches an upper or lower threshold. This means that the EV is delivering or receiving energy to or from the grid over time, and accordingly the SOC decreases or increases. The sum of P_{base} and the bid power capacity P_{cap} can however not be higher than the power capacity of the charger. Since the used V2G charger can only discharge with 9 kW, $P_{\text{base}} + P_{\text{cap}} \leq 9$ kW.

An FCR-N capacity of $P_{\text{cap}} = 6$ kW is bid for each EV, such that it can maintain the SOC using the remaining ± 3 kW or less. In a previous study, it was shown that this offset is enough to cancel out the energy content for $P_{\text{cap}} = 6$ kW and battery capacity of 40 kWh [10]. The present manuscript uses a data set of frequency measurements of 2018.

For each EV, the SOC of the battery is simulated in a continuous simulation for one year, Eq. 2. The SOC is calculated with a time resolution Δt of one hour like the spot and the FCR-N markets. The initial SOC of the first day was set to $\text{SOC}_1 = 0.5$. P_{base} is split up in a vector for charging, P_h^{c}, and a vector for discharging, P_h^{d}, for each hour, h.

The average charging and discharging efficiencies, $\eta_{\text{c}} = \eta_{\text{d}}$, were assumed to be 90 %, which results in an average energy loss of 0.26 kWh for each hour of service provision [21].

To capture the negative influence of conversion losses on the energy bias, the energy content was calculated from the battery perspective (e_n^{bat}), instead of the grid. e_n^{bat} is calculated with Eq. 3 and 4, where the nonlinear effect of the efficiency is added and integrated to an hourly energy content.

The daily energy for driving, E_h^{drive}, is consumed at the time when the work day starts and the EV is out of the aggregator's control, as shown in Eq. 5.

$$\text{SOC}_h = \text{SOC}_{h-1} + (P_h^{\text{c}}\eta_{\text{c}} + e_h^{\text{bat}} P_h^{\text{cap}} - P_h^{\text{d}} \frac{1}{\eta_{\text{d}}} - E_h^{\text{drive}}) \frac{\Delta t}{P^{\text{cap}}}. \tag{2}$$

$$\hat{y}_t = \begin{cases} y_t \eta_{\text{c}}, & \text{if } y_t \geq 0 \\ y_t \frac{1}{\eta_{\text{d}}}, & \text{if } y_t < 0 \end{cases} \tag{3}$$

$$e_n^{\text{bat}} = \frac{1}{N} \sum_{t=N\cdot(n-1)+1}^{n\cdot N} \hat{y}_t \cdot t_{\text{s}} \tag{4}$$

$$E_h^{\text{drive}} = \begin{cases} \sim \mathcal{N}(\mu,\, \sigma^2)\,, & \text{if } h = 7 + (\text{day} \cdot 24) \\ 0, & \text{else} \end{cases} \tag{5}$$

The baseline power was allocated according to the control strategy shown in Eq. 6. If the SOC was higher than the upper limit, ul, P^{base} was set to 3 kW of discharging. If the SOC was lower than the lower limit, ll, P^{base} was set to 4 kW of charging. This asymmetry was cause by the charger that can charge with 10 kW but only discharge with 9 kW. So, when 6 kW is contracted for FCR-N, there is 4 kW left for charging and 3 for discharging.

$$P_n^{\text{base}} = \begin{cases} 4 \text{ kW} & \text{if} \quad \text{SOC}_h < \text{ll} \\ -3 \text{ kW} & \text{if} \quad \text{SOC}_h > \text{ul} \end{cases} \tag{6}$$

Since the energy content can be up to 6 kWh during one hour but the balancing power can only shift up to 3 kWh during one hour, it can take several hours before the SOC starts moving in the wanted direction. It is therefore necessary to change the baseline before SOC reaches the actual limits. The limits which were found by simulating the SOC for one year and choosing the ones that maximise the allowable range, while always maintaining the SOC in an acceptable region, are presented in the results section.

The combined delivery involves that the heat pump can cancel out the 3 kW baseline change by increasing its consumption when the EV needs to reduce its consumption. This makes it possible to bid $P^{\text{cap}} = 9$ kW and still be able to maintain the SOC. The number of hours that the heat pump can consume power during each night depends on the heat consumption of the area, i.e. it varies over the year. The FCR-N capacity is therefore $P_h^{\text{cap}} = 6 \text{ kW} + P_h^{\text{hp}}$, where P_n^{hp} is either 0 kW or 3 kW per vehicle.

2) Modelling of heat pump system: In order to assess the availability for offset power delivered from the heat pump and to assess the economic feasibility of supplying combined frequency regulation, a thermodynamic model of the heat pump system was used. This model was used to simulate the operation and the corresponding total heat production cost of one year. The system model was built using the object-oriented programming language Modelica. It is described in detail in a previous publication by Meesenburg et al. [26]. The model comprised submodels of the heat pump, the storage tank, the electric boiler and the heat demand. All models were based on dynamic energy balance equations and steady-state mass and impulse balance equations. Only the storage tank model also comprised dynamic mass balance equations. Further, the model included cost balances for all components, which can be used to calculate the total production cost, including investment cost, capital cost, operation and maintenance cost and electricity cost.

Heat pump model and electric boiler model

The heat pump model was a grey box model, based on a COP that is given as a function of the load and the sink- and source temperatures. In this specific case the source temperature is directly correlated with the heat pump load, due to the control strategy in place and that the district heating return temperature was assumed to be constant. Thus, the COP function could be simplified to only be dependent on the load and the district heating forward temperature.The coefficient of performance (COP) of the heat pump was defined as

$$\text{COP} = \dot{Q}_{\text{tot}} / \dot{W}_{\text{tot}} \tag{7}$$

where $\dot{Q}_{\text{tot}}$ denoted the heat flow rate supplied by the heat pump and $\dot{W}_{\text{tot}}$ denoted the sum of the power uptake of both compressors in the heat pump. This function was obtained from a detailed dynamic model of the heat pump, described in [19] and validated against measured COP data, as presented in Fig. 3. The dynamic response of the heat pump to load changes was approximated as a first order behaviour, where the time constants were fitted to suit the experimental data of the heat pump. The electric boiler is represented as a simple control volume, with a power to heat conversion efficiency of 1.

Storage tank model

The heat storage tank model was discretised into 100 layers from top to bottom, to represent the thermal stratification in the tank. Heat transfer between layers was included. Mixing between layers and heat loss to the environment was considered as described in [26].

District heating network

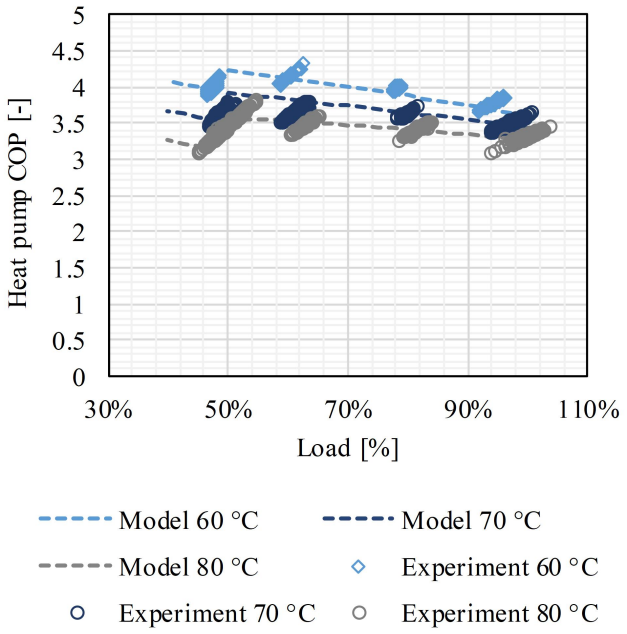

Fig. 3. COP curves for 60 °C, 70 °C and 80 °C from the function used in the model compared to experimental data, the step in the model function occurs assuming that half of the compressor cylinders are decoupled at 50 % load

The DH network supplied by the heat pump system was not modelled in detail. It was represented as a heat demand, including heat losses from the system. The pressure drop was calculated from the known pipe geometries in the network. It was assumed that the substations were controlled to always deliver a return temperature of 34 °C. This denotes a simplification, as in practice this value would vary according to heat demand and supply temperatures.

Control of the system

The control of the components of the system was coordinated using a central controller model. This was used to control the power uptake of the heat pumps and the electric boiler, the water mass flow through the heat pump and the charging/discharging of the storage tank. It was assumed that the power uptake of the heat pump can be controlled directly. The charging and discharging of the tank was controlled via the three-way-valve at the top of the tank.

Heat demand data

The heat demand data for the entire network including heat losses was obtained from measurements of the real system taken for the year 2018. The necessary supply temperatures were determined from the outdoor temperature for the Nordhavn area in Copenhagen [27], assuming that weather compensation of the supply temperature is needed below 14 °C. Both, the required supply temperature at the last customer and the temperature supplied by the heat pump system as a function of the outdoor temperature are depicted in Figure 4.

Determination of available heat pump offset operation

The available time per day t_{offset}, where the heat pump can be available to offset the EV electricity consumption is limited by the heat demand, the heat storage capacity and the

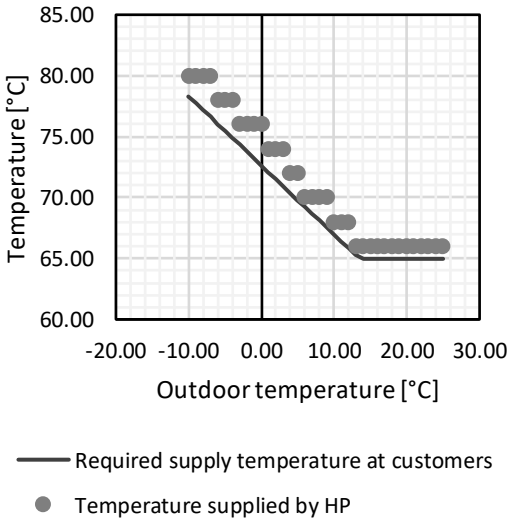

Fig. 4. Required supply temperature at the last customer and corresponding temperature supplied by the heat pump system dependent on the outdoor temperature

minimum and maximum power uptake, which depend on the heat pump COP. The minimum and maximum power uptake was calculated from the given heat demand using equation 7, taking into account that the COP varies with necessary DH forward temperature. It was assumed that the minimum load is fixed to 40 % of full load for all forward temperatures. It was assumed that the heat pump should be available for offsetting the EV operation every night. Accordingly, the maximum heat produced during offset operation needs to be less than or equal to the heat demand of the respective day, as a higher heat production would reduce the available offset operation time of the following day. Further, the heat produced during the offset operation cannot be higher than the sum of the demand during these hours and the available storage capacity. The corresponding minimum number of offset hours was rounded downwards to full hours.

$$t_{\text{offset}} \leq \min\left(\frac{Q_{\text{demand,day}}}{\dot{Q}_{\text{fullload}}}, \frac{(Q_{\text{cap,storage}} - \sum_i^t Q_{\text{demand,i}})}{\dot{Q}_{\text{fullload}}}\right) \quad (8)$$

Due to the limitations of the storage capacity within the district heating system and to avoid using the back-up electricity boiler, the heat pump was set to operate at the intermediate load between minimum part load and full load, that is:

$$\dot{W}_{\text{set,nom}} = (\dot{W}_{\text{min}} + \dot{W}_{\text{fullload}})/2 = 175\ kW \quad (9)$$

The load is changed upwards or downwards when a load shift is required by the SOC of the vehicle batteries. This results in a maximum absolute load shift of 75 kW, which is equivalent to a correction power of 3 kW, up or down, for 25 vehicles.

D. Economic evaluation of the system

1) Calculation of heat production cost: The combined provision of frequency regulation can only be feasible if the additional cost of both the HP system and the EVs can be covered. The additional income would reduce the heat generation cost. Therefore the heat cost was chosen as decisive parameter. The economic performance of the HP was evaluated using three different measures. The first one was the fuel cost of the system, i.e. the weighted average electricity price over the simulated one year period. It was calculated as the overall electricity cost divided by the overall electricity consumption in the same period.

$$\bar{c}_{\text{el}} = C_{\text{el,tot}}/W_{\text{tot}} \quad (10)$$

The second one is the operational specific heat cost, which was calculated as the total electricity cost for one year divided by the total amount of heat delivered to the district heating customers.

$$\bar{c}_{\text{heat,el}} = C_{\text{el,tot}}/Q_{\text{tot}} \quad (11)$$

The third measure is the total specific heat cost. This includes fuel cost, investment cost, capital cost and operation and maintenance cost of the components in the system. It is calculated using the model, as described in detail in [26]. The assumed values are summarized in Table I.

To calculate the total specific heat cost, the obtained total yearly cost was divided by the overall amount of heat delivered per year to the customers.

$$\bar{c}_{\text{heat,tot}} = C_{\text{heat,tot}}/Q_{\text{tot}} \quad (12)$$

The electricity price used was the historic electricity spot market prices for Eastern Denmark for the year 2018 [32], including taxes and tariffs, as summarised in table II. The expected values for 2022 are given, too, as the public service obligation (PSO) fee is being phased out before 2022 and the energy tax on electricity is reduced, according to a political agreement.

2) Calculation of V2G operation cost: V2G chargers contain more power electronics than unidirectional DC chargers and are therefore expected to be more expensive. The additional cost was neglected since expected price and lifetime for mass produced components was unknown.

The most dominant cost regarding the service provision is the conversion loss during continuous charging and discharging. The overall electricity consumption is calculated by integrating the frequency bias including conversion losses seen from the battery, scaled with the regulation capacity in the respective hour, Eq. 13.

$$E_{\text{loss}} = \sum_{h=1}^{24\cdot 365} e_h^{\text{bat}} \cdot P_h^{\text{cap}} \Delta t \quad (13)$$

The effect on the battery degradation was assuming a constant degradation per cycle equal to the value found in ref. [33], i.e. an average capacity loss of 0.0022 % cycle.

The capacity loss is proportional to the cost of using the battery. The Lithium Nickel-Manganese-Cobalt Oxides (NMC) battery which is used by most EV manufactures

TABLE I
ECONOMIC HEAT PUMP DATA USED FOR THE ANALYSIS

Unit	Total capital investment [€]	Economic lifetime [a]	Assumed average operation hours [h/a]	Fixed O&M cost [€/a]	Source
Heat pump	75300	25	6917	403	[28]
Electric heater	20200	20	3000	30	[28]
DH pump	4030	10	8760	59	[29]
GW pump	5380	10	6917	59	[30]
Storage tank	4190	40	8760	94	[28]
GW drilling	121000	40	6917	2420	[31]

TABLE II
TAXES AND TARIFFS ON ELECTRICITY FOR HEAT PRODUCTION IN DENMARK FOR 2018 AND 2022

Type	Unit	2018	2022
PSO-tariff	€/MWh	13.58	0.00
TSO-tariff	€/MWh	5.11	5.11
System tariff	€/MWh	5.65	5.65
Reduced energy tax	€/MWh	34.54	20.83
Balance tariff	€/MWh	0.13	0.13
Distribution price (2018 average values)	€/MWh	15.73	15.73

including Nissan, has a battery pack cost around 180 EUR/kWh [34]. Assuming the use in a second life application as a stationary storage, a minimum acceptable capacity, or end-of-life (EOL) of 50% of the original value was assumed.

The price of the battery degradation, c_{deg}, was therefore

$$c_{\text{deg}} = \frac{P_{\text{lost}}^{\text{cap}}}{\text{EOL}} \cdot c_{\text{pack}} \tag{14}$$

3) Calculation of income from FCR-N provision: To calculate the income from capacity payments, historic FCR-N capacity payment prices for 2018 were used [20]. The yearly performance of the heat pump system according to the schedule derived from the EV model was compared to an optimized schedule without regulation power services from 2018. This schedule was provided by the utility company owning the heat pump [35]. The difference in specific heat cost plus the additional cost of battery degradation was used to define the minimum capacity price that the system can bid into the FCR-N market. To calculate the income from capacity payments, a simple bidding strategy was applied. It was based on the assumption that the expected price in one specific hour is similar to the price in the same hour of the day before. It was assumed that in all hours, where the service could be provided the historic average value could be gained. This was a conservative assumption, as it might be possible to bid higher than average prices in the market. The same bidding strategy was assumed for combined operation and service provision of the electric vehicles alone.

E. Experimental demonstration of operation mode

It has previously been shown that the heat pump can ramp from low to high load within three to five minutes, and it can ramp downwards in four to seven minutes [36], if the power uptake is controlled directly.

The dispatching strategy to maintain the SOC was validated as part of this study. The experiment was conducted for a winter day, where the heat pump was assumed to be available for the complete regulation period, i.e. the EV could deliver FCR-N with the full capacity of 9 kW.

The experiment was conducted on a single 40 kWh Nissan EV using the described V2G charger. The frequency meter was located ca. 30 km from the installation, such that the inherent communication delay of the internet communication were captured. The frequency was measured and uploaded to a MQTT (Message Queuing Telemetry Transport) broker every 0.5 second. The controller was reacting to the measurement and calculated a setpoint for the charger. The SOC of the EV was read from the charger with the same interval. The active power was measured on the grid side and the timestamp of the local device was used for benchmarking the reaction time.

III. RESULTS

A. Offset power from heat pump

When available for supporting the EVs, the heat pump would run at 175 kW power uptake as a default if no offset power is required. The heat pump supported 25 EVs with 3 kW each and thus consumed 175 ± 75 kW. All EVs experience the same grid frequency. So their SOC moved in the same direction, but it was generally not the same as they all received a unique driving consumption. Therefore, the offset power could be less than 75 kW, as not all EVs needed support at the same time. The resulting power uptake of the heat pump is presented in Fig. 5. In the hours shown as the black area, no supporting power could be guaranteed from the heat pump. The heat pump was always supporting the EVs during the last part of the 15 hour period and was at least available for one hour between 06:00 and 07:00. In the first three hours of the regulation period the heat pump mostly ran at 175 kW, meaning no offset was required. A positive offset of 75 kW occurred most often between 23:00 and 01:00. While around 03:00 in the morning the heat pump operated most often at 100 kW power uptake, i.e. negative offset of 75 kW for the EVs. This can be explained by the shift in upper and lower SOC limit at this time that can be observed in Figure 6. This shift as introduced to ensure, that the SOC was high enough at the end of the charging period.

The simulation of the heat pump system showed that the system was available for offset power delivery in 2696 hours in the case of 2018, compared to 5475 h of availability of the EVs, i.e. the heat pump was available in 49 % of the hours, where FCR-N provision was scheduled for the EVs.

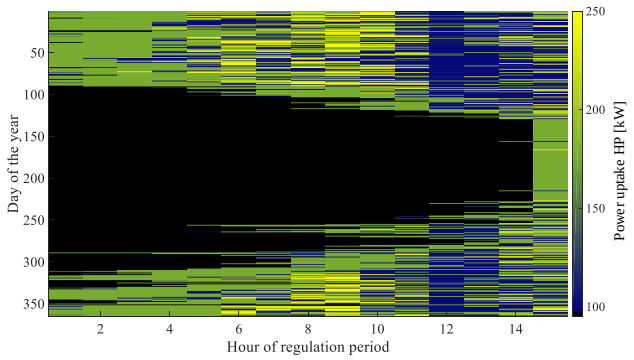

Fig. 5. Power uptake of the heat pump during the 15-hour regulation period

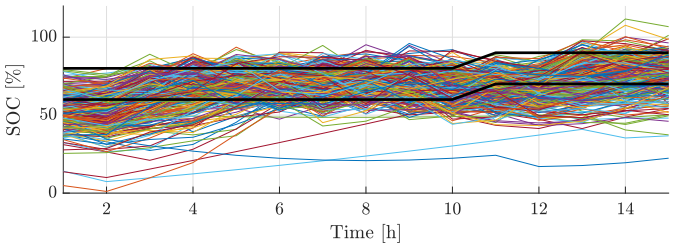

Fig. 6. SOC of 1 EV during every 15-period (16:00-07:00) for 1 year.

B. EV dispatching strategy

In Fig. 6 the SOC of one EV during every 15-period (06:00-07:00) for 1 year is shown. After each plug-in period an energy consumption around 9 kWh is subtracted for driving before the following 15 hour plug-in period begins. The initial SOC is therefore on average 22.5 % lower than the final.

The upper and lower SOC threshold, ul and ll, are shown as the thick lines in Fig. 6. The limits found, were a lower limit of 60 % for the first eleven hours and 70 % for the last four hours of the scheduled regulation period to ensure that the cars were sufficiently charged in the morning. The upper limit followed the same pattern and increases from 80 % to 90 % in the last four hours.

C. Experimental demonstration of operation mode

The ideal power response – calculated based on the frequency measurements – is seen together with the measured P_t and the calculated P_h^{base} in the top plot of Fig. 7, while the bottom plot shows the SOC of the EV. The experiment was run for a 15-hour period from 16:00 to 07:00, and shows how a single EV is reacting to the frequency measurements and the SOC.

There was only 2 s delay between a frequency change and measurement of the power response on the grid side of the charger. The response speed had a large effect on the linearity of the droop curve, where the active power is plotted against the grid frequency at the same time. The top plot in Fig. 8 shows the standalone measured power of the EV vs. the frequency. The response is linear but two additional lines occur, where the frequency power response was shifted up or down. The bottom plot shows the response when the heat

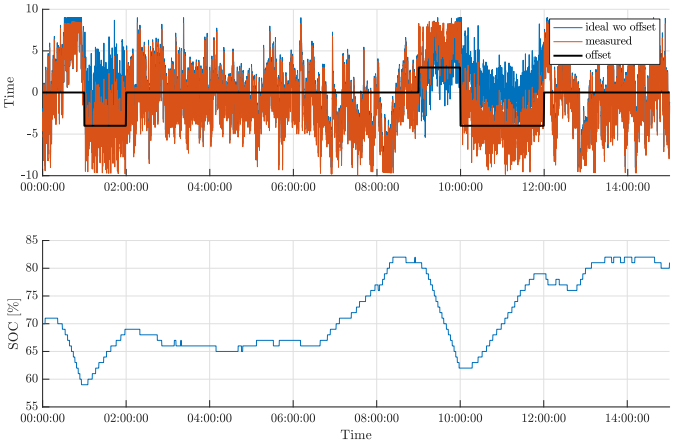

Fig. 7. Measurement of power, soc and offset for one EV during 15 hours.

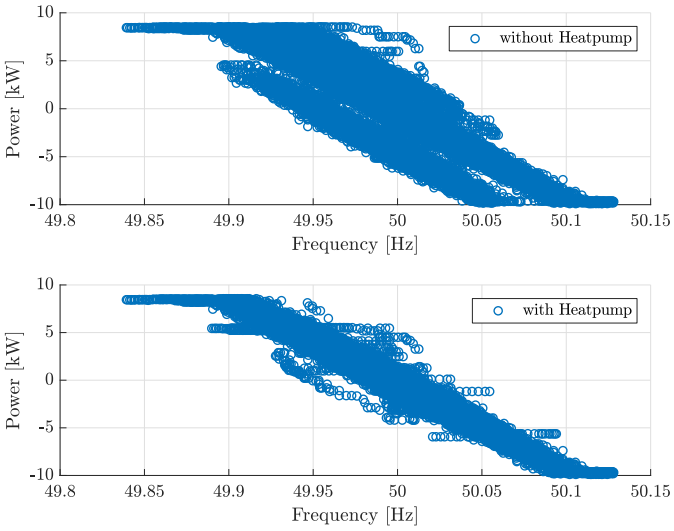

Fig. 8. Power vs. Frequency with and without the Heatpump.

pump cancelled out the EVs baseline change by making the opposite change.

D. Economic analysis of proposed operation mode

To evaluate the economic feasibility of the proposed operation strategy, the operation was simulated for the year 2018 and compared to the results of the optimally scheduled heat pump operation and FCR-N delivery from the EVs alone. The combined operation of heat pump and EVs would only be feasible if the total heat price could be reduced compared to the optimal operation schedule, and the additional cost due to increased throughput of the battery can be covered. Table III compares the overall heat, electricity uptake and the total yearly cost for the proposed provision of offset power with the optimally scheduled HP. The total fuel cost and total cost are lowest for the optimal operation schedule, as expected. However, the income from frequency regulation was high enough to outweigh the additional cost and resulted in a reduced overall cost when these revenues were taken into account. With the assumed bidding strategy, 2129 €/a could be saved, considering the data from 2018. This value results

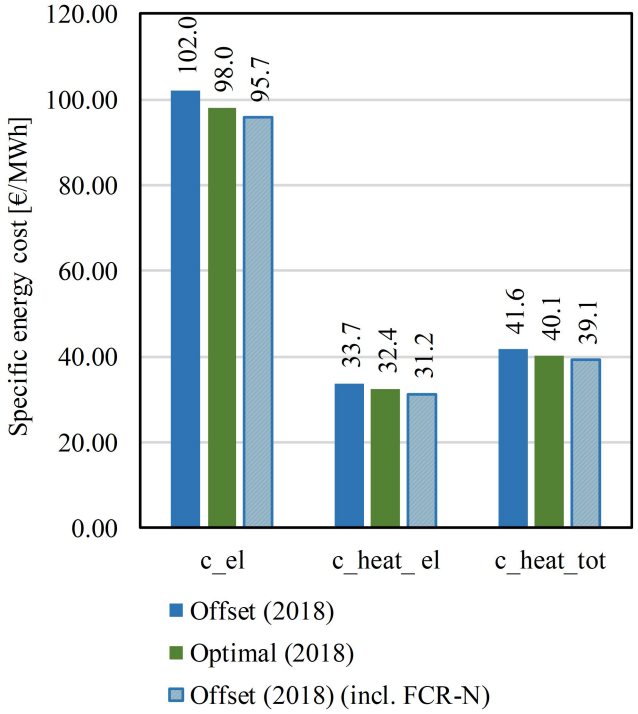

Fig. 9. Average specific electricity price, average specific operational heat cost, average specific total heat cost, excl. and incl. income from FCR-N delivery

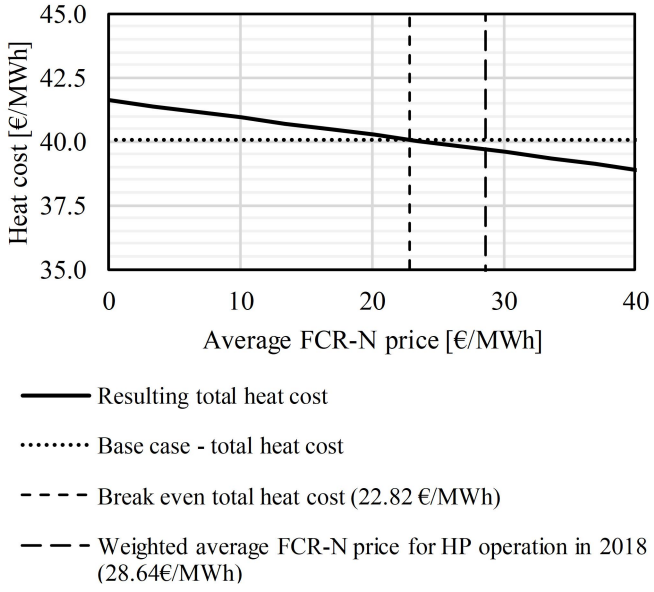

Fig. 10. Total and operational heat production cost including income from FCR-N for varying average FCR-N prices

from an additional income from capacity payments of 4435 €/a, from 305 €/a balance power price saving and additional cost of 750 €/a for additional battery operation cost and 2961 €/a total additional HP cost. These were caused by an increased heat loss in the system, as the heat production was not optimized with regard to the heat demand. Further, the operation of the heat pump was not optimized with regard to COP, as the heat pump reacted to the requirements of the grid.

Figure 9 compares the resulting average specific electricity price, operational specific heat cost and total specific heat cost for the offset operation and the optimal operation, both excluding and including the income from frequency regulation service provision and coverage of additional EV cost. Table IV shows additional losses in the battery and the corresponding cost for the combined operation compared to provision of frequency regulation from the batteries alone. As the capacity payments varied strongly over the last couple of years, a sensitivity analysis was conducted. This was done by assuming the same average FCR-N capacity price for all operation hours and varying this FCR-N capacity price. The available hours for offset power were kept constant, and it was assumed that the operation schedules for EVs and HP were kept the same. The results are presented in Figure 10 together with the break even between the offset and optimal operation, and the weighted average FCR-N capacity price for the calculated offset strategy in 2018. The average FCR-N capacity price in 2018 was 43.25 €/MW/h. The obtained weighted average price was considerably lower, as the highest prices may be obtained during summer, where the HP is seldomly available for offset power delivery.

IV. Discussion

The current study aimed at identifying the potential of combined provision of primary frequency regulation from electric vehicles and a large-scale heat pump. The study was conducted for a Danish case using data from 2018. The required regulation time for the FCR-N frequency regulation service in Eastern Denmark is 150 s, which is high compared to other primary frequency regulation services. Based on the demonstrated fast regulation times of the EVs, it is expected that the proposed operation strategy would also be valid for other primary frequency regulation services, that require faster ramping.

The year 2018 was a hot and dry summer, and it had the highest average FCR-N prices of the last years [27][32]. It may thus be expected that in colder years, the heat pump is available for offset operation for more hours, especially in early and late summer compared to the results for 2018. This would result in larger amounts of capacity payments and thus an increased income. Further, the available offset time was calculated from the maximum power uptake, i.e. full load conditions to avoid overcharging the heat storage tank. The resulting number of hours was a conservative estimate for winter days, where the heat pump is available many consecutive hours, as it is unlikely that the heat pump would be required to run at full load for the whole period. For future practical implementation this scheduling approach may be improved using statistical methods or machine learning. The need for offset power further depends on the requirement of charging the EV batteries. However, the daily driving consumption was estimated to be the same for all days of the year and the additional energy content of the batteries that might need to be offset by the HP due to missing driving consumption was disregarded. Accordingly, the heat pump offset operation might be further optimised by taking

TABLE III
RESULTS FOR HEAT PUMP SYSTEM

			Offset	Optimal
Energy related figures	Total heat delivered	MWh	1925	1925
	- Total heat delivered by HP	MWh	1916	1918
	Total electricity uptake	MWh	637	637
	- Total electricity uptake HP	MWh	540	543
	- Total electricity uptake EB	MWh	12	10
	COP HP	-	3.55	3.54
	COP system	-	3.02	3.02
Economic figures	Total yearly electricity cost	€	64893	62406
	Total yearly cost	€	80090	77128
	HP revenues from FCR-N	€	4435 + 305	0
	FCR-N operation hours HP	h	1858	0
	Weighted average FCR-N capacity price	€/MWh	35.8	0
	Total cost incl. FCR-N revenue and payments to EVs	€	74999	77128

TABLE IV
RESULTS FOR FCR-N OPERATION OF ELECTRIC VEHICLES

		Only EVs	Combined
Conversion losses	MWh	1.35	1.59
Energy Throughput	MWh	7.67	8.92
Battery capacity loss	%	0.21	0.24
Cost of electricity	€	138.00	163.00
Cost of battery degradation	€	30.24	35.20
Capacity Payment	€	1420.00	1420.00
Regulation Power prices	€	24.16	24.16
Profit	€	1277.00	1246.00

weekends and holidays into account for the EV modelling. Further, the assumed standard deviation might be too low for other EV pools. This needs to be evaluated when applying the proposed strategy to other cases. To test the influence of the average FCR-N price on the feasibility of combined FCR-N provision a simple sensitivity study was conducted. This showed, that the average FCR-N price could be reduced by 26 % before the combined provision of frequency regulation results in a negative business case. Considering that the average capacity prices in the three preceding years were 63 %, 32 % and 37 % lower respectively, this buffer cannot be considered sufficient. This means that future applications of the proposed operation strategies, should be able to switch back to the normal spot market optimal operation strategy, when the FCR-N capacity payments are too low. It also means that this operation strategy is best suited for heat pumps that are already equipped with the necessary communication interface for frequency regulation services. This would help to minimise the additional investment cost. The offset operation of the heat pump resulted in additional cost due to higher average electricity prices and due to an increased electricity consumption. This additional cost would however be reduced in future due to the expected decrease in PSO tariff and electricity tax, and thereby it would benefit the feasibility of combined FCR-N provision from EVs and large-scale HP.

In the current study, it was assumed that the electric vehicles were owned by the same company as the heat pump and thus it was not further analysed, how the income from combined operation should be divided between the EV owners, HP owner and aggregator. This is however expected to be a relevant question that has to be answered for future implementations. Different division strategies are possible, e.g. proportional to additional operation cost, a division based on factors for the different flexibility parameters, or simpler approaches. The assessment of these different strategies was beyond the scope of the current study and should be assessed in future work.

V. CONCLUSION

The current study proposed a combined delivery of primary frequency regulation (FCR-N in RG-N) using EVs and a large-scale heat pump to exploit synergies between the ability of fast regulation of batteries and the large storage capacity of thermal system. The feasibility was assessed using a model of the SOC of the EV batteries based on the frequency energy content model and a dynamic model of the heat pump system, which was previously validated against experimental data. The proposed operation of EVs was experimentally validated as part of this study. The results for the case of 2018 showed that the EVs can bid a higher capacity on the FCR-N market when the heat pump is available for offsetting the energy content of the frequency deviation. This is necessary as the allowable range of SOC of the batteries is constrained, and it has to be ensured that the EVs are fully charged in the mornings. The combined operation provided an additional income from capacity payments, which could not be generated by the EVs or the heat pump alone. This additional income was 4740 €/a. This was enough to outweigh additional operation cost of 2961 €/a for the heat pump operation and 750 €/a for the increased battery losses and resulted in a net surplus of 2129 €/a from the additional service.

VI. ACKNOWLEDGMENTS

We thank Tore Friis Gad Kjeld from HOFOR A/S for providing the optimized operation schedule for the heat pump.

This research project was financially funded by EUDP (Energy Technology Development and Demonstration) under the projects "EnergyLab Nordhavn - New Urban Energy Infrastructures" (project number: 64014-0555) and ACES (EUDPgrantnr:EUDP17-I-12499).

REFERENCES

[1] H. Lund, P. A. Østergaard, D. Connolly, B. V. Mathiesen, Smart energy and smart energy systems, Energy 137 (2017) 556–565. doi:10.1016/j.energy.2017.05.123.

[2] P. Mancarella, MES (multi-energy systems): An overview of concepts and evaluation models, Energy 65 (2014) 1–17. doi:10.1016/j.energy.2013.10.041.

[3] Y. V. Makarov, C. Loutan, J. Ma, P. de Mello, Operational impacts of wind generation on California power systems, IEEE TRANSACTIONS ON POWER SYSTEMS 24, No. 2 (2009) 1039–1050. doi:10.1109/NOMS.2002.1015622.

[4] A. Ulbig, G. Andersson, Analyzing operational flexibility of electric power systems, International Journal of Electrical Power & Energy Systems 72 (2015) 155–164. doi:10.1016/j.ijepes.2015.02.028.

[5] International Energy Agency, Global EV Outlook - Two million and counting (2017). doi:10.1787/9789264278882-en.

[6] A. González-Garrido, A. Thingvad, H. Gaztañaga, M. Marinelli, Full-scale electric vehicles penetration in the danish island of bornholm—optimal scheduling and battery degradation under driving constraints, Journal of Energy Storage 23 (2019) 381 – 391. doi:https://doi.org/10.1016/j.est.2019.03.025.

[7] A. Schuller, C. M. Flath, S. Gottwalt, Quantifying load flexibility of electric vehicles for renewable energy integration, Applied Energy 151 (2015) 335 – 344. doi:10.1016/j.apenergy.2015.04.004.

[8] M. Marinelli, S. Martinenas, K. Knezović, P. Andersen, Validating a centralized approach to primary frequency control with series-produced electric vehicles, Journal of Energy Storage 7 (2016) 63 – 73. doi:10.1016/j.est.2016.05.008.

[9] Y. V. Makarov, S. Lu, J. Ma, T. B. Nguyen, Assessing the value of regulation resources based on their time response characteristics, United States doi:10.2172/946001.

[10] A. Thingvad, C. Ziras, M. Marinelli, Economic value of electric vehicle reserve provision in the Nordic countries under driving requirements and charger losses, Journal of Energy Storage 21 (2019) 826–834. doi:10.1016/j.est.2018.12.018.

[11] European Comission, Comission staff working document - Review of available information - Accompanying the document Communication from the Commission to the European Parliament, the Council, the European Economic and Social Committee and the Committee of the Regions on an EU COM(2016) (2016) 1–99. arXiv:arXiv:1011.1669v3, doi:10.1017/CBO9781107415324.004.

[12] European Comission, Energy roadmap 2050 (COM(2011) 885 final (2012) 1–9arXiv:ISBN978-92-79-21798-2, doi:10.2833/10759.
URL http://www.roadmap2050.eu/

[13] D. Connolly, H. Lund, B. Mathiesen, S. Werner, B. Möller, U. Persson, T. Boermans, D. Trier, P. Østergaard, S. Nielsen, Heat Roadmap Europe: Combining district heating with heat savings to decarbonise the EU energy system, Energy Policy 65 (2014) 475–489. doi:10.1016/j.enpol.2013.10.035.

[14] K. M. Luc, EnergyLab Nordhavn Delivery no. 5.2b: Analysis of the potential for storing heat in district heating pipelines, Tech. rep., Technical University of Denmark (2018).

[15] K. Foteinaki, R. Li, A. Heller, C. Rode, Heating system energy flexibility of low-energy residential buildings, Energy and Buildings 180 (2018) 95–108. doi:10.1016/j.enbuild.2018.09.030.

[16] P. A. Østergaard, H. Lund, B. V. Mathiesen, Smart energy systems and 4th generation district heating, International Journal of Sustainable Energy Planning and Management 10 (2016) 1–2. doi:10.5278/ijsepm.2016.10.1.

[17] H. K. Støchkel, B. L. Paaske, K. S. Clausen, Drejebog til store varmepumpeprojekter i fjernvarmesystemet, Tech. Rep. December, Energistyrelsen & Grøn Energi (2017).

[18] ASHRAE, Ammonia as a Refrigerant, Tech. rep., Atlanta. doi:10.1016/s0140-6736(02)89201-7.

[19] W. Meesenburg, Design considerations for dynamically operated large-scale ammonia heat pumps, Proceedings of the 25th IIr International Congress of Refrigeration, Montreal (2019)doi:10.18462/iir.icr.2019.1203.

[20] Energinet.dk, Ancillary services to be delivered in denmark - tender conditions., http://energinet.dk/EN/El/Systemydelser-for-el/Sider/Systemydelserforel.aspx (2012).

[21] A. Thingvad, C. Ziras, J. Hu, M. Marinelli, Assessing the energy content of system frequency and electric vehicle charging efficiency for ancillary service provision, Proceedings of the 51st International Universities Power Engineering Conference (2017)doi:10.1109/UPEC.2017.8231947.

[22] A. Zecchino, A. Thingvad, P. B. Andersen, M. Marinelli, Test and modelling of commercial v2g chademo chargers to assess the suitability for grid services, World Electric Vehicle Journal 10(2). doi:10.3390/wevj10020021.

[23] M. Trahand, Nuvve v2g & deployments, presented at the 2nd vehicle 2 grid conference, electric vehicles for the renewable city, amsterdam university of applied sciences (2017).

[24] ACES, Project website, www.aces-bornholm.eu (2016).

[25] H. Christiansen, Dtu transport - the data and model centre, the danish national travel survey, http://www.modelcenter.transport.dtu.dk/english/TU (2017).

[26] W. Meesenburg, T. Ommen, B. Elmegaard, Dynamic exergoeconomic analysis of a heat pump system used for ancillary services in an integrated energy system, Energy 152 (2018) 154 – 165. doi:https://doi.org/10.1016/j.energy.2018.03.093.

[27] Meteoblue, Wheather data for Nordhavn 2018 (accessed via energydata.dk 11-04-2019).
URL www.meteoblue.com

[28] Energinet.dk, Technology Data for Energy Plants (2016).
URL www.ens.dk

[29] Grundfos, Product data NB 32 - 200/206 (2017).
URL https://product-selection.grundfos.com/product-detail.catalogue.productfamilies.html?from_suid=151022250390601434492979880763 7&pumpsystemid=290981485&qcid=293056119

[30] Grundfos, Product data SP 46-4 (2017).
URL https://product-selection.grundfos.com/product-detail.catalogue.productfamilies.html?from_suid=151022228811006388052718785822&pumpsystemid=280760607&qcid=271031787

[31] Energinet.dk, Technology Data for Energy Plants (2012).
URL https://ens.dk/sites/ens.dk/files/Analyser/technologydata_for_energy_plants_-_may_2012._updated_2015.pdf

[32] Energinet.dk, Energinet.dk - Markedsdata (2018).
URL http://www.energinet.dk

[33] A. Thingvad, M. Marinelli, Influence of v2g frequency services and driving on electric vehicles battery degradation in the nordic countries, in: EVS31, 2018.

[34] M. Wentker, M. Greenwood, J. Leker, A bottom-up approach to lithium-ion battery cost modeling with a focus on cathode active materials, Energies 12 (3). doi:10.3390/en12030504.

[35] Hofor A/S, Personal communication with Tore Tore Friis Gad Kjeld (2019).

[36] T. F. G. Kjeld, EnergyLab Nordhavn Delivery no.: D5.5a - Optimum supply of an island district heating grid by a local heat plant, Tech. rep. (2019).
URL http://www.energylabnordhavn.com/deliverables.html

Design considerations for dynamically operated large-scale ammonia heat pumps

Manuscript ID: 1203
DOI: 10.18462/iir.icr.2019.1203

Design considerations for dynamically operated large-scale ammonia heat pumps

Wiebke MEESENBURG[(a)], René KOFLER[(a)], Torben OMMEN[(a)], Wiebke Brix MARKUSSEN[(a)], Brian ELMEGAARD[(a)]

[(a)] Technical University of Denmark, Department of Mechanical Engineering
Kongens Lyngby, 2800, Denmark, wmeese@mek.dtu.dk

ABSTRACT

Large-scale heat pumps (HPs) are being implemented to provide heat for district heating (DH) systems from renewable heat sources. They are further expected to play a key role in integrated energy systems as flexible loads that can be used to balance the electricity grid. However, most large-scale HPs installed are designed for base load operation and are thus not optimized with regard to dynamic behaviour. Within this work, the dynamic behaviour of different HP configurations was assessed with regard to performance during load change. For this purpose, a two-stage and a one-stage ammonia HP were modelled using Modelica. Further, different adaptions of the two-stage HP to avoid condensation in the suction line were assessed. Fast ramping resulted in oscillation of the liquid level in the receivers. It would thus be necessary to design receivers carefully and include suction traps to avoid entrainment of droplets into the suction lines. The results indicated that condensation in the low-pressure suction line was a limiting factor for how fast the HPs may ramp down. This could be avoided by preheating of the suction line. In that case, the HPs under assessment were able to regulate between 100 % and 40 % load in less than five minutes, and they would thus be capable of providing secondary regulation power.

Keywords: Large-scale heat pump, dynamic operation, dynamic model, ammonia, regulation power

1. INTRODUCTION

Denmark has decided to reduce CO2 emissions drastically in order to comply with international climate change mitigation targets and national energy targets. The target is to supply all heating and electricity from renewable energy sources in 2035 (The Danish government - Energi-Forsynings- og Klimaministeriet, 2013).Renewable energy sources such as wind or solar power are fluctuating and difficult to predict. In order to secure grid stability even with high shares of fluctuating power production, flexible units on the production and demand side can be used to balance out the frequency in the grid.

Heat pumps (HPs) enable the use of ambient or low-grade heat sources for heating purposes by lifting the temperature from the source temperature to values high enough to supply the required heating service. The fuel for the cycle is most cases electricity. Thus, HPs provide a link between the electricity and the heating sector, and thereby they may act as flexible loads while supplying renewables-based heat. The flexibility is provided by the possibility to store heat in storages, the buildings or in the district heating (DH) grid.

Flexible operation of heat pumps may results in additional losses on the heating side (Meesenburg et al., 2018). However, the flexibility to adapt the electric capacity of HPs can be used to provide frequency regulation and thus act on the reserve markets. This may offer additional income for plant operators. In order to do so the regulation rate needs to be fast enough in order to comply with the standards of the transmission system operator (TSO).

While small-scale HPs can switch on and off rather quickly, large-scale HPs for DH supply are usually designed for base load operation and thus, not optimized for fast regulation (David et al., 2017). Accordingly, ramping rates in many applications are limited (Averfalk et al., 2014). In order to improve the ability of large-scale HP systems to deliver regulation services, it has to be identified what causes the limitations with regard to ramping rates and thereby, how the HP design and control can be improved (Fischer and Madani, 2017).

Danish law forbids the use of HFC refrigerants in large-scale applications because of their high global warming potential (Miljøstyrelsen, 2016). Natural refrigerants such as ammonia are mostly used for large-scale applications in Denmark today and accordingly, we chose to focus on ammonia as a refrigerant for this study.
This study focused on the description of dynamic behaviour during load change of large-scale ammonia HPs in a one-stage and a two-stage configuration. The aim was to identify what limits fast ramping up and down of the HP. Liquid formation in the suction line during ramp-down has been identified as a limitation to fast ramping. Accordingly, different strategies to avoid this were assessed. The study was based on a dynamic simulation of the HP configurations, which is further described in section 2. The results are presented in section 3 and discussed in section 4, before conclusions are presented in section 5.

2. METHOD

2.1. Heat pump application case

The HPs simulated in this study were designed to fit a real HP application, supplying DH to a small grid in the development area of Nordhavn in Copenhagen, Denmark. The design heating capacity of the system was 800 kW. As heat source groundwater at 10.5 °C was used. It was cooled down in the evaporator and ejected into the sea. This was possible as the groundwater reservoir is infiltrated by seawater anyway. The HP was able to deliver forward temperatures of 65 °C to 84 °C. For this study, we assumed a forward temperature set point of 70 °C and a constant return temperature of 35 °C. The assessed system was a two-stage ammonia HP, which comprises a flooded evaporator, separator, low-stage compressor, open flash intercooler, high-stage compressor, desuperheater, condenser, subcooler and two expansion valves as main components. Pipe models were included for both suction lines of the compressors. For better understanding of the nature of limitations during ramping of the HP, the results for the two-stage HP were compared to a one-stage ammonia HP, supplying the same services. This was comprised of flooded evaporator, separator, compressor, desuperheater, condenser, subcooler and one expansion valve. A sketch of the two configurations is shown in Figure 1.

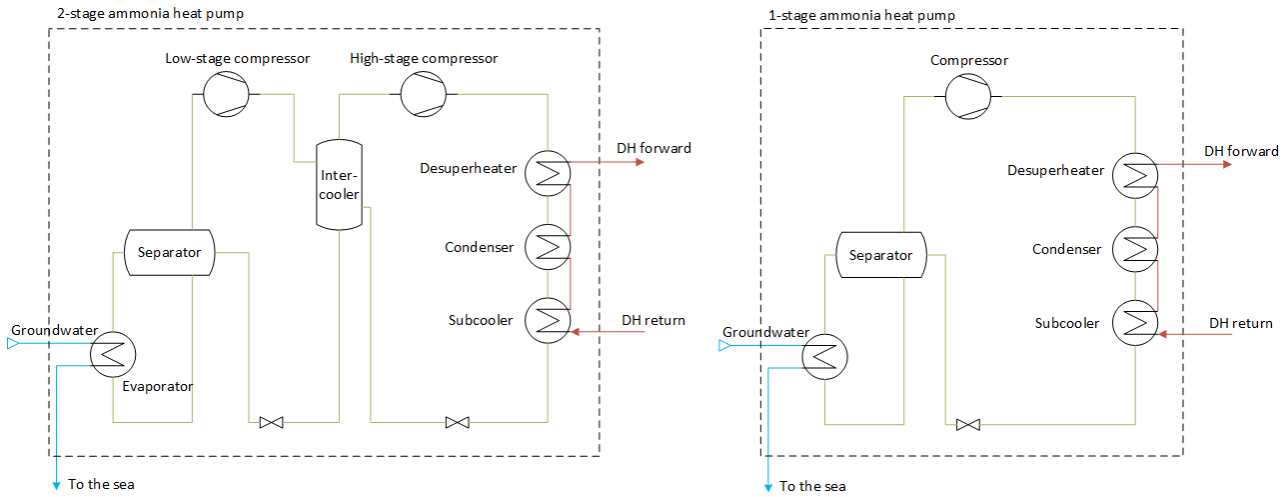

Figure 1 Sketch of 2-stage and 1-stage ammonia HP

2.2. Dynamic model

In order to simulate the behaviour of the system during up- and down ramping a dynamic model of the system was built in the object-oriented programming language Modelica (Modelica Association, 2017) using Dymola software (Dassault Systèmes, 2017) and the TIL library (TLK Thermo GmbH & IfT, 2017). The latter includes validated component models for the simulation of refrigeration systems. All components were modelled using dynamic energy and mass balances. Momentum balances were modelled using steady state equations, as the time constants for momentum balances are relative small compared to energy and mass balances.
The heat exchangers were modelled as corrugated plate heat exchangers using heat transfer correlations of Steiner (VDI, 2010) for evaporation, of Shah (VDI, 2010) for condensation and of

Gnielinski, Dittus & Boelter (Baehr and Stephan, 2011) for one-phase flow and a quadratic mass flow dependent pressure drop for ammonia. The pressure drop on the water side was neglected and the heat transfer coefficient was calculated according to (VDI, 2010). The pipe model included Dittus & Boelter heat transfer model and Konakov's pressure drop correlation for smooth pipes (VDI, 2010). Heat conduction from the ambient through steel pipe and insulation was considered.
The compressors were piston compressors equipped with variable speed drive for part-load operation. The oil-cooling was not modelled in detail, but was considered as a heat loss from the compressor. The compressor efficiencies were calculated from compressor polynomials, which were functions of condensation temperature, temperature lift, pressure ratio and compressor frequency. The displacement volumes were assumed to be 0.009425 m^3 and 0.0044 m^3 for the low-stage and high-stage compressor of the two-stage HP. The high-stage compressor polynomial was also used for the compressor in the one-stage HP, due to the high temperature tolerance (Johnson Controls, 2019). The displacement volume was 0.0088 m^3.
The separators and open-flash intercooler were modelled as ideal tanks, i.e. equilibrium between the gaseous phase and the liquid phase and uniform pressure and temperature in the tank were assumed. As the liquid levels were assumed to be low, the pressure difference between gas- and liquid outlet was neglected.

2.3. Control of the heat pumps

The aim of controlling the HPs was to ensure a certain DH forward temperature and heat output at high efficiency and safe operation of the HPs.
In the case of the two-stage HP there were 6 manipulating variables, namely the rotational speed of both compressors, the source water flow, the DH water flow and the cross sectional area of both expansion valves. The pairing of manipulating and controlled variables was deducted from a relative gain array (RGA) analysis for the two-stage and one-stage HP (Seborg et al., 2010). Resulting in the following control structures:

- *Two-stage HP*: The source water flow was fixed and the water temperature at the evaporator outlet was controlled with the low-stage compressor rotational speed. Thereby, the capacity of the HP was controlled indirectly. The rotational speed of the high-stage compressor controlled intermediate pressure level, ensuring similar pressure ratios for both compressors. The DH flow was altered to control the condensation temperature and thereby indirectly the DH forward temperature. The high-stage expansion valve controlled the fluid quality at the condenser outlet, and the low-stage expansion valve was used to control the liquid level in the separator.
- *One-stage HP*: the forward temperature was controlled by the DH water flow directly and the heat output was controlled by the compressor rotational speed. The separator level was not controlled, but the valve was used to control the condenser outlet quality of the fluid.

All controls were implemented as PI-controllers into the model. The parametrization was conducted according to the method described by Kuhn (1995).The integration time constants for the 1-stage system were reduced slightly to match those found for the two-stage cycle, in order to ensure that the results are comparable. This resulted in slightly faster regulation of the one-stage HP.

2.4. Operation strategy

In order to deliver frequency regulation, the HPs need to adapt their electricity consumption quickly. It was assumed that only upward regulation defined from an electricity supply perspective was provided. Accordingly, the HP can supply upward regulation by reducing electricity consumption. This could be achieved either by

- ramping down into part-load and ramping up again when the regulation period is over
- shutting down the HP completely and starting up again afterwards.

To avoid the necessary dead times before restart of the compressors and increased wear through recurrent starts and stops the first option was considered. Tests with the existing two-stage HP have shown that the HP can operate at part loads of down to 40 % of full load. We thus assumed that the HP capacity can be reduced by 60 % during regulation periods. The response time for frequency normal reserve (primary reserve), secondary reserve and tertiary reserve in Eastern Denmark is 150 s and 5 min and 15 min, respectively (Energinet.dk, 2017).. The frequency (normal) reserve market is the economically most attractive option and thus the aim of this study was to find out whether it could be possible to deliver the regulation power within 150 s. The electric capacity of the assessed HP is too low to bid into the markets. That means an exceptional allowance would be needed or the HP could be clustered with other flexible assets.

2.5. Evaluation criteria

The ramping time was defined as the time during which the set point of the heat load was changed, thus forcing the system to a slower or faster change of load. This value was varied to be 150 s, 100 s, 50 s and 10 s. The time between start of the ramping and reaching steady state (ss) was defined as the response time Δt_{r}

$$\Delta t_{\mathrm{r}} = t_{\mathrm{start}} - t_{\mathrm{ss}} \qquad \text{Eq. (1)}$$

Steady-state was assumed to be reached when the heat output was within a tolerance of 0.1 % of the overall heat output. This corresponded to a tolerance of < 0.2 % of the steady-state value for the power uptake.

The steady-state COP was defined as the ratio of the steady state heat output $\dot{Q}_{\mathrm{ss}}$and power consumption $\dot{W}_{\mathrm{ss}}$.

$$\mathrm{COP}_{\mathrm{ss}} = \dot{Q}_{\mathrm{ss}} \Big/ \dot{W}_{\mathrm{ss}} \qquad \text{Eq. (3)}$$

2.6. Strategies to avoid condensation in the suction line

The observed condensation in the suction line was a limiting factor to how fast the HP may be ramped down. There are a couple of possible technical solutions that may avoid condensation in the suction line during fast ramp-downs. These could help to allow a faster ramping of the HP. Here, we assessed four different strategies for the two-stage HP:

- Controlling the source outlet temperature from the evaporator to a constant temperature

The idea is to reduce the increase of evaporation pressure during fast ramp down by keeping the mean source temperature constant. This may be obtained by controlling the source outlet temperature by changing the source mass flow through the evaporator.

- Replacement of the flooded evaporator with a direct expansion evaporator (DEX)

In this case, the superheat after the evaporator could be controlled, to a value high enough to avoid liquid entering the compressor during ramp-down. The heat exchanger size of the evaporator was increased for this simulation by a factor 2, which was large enough to ensure superheating at the outlet, but it was not optimized. The superheat was controlled by the low-stage expansion valve.

- Implementation of an internal heat exchanger (IHX) to superheat the fluid in the suction line

This design would keep the flooded evaporator by installing an IHX to preheat the suction line using the liquid exiting the open-flash intercooler as heat source. The IHX was designed using manufacturer software to provide a superheating of 5 K. No further control was considered.

- Implementation of an electric preheating (el. PH) of the suction line

Ensuring superheated gas in the suction line by external electric heating is a flexible option, which may easily be added to existing systems and may allow adapting the superheating to the requirements of different operation modes. Due to simplicity for this study, we assumed a constant heating power of 2 kW throughout the simulation time.

3. RESULT

This section presents the simulation results regulation of the two-stage HP and compares them to the one-stage HP. Different possibilities of avoiding condensation in the suction line are compared.

3.1. Two-stage heat pump

The dynamic behaviour of the two-stage HP was simulated for four different ramping times. The power uptake and heat output for an exemplary case is depicted in Figure 2 and the steady state COPs were calculated as 3.45 during full-load and 3.43 at 40 % part-load. The response times of the system until steady-state are listed in Table 1.

It can be seen that the given system was not able to reach steady state in less than 150 s, which corresponds to the necessary reaction time for primary reserve in Denmark. The full regulation capacity might be delivered within 182 s to 306 s. That means that under the implemented control strategy, the system reacted too slowly to provide primary reserve, but it might be possible to provide secondary regulation power. The integration time constants of the controllers had a large influence on the system response time, i.e. optimizing the controller would allow faster ramping.

Table 1 Response time for different ramping times (change of set value) for the two- and one-stage ammonia HP cycle

Ramping time [s]	Two-stage HP		One-stage HP	
	Δt_r ramp-down [s]	Δt_r ramp up [s]	Δt_r ramp-down [s]	Δt_r ramp up [s]
150	278	306	285	303
100	238	270	240	265
50	205	221	203	232
10	182	190	179	209

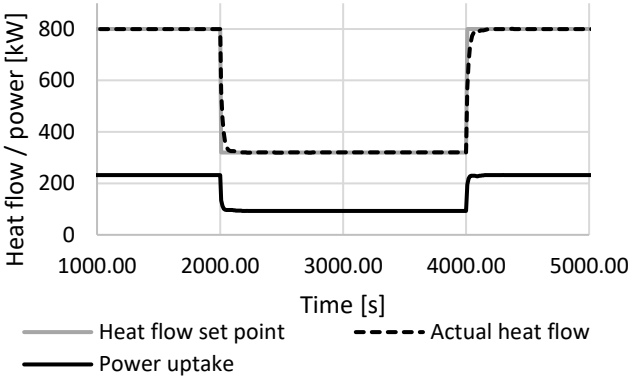

Figure 2 Operation scheme for the provision of regulation power. Depicted is the set value for the heat flow, the actual heat flow and the power uptake

The limiting factor was found to be a thermodynamic effect. As can be seen in Figure 4 the fast ramp-down from full-load into part-load led to formation of liquid in the suction line. The effect was stronger the faster the HP ramped down. This was due to a sudden increase in pressure on the low-pressure side, which caused the saturation temperature of the fluid to increase. The walls of the suction line warm up more slowly than the fluid due to the thermal inertia of the piping material. Accordingly, the wall temperature was below the saturation temperature of the fluid, which would lead to condensation along the pipe walls. The suction line in the model is only discretized in one dimension, i.e. the quality values given here are averaged over the control volumes and it is uncertain how much fluid would actually condense on the cold surface. Potentially, any droplet may however harm the reciprocating compressor and condensation in the suction line should be avoided. This limited how fast the HP capacity can be ramped down. Thus, an ammonia HP that should adapt its load quickly needs to be designed in a way that condensation in the suction line is avoided. During ramp-up, the suction line is warmer than the saturation temperature and thus there is no problem with regard to condensation.

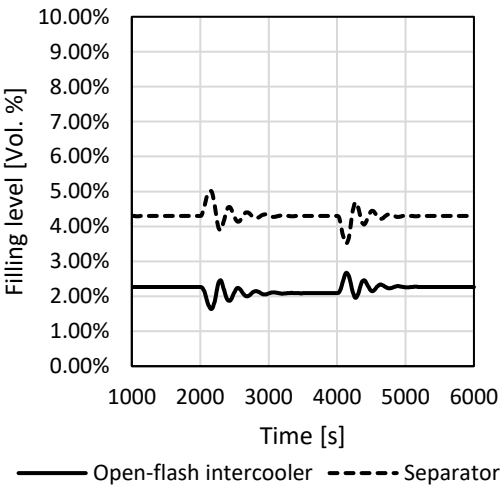

Figure 3 Filling level of intercooler and separator. Ramp-down start at 2000 s. Ramp-up starts at 4000 s.

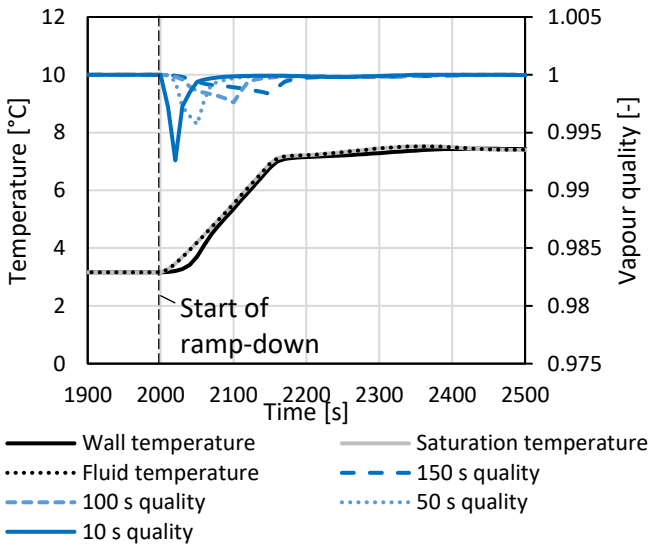

Figure 4 Fluid temperature, wall temperature, saturation temperature of the fluid and vapour quality at the end of the low-pressure suction line in a two-stage ammonia heat pump. Ramp-down into part load starts at 2000 s. Ramp-up to full load starts at 4000 s.

Figure 3 shows the liquid level of the open-flash intercooler and the separator. The fast load change induced large peaks in the filling level compared to steady-state level. This was especially critical for relatively high filling levels in steady-state, as the absolute peaks in filling level were high, too. This means that under the assumed control strategy the fast ramp down led to large agitation, which could influence the separation of liquid and vapour in the vessel negatively, and

which also influences the low and high stage pressure level - and thus the operation conditions of the heat pump. The dynamic response of the filling level depended mainly on the controller parameters chosen for the low-pressure expansion valve controller. This indicated that the applied controller design method was not sufficient for this control pair and that a more elaborate controller design is necessary.

3.2. One-stage heat pump

In order to assess whether the more simple cycle design of a one-stage HP can lead to faster response time of the HP system during ramping, a one-stage cycle with the same nominal heating capacity as the two-stage cycle was simulated.
The response time for different ramping times of the one-stage HP are presented in Table 1. The response times obtained did not differ significantly from the response times of the two-stage system. This was due to the similar time constants of the controllers.
The filling level in the separator was not controlled in the one-stage cycle. Nonetheless, the induced oscillations were as low as 3 % of the steady state filling level in full load and thus significantly lower than for the two-stage cycle. Even though no advantage in terms of response time was observed, the system reaction was more robust and fewer oscillations were induced. Thus, a more simple cycle might be well suited for flexibly operated heat pumps. However, the forward temperatures that may be delivered with a one-stage ammonia HP are limited.
As with the two-stage HP the fluid state in the suction line was in the two-phase region under fast ramp-down of the HP capacity, i.e. condensation might occur. The effect was stronger for faster ramping times.

Table 2 Results for different cycle adaptions to avoid condensation in the suction line

Design	Risk of fluid in suction line [yes/no]	Δt_r down [s]	Δt_r up [s]	COP_{ss} full-load [-]	COP_{ss} part-load [-]
Base case	yes	182	190	3.45	3.43
Source control	yes	176	159	3.41	3.24
DEX	no	205	182	3.42	3.31
IHX	no	193	206	3.40	3.39
El. PH	no	254	176	3.41	3.35

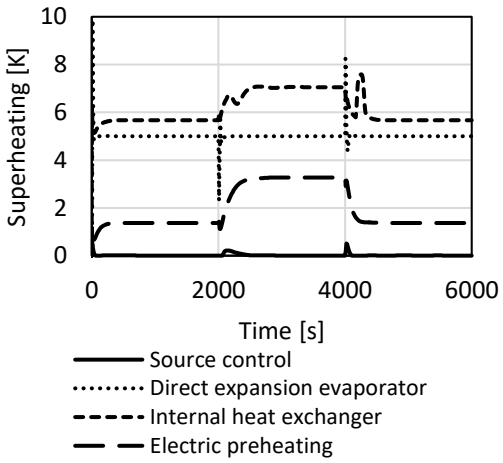

Figure 5 Superheating for four different strategies to avoid condensation in the suction line

3.3. Strategies to avoid condensation in the suction line

The results for these four adaptions to avoid condensation in the suction line are summarized in Table 2. The response times were in a similar range as for the two-stage cycle without adaption. The first option resulted in condensation in the suction line, too. Even though the increase in the evaporation pressure was less than with the original control strategy, it still increased and even peaked during ramp down. This meant that the same phenomenon as in the original cycle design occurred.
The COP in full load was highest for DEX and el. PH. In both configurations the part-load COP was comparably low. Further, Figure 5 shows that the superheating for DEX and el.PH decreased shortly during ramp-down, this means that it is crucial to design the control in a way that the superheating is large enough to accommodate this negative peak. The part-load COP of the el. PH configuration might be increased to the value of the two-stage HP base case by shutting the preheating off during part-load operation. The COP in part-load was highest for the internal heat exchanger configuration. This was advantageous in the case of the proposed operation strategy, as the heat pump would be operated in part-load during regulation periods. Thus, the loss due to

regulation would be smaller and the cost of regulation would be lower. The full-load COP in the IHX case was slightly lower than for the alternative adaptions. As shown in Figure 5, this was due to the larger superheating compared to the other technologies. The superheating increased in part load and did not show any downward peaks during ramp-down of the heat pump. It might be possible to reduce the IHX size, and thereby the set point for the superheating, and thus reduce the decrease in COP compared to the base case. In the IHX case, the reduction in COP due to superheating was partly outbalanced by the effect of additional subcooling of the liquid before entering the low-pressure expansion valve. This explains the better COP in part-load compared to the other cases.

4. DISCUSSION

The results indicated that the thermal inertia of the components as well as inertia of the system due to refrigerant migration actually had a minor impact on the system dynamics, as the system was not ramped down completely and started up again, but only the load was changed. It was observed that the dynamic behaviour is strongly influenced by the controller design. In the present study, only PI controllers were considered. It is expected that the controller design may be improved by advanced controller design methods, which may possibly reduce the reaction time of the two-stage system far enough to be able to provide frequency normal reserve (150 s response time). It should however be noted that the presented simulation results did not consider dead-times of actuators or waiting times during compressor ramping. The latter was especially relevant for the two-stage cycle, as the compressor load needs to be changed in an orchestrated way during ramping. This may possibly lead to longer actual regulation times for the two-stage HP. Further, the heat pump was controlled according to the desired heating capacity, as this is the main purpose of the heat pump. In future applications, it might be considered to control the heat pump according to the power uptake and thereby force the heat pump to follow the desired power consumption profile for frequency regulation.

The results for the one-stage cycle did not show faster regulation performance than the two-stage cycle model. However, during load change fewer oscillations occurred and the overall system performance seemed to be more robust. The one-stage ammonia cycle is usually not chosen for DH applications due to the limited supply temperatures. For 70 °C forward temperature the discharge temperature exiting the compressor in the one-stage case was calculated to be ca. 172 °C. This might still be allowable with regard to thermal stability of the lubrication oil (Ommen et al., 2015), but it is at the upper end of discharge temperatures tolerated in state-of-the-art compressor technology. However, it seems promising to investigate whether one-stage cycles with other working fluids may be more suitable for flexible operation.

Additionally, fast regulation led to sudden changes in the hold up of vessels in the system, such as receivers, open flash intercooler and separators. This can lead to increased agitation of the vapour and liquid flow, which may in extreme cases lead to two-phase flow in the lines towards compressor or valve. Both should be avoided. The effect may be decreased by improved control of the valves during the ramping routine. Further, the layout of vessels as suction traps (ASHRAE, 2006) can help to secure that no liquid enters the compressors during fast load changes.

The results showed that the crucial factor when ramping the HP down quickly was the danger of condensation in the suction line due to sudden increase of evaporation pressure. It should however be noted, that from this system level analysis it cannot be determined how much fluid actually condensates in a real system, as the flow characteristics and heat conductions along the pipe might have an influence, as well. Thus, the results only can give an indication on whether there is a risk of condensation or not. Different possible strategies to avoid this risk were compared in the results of this study. Among those, the implementation of an IHX and electric preheating of the suction line seemed most promising. The first is preferable, if the system is supposed to ramp up and down frequently, as condensation in the suction line can safely be avoided under all conditions. The part load COP is comparably high for this system. The benefit of el. PH is that the superheating control is very flexible and may be switched off during part-load or when the HP is not delivering regulation power. Further, el.PH can be added relatively easy to existing HP systems. The necessary heating power needs to be chosen carefully in order to deal with the downward peaks in superheating that were observed. Another option would be to combine the flexible approach and the IHX, by bypassing the IHX during part load operation or when no flexible operation is scheduled. This would need further implementation of three-way-valves and controllers. The influence of these on the system should be assessed further.

5. CONCLUSION

This paper assessed the dynamic behaviour of a two-stage ammonia heat pump during ramping from full-load into part-load and up to full-load again. The results were compared to a one-stage cycle. The response times for both systems was comparable, but the one-stage cycle showed less oscillation during fast ramping. By ramping the heat pump down quickly, large oscillations were observed in the filling levels of intercooler and separator in the two-stage cycle. This should be considered in controller design. Further, suction traps could avoid liquid entering the suction line.
Condensation in the low-pressure suction line was identified as a major limiting factor with regard to possible ramping times. Condensation was more likely to happen the faster the heat pump was ramped down. In order to avoid this, several possible adaptions were assessed. Out of these, an internal heat exchanger between the liquid outlet from the intercooler and the suction line and electric preheating seemed to be most feasible. If condensation could be avoided, the heat pump set up would be able to deliver secondary regulation power, i.e. response time below five minutes.

6. ACKNOWLEDGEMENT

This research project is financially supported by the Danish Energy Agency EUDP (Energy Technology Development and Demonstration Program) under the project ”EnergyLab Nordhavn - New Urban Energy Infrastructures” (project number: 64014-0555).

7. BIBLIOGRAPHY

Averfalk, H., Ingvarsson, P., Persson, U., Werner, S., Industry, D., 2014. On the use of surplus electricity in district heating systems 7–12.

Baehr, H.D., Stephan, K., 2011. Heat and mass transfer, 3rd Editio. ed, Heat and Mass Transfer. Springer- Verlag. https://doi.org/10.1007/978-981-10-1557-1

Dassault Systèmes, 2017. Dymola Systems Engineering [WWW Document]. URL https://www.3ds.com/products-services/catia/products/dymola/ (accessed 10.31.17).

David, A., Mathiesen, B.V., Averfalk, H., Werner, S., Lund, H., 2017. Heat Roadmap Europe: Large-Scale Electric Heat Pumps in District Heating Systems. Energies 10, 578. https://doi.org/10.3390/en10040578

Fischer, D., Madani, H., 2017. On heat pumps in smart grids: A review. REHVA J. https://doi.org/http://dx.doi.org/10.1016/j.rser.2016.11.182

Johnson Controls Denmark ApS, n.d. SABROE ® HPO / HPC / HPX high-pressure reciprocating compressor units [WWW Document]. URL www.sabroe.com (accessed 1.24.19).

Kuhn, U., 1995. Eine praxisnahe Einstellregel für PID-Regler: Die T-Summen-Regel (A practical parametrization rule for PID-conrollers: The T-sum-rule). Autom. Prax. 37, 10–16.

Meesenburg, W., Ommen, T., Elmegaard, B., 2018. Dynamic exergoeconomic analysis of a heat pump system used for ancillary services in an integrated energy system. Energy 152, 154–165. https://doi.org/10.1016/j.energy.2018.03.093

Miljøstyrelsen, 2016. Bekendtgørelse om regulering af visse industrielle drivhusgasser (BEK nr 1326 af 19/11/2018). Denmark.

Modelica Association, 2017. Modelica and the Modelica Standard Library [WWW Document]. URL http://www.modelica.org (accessed 10.31.17).

Ommen, T., Jensen, J.K., Markussen, W.B., Reinholdt, L., Elmegaard, B., 2015. Technical and economic working domains of industrial heat pumps: Part 1 - Single stage vapour compression heat pumps. Int. J. Refrig. 55, 168–182. https://doi.org/10.1016/j.ijrefrig.2015.02.012

Seborg, D.E., Edgar, T.F., Mellichamp, D.A., Doyle, F.J., 2010. Process dynamics and control. Wiley.

The Danish government - Energi- Forsynings- ogKlimaministeriet, 2013. The Danish Climate Policy Plan Towards a low carbon society

TLK Thermo GmbH & IfT, 2017. TIL 3.4 – Model library for thermal components and systems.

VDI - Gesellschaft Verfahrenstechnik und Chemieingenieurwesen (Ed.), 2010. VDI Heat Atlas, 2nd Editio. ed, VDI Heat Atlas. Springer-Verlag, Berlin Heidelberg. https://doi.org/DOI 10.1007/978-3-540-77877-6

Feasibility of heat pumps supplying district heating systems: case study for Austria and Denmark

FEASIBILITY OF HEAT PUMPS SUPPLYING DISTRICT HEATING SYSTEMS - CASE STUDY FOR AUSTRIA AND DENMARK

Wiebke Meesenburg[1], Roman Geyer[2], Olatz Terreros[2], Henrik Pieper[1], Torben Ommen[1], Brian Elmegaard[1]
[1] Technical University of Denmark, Department of Mechanical Engineering, Section of Thermal Energy
Nils Koppels Allé 403, 2800 Kongens Lyngby, E-mail: wmeese@mek.dtu.dk
[2] AIT Austrian Institute of Technology GmbH, Integrated Energy Systems Group, Giefinggasse 4, 1210 Wien,
E-Mail: Roman.Geyer@ait.ac.at

1 SUMMARY

The frame conditions for large-scale heat pumps (HPs) in district heating (DH) systems were studied for Denmark and Austria. While large-scale HPs are becoming more and more often implemented as DH supply units in Denmark, examples from Austria are rare. An economic analysis was conducted for both countries, comparing DH solutions based on either large-scale heat pumps or wood-fired heat only boilers to individual HPs. The results showed that large-scale HPs were beneficial compared to individual units down to linear heat demand densities of 0.85 MWh/m/a for Denmark and 0.97 MWh/m/a for Austria. The levelized cost of energy of central HPs could compete with wood-fired boilers especially for low DH temperatures (60 °C /30 °C). From a socioeconomic perspective HPs were beneficial compared to wood-fired boilers. In Austria the private economic feasibility of wood-fired boilers benefits from subsidies, which showed to decrease the competitiveness of large-scale HPs.

2 INTRODUCTION

Recently, DH has been in the focus of research as it is expected to play a key role in the transition to more energy-efficient and fossil fuel free energy supply systems [1]. DH enables exploitation of large-scale heat sources that cannot be exploited using individual units. Further, DH has also been identified as a key element in integrated energy systems [2]. This integration can be achieved using large-scale power-to-heat units, such as HPs which use electricity to supply heat and might also help to balance the power grid [3]. Large-scale HPs represent an efficient way of heat supply using electricity in combination with low temperature sources, such as groundwater, seawater or air. Centrally supplied systems are well suited for areas with high heat demand densities, i.e. densely built areas and houses with space heating (SH) and domestic hot water (DHW) demand. The feasibility of centrally supplied systems is less certain in new areas with low energy demand buildings as well as in less dense areas.

Austria and Denmark both have high shares of renewable power production [4]-[5] and the use of DH is well established in urban and rural areas [6]-[7]. However, the boundary conditions and the current policies in place are very different. Despite the fact that both countries have high shares of renewable power production, the generation mix of both power and heating are different, compare Figure 1.

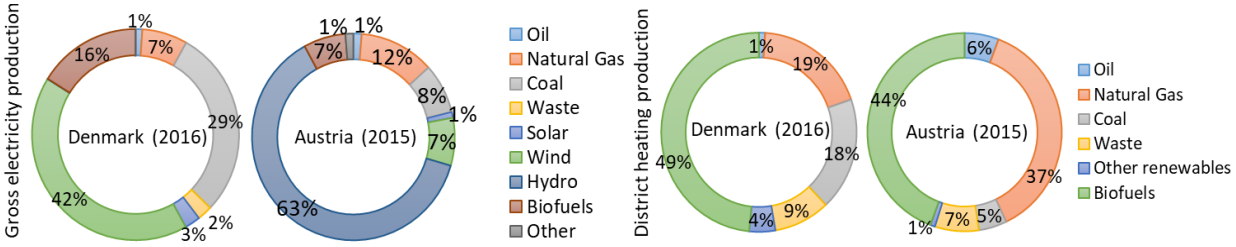

Figure 1 Composition of electricity generation and DH supply in Denmark and Austria [4], [5], [36]

This is mainly related to the geographical and meteorological conditions being different. The mountainous region in Austria provides favourable conditions for hydro power plants and just below half of the Austrian area is forestland, i.e. large resources of biomass are available. The Danish geography is especially suited for power generation from wind. The main source of biomass in Denmark is municipal waste, by-products from agricultural activities, like straw and manure, and wood-based biomass, of which ca. 50 % is imported [8]. An increase of biomass usage in Denmark would result in higher shares of imported biomass [9], which implies the risk of promoting non-sustainable land usage in other countries. As Denmark aims to achieve independency of fossil fuels, the available biomass resources might be needed in other sectors. Renewable electricity generation from non-biomass-based sources is thus expected to play a key role in the transition towards renewable supply of heat and electricity. To accommodate high shares of transient electricity generation in the energy system, the idea of an integrated energy system, utilizing synergies between different energy sectors is promoted in Denmark (e.g. [2]). This strategy has been widely acknowledged and current research and demonstration projects, and recent policy changes [10] undergird the vision of an integrated energy system. The integrated energy strategy for Austria is still in the green paper phase [11].

In both countries DH systems are common in cities and in rural areas. In Austria biomass-based DH systems are most common in rural areas. Biomass-based small-scale DH systems were supported as a subsidy for farmers, who often also own forestland in Austria, thereby exploiting synergies of sustainable forest management and creating an additional income to the farmers [12]. Nowadays, the funding has been harmonized and is available to communities and companies under the domestic environmental support scheme [13] and a quality management scheme is in place [14]. Financial support is available for heating networks and for industrial waste heat utilization for DH purposes, which can lead to indirect support of large-scale HPs. HP-specific subsidies are only available for self-supply and the use of biomass is still strongly promoted. A lack of information and dissemination has been identified as a further barrier for large-scale HPs for DH in Austria [15].

In Denmark, most rural DH networks were developed after the first oil crisis and were usually based on natural gas-fired units. DH companies in Denmark are mostly cooperatives or municipality-owned and so directly or indirectly owned by the customers [16]. They are obliged to work on a non-profit basis and a national benchmark system is in place, ensuring that the most cost-effective and environmental friendly solutions are promoted [17]. In combination with dedicated policy measures [17]-[18] this has led to high penetration of DH in Denmark (64 % in 2016 [4], compared to 25 % in Austria [19]). Today, many of the original natural gas units have been replaced by biomass-fired plants, and increasingly solar thermal plants and HPs. The diffusion of large-scale HPs benefits from research and demonstration projects, collection and dissemination of knowledge [20], and targeted tax-reduction and financial support, e.g. [10], [21].

Within this work the private and socio-economic feasibility of large-scale heat pumps supplying DH was analysed compared to supply from individual units and to wood-fired heat only boilers in Austria and Denmark. The aim was to identify beneficial boundary conditions and barrier for the implementation of large-scale HPs as supply units for DH.

3 METHOD

The feasibility of different integration possibilities of HPs into DH systems was assessed for Denmark and Austria using the district heating assessment tool (DHAT) published by the Danish Energy agency [22]. The DHAT is an MS Excel based tool that can be used to calculate the economic feasibility of establishing DH in areas currently supplied by individual units. The tool includes technical data and price projections

that are adjustable for different countries. It includes a cost-benefit analysis for the local society, customers, and the DH company. It calculates the socioeconomic feasibility of the project according to Danish guidelines [23] and the levelized cost of energy (LCOE), including the total DH network cost, and investment, fuel and O&M cost for the supply units.

The economic evaluation for the local society refers to all entities involved in the project, while the socio-economic evaluation refers to the respective country [22]. The analysis takes the socioeconomic cost of fuels, investment and emissions into consideration, while assuming that the project itself does not have an impact on the electricity or fuel price level or the labour market. The socioeconomic as well as the local society net present value (NPV) were calculated as the difference between the net present value of the DH solution and the best individual supply solution.

The DHAT as published by the Danish Energy Agency was extended to represent the HP coefficient of performance (COP) and cost in more detail to account for the characteristics of different heat sources. An estimation of the network cost and the heat losses were included to account for different DH temperatures. The analyses focussed on newly developed areas without the possibility to be connected to an existing grid. The feasibility was assessed for varying plot ratios, i.e. the ratio between the built space area and the land area supplied by DH, and thus linear heat demand densities (LHDD). The supplied area was fixed to 340,000 m^2. Five central unit types were considered - air source HP, groundwater HP, sewage water HP, wood pellet and wood chips boiler. Different DH forward and return temperature cases (80/50 °C, 70/40°C, 60/30 °C) were analysed for two heat demand scenarios. The DH solutions were compared to air-to-water HP, brine-to-water (ground source) HPs and electric boilers.

3.1 Estimation of DH network cost

To identify beneficial boundary conditions for the economic feasibility of central HPs, the network layout was not predefined. Instead the total network cost was estimated based on the plot ratio, the expected specific heat demand, the effective width and an estimated average pipe diameter, as proposed by Persson and Werner [24]. The plot ratio was varied in this analysis between 0.1 (very sparsely populated) to 1.4 (urban area). The expected specific heat demand was based on the Danish 2020 building regulation, according to which the total heat demand has to be reduced to the DHW demand only [25]. But it was expected that there still was a small SH demand due to the behaviour of the inhabitants (NB-medium). A second scenario with higher SH demand was examined to account for less energy efficient buildings (NB-high) [26], see Table 1. The piping cost were based on estimates given by Rambøll in DHAT [22]. The necessary electricity grid investment was disregarded.

Table 1 Specific heat demand scenarios

Scenario		SH demand	DHW demand	Total demand
New built (NB) medium	$[W/m^2/a]$	3	20	23
New built (NB) high	$[W/m^2/a]$	22.5	20	42.5

3.2 Heat supply units data

The central HPs for the analysis were sized to have a heat capacity which was 80 % and 65 % of the maximum demand for the NB-medium and NB-high case, respectively. The sizing criteria for the two scenarios were chosen to be different, as the scenario with very low space heating demand was dominated by daily variations of heat demand rather than seasonal variations. A restriction to less than 80 % of the

maximum demand would lead to increased utilization of peak units, in this case an electric boiler, and thus a considerably reduced system efficiency. Accordingly, the HPs' thermal capacities varied between 0.2 MW and 3.2 MW depending on the heat demand scenario and the plot ratio. Investments into a backup natural gas boiler and a heat storage were considered. The COP of the central and individual HPs was calculated from the sink and source mean logarithmic temperatures and estimated exergy efficiencies [27]. Exergy efficiencies of 0.5 for the central HPs and 0.3 for individual HPs were assumed. The source temperatures for air-source HPs were hourly values from the Danish Design Reference Year [28] and the standard temperature development for Vienna [29]. The sewage water temperature was assumed to be constant at 12.5 °C. The groundwater temperature was assumed to be 10 °C. Weather compensation was applied to the DH supply temperature for ambient air temperatures below 5 °C [30]. Cost functions and assumed lifetime of all technologies are depicted in Table 2. As the cost functions were based on only few data and many of the HPs considered in this study have capacities lower than the values given in [31], an additional power function was fitted to the data to account for insecurities.

Table 2 Investment cost and lifetime for central and decentral units

Technology	Investment [M€/MW] linear/power function		Lifetime [a]	Sources
HP Groundwater	$1.1117\ \dot{Q}_{nom}^{-0.23105}$	$1.236\ \dot{Q}_{nom}^{-0.2599}$	25	[31]
HP Sewage water	$1.2166\ \dot{Q}_{nom}^{-0.33122}$	$1.1038\ \dot{Q}_{nom}^{-0.2435}$	25	[31]
HP Air	$0.9366\ \dot{Q}_{nom}^{-0.1418}$	$1.0503\ \dot{Q}_{nom}^{-0.3078}$	25	[31]
Wood chips boiler	0.9		20	[32]
Wood pellet boiler	0.48		20	[32]
Electric boiler	0.11		20	[32]
Gas boiler	0.06		25	[32]
Indv. Air to water HP	0.95		15	[32]
Indv. Brine to water HP	1.52		20	[32]
Indv. Electric heater	0.86		30	[32]

4 RESULTS

4.1 Levelized cost of energy

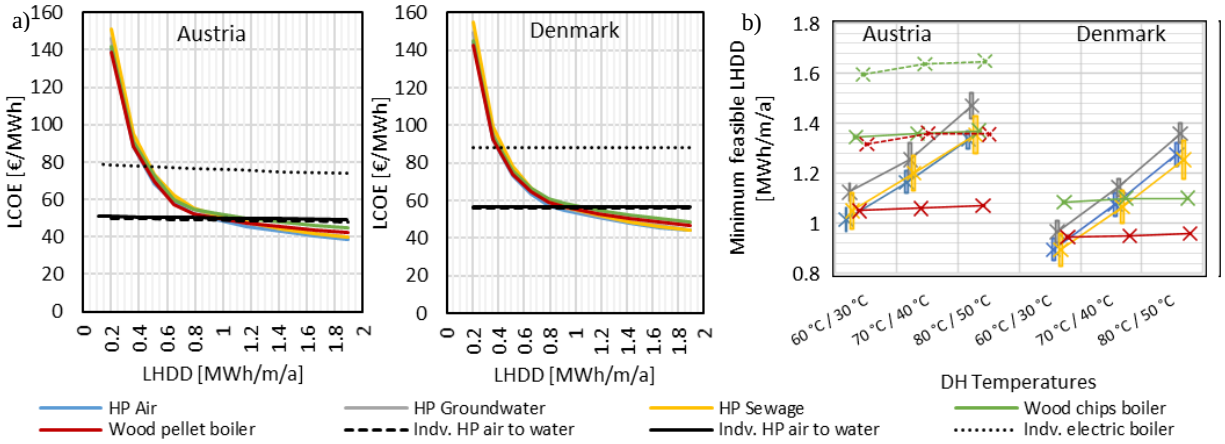

Figure 2 a) LCOE for central and individual units for Austria and Denmark, DH temperatures of 60/30 °C, NB-medium and linear HP cost functions , b) Range of minimum feasible LHDD for central solutions for different DH temperature cases, dashed lines refer to cases without subsidies

Figure 2 a) the LCOE of all central units are compared to the three decentral units for the NB-medium heat demand scenario and distribution temperature of 60 °C forward and 30 °C return for Austria and Denmark.

The cheapest individual solution was using air to water HPs. The LCOE development for decreasing LHDD was similar for all central generation units. It was lower than the LCOE from individual units for LHDD higher than 1.34 (1.08) MWh/m/a for wood chips boiler to 0.97 (0.85) MWh/m/a for air-source HPs for Austria and Denmark (in brackets), respectively. These LHDD translate to plot ratios of 0.5-0.6 with NB-medium demand buildings, this could e.g. be in suburban areas with 1-2 family houses. For lower LHDD the LCOE increase drastically. This had two major reasons, firstly the share of network cost of the total cost increased with lower LHDD. Secondly, the heat losses in the system increased as LHDD decreased. The LCOE of all technologies was lower in Austria due to differences in electricity taxation. In both cases, central heat pumps were in in the same LCOE range as wood-fired boilers.

The level of LCOE and thereby the minimum feasible LHDD depended on various factors. Figure 2 b) shows the minimum feasible LHDD for different DH temperature cases. The minimum feasible LHDD was lower in Denmark compared to Austria. The representation as bars accounts for the uncertainties in the HP cost functions, which is largest for sewage water HPs. In the Austrian case also the cost for wood-fired boilers without subsidies is shown. Compared to these all HP types would have lower minimum feasible LHDD and thus LCOE than the wood-fired boilers for DH temperatures of 70 °C/40 °C and 60 °C/30 °C. The implementation of HPs seemed especially beneficial for low DH temperatures, where the HPs benefited from better COPs due to the lower temperature lift. The calculated HP COPs can be seen in Table 3.

Air-source HPs were cheaper than groundwater HPs for NB-medium. This was due to new buildings considered, i.e. there were no large demand peaks in winter. Accordingly, the advantage from a better COP in winter for the groundwater HPs was lower and the cheaper investment cost for air source HPs made the difference. For the NB-high case the seasonal variation was considerable and the air-source HP could not compete with groundwater and sewage water HP.

The influence of the electricity and wood price (excl. taxes) on the economic feasibility of the different solutions was assessed. Figure 4 shows that the minimum feasible LHDD for central solutions increased for decreasing electricity price. This was due to the reduction in production cost in the individual unit. As the LCOE for central solutions also included the investment in the DH network, the effect of a reduction in fuel cost was less pronounced than for individual units. For increasing electricity prices wood-fired boilers became cheapest, especially for low LHDD. The variation of wood prices showed that a reduction in wood prices would decrease the minimum feasible LHDD and increase the feasibility for wood-fired boilers also for low DH forward and return temperatures. It was further studied how a variation in network cost, central HP COP and central unit investment cost influenced the minimum feasible LHDD. The results showed that the LCOE for heat sparse networks was most sensitive to a change in distribution network investment.

Table 3 COP of central HPs for different DH temperature cases and HD scenarios for Austria / Denmark

	HP air			HP groundwater			HP sewage water		
DH-Temp. [°C]	60/30	70/40	80/50	60/30	70/40	80/50	60/30	70/40	80/50
NB-medium	4.26/4.10	3.47/3.37	2.96/2.89	4.31	3.50	2.98	4.62	3.70	3.11
NB-high	4.15/3.99	3.40/3.29	2.91/2.83	4.31	3.50	2.98	4.62	3.70	3.11

4.2 Socioeconomic net present value

Figure 3shows the socioeconomic NPV of a DH project for different central solutions compared to supply by individual air-to-water HPs in Austria and Denmark. The NPV of the HP cases obtained for Denmark were slightly higher than for Austria. From a

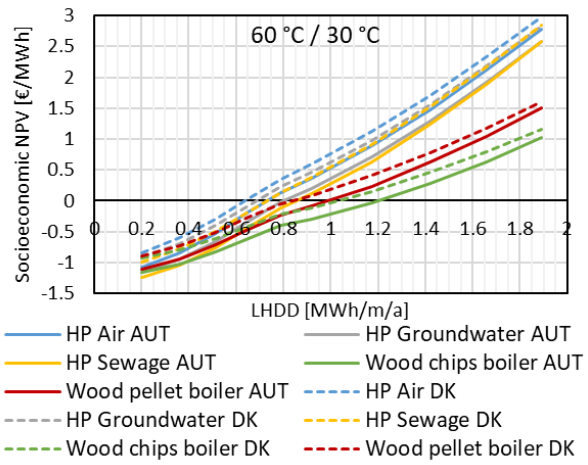

Figure 3 socioeconomic NPV for DK and AUT, DH temperatures of 60 °C/ 30°C, NB medium, lin. cost function

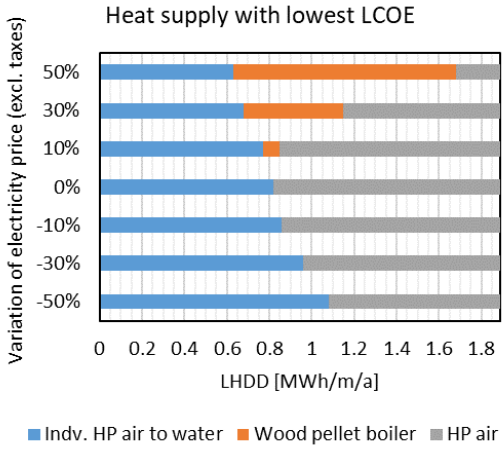

Figure 4 Solution with lowest LCOE for varying LHDD and electricity price, DH temperatures of 60 °C/ 30°C, NB medium, lin. cost function

socioeconomic perspective the DH solutions based on HPs were clearly better than the wood-fired boilers due to the emission cost caused. It has to be noted that this result was based on the assumption that the realization of the respective project will not change the countries' electricity generation portfolio.

When varying wood and electricity price it was observed that the wood-fired boilers became socioeconomically more feasible than the best HP solution, only for a reduction in wood price of 50 %. And even for an increase of 50 % in electricity price the heat pumps were socioeconomically more feasible than the boilers. Varying the DH temperature sets, it was observed that the increase in NPV with decreasing temperature was much more pronounced for HPs than for wood-fired boiler. This was due to the assumption of a constant boiler efficiency, while the HP COP changed with DH temperatures.

5 DISCUSSION

Comparing the results to current values from Denmark it was found that distribution cost, LCOE and LHDD showed to be in good agreement with the values from realised projects [33].

In areas with very low LHDD central DH solutions based on HPs have to compete with heat supply from individual units and DH supply based on biomass-fired units. The feasibility of HPs supplying DH in heat sparse areas was better in Denmark than in Austria. Lower DH-temperatures and reductions in distribution costs were beneficial. These may be obtained by new piping types, and cost efficient digging [34].

However, the case of heat sparse areas is a very special case and it needs to be mentioned that the economic feasibility of heat pumps supplying DH in terms of LCOE and socioeconomic NPV improved for larger LHDD compared to the studied alternatives. Further, the heat pump cost functions used were based on very few built heat pumps all larger than 800 kW and thus showed insecurities for smaller HP capacities. It should be kept in mind that the study presented aimed at identifying overarching trends but cannot replace a detailed planning for a specific project in question.

The feasibility of the different solutions depended on the boundary conditions in place. The available subsidies for wood-fired boilers in Austria made this type of heat supply units especially attractive for small-scale networks. As shown would central HPs be a better option for low temperature networks (60 °C / 30 °C and 70 °C / 70 °C) in Austria, without the subsidies for wood-fired boilers. As the wood used as a

fuel in Austria is often produced in close vicinity to the heating plant, it can be assumed that lower prices than the assumed market prices can be obtained. As showed this results in cheaper LCOE than central heat pump units can provide, even for low DH forward and return temperatures.

Within this study ambient heat sources were considered for the HPs. However, if industrial waste heat, even at low temperature levels was available, heat source exploitation cost could be lower compared to e.g. groundwater HPs and subsidies would be available for waste heat utilization in Austria, which would improve the economic feasibility of HPs [35]. There is however no financial support available for ambient heat sources or waste heat sources from communal sewage water.

The implementation of large-scale HPs in Denmark benefits from their socioeconomic feasibility, as heat supply projects in Denmark must prove private- and socioeconomically beneficial. Further, the Danish owner structure and regulation provides stable conditions for long-term investment into DH systems.

Finally, from an energy system perspective, HPs could play an important role in terms of system integration and thereby provide flexibility to the power system. Providing regulation power might generate further income opportunities for HPs and thereby increase the economic feasibility, also in heat sparse areas.

6 CONCLUSION

It was shown that DH supplied by central HPs compared to individual heat supply from air-to-water HPs was economically feasible in Denmark and Austria down to LHDD of 0.85 and 0.97, respectively, depending on the DH supply temperatures and the type of HP. The economic benefit increased with increasing LHDD, i.e. less energy efficient buildings or higher plot ratios. The reduction of seasonal peaks in low energy buildings benefited the economic feasibility of ambient source HPs. A barrier large-scale HPs in Austria is the promotion of wood-fired boilers as an alternative heat supply solution, while financial support to ambient source HPs is currently not available. A reduction in electricity cost would as well reduce the feasibility of central HP solution in heat-sparse areas (without a priori existing DH network), as this would decrease the LCOE of individual units more than of central units. Apart from recent tax reductions on electricity, research and dissemination activities the non-profit regulation and the condition of socioeconomic feasibility enhance the feasibility of large-scale heat pumps for DH supply in Denmark.

7 ACKNOWLEDGEMENT

This research project is financially funded by EUDP (Energy Technology Development and Demonstration) under the project ”EnergyLab Nordhavn - New Urban Energy Infrastructures” (project number: 64014-0555).

8 BIBLIOGRAPHY

[1] H. Lund *et al.*, “4th Generation District Heating (4GDH): Integrating smart thermal grids into future sustainable energy systems,” *Energy*, vol. 68, pp. 1–11, 2014.

[2] P. A. Østergaard, H. Lund, and B. V. Mathiesen, “Smart energy systems and 4th generation district heating,” *Int. J. Sustain. Energy Plan. Manag.*, vol. 10, pp. 1–2, 2016.

[3] A. David, B. V. Mathiesen, H. Averfalk, S. Werner, and H. Lund, “Heat Roadmap Europe: Large-Scale Electric Heat Pumps in District Heating Systems,” *Energies*, vol. 10, no. 4, p. 578, Apr. 2017.

[4] Danish Energy Agency, *Energy statistics 2016*. Danish Energy Agency, 2018.

[5] Energie-Control Austria, “Key Statistics 2016,” 2016.

[6] M. G. Fernández, C. Roger-Lacan, U. Gährs, and V. Aumaitre, *Efficient district heating and cooling systems in the EU*, no. December. 2016.

[7] R. Büchle *et al.*, “Bewertung des Potenzials für den Einsatz der hocheffizienten KWK und

effizienter Fernwärme- und Fernkälteversorgung," no. September 2015, p. 147, 2015.
[8] Danish Energy Agency, "Biomass | Energistyrelsen." [Online]. Available: https://ens.dk/en/our-responsibilities/bioenergy/solid-biomass. [Accessed: 13-Jun-2018].
[9] Danish Energy Agency, "Analysis of Bioenergy in Denmark (Analyse af bioenergi i Danmark)," no. March 2012, p. 160, 2014.
[10] Energi- Forsynings- og Klimaministeriet, "Forslag til Lov om ændring af lov om fremme af vedvarende energi, lov om tilskud til fremme af vedvarende energi i virksomheders produktionsprocesser og lov om elforsyning," no. 1756, pp. 11–13, 2016.
[11] C. Maurer *et al.*, "Grünbuch für eine integrierte Energie- und Klimastrategie," p. 106, 2016.
[12] R. Madlener, "Innovation diffusion, public policy, and local initiative: The case of wood-fuelled district heating systems in Austria," *Energy Policy*, vol. 35, no. 3, pp. 1992–2008, 2007.
[13] RIS, "Gesamte Rechtsvorschrift für Umweltförderungsgesetz." 2018.
[14] "QM Holzheizwerke." [Online]. Available: www.qmholzheizwerke.ch [Accessed: 25-Jul-2018].
[15] M. Hartl, P. Biermayr, A. Schneeberger, and P. Schöfmann, "Österreichische Technologie-Roadmap für Wärmepumpen," 2016.
[16] Dansk Fjernvarme, "Heat generation in Denmark," 2013.
[17] Energi- Forsynings- og Klimaministeriet, "Bekendtgørelse af lov om varmeforsyning," vol. 2017, no. 523, p. 24, 2014.
[18] Danish Government, "Reformopfølgning Regulering af fjernvarmesektoren," no. 7. april, p. 4, 2016.
[19] FGW – Fachverband der Gas- und Wärmeversorgungsunternehmungen, "Zahlenspiegel 2017 Erdgas und Fernwärme in Österreich," Wien, 2017.
[20] Danish Energy Agency, "Rejsehold for store varmepumper | Energistyrelsen." [Online]. Available: https://ens.dk/ansvarsomraader/varme/rejsehold-store-varmepumper. [Accessed: 21-Jun-2018].
[21] C. E. Fich, P. Bentzen, and S. S. Birkbak, "Tilskud til eldrevne varmepumper og rådgivning til grundbeløbsværker," no. september 2017, pp. 2017–2019, 2018.
[22] Rambøll, "District Heating Assessment Tool." Danish Energy Agency, 2017.
[23] Energistyrelsen, "Vejledning i samfundsøkonomiske analyser på energiområdet," 2005.
[24] U. Persson and S. Werner, "Heat distribution and the future competitiveness of district heating," *Appl. Energy*, 2011.
[25] C. F. Hansen and M. L. Hansen, "Executive Order on the Publication of the Danish Building Regulations 2015 (BR15)," vol. 2015, no. 1185, 2015.
[26] HOFOR, "Fjernvarmeforsyning af nordhavn," no. 6210, 2013.
[27] J. K. Jensen, T. Ommen, W. B. Markussen, and B. Elmegaard, "Design of serially connected district heating heat pumps utilising a geothermal heat source," *Energy*, 2017.
[28] P. G. Wang, M. Scharling, K. B. Wittchen, and C. Kern-Hansen, "Technical Report 13-19 2001 – 2010 Danish Design Reference Year - Reference Climate Dataset for Technical Dimensioning in Building , Construction and other Sectors," 2013.
[29] Meteotest AG, "Meteonorm: Irradiation data for every place on Earth." [Online]. Available: http://www.meteonorm.com/en/. [Accessed: 22-Jun-2018].
[30] X. Yang ,S. Svendsen, "Ultra-low temperature district heating system with central heat pump and local boosters for low-heat-density area: Analyses on a real case in Denmark," *Energy*, Jun. 2018.
[31] H. Pieper, T. Ommen, F. Bühler, and B. Lava, "Allocation of investment costs for large-scale heat pumps supplying district heating Contact information :," vol. 00, p. 64014, 2017.
[32] Energinet.dk, "Technology Data for Energy Plants," 2016. [Online]. Available: www.ens.dk. [Accessed: 12-Oct-2017].
[33] Dansk Fjernvarme, "Dansk Fjernvarmes statistik 2017," 2018. [Online]. Available: http://www.danskfjernvarme.dk/viden-om/statistik-subsection/aarsstatistik/statistik-2017. [Accessed: 20-Jun-2018].
[34] H. Zinko, B. Bøhm, H. Kristjansson, U. Ottosson, M. Rämä, and K. Sipilä, "District heating distribution in areas with low heat demand density," 2008.
[35] Kommunal Kredit Public consulting, "Informationsblatt Abwärmeauskopplung," no. 113, pp. 1–5, 2018.
[36] Bundesministerium für Wissenschaft Forschung undWirtschaft, "Energie in Österreich - Zahlen, Daten, Fakten," 2017.

DTU Mechanical Engineering
Section of Thermal Energy
Technical University of Denmark

Nils Koppels Allé, Bld. 403
DK-2800 Kgs. Lyngby
Denmark

Phone: +45 4525 4131
Fax: +45 4525 1961

www.mek.dtu.dk

January 2020

DCAMM
Danish Center for Applied Mathematics and Mechanics

Nils Koppels Allé, Bld. 404
DK-2800 Kgs. Lyngby
Denmark
Phone (+45) 4525 4250
Fax (+45) 4525 1961

www.dcamm.dk

DCAMM Special Report No. Sxxx

ISSN: 0903-1685